Development and Mechanistic Studies of Ti-Mediated C-N and N-N Coupling Reactions

A DISSERTATION

SUBMITTED TO THE FACULTY OF THE

UNIVERSITY OF MINNESOTA

BY

Yukun Cheng

IN PARTIAL FULFILLMENT OF THE REQUIREMENTS

FOR THE DEGREE OF

DOCTOR OF PHILOSOPHY

Ian A. Tonks, Advisor

November 2022

Acknowledgements

First, I would like to thank my Ph.D. advisor, Prof. Ian Tonks. Ian has always been an excellent academic advisor and mentor, and a good friend to me. He is not only knowledgeable but also resourceful, and have given many valuable advice that allowed me to understand how to do research properly and efficiently. He has also been very supportive to my career decisions and provided me with practical suggestions, despite I had changed my route multiple times during the uncertain times in the pandemic. I would like to thank his generosity of supporting me to attend various conferences, including the costly Pacificchem which is an incredibly rare opportunity for a student. Although the Pacificchem turned into a virtual conference, I still got the chance to go to Organometallic GRC instead, and the reason I got the chance to have my debut in the OM community at GRC was also largely owing to Ian's reputation. I would also like to thank him for the freedom he gave me in exploring my own research interests — I literally have been working on ideas of my own on the side from my first year to last year non-stop. This allowed me to learn various techniques and practice how to make proposals, and I can always trust Ian on guiding me back when I was too distracted from my main path.

Next, I would like to thank the people I spent the longest time with during my graduate school — the Tonks group. I have the privilege to work with some of the smartest and kindest people for more than 5 years. First, I would to thank the past grad students when I started: Drs. Peter Dunn, Zach Davis-Gilbert, Jimmy Chiu, Abby Smith, Adam Pearce, Xin Yi See, and Evan Beaumier, who all had kindly welcomed me into the lab when I was panicking with the language barrier and working in a unfamiliar research field. Jimmy, thank you for being my mentor when I started. Some of the advice you gave from those time ended up benefiting my whole grad school, *e.g.* trying different intro in every presentation for different groups of audience. Zach, your humor cheered me up a lot when I was trying to sort out the tight first year schedule. Just to let you know I still use Yukuna Matata as my name in games. Abby, thanks for the relaxing lab music and your tolerance when I crammed in the Eve box schedule in my first year. The lake house trip is an unforgettable memory to me. Adam, thanks for setting up such a good role model as an awesome chemist. I learned a lot from you on how to lead the academic atmosphere in the group as a senior grad student and I really appreciate it. Xin Yi, thanks for being the big sis in the group housekeeping both the rules and the details for so many years. We were definitely spoiled — you don't want to know how chaotic the lab space was in the month following your graduation. So thank you a lot for being so kind to everyone in the lab,

including me. Also a special thanks to Adam and Xin Yi for dragging the drowning me back to shore from the lake. Evan, I really appreciate the chemistry and Pokemon Go chats we had on the bus rides home we shared, and the numerous rides you offered me. The napping on the canoe was some of the best time I've had in MN. I will need your help again whenever I have another invisible cat hidden under my armchair. I would like to thank Drs. Gereon Yee, Ben Reiner, Yu-Ling Lien, Dan Huh, and Ross Koby, who have overlapped with me in the Tonks group in their post-doc time and have been some very knowledgeable colleagues I could learn from. Gereon, you showed me how to ask questions and how to keep a high level of curiosity to a broad scope of research, which has been very helpful to me. Ben, you and Adam gave me my initial confidence in grad school — your recognition meant a lot to the young me. Yu-Ling, the coffee time before the seminar and the chemistry chat after were always an enjoyable way to start the Tuesdays and Thursdays. I miss you and the time we worked together. Dan, thanks a ton for the tremendous help you offered during my post-doc application. From telling me the importance of Twitter to cover letters, interview strategies, offer negotiation and post-doc experience, you have covered almost every possible aspect I would come across. Besides that, thanks for contributing to the most versatile :dan: emoji. The 2022 new year party is one of the highlights in my grad school. Ross, we got along well soon after you joined, and I have been very happy working with you since — for the first time in grad school I have a colleague close to my stage sharing similar career goals. I really appreciate all the chemistry chats, grocery rides, cooking parties and that you took care of me during my dental surgery. Thanks for all the help during my post-doc search too. Besides these, I would like to sincerely thank Evan, Dan, and Ross for being great listeners. I had consulted/complained to them about various things from work stuff to career decisions. Despite being usually in different positions (as I'm an international student), they all have been very patient to my grumbles and given me good advice. I would also like to thank the now-5th year team: Steven Butler, Connor Frye, Janaya Sachs, and Shao-Yu Lo. We overlapped the longest time in grad school, and I appreciate working with every one of you. Steven, thanks for being an awesome deskmate. It has been a great pleasure working next to you and I enjoyed your funny jokes a lot. Your cheerful character is indispensable on the 6th floor. Connor, thanks for the helpful discussions that save my day multiple times. Your expertise in catalysis and calculations are always very reliable. You are also a rigorous and responsible chemist, and working with you on projects have been as easy as a breeze. Janaya, thanks for talking to me about your concerns near the end of grad school and also listening to my progress. It is heartwarming to know that there will be someone cheering for you when there's good news.

Shao-Yu, you are a great chemist and but a greater batter! Don't let covid get in the way of your softball career! Jokes aside, I really enjoy working with you — you are chilled, funny, and hardworking, and I am sure you will get well rewarded soon from your professionalism. I would like to thank all the talented younger students for providing the group a bright future so that we can always have a healthy working atmosphere: Rachel Dunscomb, Rachel Rapagnani, Kate Rynders, Michael Harris, Jaekwan Kim, Ryan Anderson, and Partha Sarathi Karmakar. In particular, I would like to thank Rachel D for always being the nicest person in the office, including helping me take photos on my defense. Michael, thank you for offering some good discussions with me in my last few years here, on both chemistry and American culture. You are curious, knowledgeable, and have plenty of passion to chemistry. I am sure success is awaiting you. Partha, as you said, we share a lot of similarity — on chemistry or not — and we sometimes think alike too. Chatting over the world map on geography with you was a lot of fun, so was the State Fair we went together. I am really happy to have worked with you, although we only overlapped for 1.5 years. I would also like to thank Dominic Egger and Tobias Kaper, who were visiting scholars in the group during my time. Dominic, your curiosity to new chemistry was so motivating to me even in the midst of covid hibernation. As the saying says, "plans can never catch up with the changes", I'm sure you are now working on some very interesting and challenging research. Tobias, thanks for sharing with me how Germany is like. I really appreciate you as a good friend dragging me out to the Minnehaha fall and the Como lake for the trips full of fun, as I would definitely be too lazy to go just by myself. The Oldenburg research symposium you introduced me to was also a very valuable experience to me. I can't wait to meet you again in Germany one day. I would also like to thank my two undergraduate mentees, Channing Klein and Xavier Murray. You have been both incredibly smart and hardworking, and I have learned a lot from the mentorship. I would like to express my appreciation to all the other people I shortly overlapped with: Alex Wheeler, Jessica Bruggen, Dr. Addison Desnoyer, Samir Ahmed, Jiawei Li, Dr. Robin Harkins, Errikos Kounalis, Dr. Carlton Folster, Zoe Stuart, Ethan Ashbrook, and all the other undergraduate researchers. I enjoy my every second working in the Tonks group, which comes from the effort of all the lab members I have worked with.

Outside the group, I would like to thank my friends in the department, in no particular order: Dr. Letitia Yao, Dr. Shuangning Xu, Dr. Brendan Graziano, Dr. Michael Dorantes, Dr. Jacob Prat, Dr. JT Moore, Josh Gavin, Dr. Roman Belli, Dr. Casey Carpenter, Andrey Joaqui, Chase Abelson, Siri Kanchanakungwankul, Bach Nguyen, Dr. Minog Kim, Dr. Xiaoxiao Yao, Dr. Lun Jin, and Yoon-Jung Jang. It has always been refreshing to chat with you from time to time, on

chemistry or not. I would like to thank Shuangning for helping me in adapting to the life in the US during my first few months here and also telling me to check out the Tonks group, which eventually led me to join the group. I would also like to thank Roman for being an awesome roommate during the GRC and allowing me to share my thoughts when I was getting nervous on the big conference atmosphere.

I would like to thank the people that allow this thesis happens. First, I would like to thank my thesis committee, Prof. Christopher Douglas, Prof. Courtney Roberts, and Prof. Courtney Aldrich. Prof. Douglas has been following up on my grad school progress step by step since my first year, and I can't thank you enough for that. I would like to thank Prof. Roberts and Prof. Aldrich for stepping up to take the spots during the uneasy time when there were only three months away from my defense. I would also like to thank Dr. Nicholas Race for serving on my preliminary exam committee. I would also like to thank the administrative staffs, Nancy Thao, Mollie Dunlap, Dan MacEwan, Justin Thao, Mark Bell and Adam Baxter, who allowed me to work smoothly during my grad school.

I have the privilege to work with many awesome collaborators. I would like to thank Dr. Joel Patrow, Dr. Cynthia Pyles, and Prof. Aaron Massari for allowing me to join their research on the Ru hydride complexes. From outside the department, I would like to thank Felix de Zwart and Prof. Bas de Bruin for their help in the low temperature EPR studies, Dr. Christian Jacobson and Prof. Naomi Halas for allowing us to join their research on Al nanoparticles, as well as Dr. Bryan Foley and Prof. Oleg Ozerov for the Ir catalyst they gifted us. I would also like to thank Dr. Kris Altus, who selflessly spent two hours teaching me COPASI at the margarita night at GRC, enjoying margarita the same time for sure.

I need to thank my old friends from college, who still chat and hang out with me despite some being on the other hemisphere. I would like to thank Shu Wang and Yifan Zhu for hosting when I visited. We had a lot of fun during the road trip to D.C. and my stay in Boston. Li Wang is another friend I must thank — you save our lives with your 20 mL vials last year when the whole US supply market was out. The long phone call chat on random stuff from chemistry to life is always something I am looking forward to. To Zhen Yang, Weiwei He, Jianfei Ma, and Zhengzhi Chen, thanks for staying connected and bearing the time zone difference with me when chatting. I also want to thank my undergraduate research advisors, Prof. Yongye Liang and Prof. Keith Man-Chung Wong. In Prof. Liang's lab I got to know what chemistry research is for the first time. Keith provided me with a lot of freedom in exploration for nearly 3 years, allowing me to have a basic understanding to several research fields and decide to take on

synthetic chemistry as my research interest. I would also like to thank an old friend of mine, Jinwen Wang, for the 24 years friendship we have despite our careers have sailed to dramatically different paths.

Lastly but most importantly, I must express my deepest gratitude to my family, dad Weixiong Cheng, mom Yongjian Gao, grandma Bilan Yang, and grandpa Guoshen Gao. Dad, me eventually becoming a scientist is all owing to you, as you have always been my role model. I am proud to be your son. Mom, thank you for always being considerate and respectful to all my decisions. Grandma, thank you for your forever lasting love to me. Grandpa, thank you for still doing readings online in your 80s to discuss grad school life with me — your wisdom and humbleness have won my utmost respect. The weekly phone calls home since COVID have given me tremendous support in mental health. It is also because of the decisions and supports from all of you that I can freely pursue my career goal. Despite being more than ten thousand miles away, I can still feel our hearts are very close.

Table of Contents

List of Tables

List of Figures

List of Abbreviations

Ac = acetyl

Alk = alkyl

Ar = aryl

PhNNPh = azobenzene

Bn = benzyl

bpy = 2,2’-bipyridine

PPN = bis(triphenylphosphine)iminium

9-BBN = 9-borabicyclo[3.3.1]nonane

^{n}Bu = *n*-butyl

COSY = correlated spectroscopy

ºC = degree Celsius

DFT = density functional theory

DCM = dichloromethane

DOSY = diffusion ordered spectroscopy

eqn = equation

EPR = electron paramagnetic resonance

ESI = electrospray ionization

equiv = equivalent

Et = ethyl

EXSY = exchange spectroscopy

Exp # = experiment notebook page number

Fc = ferrocene

Fc^{+} = ferrocenium

FID = flame ionization detector

GC = gas chromatography

g = gram(s)

HMBC = heteronuclear multiple bond correlation

HSQC = heteronuclear single quantum coherence

HMDS = hexamethyldisilazane

$HMDS^-$ = hexamethyldisilazide

HMDSO = hexamethyldisiloxane

HR = high-resolution

h = hour(s)

^{i}Pr = isopropyl

ISPCA = iterative supervised principal component analysis

LMCT = ligand-to-metal charge transfer

MS = mass spectroscopy

MHz = megahertz

Mes = mesityl

M = metal or molecular peak

Me = methyl

mg = milligram(s)

mL = milliliter(s)

MLR = multivariate linear regression

NMR = nuclear magnetic resonance

NOESY = nuclear Overhauser effect spectroscopy

ppm = parts per million

Ph = phenyl

Bpin = (pinacolato)boryl

PTFE = poly(tetrafluoroethylene)

PCA = principal component analysis

^{n}Pr = *n*-propyl

PCET = proton-coupled electron transfer

py = pyridine

[Ox] = oxidant

RNI = redox non-innocent

r.t. or RT = room temperature

R = substituent

THF = tetrahydrofuran

TEMPO = (2,2,6,6-tetramethylpiperidin-1-yl)oxyl

Tol = 4-tolyl

SnR_3 = trialkylstannyl

TMB = 1,3,5-trimethoxybenzene

TMS = trimethylsilyl

TPM = triphenylmethane

XRD = x-ray diffraction

Chapter 1: Titanium-Mediated N–X Coupling and Related Transformations

1.1 Motivation

Titanium has one of the highest elemental concentrations in the earth's crust among transition metals, only second to iron.[1] Owning to its high earth abundance, titanium has been credited as a sustainable metal in chemical synthesis. Meanwhile, titanium complexes generally undergo hydrolysis easily to the non-toxic and insoluble titanium dioxide (TiO_2). Adding to these advantages, titanium stands out as a benign metal due to its biocompatibility.[2,3] The stable titanium in the form of TiO_2 is resistant to various corrosion in biological systems, rendering titanium to be a bioorthogonal metal. This provides titanium with a higher potential than the noble metals in syntheses of pharmaceuticals, where the high natural cytotoxicity of noble metals requires extra cost in the rigorous removal of metal residue.[4]

Despite the numerous merits, titanium is significantly underrepresented in transition metal catalysis. The majority of applications of titanium in chemical synthesis are stoichiometric and catalytic Lewis acid type or insertion type chemistry, for example, the Mukaiyama aldol addition and the Ziegler-Natta polymerization.[5,6] Meanwhile, titanium mediated redox synthesis has been largely limited to fundamental reactivity studies. The biggest hindrance to titanium redox catalysis is the reduction of high valent titanium species. The low electronegativity of titanium allows the high valent titanium species to have much higher stability than the low valent counterpart. As a result, the majority of titanium complexes are in their stable Ti^{IV} form with the reduction to Ti^{II} energetically highly unfavorable.[7] To overcome this challenge, various methods have been developed following redox non-innocent (RNI) as the design concept, including RNI auxiliary ligands like *α*-diimines and substrate redox non-innocence such as the Kulinkovich reaction.[8]

Our group has developed a series of Ti-catalyzed redox nitrene transfer reactions based on Ti imido.[9] In these reactions, azobenzene serves as both the π-acceptor in stabilizing Ti^{II} and the oxidant to oxidize Ti^{II} to Ti imido. The first half of this thesis focuses on the extension of this research direction by exploring new applications of azobenzene redox chemistry in other catalytic reactions mediated by Ti imido, as well as the development of new reactions that can lead to high complexity products based on the established transformations. More recently, our group has reported a rare Ti-mediated oxidative N–N coupling pyrazole synthesis from Ti imido, while the use of oxidants stronger than diazene has made the regeneration of Ti imido increasingly difficult. The second half of the thesis aims to investigate the mechanistic details

of the Ti-mediated oxidative N–N coupling and develop catalytic N–N heterocoupling from a wider source of substrates.

1.2 C–N Coupling

Titanium mediated C–N coupling has been a thriving research area in recent decades. This section will focus on the designs and challenges in catalytic C–N coupling reactions that inspire the development of novel Ti-catalyzed redox C–N couplings. Stoichiometric Ti-mediated C–N coupling will not be covered.

1.2.1 Ti-Catalyzed C–N Coupling Categorized by Redox Process

Titanium catalyzed C–N coupling reactions can be generally divided into three categories based on the redox process: (1) redox-neutral 1,2-insertion of C–X π bond to Ti–N bond of Ti amide; (2) oxidative coupling of Ti amide and carbanion ligand (often referred to as formal C–N reductive elimination); (3) nitrene transfer of Ti imido. Nitrene transfer can be a redox-neutral process when both the Ti and imido N are involved in the transfer (*e.g.* [2+2] cycloaddition of Ti imido) or an oxidative process when only the imido N is involved (*e.g.* 1,1-insertion of carbene to imido N), as shown in Figure 1.1. Several characteristic reactions will be discussed in this section to illustrate the relationship between the redox process and the nitrogen-containing substrates.

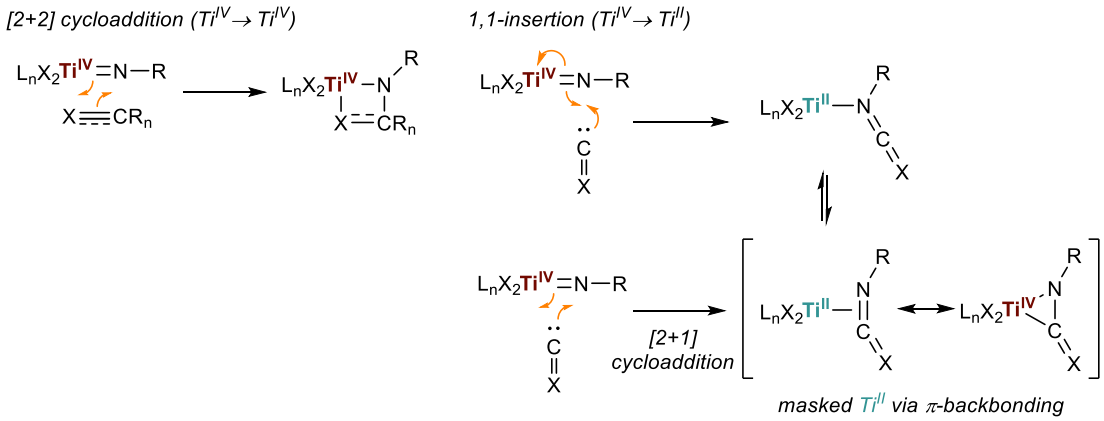

Figure 1.1. Examples of (left) redox-neutral and (right) oxidative nitrene transfer C–N coupling.

Ti-catalyzed hydroamination is one of the most prevalent Ti-mediated C–N bond formation methods. As a versatile reaction, hydroamination has found widespread synthetic applications from bioactives to polyenamines.[10–12] Initially reported in 1992, Livininghouse and Bergman pioneered the mechanistic investigation and synthetic application of group IV imido catalyzed hydroamination of alkynes with primary amines, specifically with cyclopentadienyl complexes of Ti and Zr.[10,11,13–16] Since then, a variety of catalysts have been designed in order to improve the selectivity and expand the scope of substrates, commonly featuring Ti bisamide or Ti dimethyl as the precursor to Ti imido.[17] The mechanism of Ti-catalyzed hydroamination of alkynes with primary amines is shown in Figure 1.2.[17–19] Protonolysis of Ti dimethyl precatalyst 1.1 with 2 equiv of primary amines leads to Ti bisamide **1.2**, followed by *α*-H abstraction of amide to give the active catalyst Ti imido **1.3**. The rate-determining [2+2] cycloaddition of **1.3** with alkyne yields azatitanacyclobutene **1.4**, which further undergoes protonolysis and *α*-H abstraction to regenerate Ti imido. Enamine **1.6** would tautomerize to imine **1.7** as the commonly observed reaction product. Recently, Schafer proposed an energetically more favorable process from **1.5** to **1.7** through σ-tropic rearrangement based on DFT calculations.[20] The reaction mechanism can be generally applied to Ti-catalyzed hydroamination of various C–C π bonds with primary amines, such as alkenes and allenes.[16,19,21] In this reaction, the C–N bond formation originates from the redox-neutral [2+2] cycloaddition of Ti imido. Primary amine enters the catalytic cycle as a Brønsted acid, which also serves as the nitrene source of Ti imido through further deprotonation in *α*-H abstraction.

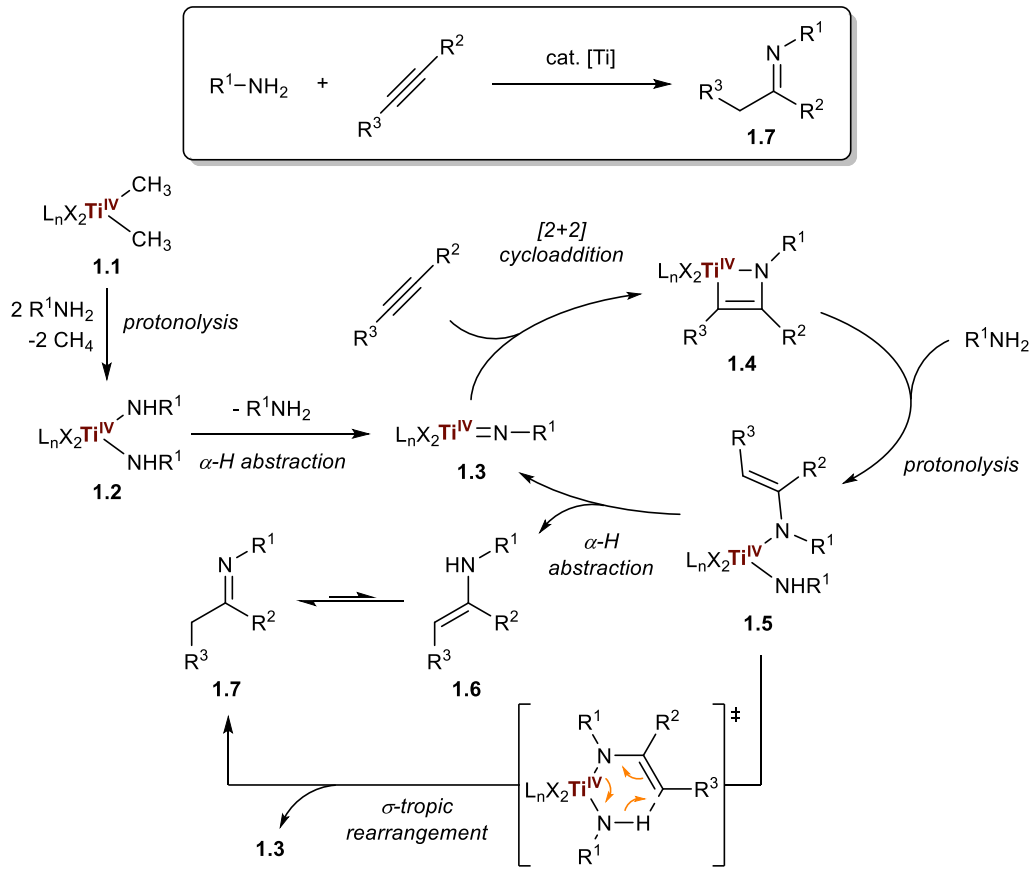

Figure 1.2. Proposed reaction mechanism of Ti-catalyzed hydroamination of alkynes with primary amines.

More sophisticated methods have been developed based on hydroamination with primary amines in order to access higher product complexity, including one-pot or tandem reactions with hydrogenation[22] and non-catalyzed cyclization.[23] An elegant example of these transformations is the Ti-catalyzed iminoamination reaction reported by Odom, where the hydroamination was “interrupted” by intercepting azatitanacyclobutene **1.4** with 1,1-insertion of isocyanide into the Ti–C bond (**1.8** and **1.9**) prior to the protonolysis with amine (Figure 1.3).[24–26] These derivatives of hydroamination share the same C–N bond formation process through [2+2] cycloaddition of Ti imido as the substrate being primary amines.

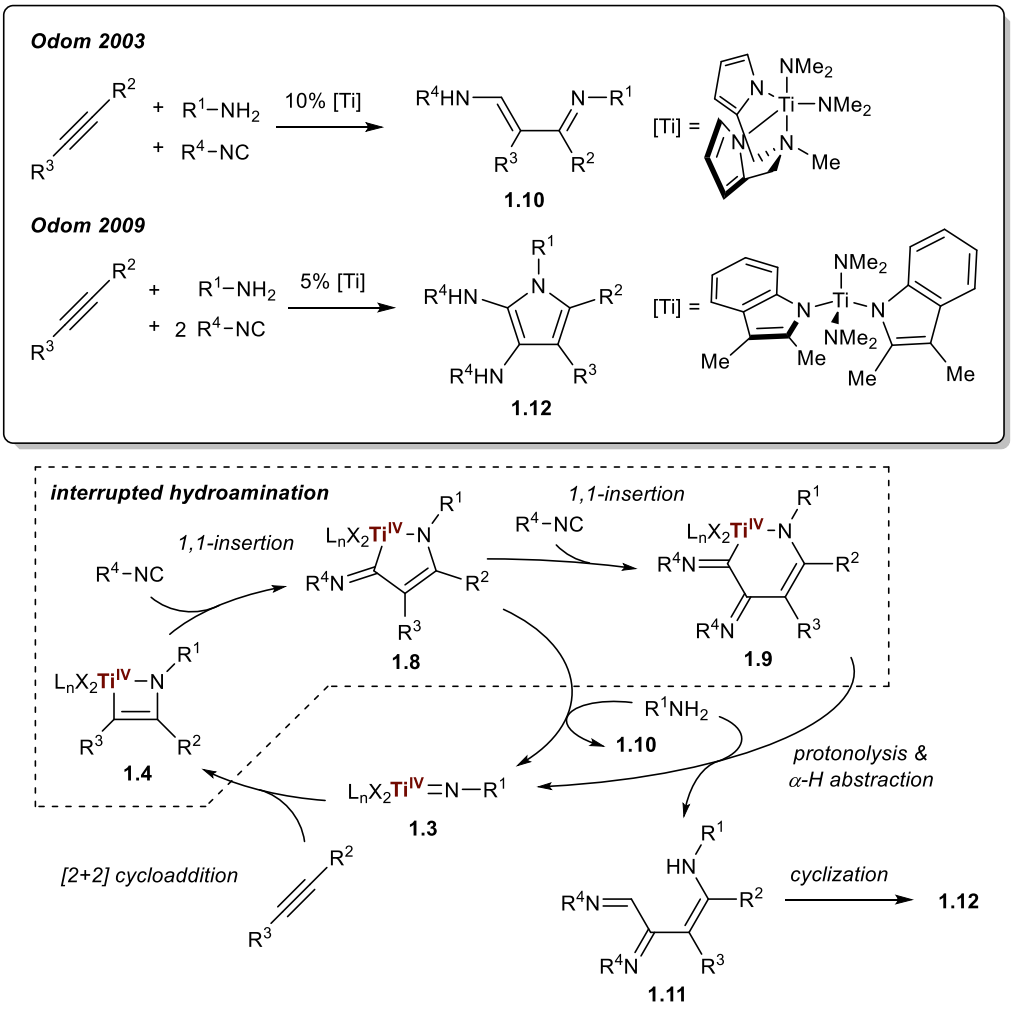

Figure 1.3. Proposed reaction mechanism of Ti-catalyzed iminoamination.

Secondary amines are also viable substrates in hydroamination of C–C π bonds using cationic Ti catalysts.[27] As disubstituted nitrogen could not further form covalent multiple bonds with metal, hydroamination with secondary amines undergoes an alternative reaction mechanism without Ti imido intermediate. Ti-catalyzed hydroamination of secondary aminoalkenes operates through a mechanism resembling hydroamination catalyzed by lanthanide metals (Figure 1.4).[17,27] Protonolysis of titanocene benzyl cation **1.15** with aminoalkene to give Ti amide complex **1.16**. **1.16** then undergoes 1,2-insertion of alkene into Ti–N bond to give **1.18** through **1.17**. Protonolysis of Ti alkyl by amine converts **1.18** to cyclic tertiary amine **1.14** and regenerates **1.16**. The C–N bond formation process in this reaction occurs through the 1,2-insertion of alkene to Ti amide, which is also a redox-neutral process.

Similar to primary amines, secondary amines also first serve as Brønsted acids to enter the catalysis through protonolysis.

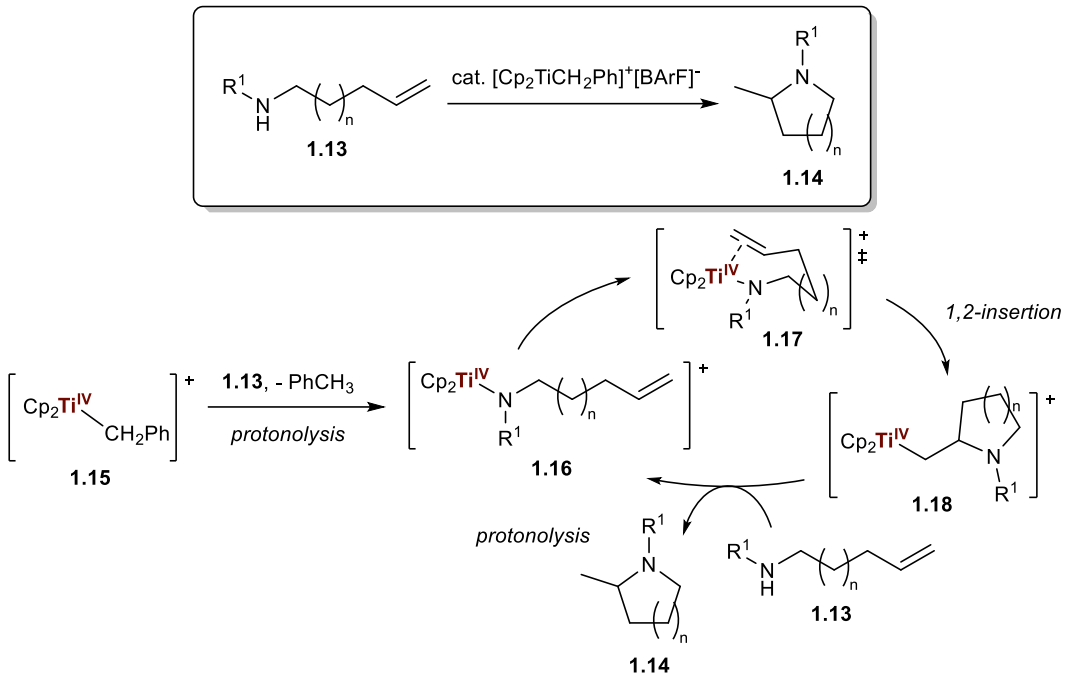

Figure 1.4. Proposed reaction mechanism of Ti-catalyzed hydroamination of secondary aminoalkenes.

Reductive elimination of Ti complexes is a very challenging process due to the high reduction potential of low valent titanium. Compared to the C–C or C–N bond being formed, the high reactivity of a non-stabilized Ti^{II} makes the reductive elimination energetically unfavorable. Meanwhile, a low valent metal can be stabilized through the formation of a π complex to become a formal high valent metal complex. The π-acceptor ligand can accept electron density from the metal through π backbonding, as explained in the Dewar-Chatt-Duncanson model.[28] Ti^{II} complexes masked by π-acceptor ligands such as alkenes and alkynes can be viewed as in resonance between the σ adduct of Ti^{II} and the Ti^{IV} metallacycle (Figure 1.5). This π stabilization effect has found its presence in a variety of Ti redox catalysis such as the Kulinkovich reaction and the Pauson-Khand reaction.[29–31]

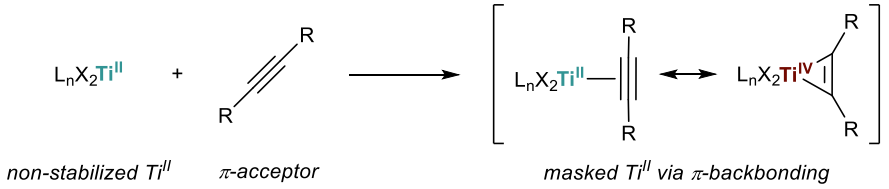

Figure 1.5. Stabilization of Ti^{II} *via* π backbonding.

Adapting the masked $Ti^{II/IV}$ redox catalysis design into C–N coupling, our group developed the Ti-catalyzed pyrrole synthesis through a formal [2+2+1] cycloaddition of Ti imido and alkynes.[32] This multicomponent reaction converts 0.5 equiv of diazene and 2 equiv of alkynes to pyrrole, featuring high atom economy and the use of simple feedstock and benign metal catalyst compared with other pyrrole synthesis methods.[33] Mechanistic investigation reveals that it undergoes a $Ti^{II/IV}$ redox cycle through Ti^{II} intermediates masked by pyrrole and diazene (Figure 1.6).[9,34] Ti-catalyzed [2+2+1] pyrrole synthesis initiates from the [2+2] cycloaddition of Ti imido **1.20** with alkyne. In the absence of amine for protonolysis, the resulting azatitanacyclobutene **1.21** undergoes the rate-determining insertion of the second alkyne to give azatitanacyclohexadiene **1.22**. After the C–N reductive elimination, **1.22** is converted to a Ti^{II}-pyrrole adduct **1.23**. The more π acidic diazene replaces pyrrole **1.19**, yielding the diazene-masked Ti^{II} **1.24**. The bimolecular diazene disproportionation process (**1.25** and **1.26**) releases half equivalent of diazene and returns Ti to Ti imido **1.20**. Two C–N bonds are formed in this reaction between the imido N and the alkynes. The first C–N bond is formed through the redox-neutral [2+2] cycloaddition of Ti imido and alkyne, which resembles the hydroamination with primary amines. The second C–N bond is formed through the formal reductive elimination of **1.22** in an electrocyclic fashion, similar to the C–C bond formation in Nazarov cyclization.[34] Thus, the second C–N bond formation can be viewed as a special class of oxidative coupling between an amide ligand and a carbanion ligand with a conjugated linker, during which Ti will be reduced from Ti^{IV} to Ti^{II}. To regenerate the high valent Ti imido catalyst, diazene is introduced as both the oxidant and the nitrene source, oxidizing the Ti^{II} **1.24** to Ti imido **1.20** through diazene disproportionation. Alternatively, alkyl azides can also be used as the oxidant and the nitrene source, oxidizing the Ti^{II} to Ti imido through a different mechanism.[35]

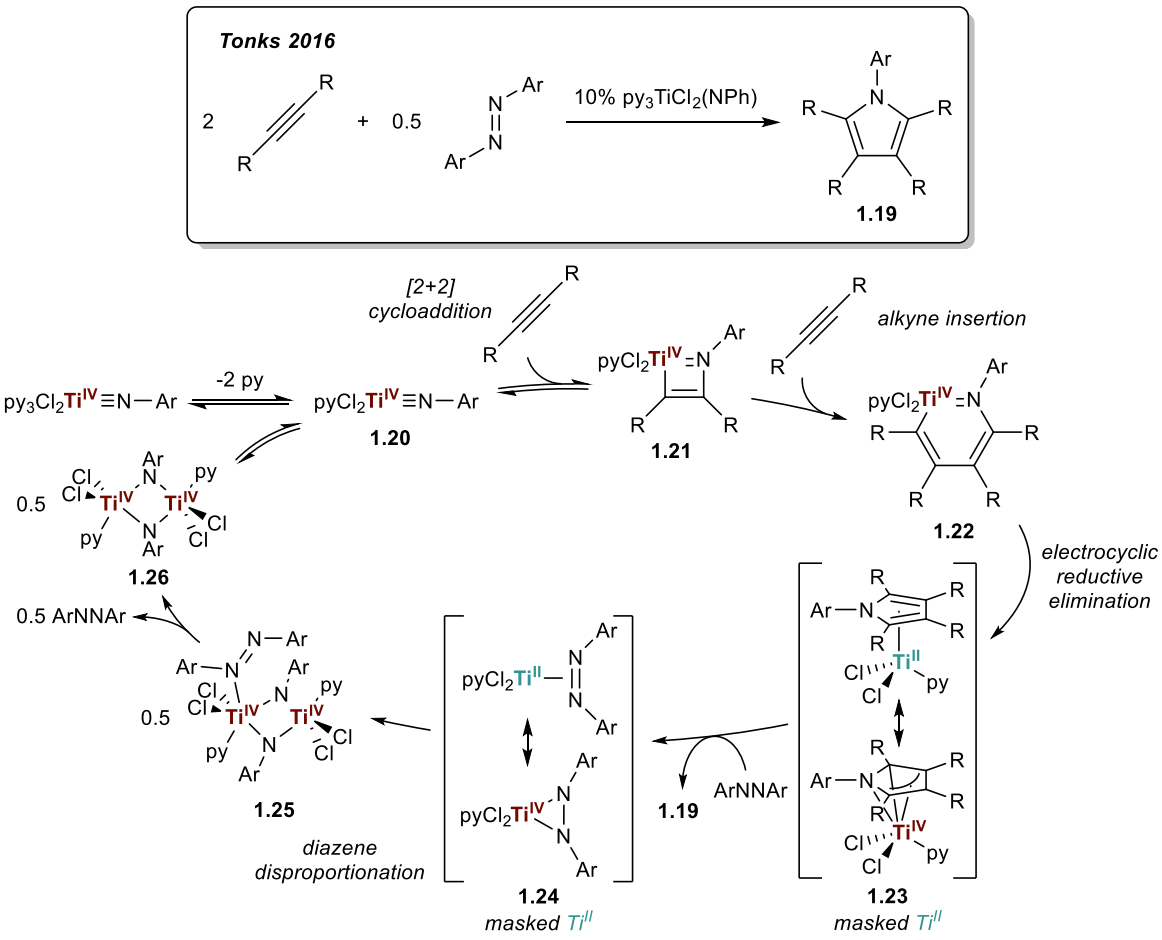

Figure 1.6. Proposed mechanism of Ti-catalyzed [2+2+1] pyrrole synthesis.

In Ti redox catalysis, masked Ti^{II} intermediates usually adopt unsaturated substrates or labile additives as the π acceptor. In the case when the ligand of the catalyst acts as the π acceptor, the ligand will be reduced while the Ti center will remain as high valent Ti. This type of ligand, commonly named redox-noninnocent (RNI) ligand, is considered an electron reservoir for the catalyst. Ti catalyst with RNI ligand can access the similar reactivity as masked Ti^{II} without the need for π backbonding. Wolczanski reported the catalytic nitrene carbonylation of Ti imido bearing a diamide-diimine (dadi) ligand (Figure 1.7, top).[36] The α-diimine in dadi ligand can undergo two-electron oxidation to become a vicinal diamide, which is a ubiquitous scaffold in RNI ligand designs. In this reaction, (dadi)Ti adamantylimido **1.27** undergoes the 1,1-insertion of CO to the imido N to give the *N*-bound η^1-adamantyl isocyanate, with the $(dadi)^{2-}$ ligand on Ti being reduced to $(dadi)^{4-}$ (**1.28**). Adamantyl azide replaces adamantyl isocyanate as the L donor (**1.29**) and oxidizes Ti $(dadi)^{4-}$ to Ti imido $(dadi)^{2-}$. A more detailed mechanism of C–N coupling has been proposed by Heyduk for the similar nitrene isocyanation

catalyzed by the Zr complex with an RNI triamide ligand. In this mechanism, the 1,1-insertion includes the [2+1] cycloaddition of Ti imido with carbene, followed by the η^2 to η^1 coordination mode change of isocynate (Figure 1.1, right, X = O).[37] Nitrene isocynation can also be catalyzed by Ti in the absence of RNI ligand (Figure 1.7, bottom). In this case, the η^1-adduct will not be formed. Instead, the Ti^{II} masked by η^2-carbodiimide (**1.31**) reacts directly with diazene to give **1.24**. Despite the C–N bond formation mechanism could vary, 1,1-insertion of carbene to imido is overall an oxidative C–N coupling that results in a reduced Ti complex in all the aforementioned examples. Thus, the regeneration of Ti imido is furnished by oxidative nitrene sources diazenes or azides.

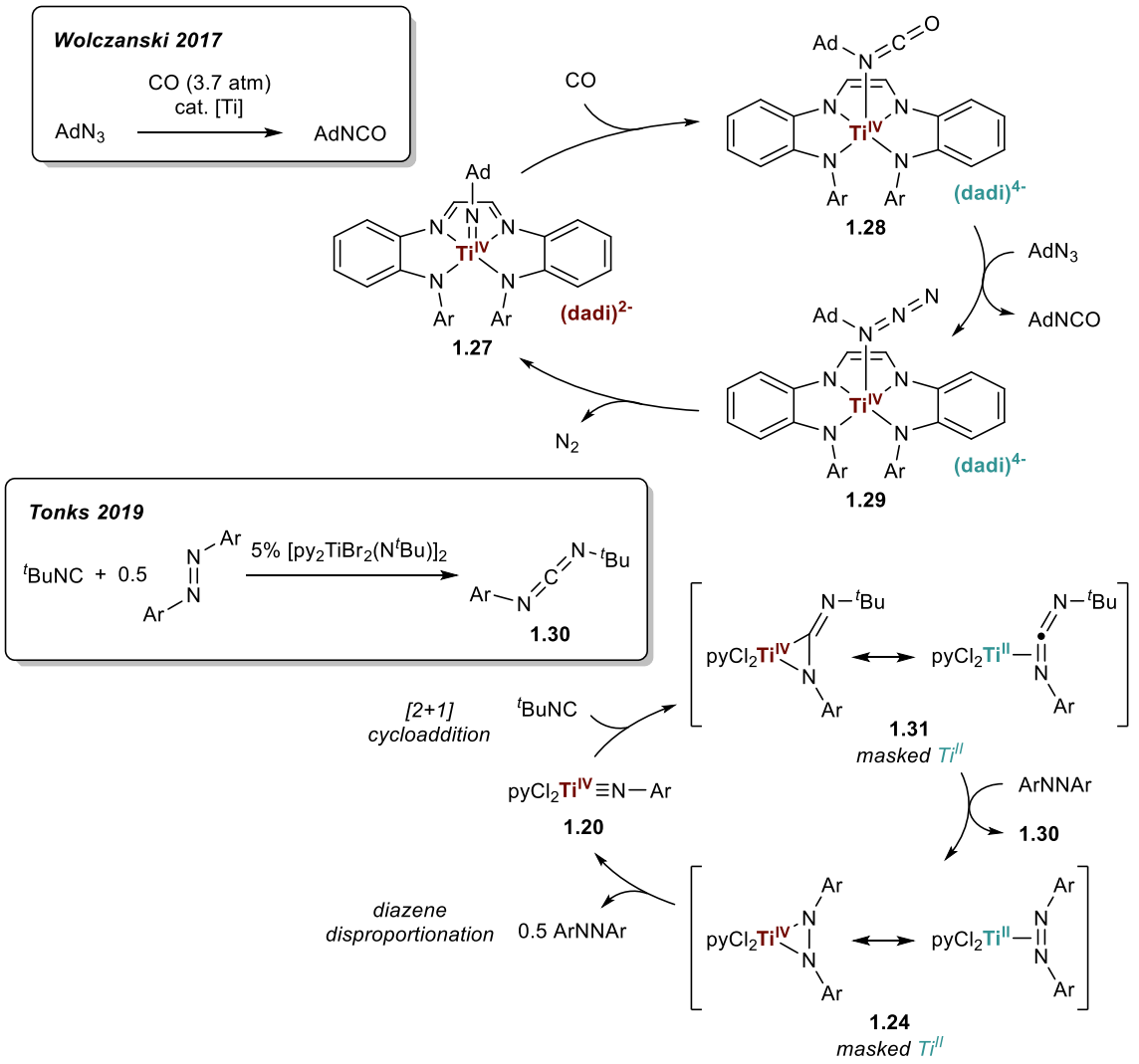

Figure 1.7. Proposed mechanism of (top) (dadi)Ti imido catalyzed nitrene carbonylation; (bottom) Ti-catalyzed nitrene isocyanation.

1.2.2 Regioselectivity and Chemoselectivity

Regioselectivity has been a long-lasting challenge for the C–N coupling reactions derived from the [2+2] cycloaddition of Ti imido. The [2+2] addition partner can adopt two orientations, resulting in Markovnikov and *anti*-Markovnikov products, respectively. The regioselectivity in this process is affected by catalyst designs, electronic and steric profiles of substrates, as well as reaction conditions.

Regioselective hydroamination has been thoroughly studied over the past three decades.[17,20,38–40] The regioselectivity largely depends on the C–N bond forming [2+2] cycloaddition as it is the rate-determining step of the reaction. Both alkyne substituents and *N*-substituent of Ti imido have a significant influence on the preferred orientation in [2+2] cycloaddition. For example, in the hydroamination of propyne with half-sandwich Ti catalyst, [2+2] cycloaddition is under steric-control when Ti imido is substituted by *tert*-butyl group (Figure 1.8).[41] The bulkier side of the alkyne coupling partner is forced to be oriented towards the sterically less hindered Ti, leading to the *anti*-Markovnikov [2+2] cycloaddition. On the other hand, electronic preference becomes the dominating factor affecting regioselectivity when Ti imido is substituted by the less bulky phenyl group. The partial charge matchup leads to a better orbital overlap between the Ti imido and the alkyne, resulting in Markovnikov [2+2] cycloaddition.[20]

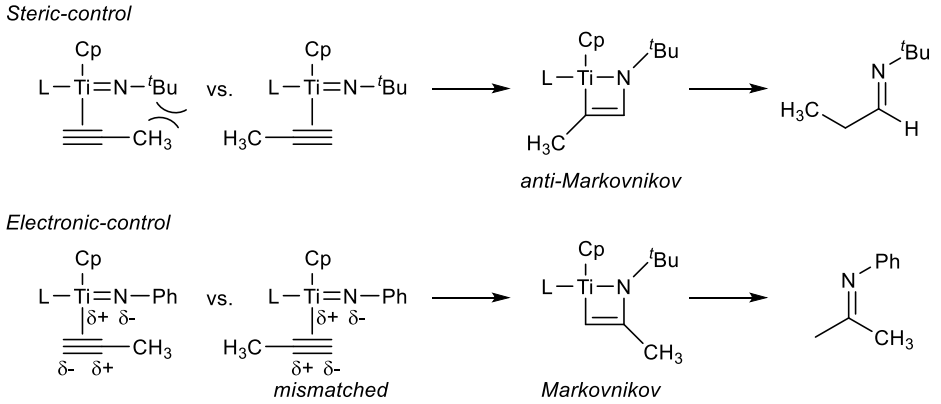

Figure 1.8. Regioselectivity of hydroamination under steric- and electronic-control of the substrates.[17]

Meanwhile, catalyst design can also alternate the regioselectivity of Ti-catalyzed hydroamination. The structure of the ligand can cause significant influence on the steric

environment, affecting the orientation of [2+2] cycloaddition partner in its pre-coordination to Ti.[20] On the other hand, the donating ability of ligand determines the polarizability of the Ti–N bond of Ti imido, changing the weights between the steric- and electronic-controlled regioselectivity. Sophisticated ligand architecture has been developed to fine-tune the regioselectivity for different substrates, including various polydentate and polyhaptic ligands. Although the orientation preference caused by substrates is usually weighed heavier in [2+2] cycloaddition, change of ligand can also lead to the switchover of regioselectivity in some cases. For example, in the hydroamination of 1-octyne catalyzed by titanocene catalysts,[41] Rosenthal's titanocene complex **1.32** was found to be selective to anti-Markovnikov products for aliphatic amines (Table 1.1, entry 1 and 3). Meanwhile, decamethyltitanocene catalyst **1.33** favored the formation of the Markovnikov product (Table 1.1, entry 2). This selectivity is unlikely to originate from the electronic difference, as the more electron-rich Ti of decamethyltitanocene would weaken the polarization of Ti imido, resulting in a less selective [2+2] cycloaddition. Hence, the Markovnikov selectivity is better to be attributed to the increased steric bulkiness around Ti. As a consequence, when the *anti*-Markovnikov-selective substrate tert-butyl amine is used with **1.33**, the hexyl group of alkyne would suffer from immense steric hindrance in both the two possible orientations, resulting in diminished reactivity (Table 1.1, entry 4).

Table 1.1. Hydroamination of 1-octyne catalyzed by titanocene catalysts[41]

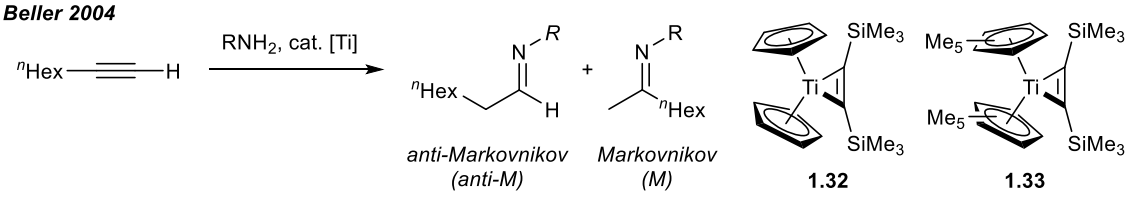

entry	R	cat. [Ti]	yield (%)	selectivity (anti-M:M)
1	CH_2Ph	10% **1.32**	46	82:18
2	CH_2Ph	10% **1.33**	51	19:81
3	^{t}Bu	2.5% **1.32**	97	99:1
4	^{t}Bu	2.5% **1.33**	0	N/A

Ti-catalyzed [2+2+1] pyrrole synthesis faces a more complicated scenario than hydroamination. The regioselectivity of pyrrole depends on not only the C–N coupling in the [2+2] cycloaddition but also the following C–C coupling in the alkyne insertion (Figure 1.6). As

a multicomponent intermolecular reaction, [2+2+1] pyrrole synthesis is also challenged by the chemoselectivity issue between homocoupling and heterocoupling products when 2 different alkynes are used. In our group's initial report, the homocoupling of unsymmetrical alkynes gave all three possible regioisomers as a product mixture, with the exception of tethered diynes and heavily biased alkynes such as terminal alkynes (Figure 1.9, top).[32] High selectivity under catalyst-control can be obtained through ligand design. Recently, our group reported the iterative supervised principal component analysis (ISPCA) as a general method for catalyst design optimization, demonstrated in regioselective pyrrole synthesis (Figure 1.9, bottom).[42] By combining statistic method (PCA), computational chemistry (DFT-calculated physical parameters) and iterative design, ISPCA offers the practical middle ground for the drawbacks of the three main-stream optimization methods — the vagueness of intuitive designs, the risk of underfitting of multivariate linear regression (MLR), and the large data set required by machine learning. Despite it enables delicate ligand optimization on the laboratory scale, ISPCA shares the same limitation as MLR in that the design is optimized for the single reporting parameter of one substrate. Hence, the optimized catalyst for regioselective synthesis is system-specific and will need to be re-subjected to optimization when the substrate is changed.

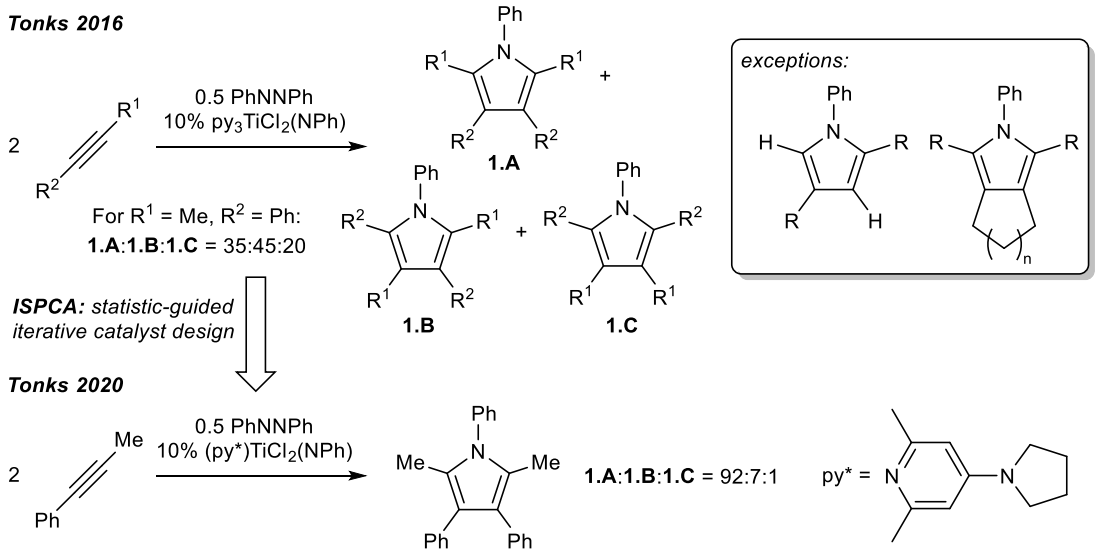

Figure 1.9. Catalyst-controlled regioselectivity in Ti-catalyzed [2+2+1] pyrrole synthesis.

Alternatively, selective [2+2+1] pyrrole synthesis can also be achieved under substrate-control. The installation of directing groups can provide a strong preference to the alkynes on their orientation in pre-coordination to Ti. Silyl groups have been found to provide a strong

directing effect in [2+2+1] pyrrole synthesis. Ti-catalyzed heterocoupled pyrrole synthesis of trimethylsilyl (TMS) alkynes and hydrocarbon alkynes yields 2-silylpyrrole in high selectivity against other 3 regioisomers and 6 homocoupling pyrrole side products (Figure 1.10).[43] Regioselectivity in this reaction is mainly influenced by the electronic character of TMS alkynes through the *α*-silyl effect.[44–46] The hyperconjugation between the σ(Si–CH_3) bond and the adjacent π(C=C) bond reinforces the polarization of the alkyne moiety, resulting in a strong preference for 1,2-insertion of alkyne and a stabilized azatitanacyclohexadiene intermediate due to strengthened Ti–C bond. Supported by the electronic bias of arylpropyne **1.35**, the *α*-silyl effect allows 2-silylpyrrole **1.36** to be the preferred regioisomer in the heterocoupled [2+2+1] pyrrole synthesis with **1.34** and **1.35**. Meanwhile, the high chemoselectivity in this reaction against the homocoupling of **1.34** and **1.35** originates from the Curtin-Hammett equilibrium.[47] The reversible [2+2] cycloaddition of Ti imido with alkynes is a fast pre-equilibrium in the catalytic cycle. Thus, under Curtin-Hammett control the product selectivity can be directly correlated to the activation barrier difference of different alkyne insertion pathways, reflected as reaction rates. Benefiting from the increased polarization due to the *α*-silyl effect, TMS alkyne **1.34** has better orbital overlap with the Ti–C bond of azatitanacyclobutene, resulting in a lower insertion barrier and faster reaction rate. Hence, the chemoselectivity is kinetically resolved to favor the heterocoupling between **1.34** and **1.35** over homocoupling of the either alkyne.

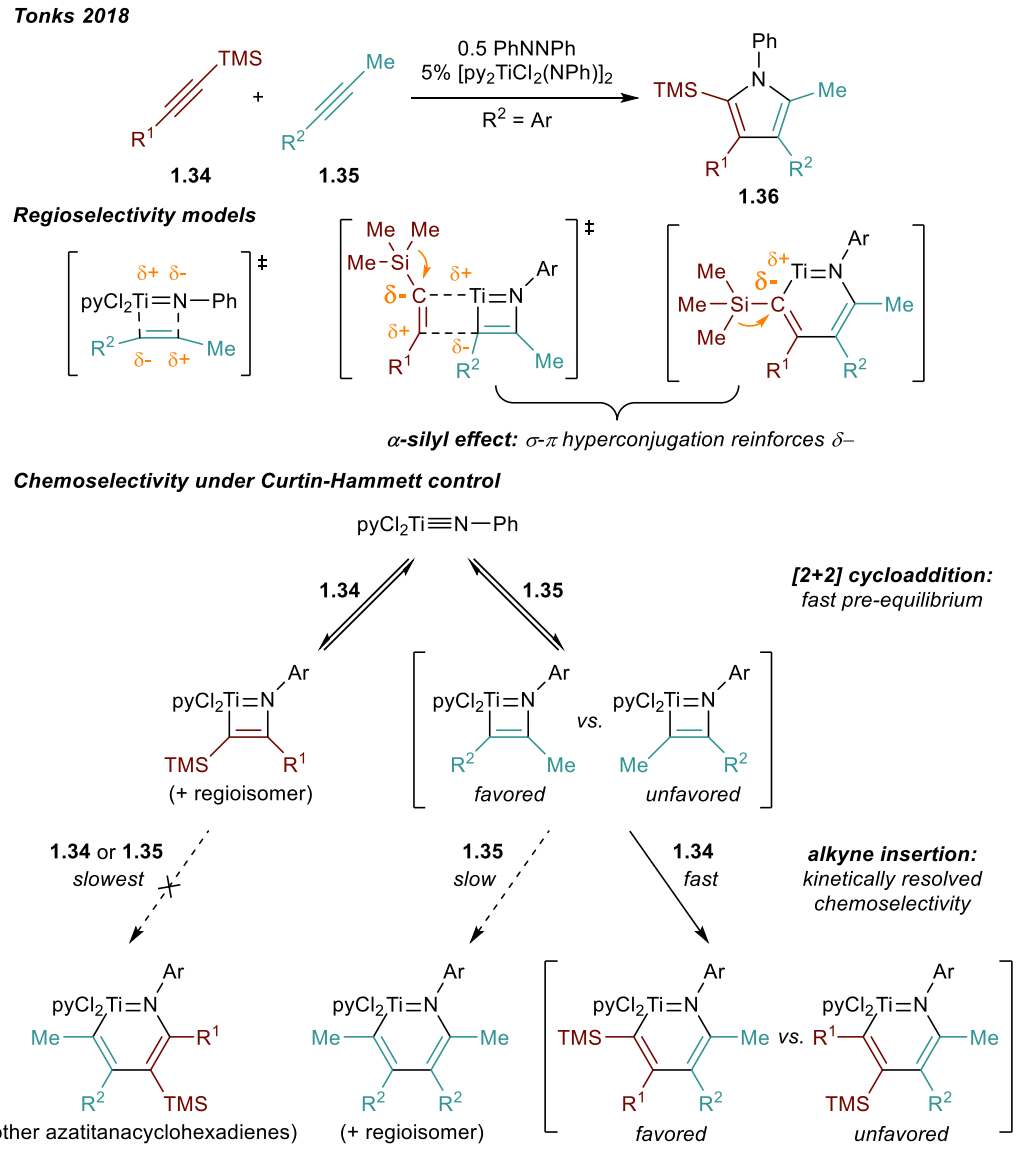

Figure 1.10. Regioselective Ti-catalyzed [2+2+1] pyrrole synthesis with TMS alkynes.

Heteroatoms with lone-pair electrons can also provide directing group effect through coordination to Ti catalyst. Our group reported that the TMS alkyne substituted with tethered N-, O-, or S-functional group can negate the directing group effect of TMS, resulting in 3-silylpyrrole (Figure 1.11).[48] The competition between the dative directing effect from coordination and the silyl directing effect from TMS was found to correlate with the Lewis acidity of the Ti catalyst, where the more acidic iodine-based catalyst $(thf)_3TiI_2(NPh)$ can provide stronger dative directing group effect through stronger binding. Therefore, $(thf)_3TiI_2(NPh)$ catalyst is more selective towards 3-silylpyrrole and allows pyrrole synthesis to

operate at a milder condition than the latter chlorine-based catalyst $[py_2TiCl_2(NPh)]_2$. Dative directing groups can also be installed on alkynes without a silyl directing group. The homocoupling of these alkynes is selective to the 2,4-regioisomer, indicating the dative directing group effect is also applicable to the transition state of the [2+2] cycloaddition step.

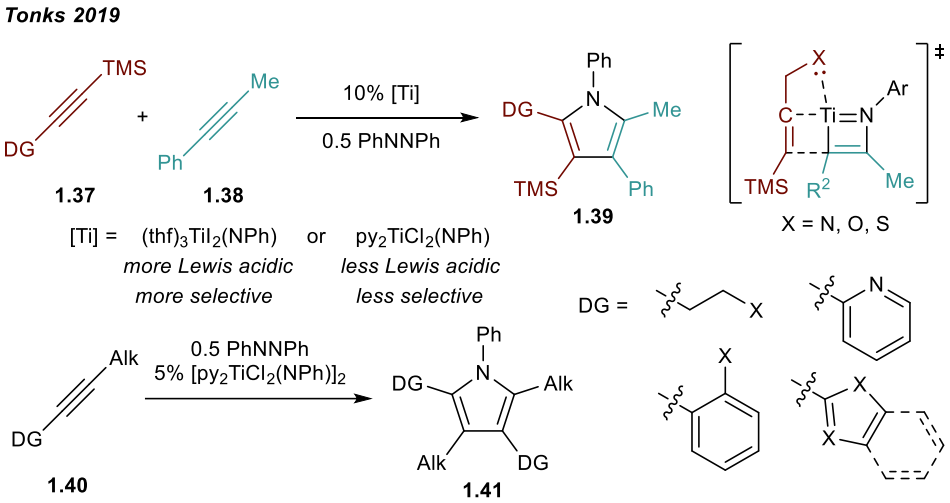

Figure 1.11. Dative directing group effects in Ti-catalyzed [2+2+1] pyrrole synthesis.

1.3 N–N Coupling

The history of N–N coupling dates back to the early 20th century when Wieland studied the homocoupling of diarylamines to tetraarylhydrazines with $KMnO_4$ and Ag_2O.[49–51] While the majority of studies on N–N coupling have been focused on the metal-free coupling of amines, N–N coupling through metal amide and imido complexes provides promising potential in the development of N–N heterocoupling reactions for high-valued unsymmetrical hydrazine and diazene products. Compared with C–N coupling, Ti-mediated N–N coupling remains under-explored with limited reports of catalytic reactions. As our ultimate goal is to develop N–N coupling Ti catalysis, this section will focus on the discussion of stoichiometric transformations mediated by Ti and relevant organometallic N–N coupling reactions with other metals. Metal-free N–N coupling such as the Mills reaction and the peroxide process will not be covered.

1.3.1 N–N Coupling of Imido

In contrast to the rich C–N bond formation chemistry *via* [2+2] cycloaddition of Ti imido, N–N coupling rarely proceeds through cycloaddition. This is largely owing to the high electronegativity of nitrogen, making the N–N coupling partner — usually an unsaturated C–N moiety such as nitrile and imine — favoring the regioselectivity for C–N coupling instead of N–N coupling. For example, Mountford reported the [2+2] cycloaddition between acetonitrile and a tethered pyridyl-bisamide substituted Ti imido (Figure 1.12, top).[52] The highly polarized C≡N bond favored the Markovnikov product **1.42** in [2+2] cycloaddition, which further resonated from tethered amide-amide to imido-imine and formed an imido-bridged dimer **1.43**. On the other hand, the [2+2] cycloaddition between the same Ti imido with *tert*-butyl phosphaalkyne yielded *anti*-Markovnikov product **1.44** (Figure 1.12, bottom). Due to the similar electronegativity of phosphorus and carbon, the C≡P bond was not significantly polarized, hence the regioselectivity was controlled by the steric hindrance from the *tert*-butyl group.

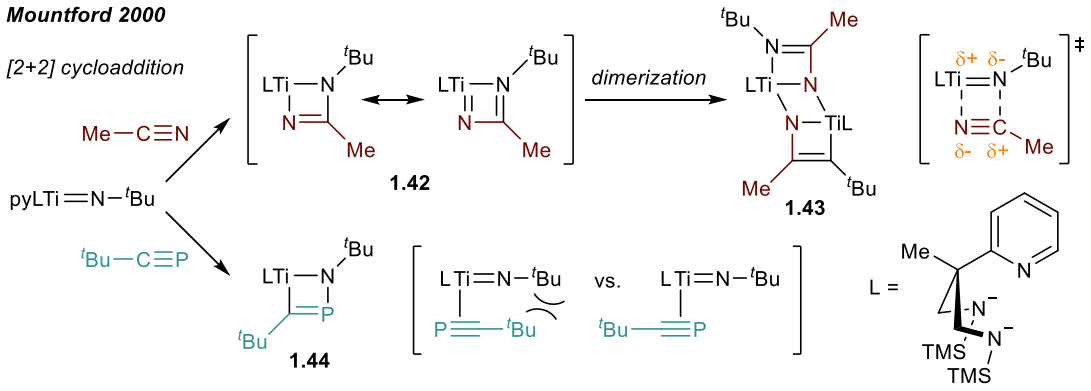

Figure 1.12. [2+2] Cycloaddition of Ti imido with nitrile and phosphaalkyne.

Oxidative N–N homocoupling and reductive N–N cleavage are the microscopic reverse processes of each other, for example, oxidation of imido versus reduction of diazene. Both the oxidation of imido to diazene and the reduction of diazene to imido and hydrazido(2-) have been widely studied for the fundamental interest in the properties of Ti imido complexes and their potential use in converting the less reactive N-N moiety to a nitrene transfer synthon. The early exploration of Ti-mediated reduction of diazene was pioneered by Floriani and Rothwell in the 80s and 90s. Floriani described the preferred bonding mode of the reduced diazene-Ti complexes as titanadiazirine — a side-on η^2-hydrazido(2-) Ti (Figure 1.13a), though exceptions of end-on η^1-hydrazido(2-) dititanium does exist depending on the reaction stoichiometry and other ligands of Ti (Figure 1.13b).[53–55] Rothwell firstly reported the reduction of diazene to terminal Ti imido **1.49** by a masked Ti^{II} bis(aryloxide) complex **1.47** (Figure 1.13c).

Disproportionation of diazene was later reported through diazatitanacycloheptadiene **1.52** (Figure 1.13d).[56] The diazene N=N bond of benzo[c]cinnoline **1.51** underwent insertion into the Ti–C bond of titanacyclopentadiene **1.50**, after which the ring contraction yielded the tethered Ti imido and pyrrole moieties (**1.53**).[57]

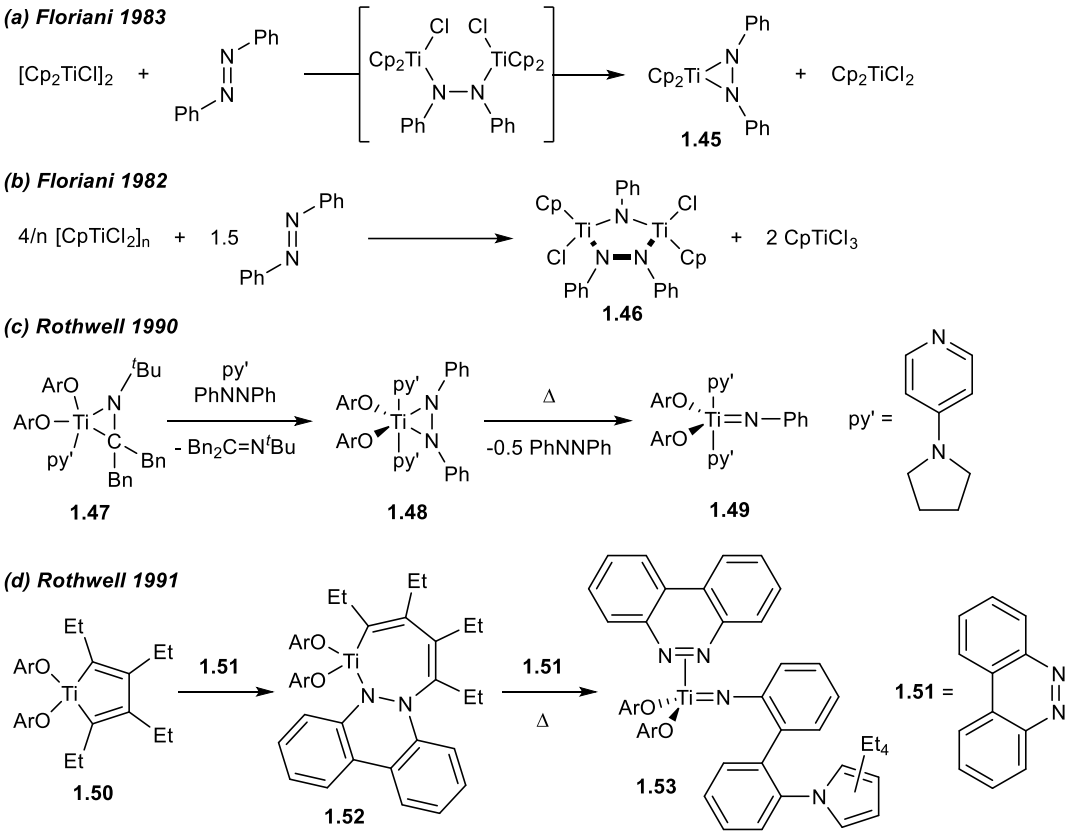

Figure 1.13. Pioneering studies on Ti-mediated diazene reduction to Ti imido and hydrazido(2-).

Building on Rothwell's discoveries, our group demonstrated the practical utility of reductive diazene disproportionation in nitrene transfer reaction.[32] Simple masked Ti^{II} dichloride complex **1.54** was found to undergo rapid disproportionation to give Ti imido **1.55** and azobenzene (Figure 1.14, top). A catalytic [2+2+1] multicomponent pyrrole synthesis was developed based on this, with the critical step of regenerating Ti imido from masked Ti^{II} going through diazene disproportionation (Figure 1.6). DFT calculations revealed a bimolecular mechanism different from Ti^{III} reduction of diazene for this step (Figure 1.14, bottom).[34] A redox tautomerization between the two diazenes was involved in the rate-determining transition state **1.57**, where a diazene was reduced from the η^2-hydrazido(2-) in **1.56** to the two μ-imido in **1.25**.

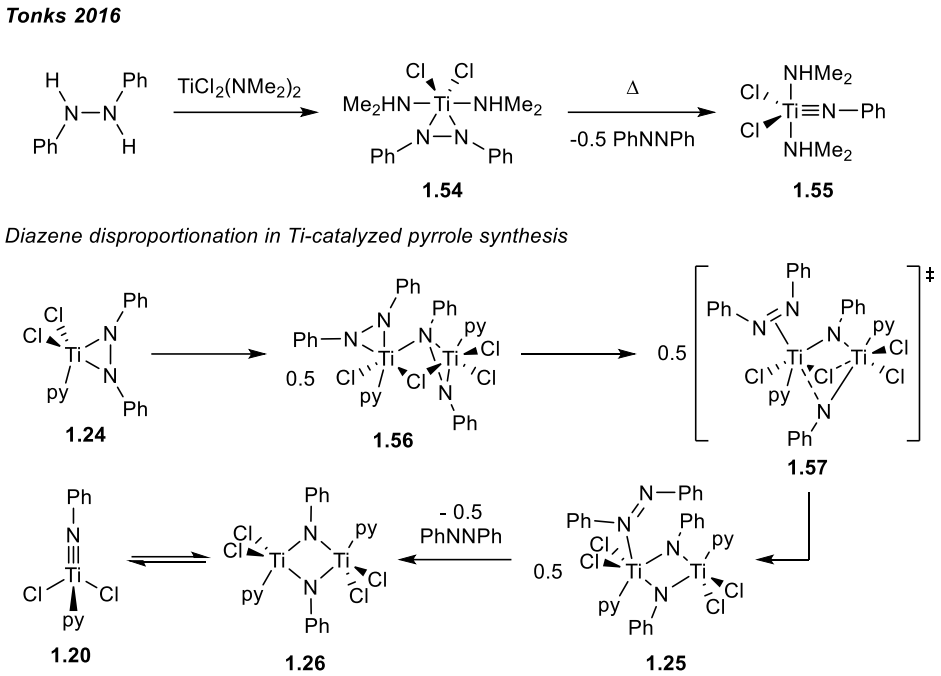

Figure 1.14. Reductive N–N cleavage in Ti-catalyzed pyrrole synthesis with diazene.

Oxidative coupling of imido to diazene undergoes a similar bimolecular mechanism due to microscopic reversibility (Figure 1.15). Although no reaction intermediate has been studied on Ti systems, a catalytic nitrene homocoupling from aryl azide to diazene has been reported using a Ta catalyst with RNI ligand through an imido-bridged ditantalum intermediate **1.60**.[58] *C*-nitroso compounds such as nitrosobenzene can also be viewed as a nitrene equivalent through oxygen abstraction to form Ti oxo. Sundermeyer reported the oxidation of phthalocyanine Ti mesitylimido with nitrosobenzene to give phthalocyanine Ti oxo and unsymmetrical diazene **1.61**, providing an interesting route for N–N heterocoupling from Ti imido.[59] Recently, our group demonstrated the *C*-nitroso oxidation of Ti imido to diazene can be applied to simple a dichlorotitanium imido complex.[60]

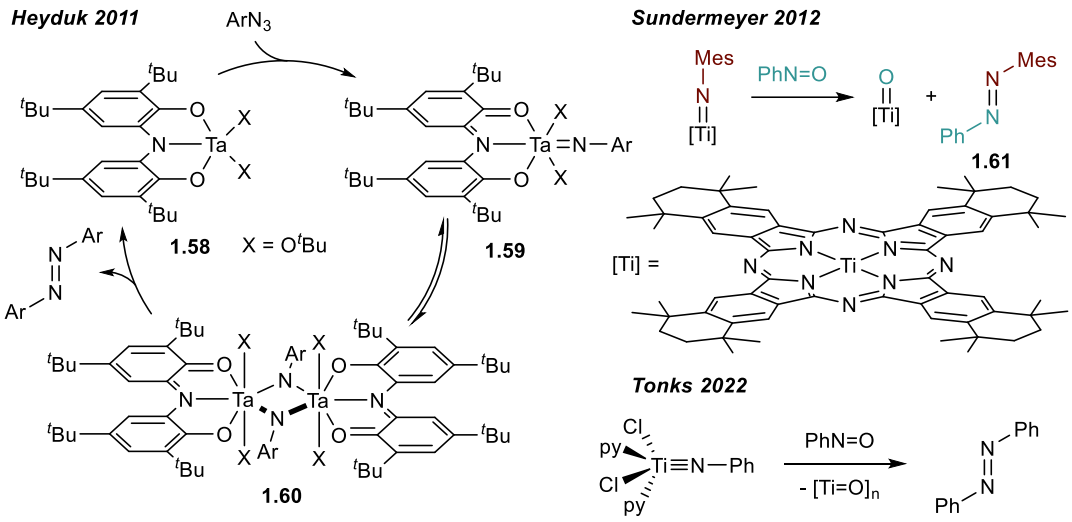

Figure 1.15. Oxidative N–N coupling of Ti imidos to diazenes.

Besides nitrene equivalents, our group has shown that imine can also serve the N–N coupling partner of Ti imido. Diazatitanacyclohexadiene **1.62** can be oxidized to pyrazole **1.63** by inner-sphere oxidants including TEMPO and various hypervalent iodine compounds (Figure 1.16).[61] The N–N bond formation in this reaction was triggered by two sequential ligand-centered oxidations, adapted from the established oxidation-induced C–C reductive elimination in late transition metal chemistry.[62–65] A series of control reactions were performed to reveal the N–N bond formation mechanism using 2-iminyl-2*H*-azirine **1.64**, which can be viewed as a structural isomer of pyrazole **1.65**. Masked titanocene **1.32** — a Ti^{II} equivalent — readily led to the ring opening of 2*H*-azirine on **1.64**, resulting in the "0e$^-$ oxidized" imido-imine titanacycle **1.66**. Meanwhile, reacting **1.64** with $Ti^{III}Cl_3(thf)_3$ yielded half equivalent of pyrazole **1.65** and half equivalent of "0e$^-$ oxidized" titanacycle **1.68**, indicating the reaction underwent a disproportionation of two Ti^{III} equivalents to one Ti^{II} and one Ti^{IV} equivalents. This process was speculated to be mediated by a "1e$^-$ oxidized" titanacycle **1.67** with a ligand-centered radical. Lastly, treating **1.64** with $Ti^{IV}Cl_4(thf)_2$ quantitatively gave **1.65** as the product *via* rapid N–N coupling of the proposed intermediate Cl-substituted "2e$^-$ oxidized" titanacycle **1.69**. Based on these observations, A mechanism was proposed for the oxidation-induced N–N reductive elimination: the "0e$^-$ oxidized" titanacycle first underwent one-electron oxidation to give the "1e$^-$ oxidized" titanacycle radical, followed by a dimeric disproportionation generating the zwitterionic "2e$^-$ oxidized" titanacycle. The rapid N–N coupling of the "2e$^-$ oxidized" titanacycle yielded pyrazole in an electrocyclic fashion similar to the Nazarov cyclization.

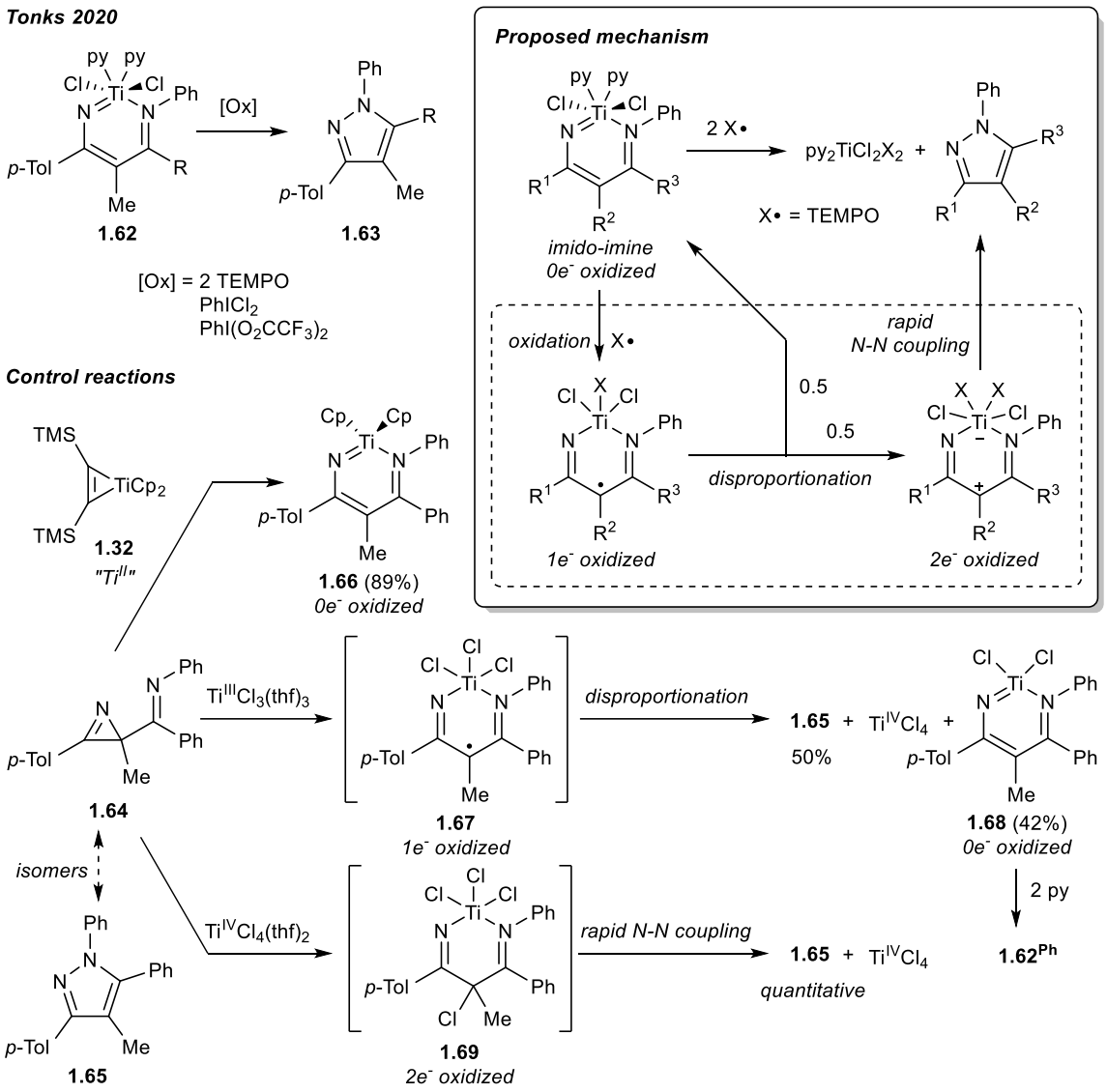

Figure 1.16. Ti-mediated pyrazole synthesis *via* oxidation-induced N–N reductive elimination.

1.3.2 N–N Coupling of Amide

To date, Ti-mediated N–N coupling *via* Ti amide remains unprecedented. Meanwhile, N–N coupling of other metal amides has been widely studied as model compounds and reaction intermediates in both stoichiometric and catalytic reactions. The closest analogs to Ti-mediated pyrazole synthesis are the Cu-catalyzed aerobic-oxidative synthesis of diazoles and triazoles. A shared key intermediate of these reactions is the diazacupracyclohexadiene in the Cu bisamide form. Imido-imine and amide-amide are the two major contributing isomers in the

electronic resonance of diazametallacyclohexadiene moiety (Figure 1.17). The imido isomer is preferred when M = Ti, as the low-lying 2p orbital of N highly polarizes the Ti–N multiple bonds, resulting in a doubly oxidized Ti and a dianionic N. Moving across the periodic table to late transition metals, Cu has a much lower 3d energy level than Ti, hence the Cu–N bond is more covalent where Cu is monooxidized and coordinated by a monoanionic N. This has been illustrated in detail in the recent isolation of a Cu triplet nitrene complex.[66]

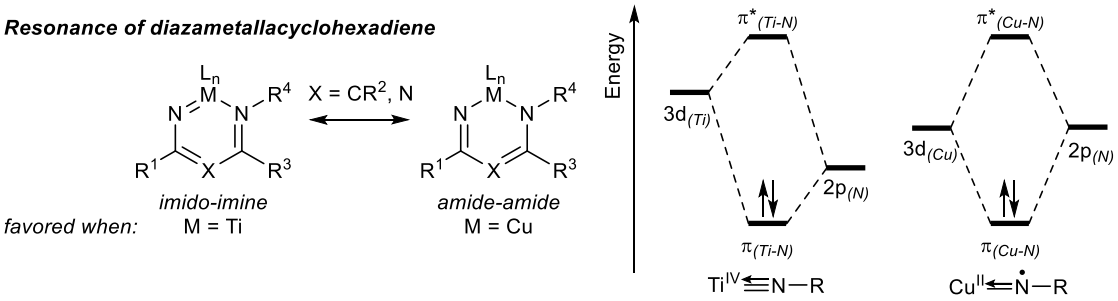

Figure 1.17. Resonance of diazametallacyclohexadiene and the bonding mode of metal-nitrogen multiple bonds.[66]

The first study on N–N coupling of diazacupracyclohexadiene dates back to the late 2000s, when a Cu-catalyzed aerobic-oxidative synthesis of triazoles was reported (Figure 1.18a).[67] 1,2,4-Triazoles **1.70** were efficiently synthesized from amidines and nitriles using CuBr as catalyst and Cs_2CO_3 as a stoichiometric base promoter. A Similar transformation could also be performed on 2-aminopyridines **1.71**, where triazole-cored products **1.72** with an extended aromatic system were generated. Following the syntheses using amidines, Glorius reported that a similar catalytic transformation can convert activated enamines **1.73** to pyrazoles **1.74** under O_2 (Figure 1.18b).[68,69] This reaction was later applied to 2-iminylanilines **1.75**, giving 1*H*-indazoles **1.76** as the product.[70] These reactions share a similar proposed mechanism. First, the imine *α*-C/N nucleophilic attacks the nitrile C on the imine and nitrile pre-coordinated Cu complex **1.77**, leading to the formation of a cupracycle. The sequential deprotonation of **1.78** and **1.79** yields diazacupracyclohexadiene **1.80** as a Cu bisamide, followed by the oxidative N–N coupling to give diazole or triazole product **1.81**. The byproduct of N–N coupling has been uncleared until the recent mechanistic investigation, where the kinetic interrogation revealed that **1.80** was oxidized by another Cu^{II} to give two Cu^{I} instead of undergoing a reductive elimination to Cu^0.[71] Lastly, the rate-determining aerobic oxidation of Cu^{I} regenerates Cu^{II} with water as the byproduct.

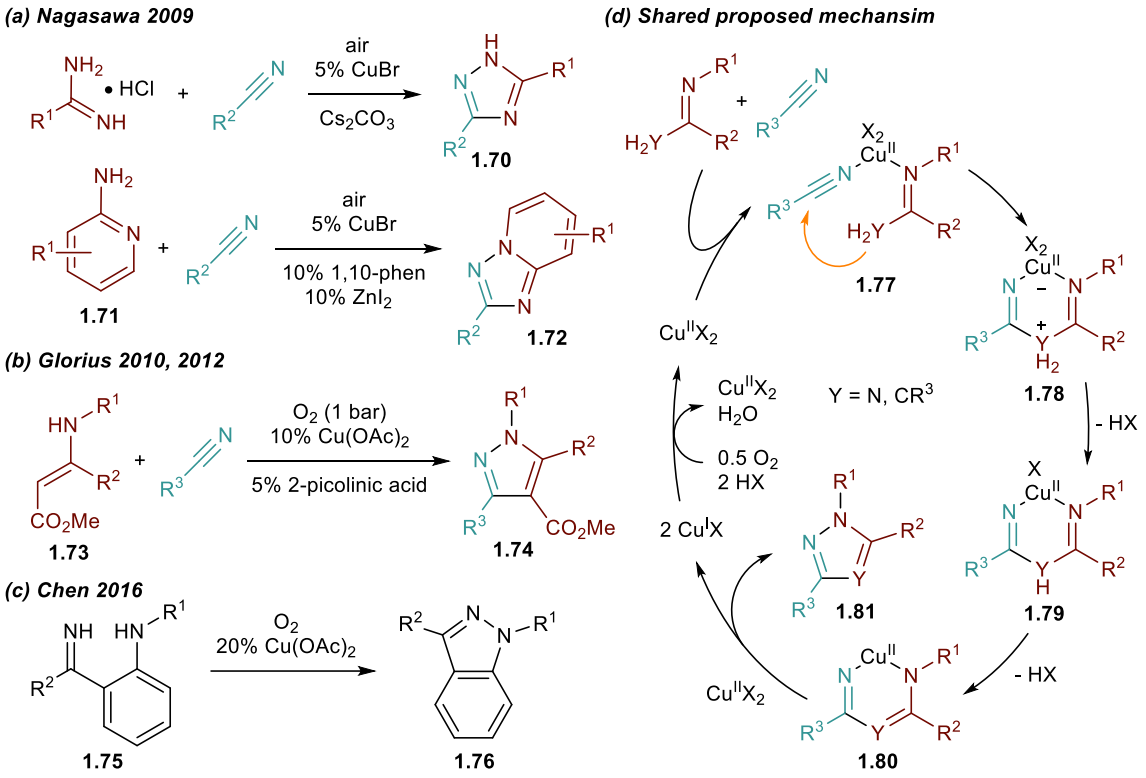

Figure 1.18. Oxidative N–N coupling of diazacupracyclohexadienes in the syntheses of diazoles and triazoles.

The more dominating reactivity of metal amides towards oxidation is the formation of aminyl radicals when the conjugated backbone for ligand-centered oxidation is absent. Cu and Fe have been well-established as catalysts for oxidative coupling of amines to hydrazines and diazenes through aminyl radicals, while in many examples it was uncleared whether the amine is directly oxidized to aminyl *via* PCET or forms a metal amide intermediate prior to the oxidation (Figure 1.19, top left).[72–75] Isolation of metal amide intermediate has been attempted on the less oxidative high valent rare earth metals. Primary and secondary amines were reported to be able to undergo aerobic oxidation to hydrazines and diazenes through the reaction with stoichiometric hexamethyldisilazide ($HMDS^-$) complexes of yttrium and various lanthanide metals, among which a reaction intermediate $Yb(HMDS)_2(NPh_2)$ was isolated and characterized crystallographically (Figure 1.19, top right).[76] Reactivity studies suggested reaction underwent the aerobic oxidation of metal bis(HMDS) monoamide complex to generate the aminyl radical. A recent study on bismuth-mediated oxidation of amines to hydrazines reported a series of homoleptic Bi^{III} triamide complexes as rare well-defined isolable intermediates (Figure 1.19, bottom).[77] Bi^{III} served as the oxidant in this reaction, rapidly

releasing aminyl radical at room temperature with the byproducts being the oligomerized Bi^{II}, Bi^{I}, and Bi^{0}.

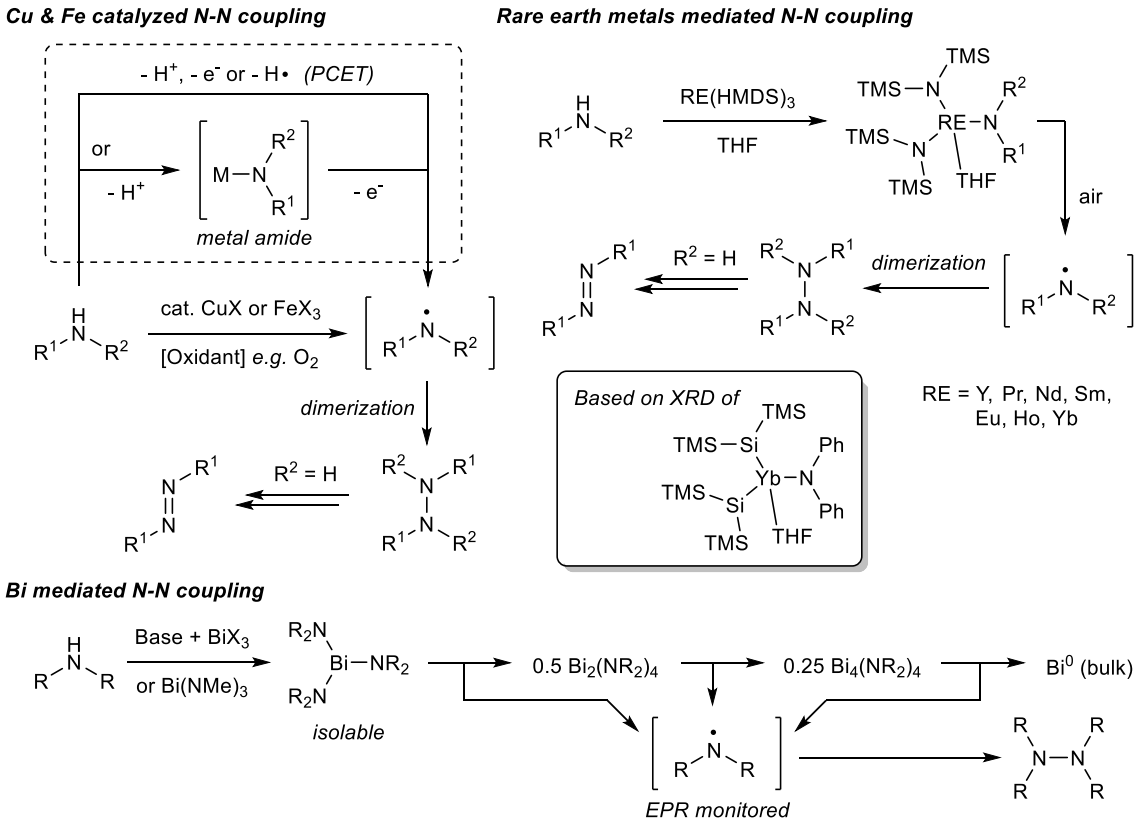

Figure 1.19. Oxidative N–N coupling of metal amides *via* aminyl radical.

Hindered by the nature of free radical chemistry, the application of N–N coupling *via* aminyl radical has been limited to N–N homocoupling reactions. Reactions between two different amines or amides will yield a statistical mixture of N–N heterocoupling and homocoupling products. An exception has been reported when diphenylamine or its derivative is used as the coupling partner. Selective heterocoupling between diarylamines **1.82** and carbazoles **1.83** can be achieved *via* Cu-catalyzed aerobic oxidation (Figure 1.20).[78] Reaction progress monitored by NMR showed that tetraarylhydrazine **1.85** was formed rapidly at the early stage of the reaction but slowly converted to heterocoupling product **1.84** as the reaction progressed, indicating **1.85** being the kinetic product while **1.84** being the thermodynamic product. Hence, the chemoselectivity was attributed to the reversibility of the N–N homocoupling of **1.82** due to the weak N–N bond strength of product **1.85**. A more recent report supports that the selectivity

originates from the substrate instead of the metal catalyst, as metal-free N–N heterocoupling between diphenylamines and carbazoles could be achieved with KI and KIO_4.[79]

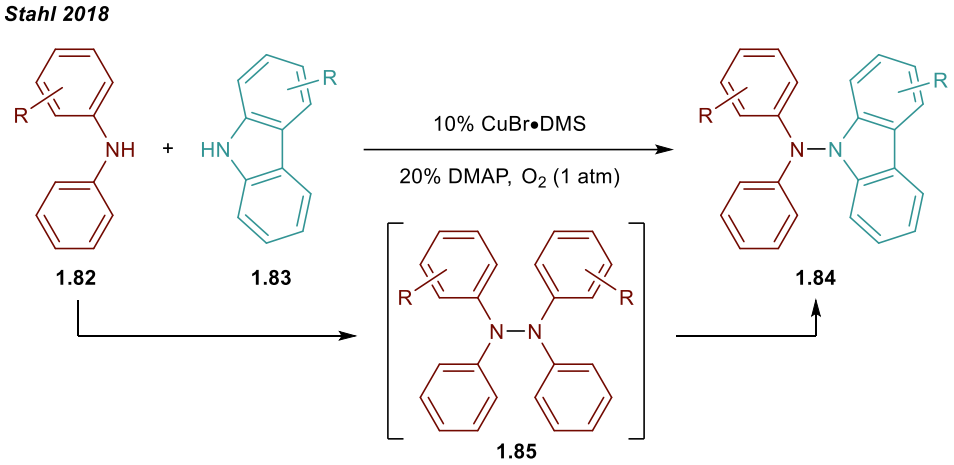

Figure 1.20. Oxidative N–N heterocoupling of diarylamines.

1.3.3 Outer-Sphere N–N Coupling

Titanium can also mediate N–N coupling without the formation of a Ti–N bond. In these reactions, the Ti complex serves as either a reductant or a Lewis acid, and the reactivity is largely dependent on the coupling reactants. A typical example is the pinacol-type reaction. Titanocene chloride dimer can reduce nitrosobenzene to azoxybenzene with *μ*-oxo bis(titanocene chloride) as the byproduct (Figure 1.21, top).[80] The reduction was proposed to undergo the dimerization of *N*-radical on monoreduced nitrosobenzene (**1.86**), followed by the oxo extrusion. Interestingly, a similar O–N–N–O scaffold can be obtained without a reductant. The reaction between $TiCl_4$ and nitrosobenzene yielded an isolable Ti complex **1.87** with a doubly oxidized diazene through dimerization of nitrosobenzene (Figure 1.21, bottom).[81] Similar dimerization can also be performed with $SnCl_4$.

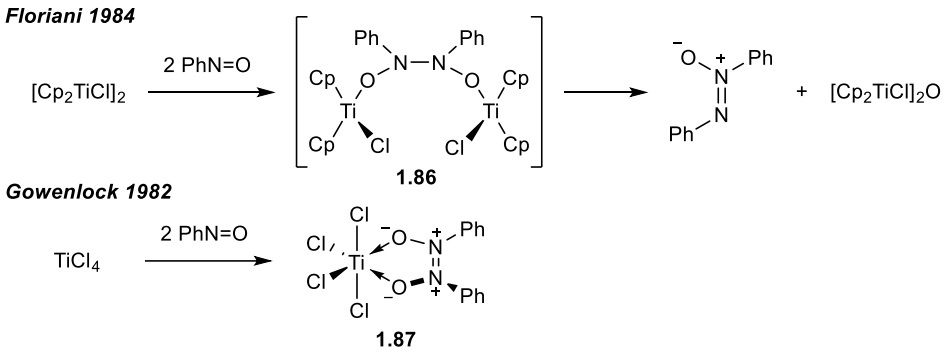

Figure 1.21. Ti-mediated pinacol-type N–N coupling.

1.4 Scope of Thesis

The objective of this thesis is to develop Ti-mediated C–N and N–N coupling reactions. This includes the exploration of the mechanism of the established reactions, the development of downstream application methods, and the design of novel transformations. The research will primarily focus on oxidative amination catalysis through two-electron redox or two sequential one-electron redox processes. Chapter 2 describes the application of boryl and stannyl alkynes in Ti-catalyzed [2+2+1] pyrrole synthesis and the subsequent Pd-catalyzed cross-coupling reactions for highly functionalized pyrroles, with an emphasis on chemo- and regioselectivity. Chapter 3 covers the exploration of the alternative nitrene source in Ti-catalyzed hydroamination, where a $Ti^{II/IV}$ redox process has been found instead of the traditional redox-neutral mechanism based on amine protonolysis. A catalytic transfer hydrogenation reaction has been developed based on this discovery. Chapter 4 details the mechanistic investigation of the sequential one-electron oxidation processes in the oxidative pyrazole synthesis from diazatitanacyclohexadiene. The study features the isolation of the dititanium diradical as the model compound of the $1e^-$-oxidized intermediate, and the coordination effect of chloride counteranion in enabling outer-sphere oxidation in the inner-sphere-like oxidation. In chapter 5, a preliminary study on N–N coupled indazole synthesis from diazatitanacyclohexadiene with an extended aromatic system is reported. This study also aims to develop a general strategy for Ti-mediated N–N heterocoupling with one-electron oxidants, where a conjugated tethered linker has been found to be critical. The mechanistic studies and method development in this thesis will hopefully provide inspiration for the exploration of oxidative amination reactions mediated by group IV metals in the future.

Chapter 2: Synthesis of Pentasubstituted 2-Aryl Pyrroles from Boryl and Stannyl Alkynes *via* One-Pot Sequential Ti-Catalyzed [2+2+1] Pyrrole Synthesis/Cross Coupling Reactions

Reprinted (adapted) with permission from:

Cheng, Y.; Klein, C. K.; Tonks, I. A.

Synthesis of Pentasubstituted 2-Aryl Pyrroles from Boryl and Stannyl Alkynes *via* One-Pot Sequential Ti-Catalyzed [2+2+1] Pyrrole Synthesis/Cross Coupling Reactions.

Chem. Sci. **2020**, *11*, 10236–10242.

2.1 Overview

Multisubstituted pyrroles are commonly found in many bioactive small molecule scaffolds, yet the synthesis of highly-substituted pyrrole cores remains challenging. Herein, we report an efficient catalytic synthesis of 2-heteroatom-substituted (9-BBN or SnR_3) pyrroles *via* Ti-catalyzed [2+2+1] heterocoupling of heteroatom-substituted alkynes. In particular, the 9-BBN-alkyne coupling reactions were found to be very sensitive to Lewis basic ligands in the reaction: exchange of pyridine ligands from Ti to B inhibited catalysis, as evidenced by *in situ* ^{11}B NMR studies. The resulting 2-boryl substituted pyrroles can then be used in Suzuki reactions in a one-pot sequential fashion, resulting in pentasubstituted 2-aryl pyrroles that are inaccessible via previous [2+2+1] heterocoupling strategies. This reaction provides a complementary approach to previous [2+2+1] heterocouplings of TMS-substituted alkynes, which could be further functionalized via electrophilic aromatic substitution.

2.2 Introduction

Pyrroles are important heterocycles found in diverse applications from pharmaceuticals to conducting materials.[82–87] However, their ubiquity belies significant challenges in the facile synthesis of highly substituted pyrrole cores. Many of the synthetic routes such as the Paal-Knorr condensation require multi-steps backbone synthesis, which add difficulties to late-stage substituent diversification.[88,89] Multicomponent reactions provide a shortcut to the construction of structures with high complexity. A series of pioneering studies has been reported by Odom on Ti-catalyzed multicomponent pyrrole synthesis based on hydroamination and iminoamination.[23,25,90] Following a slightly different strategy, we recently developed a multicomponent [2+2+1] Ti-catalyzed pyrrole forming reaction that yields the heterocycle in a single step.[32] Chemo- and regioselective intermolecular reactions can be achieved via the heterocoupling of trialkylsilyl-protected alkynes, which selectively engage in migratory insertion into a key azatitanacyclobutene [2+2] cycloadduct intermediate.[43] (Figure 2.1, top).

Although the TMS-substituted pyrrole heterocoupling products were good candidates for further diversification through electrophilic aromatic substitution of the electron-rich silylpyrrole, we were not able to directly install aryl groups into either the 2- or 5-position around the pyrrole. This limitation arises from the polarization of the Ti-imido bond in [2+2] cycloaddition, as well as the limited utility of TMS-substituted arenes in C_{sp2}-C_{sp2} bond forming reactions. Thus, we

envisioned that the development of other heteroatom-substituted alkyne heterocoupling reactions would lead to alternative strategies for pyrrole diversification.

Given the enormous library of well-established group to metal-catalyzed cross coupling reactions, we were interested in the direct synthesis of pyrroles with heteroatoms that could potentially serve as good transmetallation partners.[91–98] Herein, we report the application of B-alkynyl 9-borabicyclo[3,3,1]nonanes and alkynyl stannanes in selective Ti-catalyzed [2+2+1] pyrrole synthesis (Figure 2.1, bottom). These reactions provide efficient methods for the construction of versatile polysubstituted pyrrole building blocks, and also provide the opportunity for further diversification into otherwise-inaccessible 2-arylpyrroles through one-pot alkyne cyclization/Suzuki coupling reactions. Preliminary results with other heteroatom-substituted alkynes such as B-alkynyl pinacolborane and copper acetylides are also presented.

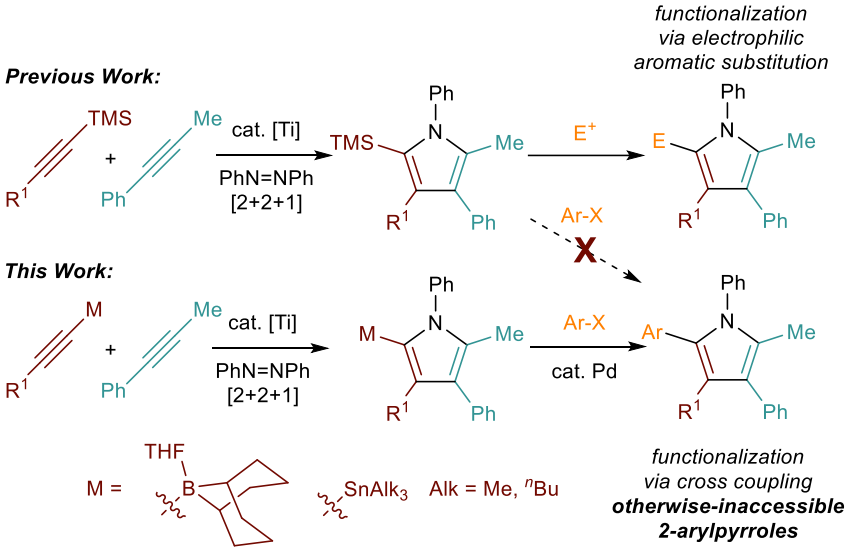

Figure 2.1. Heterocoupling strategies for selective [2+2+1] pyrrole synthesis.

2.3 Result and Discussion

First, several potential heteroatom-substituted alkynes were examined as candidates for the [2+2+1] reaction, focusing on heteroatomic groups that could later be good transmetallation partners in cross-coupling catalysis (Table 2.1). The functional groups involved in the initial screen included boronic acid pinacol ester (Table 2.1, entry 1, **2.1a-Bpin**) and the THF adduct of 9-borabicyclo[3,3,1]nonane (Table 2.1, entry 2, **1a-BBN**), $SnMe_3$ (Table 2.1, entry 3, **2.1a-SnMe$_3$**), and Cu (Table 2.1, entry 4, **2.1a-Cu**). Initial reaction conditions were

based off from previously successful conditions for TMS-substituted alkyne substrates,[43] using chloride-based Ti catalysts that are typically most robust for [2+2+1] reactions.[42,99] All new heteroatom-substituted reactions resulted in significantly lower yields than the corresponding TMS-substituted alkyne reactions, highlighting the challenges of conserving a reactive transmetallating agent through another organometallic transformation.

Table 2.1. Examination of potential heteroatom-substituted alkyne partners in Ti-catalyzed [2+2+1] heterocoupling.[a]

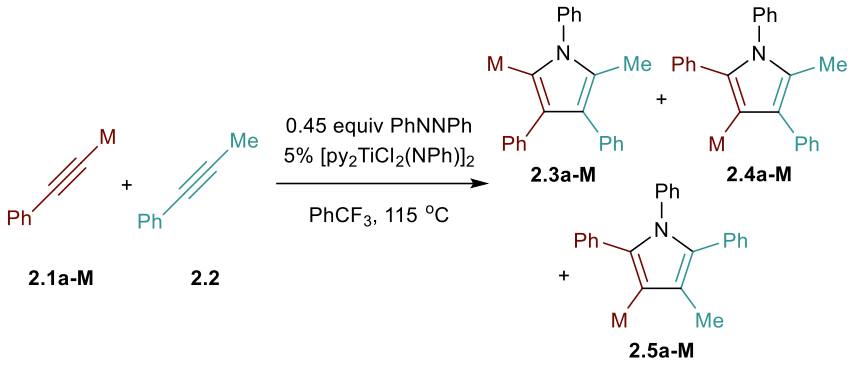

2.1a-M 2.2 2.3a-M 2.4a-M 2.5a-M

Entry	X	Product	Yield	Selectivity[b]
1[d]	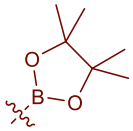 2.1a-Bpin	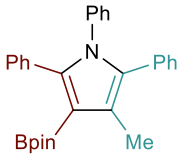 2.5a-Bpin	19%	2.5:1 (1.1:1)[d]
2[e]	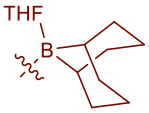 2.1a-BBN	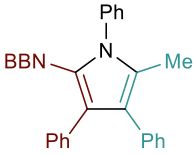 2.3a-BBN	7%	22.3:1 (12.5:1)
3[e]	 2.1a-SnMe$_3$	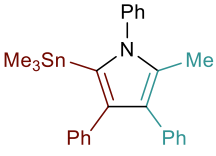 2.3a-SnMe$_3$	51%	6.4:1 (4.5:1)

4[d]	 **2.1a-Cu**	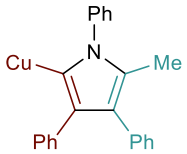 **2.3a-Cu**	7%	n.d.[f]

[a]Conc. = 0.2 M. [b]Selectivity with respect to all heterocoupling pyrrole regioisomer products. Selectivity = **2.3a-M** / (**2.4a-M** + **2.5a-M**). In parenthesis: selectivity with respect to all possible pyrrole products. Selectivity in parenthesis = **2.3a-M** / (**2.4a-M** + **2.5a-M** + homocoupled products of **2.2**). [d]Selectivities calculated for major heterocoupling product **2.5a-M** instead of **2.3a-M**. [d]t = 16 h. [e]t = 20 h. [f]Other pyrrole products cannot be quantified due to their low yield and peak overlapping.

The reaction of PhCCBpin (**2.1a-Bpin**) with PhCCMe yielded 3-Bpin-substituted pyrrole **2.5a-Bpin** as the major product of the reaction (Table 2.1 entry 1); however, the heterocoupling selectivity with respect to **2.3a-Bpin** and **2.4a-Bpin** (2.5:1) and overall selectivity toward **2.5a-Bpin** (1.1:1) was poor. Additionally, there was obvious decomposition of the Bpin moiety, indicated by the observation of white Ti-oxo precipitates. This leads us to speculate that oxophilic Ti may be transmetallating or otherwise reacting with the Bpin B-O bonds.[48] Further optimization attempts with Bpin-substituted alkynes were unsuccessful (Figure 2.16). Although alkynyl borates exhibited compatibility issues with our catalytic system, a recent report from Schafer has demonstrated a borane-functionalized alkyne as a hydroamination substrate in Ti hydroamination catalysis.[100] Thus, we next examined PhCC-BBN·THF (**2.1a-BBN**) (Table 2.1, entry 2). Although **2.1a-BBN** gave a low yield of **2.3a-BBN** as the major product, both the heterocoupling selectivity and overall selectivity of the reaction were very high. Retention of the 9-BBN moiety in this reaction was encouraging, given the diverse modes of reactivity and transmetallation of the boryl unit with transition metals and unsaturated species.[101–106] In fact, there are no reports of organometallic reactions of 9-BBN-substituted alkynes that retain the 9-BBN group. Similar to **2.1a-BBN**, reaction of PhCCSnMe$_3$ (**2.1a-SnMe$_3$**) resulted in the chemo- and regioselective formation of **2.3a-SnMe$_3$** (Table 2.1, entry 3). **2.3a-SnMe$_3$** is also stable to aqueous workup, making stannyl alkynes another attractive candidate class for optimization and method development. Regioselectivity in these reactions results from the polarized C-C triple bond (Figure 2.2).[107–109] In the case of 9-BBN, polarization is a result of the B mesomeric effect,[101] while for SnMe$_3$ polarization results from hyperconjugation between $\sigma_{\mathrm{Sn-R}}$ and $\pi^*_{\mathrm{C-C}}$ in a manner similar to TMS-protected alkynes.[43]

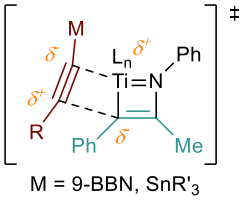

Figure 2.2. Alkyne polarization results in high regioselectivity for 2nd insertion into the putative azatitanacyclobutadiene intermediate.

[PhCCCu]$_n$ (**2.1a-Cu**) exhibited excellent regioselectivity for the formation of **2.3a-Cu** (Table 2.1, entry 4; Figure 2.15); however, the yield and overall chemoselectivity for the heterocoupled product was very low owing to the insolubility of polymeric **2.1a-Cu**. Further, significant protodecupration occurred in all attempts with **2.1a-Cu**, hampering potential utility. Despite these initial challenges with Cu, a recent report from Schafer on Ti-catalyzed hydroamination of NHC-Cu alkynes indicates that alkynylcuprates could yet be good candidates for [2+2+1] pyrrole synthesis.[110]

Having identified 9-BBN- and Sn-substituted alkynes as potential heterocoupling candidates, we next optimized these reactions and explored their substrate scope. Optimization experiments for PhCC-BBN·THF (**2.1a-BBN**) are presented in Table 2.2, while optimization of PhCC-SnMe$_3$ (**2.1a-SnMe$_3$**) are presented in Table 2.7. Increasing Ti catalyst loading to 10% and changing the solvent from PhCF$_3$ to C$_6$D$_5$Br resulted in significant increases to the yield of **2.3a** without erosion of the overall selectivity. Under these optimized conditions, the reactions were completed within 0.5 h (Table 2.2, entry 8).

Surprisingly, the yield of **2.3a** dropped from 74% to 65% upon increasing the catalyst loading from 10 mol% to 15 mol% (Table 2.2, entries 3 and 4). We hypothesized that B and Ti may be undergoing dative ligand (THF or py) exchange and that the resulting B-L/Ti-L speciation may be impacting catalysis. Thus, several experiments were conducted where the L donor identities and molar ratios were changed (Figure 2.3). First, reaction of **2.1a-BBN** with pyridine-free catalyst [TiCl$_2$(NPh)]$_n$ (Figure 2.3A) resulted in dramatically lower yields, indicating that pyridine is needed for productive catalysis (in part, at least, due to catalyst solubility). Excess **2.1a-BBN** (Figure 2.3B) resulted in a lower yield of **2.3a**, and monitoring by ^{11}B NMR (Figure 2.78) indicated that remaining **2.1a-BBN** had abstracted pyridine from the catalyst forming PhCC-BBN·py (**1a-BBN-py**). Reaction of preformed **2.1a-BBN-py** resulted in very slow conversion to **2.3a** (Figure 2.3C). *In situ* ^{11}B NMR analysis of the optimized reaction of **2.1a-BBN** (Table 2.2, entry 8) and the reaction of **2.1a-BBN-py** are shown in Figure 2.4. In

both cases, **2.1a-BBN-py** is evident at t = 0 and is not fully consumed at the end of the reaction at t = 0.5 h. These results indicate that a careful stoichiometric balance of pyridine must be struck with these Lewis acidic substrates: the Ti catalyst needs py bound for productive catalysis, but py-bound **2.1a-BBN-py** undergoes significantly slower reaction than THF-bound **2.1a-BBN** or free PhCC-BBN (Figure 2.3D).

Table 2.2. Optimization of the Ti-catalyzed [2+2+1] heterocoupling of **2.1a-BBN** with **2.2**.[a]

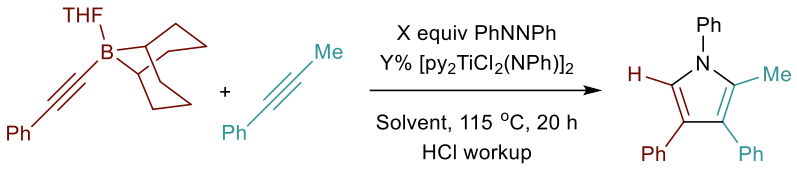

2.1a-BBN **2.2** **2.3a**

Entry	%[Ti][b]	Solvent	[py] equiv.[c]	Yield[d] (Selectivity[e])
1	5	$PhCF_3$	0.2	7% (12.5:1)
2	5	C_6D_5Br	0.2	22% (6.2:1)
3	10	C_6D_5Br	0.4	74% (17.1:1)
4	15	C_6D_5Br	0.6	65% (13.2:1)
5	10	$PhCH_3$	0.4	67% (19.6:1)
6	10	$PhCF_3$	0.4	55% (15.7:1)
7	10	$PhOCH_3$	0.4	20% (9.6:1)
8[f]	10	C_6D_5Br	0.4	66% (22.7:1)

[a]Conc. = 0.2 M. [b][PhNNPh] was adjusted coordinatingly to the change in [Ti] to keep the nitrene equivalent as 1, on basis of the relationship [Nitrene] = [Ti] + 2[PhNNPh]. [c]Total equivalent of pyridine in the reaction. [d]Yield determined by GC-FID. [e]Selectivity with respective to all possible pyrrole products. [f]t = 0.5 h.

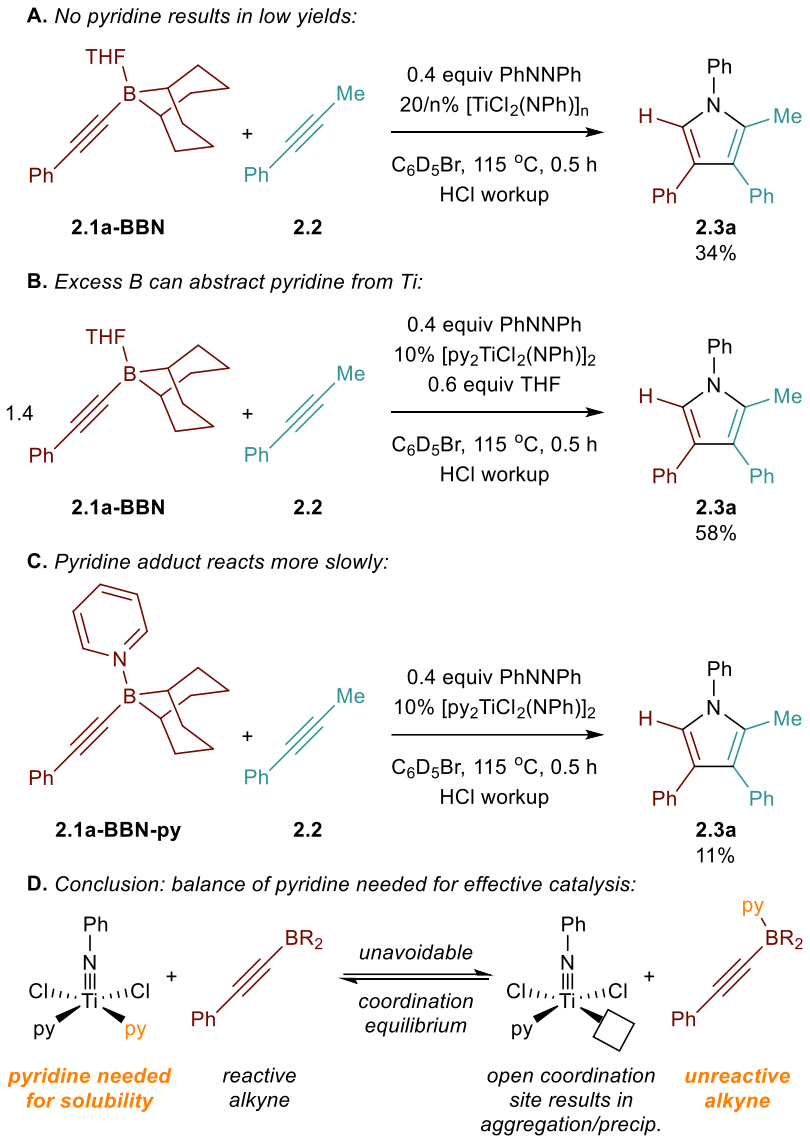

Figure 2.3. Control reactions studying the effect of L donor on the Ti-catalyzed [2+2+1] heterocoupling of **2.1a-BBN** with **2.2**. (A) Reaction with 0 equiv pyridine. (B) Excess **2.1a-BBN** acts as a pyridine scavenger. (C) Pyridine-bound **2.1a-BBN-py** reacts significantly slower than **2.1a-BBN**. (D) Schematic demonstrating pyridine coordination equilibrium effects.

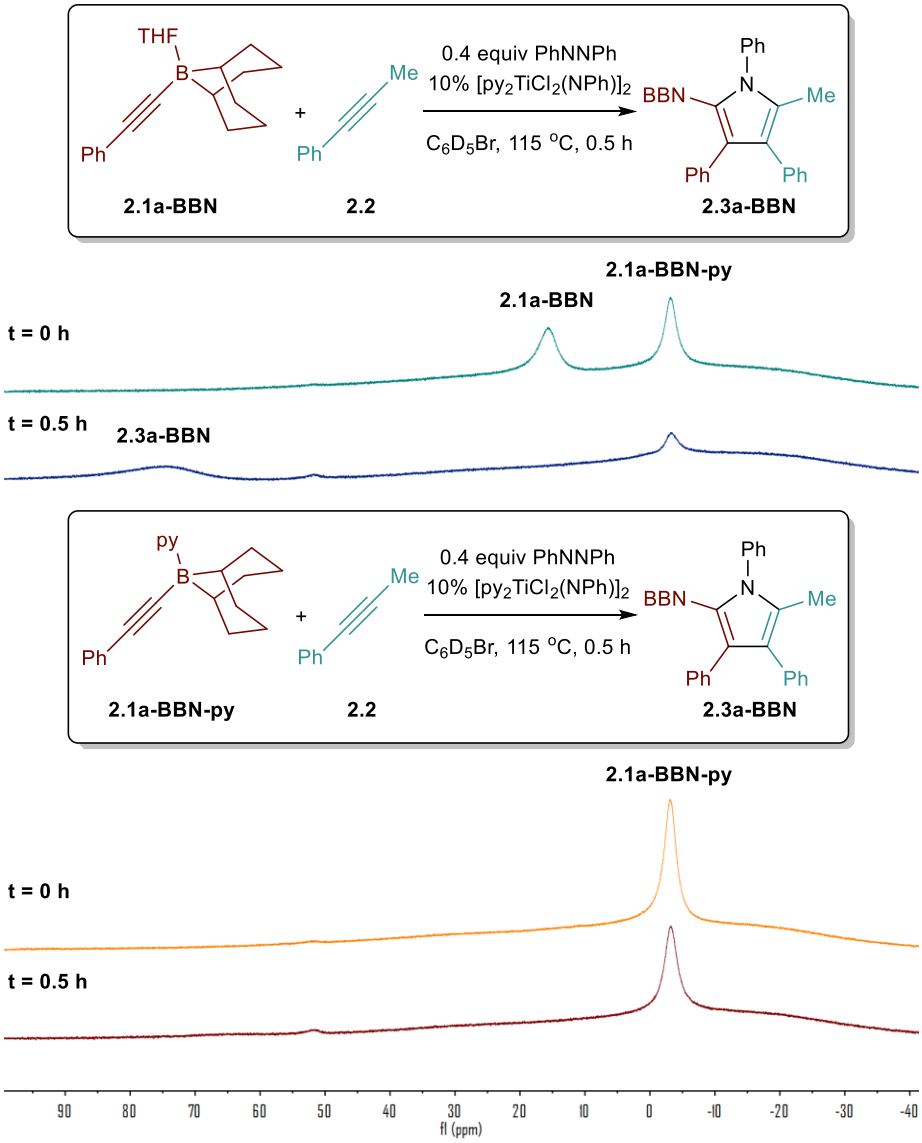

Figure 2.4. ^{11}B NMR study demonstrating pyridine-bound **2.1a-BBN-py** (bottom) reacts more slowly than **2.1a-BBN** (top).

Next, a small scope of 9-BBN-substituted and SnR_3-substituted alkynes was examined in heterocoupling with **2.2** (Table 2.3). Reactions of the alkynes examined resulted in good selectivity and yield of the corresponding 2-borylpyrroles and 2-stannylpyrroles, which were hydrolyzed with HCl in methanol to simplify analysis. Neither electronics or sterics on the arylalkyne significantly impacted yield and selectivity: electron-rich (**2.1b-BBN**, **2.1b-SnMe$_3$**) and electron-deficient (**2.1c-BBN**, **2.1c-SnMe$_3$**) arylalkynylboranes reacted equally well, as did the more sterically encumbered *o*-tolyl-alkynylborane (**2.1d-BBN**, **2.1d-SnMe$_3$**). Lastly, the

reaction of alkyl-substituted alkynes ^{n}BuCC-BBN·THF (**2.1e-BBN**) and MeCC-Sn^{n}Bu$_3$ (**2.1f-Sn^{n}Bu$_3$**) were also highly selective.

Table 2.3. Substrate scope of 9-BBN- and R$_3$Sn-alkynes in [2+2+1] pyrrole synthesis.

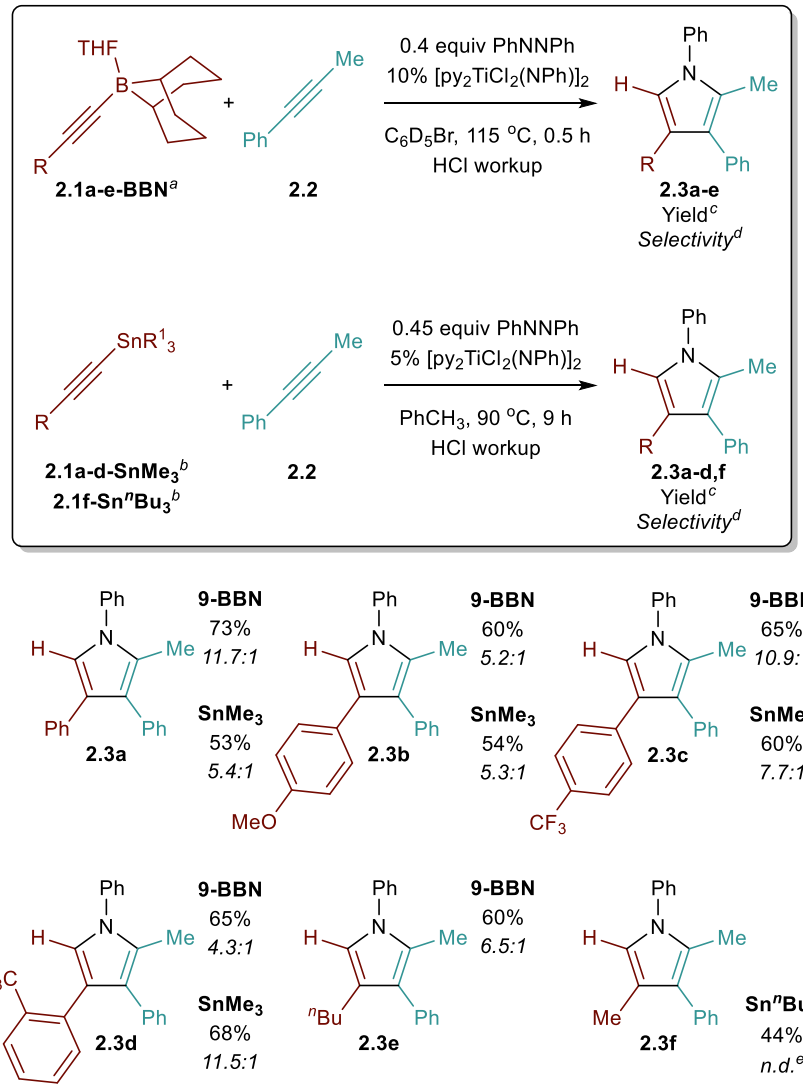

[a]Conc. = 0.2 M. [b]Conc. = 0.8 M. [c]Yield determined by NMR. [d]Selectivity with respect to all possible pyrrole products. [e]Other regioisomers cannot quantified due to their low yield.

Further, we investigated the [2+2+1] heterocoupling reactions with different hydrocarbon alkynes (Table 2.4). Various symmetric internal alkyne (**2.2g-j**) demonstrated productive heterocoupling reactivity. The non-polarized nature of the C≡C bond of these symmetric alkynes led to lower reactivity in [2+2] cycloaddition, resulting in lower yields. However, these less reactive alkynes were also less prone to competitive insertion chemistry, contributing to

the higher overall selectivity (> 50:1 in the case of **2.3j**) of these reactions. Lastly, a terminal alkyne (**2.2k**) was also tested, which resulted in mostly alkyne trimerization instead of productive reactivity (Figure 2.188-2.192).

Table 2.4. Alkyne scope in B- and Sn-functionalized [2+2+1] pyrrole synthesis.

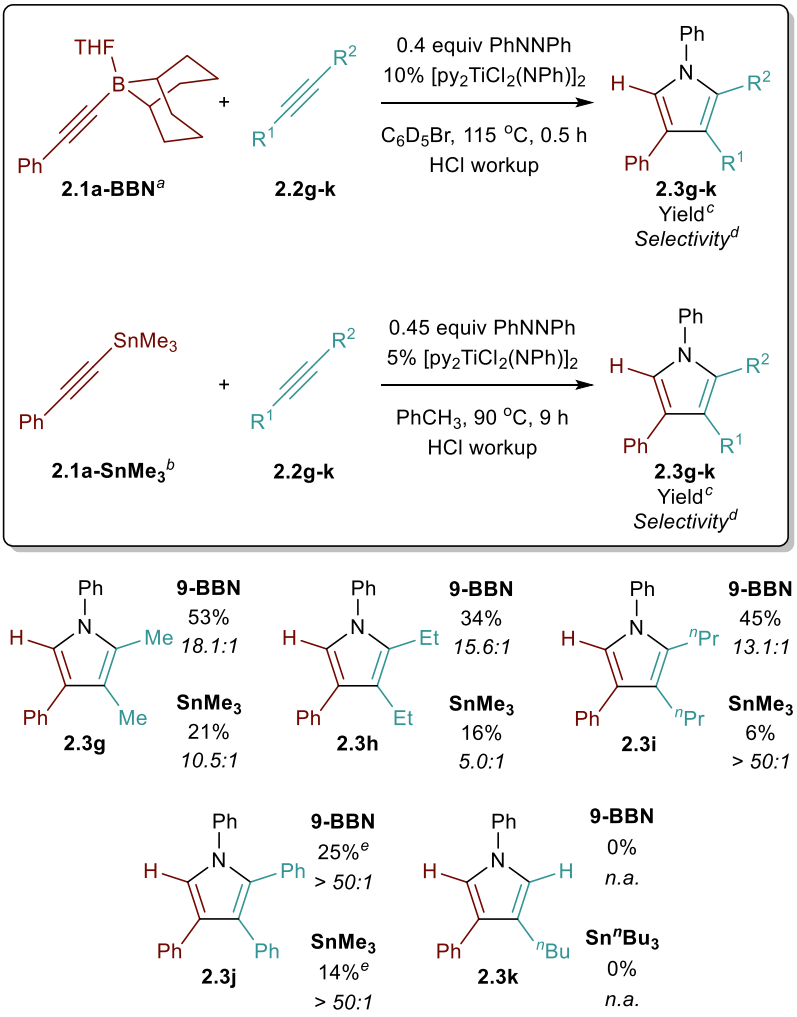

[a]Conc. = 0.2 M. [b]Conc. = 0.8 M. [c]Yield determined by NMR. [d]Selectivity with respect to all possible pyrrole products. [e]Yield determined by GC.

Though 9-BBN is frequently used in Suzuki cross coupling reactions between C_{sp^3}-9-BBN and various C-X electrophiles,[111–115] the sp^2-sp^2 Suzuki cross coupling of aryl-9-BBN nucleophiles is rare.[116] Nonetheless, we sought to develop a one-pot sequential [2+2+1] pyrrole synthesis and arylation procedure (Table 2.5). Reaction of **2.1a-BBN** with **2.2** in $PhCH_3$ *in situ* produces **2.3a-BBN**; after formation of the pyrrole, addition of *p*-iodofluorobenzene

(**2.6a**), 10% $Pd(PPh_3)_4$, and 2.5 equiv NaO^tBu generates the pentasubstituted pyrrole product **2.7aa** in good (58%) overall yield. Since these Ti redox catalytic reactions are tolerant of aryl halide functional groups, the reaction can also be carried in the desired aryl halide solvent in similar overall yield (40% for **2.7aa**) and shorter [2+2+1] reaction time. This one-pot procedure provides convenient access to unsymmetrical pentasubstituted 2-aryl pyrroles that cannot be accessed via previous [2+2+1] heterocoupling protocols, which could only install aryl groups at the N-, 3-, and 4-positions. Further exploration on the scope of the one-pot pyrrole synthesis/arylation revealed that productive chemistry can be performed on a broad scope of alkynylborane substrates and aryl halides, giving moderate to good yields over the two-step sequence. In general, the substrate scope revealed limited effect on the yield of [2+2+1] step (as seen in Table 2.3), but large effects on the arylation step. For example, the arylation step is very sensitive to steric hindrance: formation of **2.7da**, which requires transmetallation[117] of a sterically encumbered 3-tolyl-2-(9-BBN)pyrrole, resulted in large amount of protodeborylated **2.3d** (Figure 2.128) and only 19% **2.7da**. In contrast, in the formation of **2.7ac** (where the aryl and tolyl groups are transposed, resulting in a less bulky 3-phenyl-2-(9-BBN)pyrrole), there was a smaller amount of protodeborylated **2.3a** observed (Figure 2.146). Similarly, the arylation to form **2.7ea** is much higher yielding, with only trace amount of **2.3e** formed (Figure 2.135). The aryl ether substrate **2.6b** underwent coupling to form **2.7ab** with moderate yield, although some demethoxylation was evident. Other oxygenated substrates such as **2.6d** and **2.6e** were poor cross coupling partners. Although nitro groups and esters are commonly tolerated in Suzuki reactions, ^{11}B NMR spectroscopic evidence indicates that deleterious chemistry with the 9-BBN group may be taking place (Figure 2.155). In addition to sp^2-sp^2 Suzuki cross coupling, we also attempted C_{sp^3}-C-X cross couplings with aryl-9-BBN. These reactions are also rarely studied, although Fu has several demonstrations with aryl and vinyl 9-BBN substrates.[95,118] Unfortunately, rapid protiodemetalation of the 9-BBN pyrrole was observed in all attempts.

Table 2.5. One-pot sequential pyrrole synthesis/arylation.[a]

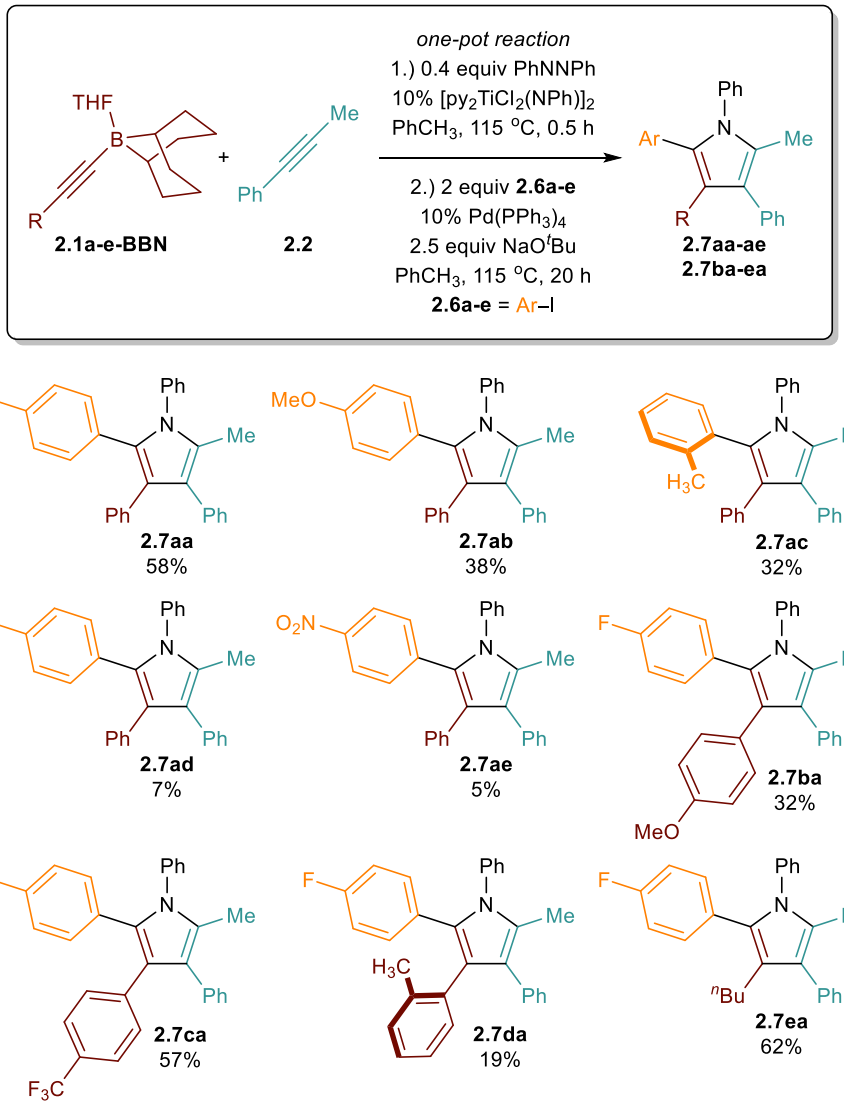

[a]Conc. = 0.2 M. Yields determined by ^{1}H NMR. [b]In parenthesis: reaction solvent = **2.6a**, time = 0.5 h (1st step), 20 h (2nd step).

Finally, given that 9-BBN and Sn alkynes undergo coupling with similar chemo- and regioselectivity to TMS-protected alkynes,[43] intramolecular competition experiments were conducted to determine the relative directing ability of the two functional groups compared to TMS (Figure 2.5). There are few points of comparison for the regioselectivity of insertion into these types of doubly-functionalized alkynes. Studies of protodetmetallation of TMS-CC-M (M = Si, Ge, Sn) indicate that β-hyperconjugative stabilization of putatitve vinyl carbocation intermediates increases Si < Ge << Sn,[119] which could potentially also stabilize the building δ^+ on the β-C during 1,2-insertion of the alkyne into the Ti-C bond of the azatitanacyclobutadiene

intermediate. If this were the dominant mechanism of regiocontrol, Sn would be a stronger director than Si. Reaction of TMSCC-BBN·THF (**2.1g-BBN**) with **2.2** resulted in formation of 10% **2.3g-BBN** and 25% **2.4g-BBN** (Figure 2.5, top), while reaction of TMSCCSn^{n}Bu$_3$ (**2.1g-Sn^{n}Bu$_3$**) with **2.2** resulted in the formation of 6% **2.3g-Sn^{n}Bu$_3$** and 12% **2.4g-Sn^{n}Bu$_3$**. Thus, TMS is a stronger directing group for insertion than both 9-BBN and Sn^{n}Bu$_3$ (Figure 2.5, bottom). Thus, the β-stabilization from the alkyne substituent does not play a dominant role in determining relative selectivity, and other factors such as the relative strength of the forming Ti-C$_{Si}$ bond *vs.* Ti-C$_M$ bond may also be involved: for example, Micalizio has demonstrated that insertion into 2-silyl-3-stannyltitanacyclopropenes will occur on the Ti-C$_{Sn}$ bond compared to the Ti-C$_{Si}$ bond.[120,121]

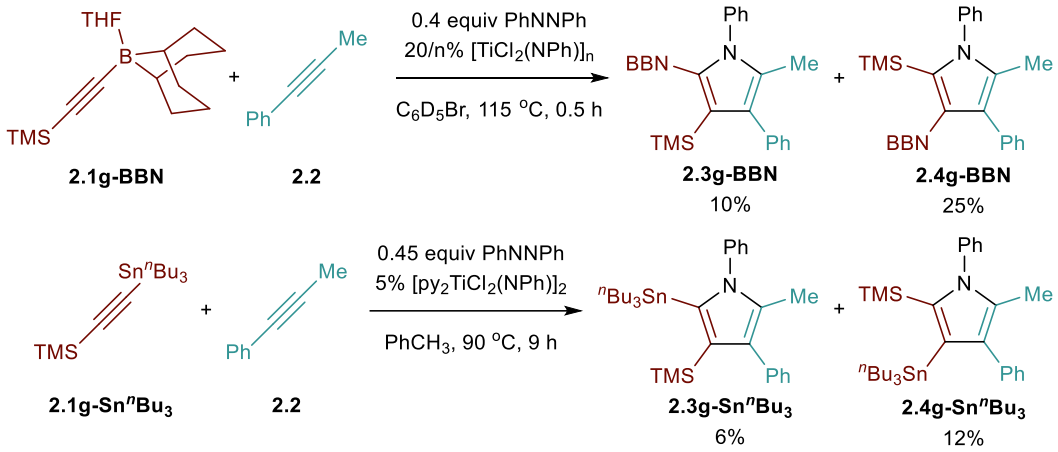

Figure 2.5. Directing group strength comparisons.

2.4 Conclusion

In summary, both alkynyl boranes and stannanes are efficient alkyne heterocoupling partners in titanium-catalyzed [2+2+1] pyrrole synthesis, generating the corresponding heteroatom-substituted pyrroles with high chemo- and regioselectivity. The resulting products are candidates for further functionalization through cross coupling, as demonstrated by a one-pot sequential [2+2+1] boryl pyrrole synthesis/Suzuki coupling reaction. These one-pot sequential reactions provide access to unique, highly decorated pentasubstituted pyrroles that are otherwise inaccessible *via* [2+2+1] heterocoupling protocols or classical pyrrole synthetic strategies.

2.5 Experimental

2.5.1 General Considerations

All air- and moisture-sensitive compounds were manipulated in a glovebox under nitrogen atmosphere. Solvents for air- and moisture-sensitive reactions ($PhCF_3$, $PhCH_3$, C_6H_6) were dried through activated alumina on a Pure Process Technology solvent purification system. $PhOCH_3$ and NMR solvents ($CDCl_3$ and C_6D_6) were dried over CaH_2 or Na^0/Ph_2CO and vacuum transferred before passing through activated alumina and storing over activated 3 Å molecular sieves in the glovebox. C_6D_5Br was synthesized following a reported procedure[122] and passed through activated alumina before storing over activated 3 Å molecular sieves in the glovebox. **2.1a-SnMe$_3$**, **2.1f-Sn^{n}Bu$_3$**, **2.1g-Sn^{n}Bu$_3$**, **2.2**, *n*-butyllithium, *B*-methoxy-9-borabicyclo[3,3,1]nonane solution in hexanes and Me_3SnCl solution in hexanes were purchased from Millipore-Sigma. Azobenzene was purchased from TCI Chemicals and purified by hexane/water extraction three times. Terminal alkynes were purchased from Oakwood Products, Inc. and Millipore-Sigma. **2.1a-BBN**,[123] **2.1e-BBN**,[124] **2.1g-BBN**,[125] **2.1a-Cu**,[126] and $[py_2TiCl_2(NPh)]_2$[127] were prepared following the reported procedures.

GC chromatographs were collected on Agilent 7890B GC system equipped with the HP-5 column (30 m, 0.32 mm, 0.25 µm, 7 inch cage), an oxidation-methanation reactor (Polyarc® System, Activated Research Company), and a FID detector for quantitative carbon detection.[128,129] ^1H, ^{11}B, $^{13}C\{^1H\}$, $^{19}F\{^1H\}$, $^{119}Sn\{^1H\}$, ^1H–^{13}C and ^1H–^{15}N HMBC, NOESY, and No-D ^1H NMR were collected on Bruker Avance III HD NanoBay 400 MHz or Bruker Avance III HD 500 MHz spectrometers. Chemical shifts are reported with respect to residual protio-solvent impurity for ^1H (s, 7.26 ppm for $CDCl_3$; s, 7.16 ppm for C_6D_6) and ^{13}C (t, 77.16 ppm for $CDCl_3$; t, 128.06 ppm for C_6D_6). ^{11}B NMR was externally referenced to $BF_3{\cdot}OEt_2$ in the corresponding solvent as 0.0 ppm. $^{119}Sn\{^1H\}$ NMR in $CDCl_3$ was externally referenced to Me_4Sn in $CDCl_3$ as 0.00 ppm. $^{119}Sn\{^1H\}$ NMR in toluene was referenced to the chemical shifts of the corresponding stannyl alkynes in C_6D_6 (**2.1a-SnMe$_3$**,[130] **2.1g-Sn^{n}Bu$_3$**[131]) or $CDCl_3$ (**2.1b-SnMe$_3$**, **2.1c-SnMe$_3$**, **2.1d-SnMe$_3$**). No-D ^1H NMR was referenced to the proton signal of the internal standard triphenylmethane (Ph_3CH, s, 5.54 ppm in $PhCF_3$; s, 5.34 ppm in $PhCH_3$). ^1H NMR of catalytic reactions in C_6D_5Br were referenced to the proton signal of the internal standard triphenylmethane (Ph_3CH, s, 5.45 ppm).

2.5.2 Initial Screening of Heteroatom-Substituted Alkynes (Table 1)

General Procedure for Initial Screening of Heteroatom-Substituted Alkynes as Heterocoupling Partner (Procedure 2.A)

$[py_2TiCl_2(NPh)]_2$ (3.7 mg, 0.005 mmol, 0.05 equiv), heteroatom-substituted 2-phenylethyne (**2.1a-M**, 0.1 mmol, 1 equiv) and 0.5 mL of $PhCF_3$ stock solution containing 1-phenyl-1-propyne (**2.2**) (11.6 mg, 0.1 mmol, 1 equiv), azobenzene (8.2 mg, 0.045 mmol, 0.45 equiv) and triphenylmethane (4.9 mg, 0.02 mmol, 0.2 equiv, internal standard) were added to an NMR tube. The reaction was then sealed and heated in a preheated oil bath at 115 ℃. No-D NMR spectra were collected before and after heating to monitor the reaction. The reaction was quenched with 5% HCl in methanol and extracted with $EtOAc/H_2O$. The organic phase was dried over $MgSO_4$ and evaporated under vacuum. The crude product mixture was characterized by GC-Polyarc®/FID to calculate the yield and selectivity.

Reaction of **2.1a-Bpin (Table 2.1, Entry 1)**

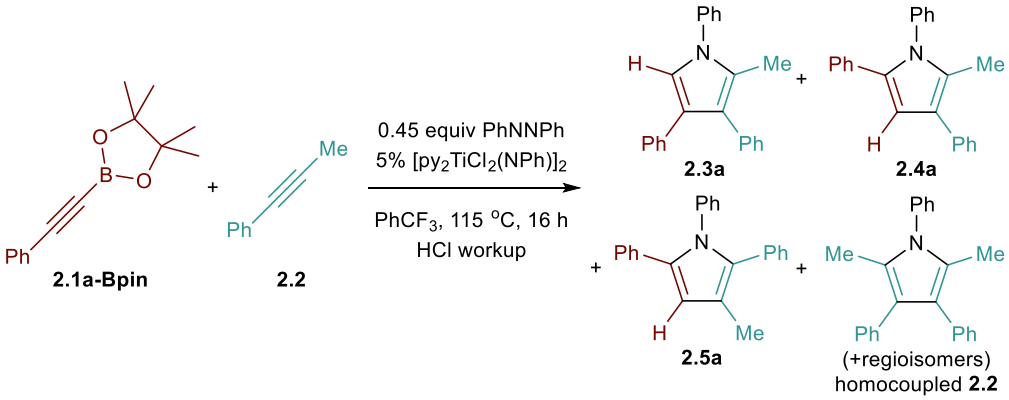

The reaction was performed following **Procedure 2.A** using **2.1a-Bpin** (22.8 mg, 0.1 mmol, 1 equiv) with the reaction being heated for 16 h. Selectivity calculated for the major regioisomer of the heterocoupling, product **2.5a**.

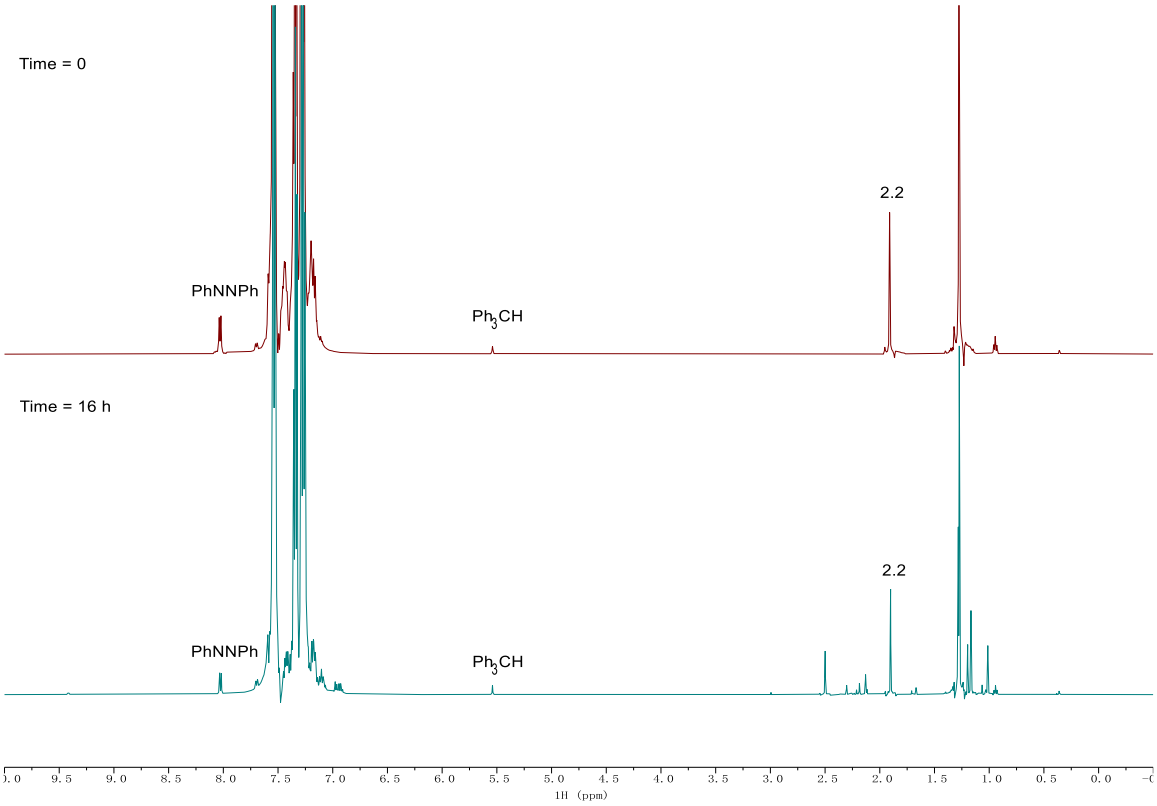

Figure 2.6. No-D ^{1}H NMR of the reaction of **2.1a-Bpin** at time = 0 (top), time = 16 h (bottom) in $PhCF_3$. *Taken from (top) YC-2019-0021-NoD-TFT-0h and (bottom) YC-2019-0020-NoD-TFT-22h.*

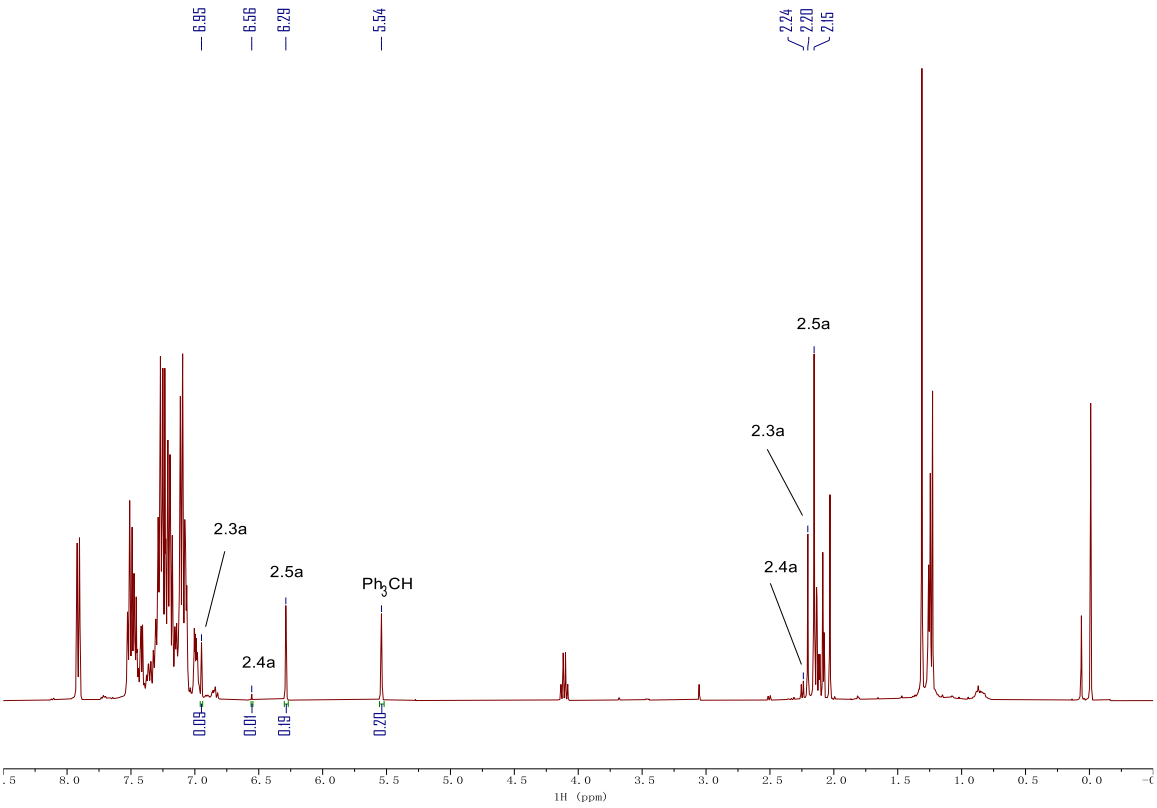

Figure 2.7. ^{1}H NMR of the reaction of **2.1a-Bpin** in $CDCl_3$ after HCl workup. *Taken from YC-2019-0021-Deborylated-2H.*

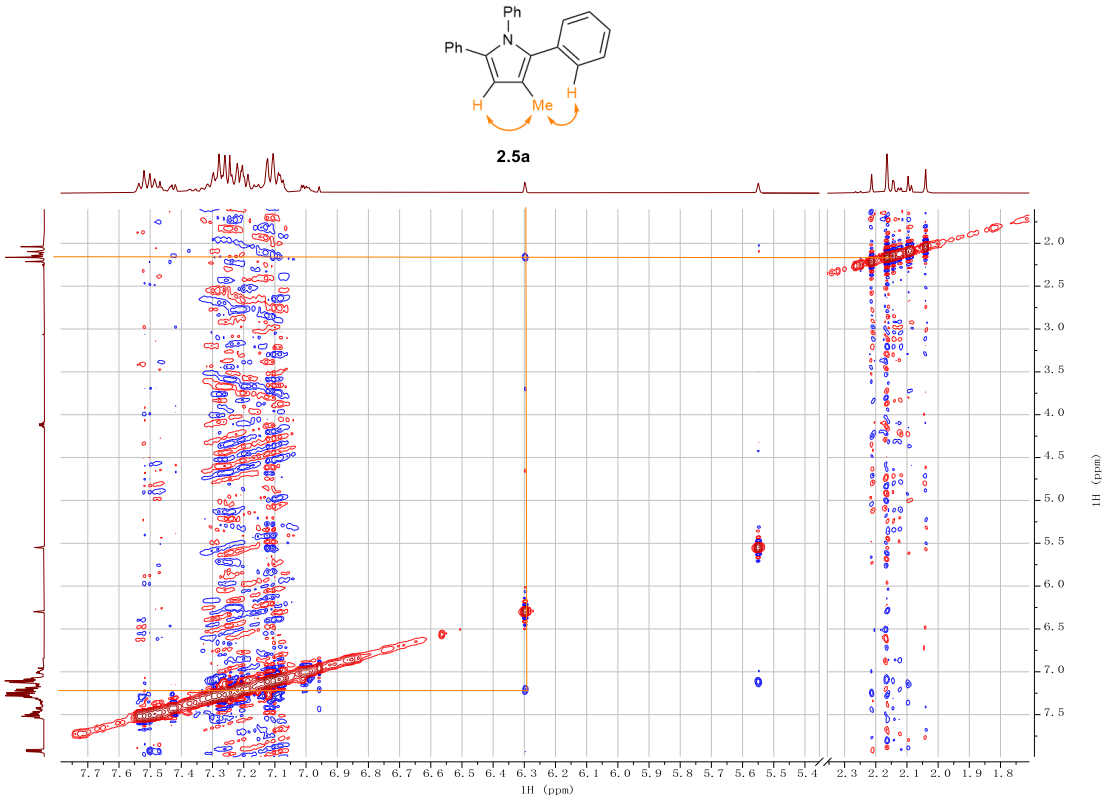

Figure 2.8. NOESY NMR spectrum of the reaction of **2.1a-Bpin** in $CDCl_3$ after HCl workup. *Taken from YC-2019-0021-Deborylated-2NOESY.*

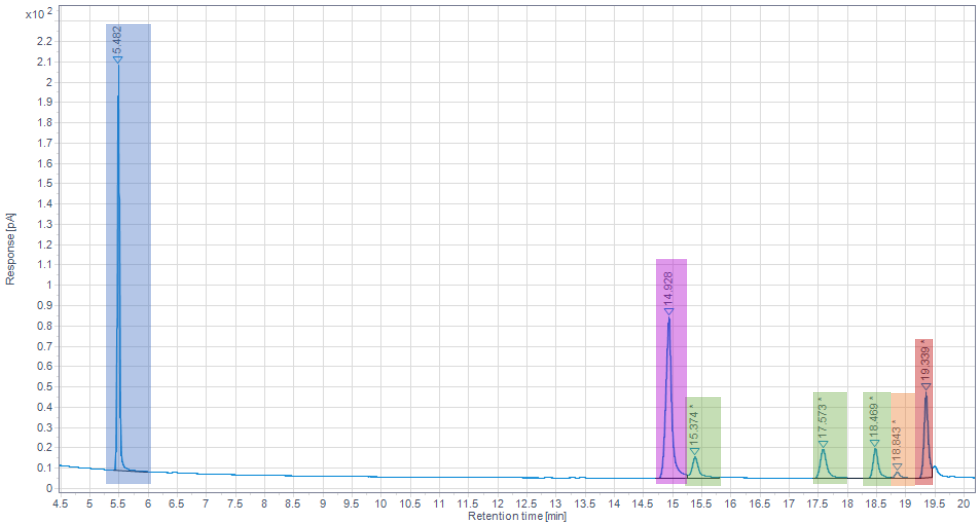

	Retention Time (min)	Surface Area	# of C	Yield (%)
Ph_3CH	5.48	479.301	19	n.a.
2.3a	19.34	208.919	23	9.1

2.4a	18.84	17.921	23	0.6
2.5a	14.93	560.266	23	19.3
homocoupled **2.2**	15.37, 17.57, 18.47	295.586	24	9.8

Figure 2.9. Quantitative GC-FID chromatograph of the reaction of **2.1a-Bpin** after HCl workup. *Taken from YC-2019-0024-1FID.*

Sample yield calculation based on quantitative carbon detection:

$$Yield\ of\ \mathbf{2.3a} = \frac{Surface\ Area\ of\ \mathbf{2.3a}}{\#\ of\ C\ of\ \mathbf{2.3a}} \times \frac{\#\ of\ C\ of\ Ph_3CH}{Surface\ Area\ of\ Ph_3CH} \times equiv\ of\ Ph_3CH \times 100\%$$

Reaction of **2.1a-BBN (Table 2.1, Entry 2)**

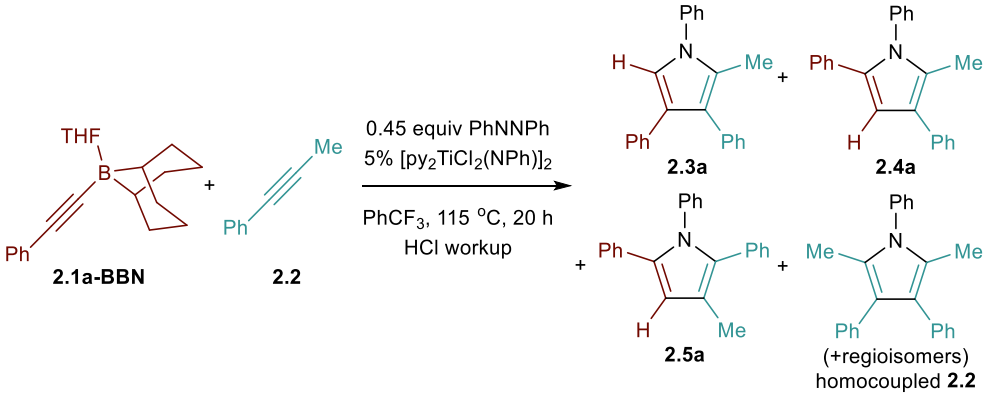

The reaction was performed following **Procedure 2.A** using **2.1a-BBN** (29.4 mg, 0.1 mmol, 1 equiv) with the reaction being heated for 20 h. Selectivity calculated for the major regioisomer of the heterocoupling, product **2.3a**.

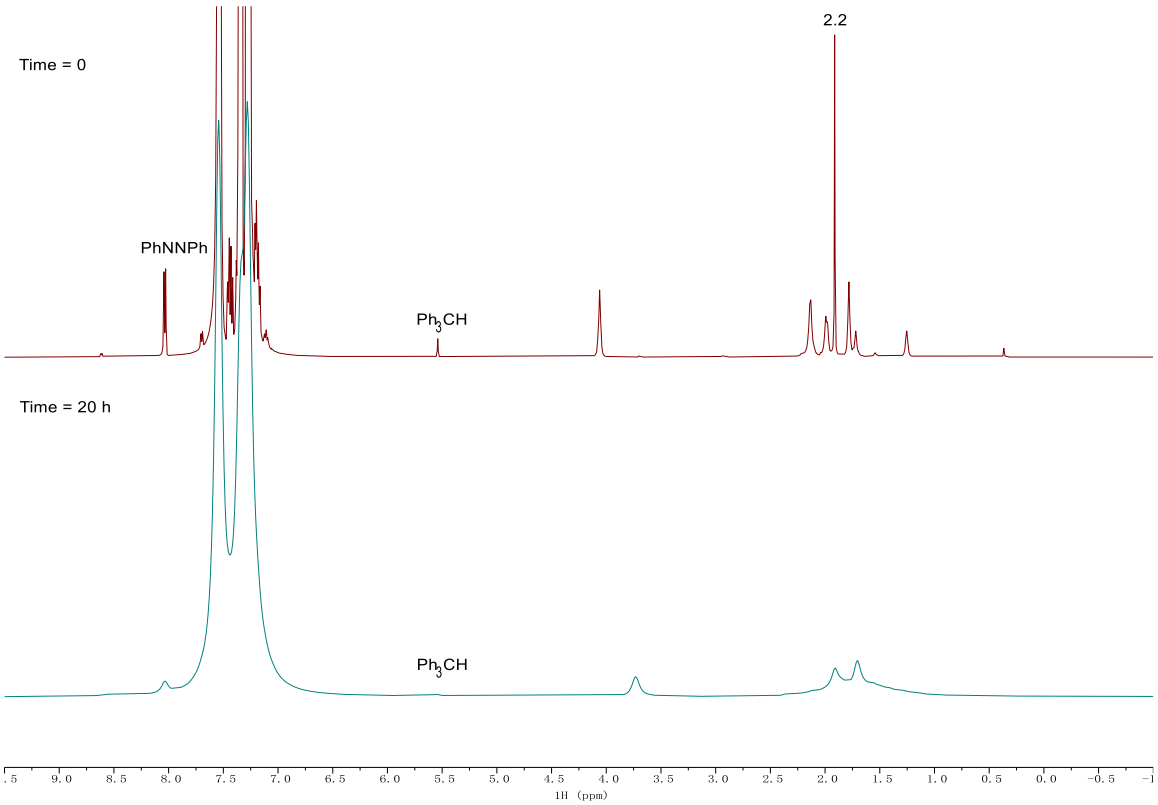

Figure 2.10. No-D ^{1}H NMR of the reaction of **2.1a-BBN** at time = 0 (top), time = 20 h (bottom) in $PhCF_3$. *Taken from (top) YC-2019-0095-NoD-TFT-0h and (bottom) YC-2019-0095-NoD-TFT-20h.*

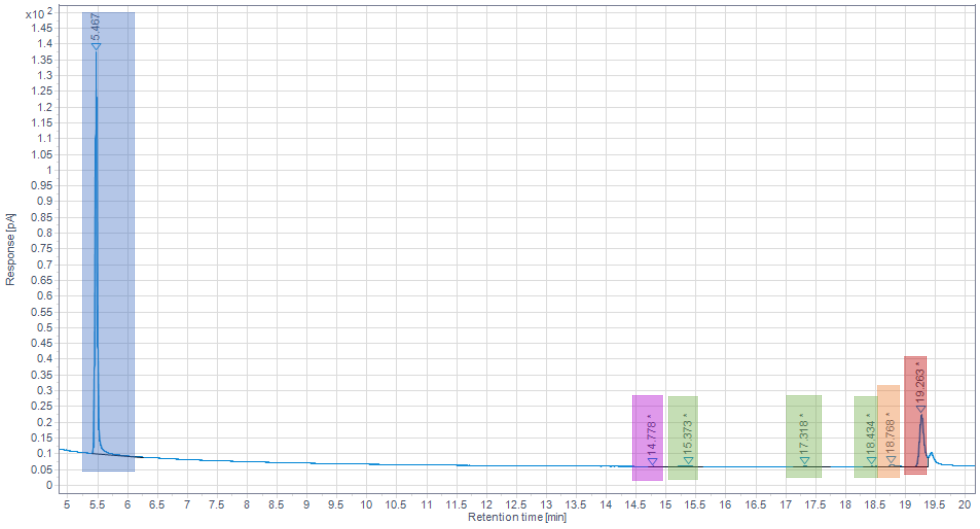

	Retention Time (min)	Surface Area	# of C	Yield (%)
Ph_3CH	5.47	313.838	19	n.a.
2.3a	19.26	125.569	23	6.6
2.4a	18.77	5.332	23	0.3
2.5a	14.78	0.287	23	< 0.1
homocoupled **2.2**	15.37, 17.32, 18.43	4.602	24	0.2

Figure 2.11. Quantitative GC-FID chromatograph of the reaction of **2.1a-BBN** after HCl workup. *Taken from YC-2019-0095-6FID.*

Reaction of **2.1a-SnMe$_3$ (Table 2.1, Entry 3)**

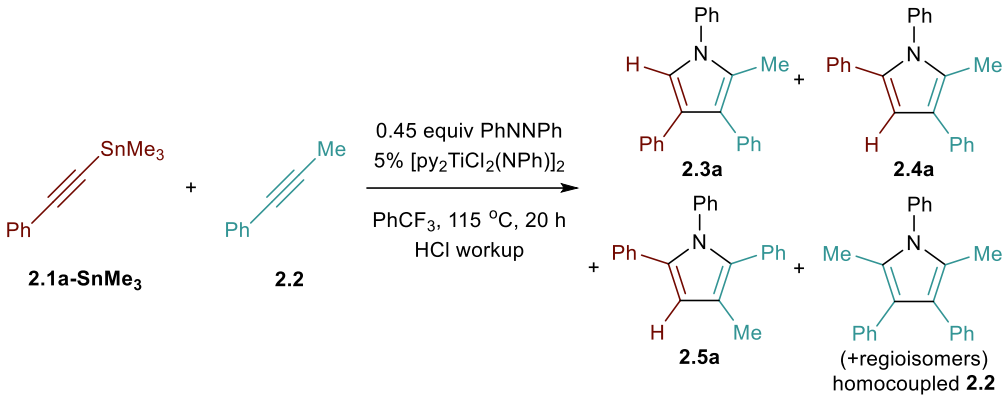

The reaction was performed following **Procedure 2.A** using **2.1a-SnMe$_3$** (26.5 mg, 0.1 mmol, 1 equiv) with the reaction being heated for 20 h. Selectivity calculated for the major regioisomer of the heterocoupling, product **2.3a**.

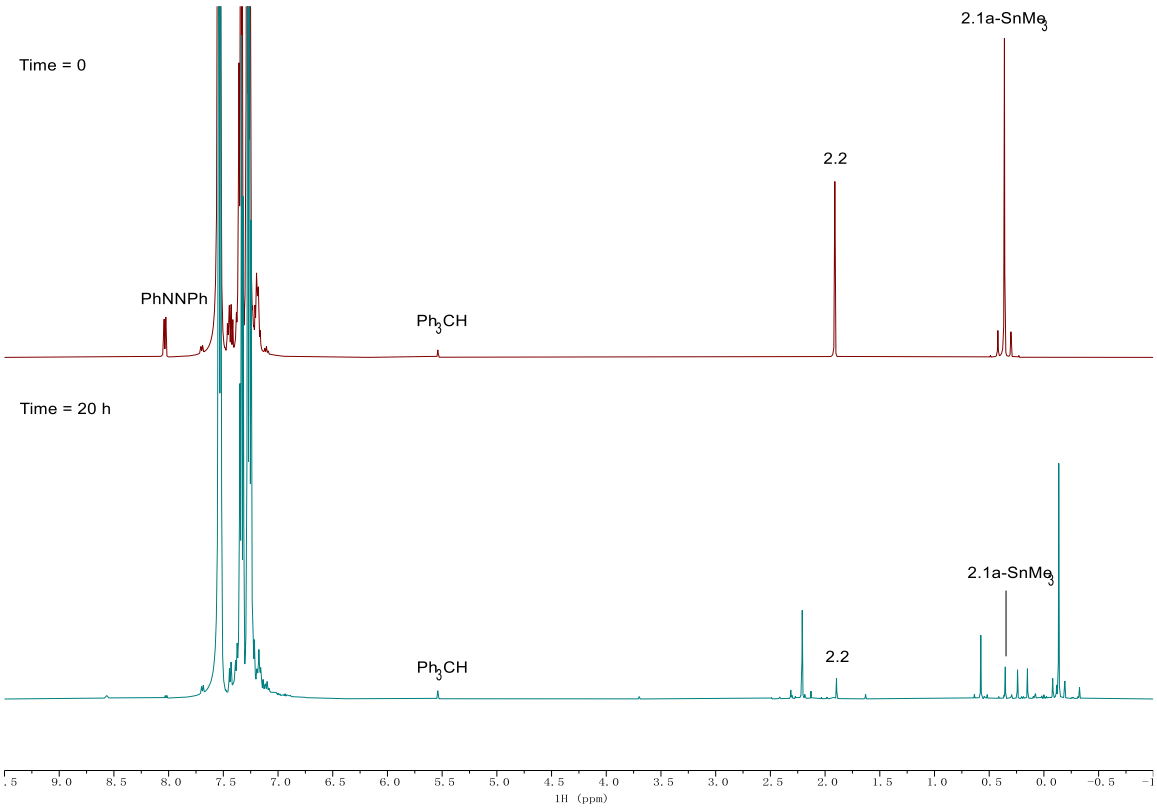

Figure 2.12. No-D ^{1}H NMR of the reaction of **2.1a-SnMe$_3$** at time = 0 (top), time = 20 h (bottom) in $PhCF_3$. *Taken from (top) YC-2019-0100-NoD-TFT-0h and (bottom) YC-2019-0100-NoD-TFT-20h.*

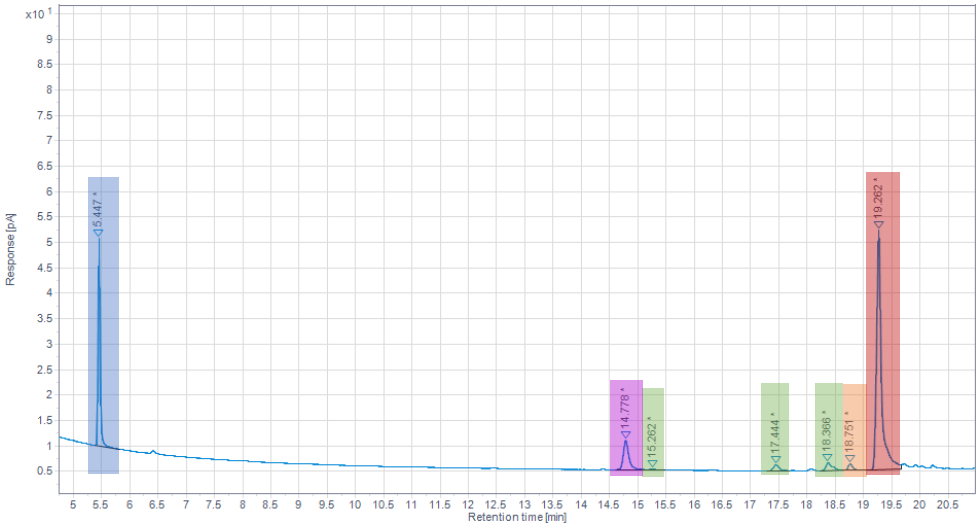

	Retention Time (min)	Surface Area	# of C	Yield (%)
Ph_3CH	5.45	97.101	19	n.a.
2.3a	19.26	297.256	23	50.6
2.4a	18.75	7.061	23	1.2
2.5a	14.78	39.048	23	6.6
homocoupled **2.2**	15.26, 17.44, 18.37	20.440	24	3.3

Figure 2.13. Quantitative GC-FID chromatograph of the reaction of **2.1a-SnMe$_3$** after HCl workup. *Taken from YC-2019-0100-2FID.*

Reaction of **2.1a-Cu (Table 2.1, Entry 4)**

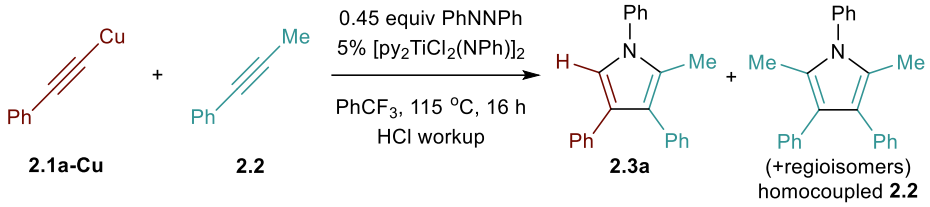

The reaction was performed following **Procedure 2.A** using **2.1a-Cu** (16.5 mg, 0.1 mmol, 1 equiv) with the reaction being heated for 16 h. Yield of **2.3a** was found to be 7%. **2.4a** and **2.5a** were not found. Selectivity was not determined due to the peak overlapping with homocoupled **2.2**.

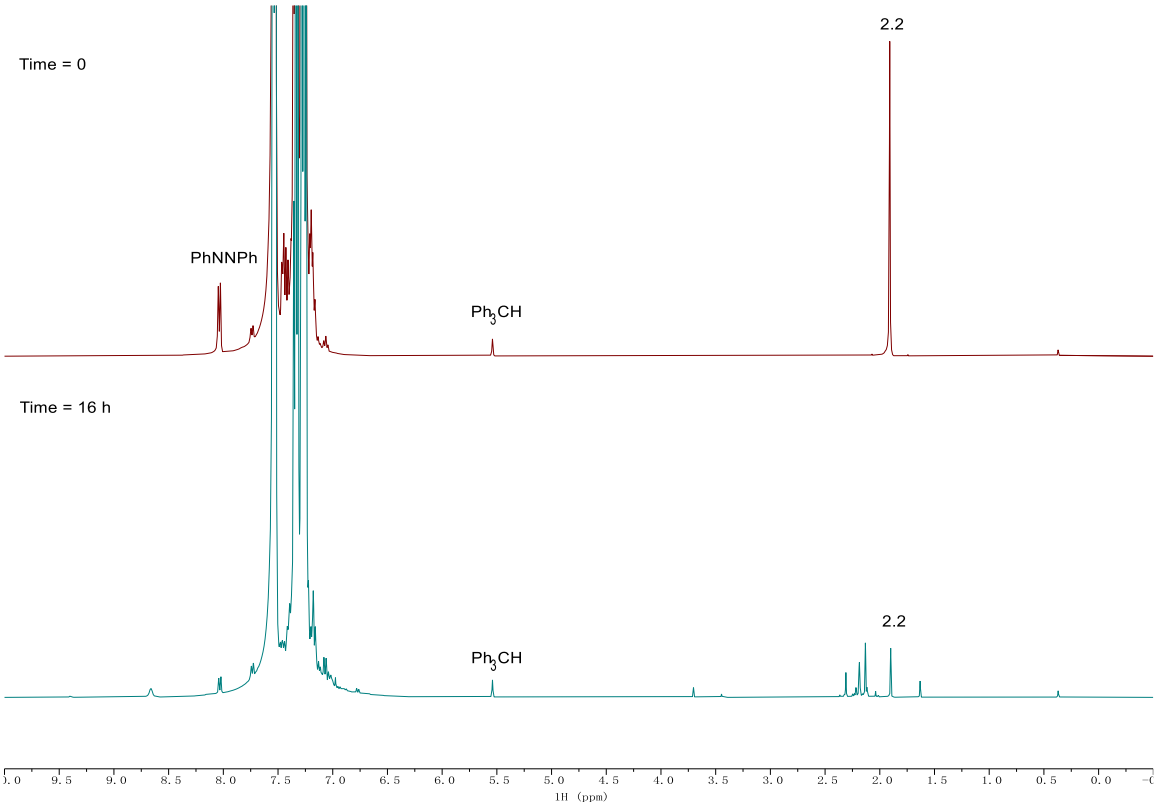

Figure 2.14. No-D ^{1}H NMR of the reaction of **2.1a-Cu** at time = 0 (top), time = 16 h (bottom) in $PhCF_3$. *Taken from (top) YC01038-A-NoD-TFT-0h and (bottom) YC01038-A-NoD-TFT-16h-1H.*

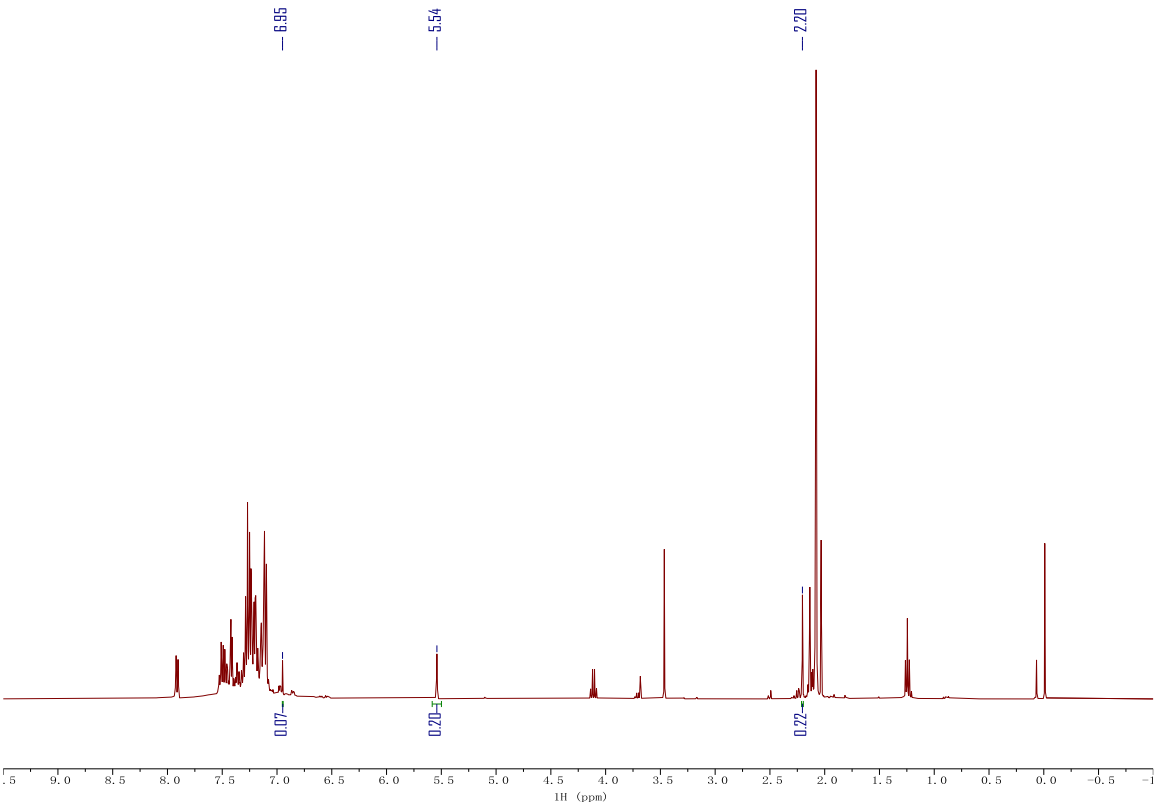

Figure 2.15. ^{1}H NMR of the reaction of **2.1a-Cu** after HCl workup. *Taken from YC01038-A-3H.*

2.5.3 Optimization of Reaction Conditions

Attempted Optimization of Catalysis with 2.1a-Bpin as Heterocoupling Partner

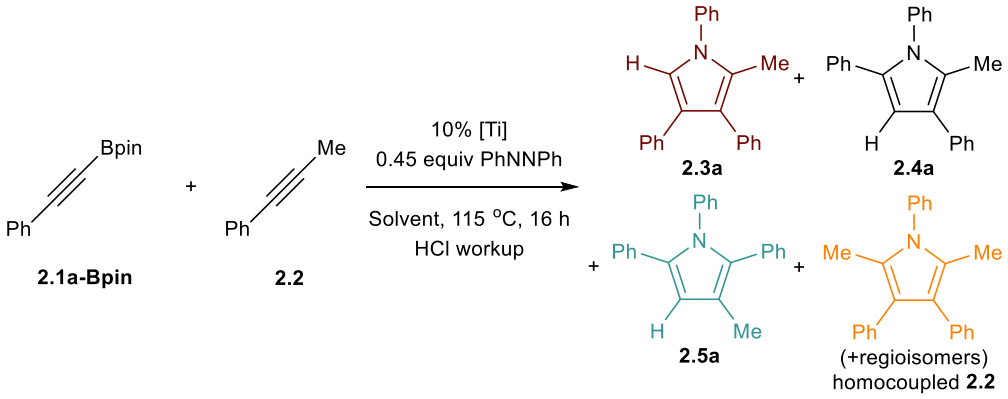

Ti catalyst (0.01 mmol, absolute quantity of titanium, 0.1 equiv), azobenzene (8.2 mg, 0.045 mmol, 0.45 equiv), 2-phenylethynyl-4,4,5,5-tetramethyl-1,3,2-dioxaborolane (**2.1a-Bpin**) (22.8 mg, 0.1 mmol, 1 equiv), 1-phenyl-1-propyne (**2.2**) (11.6 mg. 0.1 mmol, 1 equiv), triphenylmethane (4.9 mg, 0.02 mmol, 0.2 equiv, internal standard) and 0.5 mL of solvent were added to a 4 mL scintillation vial equipped with a stir bar in the glovebox. The vial was then sealed with a PTFE-lined Teflon screw cap, brought out of the glovebox and heated at 115 ℃ on an aluminum well plate for 16 h. After cooling down to room temperature, the reaction was quenched with 5% HCl in methanol and extracted with EtOAc/H_2O. The organic phase was dried over $MgSO_4$ and evaporated to yield a mixture containing **2.3a**, **2.5a** and the regioisomers from the homocoupling of **2.2**. The yields and selectivity were determined by GC-Polyarc®/FID. The yield of **2.4a** was lower than 1% throughout the whole optimization and was considered negligible.

A trend can be found that the sum yield of heterocoupling (**2.3a** and **2.5a**) as well as the yield of homocoupling of **2.2** are solvent dependent. Further, the ratio of the heterocoupling product (**2.3a**/**2.5a**) increases the catalyst ancillary halogen is changed from Cl, Br, to I, indicating that a more electron-deficient Ti center favors **2.3a** over **2.5a** (Figure 2.16 and 2.17). However, none of the attempted reactions ultimately led to high-yielding, selective outcomes.

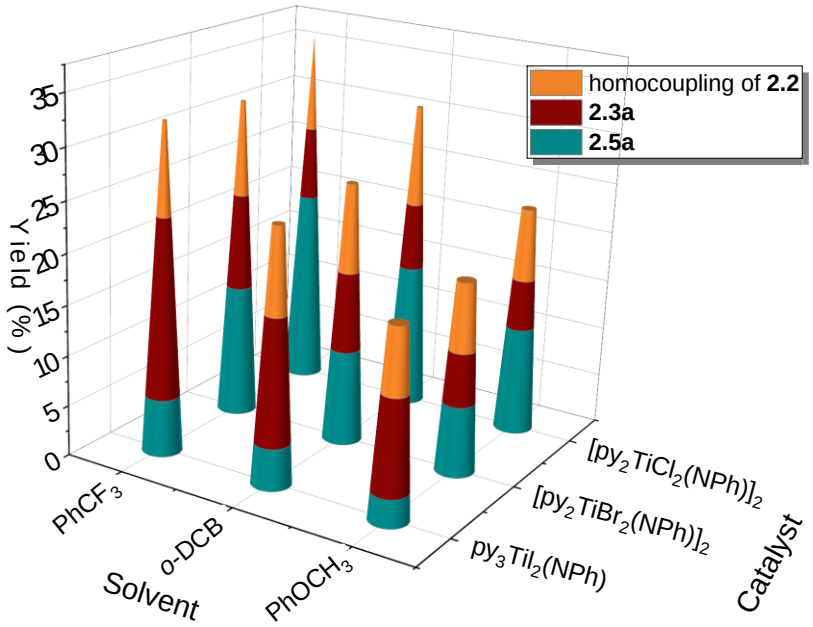

Figure 2.16. Scope of catalyst and solvent.

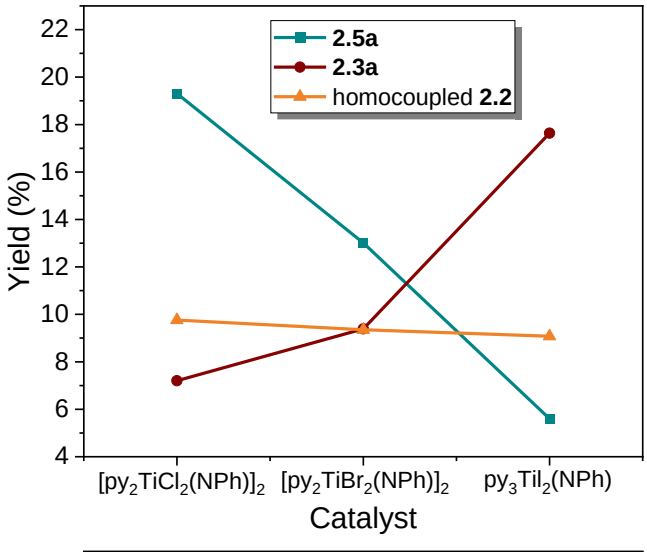

Figure 2.17. Yield distribution in $PhCF_3$.

Optimization of Catalysis with 2.1a-BBN as Heterocoupling Partner

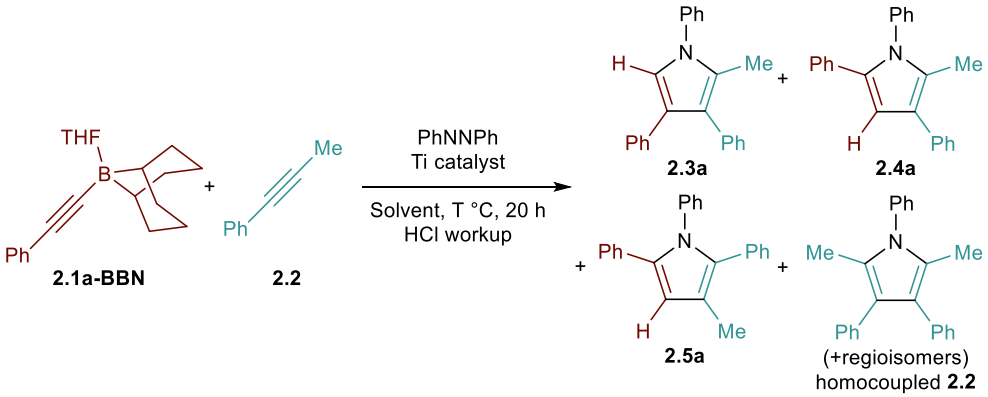

[$py_2TiCl_2(NPh)]_2$, azobenzene, *B*-phenylethynyl-9-borabicyclo[3,3,1]nonane (**2.1a-BBN**, 29.4 mg, 0.1 mmol, 1 equiv), 1-phenyl-1-propyne (11.6 mg, 0.1 mmol, 1 equiv), triphenylmethane (4.9 mg, 0.02 mmol, 0.2 equiv, internal standard) and 0.5 mL solvent were added to an NMR tube. The total nitrene equivalent was kept as 1 by adjusting the molar quantity of azobenzene according to the Ti catalyst loading, following the relationship of:

$$Equiv_{nitrene} = Equiv_{[py_2TiCl_2(NPh)]_2} + Equiv_{azobenzene} \times 2$$

The reaction was then sealed and heated in a preheated oil bath for 20 h. The reaction was quenched with 5% HCl in methanol and extracted with EtOAc/H_2O. The organic phase was dried over $MgSO_4$ and evaporated under vacuum. The crude product mixture was characterized by GC-Polyarc®/FID to determine the yield and selectivity.

Table 2.6. Optimization of the catalysis using **2.1a-BBN** as heterocoupling partner.

Entry	%[Ti]	Solvent	T (°C)	**2.3a** (%)	**2.4a** (%)	**2.5a** (%)	homocoupled **2.2** (%)	Selectivity[a]
1	5	$PhCF_3$	115	**6.6**	0.3	< 0.1	0.2	22.3:1 (12.5:1)
2	5	C_6D_5Br	115	**21.8**	0.5	0.1	2.9	36.2:1 (6.2:1)
3	10	C_6D_5Br	115	**74.3**	1.2	0.1	3.0	55.8:1 (17.1:1)
4	15	C_6D_5Br	115	**64.9**	1.2	0.1	3.6	50.7:1 (13.2:1)
5	10	$PhCH_3$	115	**66.6**	2.0	0.1	1.3	31.5:1 (19.6:1)
6	10	$PhCF_3$	115	**54.6**	1.2	0.1	2.2	41.8:1 (15.7:1)
7	10	$PhOCH_3$	115	**20.0**	0.4	0.1	1.6	41.2:1 (9.6:1)
8	10[b]	C_6D_5Br	115	**3.3**	0.3	0.2	0.2	7.4:1 (4.9:1)
9	20[c]	C_6D_5Br	115	**3.2**	0.1	0.1	0.2	20.1:1 (9.2:1)
10	10	C_6D_5Br	90	**45.2**	0.9	0.1	3.1	48.5:1 (11.3:1)
11	10	C_6D_5Br	145	**60.5**	1.4	0.2	1.9	38.7:1 (17.6:1)
12[d]	10	C_6D_5Br	115	**65.9**	1.4	< 0.1	1.5	45.5:1 (22.7:1)

[a]Selectivity with respect to all heterocoupling pyrrole regioisomer products. Selectivity = **2.3a**/(**2.4a**+**2.5a**). In parenthesis: selectivity with respect to all possible pyrrole products. Selectivity in parenthesis = **2.3a**/(**2.4a**+**2.5a**+homocoupled **2.2**). [b]Ti catalyst = $[py_2TiBr_2(NPh)]_2$. [c]Ti catalyst = $py_3TiI_2(NPh)$. [d]Time = 0.5 h.

Catalysis with 2.1a-$SnMe_3$ as Heterocoupling Partner

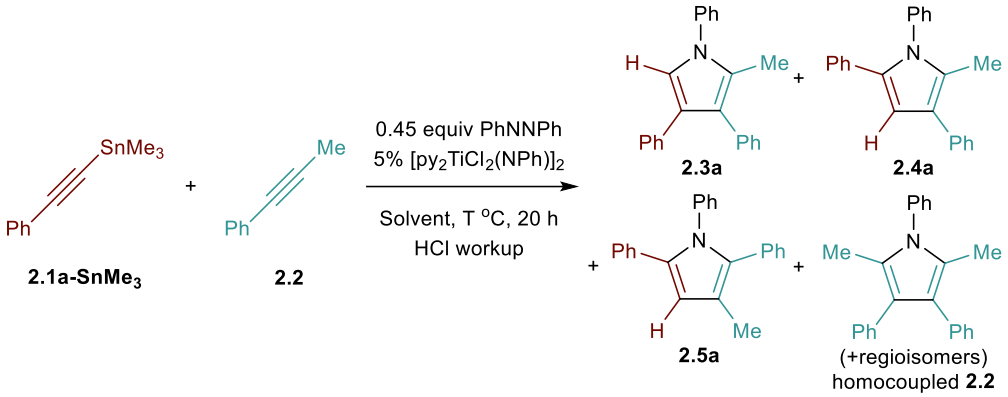

[$py_2TiCl_2(NPh)]_2$ (3.7 mg, 0.005 mmol, 0.05 equiv), azobenzene (8.2 mg, 0.045 mmol, 0.45 equiv), phenylethynyl trimethylstannane (**2.1a-SnMe$_3$**, 26.5 mg, 0.1 mmol, 1 equiv), 1-phenyl-1-propyne (11.6 mg, 0.1 mmol, 1 equiv), triphenylmethane (4.9 mg, 0.02 mmol, 0.2 equiv, internal standard) and 0.5 mL solvent were added to an NMR tube. The reaction was then sealed and heated in a preheated oil bath for 20 h. The reaction was quenched with 10% HCl in methanol and extracted with EtOAc/H_2O. The organic phase was dried over $MgSO_4$ and evaporated under vacuum. The crude product mixture was characterized by GC-Polyarc®/FID to determine the yield and selectivity.

Precaution: Trialkyltin species are highly toxic. Proper PPE is required. All the chemical and labware waste should be handled separately from the normal waste stream and quenched thoroughly.

Table 2.7. Optimization of the catalysis using **2.1a-SnMe$_3$** as heterocoupling partner.

Entry	Solvent	T (°C)	Conc. (M)	**2.3a** (%)	**2.4a** (%)	**2.5a** (%)	homocoupled **2.2** (%)	Selectivity[a]
1	$PhCF_3$	115	0.2	**50.6**	1.2	6.6	3.3	6.4:1 (4.5:1)
2	C_6D_5Br	115	0.2	**47.5**	1.1	3.3	4.4	10.7:1 (5.4:1)
3	C_6D_5Br	60	0.2	**30.4**	0.7	2.0	0.9	11.1:1 (8.4:1)
4	$PhCH_3$	115	0.2	**51.1**	1.2	6.0	2.7	7.1:1 (5.1:1)
5[b]	$PhCH_3$	115	0.2	**46.2**	0.9	4.6	4.2	8.3:1 (4.7:1)
6	$PhCH_3$	90	0.2	**57.7**	1.3	4.9	2.6	9.3:1 (6.6:1)
7	$PhCH_3$	75	0.2	**41.4**	1.1	3.3	3.6	9.3:1 (5.2:1)
8	$PhCH_3$[c]	90	0.2	**28.1**	0.9	3.8	0.5	6.0:1 (5.4:1)
9	$PhCH_3$	90	0.07	**18.8**	0.5	1.8	0.4	8.3:1 (7.2:1)
10	$PhCH_3$	90	0.8	**66.0**	1.8	4.6	2.9	10.3:1 (7.1:1)

11	$PhCH_3$	90	2.0	**64.5**	2.0	3.9	2.8	10.9:1 (7.4:1)
12[d]	$PhCH_3$	90	0.8	**68.5**	2.1	4.5	1.5	10.4:1 (8.4:1)

[a]Selectivity with respect to all heterocoupling pyrrole regioisomer products. Selectivity = **2.3a**/(**2.4a**+**2.5a**). In parenthesis: selectivity with respect to all possible pyrrole products. Selectivity in parenthesis = **2.3a**/(**2.4a**+**2.5a**+homocoupled **2.2**). [b]10% $[py_2TiCl_2(NPh)]_2$. [c]2 equiv **2.1a-SnMe$_3$**. [d]Time = 9 h.

2.5.4 Catalyst Synthesis

Synthesis of $[TiCl_2(NPh)]_n$

$$TiCl_4 + PhN(SiMe_3)_2 \xrightarrow[50\ °C,\ overnight]{CH_2Cl_2} 1/n\ [TiCl_2(NPh)]_n + 2\ Me_3SiCl$$

The synthesis of $[TiCl_2(NPh)]_n$ was modified from the synthetic procedure of $py_3TiBr_2(NTol)$.[127] $TiCl_4$ (2.000 g, 10.5 mmol), *N*-phenyl-*N*,*N*-bis(trimethylsilyl)amine (2.500 g, 10.5 mmol), 20 mL of CH_2Cl_2 and a stirbar were added to a 20 mL scintillation vial in the glovebox. The reaction was then sealed with a PTFE-lined Teflon screw cap and heated at 50 ℃ overnight while stirring. After cooling down, the suspension was filtered through a fine frit and washed with CH_2Cl_2 until the fresh filtrate changed from yellow to colorless. The precipitate was further washed by 20 mL of pentane twice to remove the remaining CH_2Cl_2. After drying under vacuum for 3 h, $[TiCl_2(NPh)]_n$ was obtained as black powder. Yield: 1.003 g (4.78 mmol, 45%). Attempts in characterizing the compound by ^{1}H NMR failed due to its low solubility in common organic solvents. Further addition of THF to the compound yielded $[(THF)_2TiCl_2(NPh)]_2$ in 95% yield.[132]

2.5.5 Substrate Syntheses

Synthesis of 2-phenylethynyl-4,4,5,5-tetramethyl-1,3,2-dioxaborolane (2.1a-Bpin)

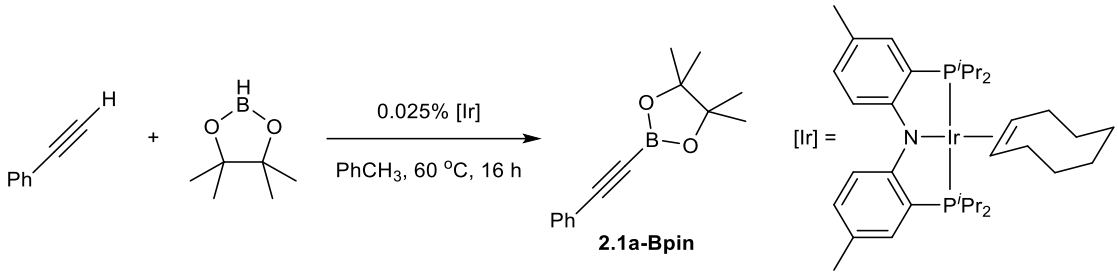

The synthesis was performed following a reported procedure using phenylacetylene (4.086 g, 40 mmol, limiting reagent) as the terminal alkyne reactant.[133,134] **2.1a-Bpin** was obtained as white needled-shaped crystals in 76% yield (6.900 g). Spectra data was consistent with literature values.[135]

^{1}H NMR ($CDCl_3$, 400 MHz): δ 7.54-7.51 (m, 2H), 7.38-7.28 (m, 3H), 1.32 (s, 12H) ppm.

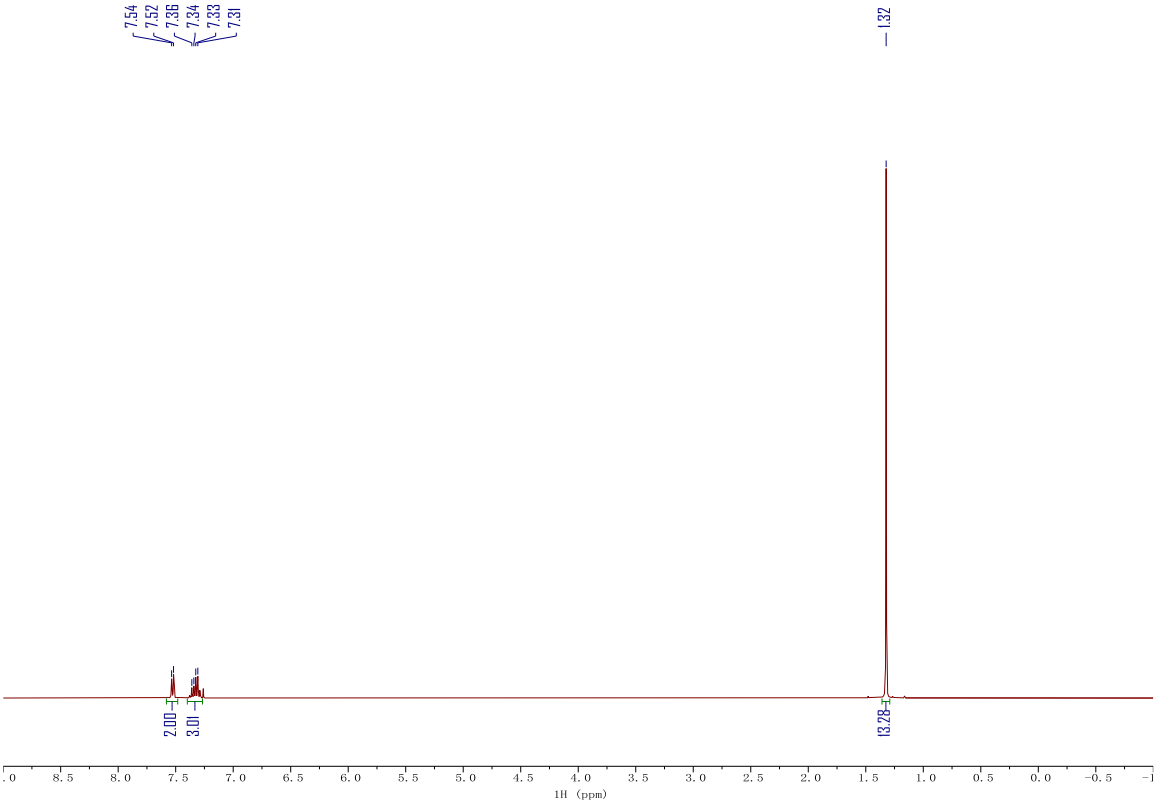

Figure 2.18. ^{1}H NMR spectrum of **2.1a-Bpin** in $CDCl_3$. *Taken from YC-2019-0049-R1-1H.*

General Synthetic Procedure for *B*-Arylethynyl-9-Borabicyclo[3,3,1]nonanes (2.1b-d-BBN)

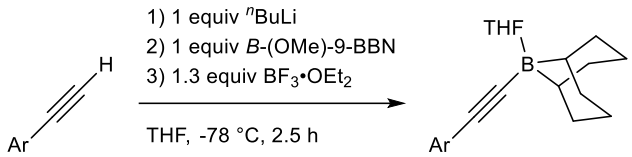

2.1b-d-BBN

The synthesis was performed following a modification of the reported procedure.[123] Terminal aryl alkyne (10 mmol), dry THF (15 mL) and a stir bar were added to a N_2-filled 50 mL Schlenk flask and cooled at -78 ℃. *n*-BuLi solution in hexanes (2.5 M, 4.0 mL, 10 mmol, 1.0 equiv) was slowly added to the mixture and stirred for 15 min at -78 ℃. *B*-methoxy-9-BBN solution in hexanes (1.0 M, 10 mL, 10 mmol, 1.0 equiv) was added and the mixture was stirred for 1.5 h at -78 ℃. $BF_3{\cdot}OEt_2$ (1.6 mL, 13 mmol, 1.3 equiv) was added, after which the reaction was further stirred at -78 ℃ for 0.5 h before warming up to room temperature. All volatiles were removed under vacuum, and the mixture was dissolved in dry benzene (15 mL). The suspension was then filtered via cannula filtration into another N_2-filled 50 mL Schlenk flask. The resulting solution was concentrated under vacuum, yielding the white-pale yellow crude product. The Schlenk flask was then transferred into the glovebox, and the crude product was washed sequentially with pentane (3 x 10 mL). Redissolving the white solid in 30 mL of benzene separated the product from remaining $LiBF_4$ after filtration through a medium frit. The filtrate was concentrated to yield the *B*-arylethynyl-9-BBN after drying.

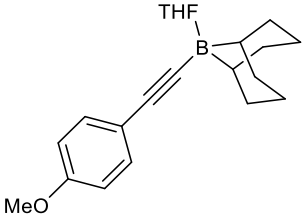

***B*-(*p*-methoxyphenyl)ethynyl-9-borabicyclo[3,3,1]nonane (2.1b-BBN)** off-white powder, 43% yield.

^{1}H NMR (C_6D_6, 400 MHz): δ 7.49 (d, *J* = 8.3 Hz, 2H), 6.65 (d, *J* = 8.3 Hz, 2H), 3.75-3.72 (br, 4H), 3.20 (s, 3H), 2.25-2.02 (m, 10H), 1.83-1.69 (m, 2H), 1.40 (s, 3H), 1.29-1.17 (br, 4H) ppm.

^{13}C{^{1}H} NMR (C_6D_6, 101 MHz): δ 159.48, 133.57, 118.48, 114.20, 104.44, 102.05 (br), 70.21, 54.75, 32.49, 26.96 (br), 25.08, 24.74 ppm.

^{11}B NMR (C_6D_6, 128 MHz): δ 22.8 ppm.

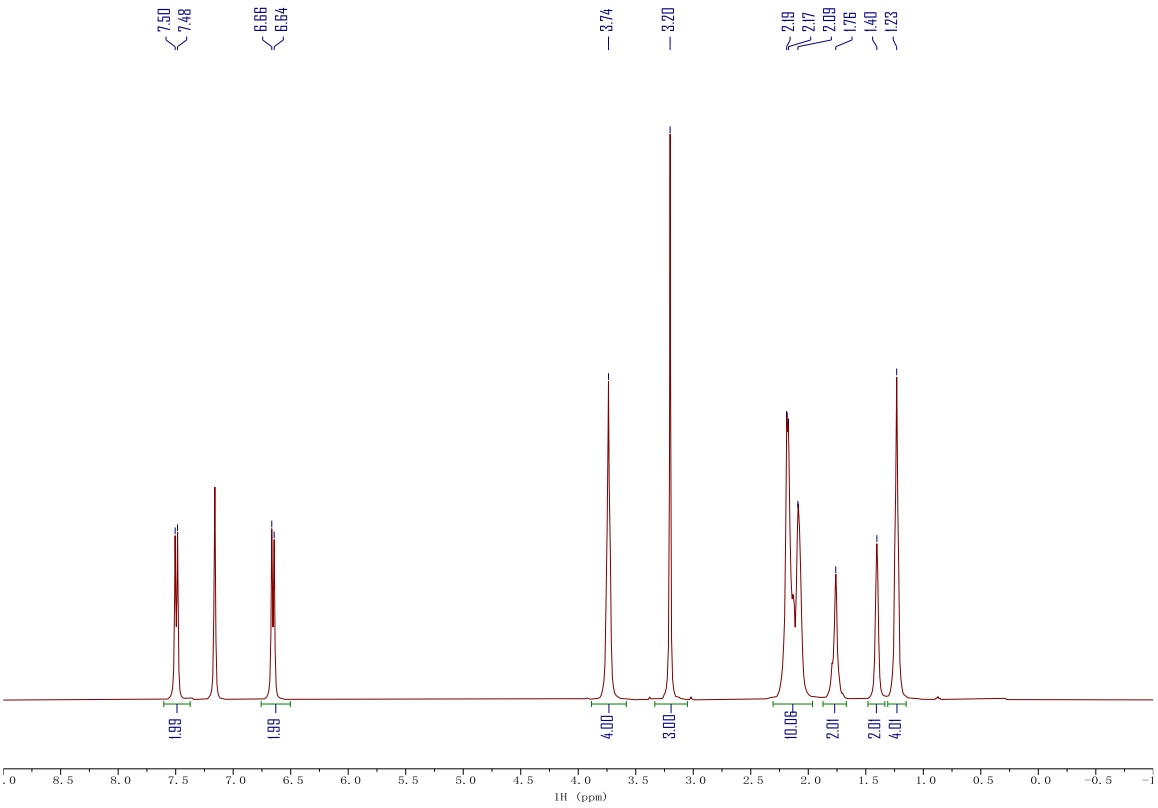

Figure 2.19. ^{1}H NMR spectrum of **2.1b-BBN** in C_6D_6. *Taken from YC-2019-0165-1.*

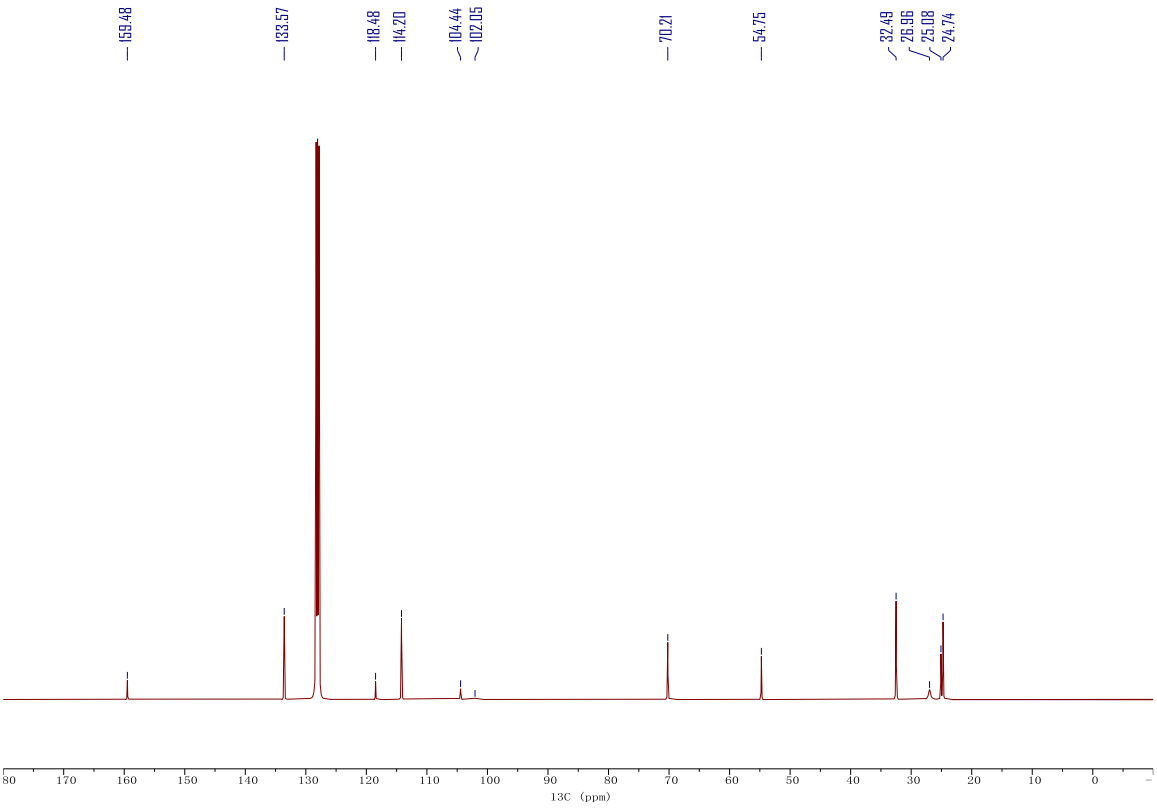

Figure 2.20. $^{13}C\{^{1}H\}$ spectrum of **2.1b-BBN** in C_6D_6. *Taken from YC-2019-0165-1C.*

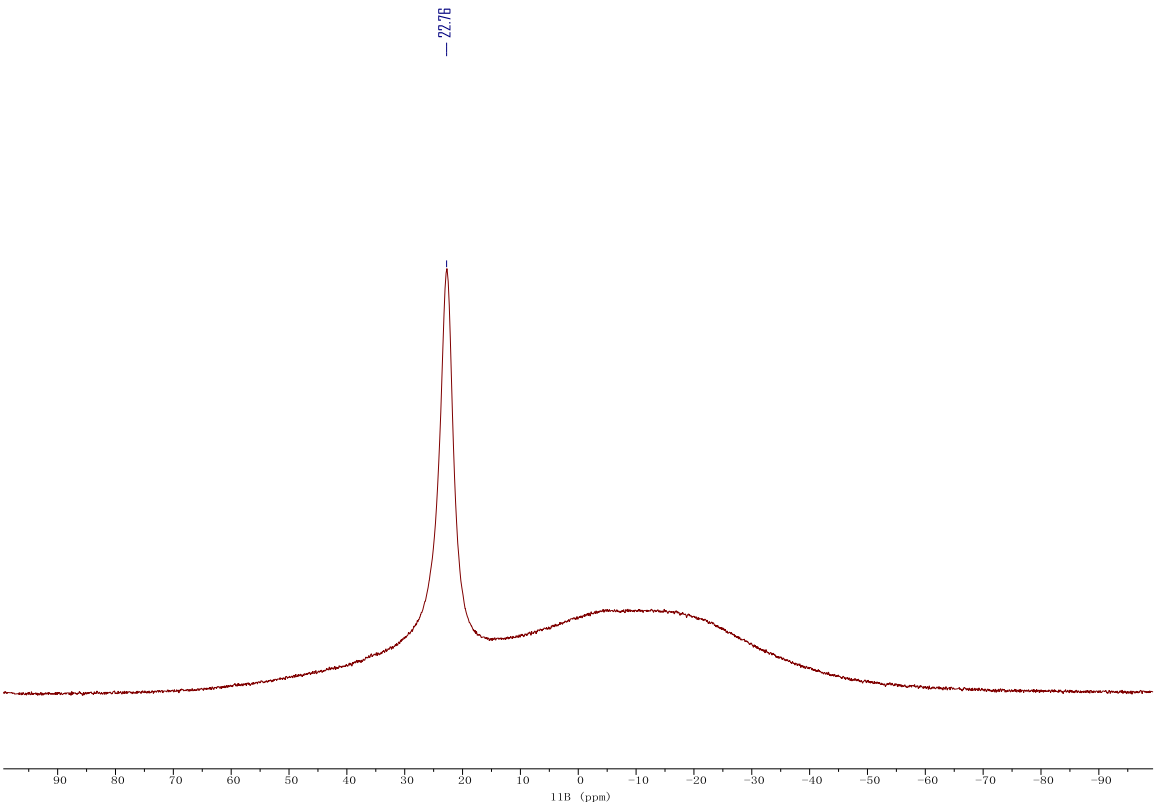

Figure 2.21. ^{11}B NMR spectrum of **2.1b-BBN** in C_6D_6. *Taken from YC-2019-0165-1B.*

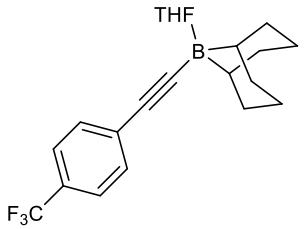

***B*-(*p*-(trifluoromethyl)phenyl)ethynyl-9-borabicyclo[3,3,1]nonane (2.1c-BBN)** The crude product was further recrystallized from the saturated pentane solution at 0 ℃ overnight. Product was obtained as white crystalline solid after filtration and drying in 40% yield.

^{1}H NMR (C_6D_6, 500 MHz): δ 7.30 (d, *J* = 8.1 Hz, 2H), 7.22 (d, *J* = 8.2 Hz, 2H), 3.69-3.64 (m, 4H), 2.24-2.04 (m, 10H), 1.82-1.74 (m, 2H), 1.30 (s, 3H), 1.21-1.15 (m, 4H) ppm.

^{13}C{^{1}H} NMR (C_6D_6, 101 MHz): δ 131.98, 130.07 (q, *J* = 1.5 Hz), 128.75 (q, *J* = 32.4 Hz), 125.35 (q, *J* = 3.7 Hz), 124.94 (q, *J* = 271.9 Hz), 100.92, 70.72, 32.14, 25.93 (br), 25.11, 24.56 ppm.

^{11}B NMR (C_6D_6, 161 MHz): δ 19.4 ppm.

^{19}F{^{1}H} NMR (C_6D_6, 471 MHz): δ -62.31 ppm.

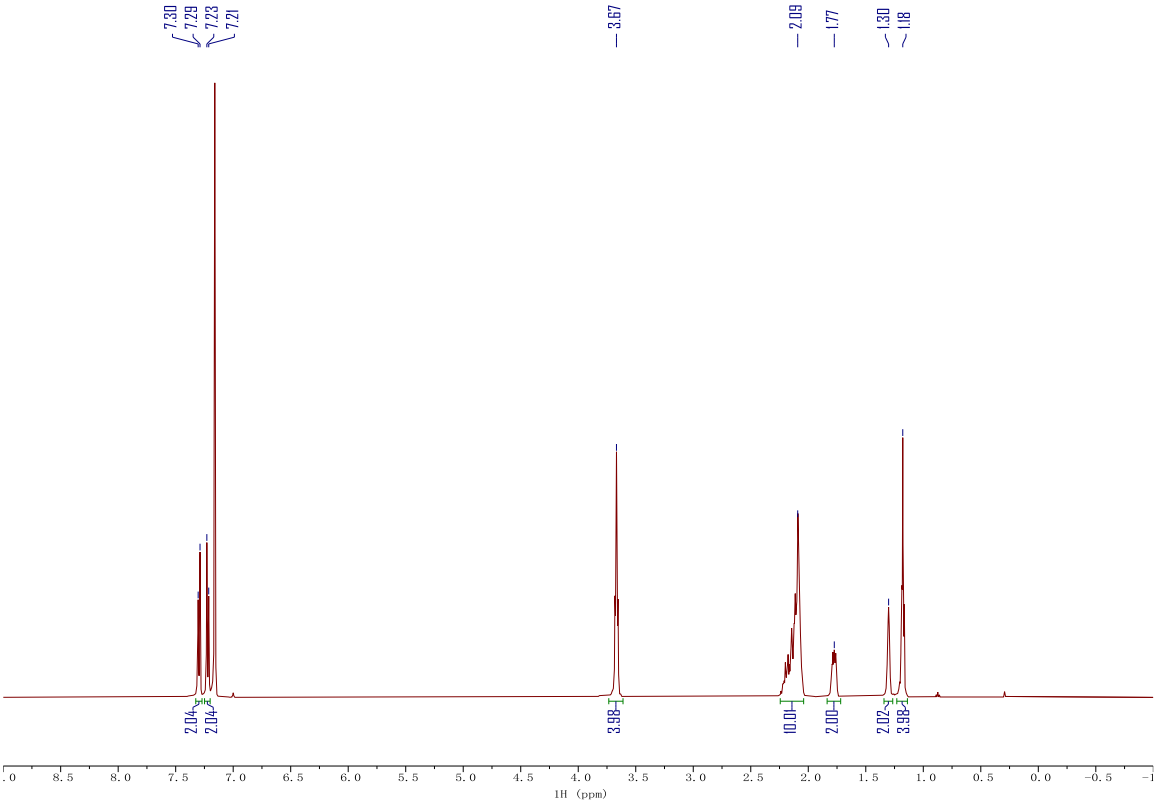

Figure 2.22. ^{1}H NMR spectrum of **2.1c-BBN** in C_6D_6. *Taken from CKK-2019-0009-5H.*

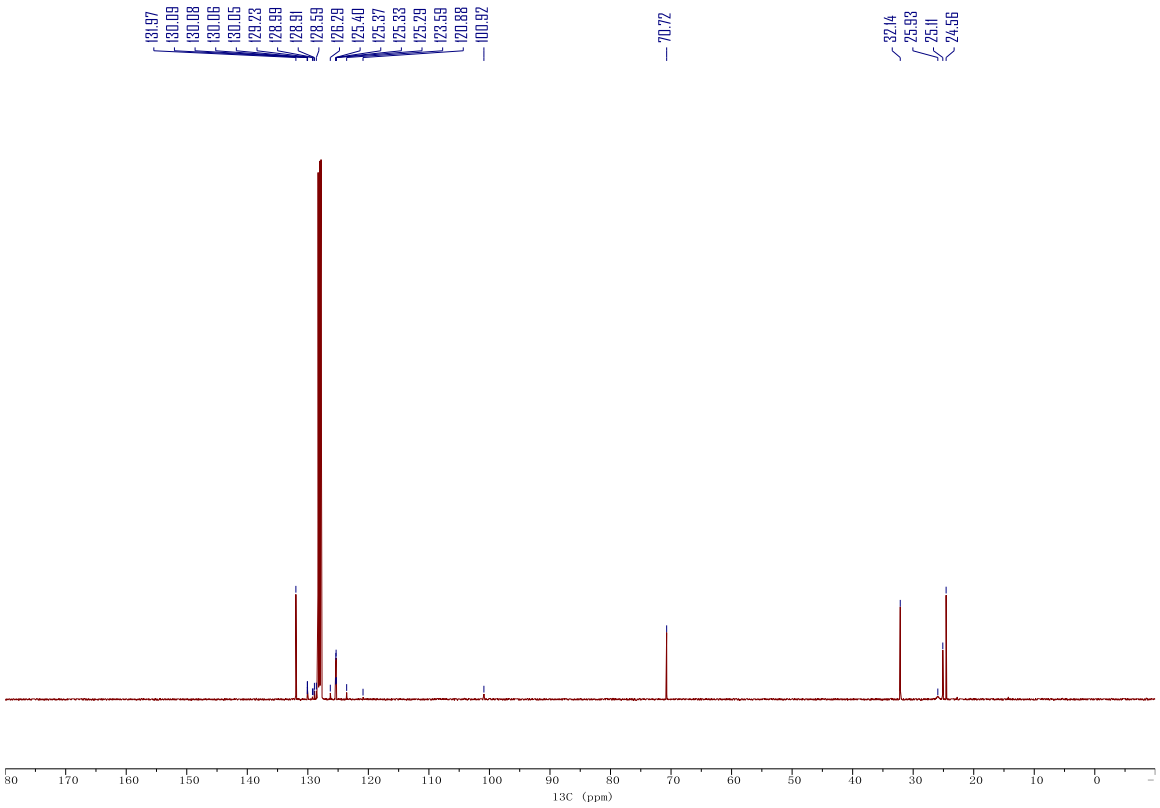

Figure 2.23. $^{13}C\{^{1}H\}$ NMR spectrum of **2.1c-BBN** in C_6D_6. *Taken from CKK-2019-0009-8C.*

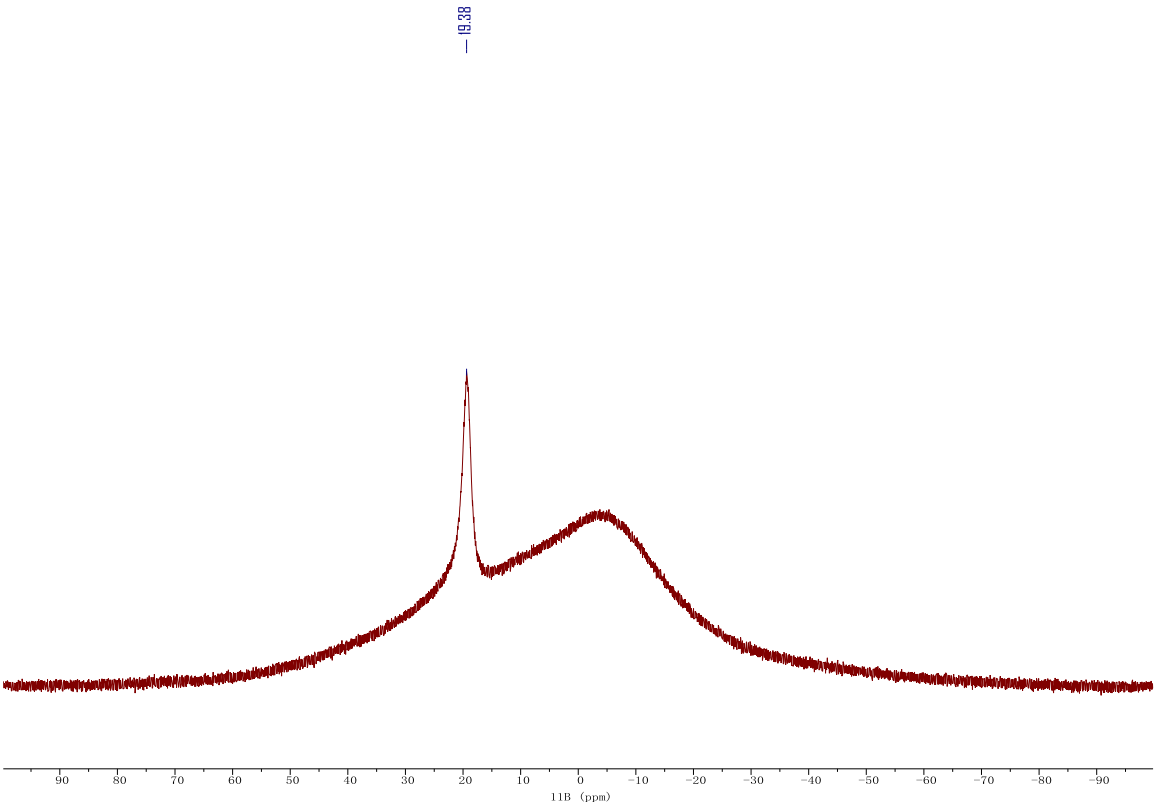

Figure 2.24. ^{11}B NMR spectrum of **2.1c-BBN** in C_6D_6. *Taken from CKK-2019-0009-5B.*

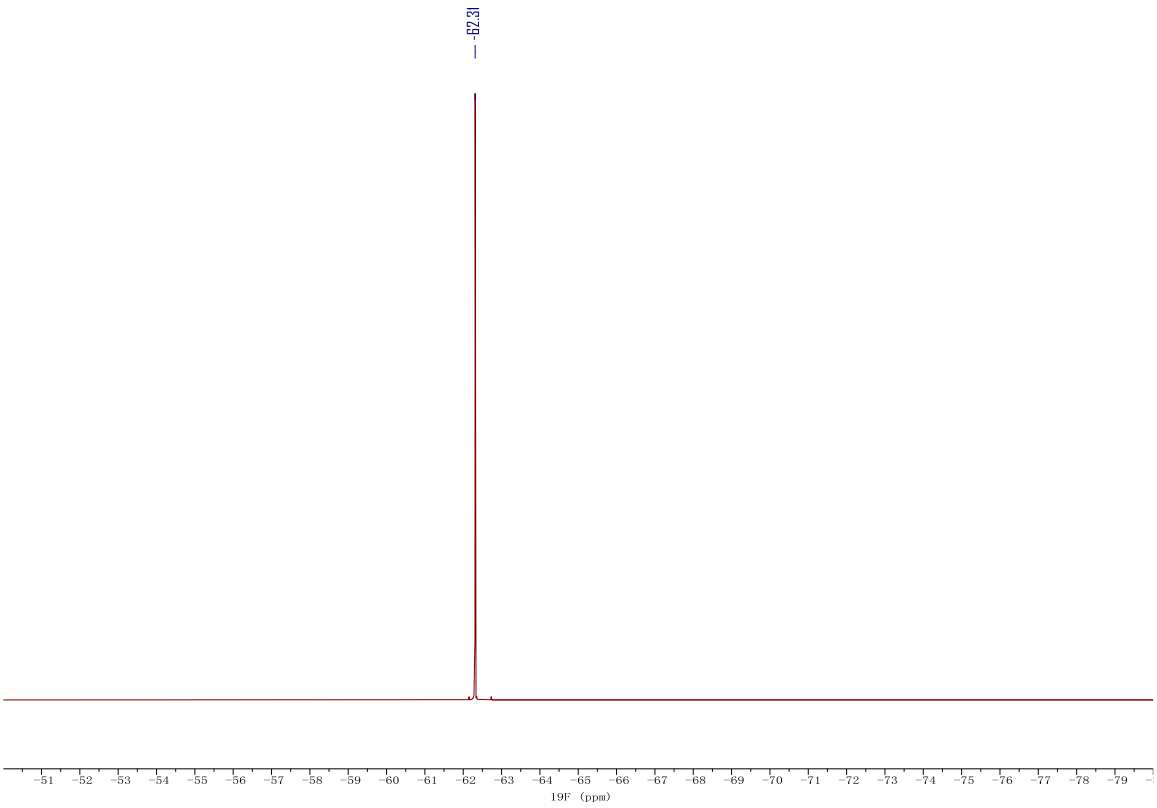

Figure 2.25. $^{19}F\{^{1}H\}$ NMR spectrum of **2.1c-BBN** in C_6D_6. *Taken from CKK-2019-0009-5F.*

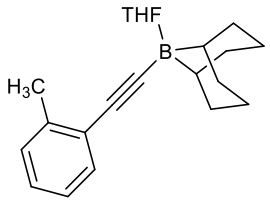

***B*-(*o*-tolyl)ethynyl-9-borabicyclo[3,3,1]nonane (2.1d-BBN)** isolated as alkynylborane:THF = 1/1.25 adduct, white powder, 46% yield.

^{1}H NMR (C_6D_6, 500 MHz): δ 7.54 (dd, *J* = 7.2, 1.8 Hz, 1H), 7.04-6.91 (m, 3H), 3.70-3.62 (m, 5H), 2.49 (s, 3H), 2.21-2.00 (m, 10H), 1.77-1.67 (m, 2H), 1.43 (s, 2H), 1.30-1.18 (m, 5H) ppm.

$^{13}C\{^{1}H\}$ NMR (C_6D_6, 101 MHz): δ 139.74, 131.92, 129.31, 125.44, 69.24, 32.22, 24.62, 24.58, 20.89 ppm.

^{11}B NMR (C_6D_6, 161 MHz): δ 26.7 ppm.

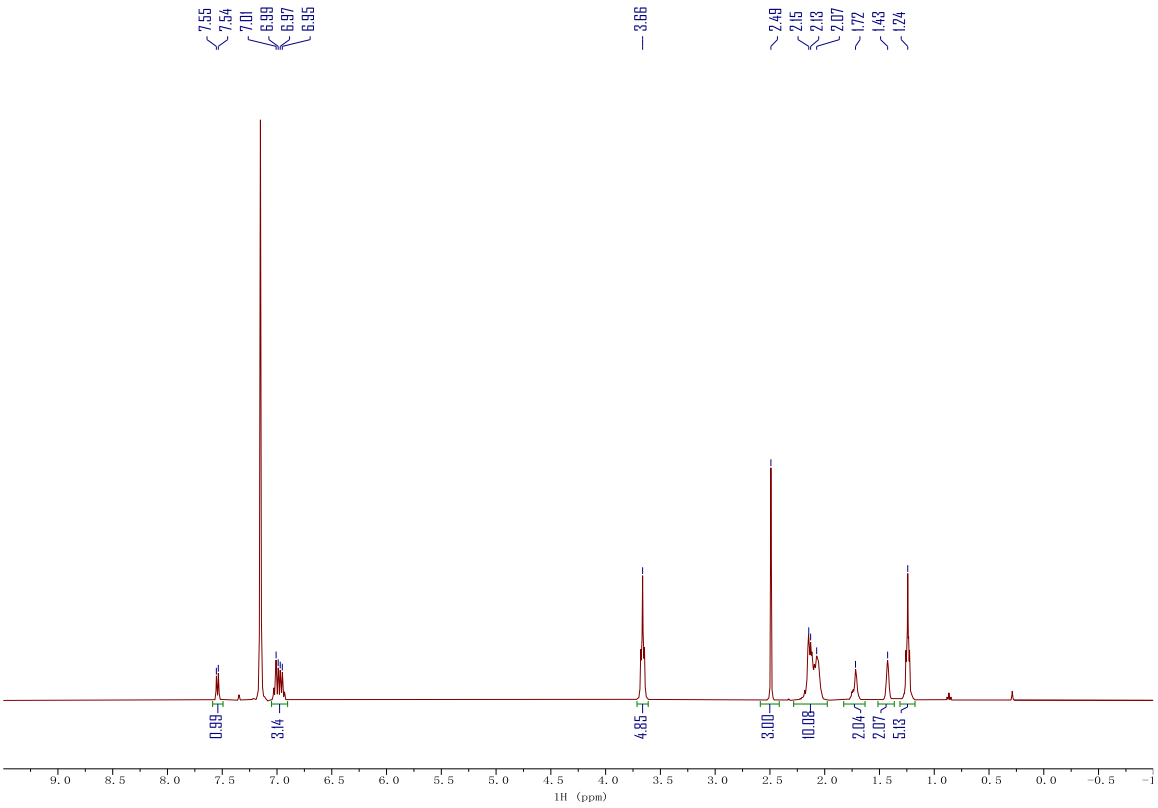

Figure 2.26. ^{1}H NMR spectrum of **2.1d-BBN** in C_6D_6. *Taken from CKK-2019-0007-2H.*

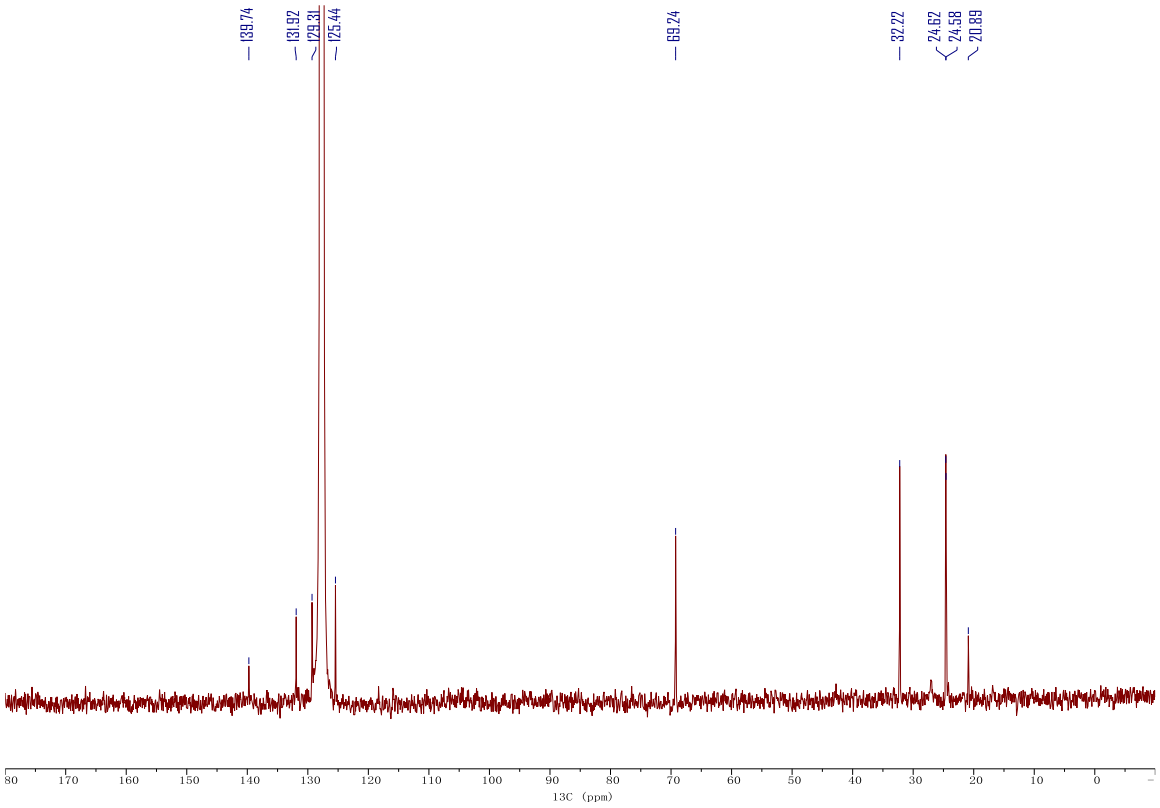

Figure 2.27. $^{13}C\{^{1}H\}$ NMR spectrum of **2.1d-BBN** in C_6D_6. *Taken from CKK-2019-0007-2C.*

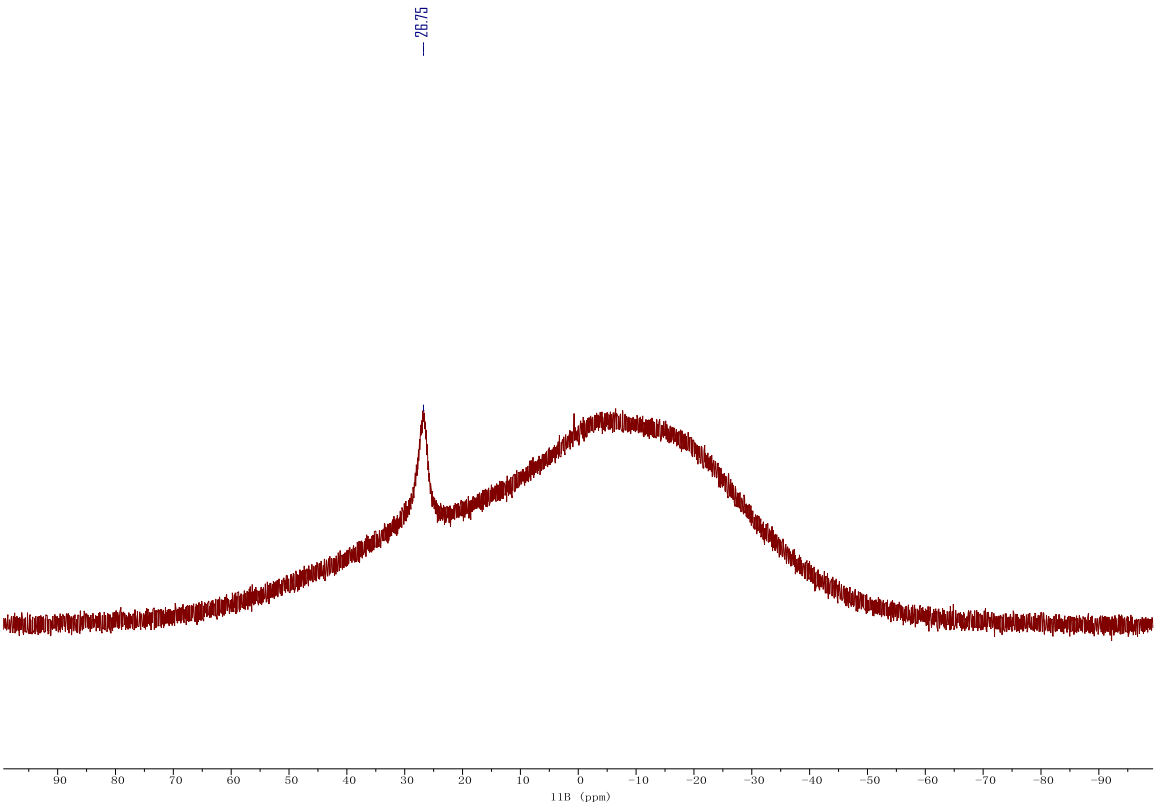

Figure 2.28. ^{11}B NMR spectrum of **2.1d-BBN** in C_6D_6. *Taken from CKK-2019-0007-2B.*

Synthesis of Pyridine-Adduct of *B*-phenylethynyl-9-BBN (2.1a-BBN-py)

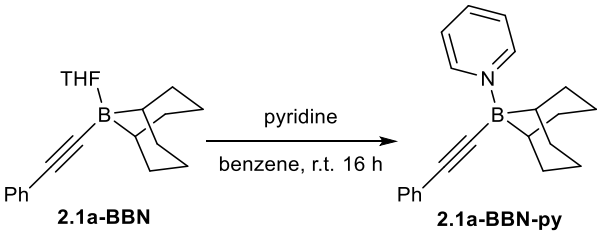

The synthesis of **2.1a-BBN-py** was adopted from the reported procedure for the synthesis of pyridine-adduct of *B*-(1-propynyl)-9-BBN, using **2.1a-BBN** instead as the *B*-alkynyl-9-BBN reactant and benzene as solvent. **2.1a-BBN-py** was obtained in quantitative yield.

^{1}H NMR (C_6D_6, MHz): δ 8.29 (d, *J* = 5.0 Hz, 2H), 7.53 (d, *J* = 6.9 Hz, 2H), 6.97 (t, *J* = 7.3 Hz, 2H), 6.90 (t, , *J* = 7.3 Hz, 1H), 6.58 (t, *J* = 7.6 Hz, 1H), 6.28 (t, *J* = 7.1 Hz, 2H), 3.20-3.06 (br, 2H), 2.44-2.11 (m, 5H), 2.09-1.97 (m, 2H), 1.64 (s, 2H), 1.55-1.41 (m, 3H) ppm.

$^{13}C\{^{1}H\}$ NMR (C_6D_6, MHz): δ 145.59, 138.94, 131.81, 128.59, 126.37, 125.10, 34.07, 29.89, 25.61, 25.02 ppm.

^{11}B NMR (C_6D_6, MHz): δ -3.2 ppm.

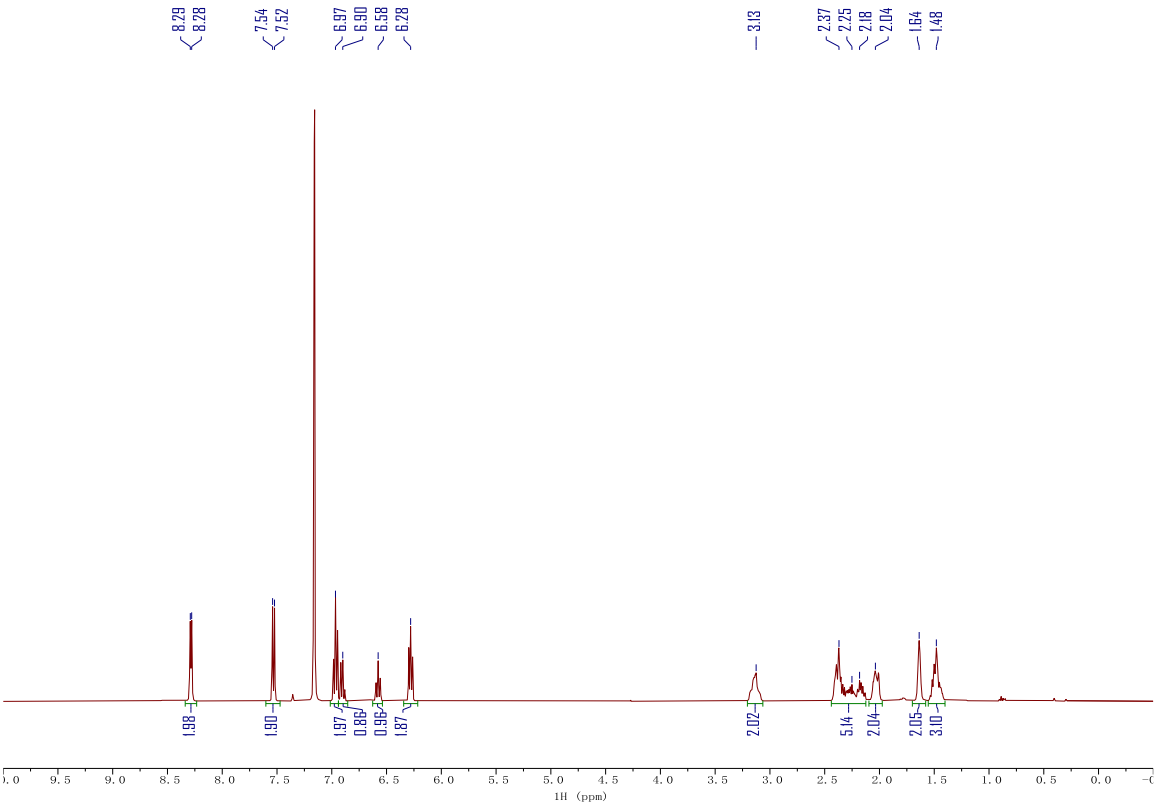

Figure 2.29. ^{1}H NMR spectrum of **2.1a-BBN-py** in C_6D_6. *Taken from YC-2020-ReagentPurity-PhCCBBN(py)-0224-3H.*

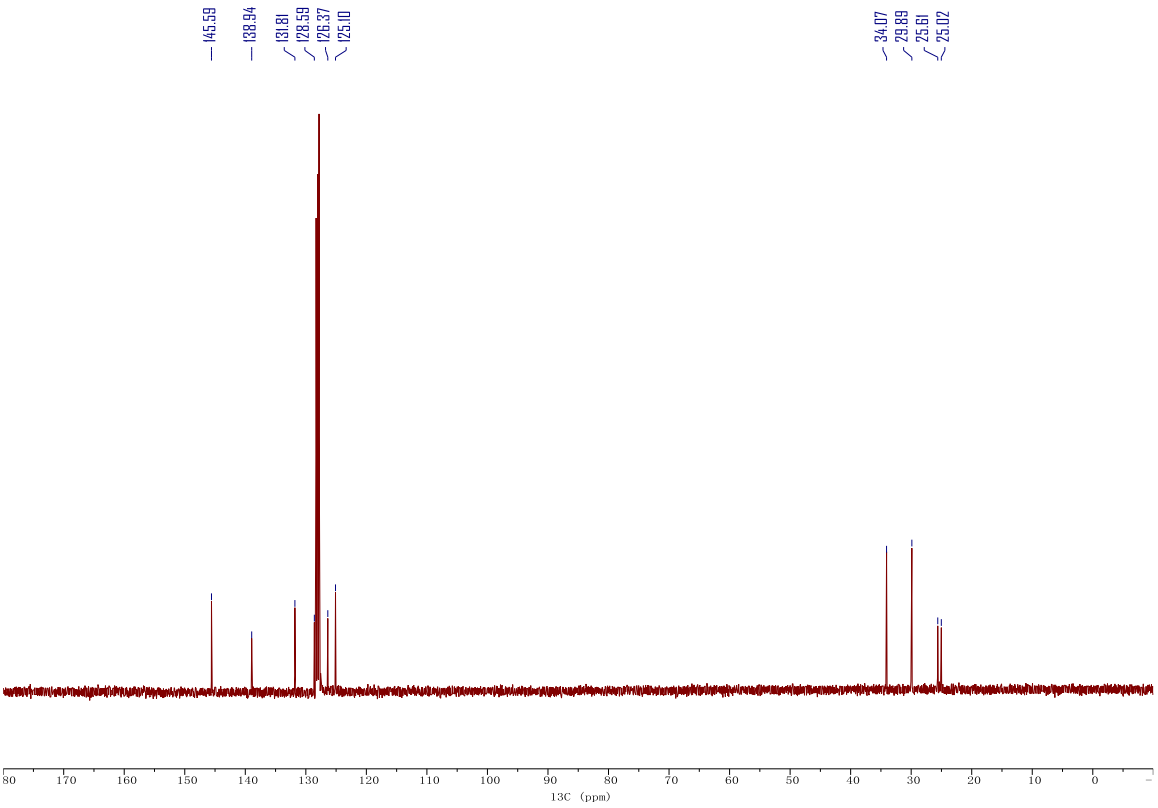

Figure 2.30. $^{13}C\{^{1}H\}$ NMR spectrum of **2.1a-BBN-py** in C_6D_6. *Taken from YC-2020-ReagentPurity-PhCCBBN(py)-0224-3C.*

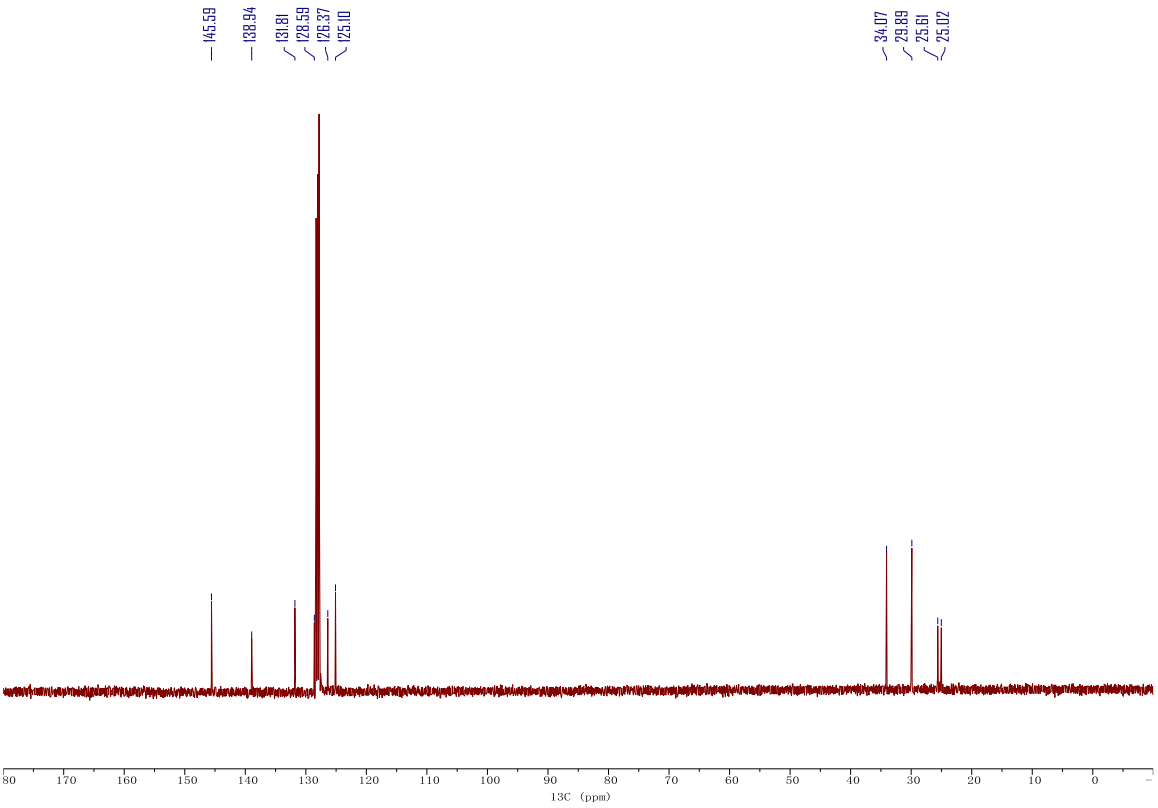

Figure 2.31. ^{11}B NMR spectrum of **2.1a-BBN-py** in C_6D_6. *Taken from YC-2020-ReagentPurity-PhCCBBN(py)-0224-B.*

General Synthetic Procedure for Arylethynyl Trimethylstannanes (2.1b-d-SnMe$_3$)

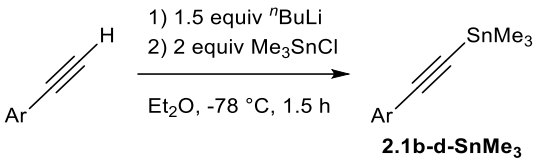

2.1b-d-SnMe$_3$

The synthesis was performed following a modification of the reported procedure.[136] Terminal aryl alkyne (2.5 mmol), dry diethyl ether (5 mL) and a stir bar were added to a N_2-filled 50 mL Schlenk flask and cooled at -78 ℃. n-BuLi solution in hexanes (2.5 M, 1.5 mL, 3.8 mmol, 1.5 equiv) was slowly added to the mixture and stirred for 15 min at -78 ℃. Trimethyltin chloride solution in hexanes (1.0 M, 5 mL, 5 mmol, 2.0 equiv) was added via syringe. The resulting white suspension was stirred for an hour at room temperature. All volatiles were carefully removed under vacuum. Pentane (5 mL) was added to the white mixture, and the

resulting suspension was washed by 3 x 10 mL of water. After drying over $MgSO_4$ and evaporation under vacuum, arylethynyl trimethylstannane was obtained as yellow or colorless oil.

Precaution: Trialkyltin species are highly toxic. Proper PPE is required. A secondary cold trap is recommended for evacuation of the crude reaction mixture. All the chemical and labware waste should be handled separately from the normal waste stream and quenched thoroughly.

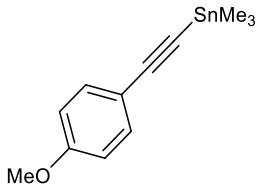

(p-methoxyphenyl)ethynyl trimethylstannane (2.1b-$SnMe_3$) 55% yield.

^{1}H NMR ($CDCl_3$, 500 MHz): δ 7.40 (d, 8.7 Hz, 2H), 6.81 (d, 8.7 Hz, 2H), 3.80 (s, 3H), 0.34 (s, 9H) ppm.

$^{13}C\{^1H\}$ NMR ($CDCl_3$, 101 MHz): δ 159.58, 133.54, 115.95, 113.92, 109.11, 91.54, 55.40, -7.50 ppm.

$^{119}Sn\{^1H\}$ NMR ($CDCl_3$, 187 MHz): δ -66.21 ppm.

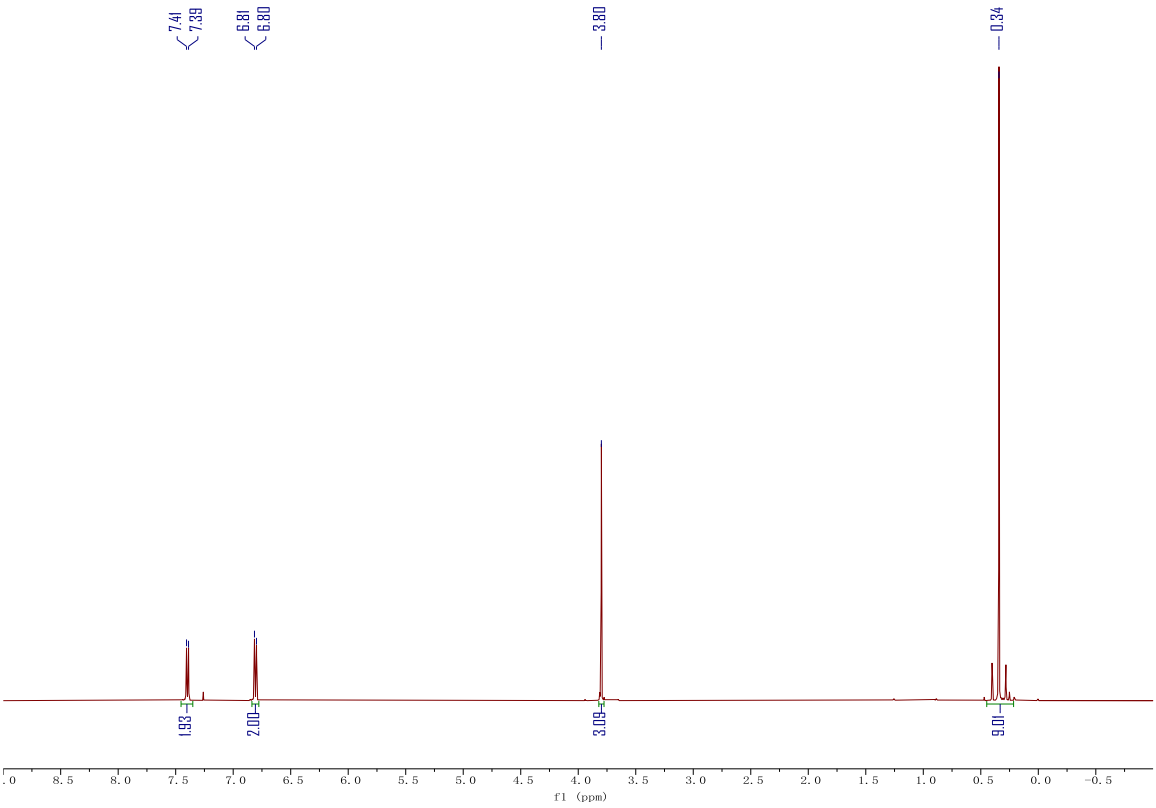

Figure 2.32. ^{1}H NMR spectrum of **2.1b-SnMe$_3$** in $CDCl_3$. *Taken from YC-2019-0185-4-H.*

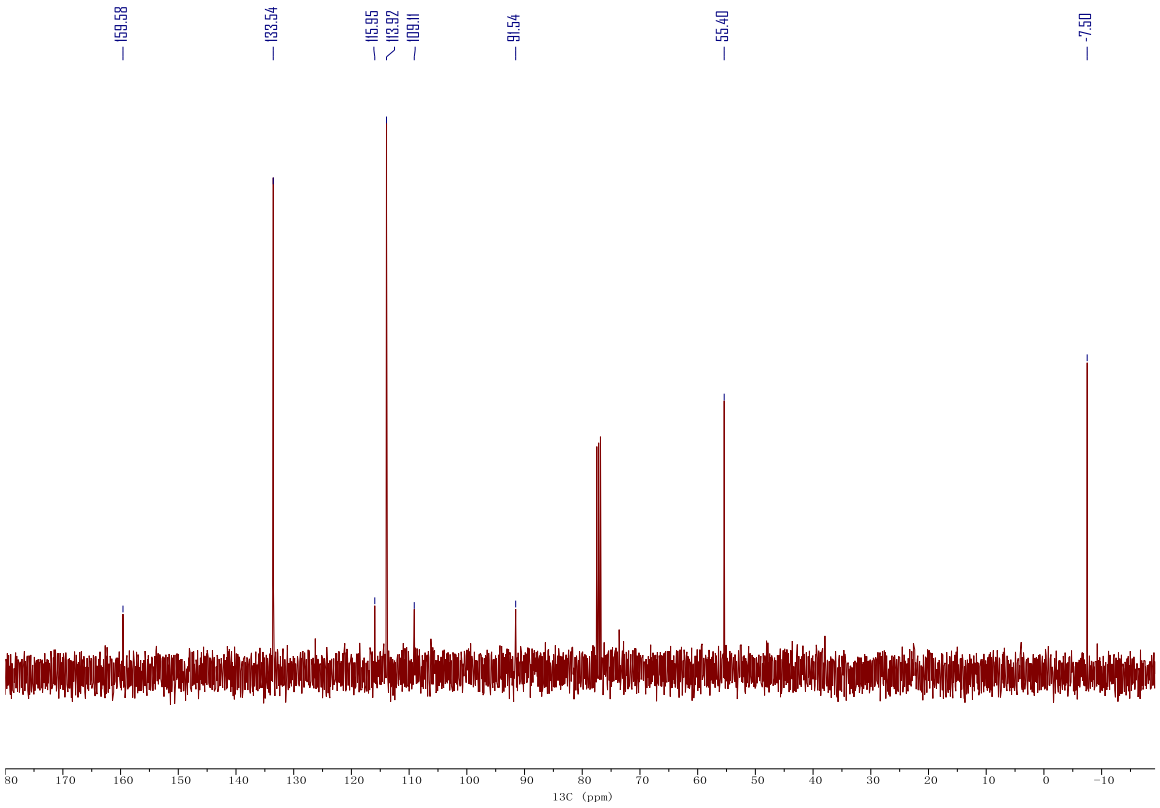

Figure 2.33. $^{13}C\{^{1}H\}$ NMR spectrum of **2.1b-SnMe$_3$** in $CDCl_3$. *Taken from YC-2019-0185-4-C.*

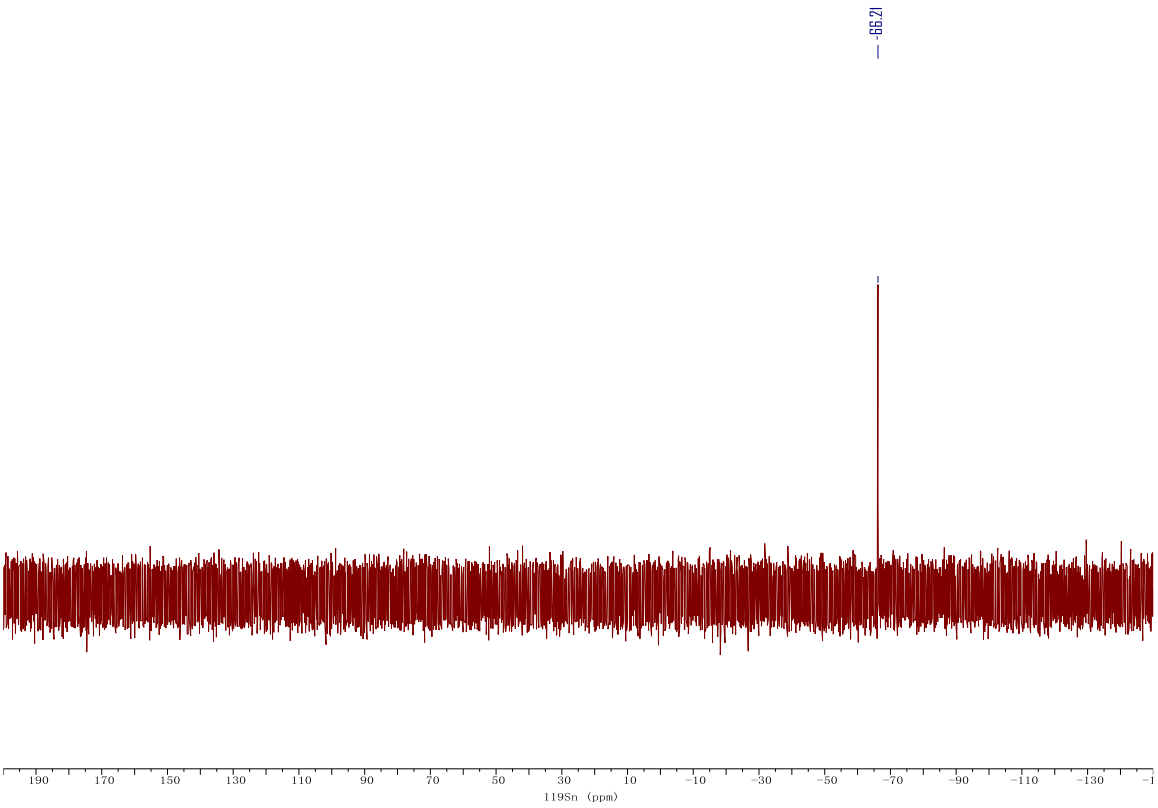

Figure 2.34. $^{119}Sn\{^{1}H\}$ NMR spectrum of **2.1b-SnMe$_3$** in $CDCl_3$. *Taken from YC-2019-RefSnNMR-MeOC6H4CCSnMe3.*

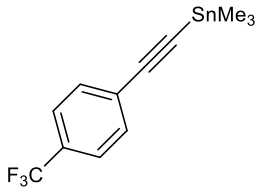

(*p*-(trifluoromethyl)phenyl)ethynyl trimethylstannane (2.1c-SnMe$_3$) 59% yield.

^{1}H NMR ($CDCl_3$, 400 MHz): δ 7.54 (s, 4H), 0.37 (s, 9H) ppm.

$^{13}C\{^{1}H\}$ NMR ($CDCl_3$, 101 MHz): δ 132.26, 125.25, -7.55 ppm.

$^{119}Sn\{^{1}H\}$ NMR ($CDCl_3$, 187 MHz): δ -63.29 ppm.

$^{19}F\{^{1}H\}$ NMR ($CDCl_3$, MHz): δ -62.79 ppm.

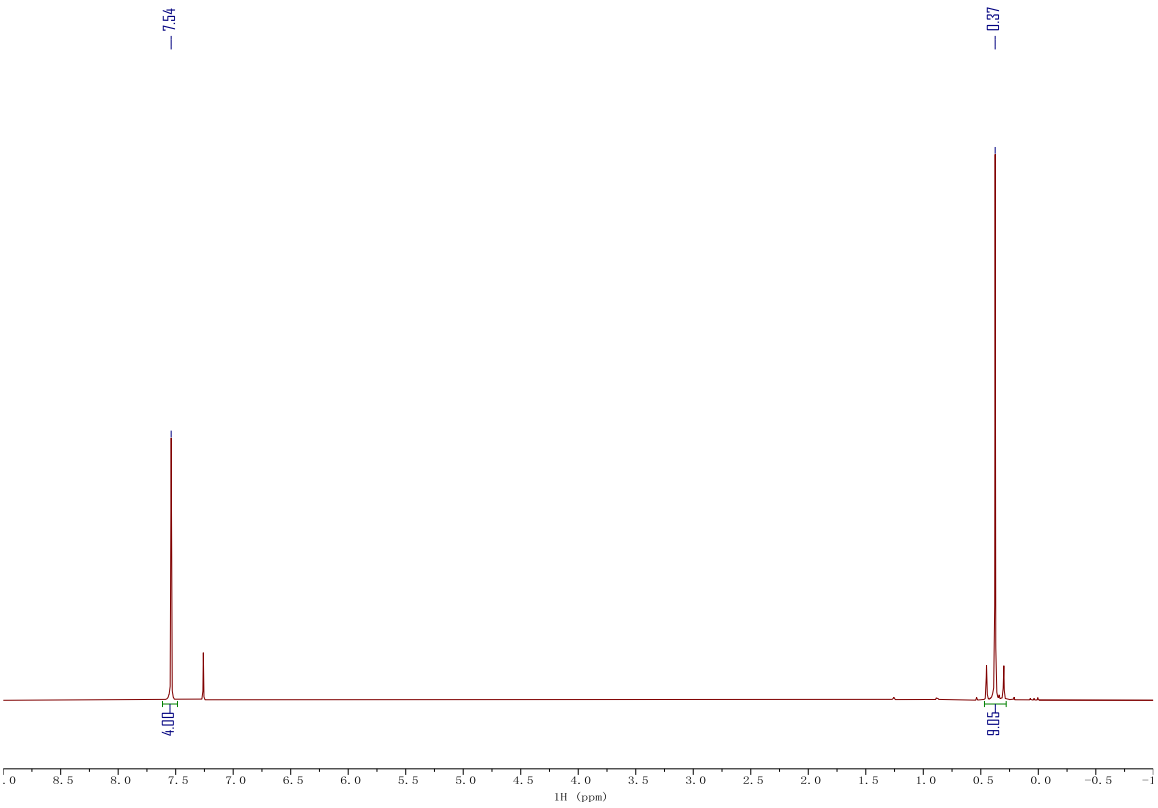

Figure 2.35. ^{1}H NMR spectrum of **2.1c-SnMe$_3$** in $CDCl_3$. *Taken from YC-2019-0188-1-H-2.*

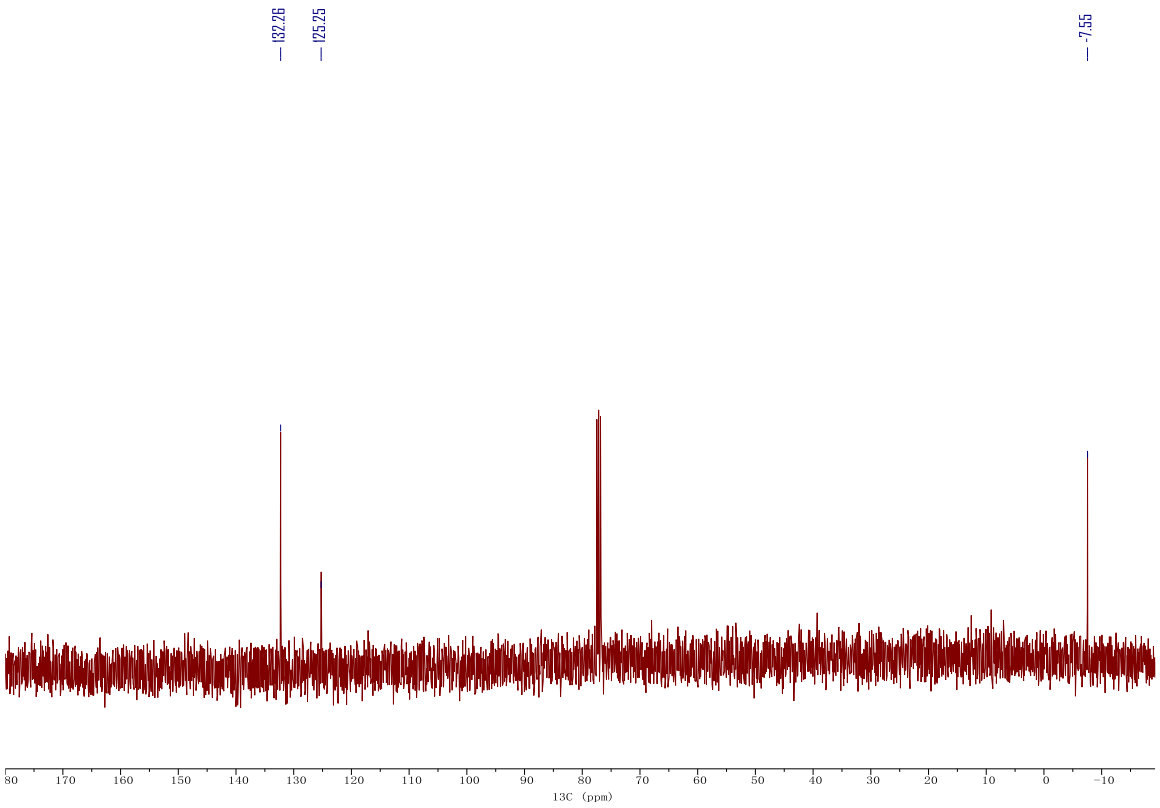

Figure 2.36. $^{13}C\{^{1}H\}$ NMR spectrum of **2.1c-SnMe$_3$** in $CDCl_3$. *Taken from YC-2019-0188-1-C.*

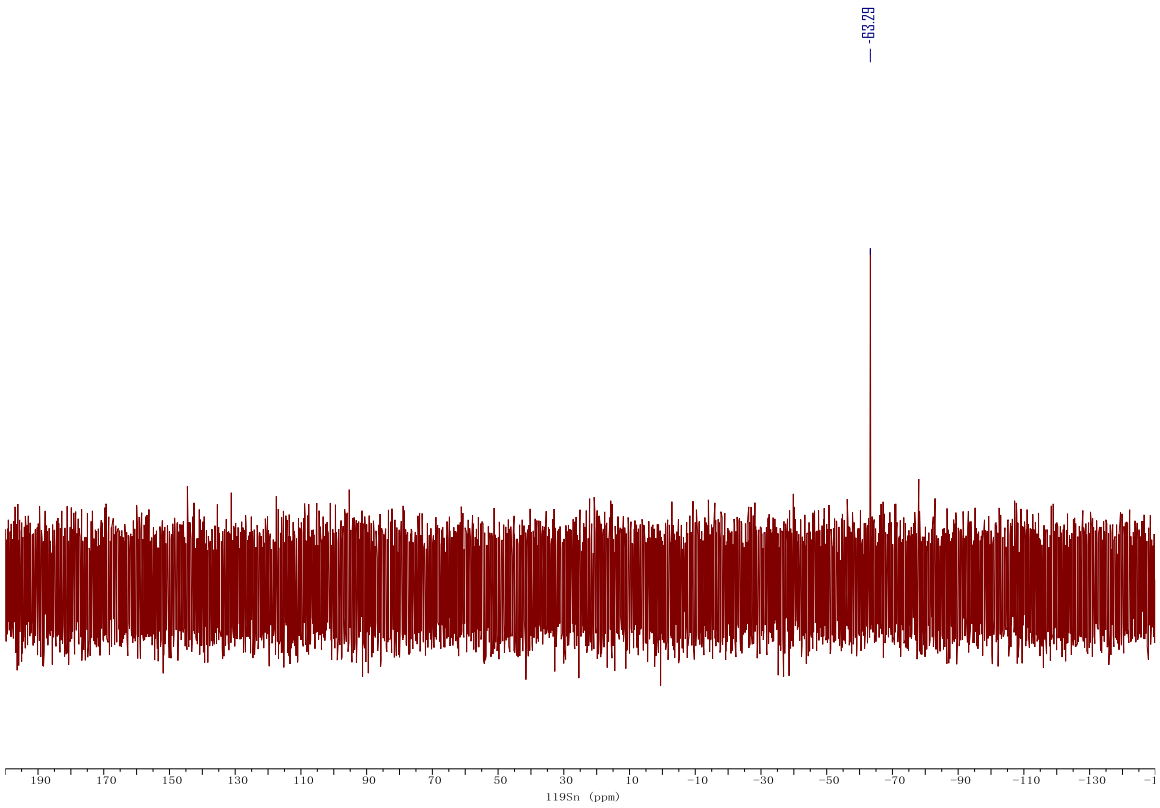

Figure 2.37. $^{119}Sn\{^{1}H\}$ NMR spectrum of **2.1c-SnMe$_3$** in $CDCl_3$. *Taken from YC-2019-RefSnNMR-F3CC6H4CCSnMe3*

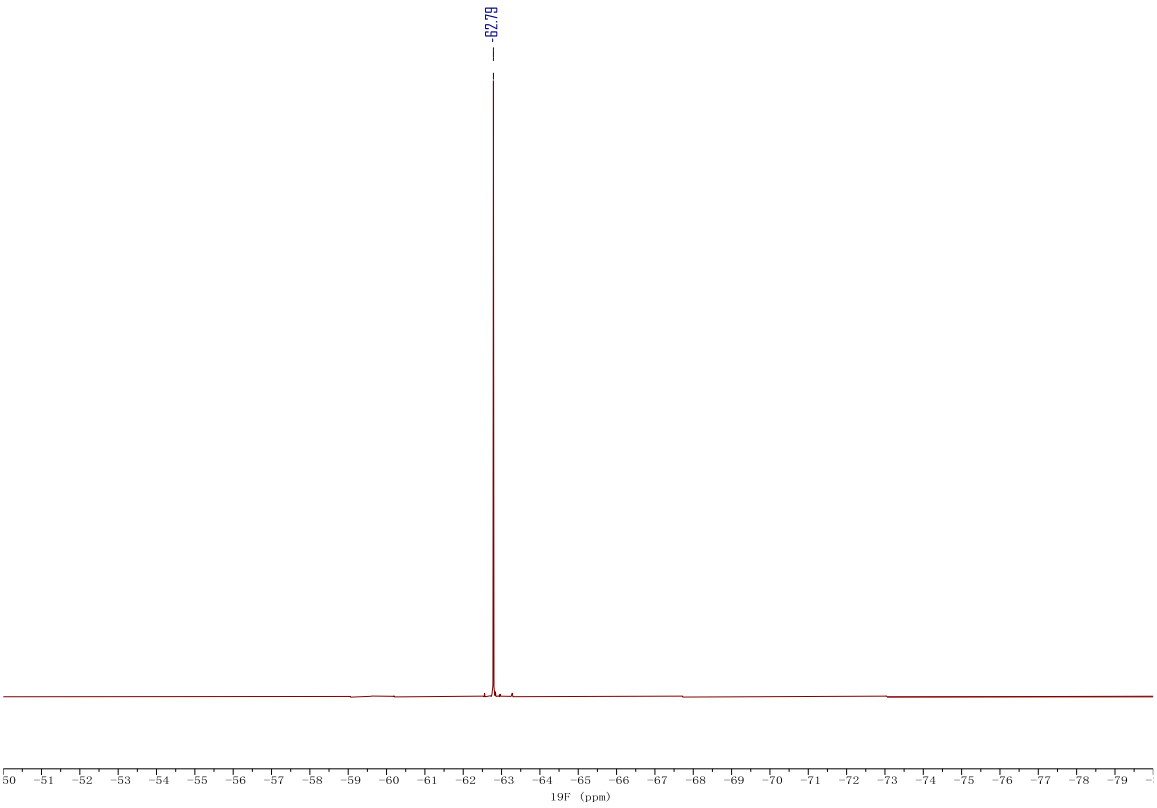

Figure 2.38. $^{19}F\{^{1}H\}$ NMR spectrum of **2.1c-SnMe$_3$** in $CDCl_3$. *Taken from YC-2020-ReagentPurity-F3CPhCCSnMe3-0224-F.*

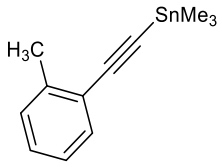

(*o*-tolyl)ethynyl trimethylstannane (2.1d-SnMe$_3$) 40% yield.

^{1}H NMR ($CDCl_3$, 500 MHz): δ 7.42 (d, 7.5 Hz, 1H), 7.20-7.14 (m, 2H), 7.13-7.07 (m, 1H), 2.44 (s, 3H), 0.36 (s, 9H) ppm.

$^{13}C\{^{1}H\}$ NMR ($CDCl_3$, 101 MHz): δ 140.52, 132.26, 129.43, 128.17, 125.53, 123.58, 107.97, 97.47, 20.93, -7.47 ppm.

$^{119}Sn\{^{1}H\}$ NMR ($CDCl_3$, 187 MHz): δ -65.64 ppm.

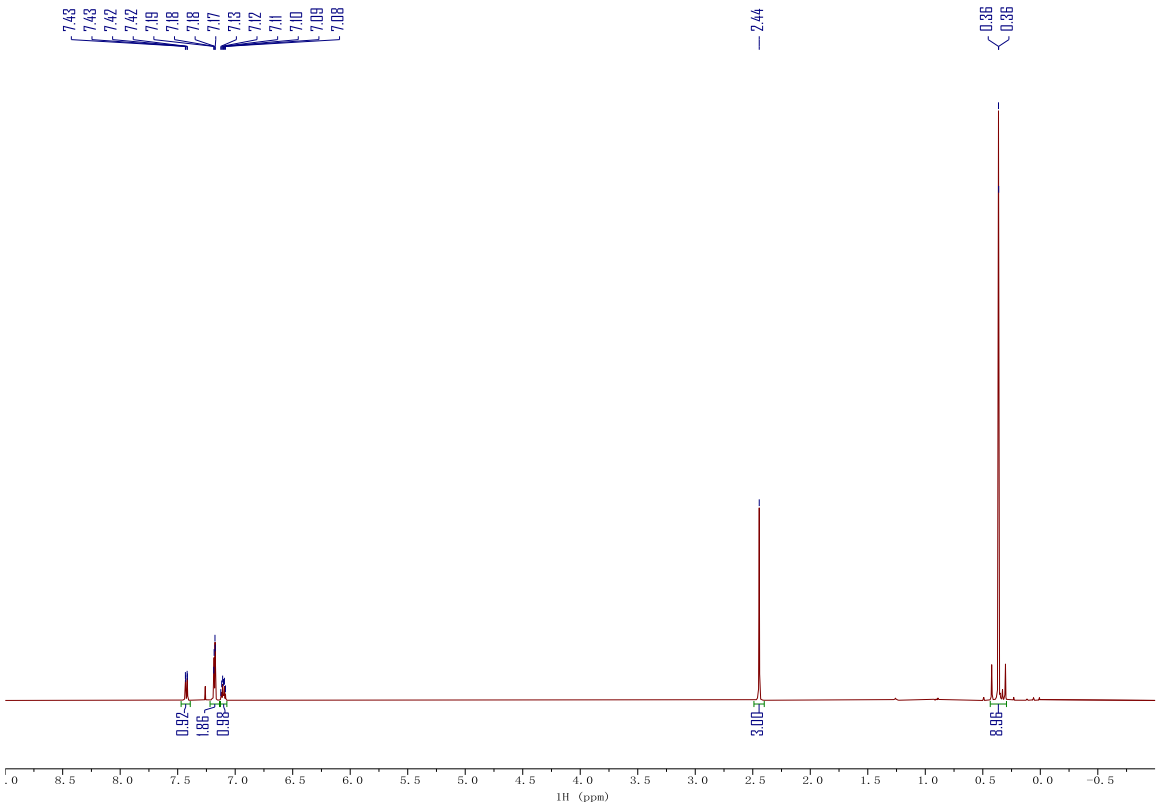

Figure 2.39. ^{1}H NMR spectrum of **2.1d-SnMe$_3$** in $CDCl_3$. *Taken from YC-2019-0187-3-H.*

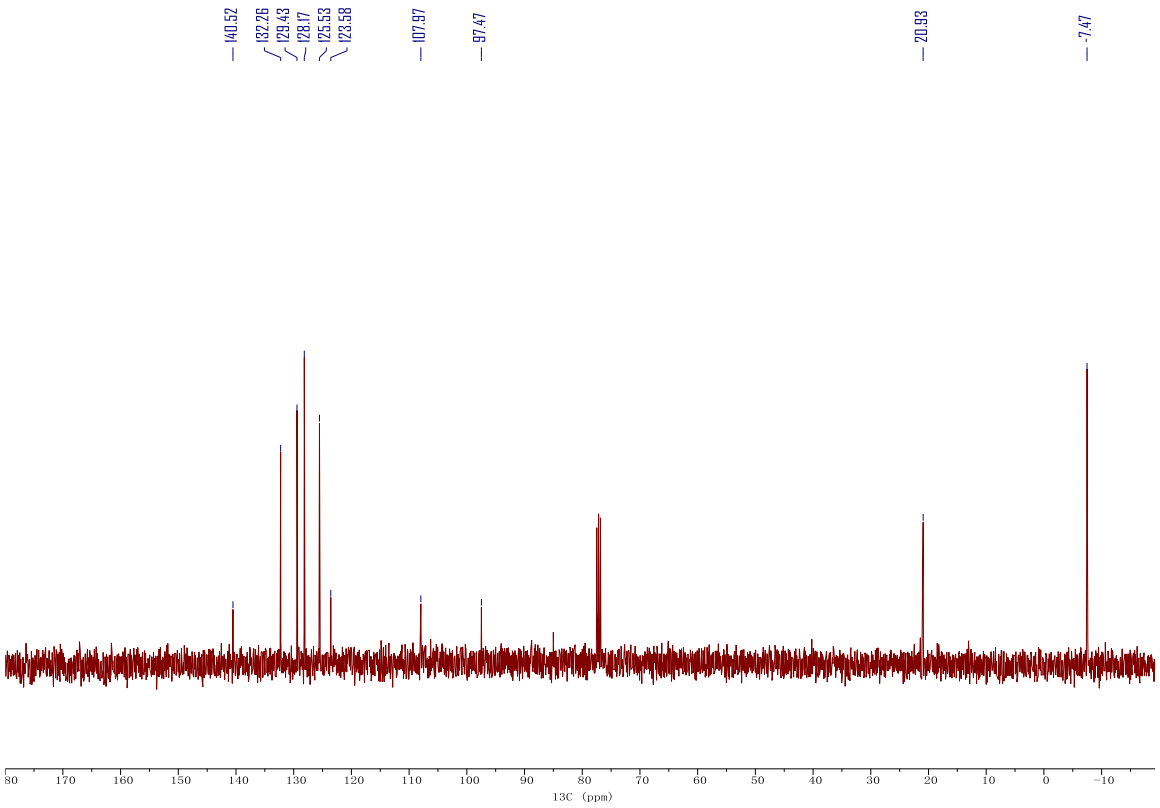

Figure 2.40. $^{13}C\{^{1}H\}$ NMR spectrum of **2.1d-SnMe$_3$** in $CDCl_3$. *Taken from YC-2019-0187-3-C.*

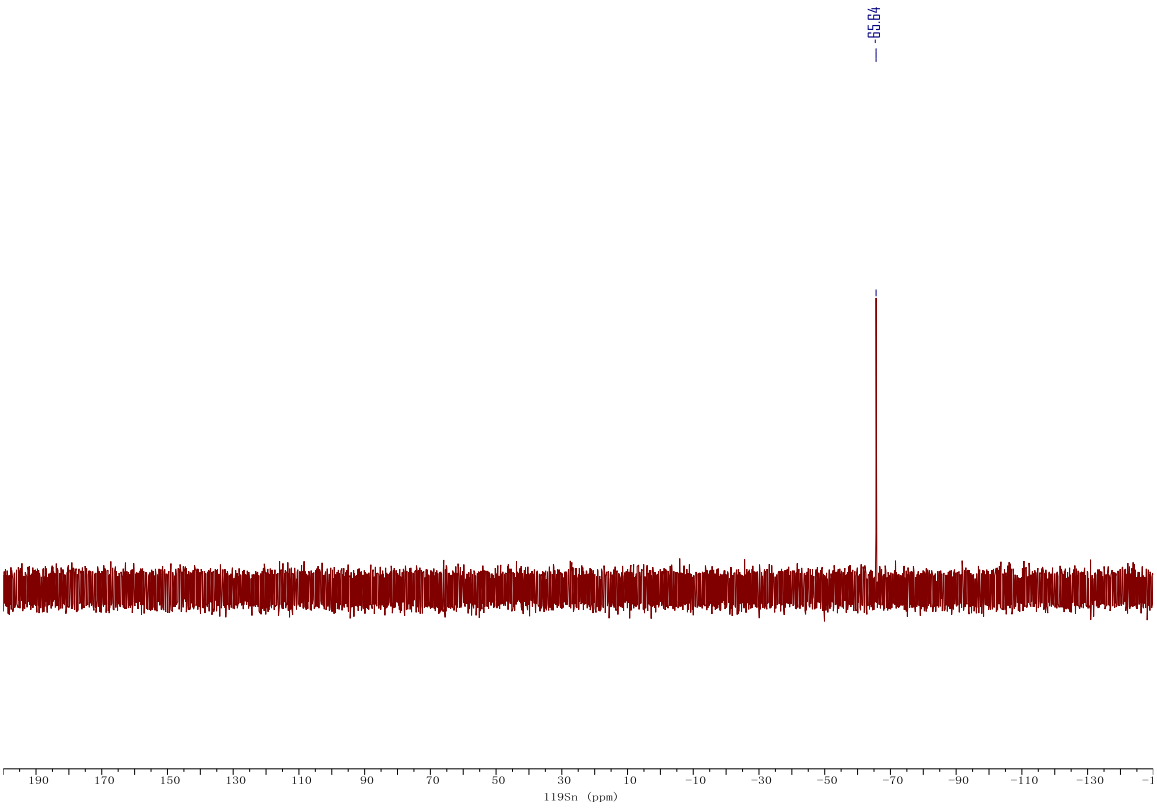

Figure 2.41. $^{119}Sn\{^{1}H\}$ NMR spectrum of **2.1d-SnMe$_3$** in $CDCl_3$. *Taken from YC-2019-RefSnNMR-TolCCSnMe3.*

2.5.6 Catalytic Pyrrole Syntheses: Alkynyl BBN and Alkynyl Stannanes Scopes (Table 2.3)

General Procedure for Catalysis with *B*-alkynyl-9-BBN as Substrate (Procedure 2.B)

$[py_2TiCl_2(NPh)]_2$ (7.4 mg, 0.01 mmol, 0.1 equiv), *B*-alkynyl-9-BBN (0.1 mmol, 1 equiv) and 0.5 mL of C_6D_5Br stock solution containing 1-phenyl-1-propyne (11.6 mg, 0.1 mmol, 1 equiv), azobenzene (7.3 mg, 0.04 mmol, 0.4 equiv) and triphenylmethane (4.9 mg, 0.02 mmol, 0.2 equiv, internal standard) were added to an NMR tube. The reaction was then sealed and heated in a preheated oil bath at 115 ℃ for 0.5 h. NMR spectra were collected before and after heating to monitor the reaction. The reaction was quenched with 5% HCl in methanol and extracted with EtOAc/H_2O. The organic phase was dried over $MgSO_4$, evaporated and characterized by NMR. The peak assignment of pyrrole products were performed based on the reported chemical shifts,[32,43,137] and the yields were calculated by the comparison of peak

area integral with respect to the internal standard. The peak area of selected ^{1}H NMR peaks were calculated by Gaussian-Lorentzian fitting to omit the influence from minor baseline overlapping.[138]

Catalytic Reaction of **2.1a-BBN** with 1-phenyl-1-propyne **(Table 2.3)**

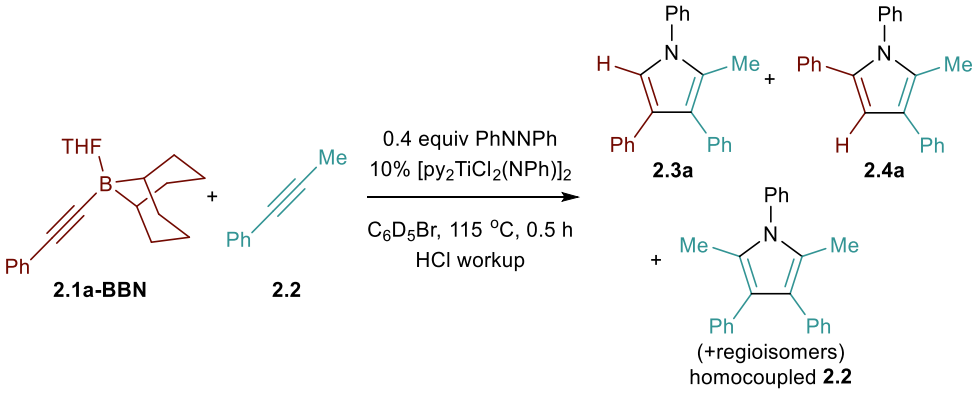

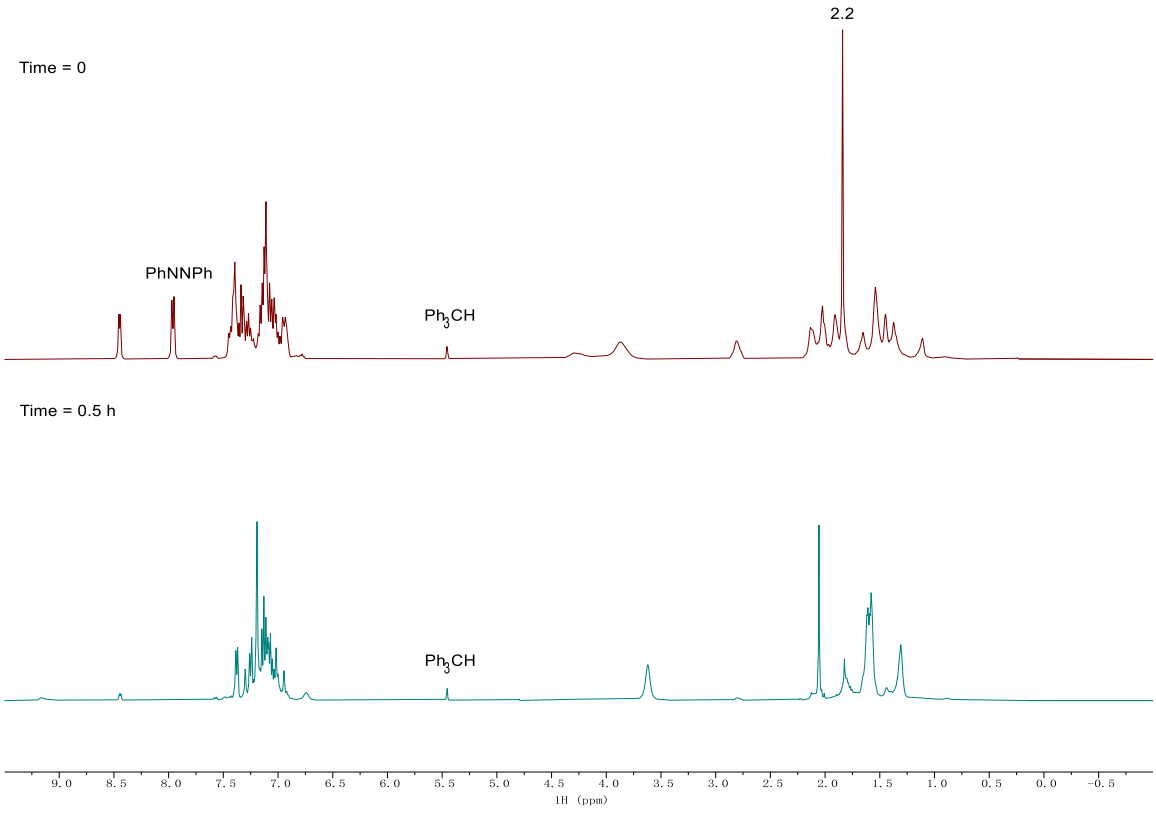

Figure 2.42. ^{1}H NMR of the reaction of **2.1a-BBN** with 1-phenyl-1-propyne at time = 0 (top), time = 0.5 h (bottom) in C_6D_5Br. *Taken from (top) YC-2019-0181-0h-H and (bottom) YC-2019-0181-30min-H.*

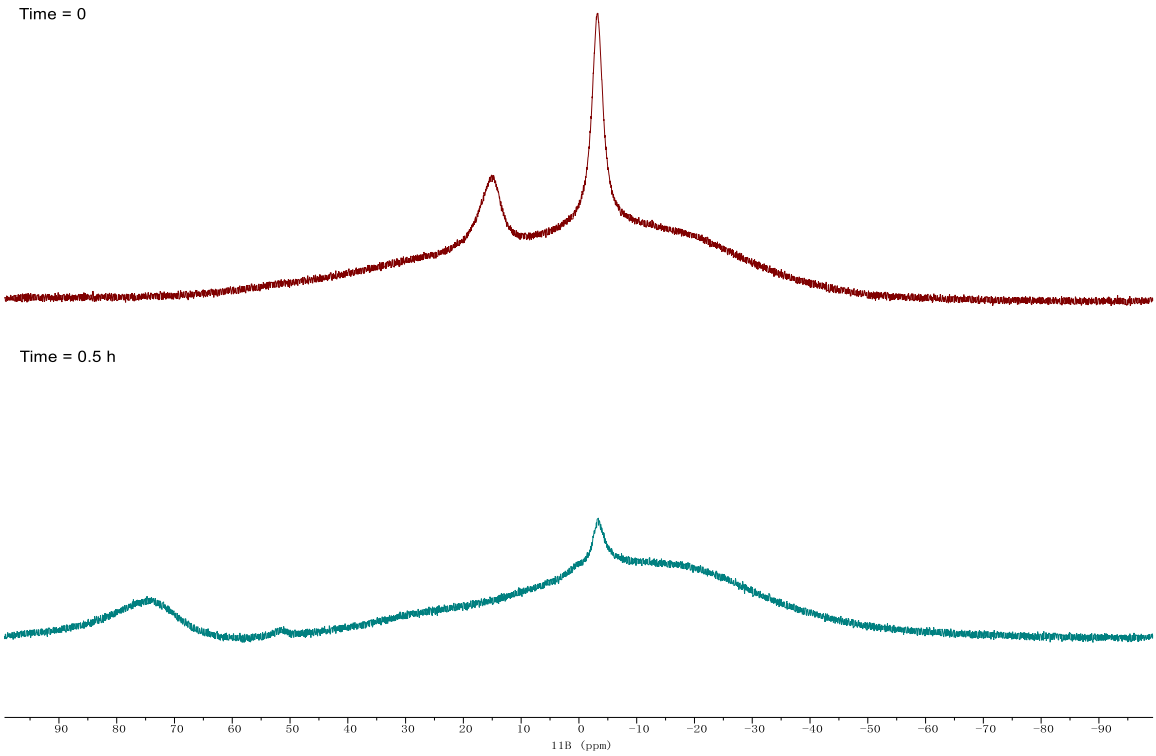

Figure 2.43. ^{11}B NMR of the reaction of **2.1a-BBN** with 1-phenyl-1-propyne at time = 0 (top), time = 0.5 h (bottom) in C_6D_5Br. *Taken from (top) YC-2019-0181-0h-B and (bottom) YC-2019-0181-30min-B.*

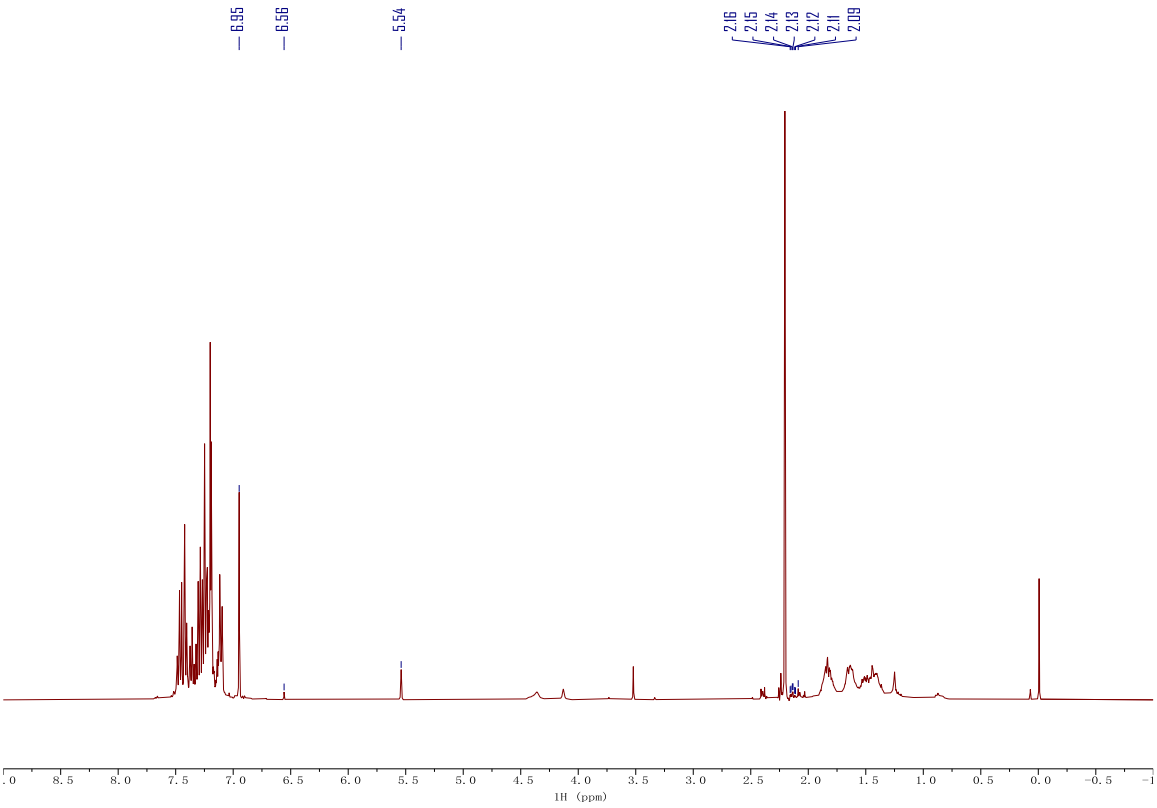

	δ (ppm)	Assignment	# of H	Peak Area	Yield (%)
Ph_3CH	5.54	Ph_3C-H	1	3363.3	n.a.
2.3a	6.95	$H_{pyrrolyl}$	1	12234.0	72.8
2.4a	6.56	$H_{pyrrolyl}$	1	534.5	3.2
homocoupled **2.2**	2.16, 2.15, 2.14, 2.13, 2.12, 2.11, 2.09	$Me_{pyrrolyl}$ (2 per molecule)	6	3040.3	3.0

Figure 2.44. ^{1}H NMR of the reaction of **2.1a-BBN** with 1-phenyl-1-propyne in $CDCl_3$ after HCl workup. *Taken from YC-2019-0181-3H.*

Sample yield calculation based on ^{1}H NMR peak area:

$$Yield\ of\ \mathbf{2.3a} = \frac{Peak\ Area\ of\ \mathbf{2.3a}}{\#\ of\ H\ of\ \mathbf{2.3a}} \times \frac{\#\ of\ H\ of\ Ph_3CH}{Peak\ Area\ of\ Ph_3CH} \times equiv\ of\ Ph_3CH \times 100\%$$

Catalytic Reaction of **2.1b-BBN** with 1-phenyl-1-propyne **(Table 2.3)**

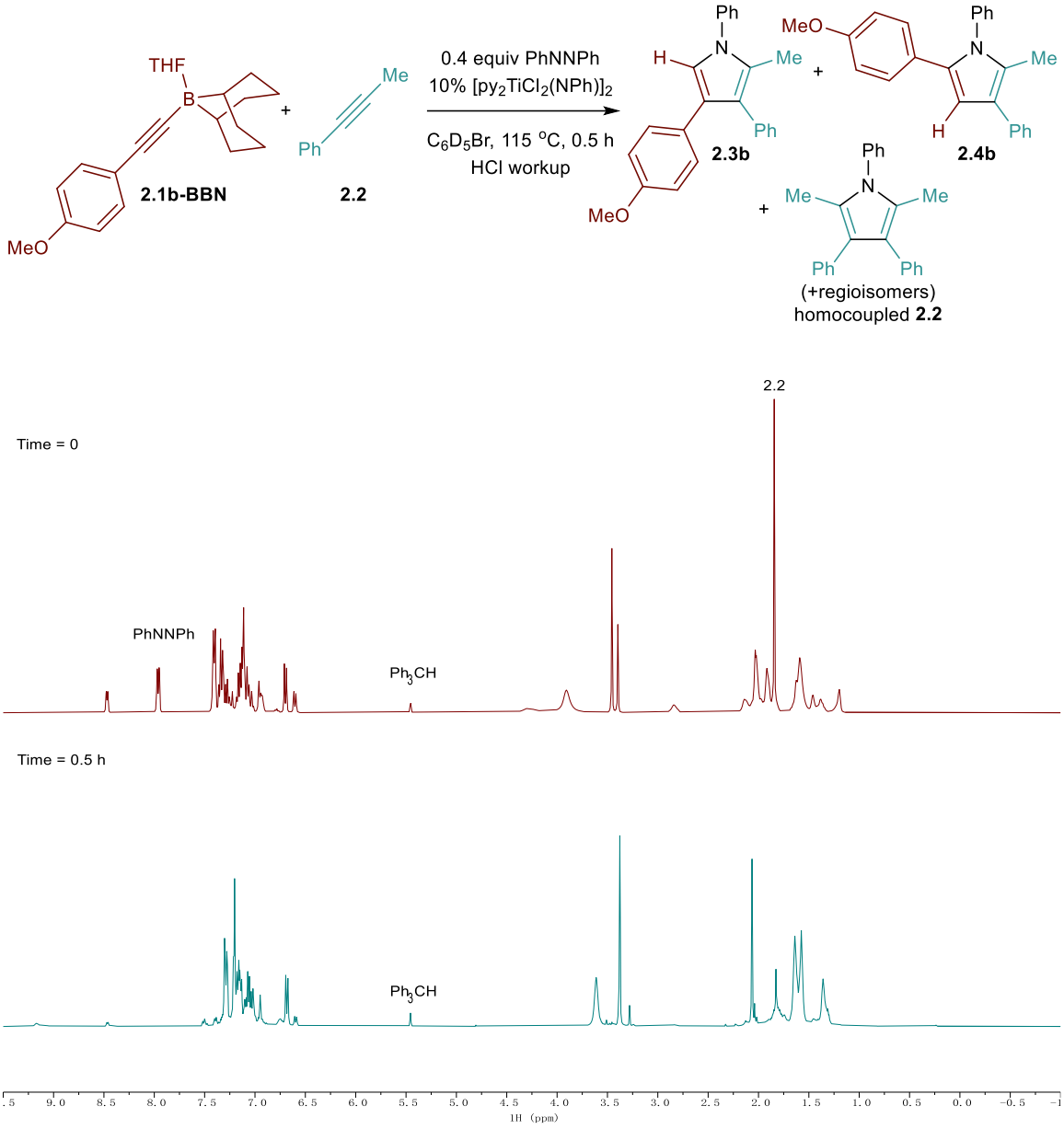

Figure 2.45. ^{1}H NMR of the reaction of **2.1b-BBN** with 1-phenyl-1-propyne at time = 0 (top), time = 0.5 h (bottom) in C_6D_5Br. *Taken from (top) YC-2019-0182-0h-H and (bottom) YC-2019-0182-30min-H.*

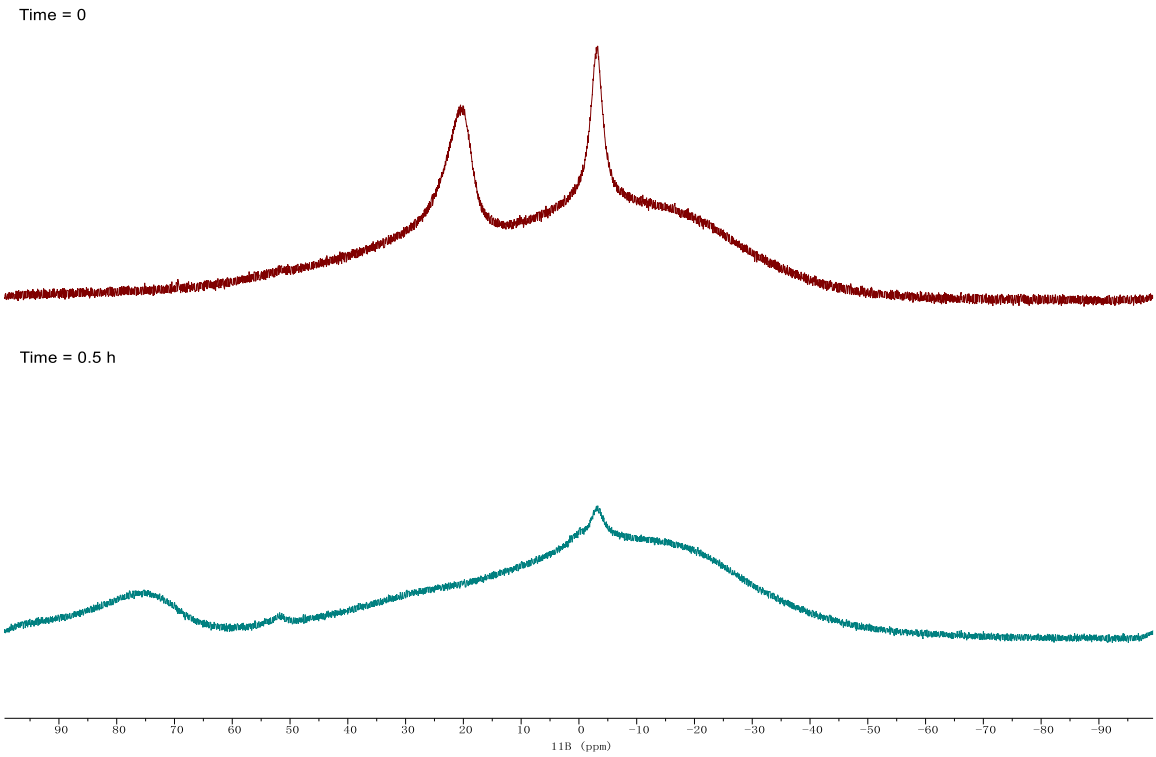

Figure 2.46. ^{11}B NMR of the reaction of **2.1b-BBN** with 1-phenyl-1-propyne at time = 0 (top), time = 0.5 h (bottom) in C_6D_5Br. *Taken from (top) YC-2019-0182-0h-B and (bottom) YC-2019-0182-30min-B.*

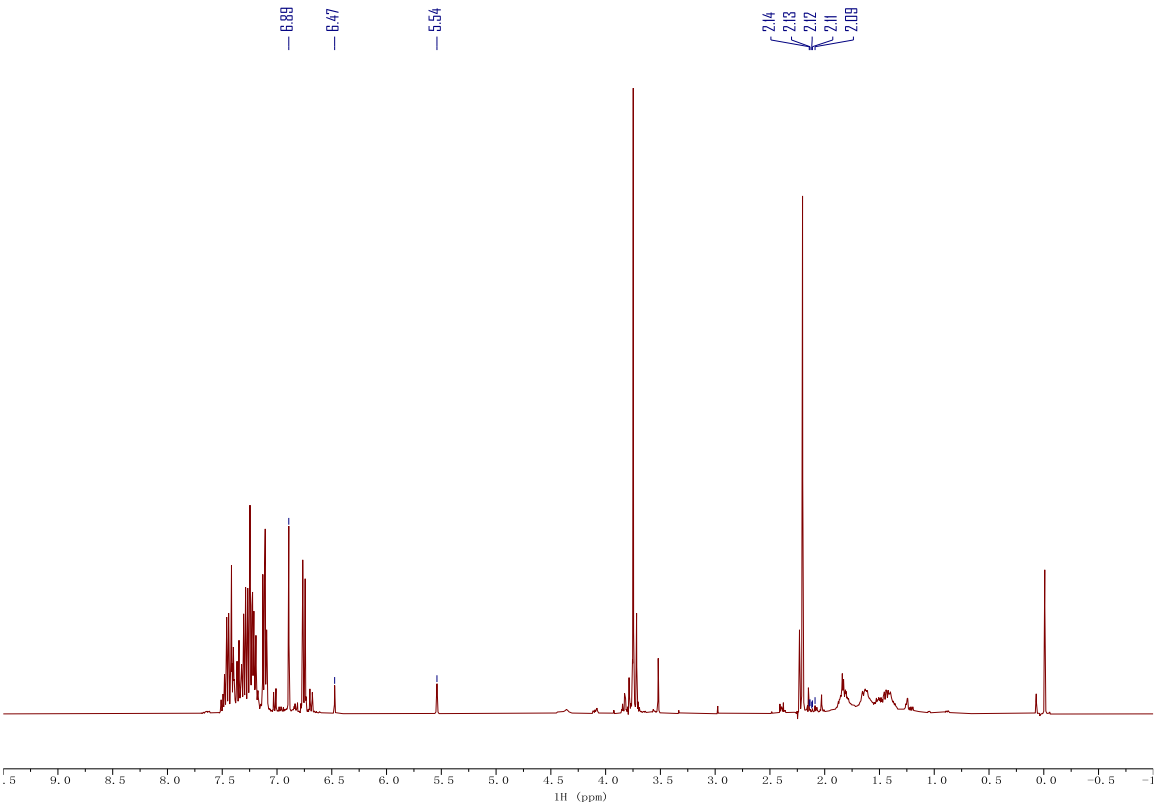

	δ (ppm)	Assignment	# of H	Peak Area	Yield (%)
Ph_3CH	5.54	Ph_3C-H	1	3296.7	n.a.
2.3b	6.89	$H_{pyrrolyl}$	1	9824.6	59.6
2.4b	6.47	$H_{pyrrolyl}$	1	1560.1	9.5
homocoupled **2.2**	2.14, 2.13, 2.12, 2.11, 2.09	$Me_{pyrrolyl}$ (2 per molecule)	6	2025.7	2.1

Figure 2.47. ^{1}H NMR of the reaction of **2.1b-BBN** with 1-phenyl-1-propyne in $CDCl_3$ after HCl workup. *Taken from YC-2019-0194-1H.*

Catalytic Reaction of **2.1c-BBN** with 1-phenyl-1-propyne **(Table 2.3)**

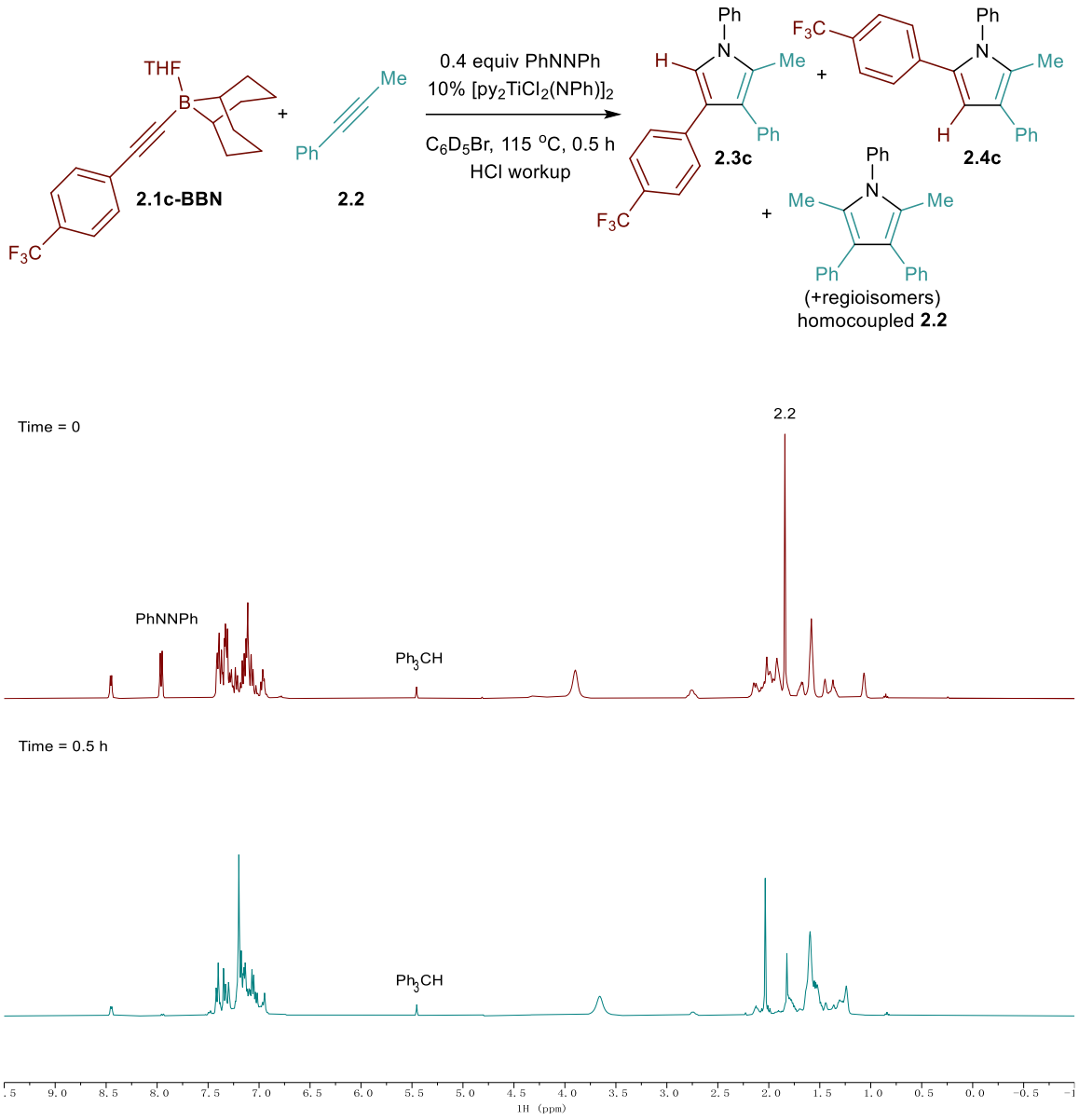

Figure 2.48. ^{1}H NMR of the reaction of **2.1c-BBN** with 1-phenyl-1-propyne at time = 0 (top), time = 0.5 h (bottom) in C_6D_5Br. *Taken from (top) YC-2019-0198-0h-H and (bottom) YC-2019-0198-30min-H.*

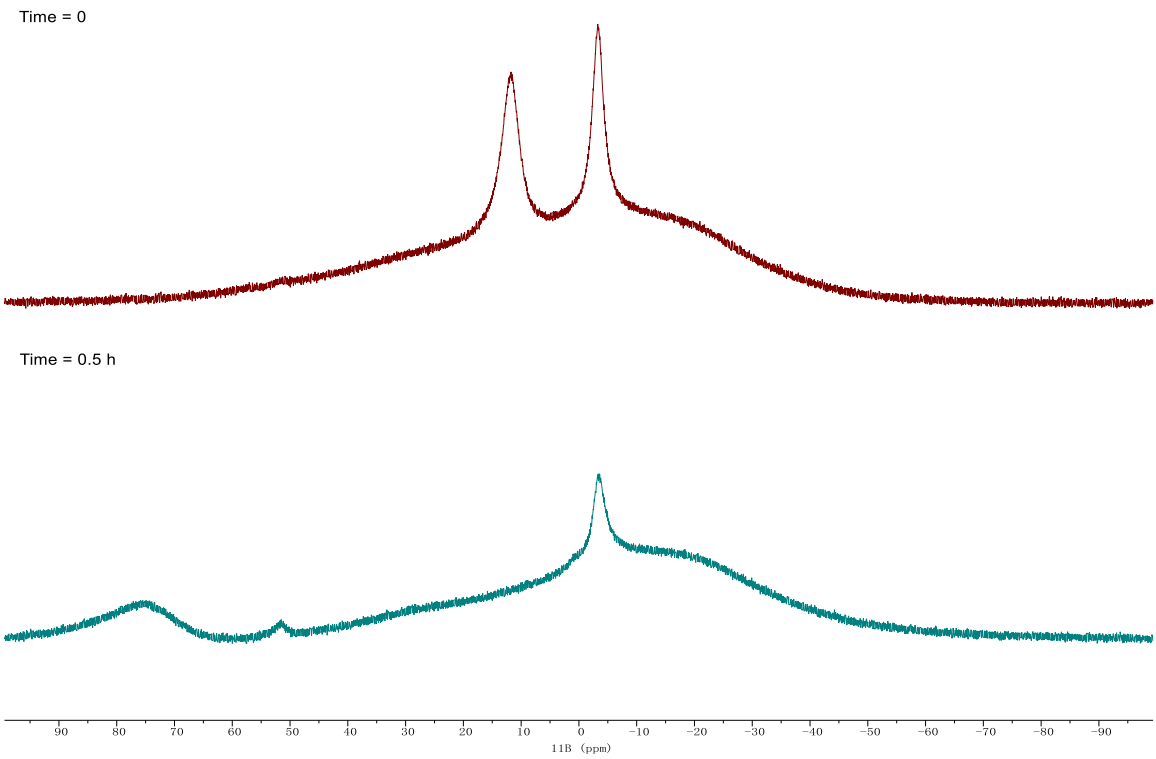

Figure 2.49. ^{11}B NMR of the reaction of **2.1c-BBN** with 1-phenyl-1-propyne at time = 0 (top), time = 0.5 h (bottom) in C_6D_5Br. *Taken from (top) YC-2019-0198-0h-B and (bottom) YC-2019-0198-30min-B.*

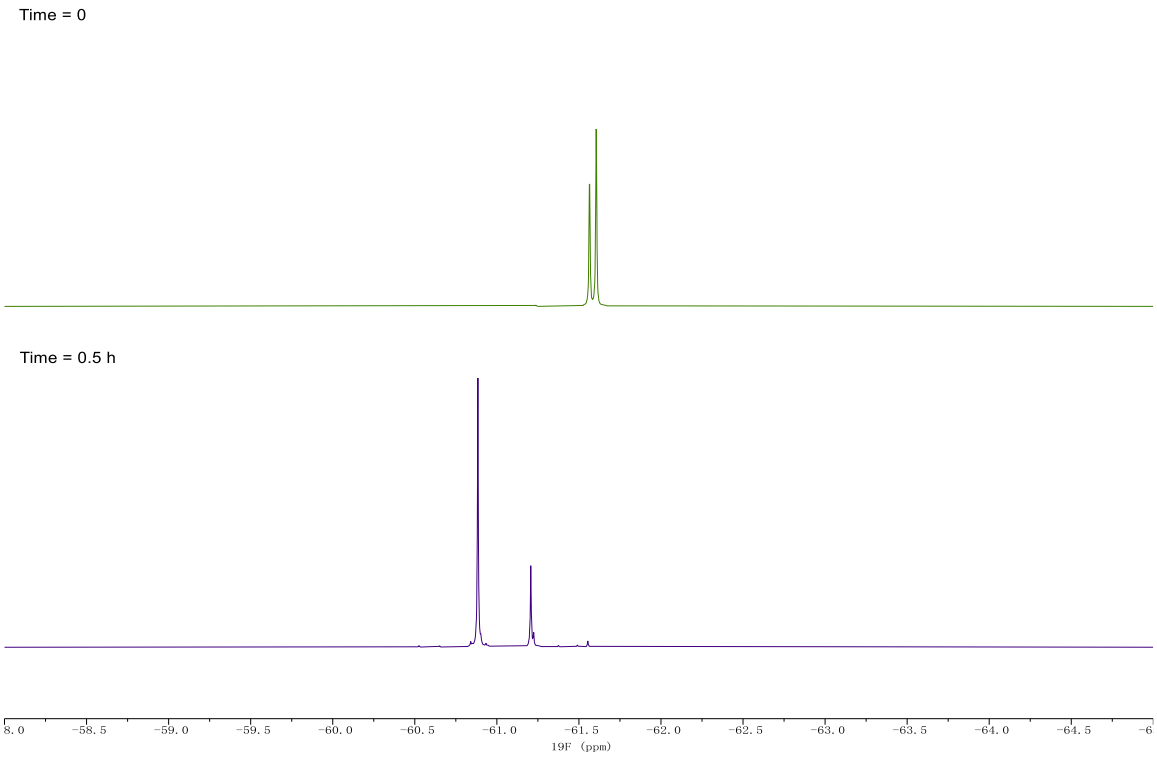

Figure 2.50. $^{19}F\{^{1}H\}$ NMR of the reaction of **2.1c-BBN** with 1-phenyl-1-propyne at time = 0 (top), time = 0.5 h (bottom) in C_6D_5Br. *Taken from (top) YC-2019-0198-0h-F and (bottom) YC-2019-0198-30min-F.*

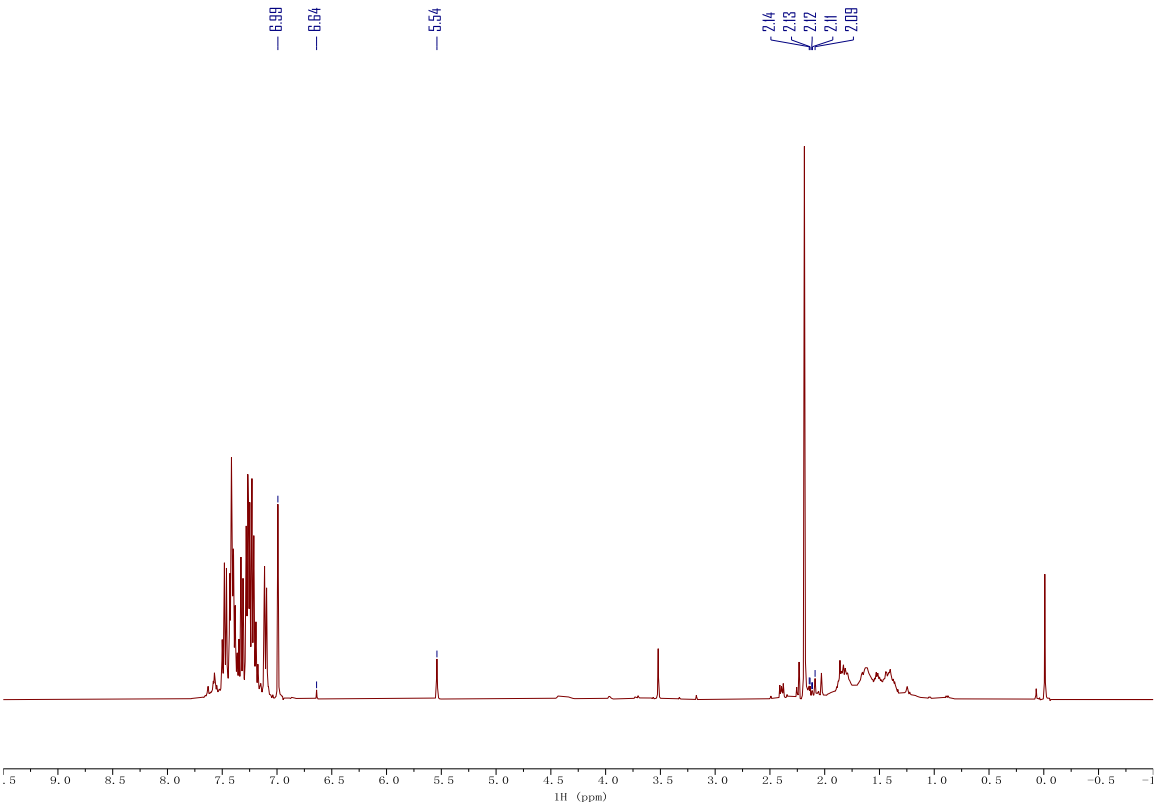

	δ (ppm)	Assignment	# of H	Peak Area	Yield (%)
Ph_3CH	5.54	Ph_3C-H	1	3643.1	n.a.
2.3c	6.99	$H_{pyrrolyl}$	1	11843.5	65.0
2.4c	6.64	$H_{pyrrolyl}$	1	605.9	3.3
homocoupled **2.2**	2.14, 2.13, 2.12, 2.11, 2.09	$Me_{pyrrolyl}$ (2 per molecule)	6	2869.3	2.6

Figure 2.51. ^{1}H NMR of the reaction of **2.1c-BBN** with 1-phenyl-1-propyne in $CDCl_3$ after HCl workup. *Taken from YC-2019-0198-3H.*

Catalytic Reaction of **2.1d-BBN** with 1-phenyl-1-propyne **(Table 2.3)**

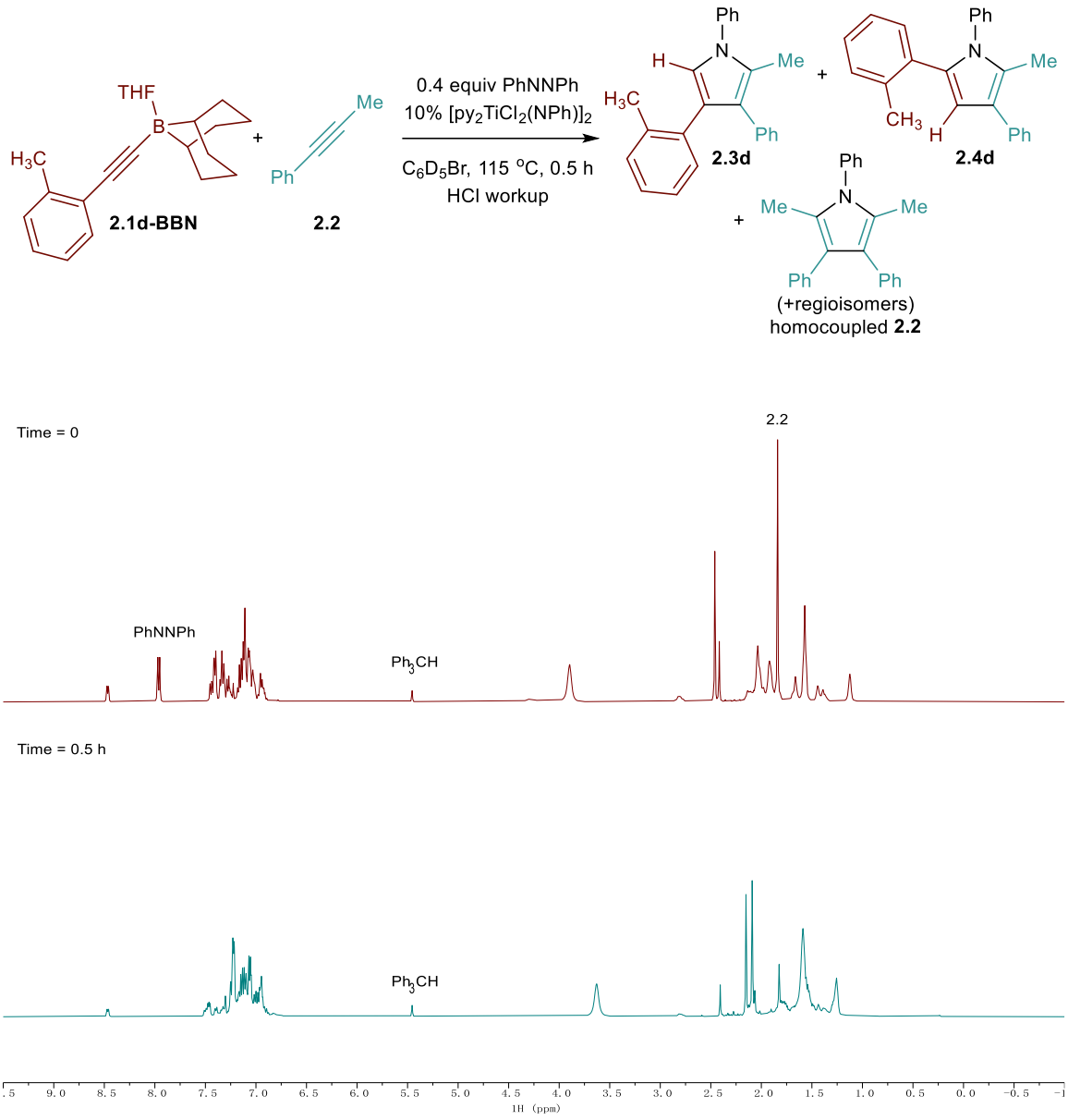

Figure 2.52. ^{1}H NMR of the reaction of **2.1d-BBN** with 1-phenyl-1-propyne at time = 0 (top), time = 0.5 h (bottom) in C_6D_5Br. *Taken from (top) YC-2019-0201-0h-H and (bottom) YC-2019-0201-30min-H.*

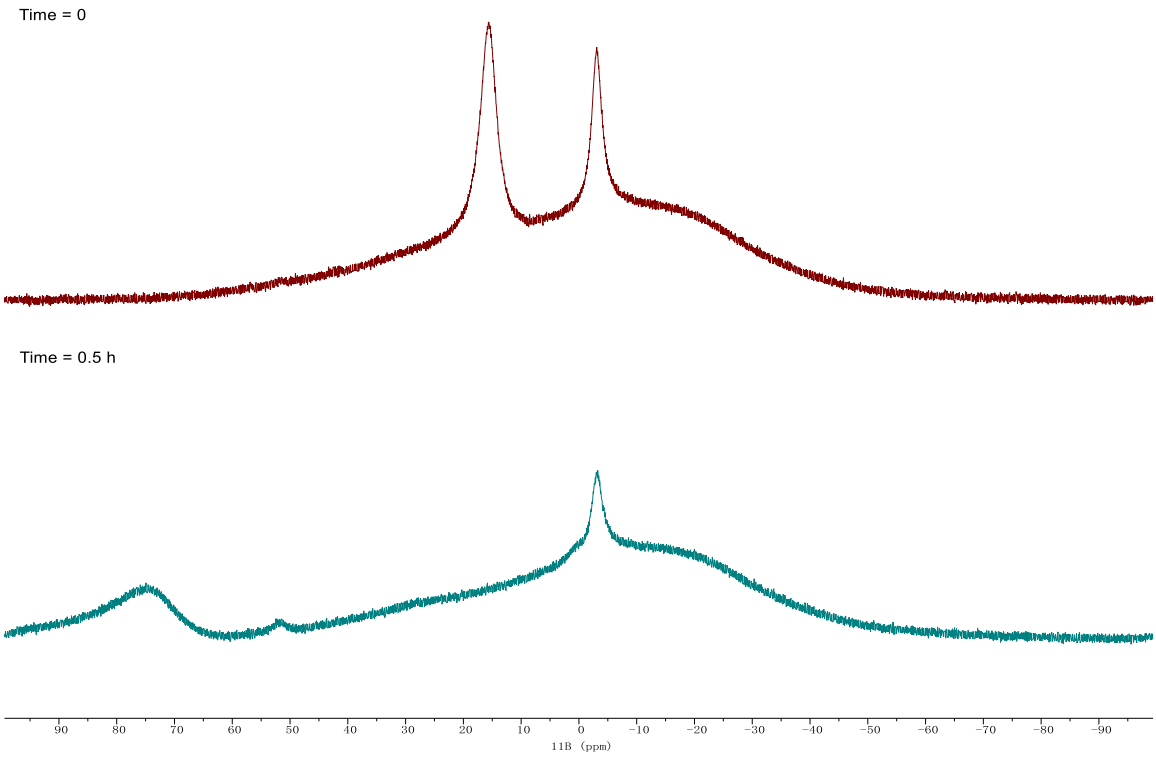

Figure 2.53. ^{11}B NMR of the reaction of **2.1d-BBN** with 1-phenyl-1-propyne at time = 0 (top), time = 0.5 h (bottom) in C_6D_5Br. *Taken from (top) YC-2019-0201-0h-B and (bottom) YC-2019-0201-30min-B.*

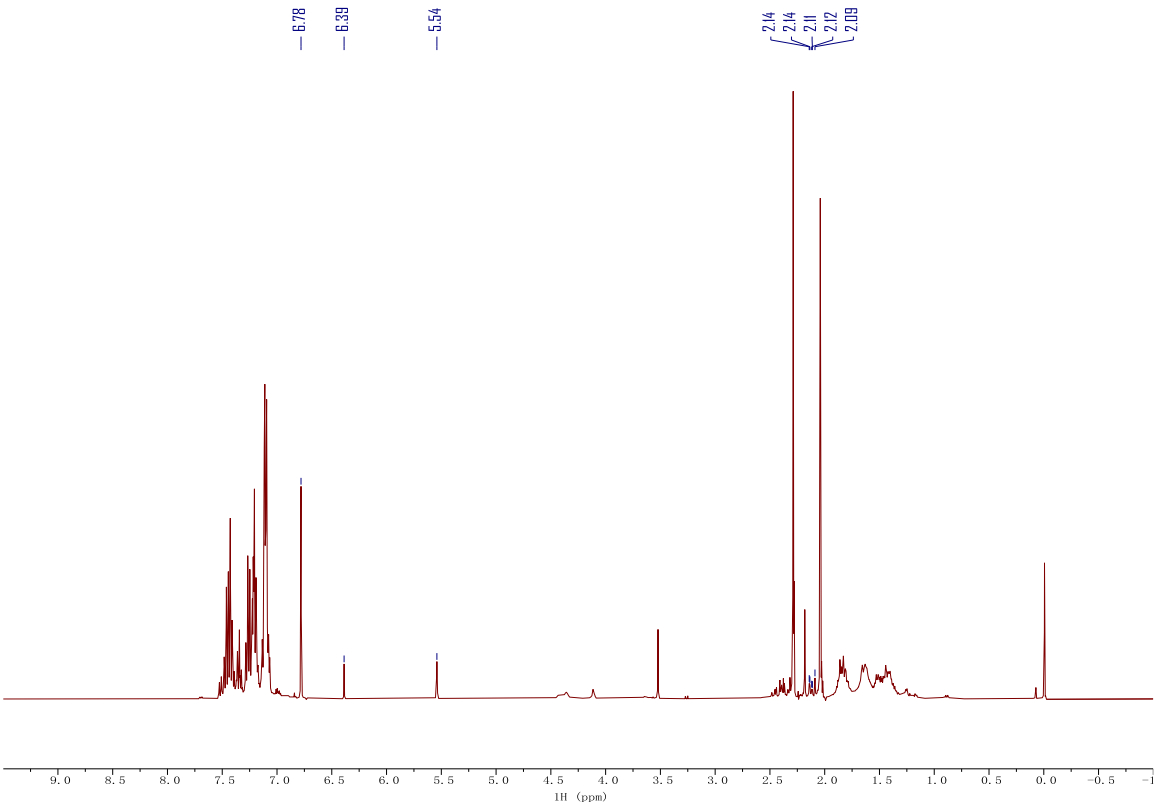

	δ (ppm)	Assignment	# of H	Peak Area	Yield (%)
Ph_3CH	5.54	Ph_3C-H	1	3098.0	n.a.
2.3d	6.78	$H_{pyrrolyl}$	1	10013.2	64.6
2.4d	6.39	$H_{pyrrolyl}$	1	1831.5	11.8
homocoupled **2.2**	2.14, 2.13, 2.12, 2.11, 2.09	$Me_{pyrrolyl}$ (2 per molecule)	6	3011.5	3.2

Figure 2.54. ^{1}H NMR of the reaction of **2.1d-BBN** with 1-phenyl-1-propyne in $CDCl_3$ after HCl workup. *Taken from YC-2019-0201-3H.*

Catalytic Reaction of **2.1e-BBN** with 1-phenyl-1-propyne **(Table 2.3)**

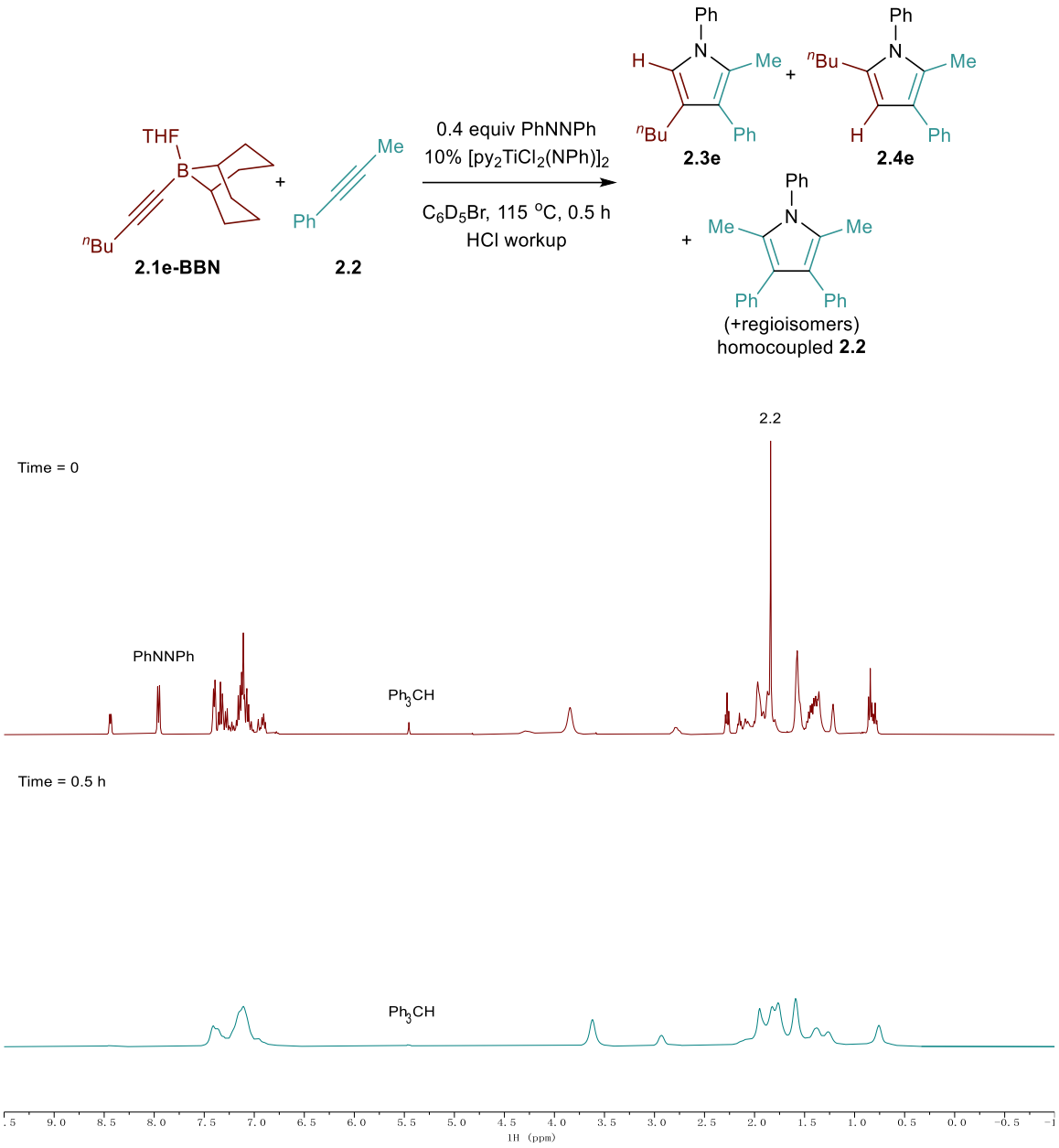

Figure 2.55. ^{1}H NMR of the reaction of **2.1e-BBN** with 1-phenyl-1-propyne at time = 0 (top), time = 0.5 h (bottom) in C_6D_5Br. *Taken from (top) YC-2019-0200-0h-H and (bottom) YC-2019-0200-30min-H.*

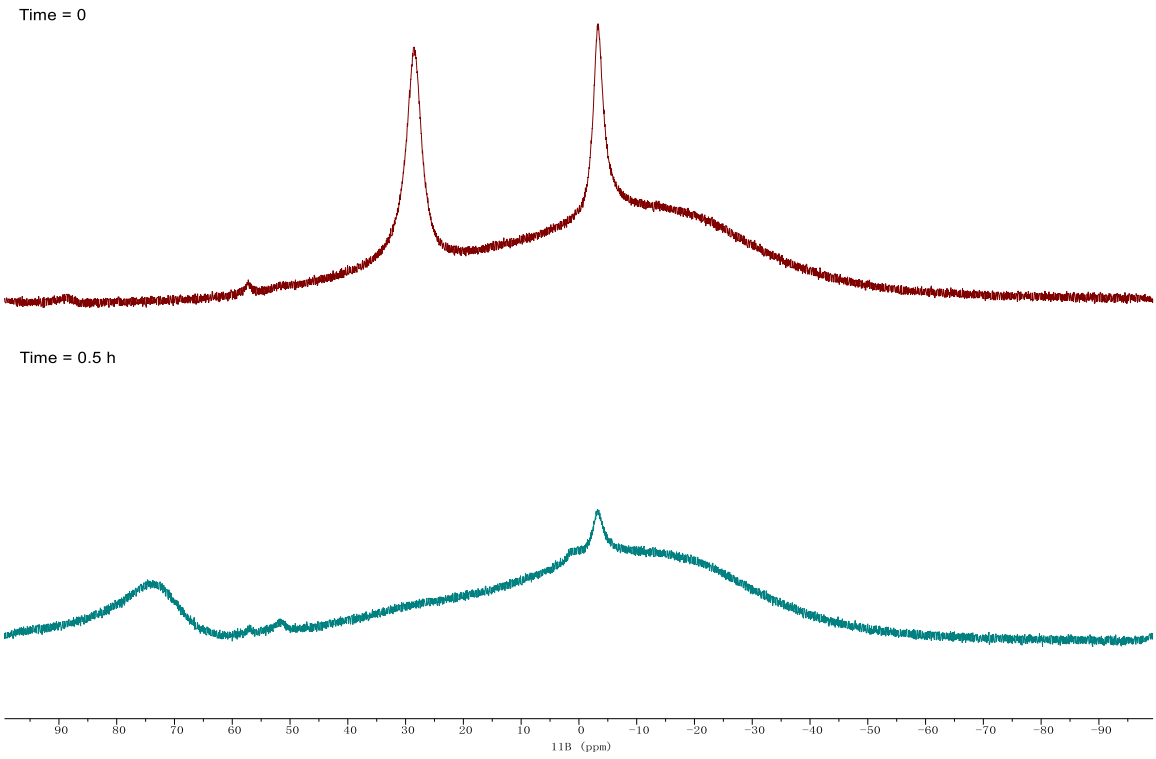

Figure 2.56. ^{11}B NMR of the reaction of **2.1e-BBN** with 1-phenyl-1-propyne at time = 0 (top), time = 0.5 h (bottom) in C_6D_5Br. *Taken from (top) YC-2019-0200-0h-B and (bottom) YC-2019-0200-30min-B.*

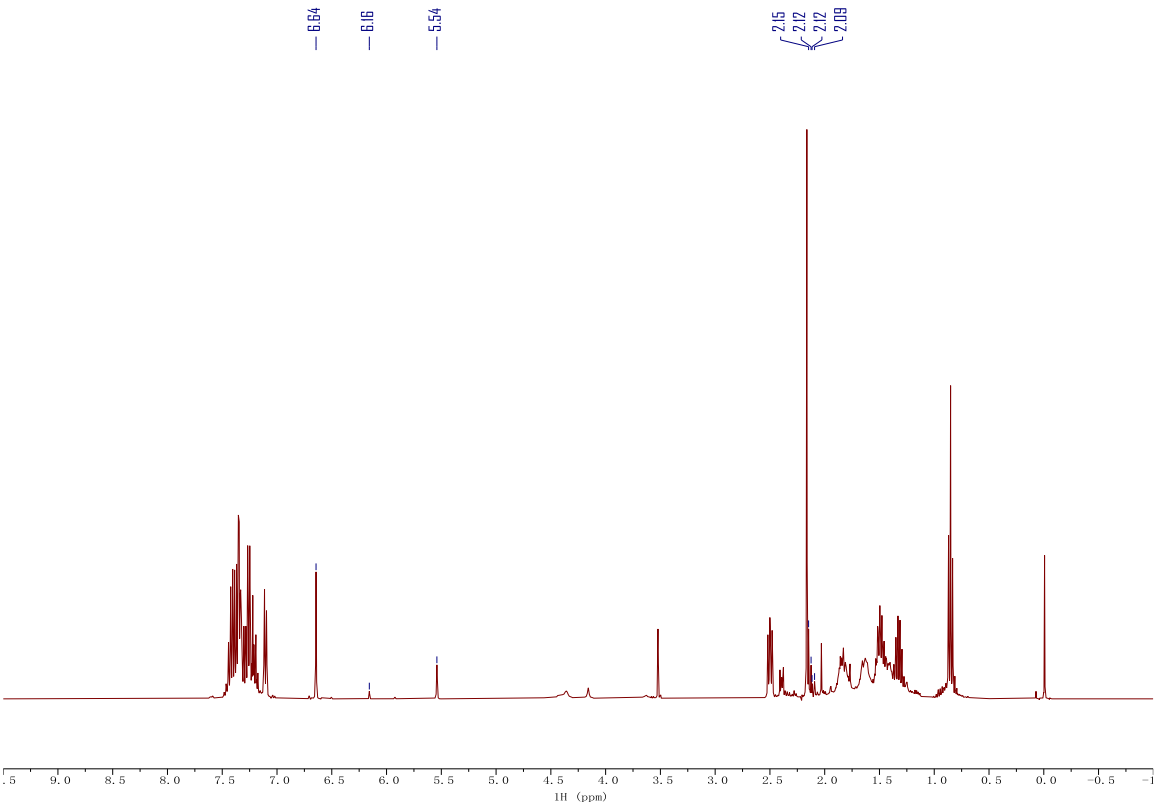

	δ (ppm)	Assignment	# of H	Peak Area	Yield (%)
Ph_3CH	5.54	Ph_3C-H	1	3527.4	n.a.
2.3e	6.64	$H_{pyrrolyl}$	1	10587.6	60.0
2.4e	6.16	$H_{pyrrolyl}$	1	587.4	3.3
homocoupled **2.2**	2.15, 2.12, 2.12, 2.09	$Me_{pyrrolyl}$ (2 per molecule)	6	6246.3	5.9

Figure 2.57. ^{1}H NMR of the reaction of **2.1e-BBN** with 1-phenyl-1-propyne in $CDCl_3$ after HCl workup. *Taken from YC-2019-0200-3H.*

General Procedure for Catalysis with Alkynyl Trialkylstannane as Substrate (Procedure 2.C) (Table 2.3)

$[py_2TiCl_2(NPh)]_2$ (14.7 mg, 0.02 mmol, 0.05 equiv), alkynyl trialkylstannane (0.4 mmol, 1 equiv) and 0.5 mL of toluene stock solution containing 1-phenyl-1-propyne (46.5 mg, 0.4 mmol, 1

equiv), azobenzene (32.8 mg, 0.18 mmol, 0.45 equiv) and triphenylmethane (19.5 mg, 0.08 mmol, 0.2 equiv, internal standard) were added to an NMR tube. The reaction was then sealed and heated in a preheated oil bath at 90 ℃ for 9 h. No-D NMR spectra were collected before and after heating to monitor the reaction. The reaction was quenched with 10% HCl in methanol and extracted with EtOAc/H_2O. The organic phase was dried over $MgSO_4$, evaporated and characterized by NMR. The peak assignment of pyrrole products were performed based on the reported chemical shifts,[32,43,137,139–141] and the yields were calculated by the comparison of peak area integral with respect to the internal standard. The peak area of selected ^1H NMR peaks were calculated by Gaussian-Lorentzian fitting to omit the influence from minor baseline overlapping.[138]

Precaution: Trialkyltin species are highly toxic. Proper PPE is required. All the chemical and labware waste should be handled separately from the normal waste stream and quenched thoroughly.

Catalytic Reaction of **2.1a-SnMe$_3$** with 1-phenyl-1-propyne **(Table 2.3)**

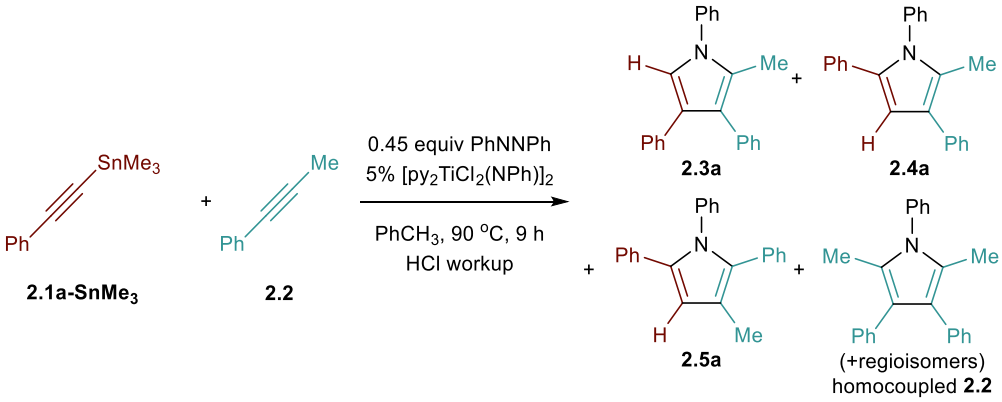

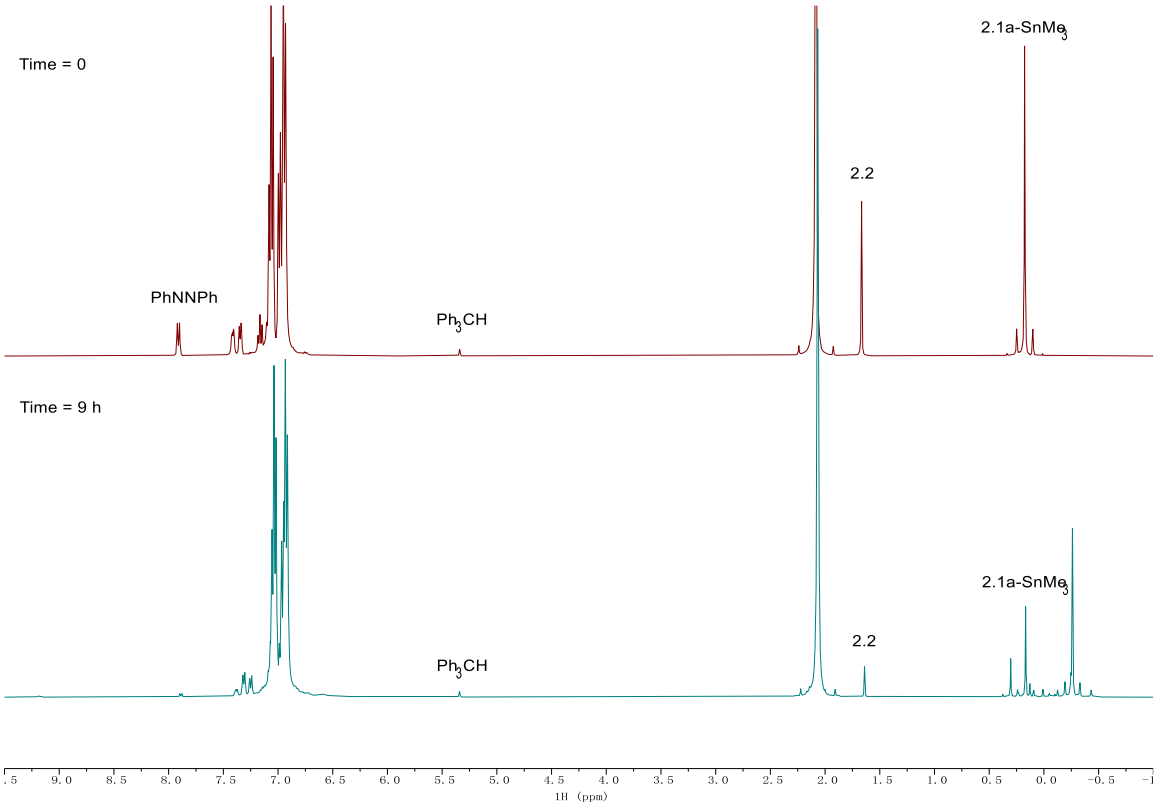

Figure 2.58. No-D ^{1}H NMR of the reaction of **2.1a-SnMe$_3$** with 1-phenyl-1-propyne at time = 0 (top), time = 9 h (bottom) in $PhCH_3$. *Taken from (top) YC-2020-0006-NoD-Tol-0h-H and (bottom) YC-2020-0006-NoD-Tol-9h-H.*

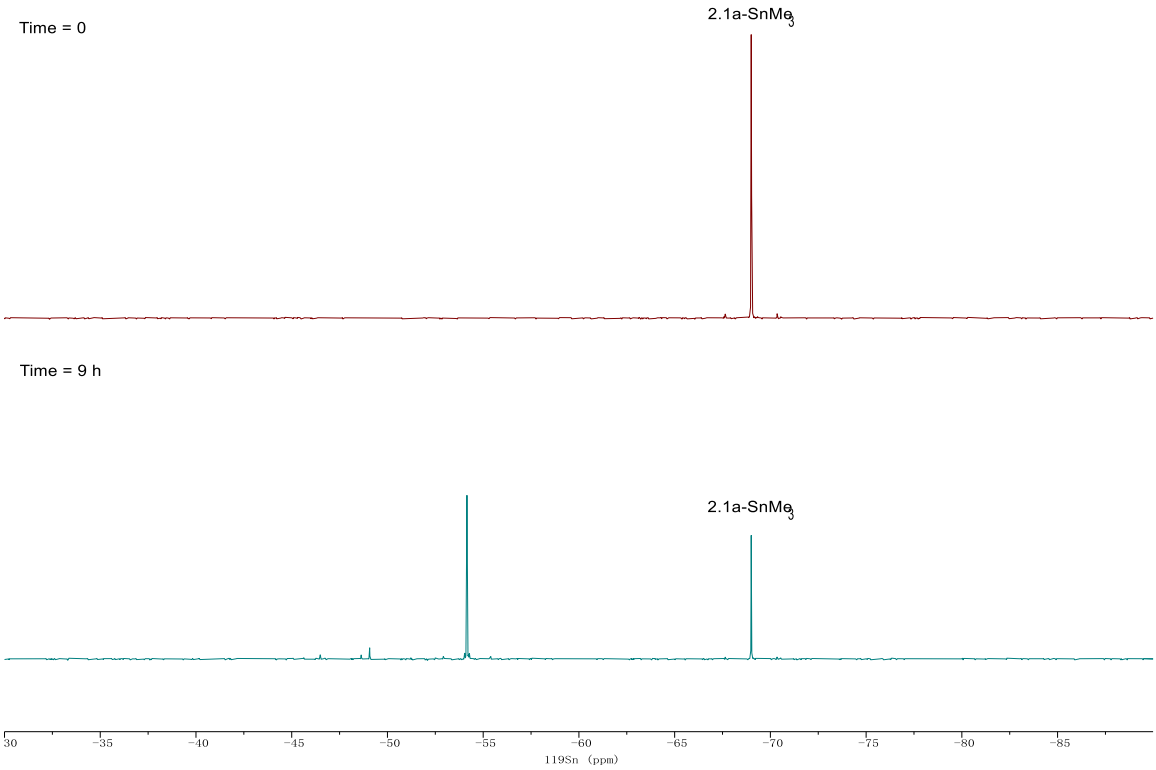

Figure 2.59. $^{119}Sn\{^{1}H\}$ NMR of the reaction of **2.1a-SnMe$_3$** with 1-phenyl-1-propyne at time = 0 (top), time = 9 h (bottom) in $PhCH_3$. *Taken from (top) YC-2020-0006-NoD-Tol-0h-Sn and (bottom) YC-2020-0006-NoD-Tol-9h-Sn.*

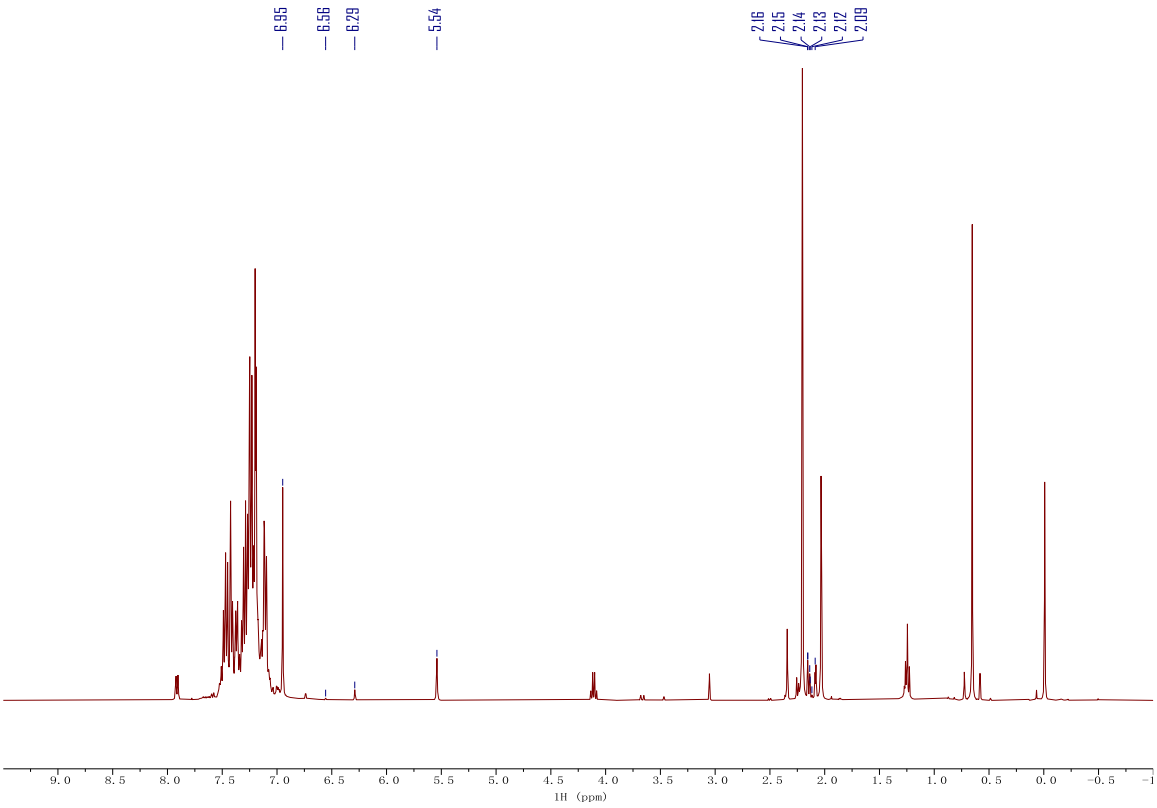

	δ (ppm)	Assignment	# of H	Peak Area	Yield (%)
Ph_3CH	5.54	Ph_3C-H	1	5049.3	n.a.
2.3a	6.95	$H_{pyrrolyl}$	1	13354.3	52.9
2.4a	6.56	$H_{pyrrolyl}$	1	125.2	0.5
2.5a	6.29	$H_{pyrrolyl}$	1	1185.1	4.7
homocoupled **2.2**	2.16, 2.15, 2.14, 2.13 2.12, 2.09	$Me_{pyrrolyl}$ (2 per molecule)	6	7087.7	4.7

Figure 2.60. ^{1}H NMR of the reaction of **2.1a-SnMe$_3$** with 1-phenyl-1-propyne in $CDCl_3$ after HCl workup. *Taken from (top) YC-2020-0006-3-H*

Catalytic Reaction of **2.1b-SnMe$_3$** with 1-phenyl-1-propyne **(Table 2.3)**

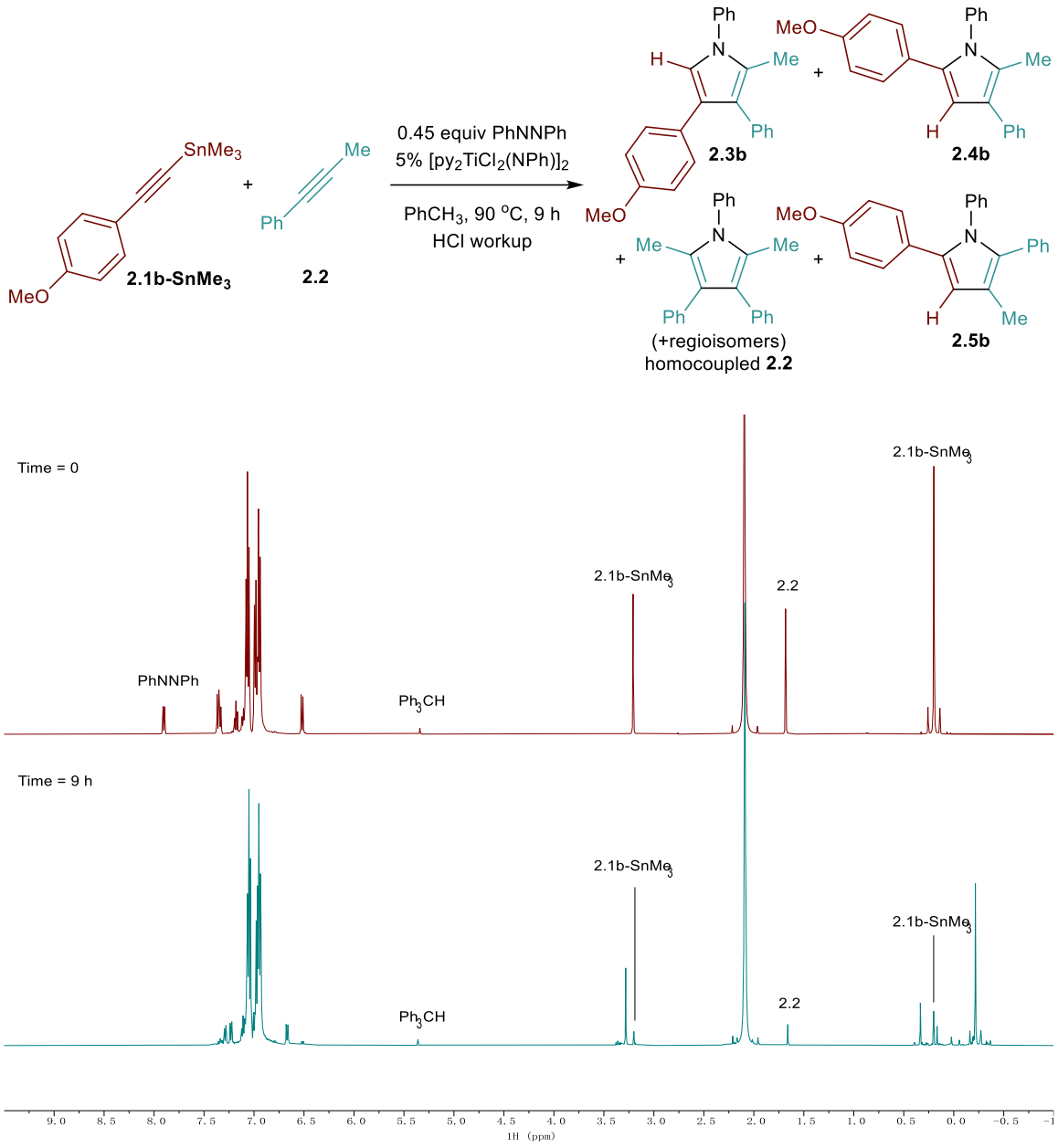

Figure 2.61. No-D ^{1}H NMR of the reaction of **2.1b-SnMe$_3$** with 1-phenyl-1-propyne at time = 0 (top), time = 9 h (bottom) in $PhCH_3$. *Taken from (top) YC-2019-0203-NoD-Tol-0h-H and (bottom) YC-2019-0203-NoD-Tol-9h-H.*

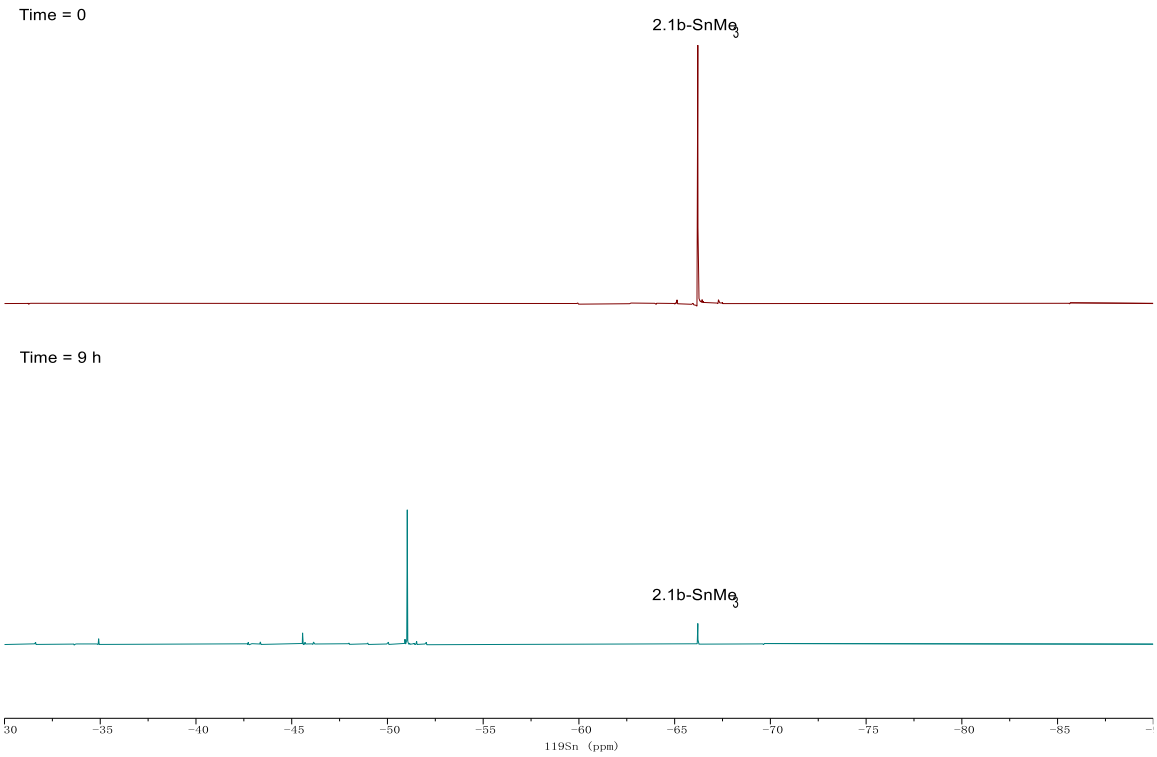

Figure 2.62. $^{119}Sn\{^{1}H\}$ NMR of the reaction of **2.1b-SnMe$_3$** with 1-phenyl-1-propyne at time = 0 (top), time = 9 h (bottom) in $PhCH_3$. *Taken from (top) YC-2019-0203-NoD-Tol-0h-Sn and (bottom) YC-2019-0203-NoD-Tol-9h-Sn.*

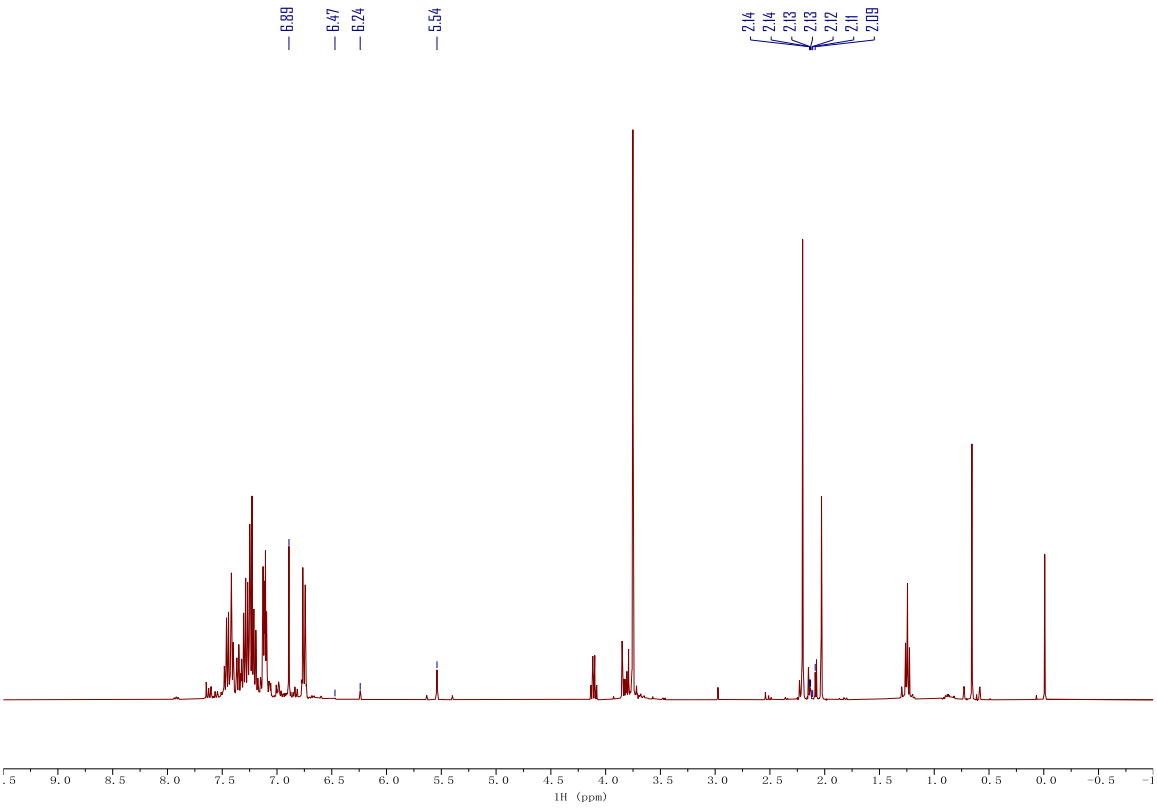

	δ (ppm)	Assignment	# of H	Peak Area	Yield (%)
Ph_3CH	5.54	Ph_3C-H	1	3542.0	n.a.
2.3b	6.89	$H_{pyrrolyl}$	1	9469.0	53.5
2.4b	6.47	$H_{pyrrolyl}$	1	158.8	0.9
2.5b	6.24	$H_{pyrrolyl}$	1	980.0	5.5
homocoupled **2.2**	2.14, 2.14, 2.13, 2.13, 2.12, 2.11, 2.09	$Me_{pyrrolyl}$ (2 per molecule)	6	3861.5	3.6

Figure 2.63. ^{1}H NMR of the reaction of **2.1b-SnMe$_3$** with 1-phenyl-1-propyne in $CDCl_3$ after HCl workup. *Taken from YC-2019-0203-4H.*

Catalytic Reaction of **2.1c-SnMe$_3$** with 1-phenyl-1-propyne **(Table 2.3)**

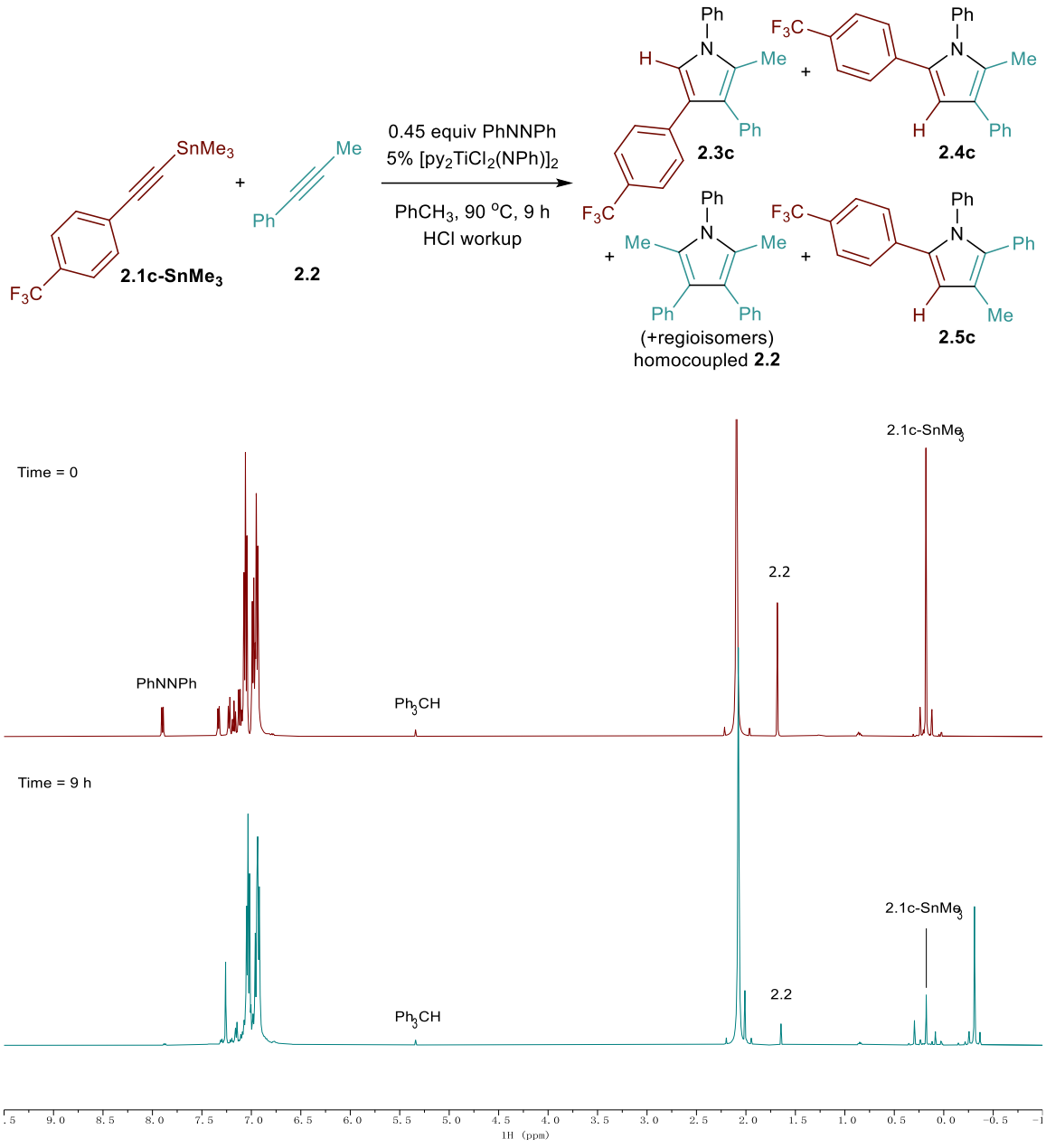

Figure 2.64. No-D ^{1}H NMR of the reaction of **2.1c-SnMe$_3$** with 1-phenyl-1-propyne at time = 0 (top), time = 9 h (bottom) in $PhCH_3$. *Taken from (top) YC-2019-0204-NoD-Tol-0h-H and (bottom) YC-2019-0204-NoD-Tol-9h-H.*

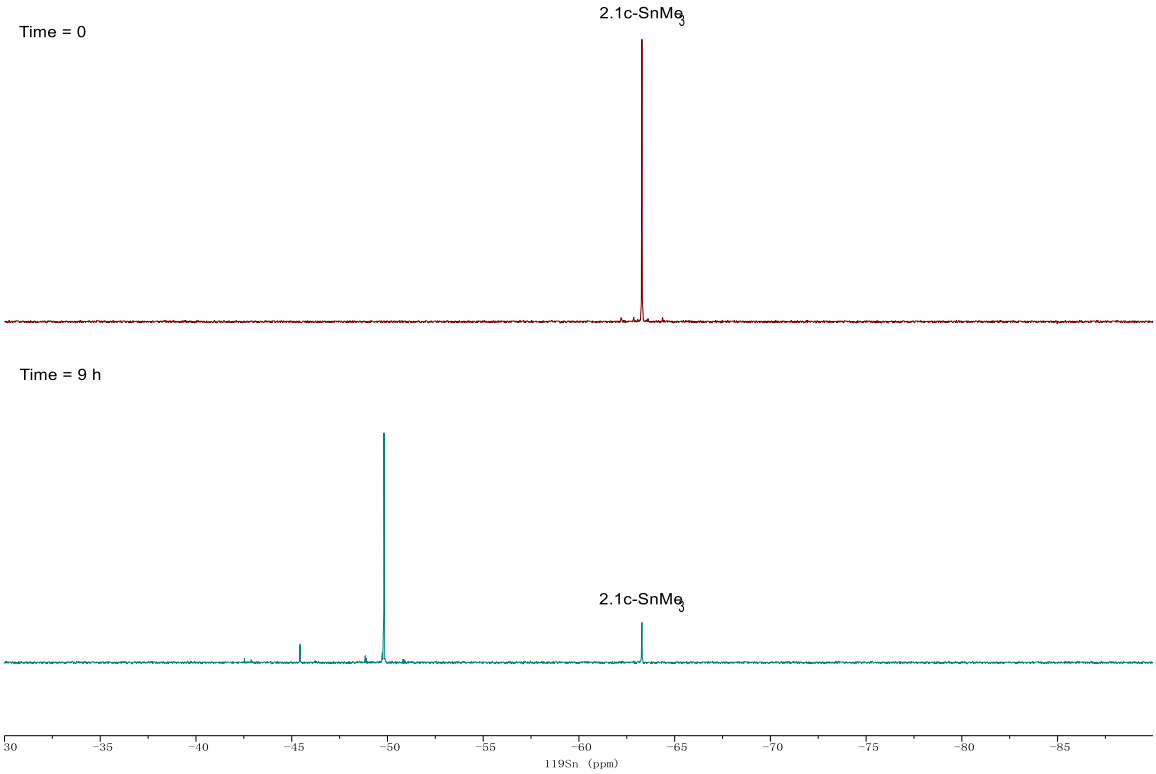

Figure 2.65. $^{119}Sn\{^{1}H\}$ NMR of the reaction of **2.1c-SnMe$_3$** with 1-phenyl-1-propyne at time = 0 (top), time = 9 h (bottom) in $PhCH_3$. *Taken from (top) YC-2019-0204-NoD-Tol-0h-Sn and (bottom) YC-2019-0204-NoD-Tol-9h-Sn.*

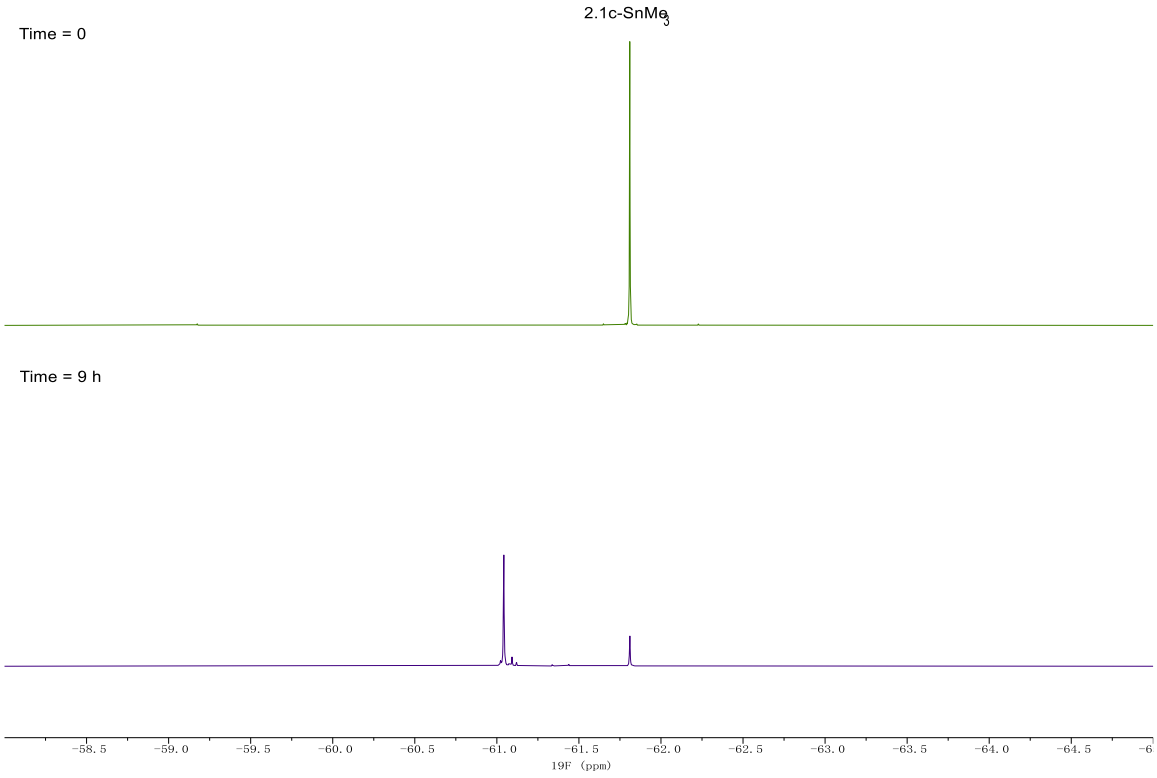

Figure 2.66. $^{19}F\{^{1}H\}$ NMR of the reaction of **2.1c-SnMe$_3$** with 1-phenyl-1-propyne at time = 0 (top), time = 9 h (bottom) in $PhCH_3$. *Taken from (top) YC-2019-0204-NoD-Tol-0h-F and (bottom) YC-2019-0204-NoD-Tol-9h-F.*

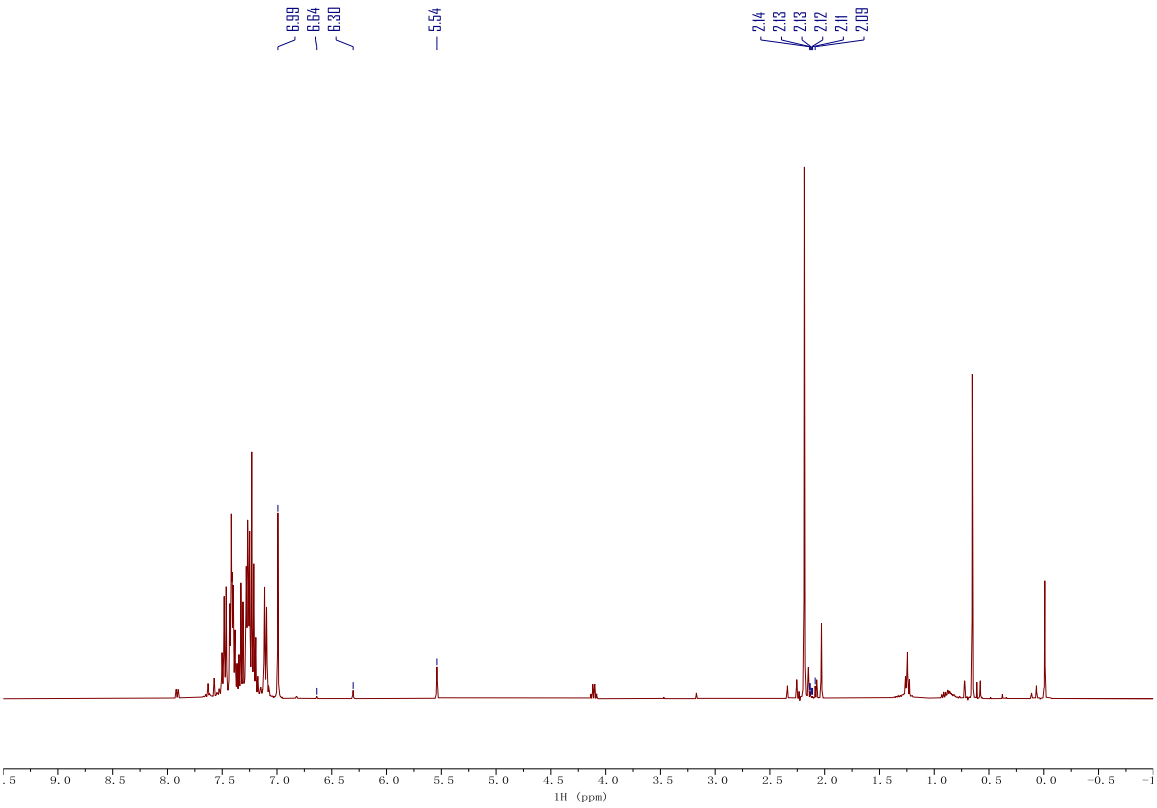

	δ (ppm)	Assignment	# of H	Peak Area	Yield (%)
Ph_3CH	5.54	Ph_3C-H	1	5789.5	n.a.
2.3c	6.99	$H_{pyrrolyl}$	1	17397.6	60.1
2.4c	6.64	$H_{pyrrolyl}$	1	324.5	1.1
2.5c	6.30	$H_{pyrrolyl}$	1	1437.4	5.0
homocoupled **2.2**	2.14, 2.14, 2.13, 2.13, 2.12, 2.11, 2.09	$Me_{pyrrolyl}$ (2 per molecule)	6	3061.2	1.8

Figure 2.67. ^{1}H NMR of the reaction of **2.1c-SnMe$_3$** with 1-phenyl-1-propyne in $CDCl_3$ after HCl workup. *Taken from YC-2019-0204-3H.*

Catalytic Reaction of **2.1d-SnMe$_3$** with 1-phenyl-1-propyne **(Table 2.3)**

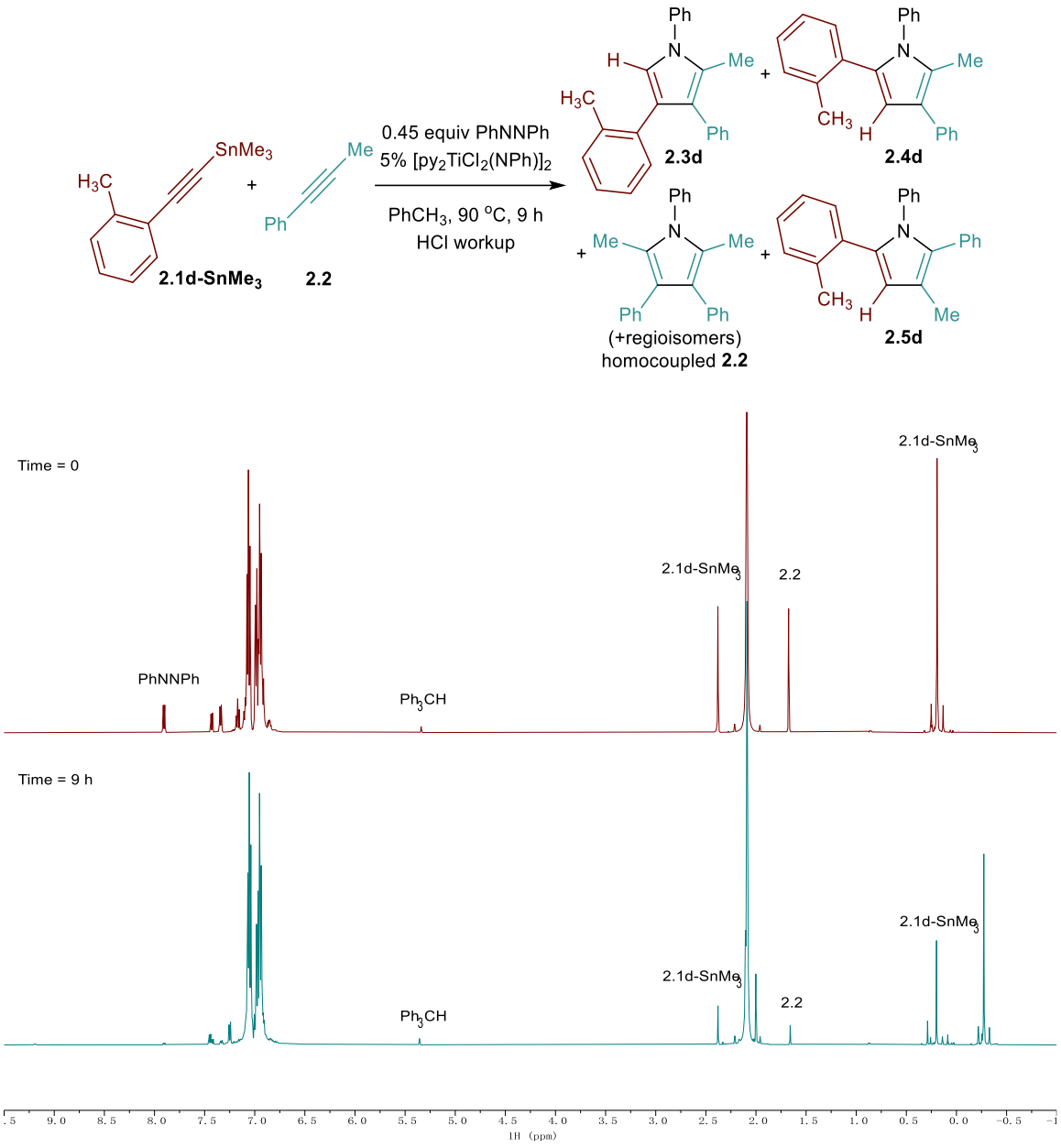

Figure 2.68. No-D ^{1}H NMR of the reaction of **2.1d-SnMe$_3$** with 1-phenyl-1-propyne at time = 0 (top), time = 9 h (bottom) in $PhCH_3$. *Taken from (top) YC-2019-0202-NoD-Tol-0h-H and (bottom) YC-2019-0202-NoD-Tol-9h-H.*

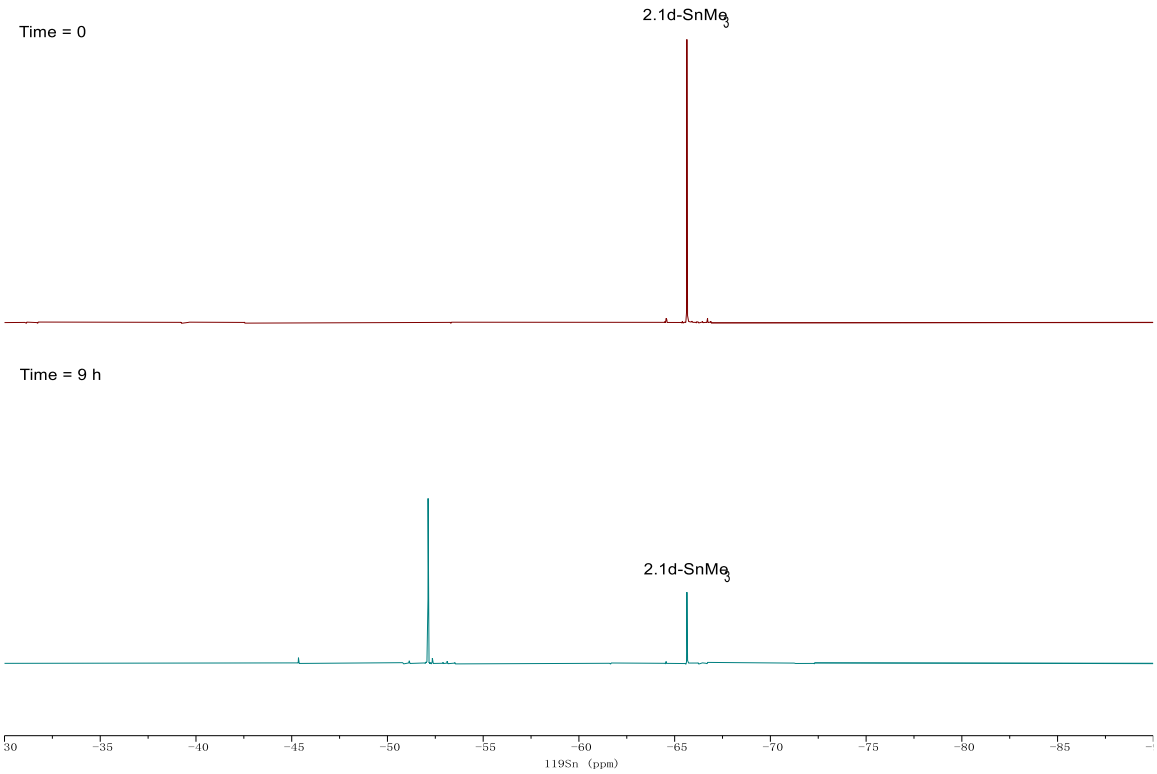

Figure 2.69. $^{119}Sn\{^{1}H\}$ NMR of the reaction of **2.1d-SnMe$_3$** with 1-phenyl-1-propyne at time = 0 (top), time = 9 h (bottom) in $PhCH_3$. *Taken from (top) YC-2019-0202-NoD-Tol-0h-Sn and (bottom) YC-2019-0202-NoD-Tol-9h-Sn.*

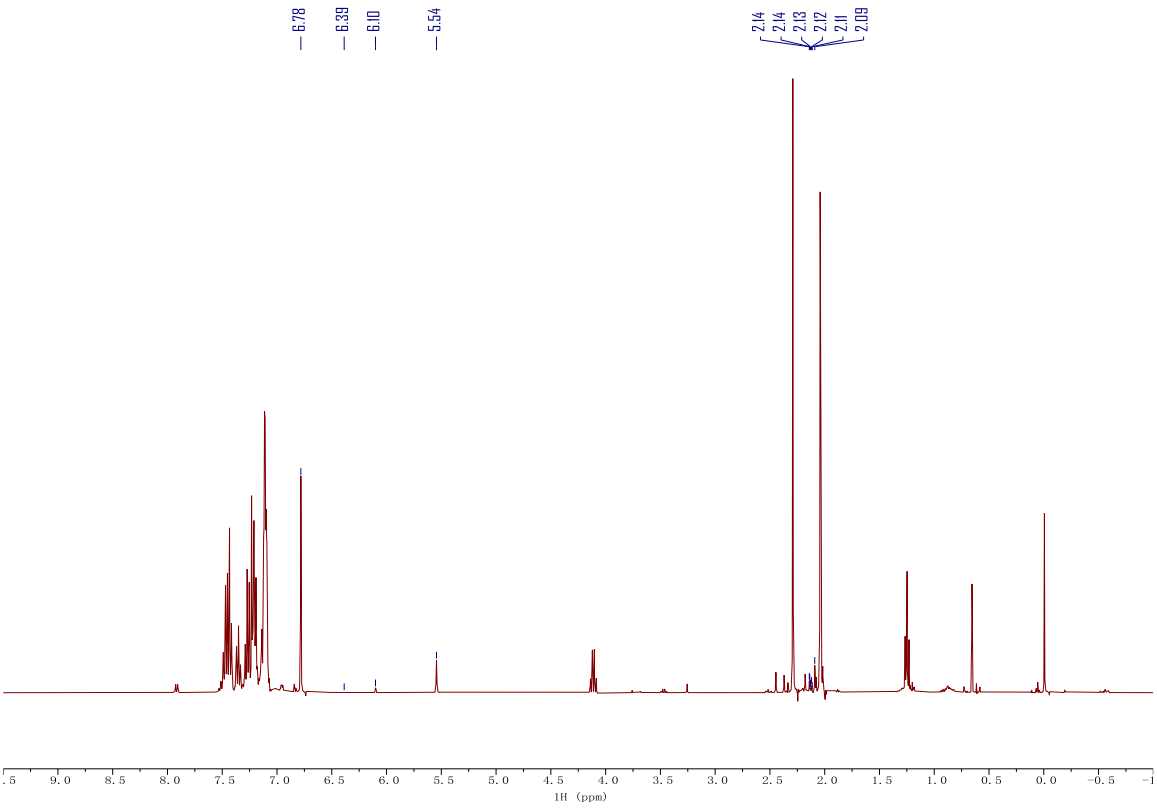

	δ (ppm)	Assignment	# of H	Peak Area	Yield (%)
Ph_3CH	5.54	Ph_3C-H	1	5252.4	n.a.
2.3d	6.78	$H_{pyrrolyl}$	1	17946.9	68.3
2.4d	6.39	$H_{pyrrolyl}$	1	113.0	0.4
2.5d	6.10	$H_{pyrrolyl}$	1	662.8	2.5
homocoupled **2.2**	2.14, 2.14, 2.13, 2.12, 2.11, 2.09	$Me_{pyrrolyl}$ (2 per molecule)	6	4672.7	3.0

Figure 2.70. ^{1}H NMR of the reaction of **2.1d-SnMe$_3$** with 1-phenyl-1-propyne in $CDCl_3$ after HCl workup. *Taken from YC-2019-0202-4H.*

Catalytic Reaction of **2.1f-Sn^{n}Bu$_3$** with 1-phenyl-1-propyne **(Table 2.3)**

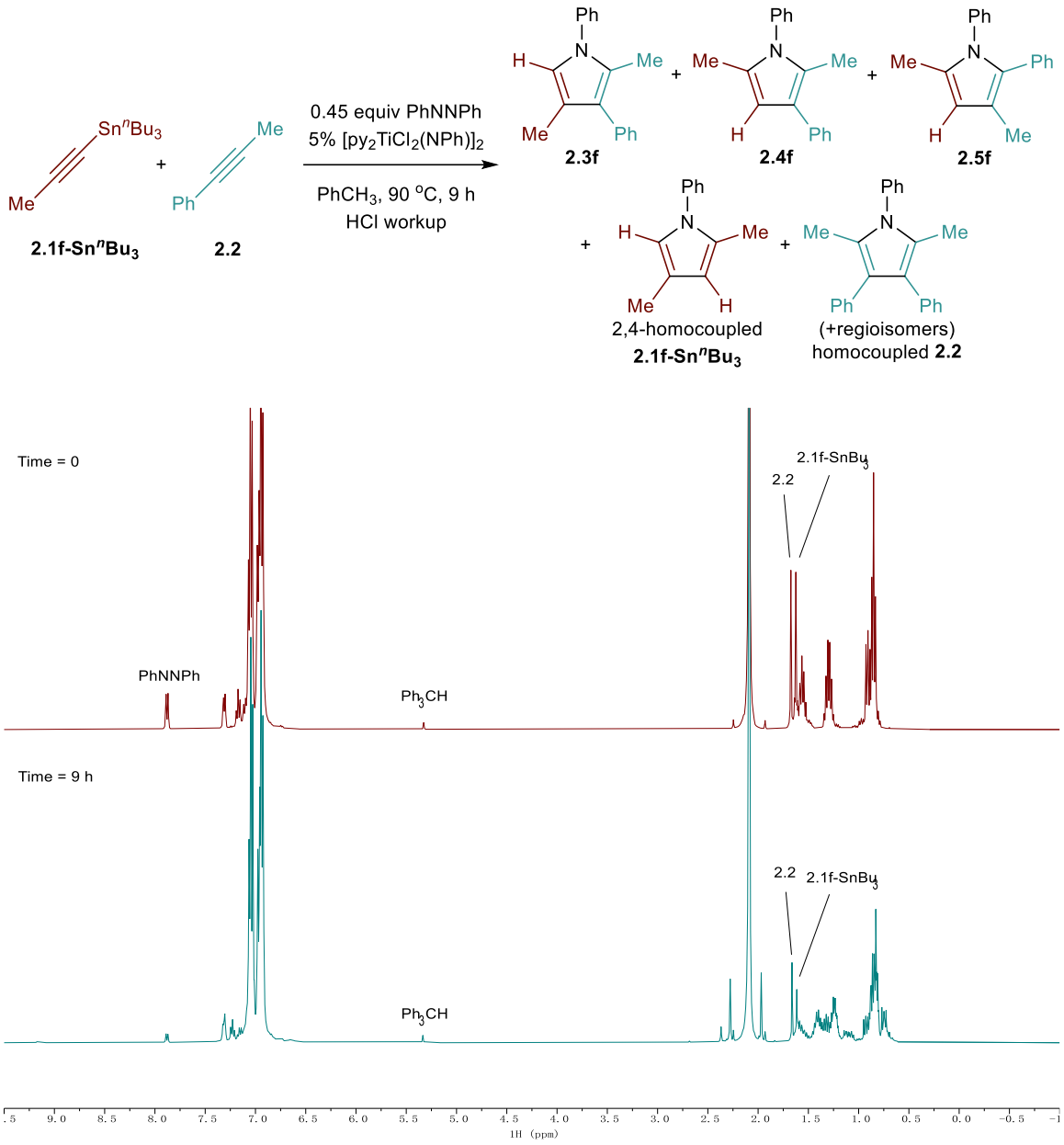

Figure 2.71. No-D ^{1}H NMR of the reaction of **2.1f-Sn^{n}Bu$_3$** with 1-phenyl-1-propyne at time = 0 (top), time = 9 h (bottom) in $PhCH_3$. *Taken from (top) YC-2020-0007-NoD-Tol-0h-H and (bottom) YC-2020-0007-NoD-Tol-9h-H.*

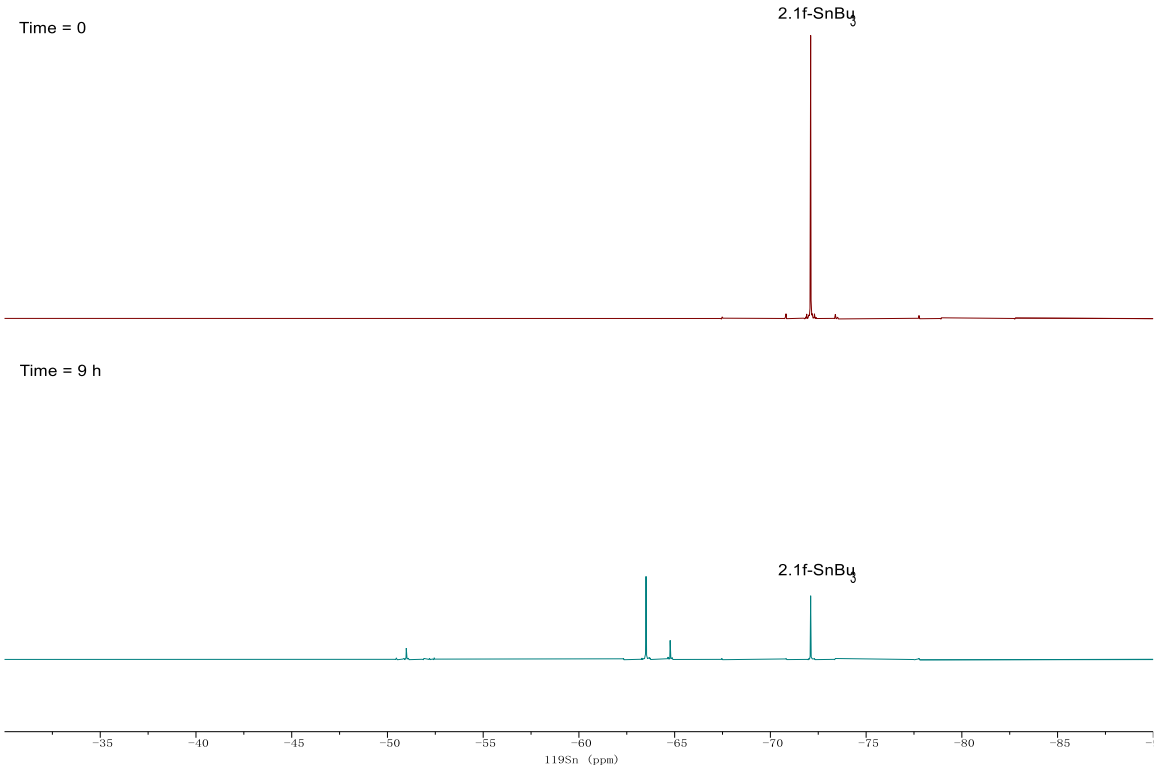

Figure 2.72. $^{119}Sn\{^{1}H\}$ NMR of the reaction of **2.1f-Sn^{n}Bu$_3$** with 1-phenyl-1-propyne at time = 0 (top), time = 9 h (bottom) in $PhCH_3$. *Taken from (top) YC-2020-0007-NoD-Tol-0h-Sn and (bottom) YC-2020-0007-NoD-Tol-9h-Sn.*

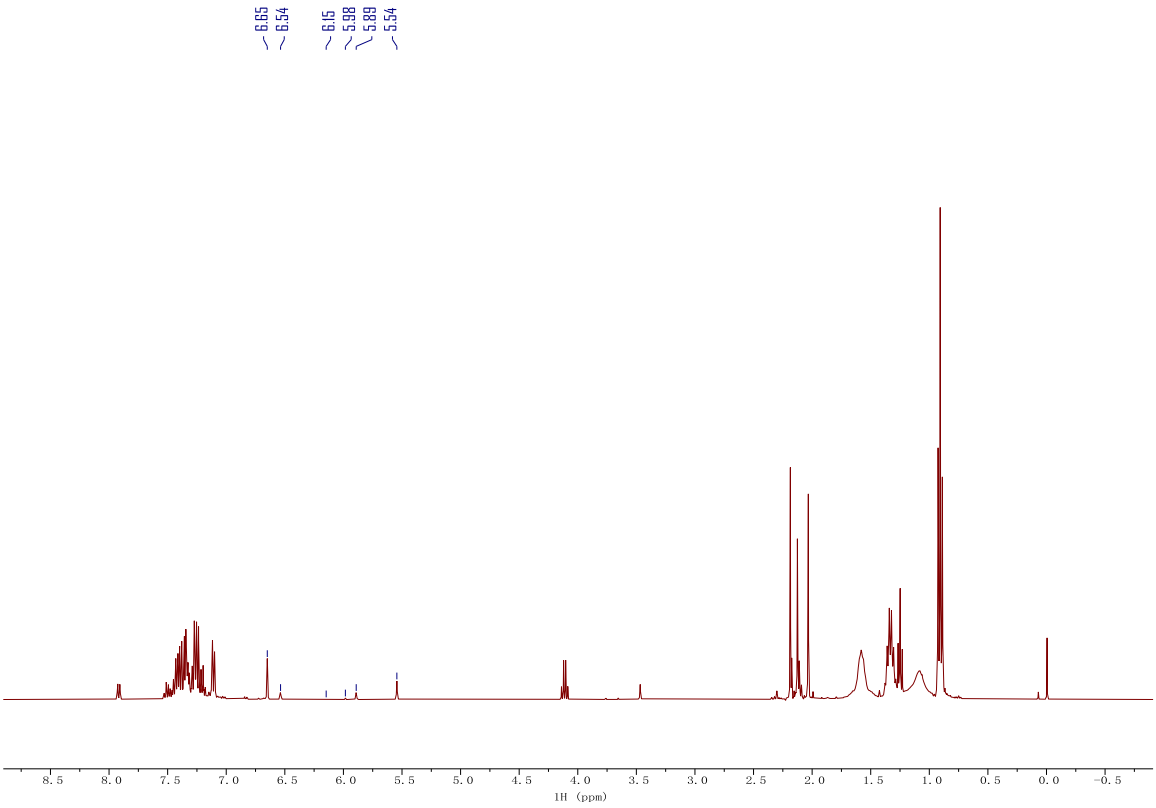

	δ (ppm)	Assignment	# of H	Peak Area	Yield (%)
Ph_3CH	5.54	Ph_3C-H	1	3941.1	n.a.
2.3f	6.65	$H_{pyrrolyl}$	1	8607.3	43.7
2.4f	6.15	$H_{pyrrolyl}$	1	98.0	0.5
2.5f	5.98	$H_{pyrrolyl}$	1	282.9	1.4
2,4-homocoupled **2.1f-Sn^{n}Bu$_3$**	6.54, 5.89	$H_{pyrrolyl}$ (2 per molecule)	2	4117.4	10.4
homocoupled **2.2**	overlap[a]	$Me_{pyrrolyl}$ (2 per molecule)	6	n.d.	n.d.

[a]Peaks overlapped with the $Me_{pyrrolyl}$ peaks of **2.4f**, **2.4f'** and 2,4-homocoupled of **2.1f-Sn^{n}Bu$_3$**.

Figure 2.73. ^{1}H NMR of the reaction of **2.1f-Sn^{n}Bu$_3$** with 1-phenyl-1-propyne in $CDCl_3$ after HCl workup. *Taken from YC-2020-0007-5H.*

2.5.7 L Donor Effect Study

Reaction with No Pyridine (Figure 2.3A)

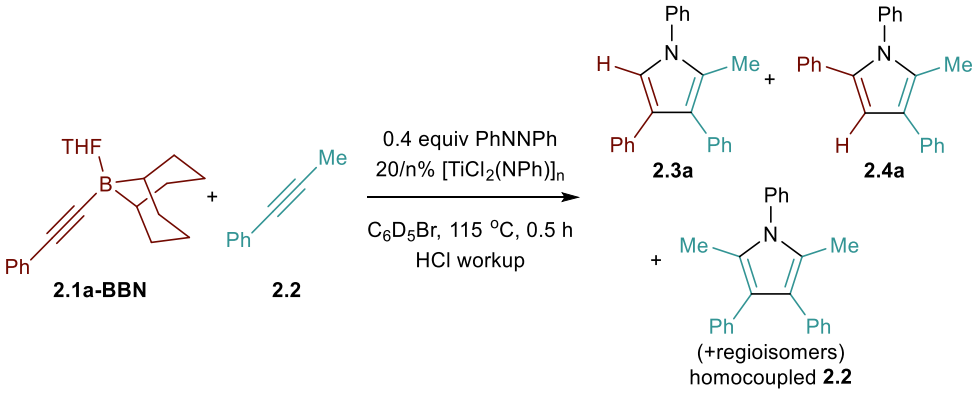

The reaction was performed following **Procedure 2.B** using $[TiCl_2(NPh)]_n$ (4.2 mg, 0.02 mmol, absolute quantity of titanium, 0.2 equiv) as catalyst instead of $[py_2TiCl_2(NPh)]_2$.

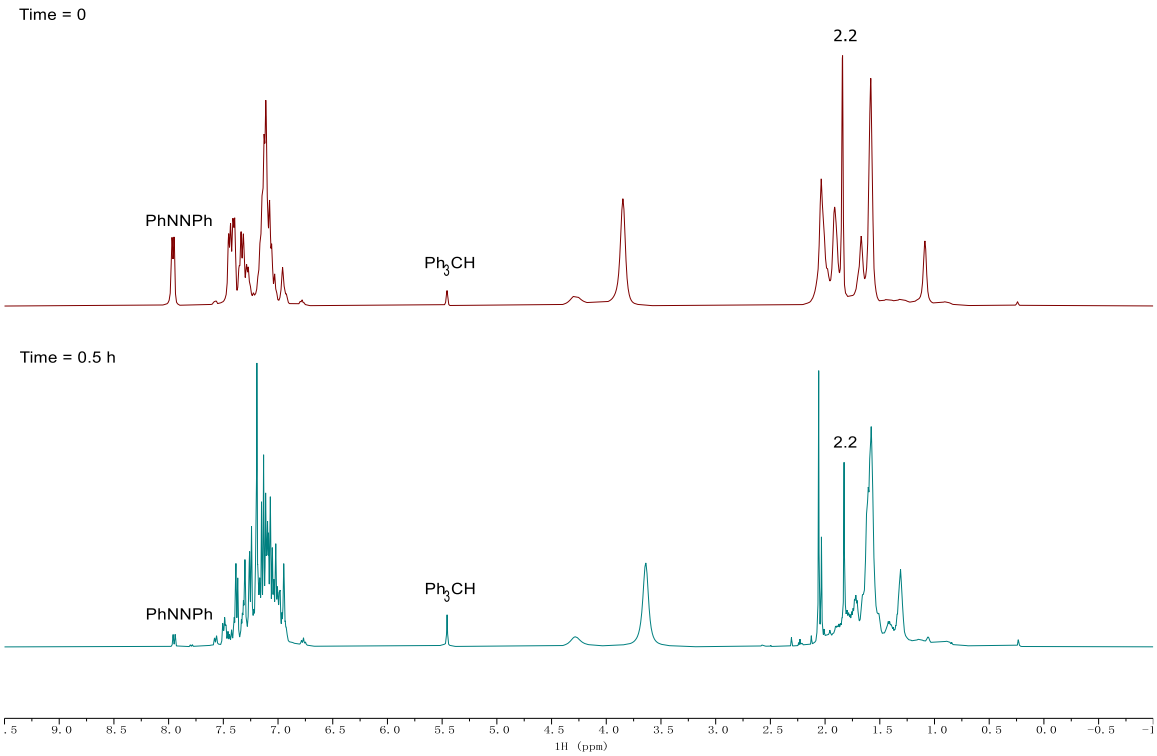

Figure 2.74. ^1H NMR of the reaction using $[TiCl_2(NPh)]_n$ at time = 0 (top), time = 0.5 h (bottom) in C_6D_5Br. *Taken from (top) YC-2019-0192-0h-H and (bottom) YC-2019-0192-30min-H.*

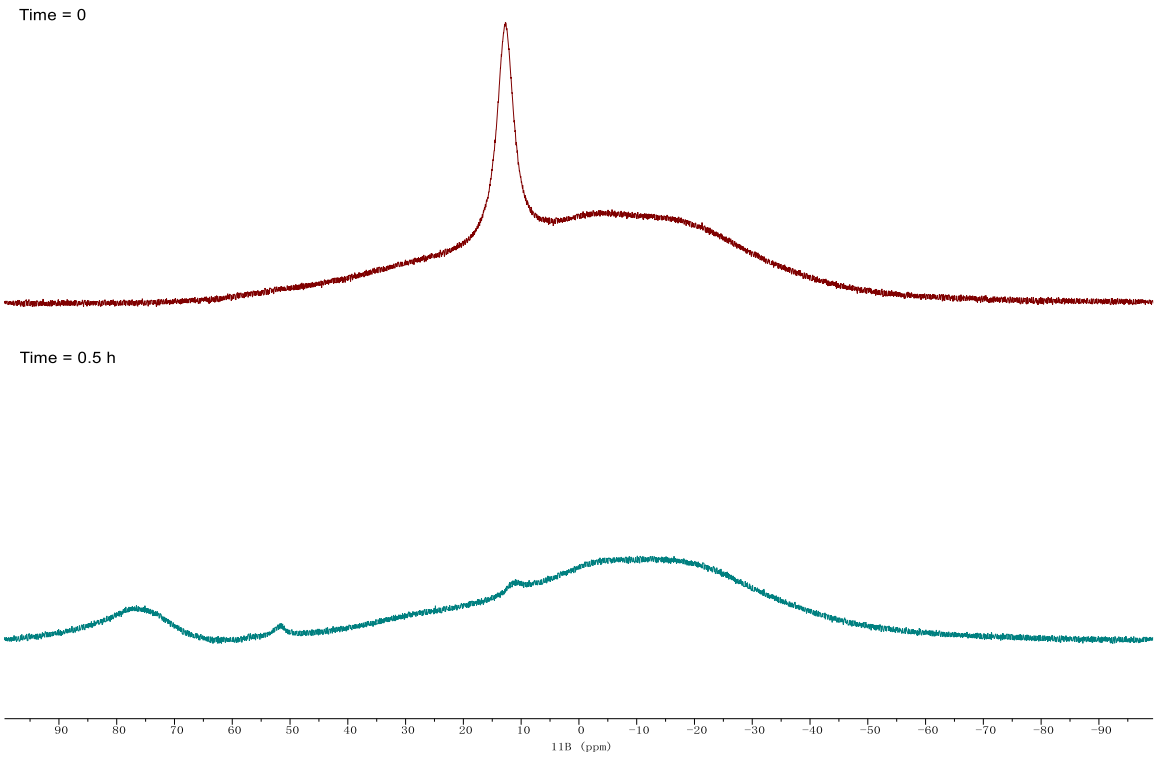

Figure 2.75. ^{11}B NMR of the reaction using $[TiCl_2(NPh)]_n$ at time = 0 (top), time = 0.5 h (bottom) in C_6D_5Br. *Taken from (top) YC-2019-0192-0h-B and (bottom) YC-2019-0192-30min-B.*

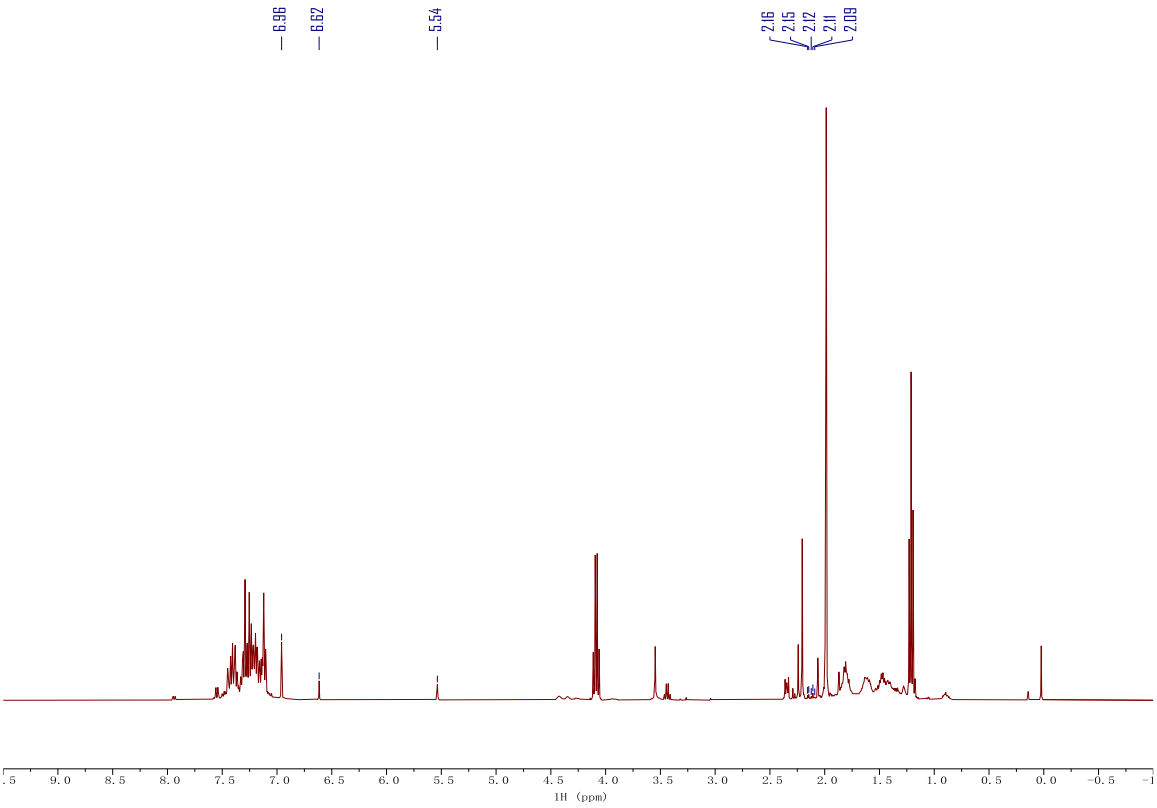

	δ (ppm)	Assignment	# of H	Peak Area	Yield (%)
Ph_3CH	5.54	Ph_3C-H	1	2708.9	n.a.
2.3a	6.96	$H_{pyrrolyl}$	1	4589.7	33.9
2.4a	6.62	$H_{pyrrolyl}$	1	1765.2	13.0
homocoupled **2.2**	2.16, 2.15, 2.12, 2.11, 2.09	$Me_{pyrrolyl}$ (2 per molecule)	6	3603.2	4.4

Figure 2.76. ^1H NMR of the reaction using $[TiCl_2(NPh)]_n$ in $CDCl_3$ after HCl workup. *Taken from YC-2019-0192-3H.*

Reaction with Excess *B*-phenylethynyl-9-BBN as Pyridine Scavenger (Figure 2.3B)

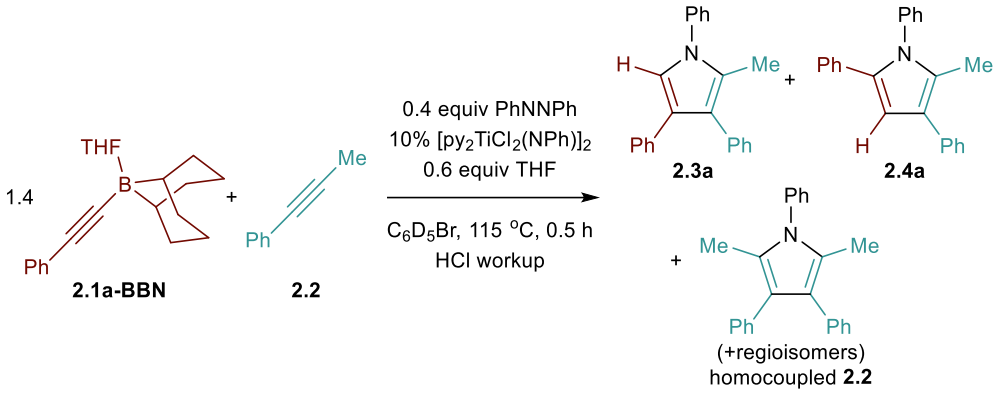

The reaction was performed following **Procedure 2.B** with higher **2.1a-BBN** (41.2 mg, 0.14 mmol, 1.4 equiv) loading and THF (4.3 mg, 0.06 mmol, 0.6 equiv) as additive.

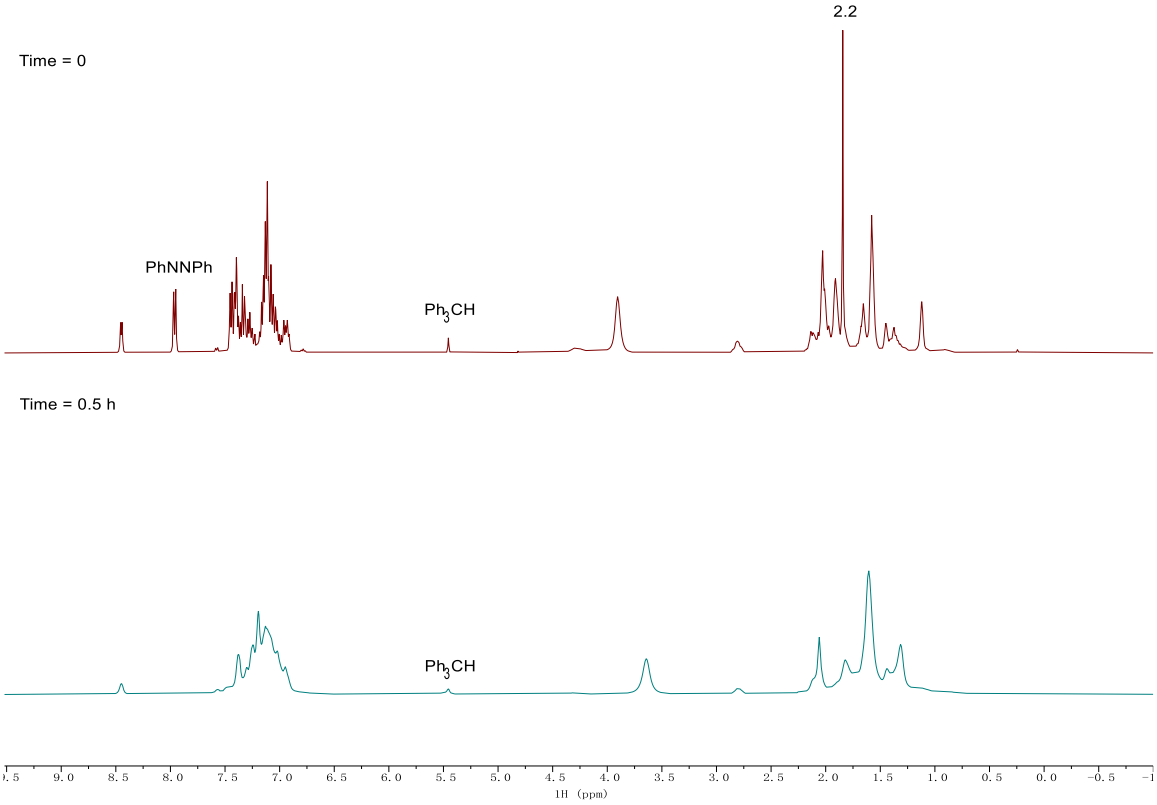

Figure 2.77. ^{1}H NMR of the reaction with excess **2.1a-BBN** at time = 0 (top), time = 0.5 h (bottom) in C_6D_5Br. *Taken from (top) YC-2019-0193-0h-H and (bottom) YC-2019-0193-30min-H.*

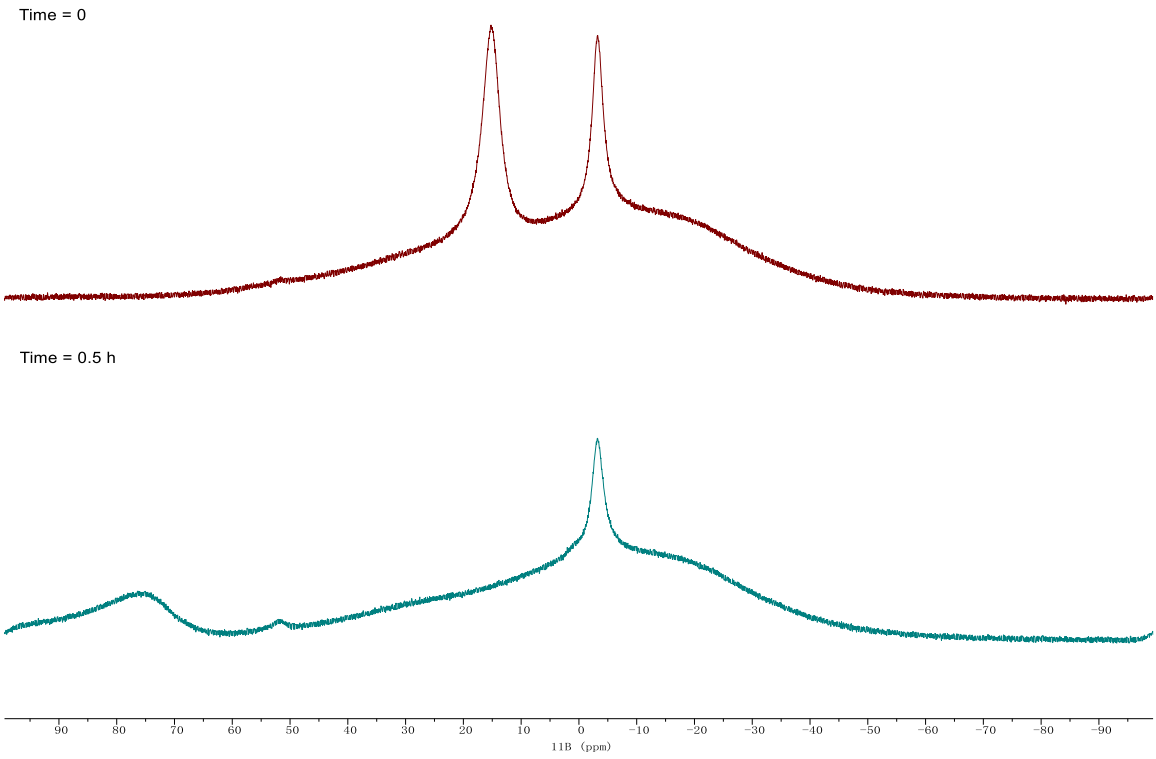

Figure 2.78. ^{11}B NMR of the reaction with excess **2.1a-BBN** at time = 0 (top), time = 0.5 h (bottom) in C_6D_5Br. *Taken from (top) YC-2019-0193-0h-B and (bottom) YC-2019-0193-30min-B.*

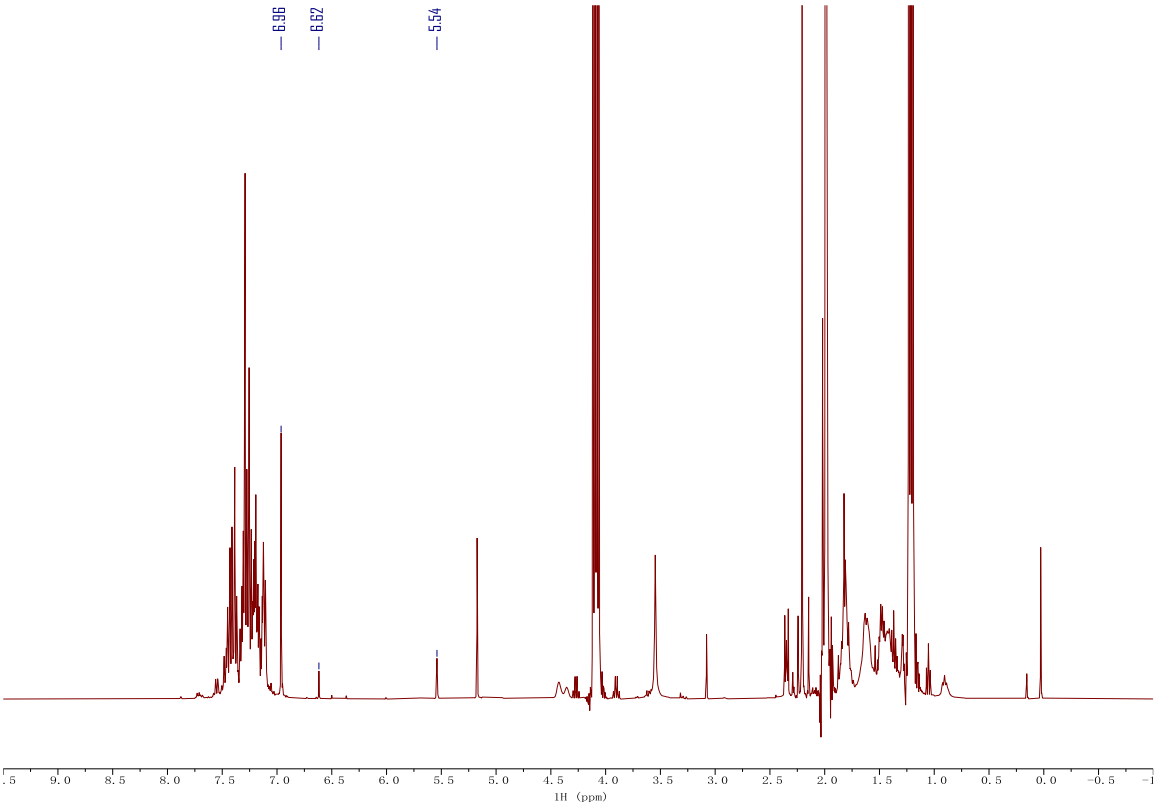

	δ (ppm)	Assignment	# of H	Peak Area	Yield (%)
Ph_3CH	5.54	Ph_3C-H	1	1342.0	n.a.
2.3a	6.96	$H_{pyrrolyl}$	1	3910.8	58.3
2.4a	6.62	$H_{pyrrolyl}$	1	444.7	6.6
homocoupled **2.2**	not found	$Me_{pyrrolyl}$ (2 per molecule)	6	n.a.	n.d.

Figure 2.79. ^{1}H NMR of the reaction with excess **2.1a-BBN** in $CDCl_3$ after HCl workup. *Taken from YC-2019-0193-3H.*

Reaction with Pyridine-Adduct of *B*-phenylethynyl-9-BBN (Figure 2.3C)

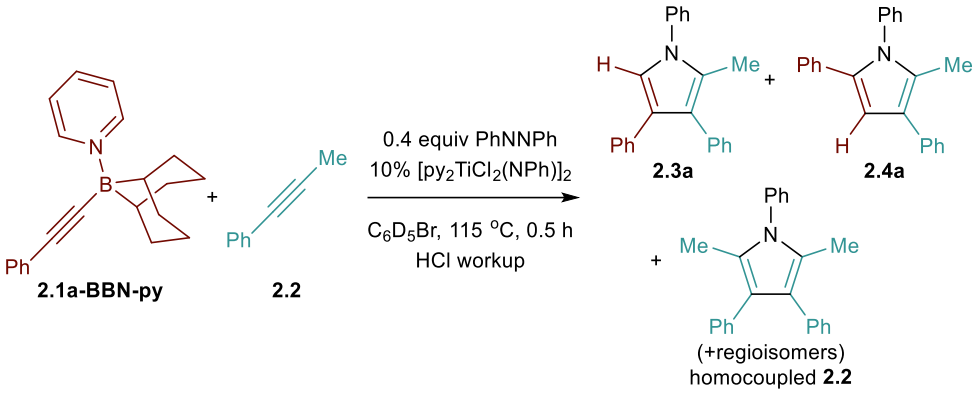

The reaction was performed following **Procedure 2.B** using **2.1a-BBN-py** (30.1 mg, 0.1 mmol, 1 equiv) as heterocoupling partner instead of **2.1a-BBN**.

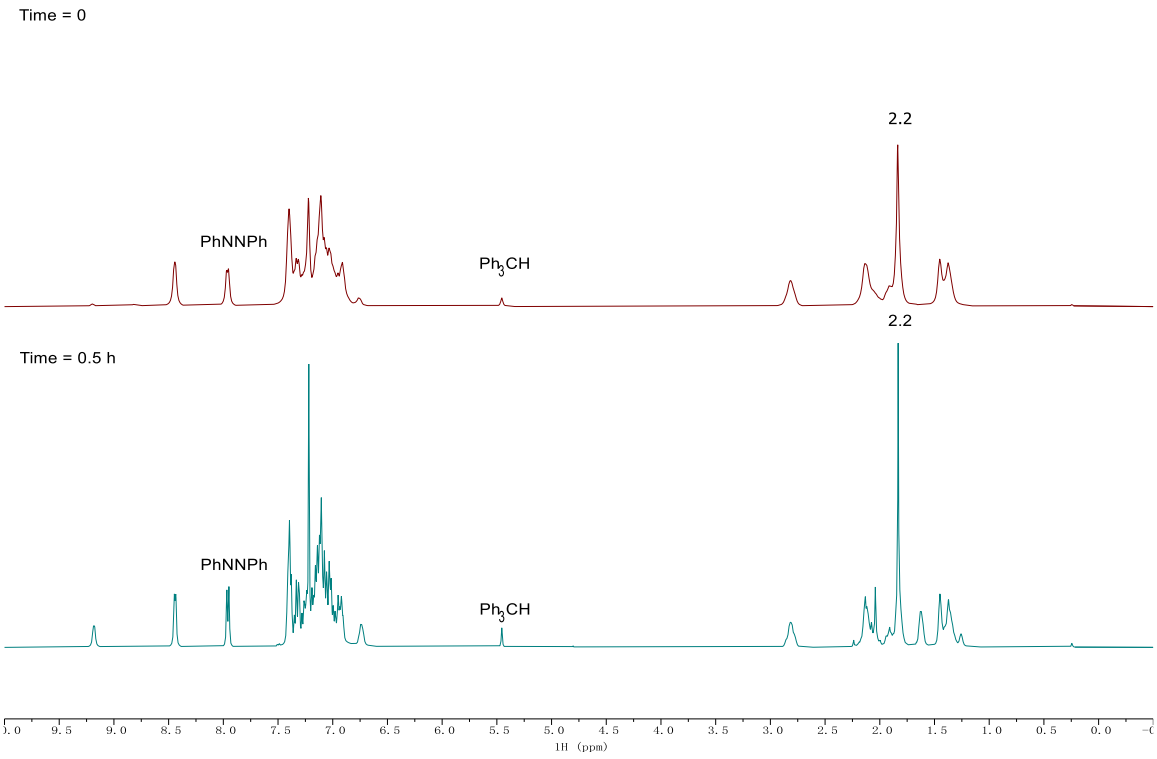

Figure 2.80. ^{1}H NMR of the reaction of **2.1a-BBN-py** at time = 0 (top), time = 0.5 h (bottom) in C_6D_5Br. *Taken from (top) YC-2020-0009-0h-H and (bottom) YC-2020-0009-30min-H.*

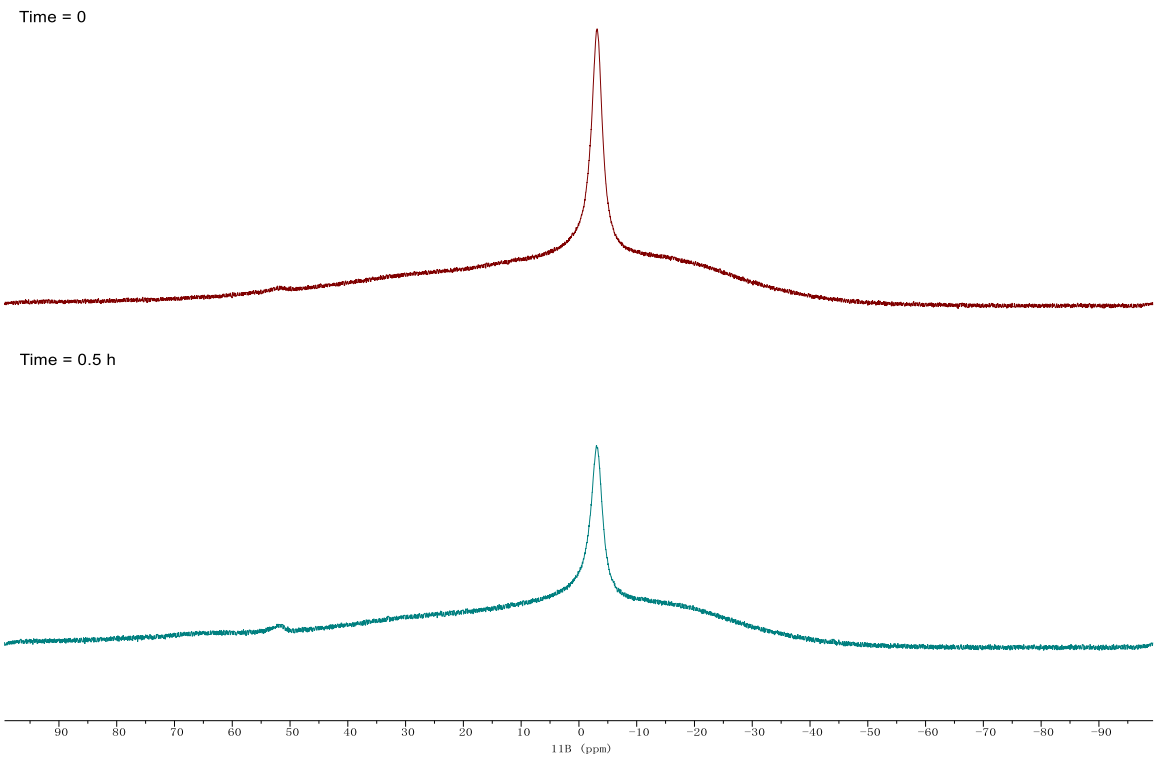

Figure 2.81. ^{11}B NMR of the reaction of **2.1a-BBN-py** at time = 0 (top), time = 0.5 h (bottom) in C_6D_5Br. *Taken from (top) YC-2020-0009-0h-B and (bottom) YC-2020-0009-30min-B.*

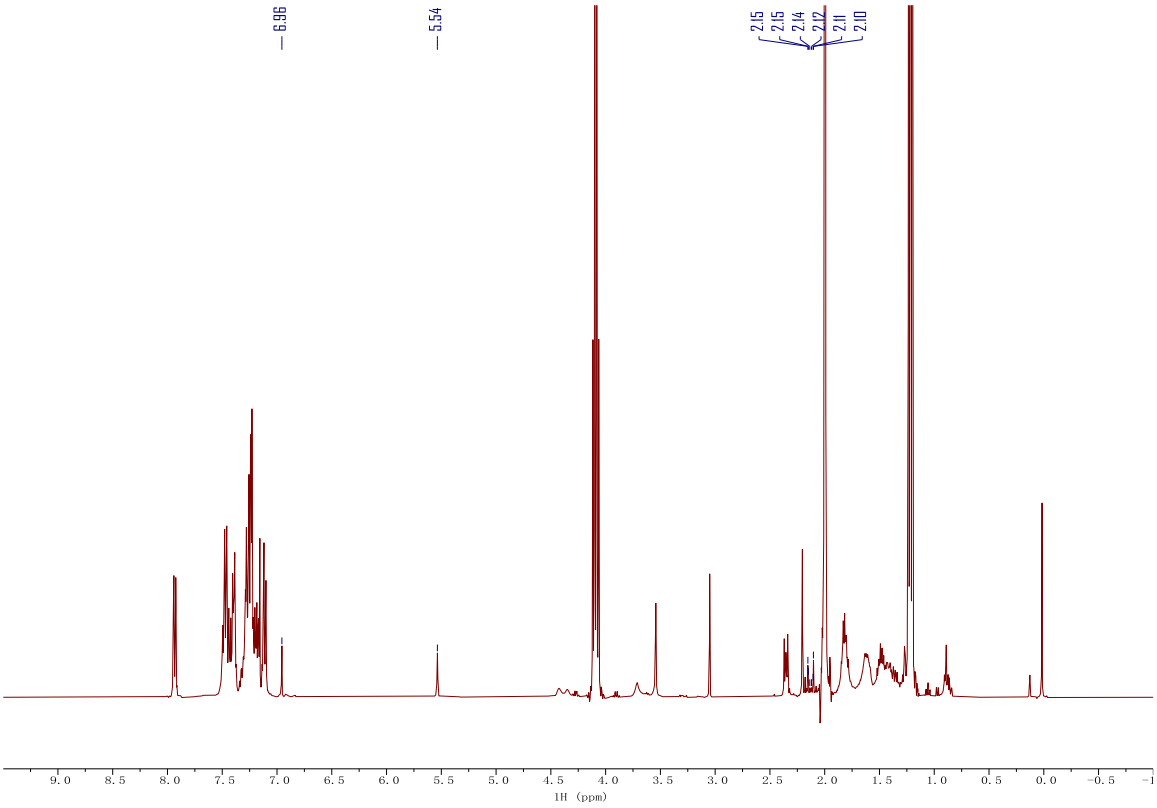

	δ (ppm)	Assignment	# of H	Peak Area	Yield (%)
Ph_3CH	5.54	Ph_3C-H	1	2978.9	n.a.
2.3a	6.96	$H_{pyrrolyl}$	1	1654.2	11.1
2.4a	not found	$H_{pyrrolyl}$	1	n.a.	n.d.
homocoupled **2.2**	2.15, 2.15, 2.14, 2.12, 2.11, 2.10	$Me_{pyrrolyl}$ (2 per molecule)	6	2281.8	2.6

Figure 2.82. ^{1}H NMR of the reaction of **2.1a-BBN-py** in $CDCl_3$ after HCl workup. *Taken from YC-2020-0009-3H.*

2.5.8 Directing Group Strength Comparisons

Comparison Between TMS and 9-BBN (Figure 2.5, Top)

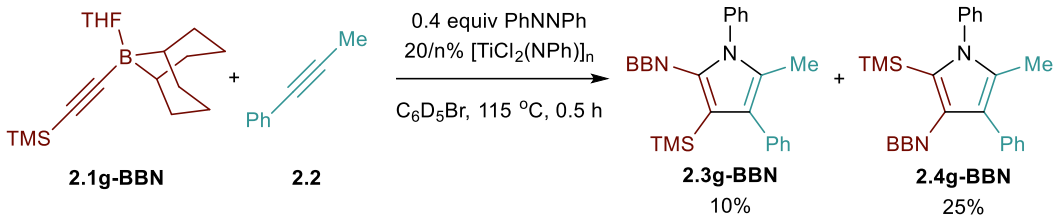

The reaction of **2.1g-BBN** was performed following **Procedure 2.B** using $[TiCl_2(NPh)]_2$ as catalyst (4.2 mg, 0.02 mmol, absolute quantity of titanium, 0.2 equiv) as catalyst instead of $[py_2TiCl_2(NPh)]_2$, and the reaction was not quenched by the HCl workup. Instead the NMR tube was transferred into the glovebox after heating and taking t = 0.5 h NMR spectra. C_6D_6 (0.5 mL) was added to the reaction mixture, and the NMR tube was re-sealed and taken out of the glovebox. The reaction mixture was then characterized by ^1H NMR, ^1H–^{15}N HMBC and NOESY. **2.4g-BBN** was found to be the major product.

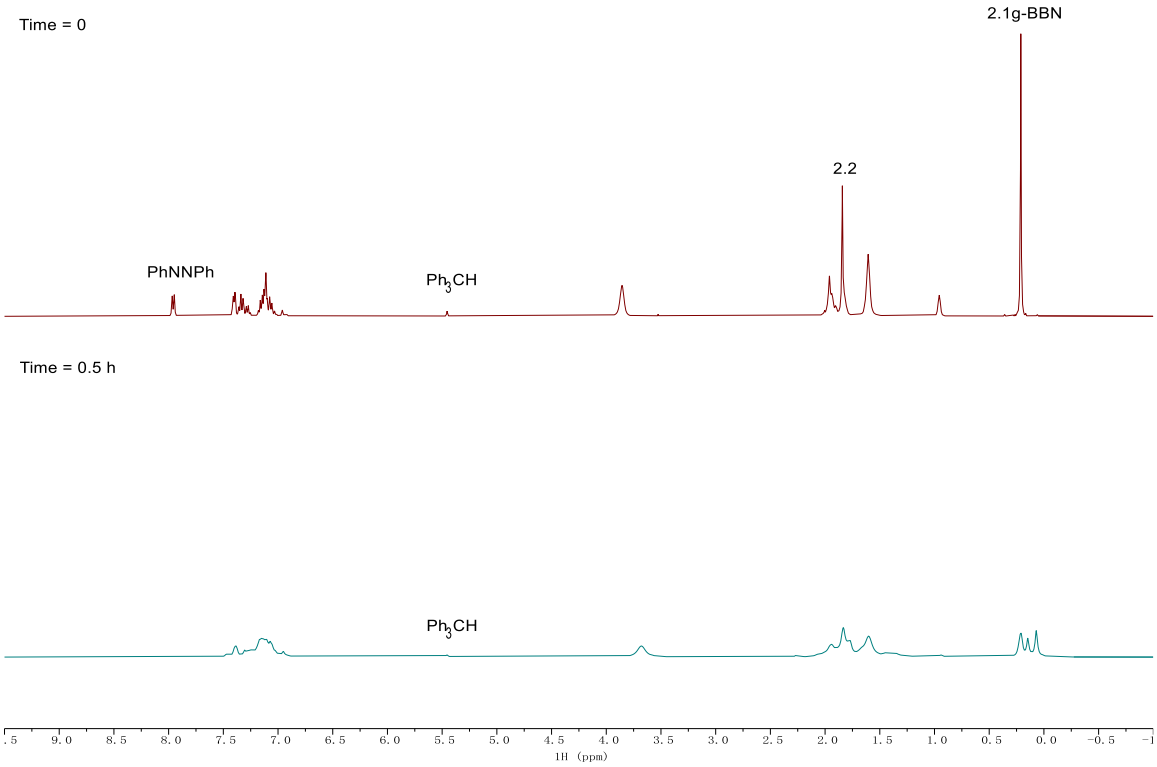

Figure 2.83. ^1H NMR in C_6D_5Br of the reaction of **2.1g-BBN** at time = 0 (top), time = 0.5 h (bottom). *Taken from (top) YC-2019-0197-0h-H and (bottom) YC-2019-0197-30min-H.*

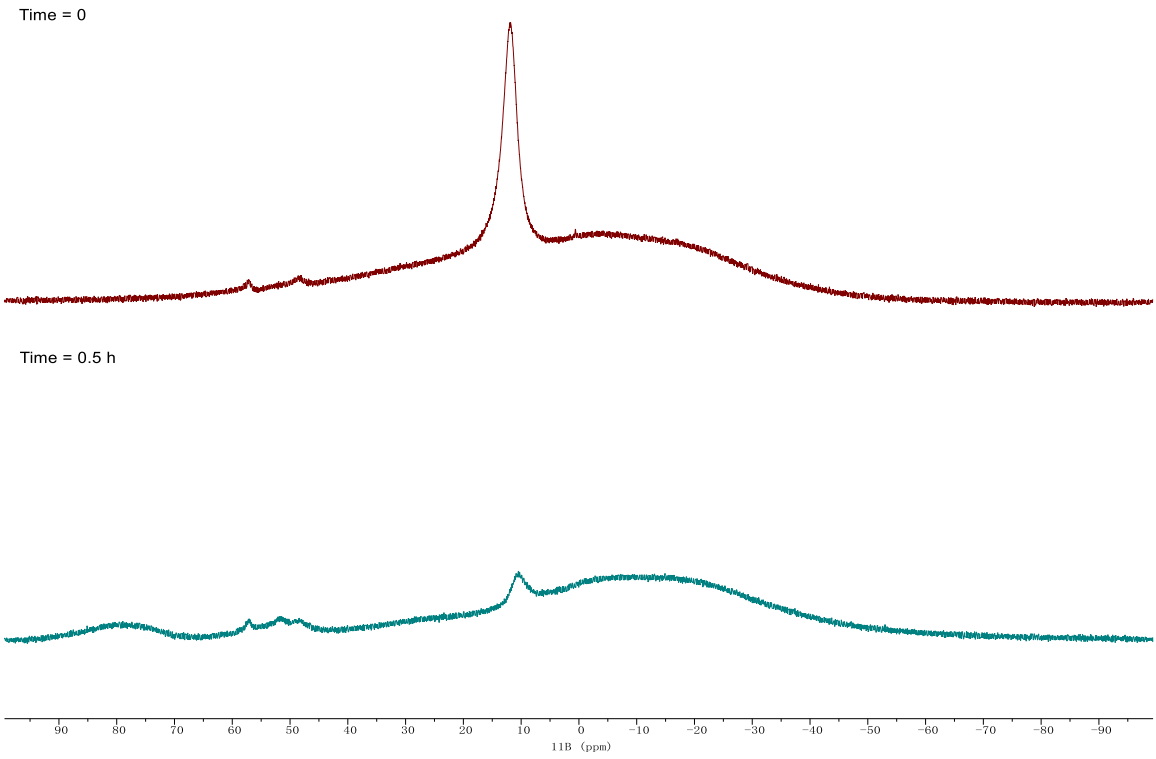

Figure 2.84. ^{11}B NMR in C_6D_5Br of the reaction of **2.1g-BBN** at time = 0 (top), time = 0.5 h (bottom). *Taken from (top) YC-2019-0197-0h-B and (bottom) YC-2019-0197-30min-B.*

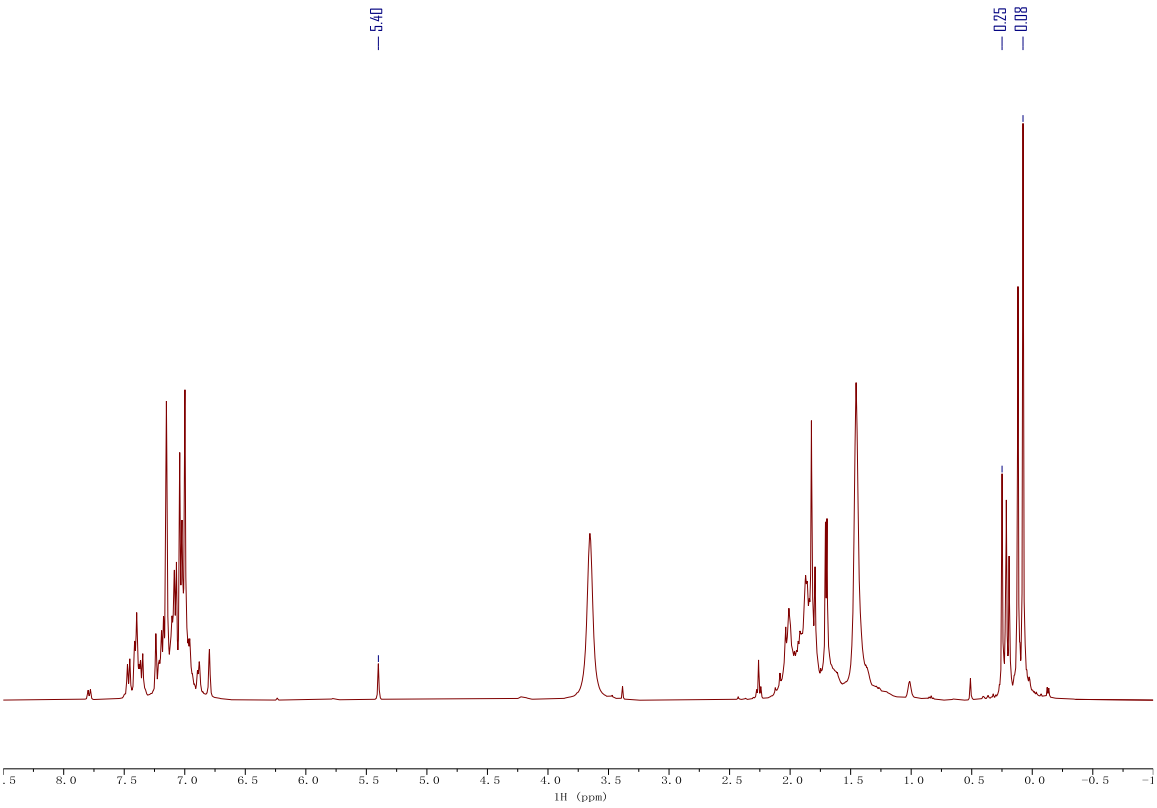

	δ (ppm)	Assignment	# of H	Peak Area	Yield (%)
Ph_3CH	5.40	Ph_3C-H	1	2637.0	n.a.
2.3g-BBN	0.25	$TMS_{pyrrolyl}$	9	11494.0	9.7
2.4g-BBN	0.08	$TMS_{pyrrolyl}$	9	30159.4	25.4

Figure 2.85. ^1H NMR of the reaction product mixture of **2.1g-BBN** in C_6D_5Br/C_6D_6 (1:1, v/v). Chemical shifts were referenced to the proton signal of the internal standard triphenylmethane (Ph_3CH, s, 5.40 ppm). *Taken from YC-2019-0199-5-H_C6D6.*

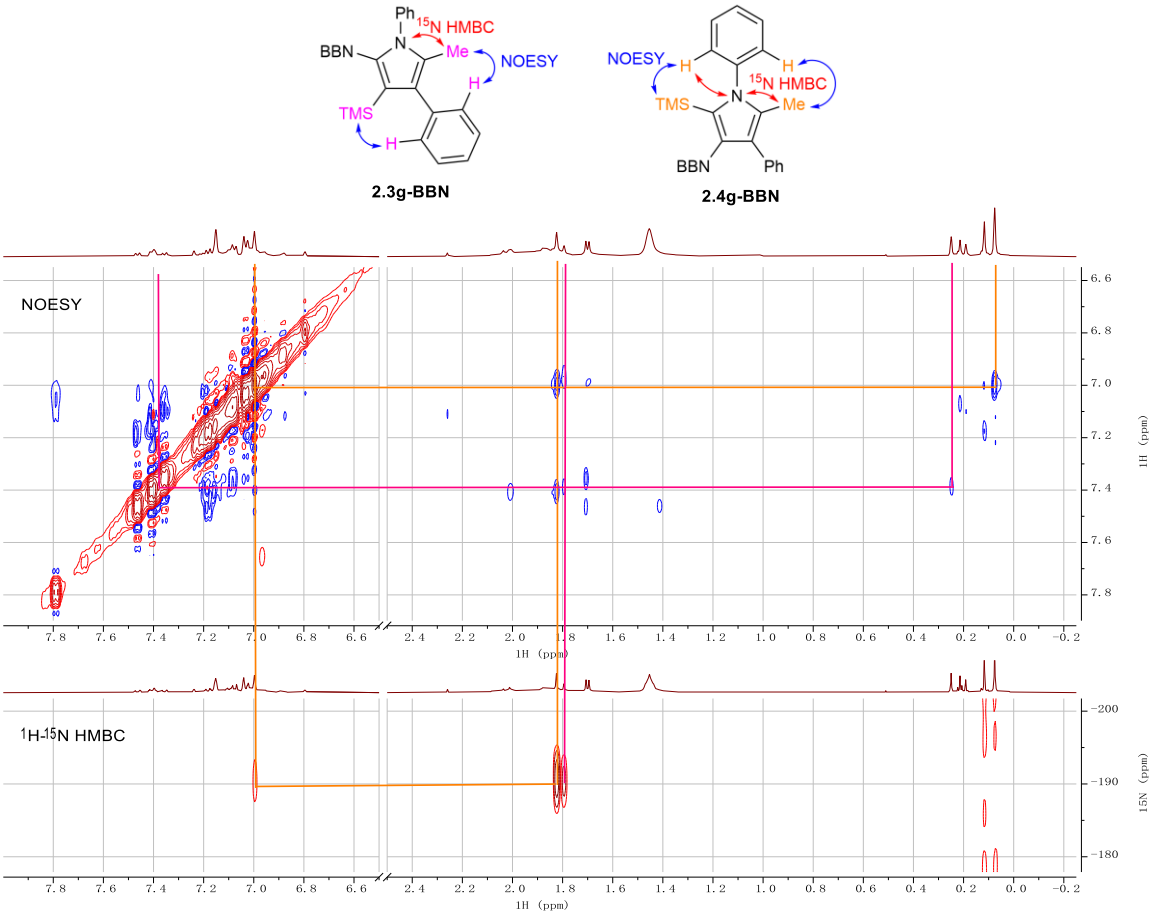

Figure 2.86. NOESY (top) and ^{1}H–^{15}N HMBC (bottom) NMR spectra of the reaction product mixture of **2.1g-BBN** in C_6D_5Br/C_6D_6 (1:1, v/v). *Taken from (top) YC-2019-0199-6-NOESY and (bottom) YC-2019-0199-7-NHMBC.*

Comparison Between TMS and Sn^{n}Bu$_3$ (Figure 2.5, Bottom)

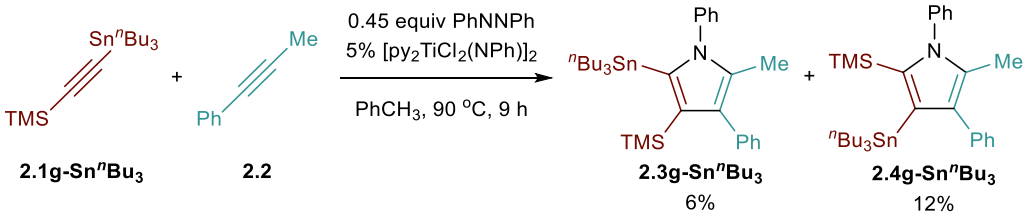

2.1g-Sn^{n}Bu$_3$ **2.2** **2.3g-Sn^{n}Bu$_3$** 6% **2.4g-Sn^{n}Bu$_3$** 12%

The reaction of **2.1g-Sn^{n}Bu$_3$** was performed following **Procedure 2.C** without being quenched by the HCl workup. Instead, the NMR tube was transferred into the glovebox after heating and taking t = 0.5 h NMR spectra. The reaction was diluted with toluene, filtered and evaporated

under vacuum. The crude mixture was dissolved in CD_2Cl_2 and characterized by ^1H NMR and NOESY. The solution was then extracted by EtOAc/H_2O, during which the TMS moiety was hydrolyzed while the Sn^nBu_3 moiety remained. The organic phase was then dried by $MgSO_4$, evaporated, redissoved in $CDCl_3$ and characterized by ^1H NMR, ^1H–^{13}C and ^1H–^{15}N HMBC and NOESY. **2.4g-Sn^{n}Bu$_3$** was found to be the major product.

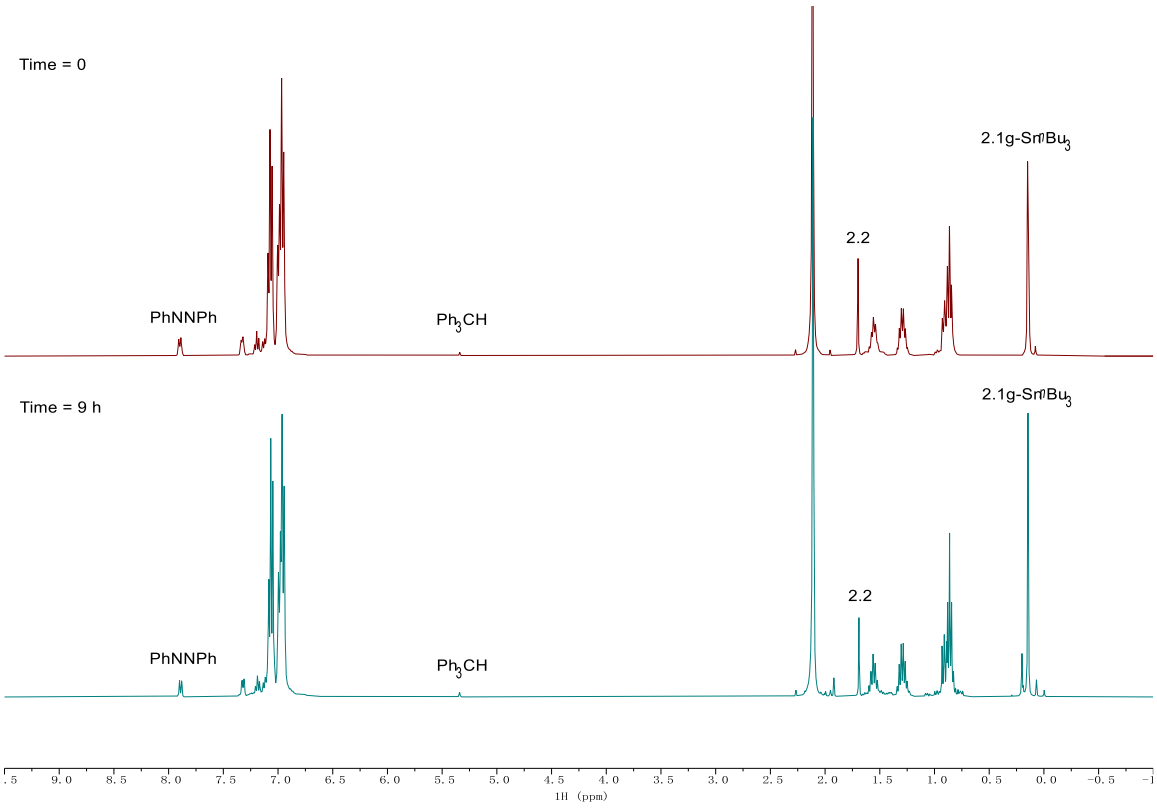

Figure 2.87. No-D ^1H NMR of the reaction of **2.1g-Sn^{n}Bu$_3$** at time = 0 (top), time = 9 h (bottom) in $PhCH_3$. *Taken from (top) YC-2020-0008-NoD-Tol-0h-H and (bottom) YC-2020-0008-NoD-Tol-9h-H.*

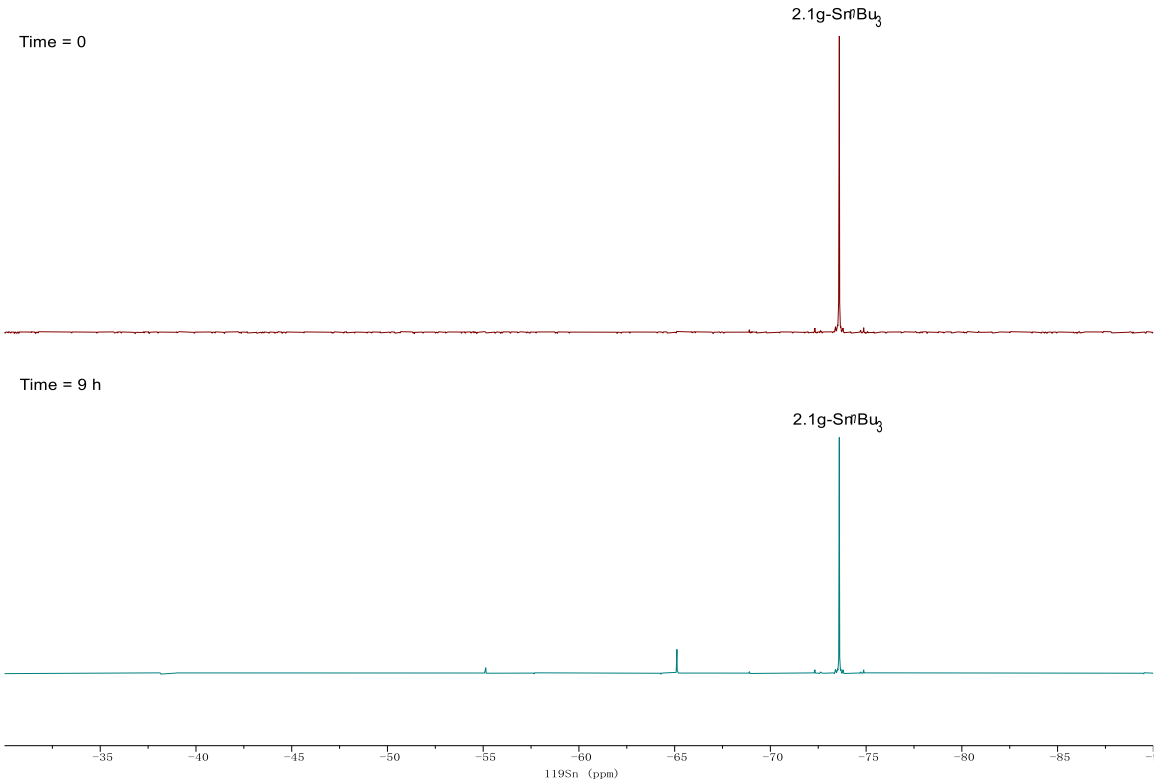

Figure 2.88. $^{119}Sn\{^{1}H\}$ NMR of the reaction of **2.1g-Sn^{n}Bu$_3$** at time = 0 (top), time = 9 h (bottom) in $PhCH_3$. Two new $^{119}Sn\{^{1}H\}$ signals observed. *Taken from (top) YC-2020-0008-NoD-Tol-0h-Sn and (bottom) YC-2020-0008-NoD-Tol-9h-Sn.*

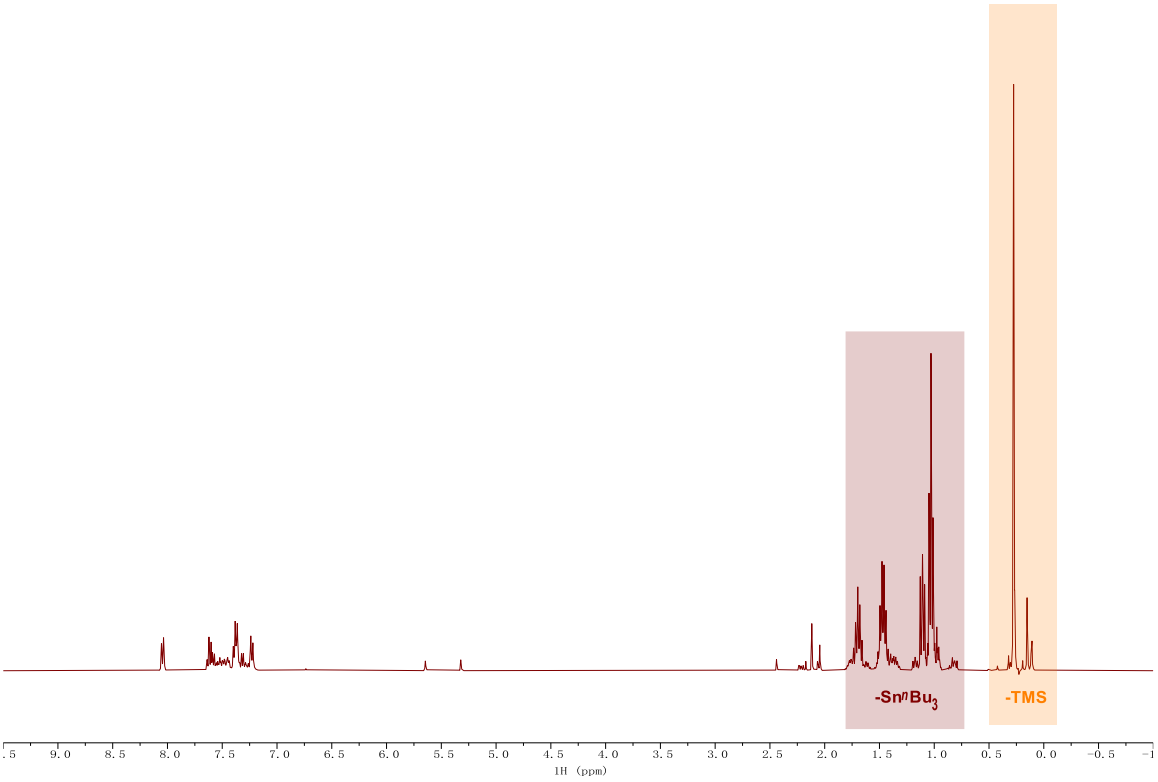

Figure 2.89. ^{1}H NMR of the reaction of **2.1g-Sn^{n}Bu$_3$** in CD_2Cl_2. *Taken from YC-2020-0008-4H.*

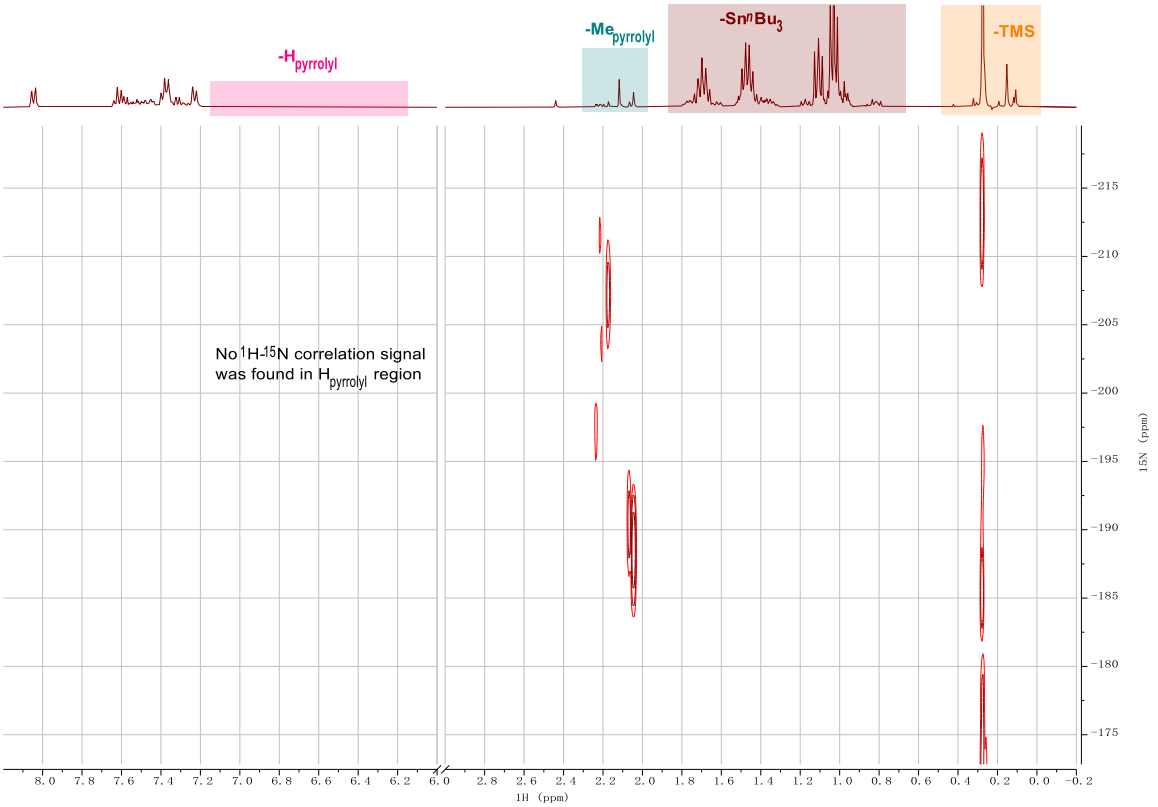

Figure 2.90. $^{1}H–^{15}N$ HMBC of the reaction of **2.1g-Sn^{n}Bu$_3$** in CD_2Cl_2. *Taken from YC-2020-0008-4NHMBC.*

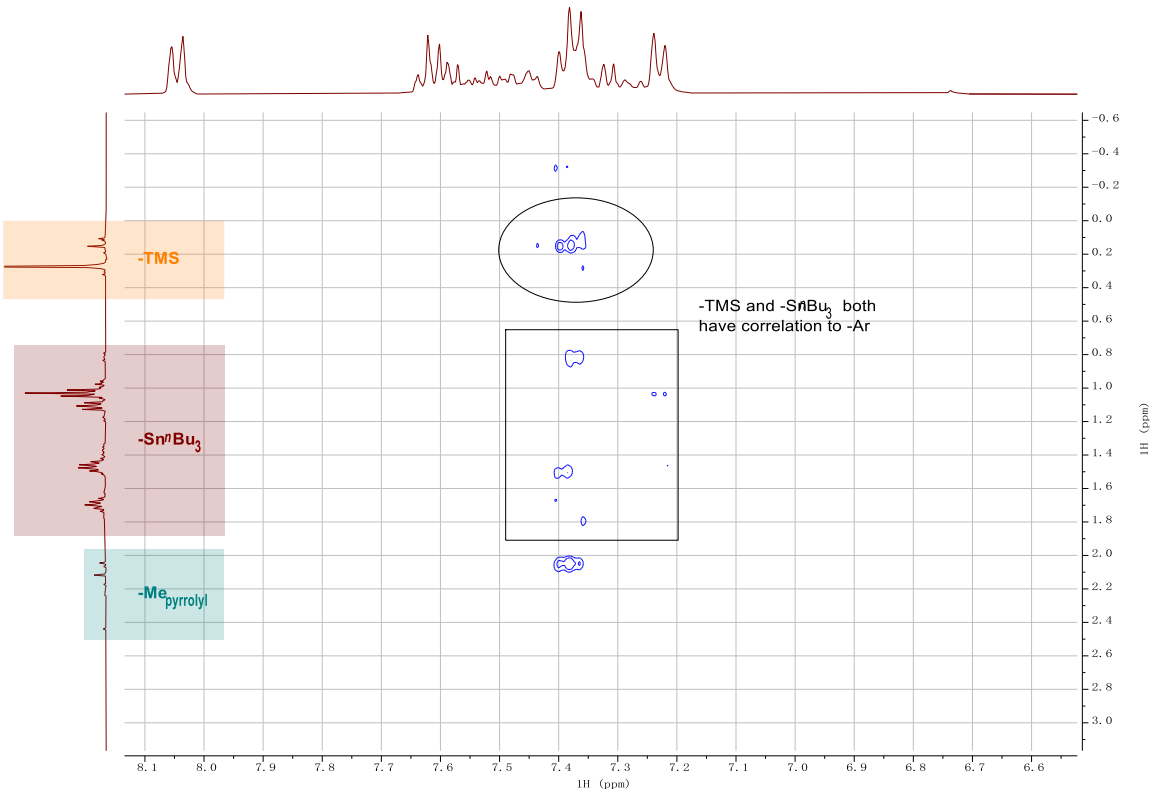

Figure 2.91. NOESY NMR spectrum of the reaction of **2.1g-Sn^{n}Bu$_3$** in CD_2Cl_2. *Taken from YC-2020-0008-4NOESY.*

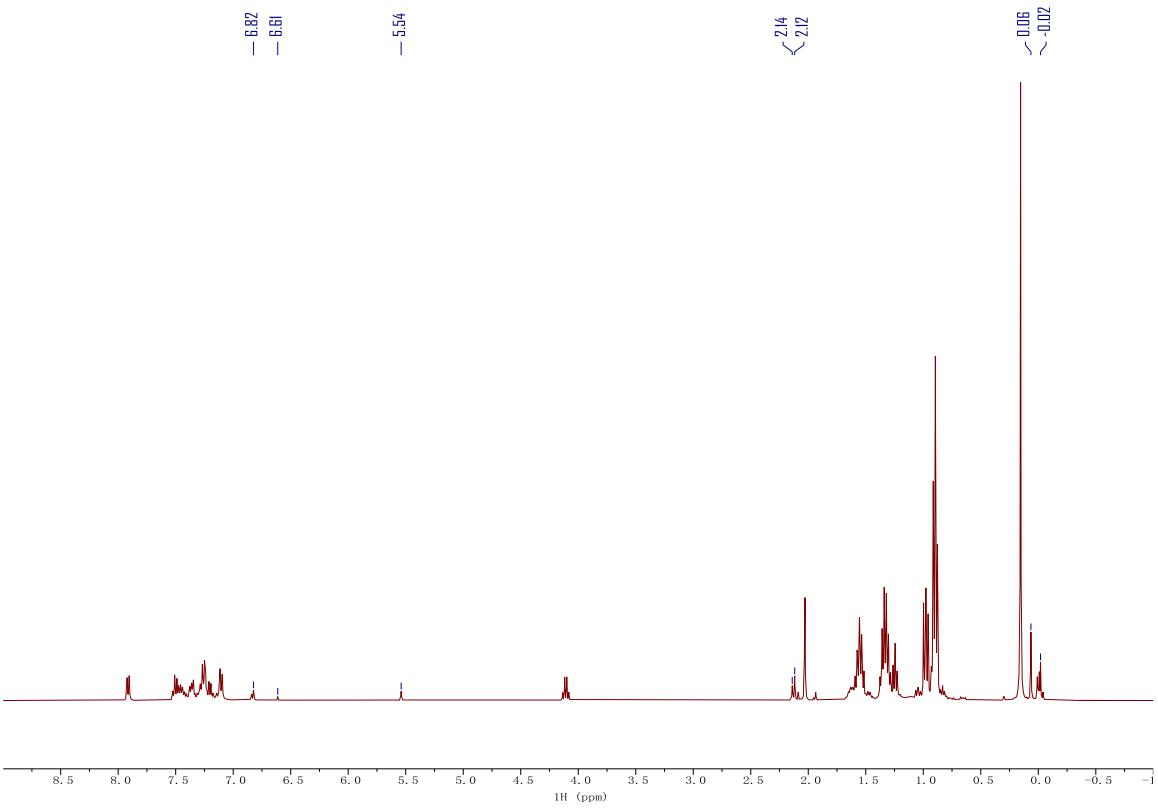

Figure 2.92. ^{1}H NMR of the reaction of **2.1g-Sn^{n}Bu$_3$** in $CDCl_3$ after extraction. *Taken from YC-2020-0008-7H.*

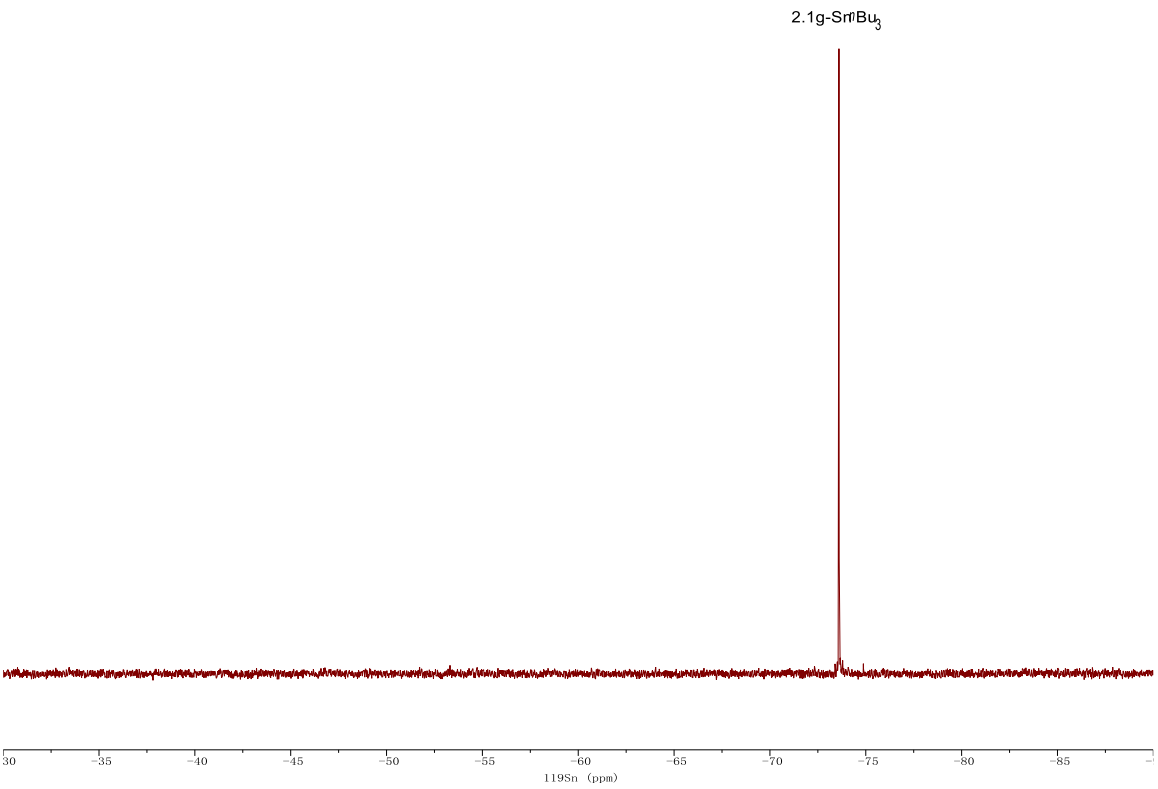

Figure 2.93. $^{119}Sn\{^{1}H\}$ NMR of the reaction of **2.1g-Sn^{n}Bu$_3$** in $CDCl_3$ after extraction. *Taken from YC-2020-0008-9-Sn.*

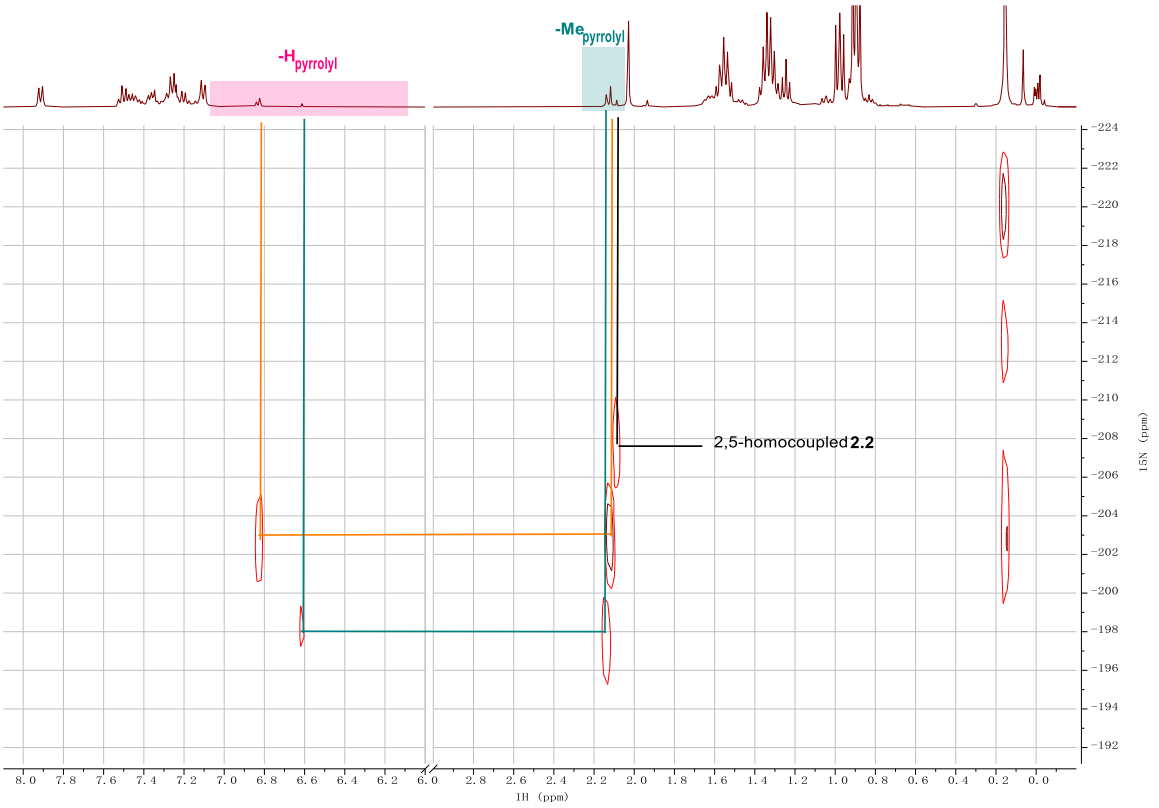

Figure 2.94. $^{1}H–^{15}N$ HMBC of the reaction of **2.1g-Sn^{n}Bu$_3$** in $CDCl_3$ after extraction. *Taken from YC-2020-0008-7NHMBC.*

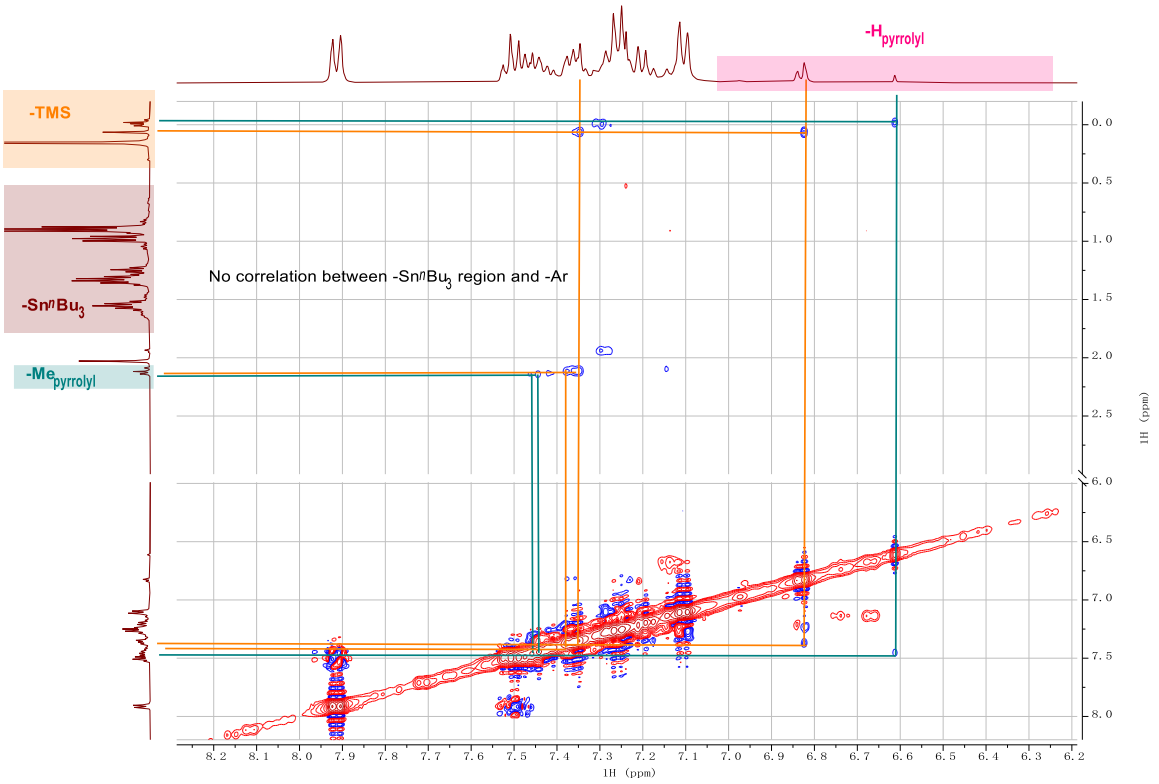

List of correlations (chemical shifts in ppm):

Peak — Peak		Peak — Peak	
6.82 (–H)	0.06 (–TMS)	6.61 (–H)	-0.02 (–TMS)
6.82 (–H)	7.38 (–Ph)	6.61 (–H)	7.45 (–Ph)
2.12 (–Me)	7.38 (–Ph)	2.14 (–Me)	7.45 (–Ph)
2.12 (–Me)	7.35 (–Ph)	2.14 (–Me)	7.46 (–Ph)
0.06 (–TMS)	7.35 (–Ph)		

Figure 2.95. NOESY NMR spectrum of the reaction of **2.1g-Sn^{n}Bu$_3$** in $CDCl_3$ after extraction. *Taken from YC-2020-0008-7NOESY.*

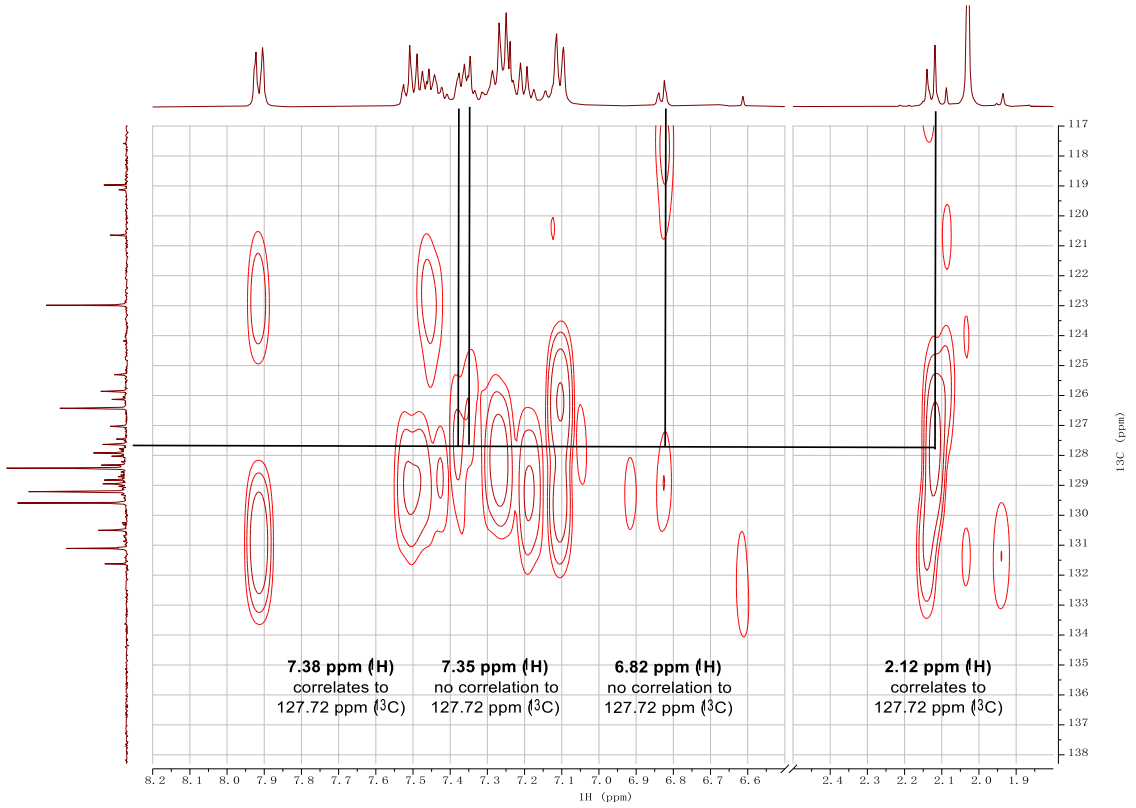

Figure 2.96. ^{1}H–^{13}C HMBC of the reaction of **2.1g-Sn^{n}Bu$_3$** in $CDCl_3$ after extraction. *Taken from YC-2020-0008-8HMBC.*

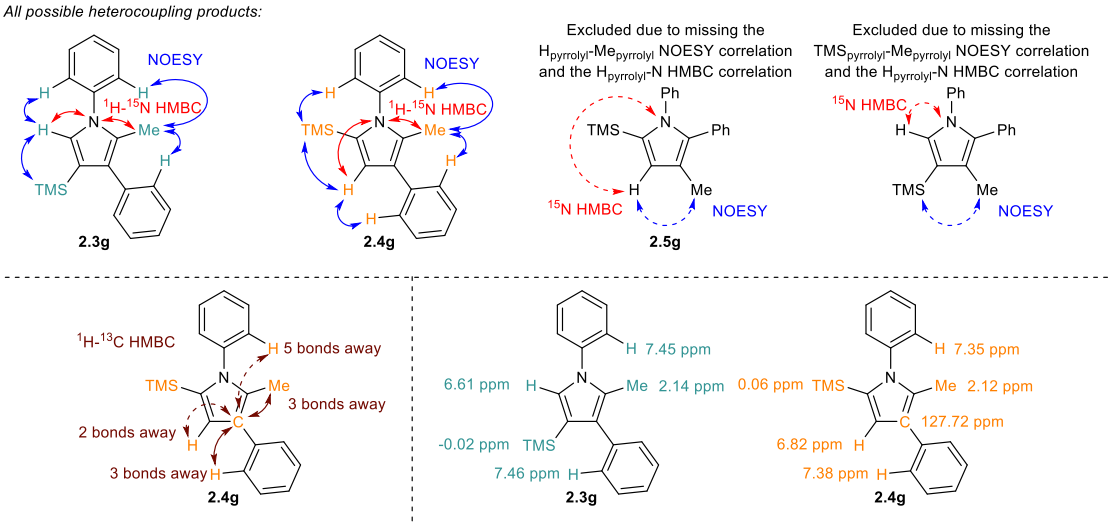

	δ (ppm)	Assignment	# of H	Peak Area	Yield (%)
Ph_3CH	5.40	Ph_3C-H	1	8903.9	n.a.

2.3g	6.61	$H_{pyrrolyl}$	1	2588.2	5.8
2.4g	2.12	$Me_{pyrrolyl}$	3	15998.7	12.0

Figure 2.97. Determination of regioisomers and yields.

2.5.9 One-Pot Reactions

One-Pot Pyrrole Synthesis/Arylation in *p*-Fluoroiodobenzene

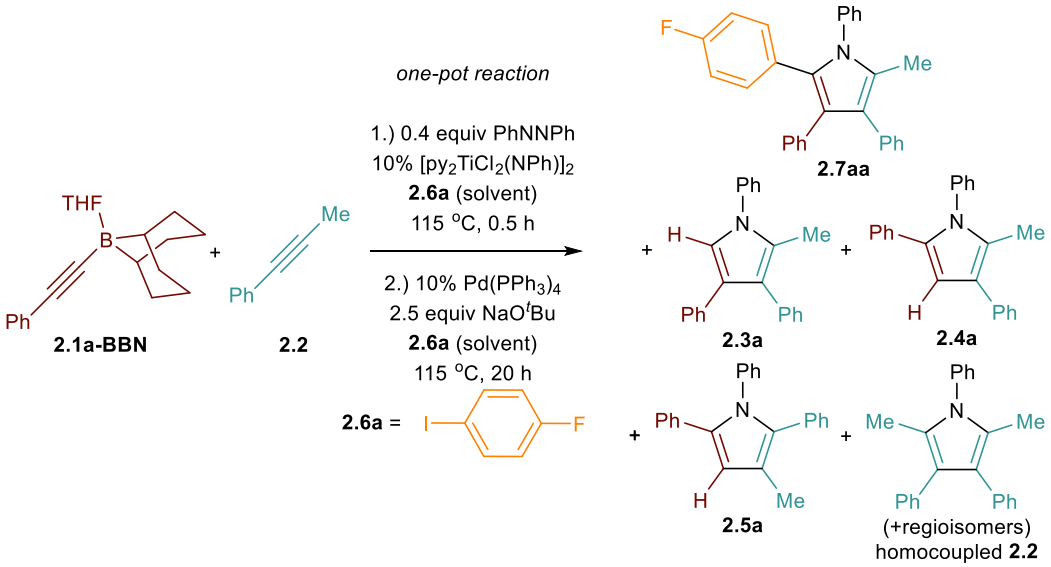

$[py_2TiCl_2(NPh)]_2$ (7.4 mg, 0.01 mmol, 0.1 equiv), *B*-alkynyl-9-BBN (0.1 mmol, 1 equiv), 1-phenyl-1-propyne (11.6 mg, 0.1 mmol, 1 equiv), azobenzene (7.3 mg, 0.04 mmol, 0.4 equiv) and triphenylmethane (2.7 mg, 0.011 mmol, 0.11 equiv, internal standard) and 0.5 mL of *p*-fluoroiodobenzene (**2.6a**) were added to an NMR tube. The reaction was then sealed and heated in a preheated oil bath at 115 ℃ for 0.5 h. NMR spectra were collected before and after heating to monitor the reaction. The NMR tube was then transferred into the glovebox. $Pd(PPh_3)_4$ (11.6 mg, 0.01 mmol, 0.1 equiv) and NaO^tBu (24.0 mg, 0.25 mmol, 2.5 equiv) were added to the reaction, the NMR tube was re-sealed and heated in a preheated oil bath at 115 ℃ for 20 h. NMR spectra were collected before and after the reaction. The reaction was then quenched with 5% HCl in methanol and extracted with EtOAc/H_2O. The organic phase was dried over $MgSO_4$ and evaporated under vacuum. The crude product mixture was characterized by NMR and GC-Polyarc®/FID to calculate the yield and selectivity.

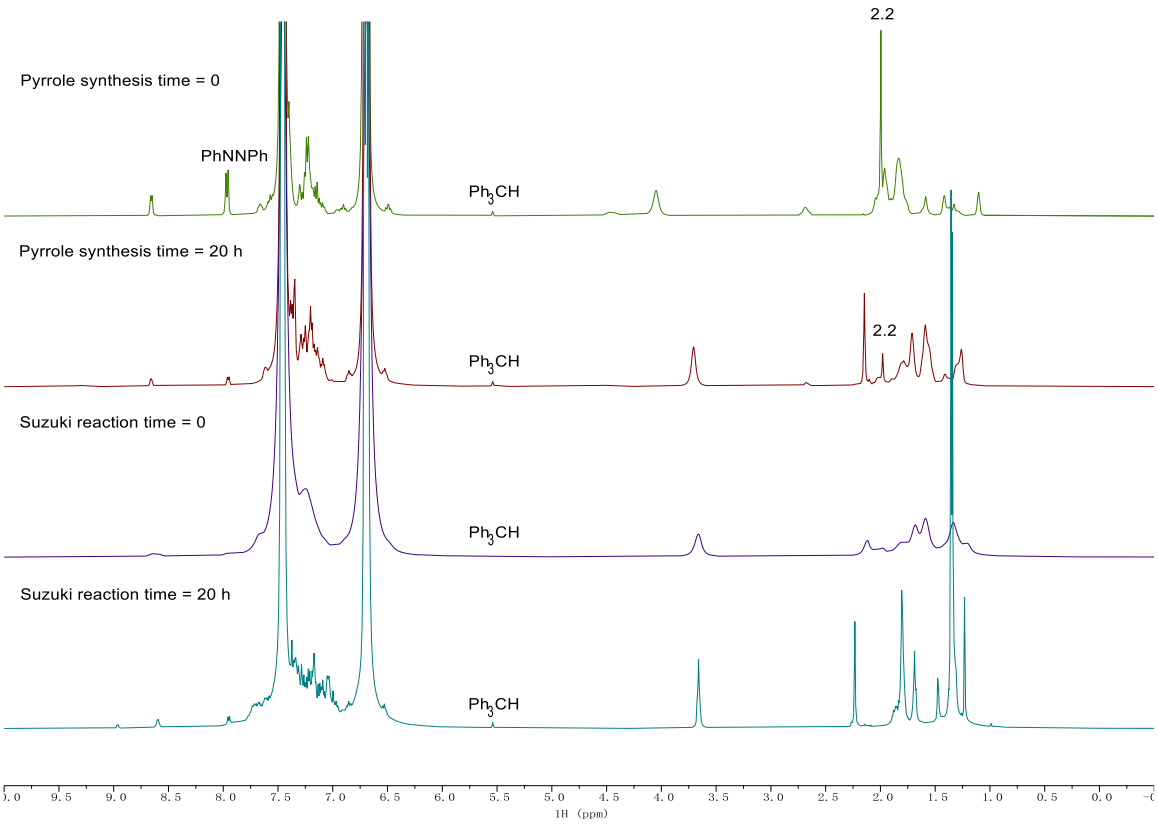

Figure 2.98. No-D ^{1}H NMR of the one-pot pyrrole synthesis/arylation of **2.1a-BBN** and **2.6a** at time = 0, time = 20 h of pyrrole synthesis, time = 0 and time = 20 h of Suzuki reaction in *p*-fluoroiodobenzene. Chemical shifts were referenced to the proton signal of the internal standard triphenylmethane (Ph_3CH, s, 5.40 ppm). *Taken from (top to bottom) (1) YC-2020-0018-NoD-FC6H4I-0h-H; (2) YC-2020-0018-NoD-FC6H4I-30min-H; (3) YC-2020-0018-NoD-FC6H4I-tandem-0h-H; (4) YC-2020-0018-NoD-FC6H4I-tandem-20h-H.*

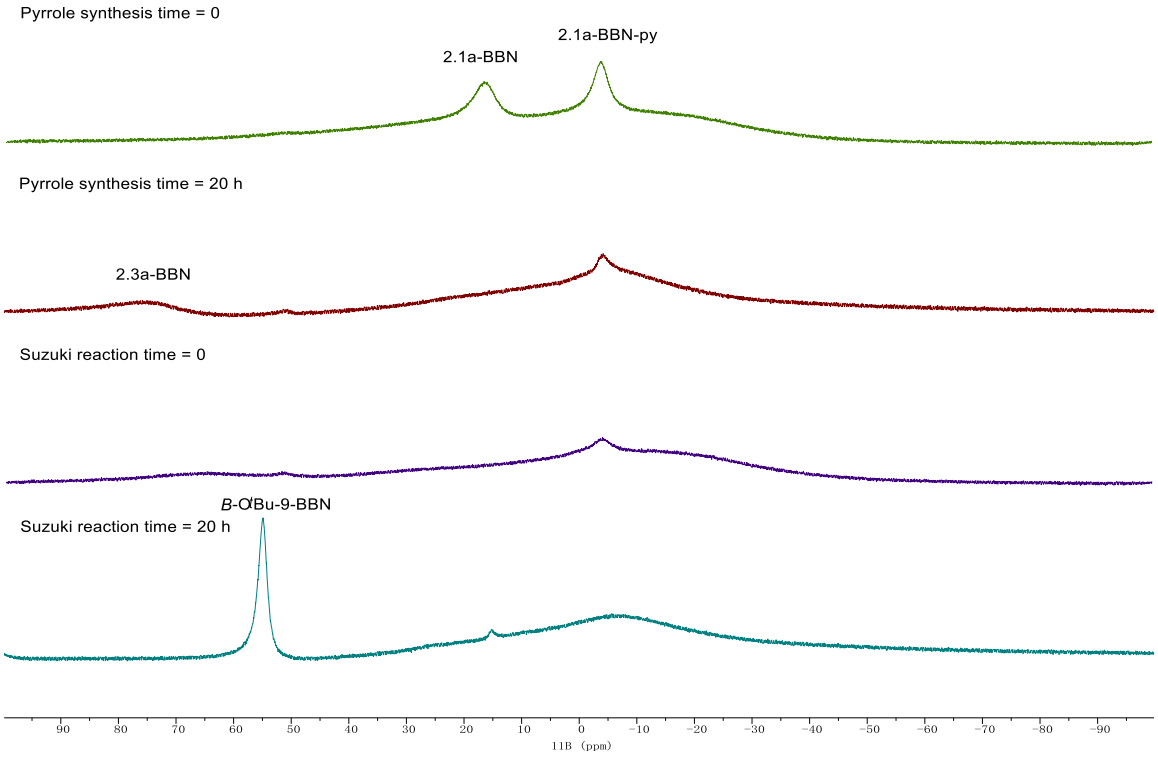

Figure 2.99. ^{11}B NMR of the one-pot pyrrole synthesis/arylation of **2.1a-BBN** and **2.6a** at time = 0, time = 20 h of pyrrole synthesis, time = 0 and time = 20 h of Suzuki reaction in *p*-fluoroiodobenzene. *Taken from (top to bottom) (1) YC-2020-0018-NoD-FC6H4I-0h-B; (2) YC-2020-0018-NoD-FC6H4I-30min-B; (3) YC-2020-0018-NoD-FC6H4I-tandem-0h-B; (4) YC-2020-0018-NoD-FC6H4I-tandem-20h-B.*

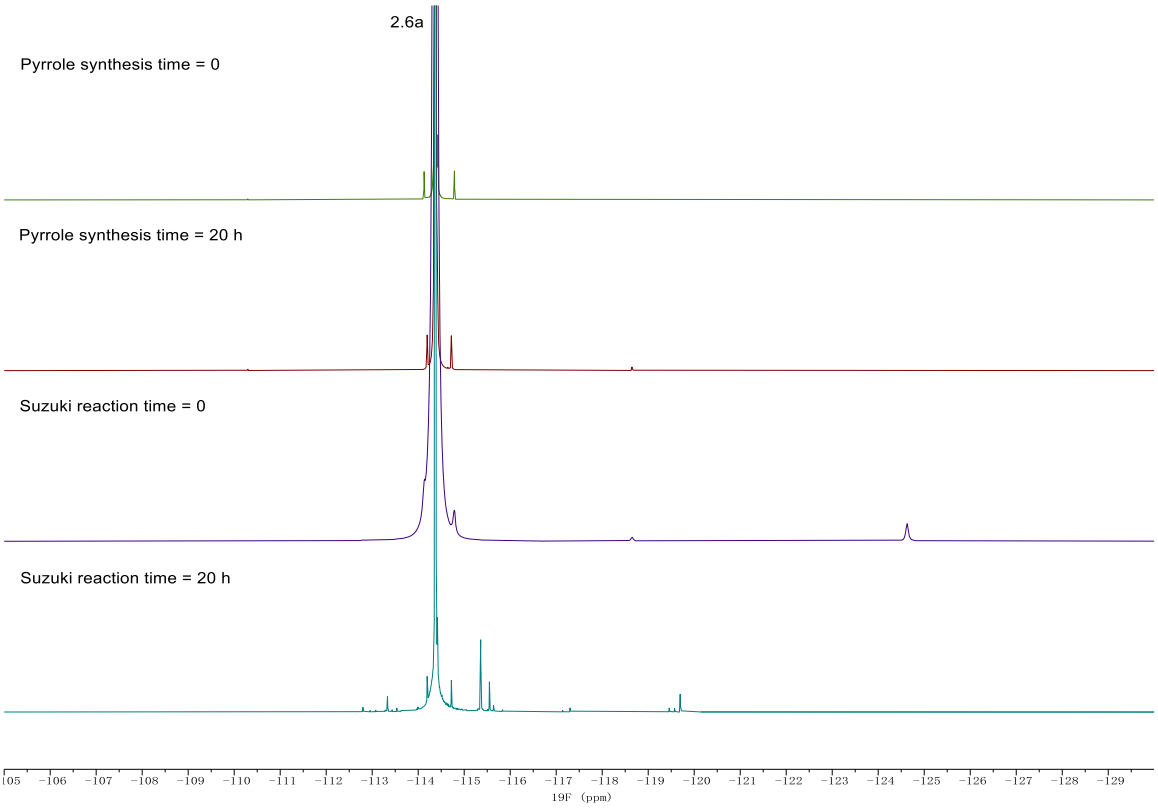

Figure 2.100. $^{19}F\{^{1}H\}$ NMR of the one-pot pyrrole synthesis/arylation of **2.1a-BBN** and **2.6a** at time = 0, time = 20 h of pyrrole synthesis, time = 0 and time = 20 h of Suzuki reaction in *p*-fluoroiodobenzene. *Taken from (top to bottom) (1) YC-2020-0018-NoD-FC6H4I-0h-F; (2) YC-2020-0018-NoD-FC6H4I-30min-F; (3) YC-2020-0018-NoD-FC6H4I-tandem-0h-F; (4) YC-2020-0018-NoD-FC6H4I-tandem-20h-F.*

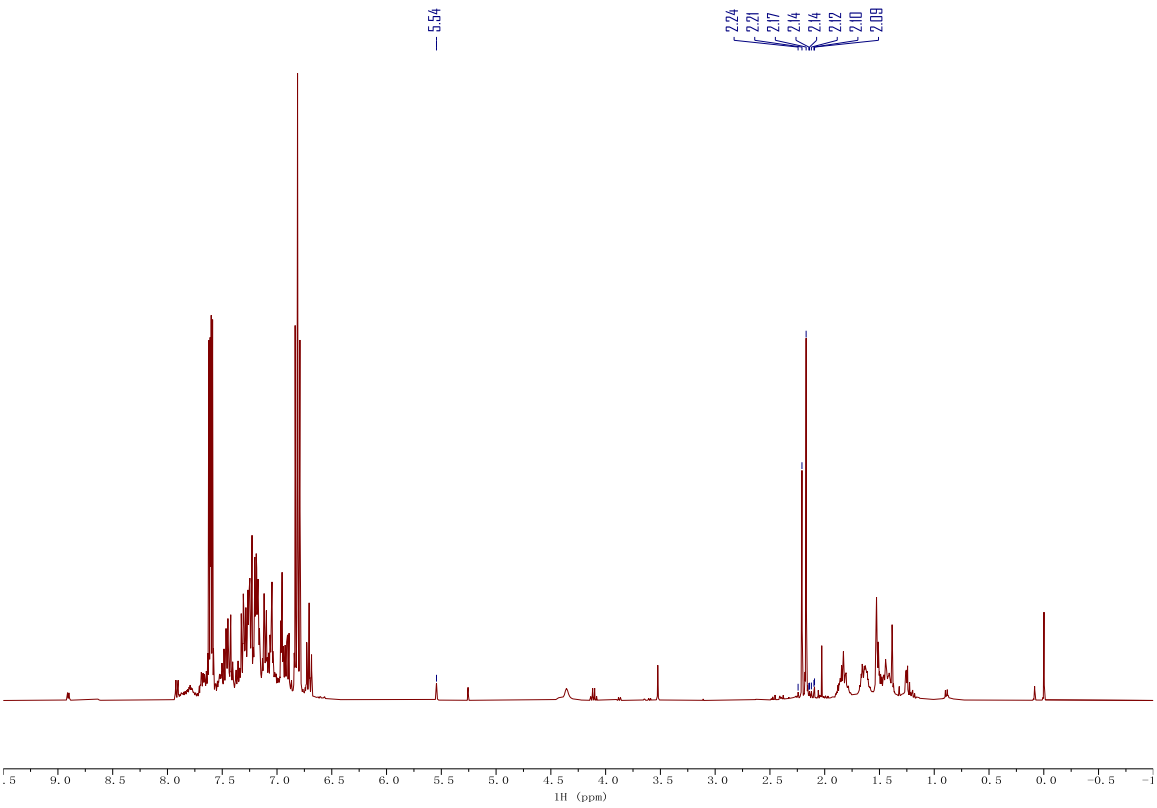

	δ (ppm)	Assignment	# of H	Peak Area	Yield (%)
Ph_3CH	5.54	Ph_3C-H	1	1945.8	n.a.
2.7aa	2.17	$Me_{pyrrolyl}$	3	21284.0	40.1
2.3a	2.21	$Me_{pyrrolyl}$	3	12903.9	24.3
2.4a	2.24	$Me_{pyrrolyl}$	3	700.8	1.3
2.5a	not found	$H_{pyrrolyl}$	1	n.a.	n.d.
homocoupled **2.2**	2.14, 2.14, 2.12, 2.10, 2.09	$Me_{pyrrolyl}$ (2 per molecule)	6	2941.0	2.8

Figure 2.101. ^1H NMR of the one-pot pyrrole synthesis/arylation of **2.1a-BBN** and **2.6a** in $CDCl_3$ after HCl workup. *Taken from YC-2020-0018-5H.*

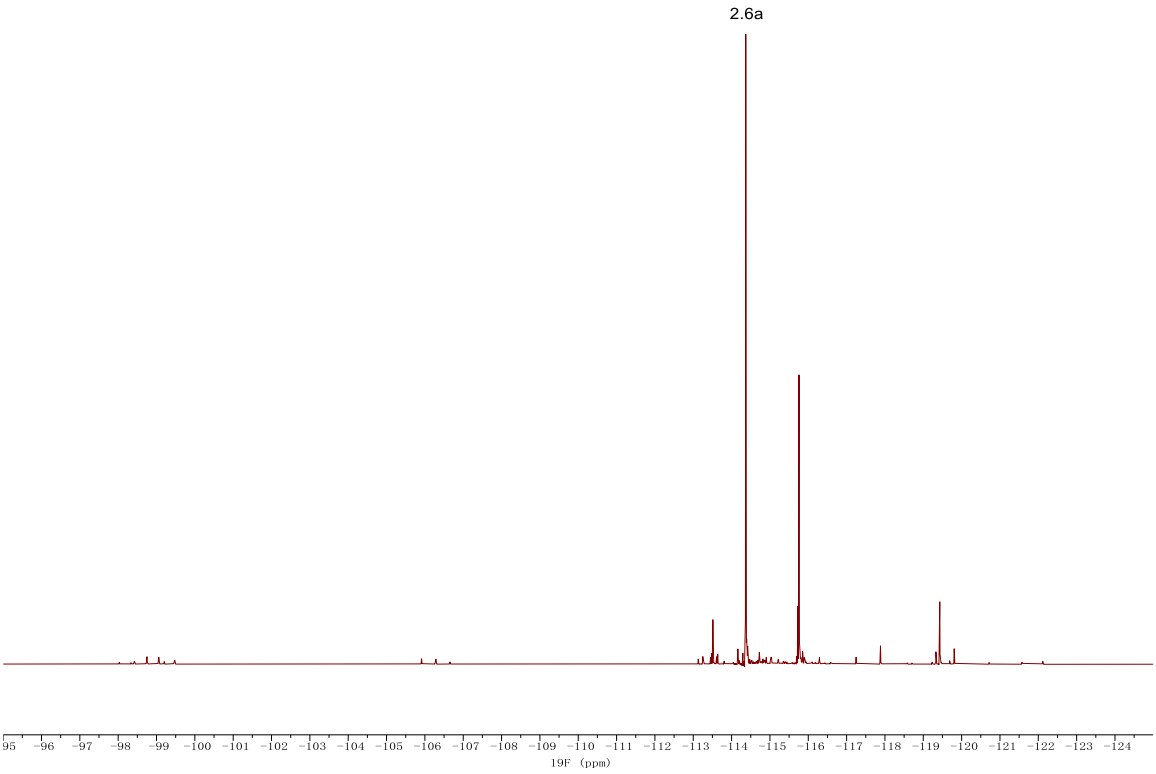

Figure 2.102. $^{19}F\{^{1}H\}$ NMR of the one-pot pyrrole synthesis/arylation of **2.1a-BBN** and **2.6a** in $CDCl_3$ after HCl workup. *Taken from YC-2020-0018-6F.*

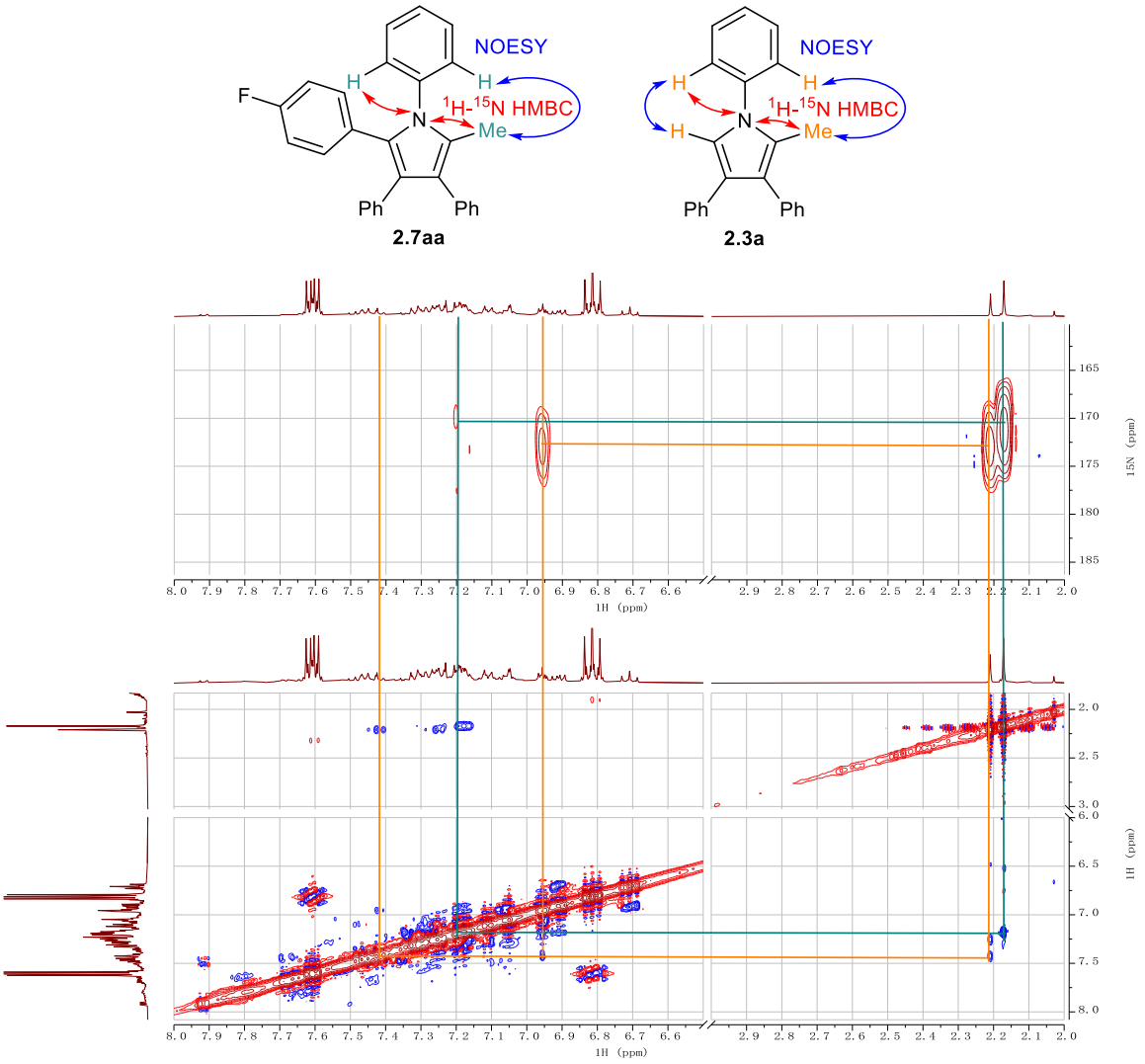

Figure 2.103. ^{1}H–^{15}N HMBC (top) and NOESY (bottom) NMR spectra of the one-pot pyrrole synthesis/arylation of **2.1a-BBN** and **2.6a** in $CDCl_3$ after HCl workup. *Taken from (top) YC-2020-0018-5NHMBC and (bottom) YC-2020-0018-5NOESY.*

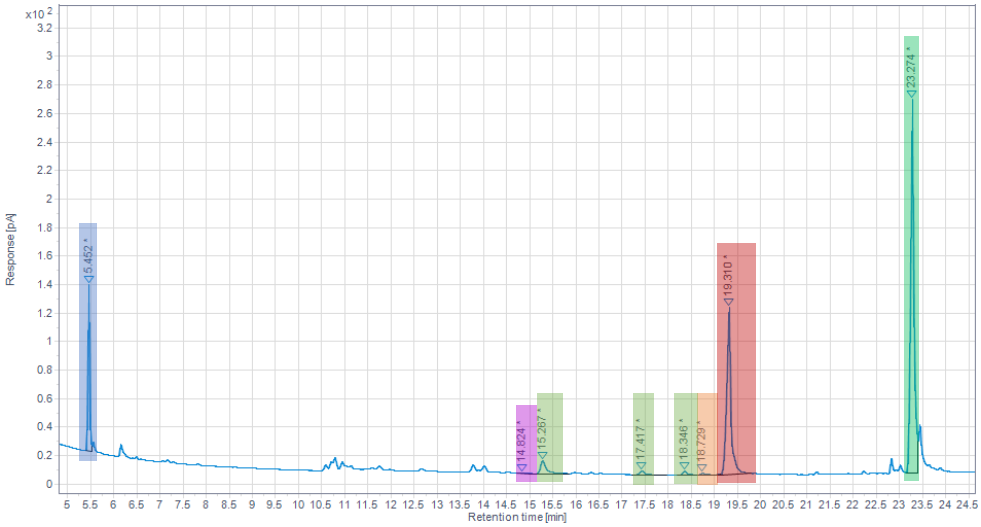

	Retention Time (min)	Surface Area	# of C	Yield (%)
Ph_3CH	5.45	281.717	19	n.a.
2.7aa	23.27	1508.02	29	38.6
2.3a	19.31	736.615	23	23.8
2.4a	18.73	11.991	23	0.4
2.5a	14.82	1.801	23	0.1
homocoupled **2.2**	15.27, 17.42, 18.35	116.179	24	3.6

Figure 2.104. Quantitative GC-FID chromatograph of the one-pot pyrrole synthesis/arylation of **2.1a-BBN** and **2.6a** after HCl workup. *Taken from YC-2020-0018-2FID.*

General Procedure for One-Pot Pyrrole Synthesis/Arylation in Toluene (Procedure 2.D) (Table 2.4)

$[py_2TiCl_2(NPh)]_2$ (7.4 mg, 0.01 mmol, 0.1 equiv), *B*-alkynyl-9-BBN (0.1 mmol, 1 equiv) and 0.5 mL of $PhCH_3$ stock solution containing 1-phenyl-1-propyne (11.6 mg, 0.1 mmol, 1 equiv), azobenzene (7.3 mg, 0.04 mmol, 0.4 equiv) and triphenylmethane (4.9 mg, 0.02 mmol, 0.2 equiv, internal standard) were added to an NMR tube. The reaction was then sealed and heated in a preheated oil bath at 115 ℃ for 20 h. NMR spectra were collected before and after heating to monitor the reaction. The NMR tube was then transferred into the glovebox. $Pd(PPh_3)_4$ (11.6 mg, 0.01 mmol, 0.1 equiv), aryl iodide (0.2 mmol, 2 equiv), NaO^tBu (24.0 mg, 0.25 mmol, 2.5 equiv) and 0.2 mL of $PhCH_3$ were added to the reaction, the NMR tube was

re-sealed and heated in a preheated oil bath at 115 ℃ for 20 h. NMR spectra were collected before and after the reaction. The reaction was then quenched with 5% HCl in methanol and extracted with EtOAc/H_2O. The organic phase was dried over $MgSO_4$ and evaporated under vacuum. The crude product mixture was characterized by NMR and GC-Polyarc®/FID to calculate the yield and selectivity.

One-Pot Pyrrole Synthesis/Arylation for 2.1a-BBN and *p*-Fluoroiodobenzene

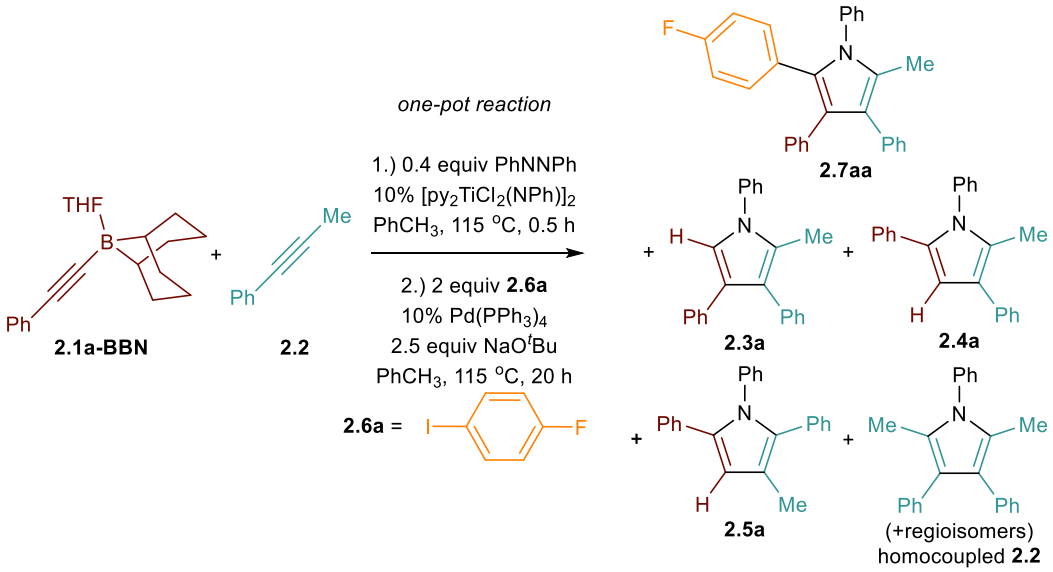

The reaction was performed following **Procedure 2.D** using **2.1a-BBN** (29.4 mg, 0.1 mmol, 1 equiv) as alkynylborane and *p*-fluoroiodobenzene (**2.6a**, 44.4 mg, 0.2 mmol, 2 equiv) as aryl iodide.

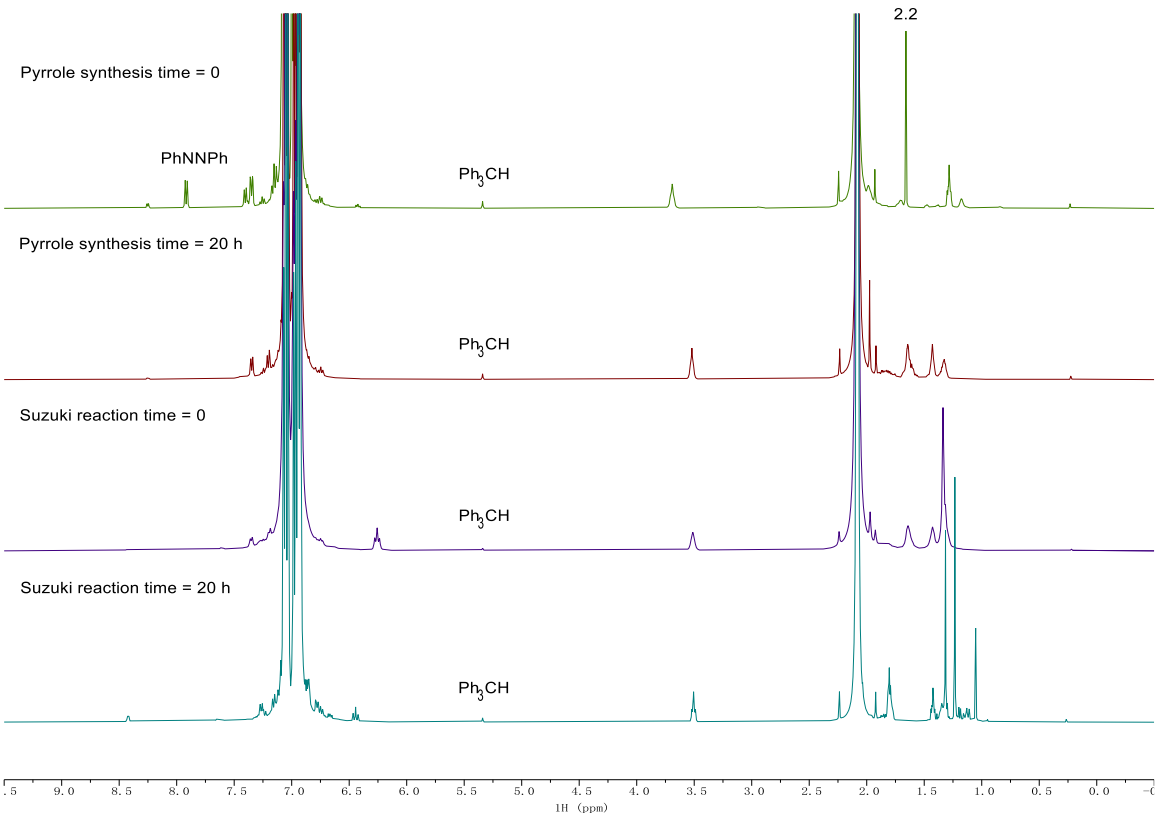

Figure 2.105. No-D ^{1}H NMR of the one-pot pyrrole synthesis/arylation of **2.1a-BBN** and **2.6a** at time = 0, time = 20 h of pyrrole synthesis, time = 0 and time = 20 h of Suzuki reaction in $PhCH_3$. *Taken from (top to bottom) (1) YC-2020-0017-NoD-Tol-0h-H; (2) YC-2020-0017-NoD-Tol-20h-H; (3) YC-2020-0017-NoD-Tol-tandem-0h-H; (4) YC-2020-0017-NoD-Tol-tandem-20h-H.*

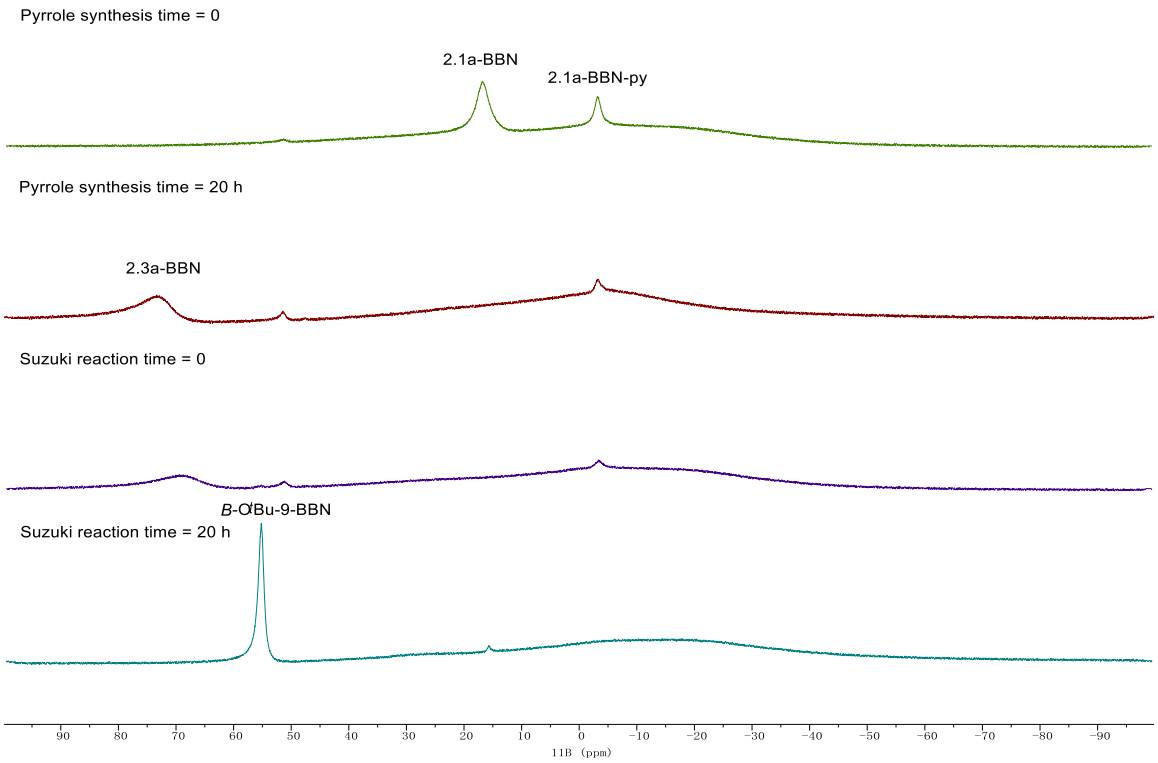

Figure 2.106. ^{11}B NMR of the one-pot pyrrole synthesis/arylation of **2.1a-BBN** and **2.6a** at time = 0, time = 20 h of pyrrole synthesis, time = 0 and time = 20 h of Suzuki reaction in $PhCH_3$. *Taken from (top to bottom) (1) YC-2020-0017-NoD-Tol-0h-B; (2) YC-2020-0017-NoD-Tol-20h-B; (3) YC-2020-0017-NoD-Tol-tandem-0h-B; (4) YC-2020-0017-NoD-Tol-tandem-20h-B.*

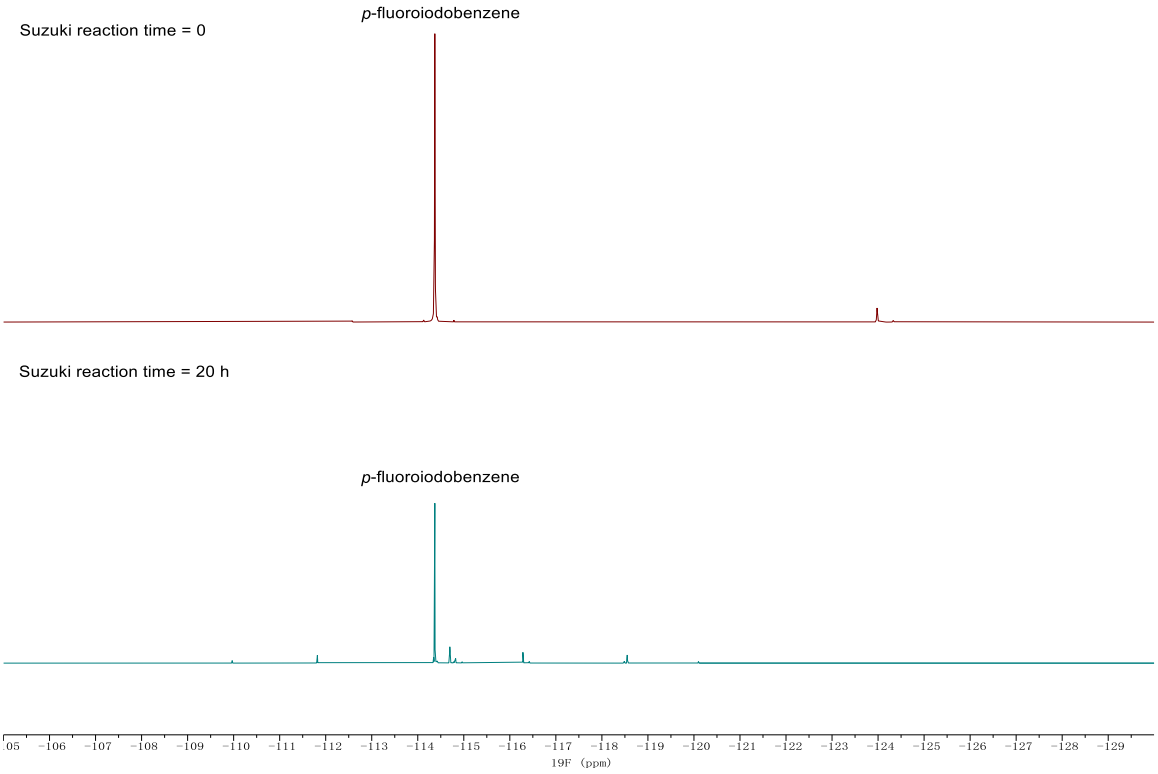

Figure 2.107. $^{19}F\{^{1}H\}$ NMR of the one-pot pyrrole synthesis/arylation of **2.1a-BBN** and **2.6a** at time = 0 and time = 20 h of Suzuki reaction in $PhCH_3$. *Taken from (top) YC-2020-0017-NoD-Tol-tandem-0h-F and (bottom) YC-2020-0017-NoD-Tol-tandem-20h-F.*

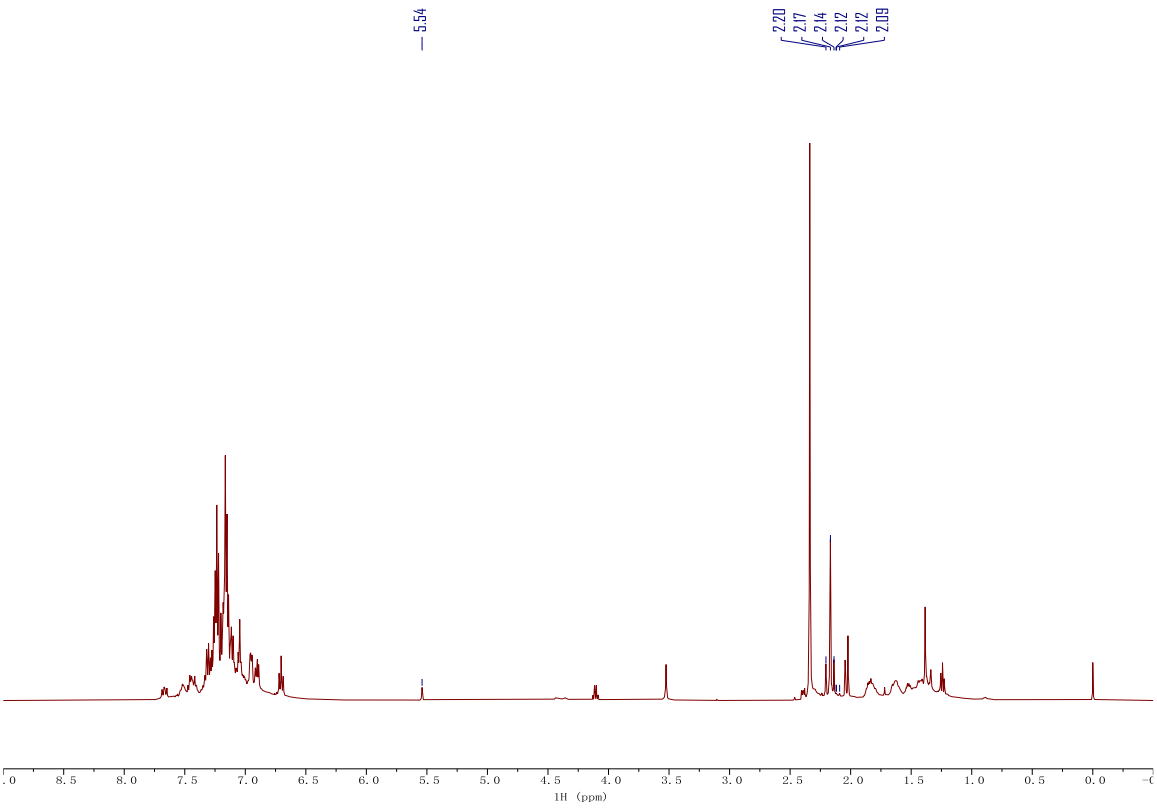

	δ (ppm)	Assignment	# of H	Peak Area	Yield (%)
Ph_3CH	5.54	Ph_3C-H	1	1745.7	n.a.
2.7aa	2.17	$Me_{pyrrolyl}$	3	15242.5	58.2
2.3a	2.20	$Me_{pyrrolyl}$	3	2800.3	10.7
2.4a	not found	$H_{pyrrolyl}$	1	n.a.	n.d.
2.5a	not found	$H_{pyrrolyl}$	1	n.a.	n.d.
homocoupled **2.2**	2.14, 2.12, 2.12, 2.09	$Me_{pyrrolyl}$ (2 per molecule)	6	4165.5	8.0

Figure 2.108. ^1H NMR of the one-pot pyrrole synthesis/arylation of **2.1a-BBN** and **2.6a** in $CDCl_3$ after HCl workup. *Taken from YC-2020-0017-3H.*

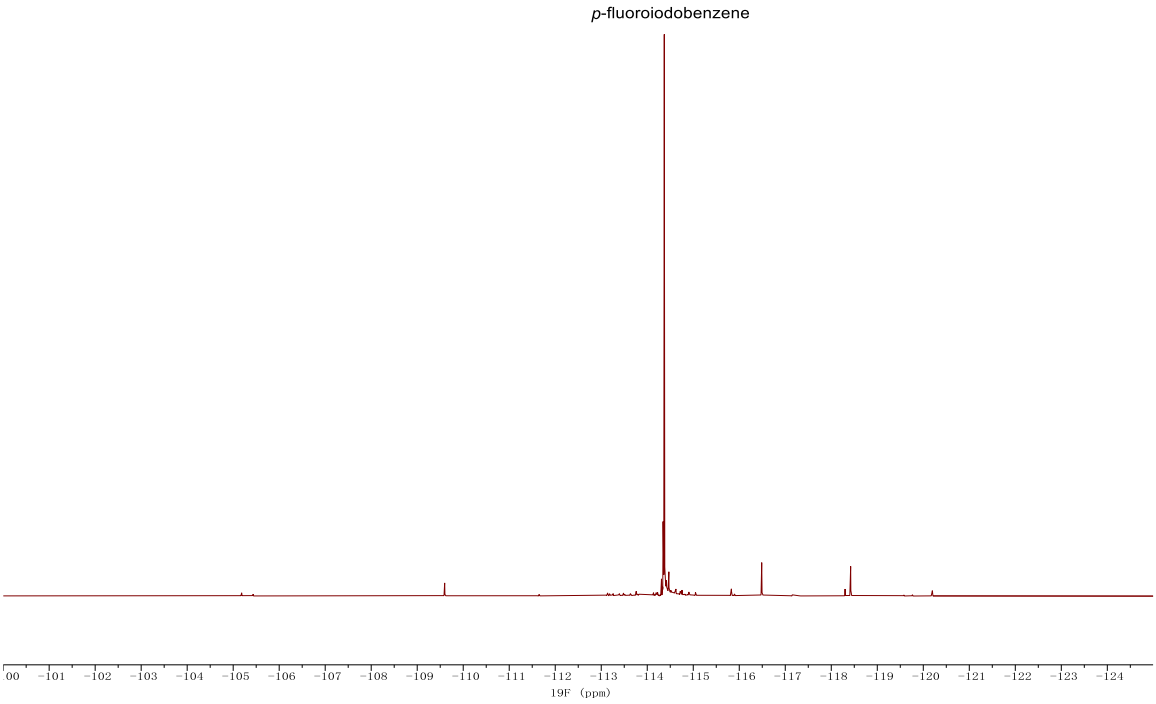

Figure 2.109. $^{19}F\{^{1}H\}$ NMR of the one-pot pyrrole synthesis/arylation of **2.1a-BBN** and **2.6a** in $CDCl_3$ after HCl workup. *Taken from YC-2020-0017-3F.*

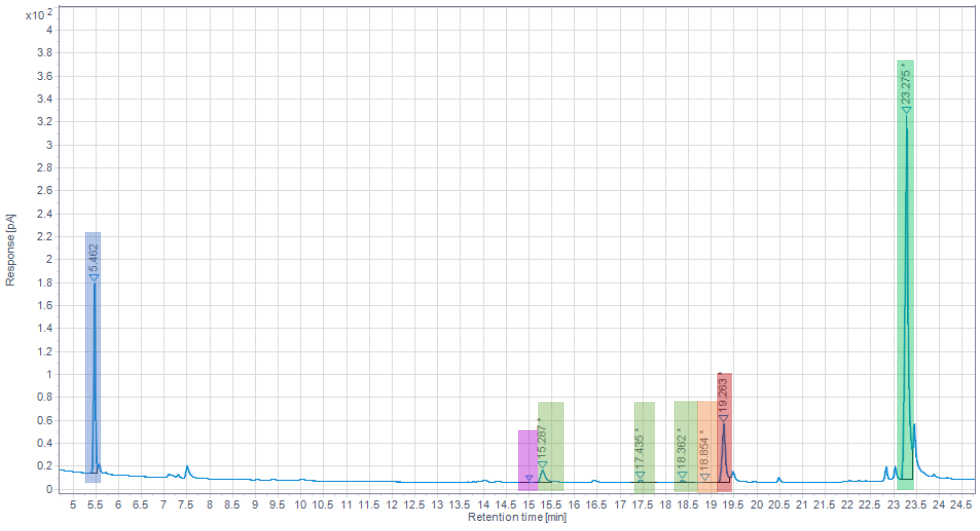

	Retention Time (min)	Surface Area	# of C	Yield (%)

Ph_3CH	5.46	394.879	19	n.a.
2.7aa	23.28	1732.741	29	57.5
2.3a	19.26	258.055	23	10.8
2.4a	18.85	1.164	23	< 0.1
2.5a	14.99	0.022	23	< 0.1
homocoupled **2.2**	15.29, 17.44, 18.36	109.487	24	4.4

Figure 2.110. Quantitative GC-FID chromatograph of the one-pot pyrrole synthesis/arylation of **2.1a-BBN** and **2.6a** after HCl workup. *Taken from YC-2020-0017-1FID.*

One-Pot Pyrrole Synthesis/Arylation for 2.1b-BBN and *p*-Fluoroiodobenzene

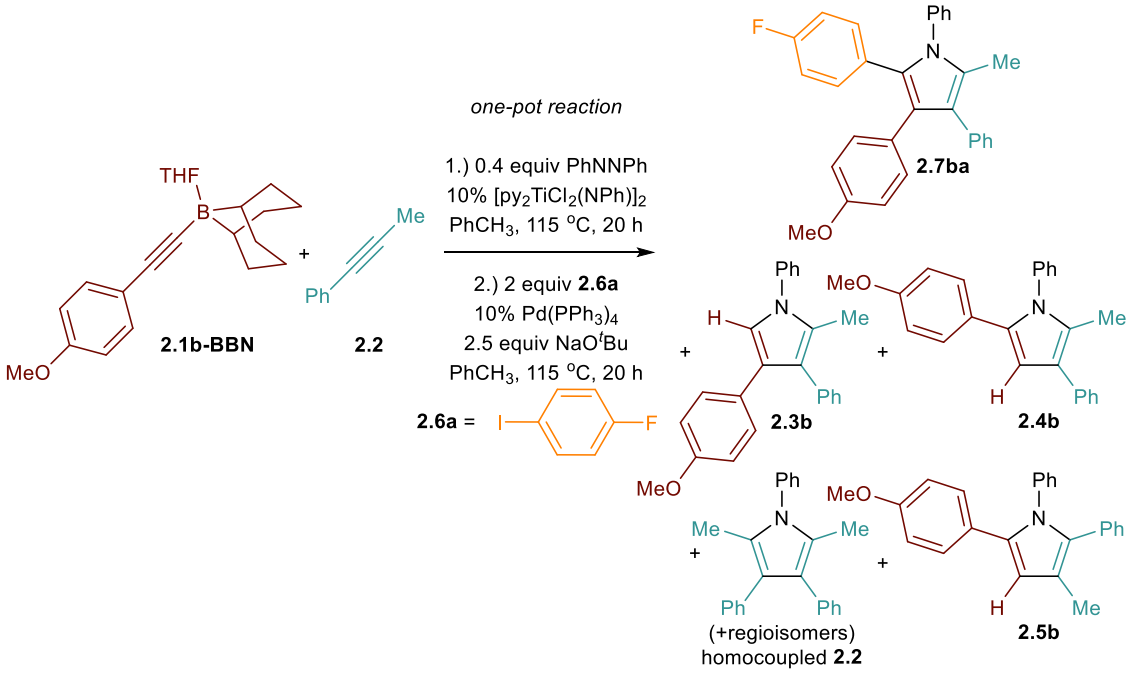

The reaction was performed following **Procedure 2.D** using **2.1b-BBN** (32.4 mg, 0.1 mmol, 1 equiv) as alkynylborane and *p*-fluoroiodobenzene (**2.6a**, 44.4 mg, 0.2 mmol, 2 equiv) as aryl iodide.

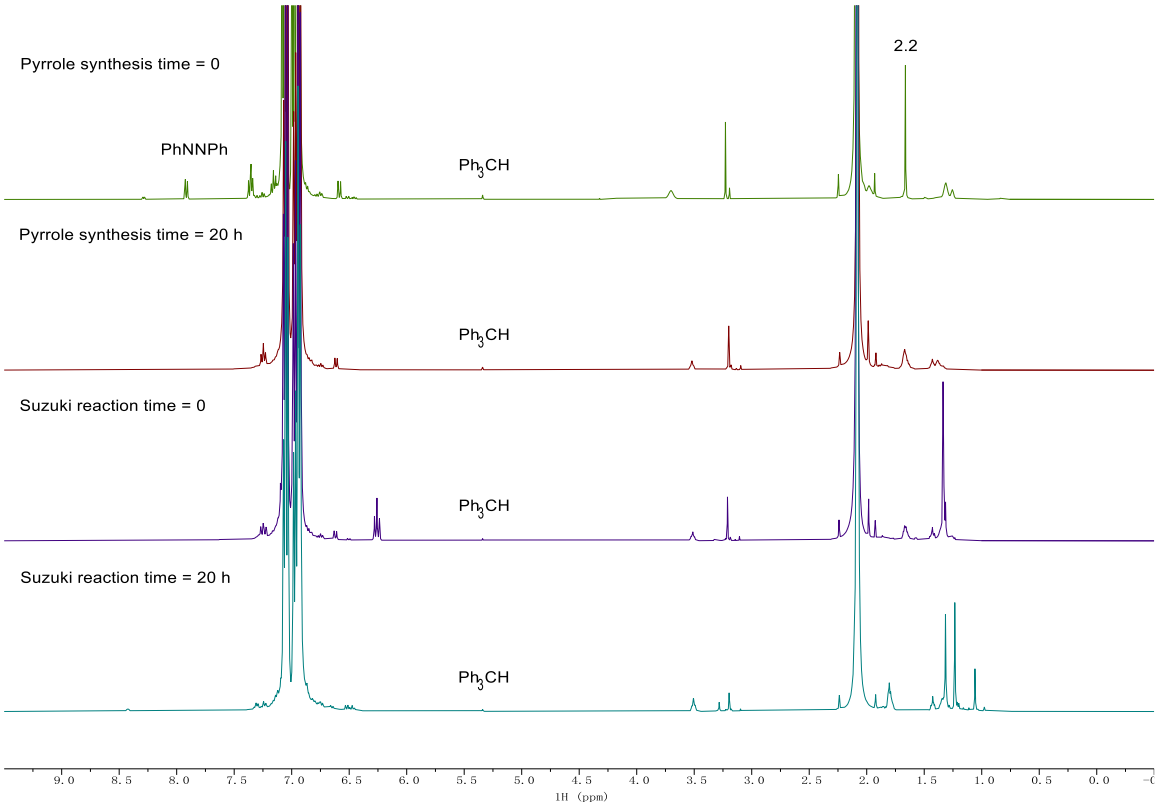

Figure 2.111. No-D ^{1}H NMR of the one-pot pyrrole synthesis/arylation of **2.1b-BBN** and **2.6a** at time = 0, time = 20 h of pyrrole synthesis, time = 0 and time = 20 h of Suzuki reaction in $PhCH_3$. *Taken from (top to bottom) (1) YC-2020-0024-NoD-Tol-0h-H; (2) YC-2020-0024-NoD-Tol-20h-H; (3) YC-2020-0024-NoD-Tol-tandem-0h-H; (4) YC-2020-0024-NoD-Tol-tandem-20h-H.*

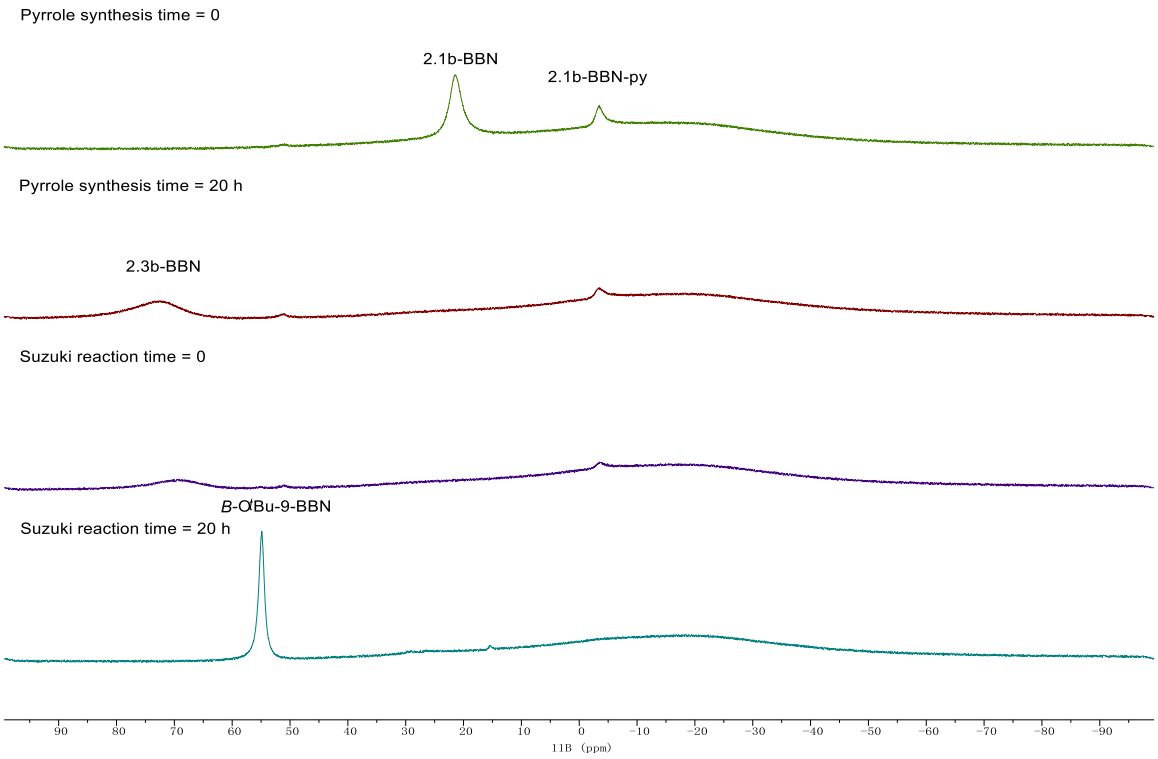

Figure 2.112. ^{11}B NMR of the one-pot pyrrole synthesis/arylation of **2.1b-BBN** and **2.6a** at time = 0, time = 20 h of pyrrole synthesis, time = 0 and time = 20 h of Suzuki reaction in $PhCH_3$. *Taken from (top to bottom) (1) YC-2020-0024-NoD-Tol-0h-B; (2) YC-2020-0024-NoD-Tol-20h-B; (3) YC-2020-0024-NoD-Tol-tandem-0h-B; (4) YC-2020-0024-NoD-Tol-tandem-20h-B.*

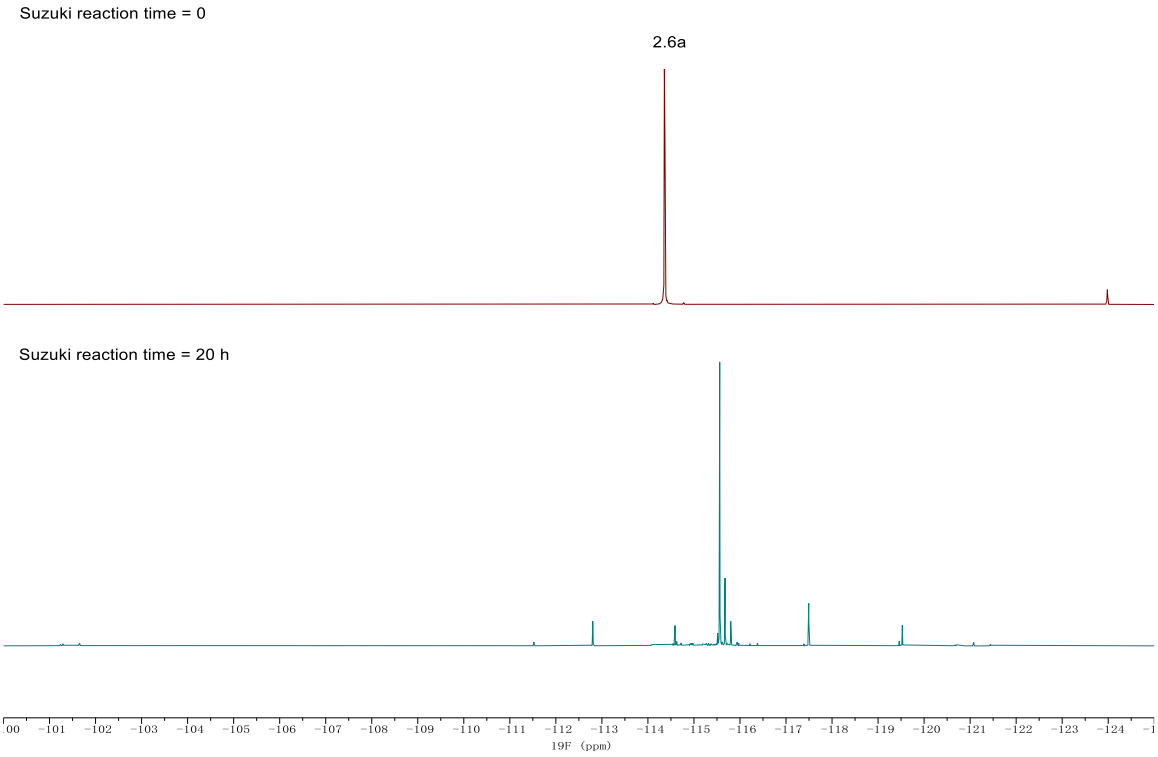

Figure 2.113. $^{19}F\{^{1}H\}$ NMR of the one-pot pyrrole synthesis/arylation of **2.1b-BBN** and **2.6a** at time = 0 and time = 20 h of Suzuki reaction in $PhCH_3$. *Taken from (top) YC-2020-0024-NoD-Tol-tandem-0h-F and (bottom) YC-2020-0024-NoD-Tol-tandem-20h-F.*

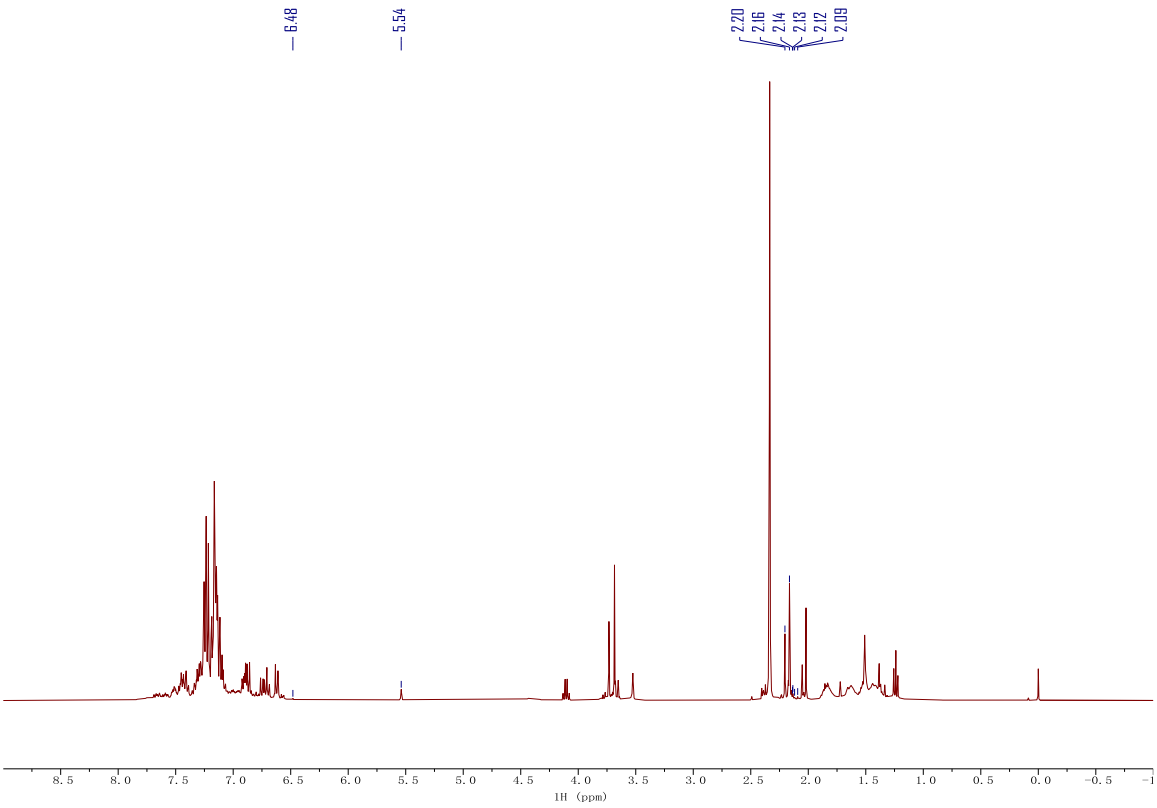

	δ (ppm)	Assignment	# of H	Peak Area	Yield (%)
Ph_3CH	5.54	Ph_3C-H	1	1956.4	n.a.
2.7ba	2.16	$Me_{pyrrolyl}$	3	9315.6	31.7
2.3b	2.20	$Me_{pyrrolyl}$	3	6711.6	22.9
2.4b	6.48	$H_{pyrrolyl}$	1	80.5	0.8
2.5b	not found	$H_{pyrrolyl}$	1	n.a.	n.d.
homocoupled **2.2**	2.14, 2.13, 2.12, 2.09	$Me_{pyrrolyl}$ (2 per molecule)	6	1959.8	3.3

Figure 2.114. ^1H NMR of the one-pot pyrrole synthesis/arylation of **2.1b-BBN** and **2.6a** in $CDCl_3$ after HCl workup. *Taken from YC-2020-0024-5H.*

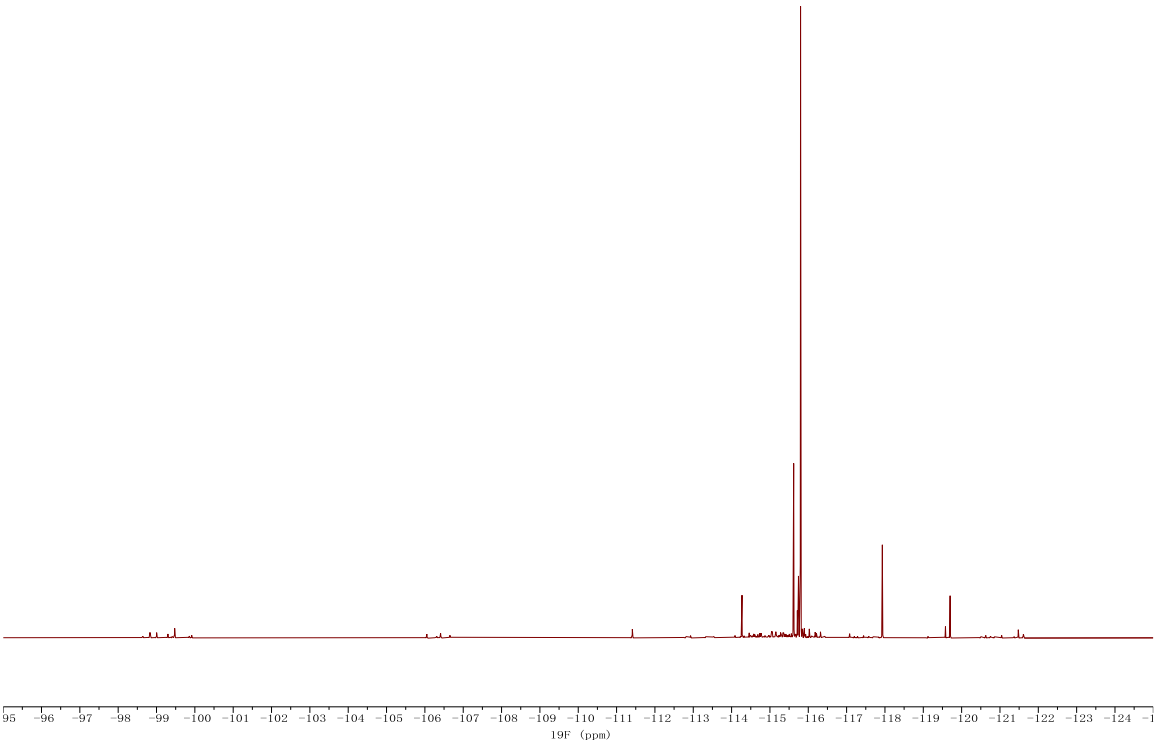

Figure 2.115. $^{19}F\{^{1}H\}$ NMR of the one-pot pyrrole synthesis/arylation of **2.1b-BBN** and **2.6a** in $CDCl_3$ after HCl workup. *Taken from YC-2020-0024-5F.*

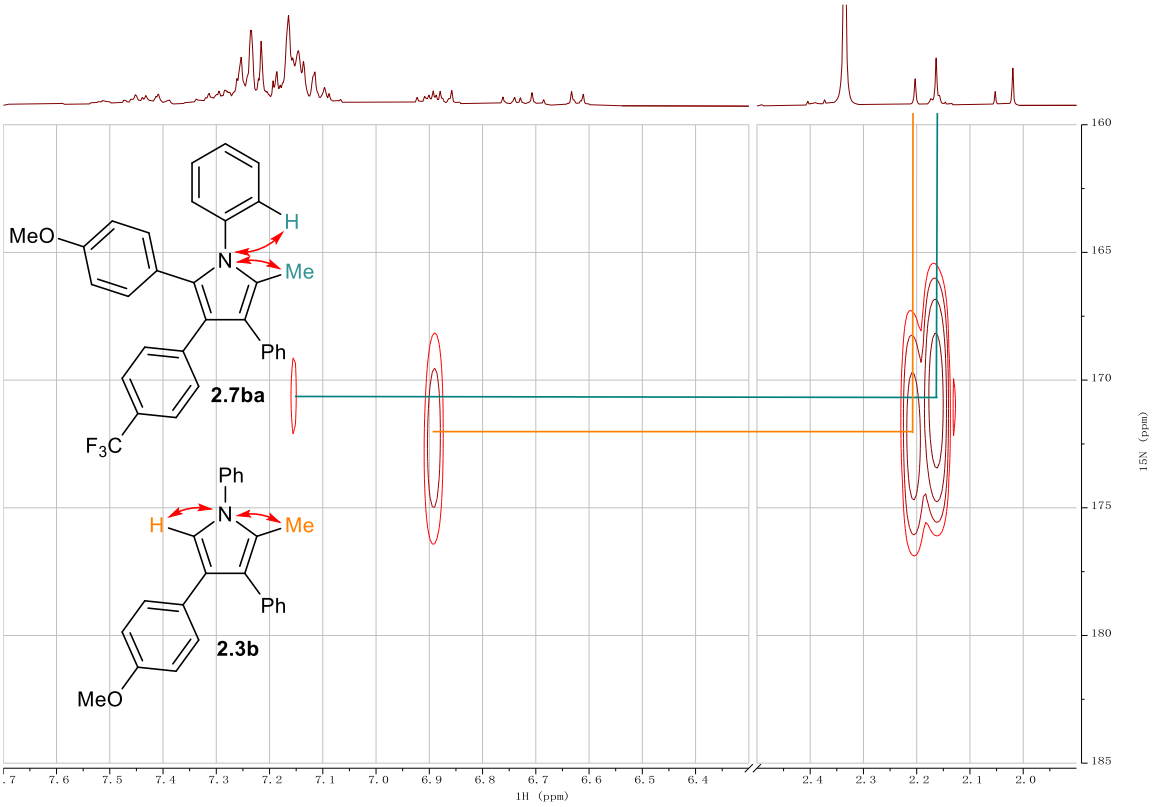

Figure 2.116. ^{1}H–^{15}N HMBC of the one-pot pyrrole synthesis/arylation of **2.1b-BBN** and **2.6a** in $CDCl_3$ after HCl workup. *Taken from YC-2020-0024-5NHMBC.*

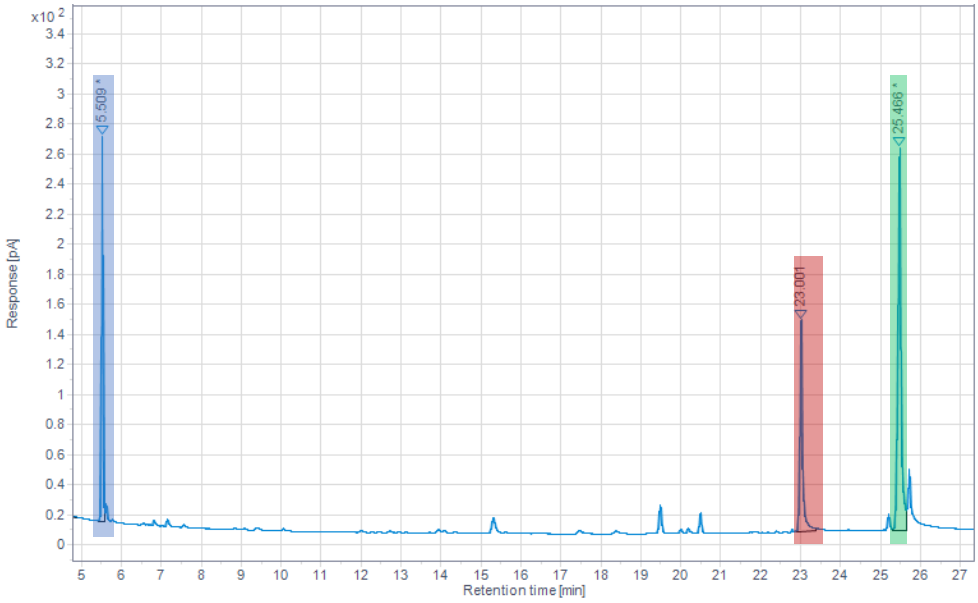

	Retention Time (min)	Surface Area	# of C	Yield (%)
Ph_3CH	5.51	603.790	19	n.a.
2.7ba	25.47	1336.157	30	28.0
2.3b	23.00	598.320	24	15.7

Figure 2.117. Quantitative GC-FID chromatograph of the one-pot pyrrole synthesis/arylation of **2.1b-BBN** and **2.6a** after HCl workup. *Taken from YC-2020-0024-1FID.*

One-Pot Pyrrole Synthesis/Arylation for 2.1c-BBN and *p*-Fluoroiodobenzene

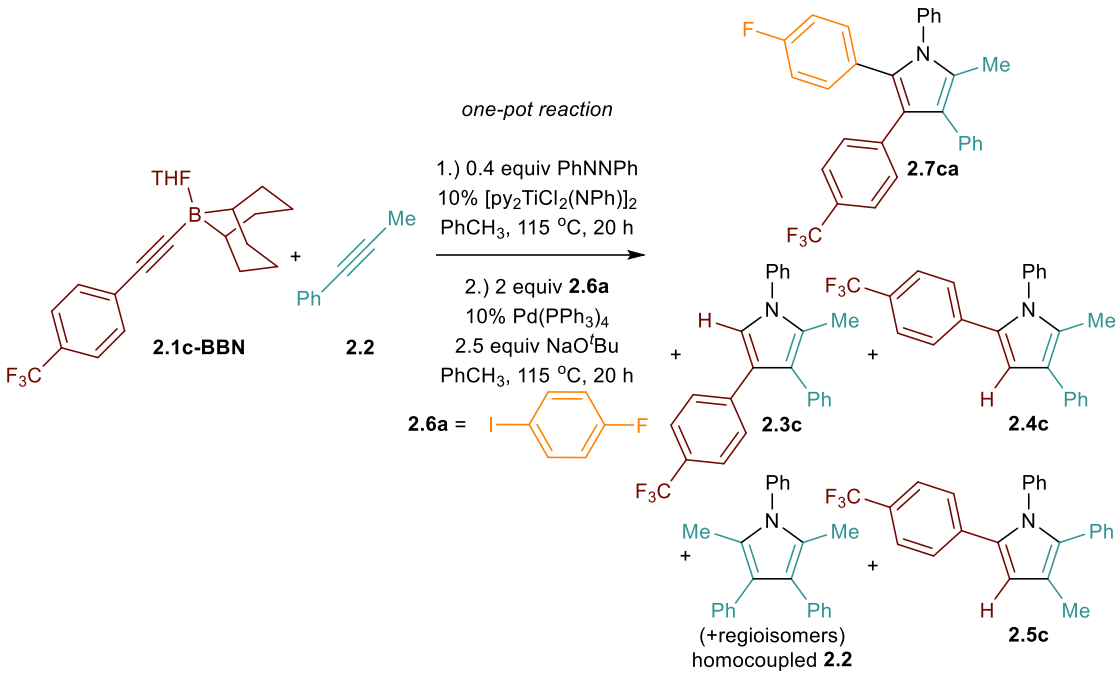

The reaction was performed following **Procedure 2.D** using **2.1c-BBN** (36.2 mg, 0.1 mmol, 1 equiv) as alkynylborane and *p*-fluoroiodobenzene (**2.6a**, 44.4 mg, 0.2 mmol, 2 equiv) as aryl iodide.

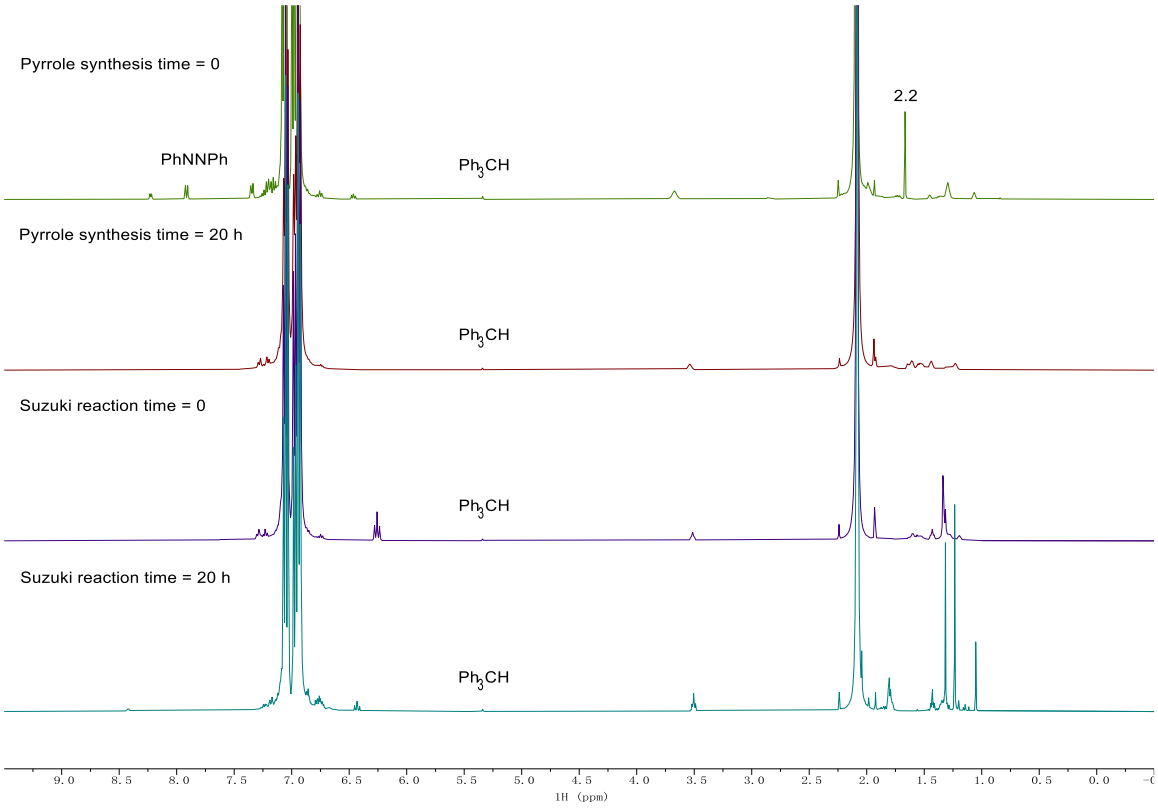

Figure 2.118. No-D ^{1}H NMR of the one-pot pyrrole synthesis/arylation of **2.1c-BBN** and **2.6a** at time = 0, time = 20 h of pyrrole synthesis, time = 0 and time = 20 h of Suzuki reaction in $PhCH_3$. *Taken from (top to bottom) (1) YC-2020-0025-NoD-Tol-0h-H; (2) YC-2020-0025-NoD-Tol-20h-H; (3) YC-2020-0025-NoD-Tol-tandem-0h-H; (4) YC-2020-0025-NoD-Tol-tandem-20h-H.*

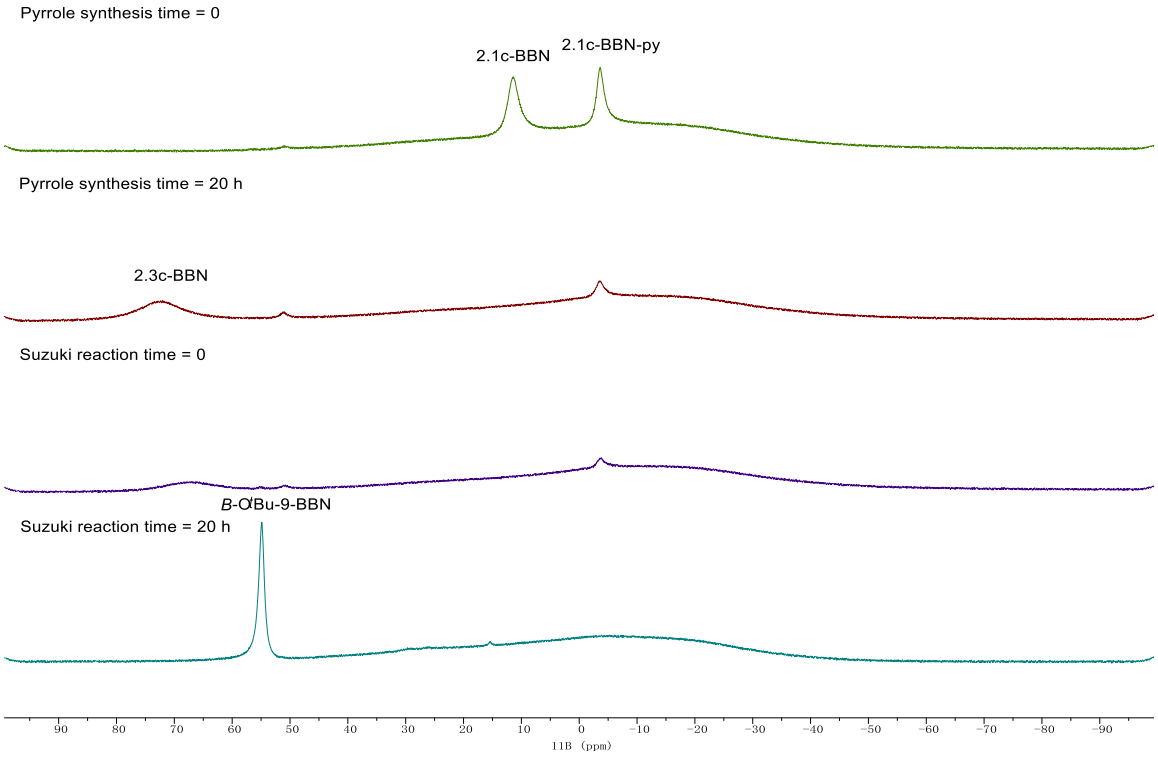

Figure 2.119. ^{11}B NMR of the one-pot pyrrole synthesis/arylation of **2.1c-BBN** and **2.6a** at time = 0, time = 20 h of pyrrole synthesis, time = 0 and time = 20 h of Suzuki reaction in $PhCH_3$. *Taken from (top to bottom) (1) YC-2020-0025-NoD-Tol-0h-B; (2) YC-2020-0025-NoD-Tol-20h-B; (3) YC-2020-0025-NoD-Tol-tandem-0h-B; (4) YC-2020-0025-NoD-Tol-tandem-20h-B.*

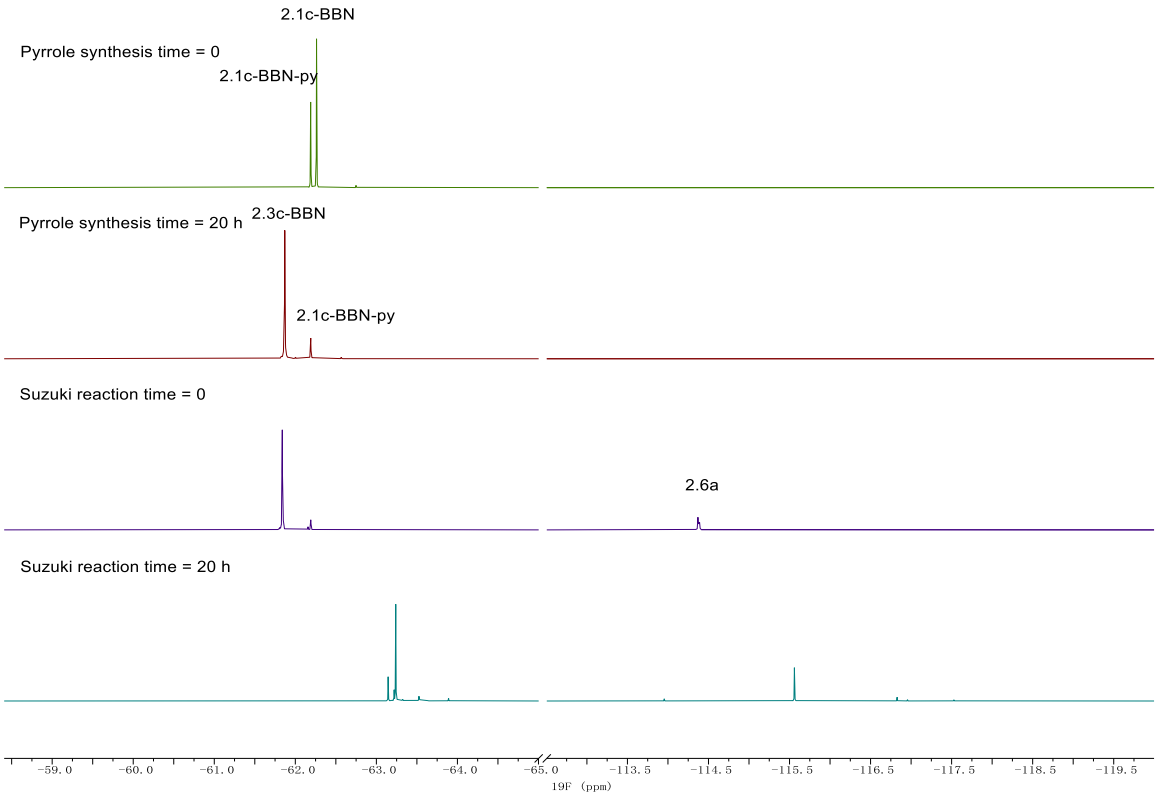

Figure 2.120. $^{19}F\{^{1}H\}$ NMR of the one-pot pyrrole synthesis/arylation of **2.1c-BBN** and **2.6a** at time = 0, time = 20 h of pyrrole synthesis, time = 0 and time = 20 h of Suzuki reaction in $PhCH_3$. *Taken from (top to bottom) (1) YC-2020-0025-NoD-Tol-0h-F; (2) YC-2020-0025-NoD-Tol-20h-F; (3) YC-2020-0025-NoD-Tol-tandem-0h-F; (4) YC-2020-0025-NoD-Tol-tandem-20h-F.*

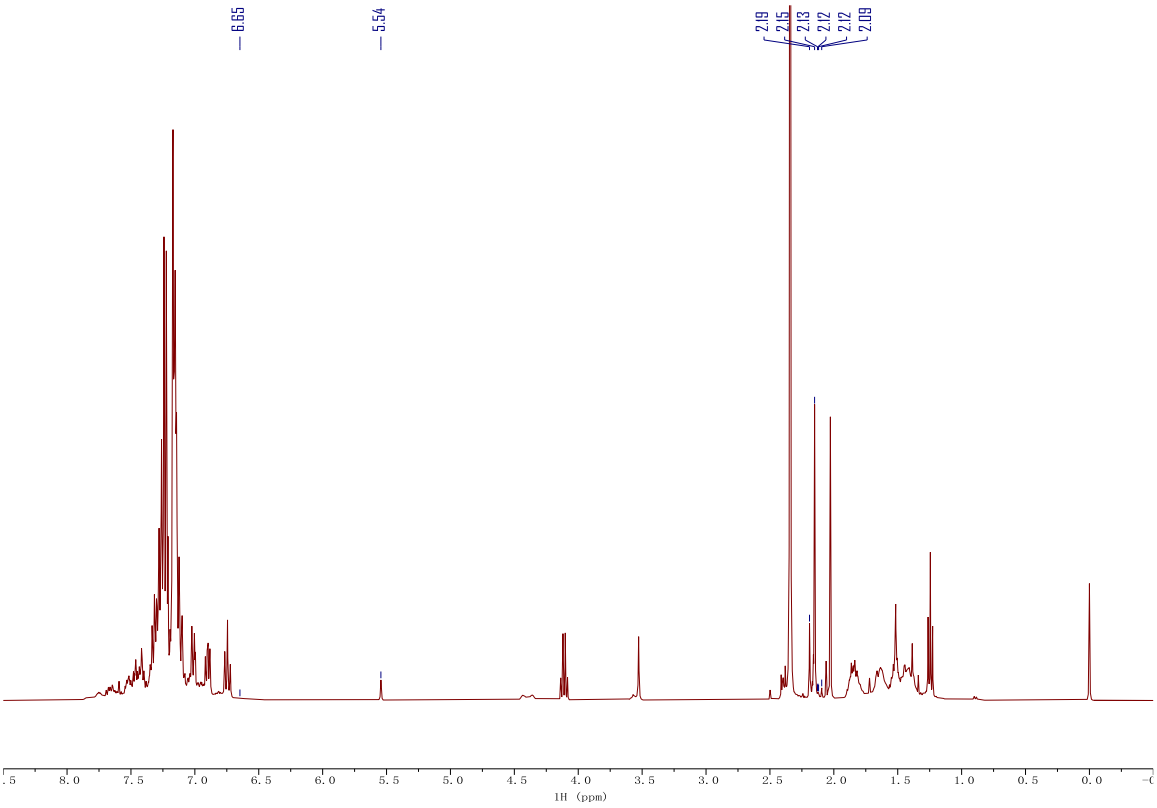

	δ (ppm)	Assignment	# of H	Peak Area	Yield (%)
Ph_3CH	5.54	Ph_3C-H	1	2089.5	n.a.
2.7ca	2.15	$Me_{pyrrolyl}$	3	17925.1	57.2
2.3c	2.19	$Me_{pyrrolyl}$	3	4156.4	13.3
2.4c	6.65	$H_{pyrrolyl}$	1	44.7	0.4
2.5c	not found	$H_{pyrrolyl}$	1	n.a.	n.d.
homocoupled **2.2**	2.13, 2.12, 2.12, 2.09	$Me_{pyrrolyl}$ (2 per molecule)	6	1043.1	1.7

Figure 2.121. ^{1}H NMR of the one-pot pyrrole synthesis/arylation of **2.1c-BBN** and **2.6a** in $CDCl_3$ after HCl workup. *Taken from YC-2020-0025-5H.*

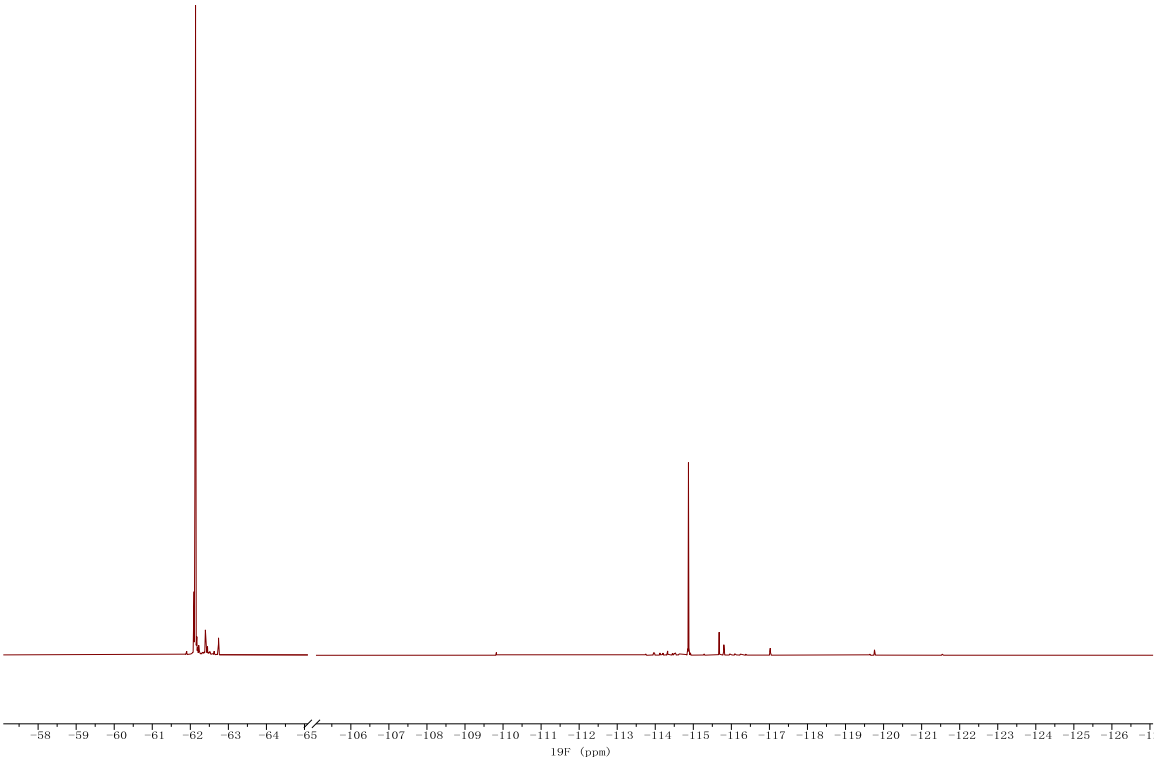

Figure 2.122. $^{19}F\{^{1}H\}$ NMR of the one-pot pyrrole synthesis/arylation of **2.1c-BBN** and **2.6a** in $CDCl_3$ after HCl workup. *Taken from YC-2020-0025-5F.*

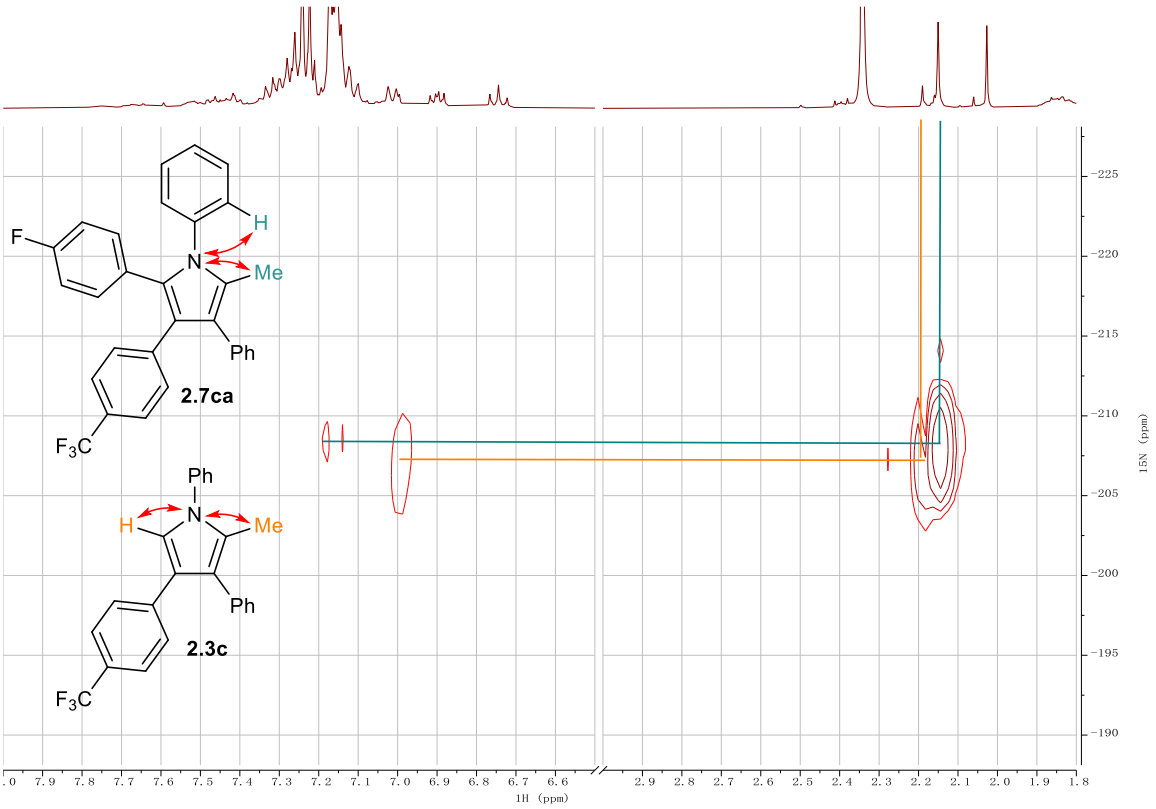

Figure 2.123. ^{1}H–^{15}N HMBC of the one-pot pyrrole synthesis/arylation of **2.1c-BBN** and **2.6a** in $CDCl_3$ after HCl workup. *Taken from YC-2020-0025-5NHMBC.*

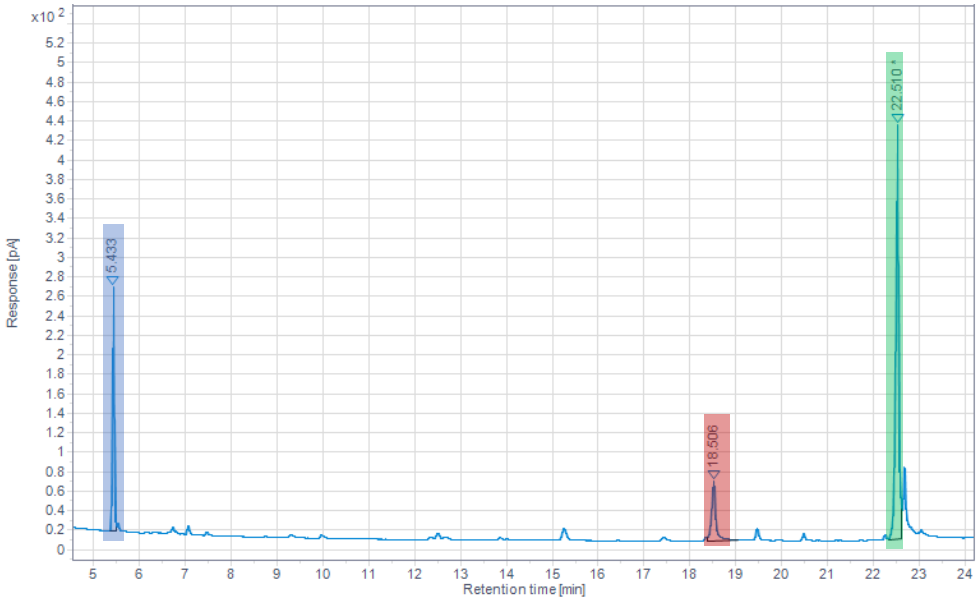

	Retention Time (min)	Surface Area	# of C	Yield (%)
Ph_3CH	5.43	593.967	19	n.a.
2.7ca	22.51	2204.875	30	47.0
2.3c	18.51	388.869	24	10.4

Figure 2.124. Quantitative GC-FID chromatograph of the one-pot pyrrole synthesis/arylation of **2.1c-BBN** and **2.6a** after HCl workup. *Taken from YC-2020-0025-1FID.*

One-Pot Pyrrole Synthesis/Arylation for 2.1d-BBN and *p*-Fluoroiodobenzene

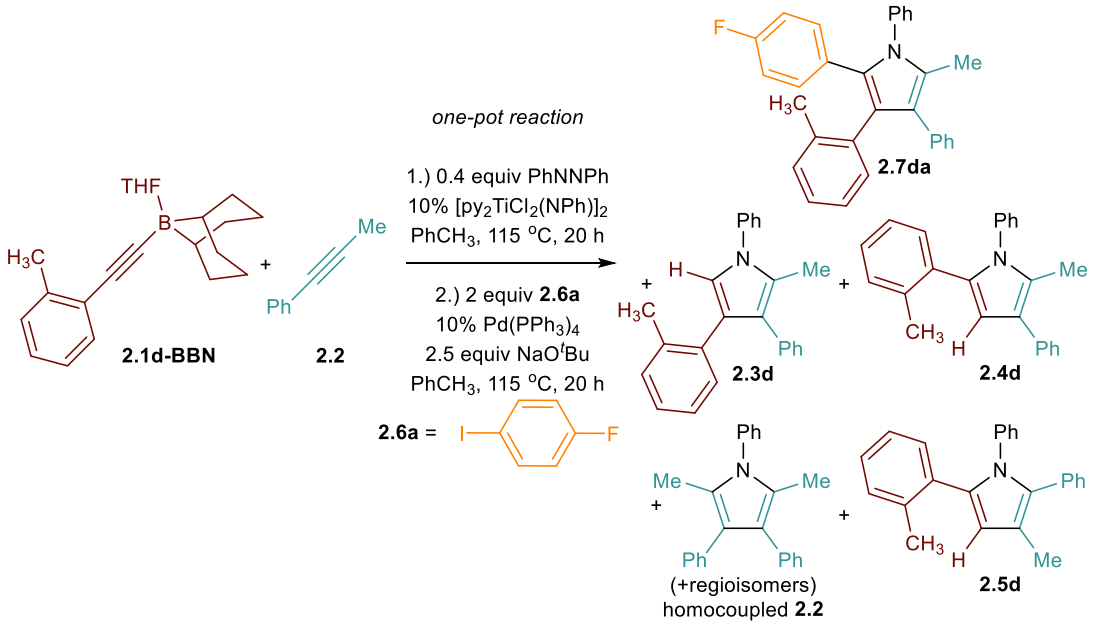

The reaction was performed following **Procedure 2.D** using **2.1d-BBN** (30.8 mg, 0.1 mmol, 1 equiv) as alkynylborane and *p*-fluoroiodobenzene (**2.6a**, 44.4 mg, 0.2 mmol, 2 equiv) as aryl iodide.

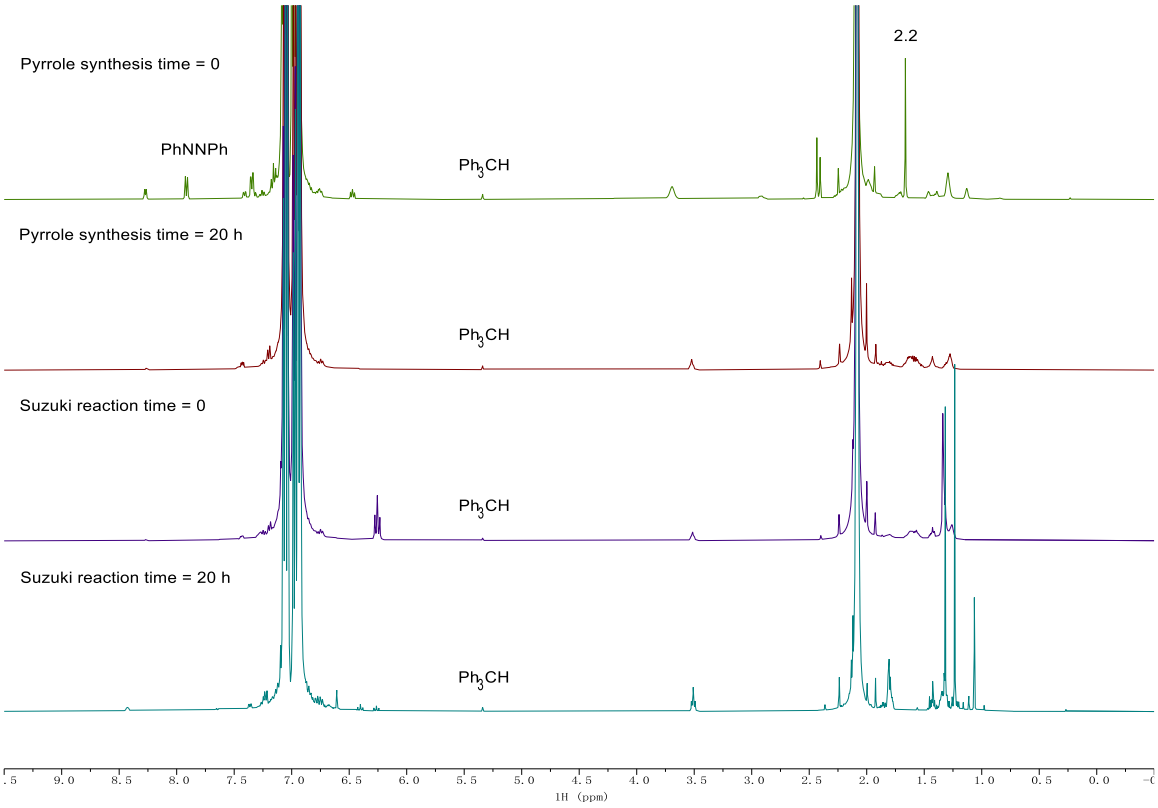

Figure 2.125. No-D ^{1}H NMR of the one-pot pyrrole synthesis/arylation of **2.1d-BBN** and **2.6a** at time = 0, time = 20 h of pyrrole synthesis, time = 0 and time = 20 h of Suzuki reaction in $PhCH_3$. *Taken from (top to bottom) (1) YC-2020-0026-NoD-Tol-0h-H; (2) YC-2020-0026-NoD-Tol-20h-H; (3) YC-2020-0026-NoD-Tol-tandem-0h-H; (4) YC-2020-0026-NoD-Tol-tandem-20h-H.*

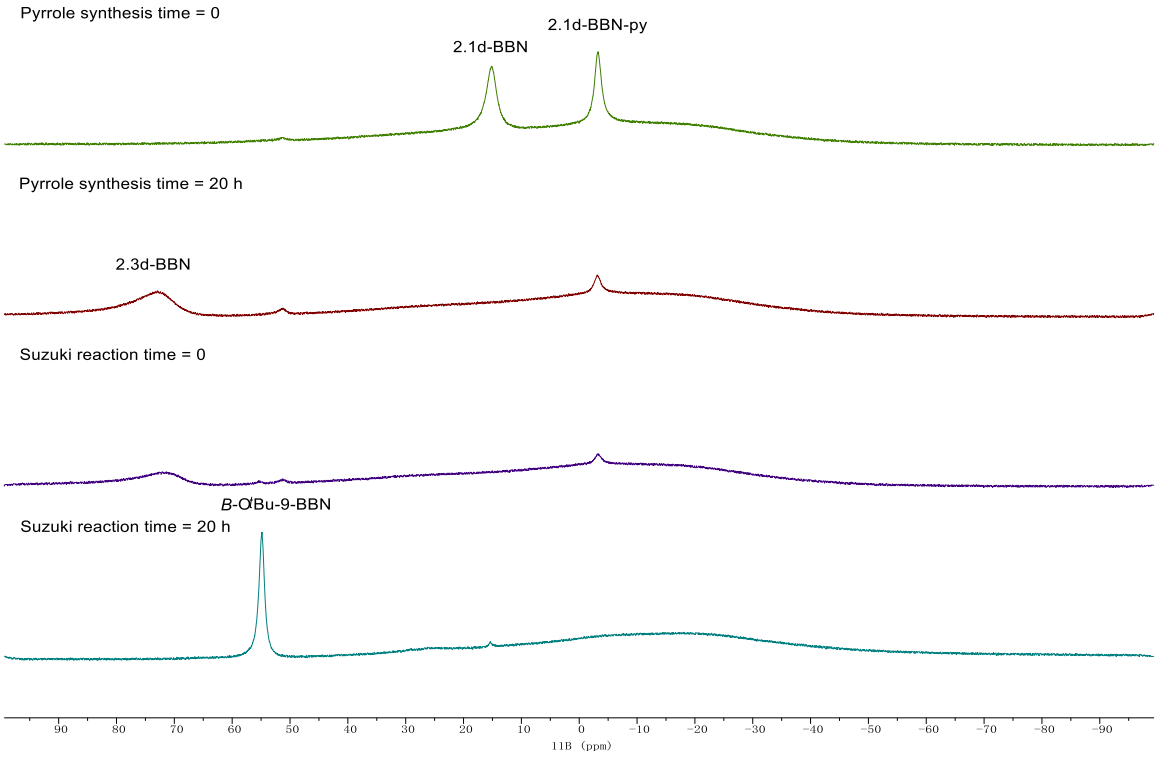

Figure 2.126. ^{11}B NMR of the one-pot pyrrole synthesis/arylation of **2.1d-BBN** and **2.6a** at time = 0, time = 20 h of pyrrole synthesis, time = 0 and time = 20 h of Suzuki reaction in $PhCH_3$. *Taken from (top to bottom) (1) YC-2020-0026-NoD-Tol-0h-B; (2) YC-2020-0026-NoD-Tol-20h-B; (3) YC-2020-0026-NoD-Tol-tandem-0h-B; (4) YC-2020-0026-NoD-Tol-tandem-20h-B.*

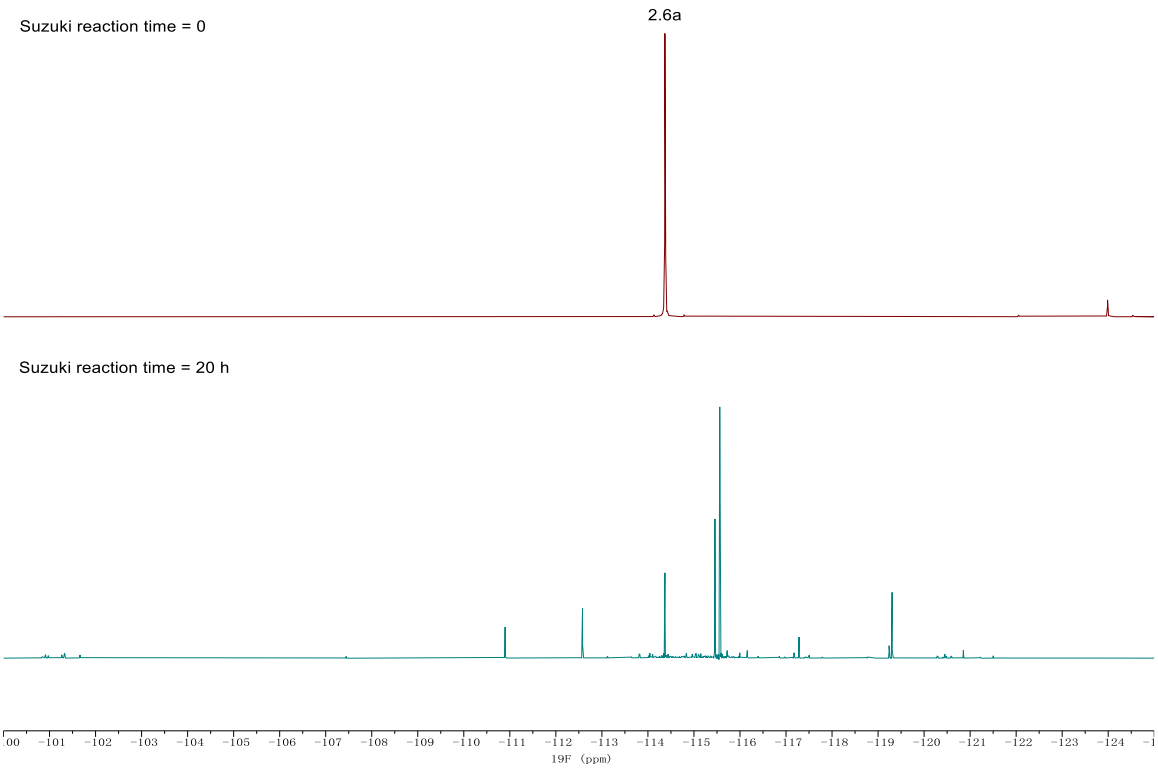

Figure 2.127. $^{19}F\{^{1}H\}$ NMR of the one-pot pyrrole synthesis/arylation of **2.1d-BBN** and **2.6a** at time = 0 and time = 20 h of Suzuki reaction in $PhCH_3$. *Taken from (top) YC-2020-0026-NoD-Tol-tandem-0h-F and (bottom) YC-2020-0026-NoD-Tol-tandem-20h-F.*

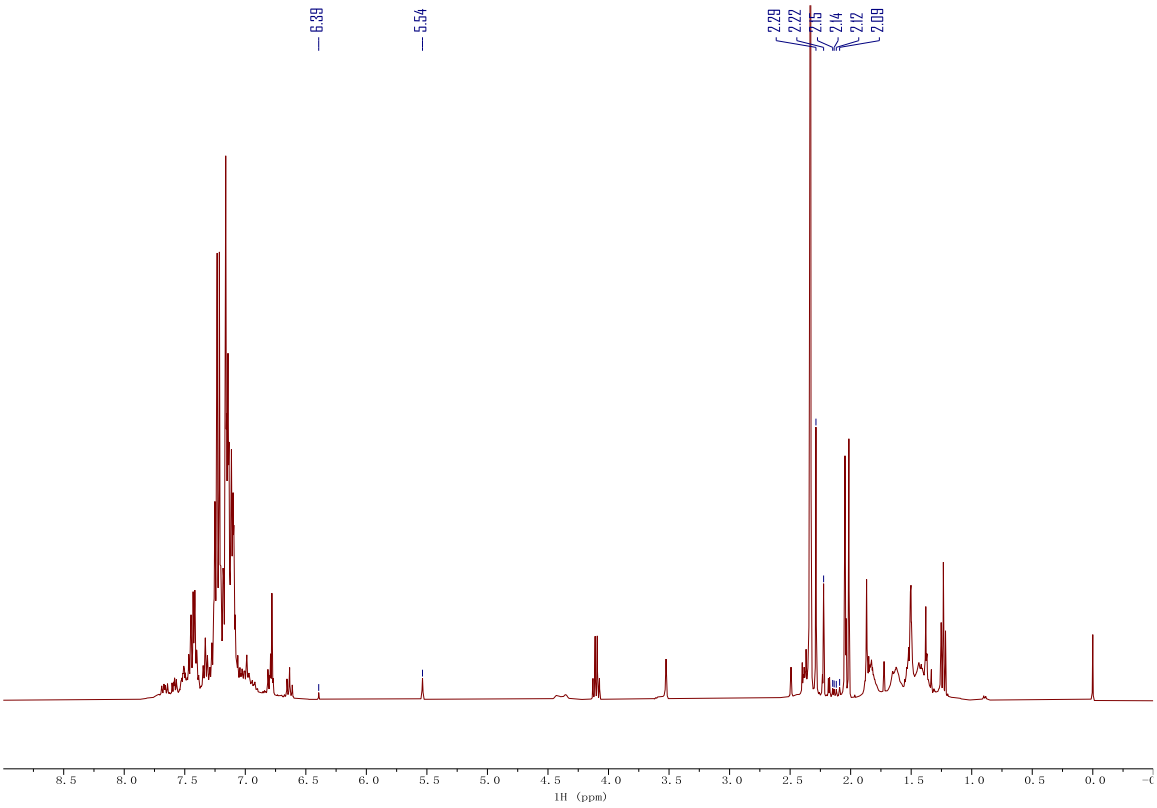

	δ (ppm)	Assignment	# of H	Peak Area	Yield (%)
Ph_3CH	5.54	Ph_3C-H	1	1645.6	n.a.
2.7da	2.22	$Me_{pyrrolyl}$	3	4649.1	18.8
2.3d	2.29	$Me_{pyrrolyl}$	3	11361.0	46.0
2.4d	6.39	$H_{pyrrolyl}$	1	273.2	3.3
2.5d	not found	$H_{pyrrolyl}$	1	n.a.	n.d.
homocoupled **2.2**	2.15, 2.14, 2.12, 2.09	$Me_{pyrrolyl}$ (2 per molecule)	6	1477.0	3.0

Figure 2.128. ^1H NMR of the one-pot pyrrole synthesis/arylation of **2.1d-BBN** and **2.6a** in $CDCl_3$ after HCl workup. *Taken from YC-2020-0026-5H.*

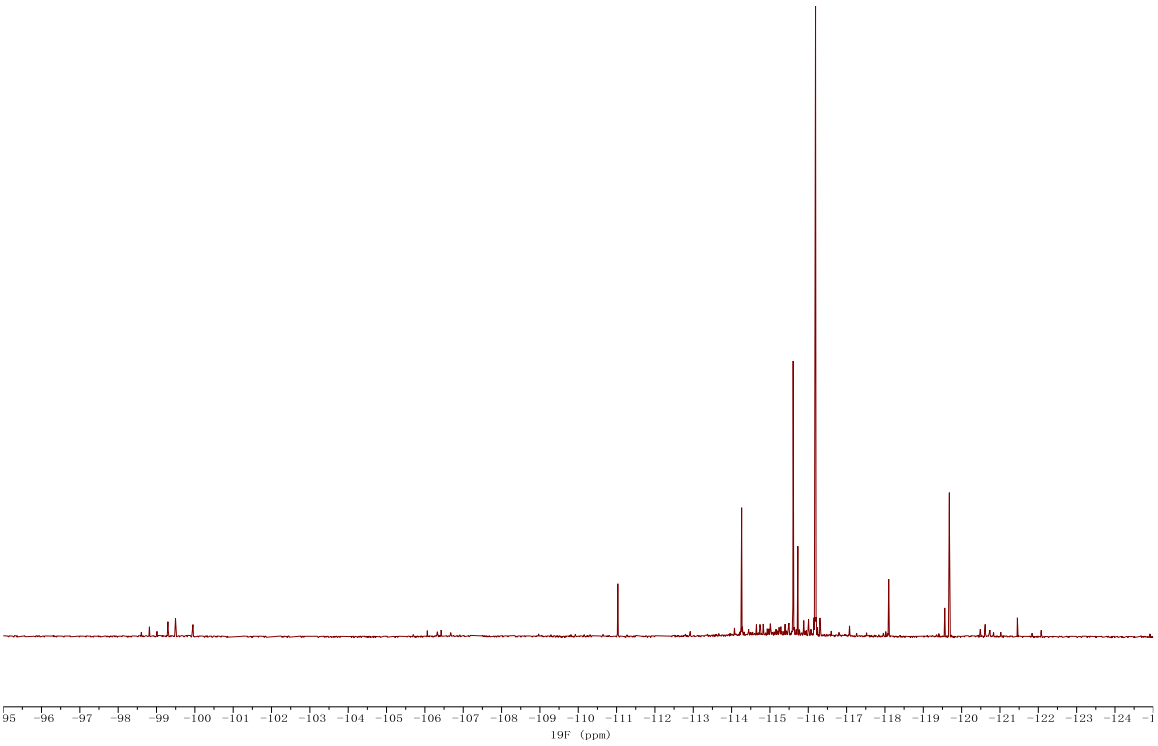

Figure 2.129. $^{19}F\{^{1}H\}$ NMR of the one-pot pyrrole synthesis/arylation of **2.1d-BBN** and **2.6a** in $CDCl_3$ after HCl workup. *Taken from YC-2020-0026-5F.*

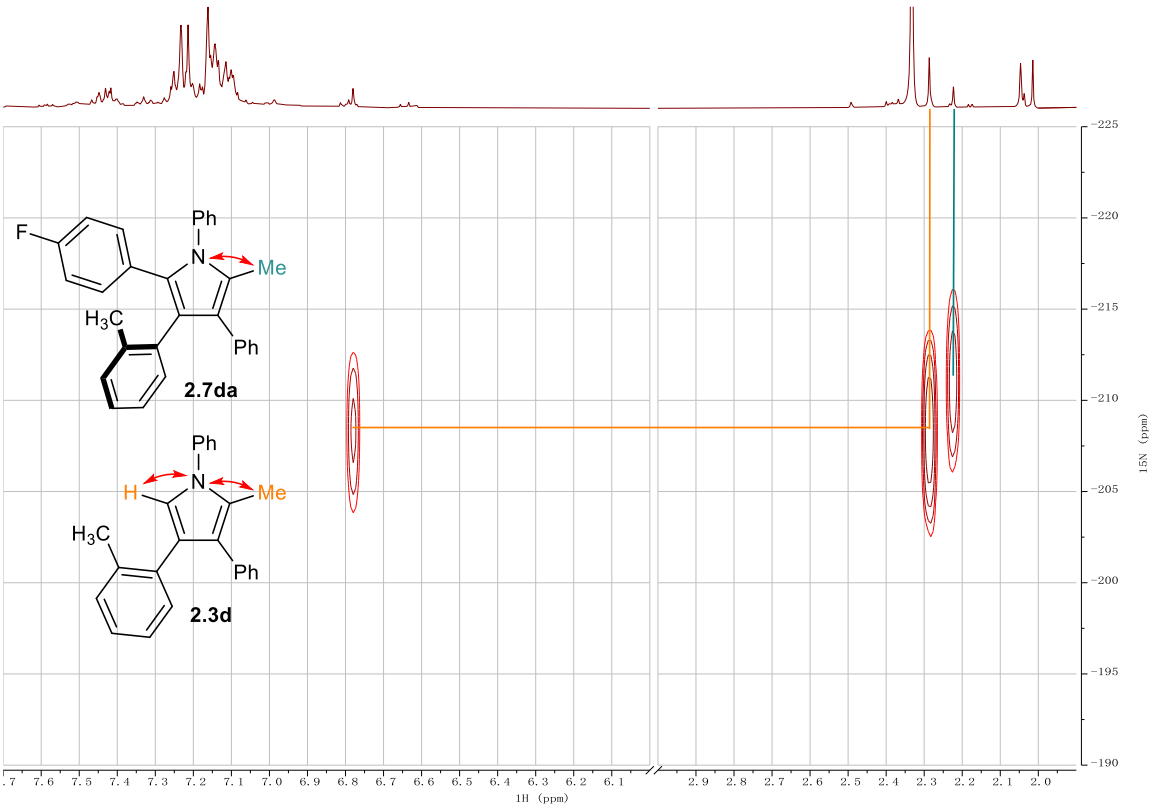

Figure 2.130. ^{1}H–^{15}N HMBC of the one-pot pyrrole synthesis/arylation of **2.1d-BBN** and **2.6a** in $CDCl_3$ after HCl workup. *Taken from YC-2020-0026-5NHMBC.*

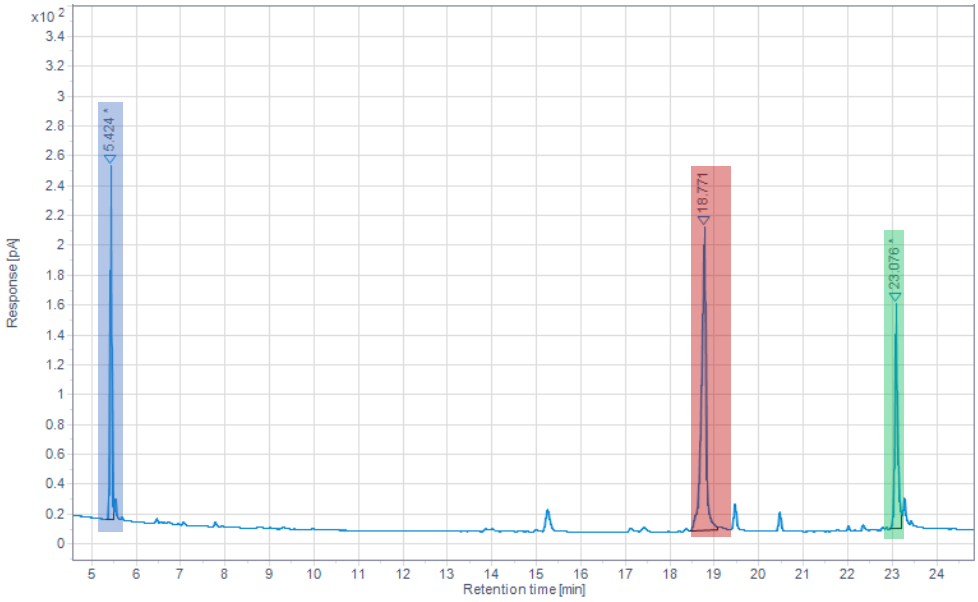

	Retention Time (min)	Surface Area	# of C	Yield (%)
Ph_3CH	5.42	555.761	19	n.a.
2.7da	23.08	710.741	30	16.2
2.3d	18.77	1403.187	24	40.0

Figure 2.131. Quantitative GC-FID chromatograph of the one-pot pyrrole synthesis/arylation of **2.1d-BBN** and **2.6a** after HCl workup. *Taken from YC-2020-0026-1FID.*

One-Pot Pyrrole Synthesis/Arylation for 2.1e-BBN and *p*-Fluoroiodobenzene

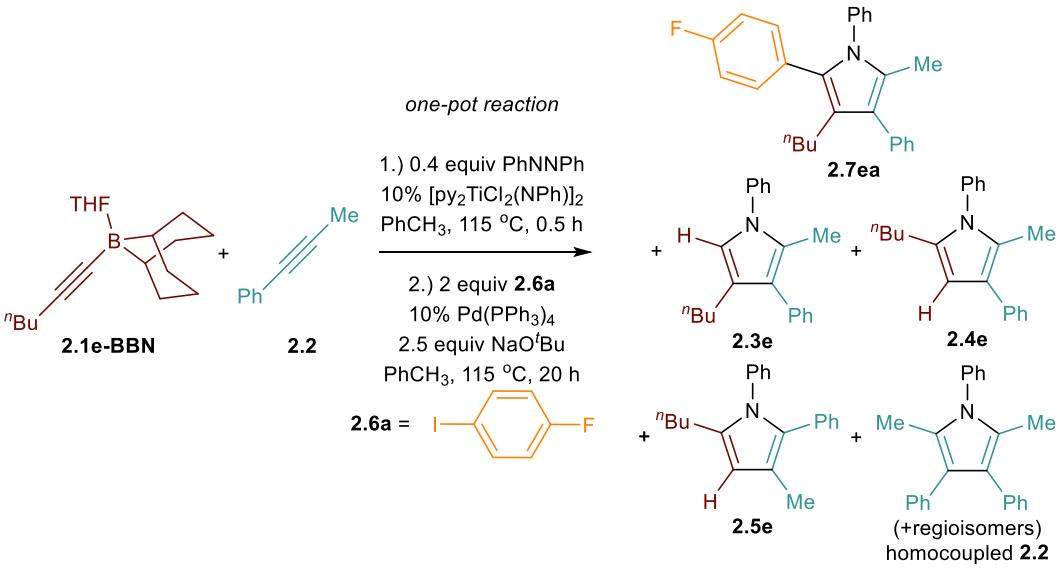

The reaction was performed following **Procedure 2.D** using **2.1e-BBN** (27.4 mg, 0.1 mmol, 1 equiv) as alkynylborane and *p*-fluoroiodobenzene (**2.6a**, 44.4 mg, 0.2 mmol, 2 equiv) as aryl iodide.

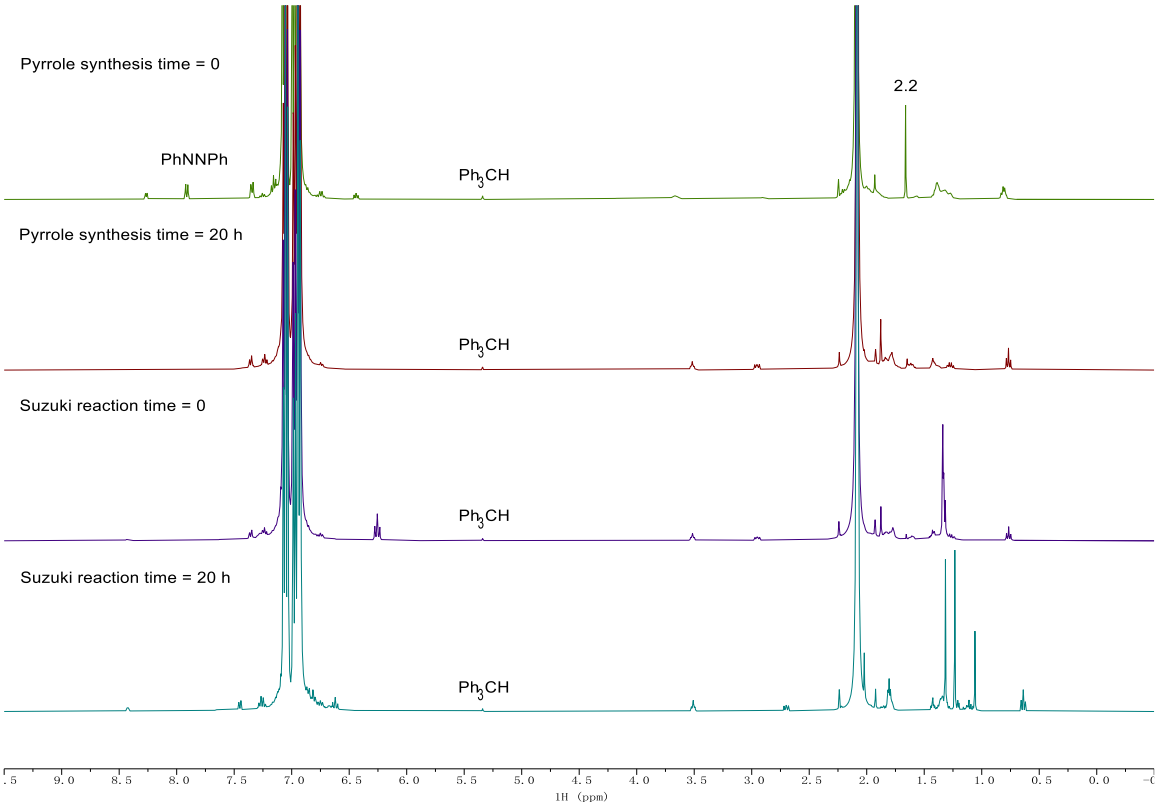

Figure 2.132. No-D ^{1}H NMR of the one-pot pyrrole synthesis/arylation of **2.1e-BBN** and **2.6a** at time = 0, time = 20 h of pyrrole synthesis, time = 0 and time = 20 h of Suzuki reaction in $PhCH_3$. *Taken from (top to bottom) (1) YC-2020-0027-NoD-Tol-0h-H; (2) YC-2020-0027-NoD-Tol-20h-H; (3) YC-2020-0027-NoD-Tol-tandem-0h-H; (4) YC-2020-0027-NoD-Tol-tandem-20h-H.*

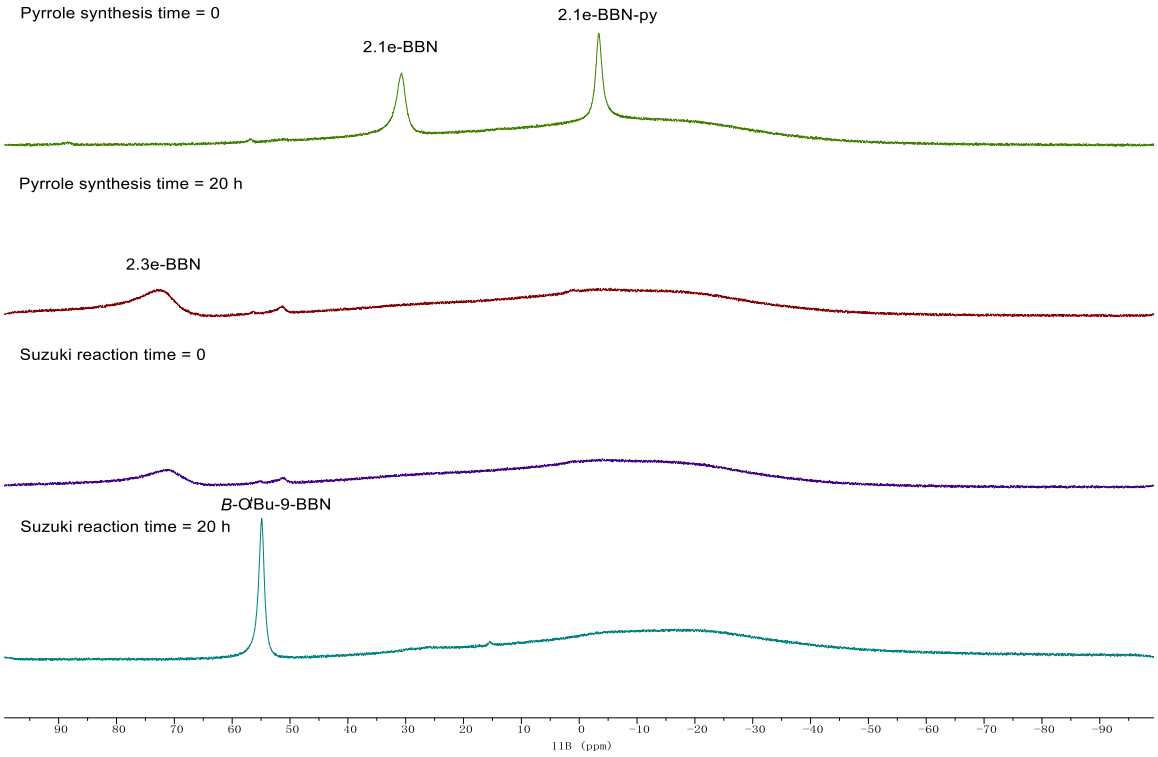

Figure 2.133. ^{11}B NMR of the one-pot pyrrole synthesis/arylation of **2.1e-BBN** and **2.6a** at time = 0, time = 20 h of pyrrole synthesis, time = 0 and time = 20 h of Suzuki reaction in $PhCH_3$. *Taken from (top to bottom) (1) YC-2020-0027-NoD-Tol-0h-B; (2) YC-2020-0027-NoD-Tol-20h-B; (3) YC-2020-0027-NoD-Tol-tandem-0h-B; (4) YC-2020-0027-NoD-Tol-tandem-20h-B.*

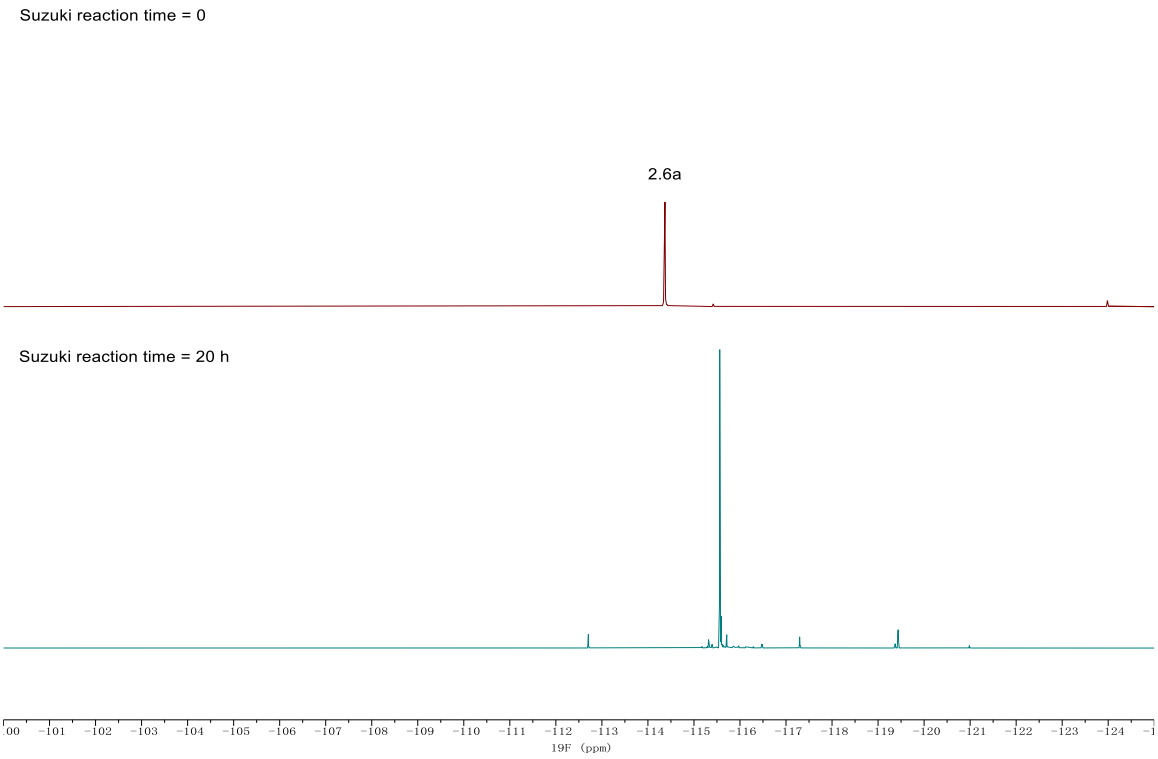

Figure 2.134. $^{19}F\{^{1}H\}$ NMR of the one-pot pyrrole synthesis/arylation of **2.1e-BBN** and **2.6a** at time = 0 and time = 20 h of Suzuki reaction in $PhCH_3$. *Taken from (top) YC-2020-0027-NoD-Tol-tandem-0h-F and (bottom) YC-2020-0027-NoD-Tol-tandem-20h-F.*

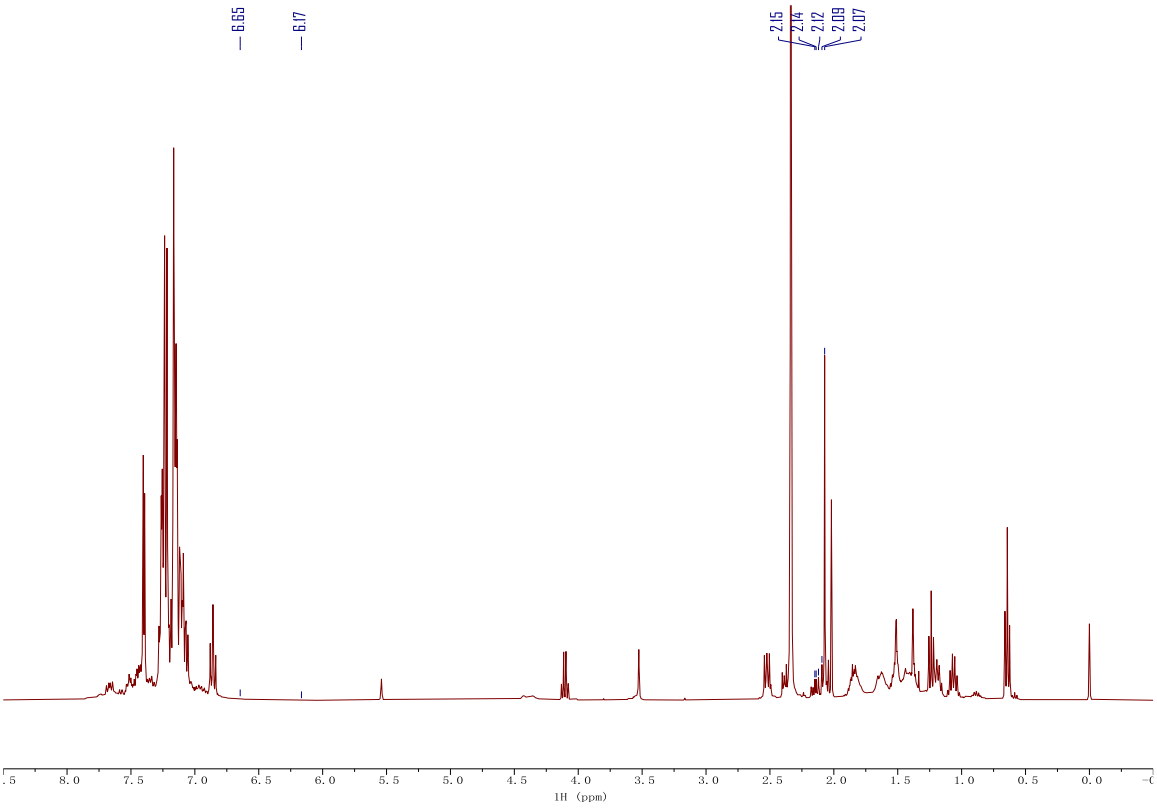

	δ (ppm)	Assignment	# of H	Peak Area	Yield (%)
Ph_3CH	5.54	Ph_3C-H	1	1777.6	n.a.
2.7ea	2.07	$Me_{pyrrolyl}$	3	16573.1	62.2
2.3e	6.65	$H_{pyrrolyl}$	1	93.6	1.1
2.4e	6.17	$H_{pyrrolyl}$	1	54.8	0.6
2.5e	not found	$H_{pyrrolyl}$	1	n.a.	n.d.
homocoupled **2.2**	2.15, 2.14, 2.12, 2.09	$Me_{pyrrolyl}$ (2 per molecule)	6	5062.5	9.5

Figure 2.135. ^{1}H NMR of the one-pot pyrrole synthesis/arylation of **2.1e-BBN** and **2.6a** in $CDCl_3$ after HCl workup. *Taken from YC-2020-0027-5H.*

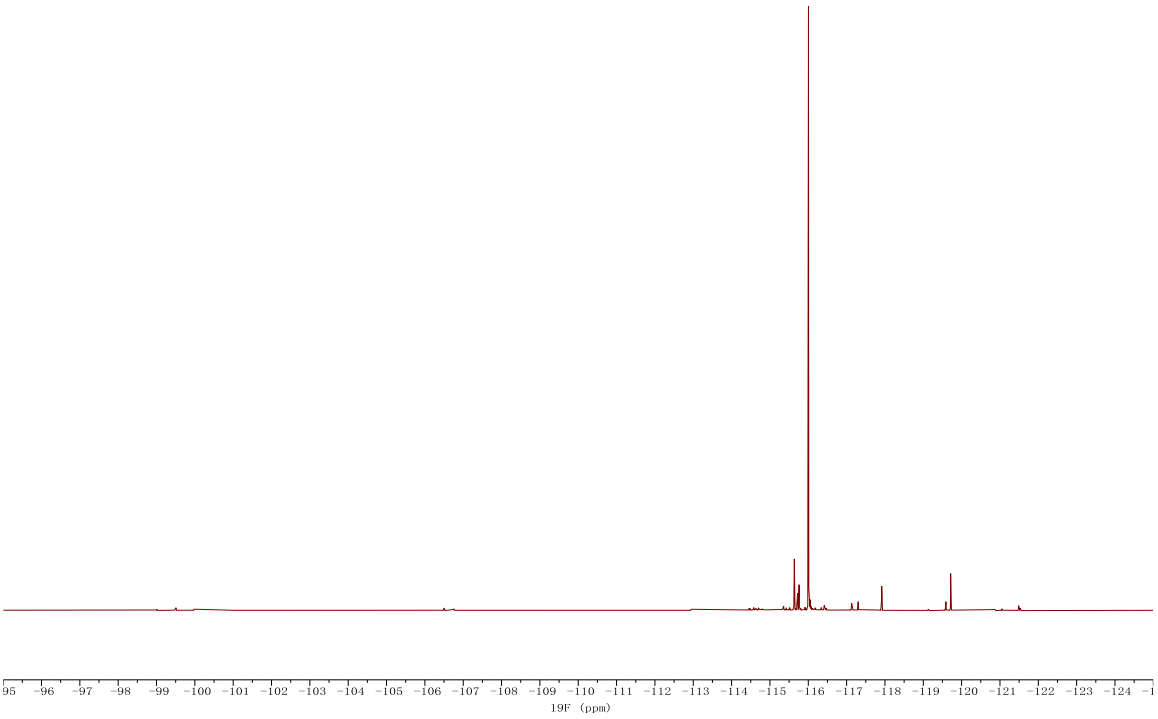

Figure 2.136. $^{19}F\{^{1}H\}$ NMR of the one-pot pyrrole synthesis/arylation of **2.1e-BBN** and **2.6a** in $CDCl_3$ after HCl workup. *Taken from YC-2020-0027-5F.*

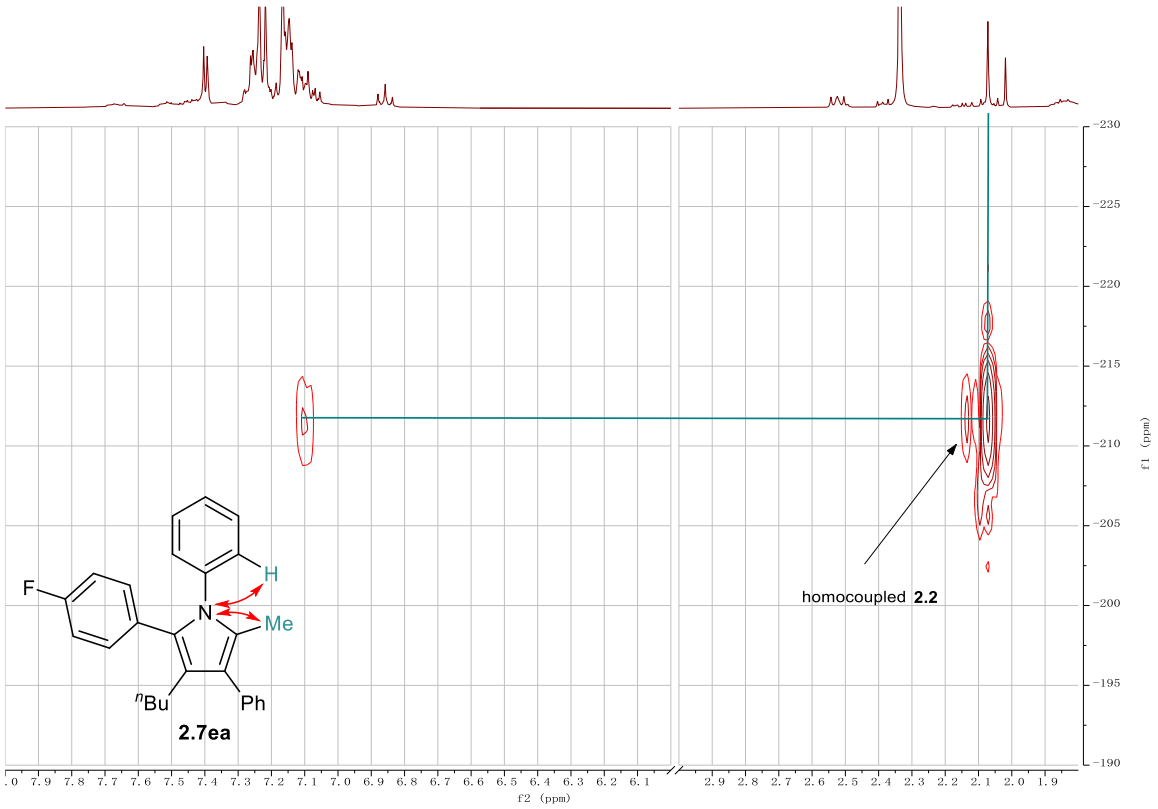

Figure 2.137. ^{1}H–^{15}N HMBC of the one-pot pyrrole synthesis/arylation of **2.1e-BBN** and **2.6a** in $CDCl_3$ after HCl workup. *Taken from YC-2020-0027-5NHMBC.*

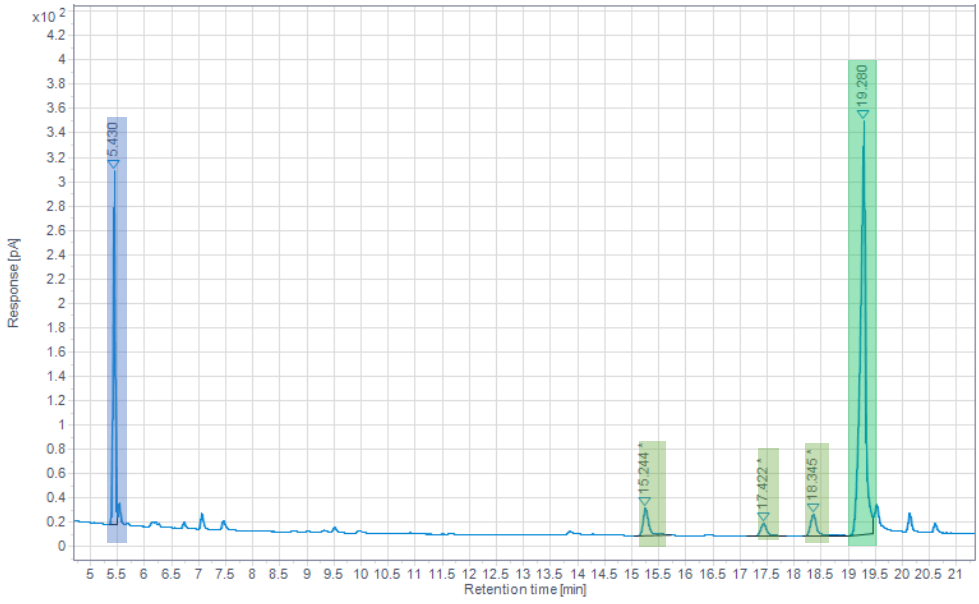

	Retention Time (min)	Surface Area	# of C	Yield (%)
Ph_3CH	5.43	705.418	19	n.a.
2.7ea	19.28	2349.471	27	46.9
2.3e	not found[a]	n.d.	21	n.a.
homocoupled **2.2**	15.24, 17.42, 18.35	385.400	24	8.7

[a]The yield was too low to be identified.

Figure 2.138. Quantitative GC-FID chromatograph of the one-pot pyrrole synthesis/arylation of **2.1e-BBN** and **2.6a** after HCl workup. *Taken from YC-2020-0027-1FID.*

One-Pot Pyrrole Synthesis/Arylation for 2.1a-BBN and *p*-Iodoanisole

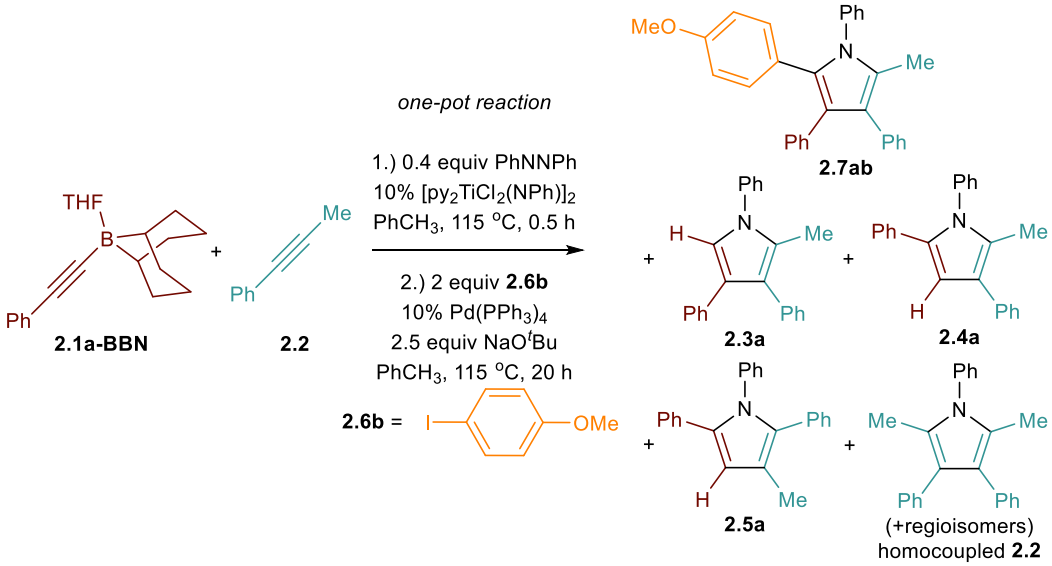

The reaction was performed following **Procedure 2.D** using **2.1a-BBN** (29.4 mg, 0.1 mmol, 1 equiv) as alkynylborane and *p*-iodoanisole (**2.6b**, 46.8 mg, 0.2 mmol, 2 equiv) as aryl iodide. The extraction was performed with CH_2Cl_2/H_2O.

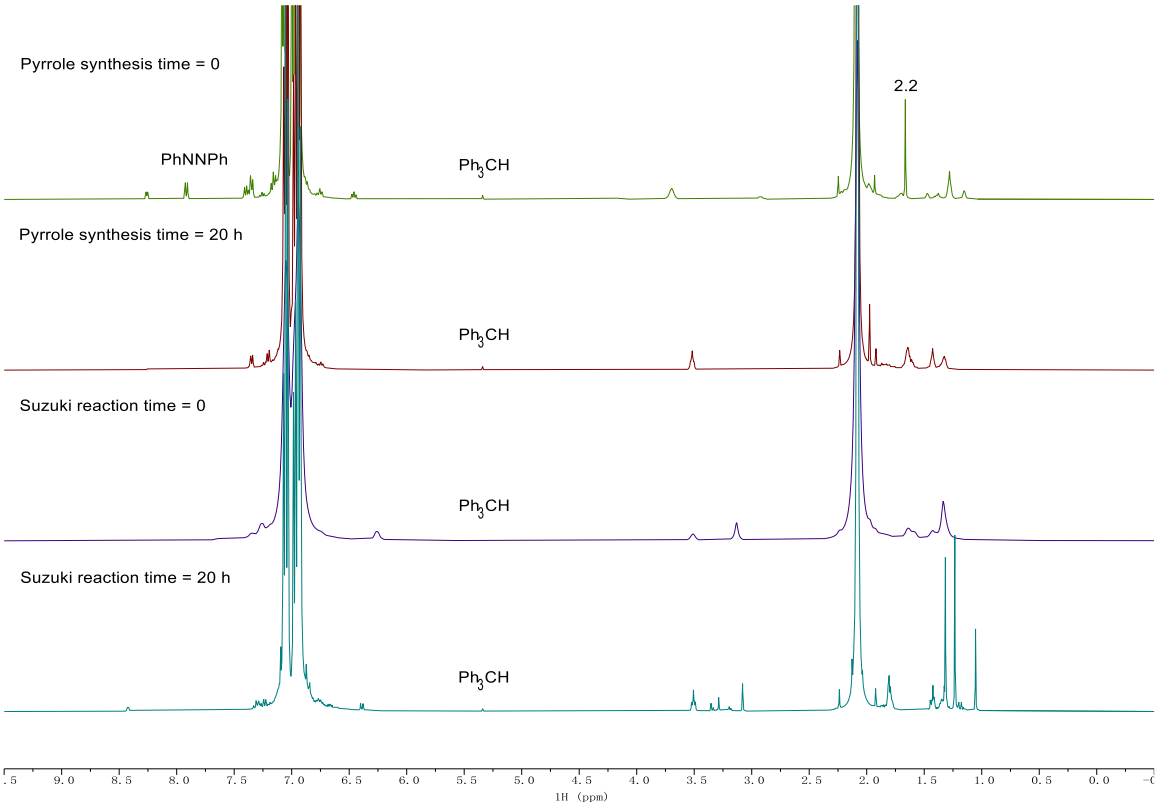

Figure 2.139. No-D ^{1}H NMR of the one-pot pyrrole synthesis/arylation of **2.1a-BBN** and **2.6b** at time = 0, time = 20 h of pyrrole synthesis, time = 0 and time = 20 h of Suzuki reaction in $PhCH_3$. *Taken from (top to bottom) (1) YC-2020-0020-NoD-Tol-0h-H; (2) YC-2020-0020-NoD-Tol-20h-H; (3) YC-2020-0020-NoD-Tol-tandem-0h-H; (4) YC-2020-0020-NoD-Tol-tandem-20h-H.*

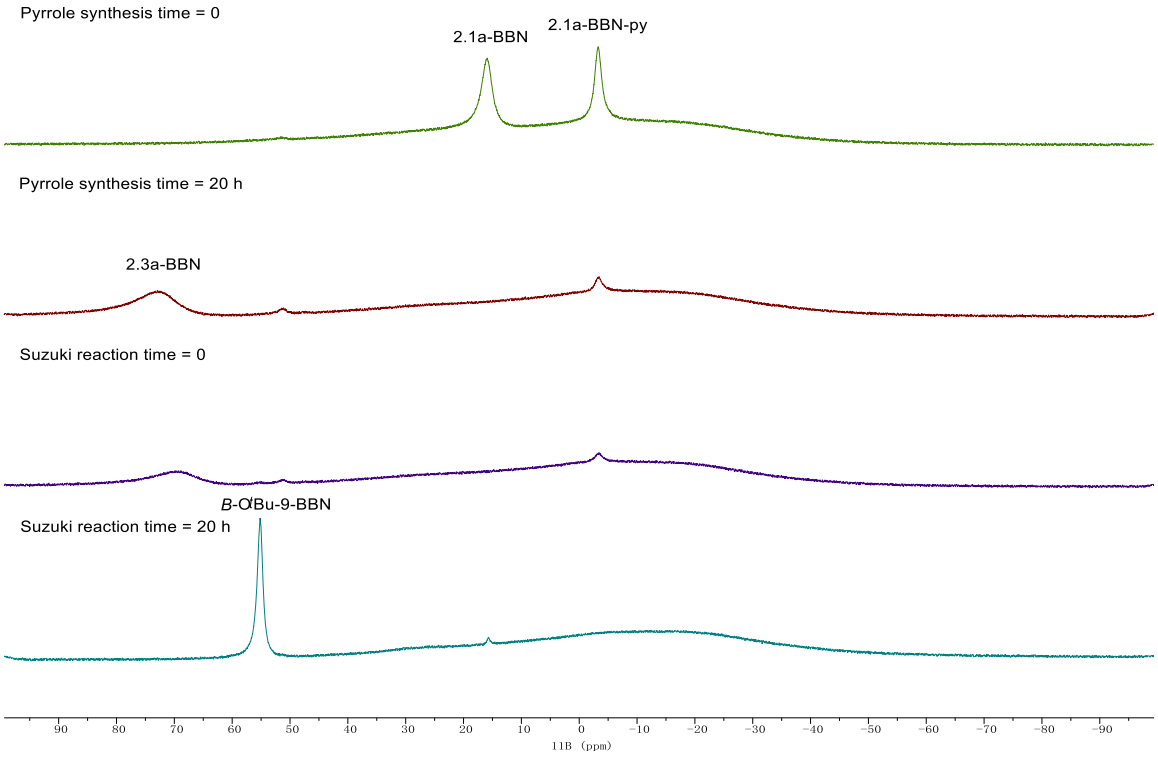

Figure 2.140. ^{11}B NMR of the one-pot pyrrole synthesis/arylation of **2.1a-BBN** and **2.6b** at time = 0, time = 20 h of pyrrole synthesis, time = 0 and time = 20 h of Suzuki reaction in $PhCH_3$. *Taken from (top to bottom) (1) YC-2020-0020-NoD-Tol-0h-B; (2) YC-2020-0020-NoD-Tol-20h-B; (3) YC-2020-0020-NoD-Tol-tandem-0h-B; (4) YC-2020-0020-NoD-Tol-tandem-20h-B.*

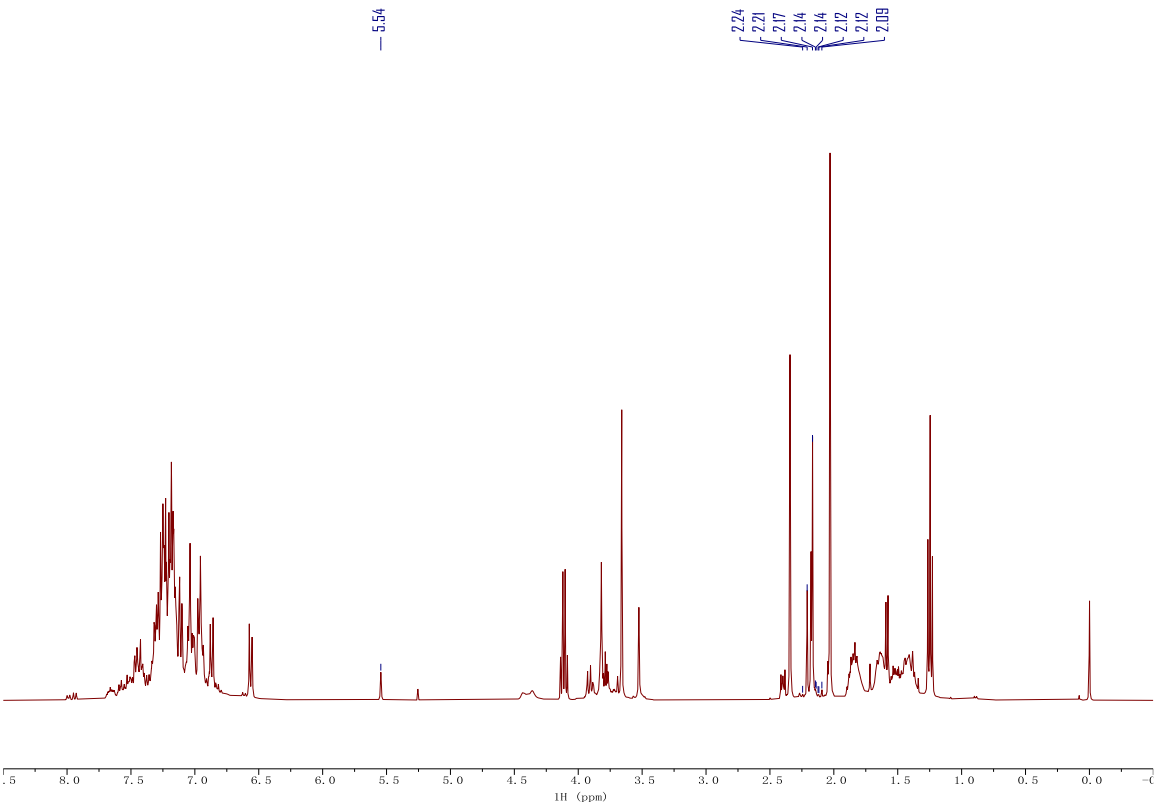

	δ (ppm)	Assignment	# of H	Peak Area	Yield (%)
Ph_3CH	5.54	Ph_3C-H	1	3010.6	n.a.
2.7ab	2.17	$Me_{pyrrolyl}$	3	17318.6	38.4
2.3a	2.20	$Me_{pyrrolyl}$	3	6484.8	14.4
2.4a	2.24	$Me_{pyrrolyl}$	3	309.1	0.7
2.5a	not found	$H_{pyrrolyl}$	1	n.a.	n.d.
homocoupled **2.2**	2.14, 2.14, 2.12, 2.12, 2.09	$Me_{pyrrolyl}$ (2 per molecule)	6	1213.1	1.3

Figure 2.141. ^1H NMR of the one-pot pyrrole synthesis/arylation of **2.1a-BBN** and **2.6b** in $CDCl_3$ after HCl workup. *Taken from YC-2020-0020-5H.*

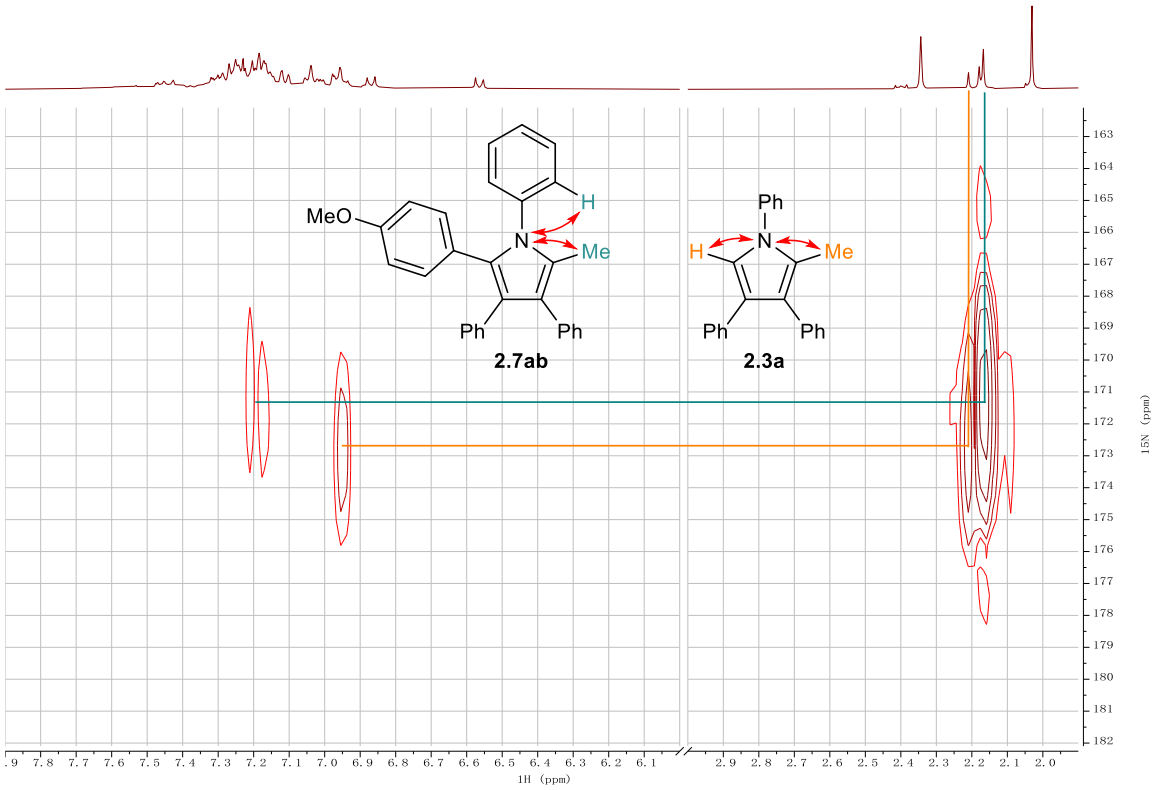

Figure 2.142. ^{1}H–^{15}N HMBC of the one-pot pyrrole synthesis/arylation of **2.1a-BBN** and **2.6b** in $CDCl_3$ after HCl workup. *Taken from YC-2020-0020-5NHMBC.*

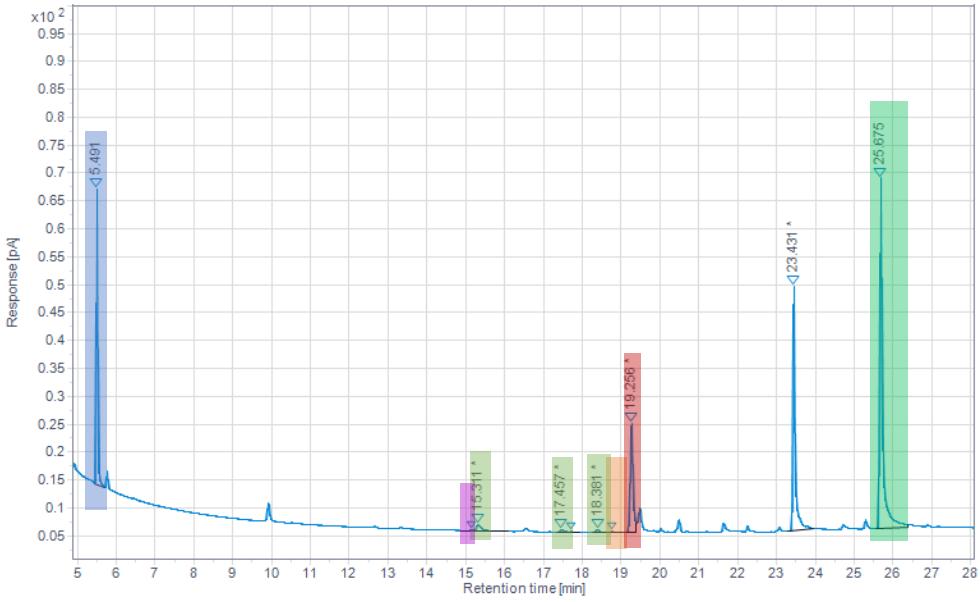

	Retention Time (min)	Surface Area	# of C	Yield (%)
Ph_3CH	5.49	127.128	19	n.a.
2.7ab	25.68	306.060	30	30.5
2.3a	19.26	96.947	23	12.6
2.4a	18.76	1.783	23	0.2
2.5a	15.14	1.131	23	0.1
homocoupled **2.2**	15.31, 17.46, 18.38	17.406	24	2.2

Figure 2.143. Quantitative GC-FID chromatograph of the one-pot pyrrole synthesis/arylation of **2.1a-BBN** and **2.6b** after HCl workup. *Taken from YC-2020-0020-3FID.*

One-Pot Pyrrole Synthesis/Arylation for 2.1a-BBN and *o*-Iodotoluene

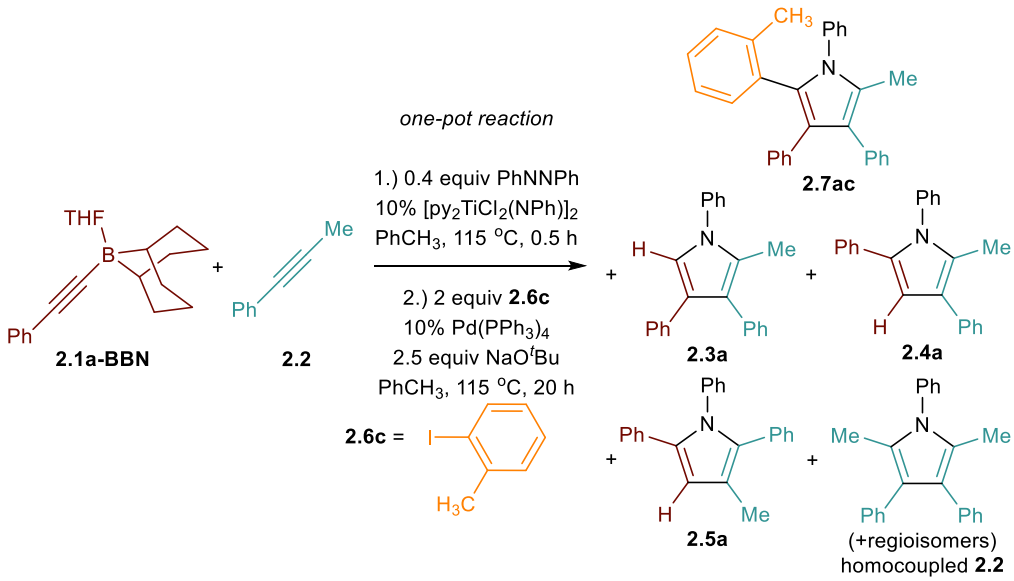

The reaction was performed following **Procedure 2.D** using **2.1a-BBN** (29.4 mg, 0.1 mmol, 1 equiv) as alkynylborane and *o*-iodotoluene (**2.6c**, 43.6 mg, 0.2 mmol, 2 equiv) as aryl iodide.

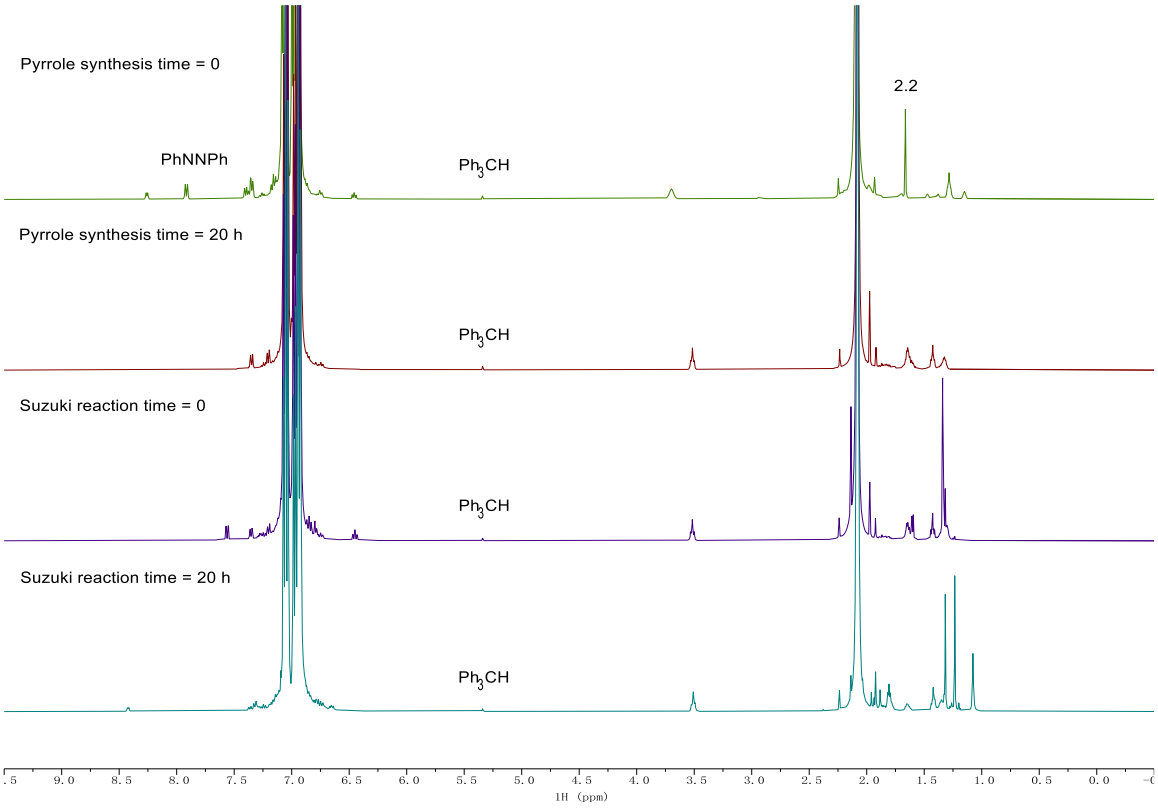

Figure 2.144. No-D ^{1}H NMR of the one-pot pyrrole synthesis/arylation of **2.1a-BBN** and **2.6c** at time = 0, time = 20 h of pyrrole synthesis, time = 0 and time = 20 h of Suzuki reaction in $PhCH_3$. *Taken from (top to bottom) (1) YC-2020-0023-NoD-Tol-0h-H; (2) YC-2020-0023-NoD-Tol-20h-H; (3) YC-2020-0023-NoD-Tol-tandem-0h-H; (4) YC-2020-0023-NoD-Tol-tandem-20h-H.*

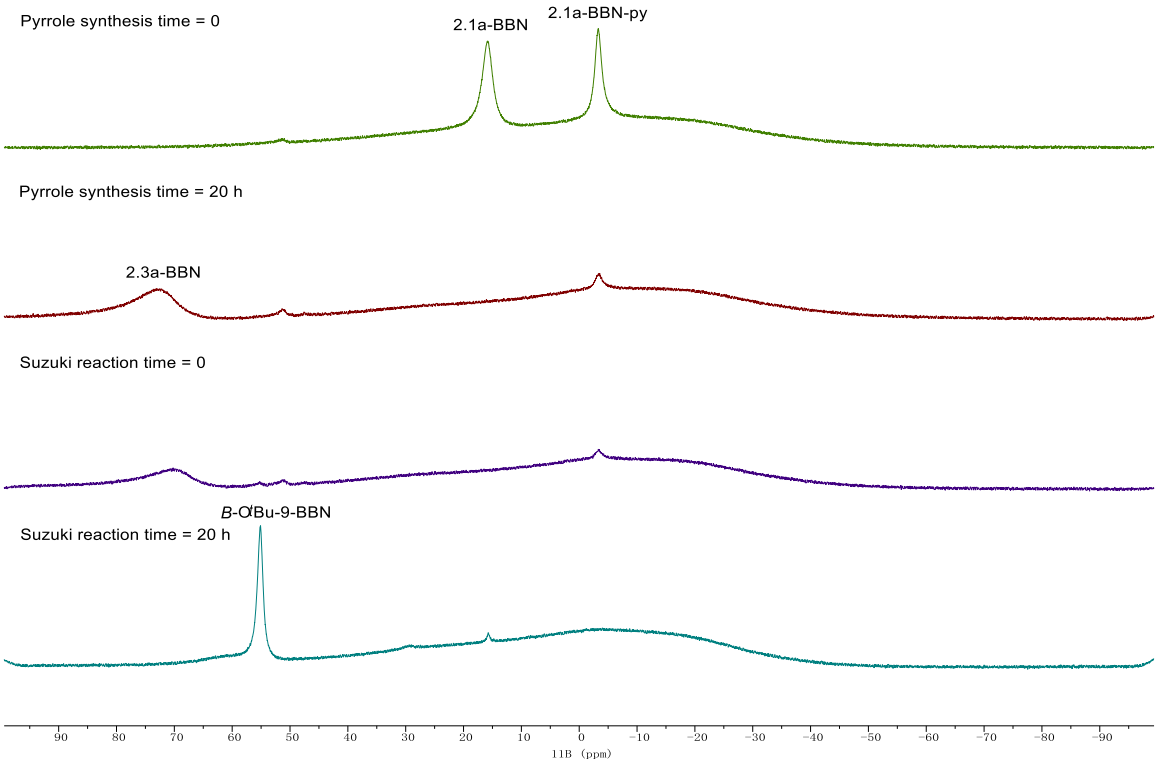

Figure 2.145. ^{11}B NMR of the one-pot pyrrole synthesis/arylation of **2.1a-BBN** and **2.6c** at time = 0, time = 20 h of pyrrole synthesis, time = 0 and time = 20 h of Suzuki reaction in $PhCH_3$. *Taken from (top to bottom) (1) YC-2020-0023-NoD-Tol-0h-B; (2) YC-2020-0023-NoD-Tol-20h-B; (3) YC-2020-0023-NoD-Tol-tandem-0h-B; (4) YC-2020-0023-NoD-Tol-tandem-20h-B.*

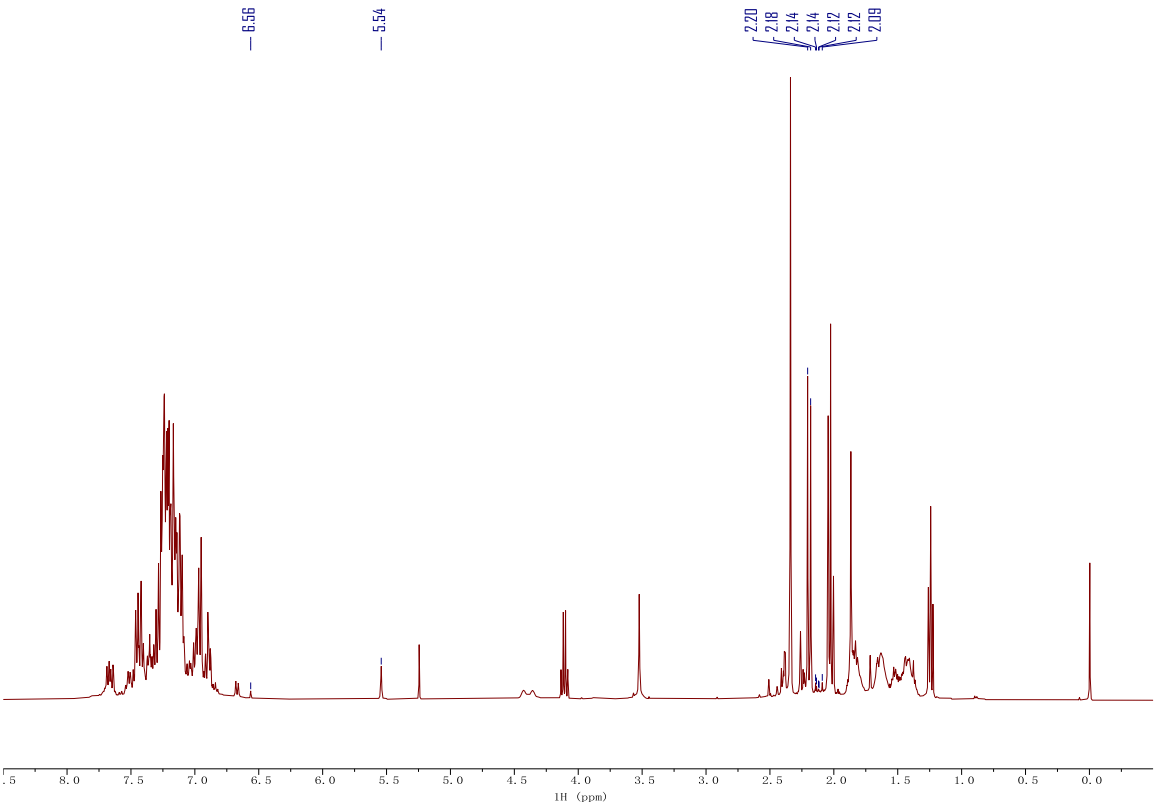

	δ (ppm)	Assignment	# of H	Peak Area	Yield (%)
Ph_3CH	5.54	Ph_3C-H	1	2996.5	n.a.
2.7ac	2.17	$Me_{pyrrolyl}$	3	14251.9	31.7
2.3a	2.20	$Me_{pyrrolyl}$	3	15108.3	33.6
2.4a	6.56	$H_{pyrrolyl}$	1	356.2	2.4
2.5a	not found	$H_{pyrrolyl}$	1	n.a.	n.d.
homocoupled **2.2**	2.14, 2.14, 2.12, 2.12, 2.09	$Me_{pyrrolyl}$ (2 per molecule)	6	2009.3	2.2

Figure 2.146. ^1H NMR of the one-pot pyrrole synthesis/arylation of **2.1a-BBN** and **2.6c** in $CDCl_3$ after HCl workup. *Taken from YC-2020-0023-5H.*

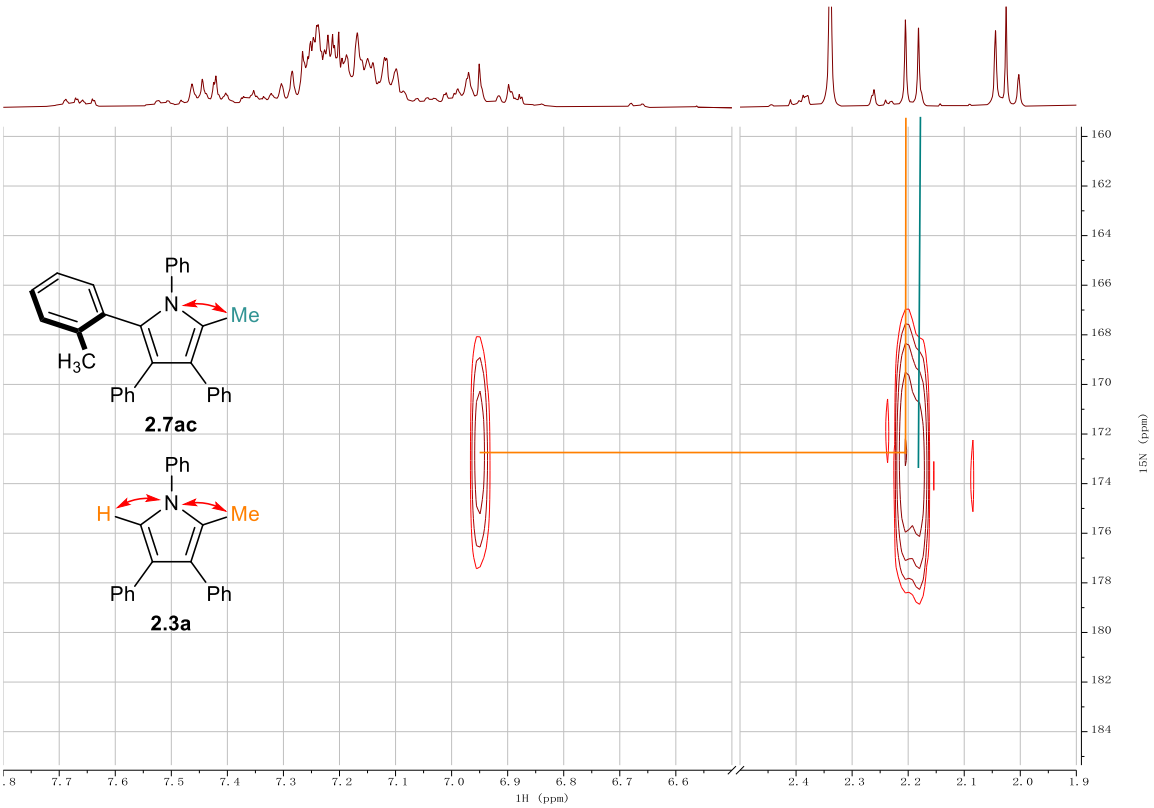

Figure 2.147. ^{1}H–^{15}N HMBC of the one-pot pyrrole synthesis/arylation of **2.1a-BBN** and **2.6c** in $CDCl_3$ after HCl workup. *Taken from YC-2020-0023-5NHMBC.*

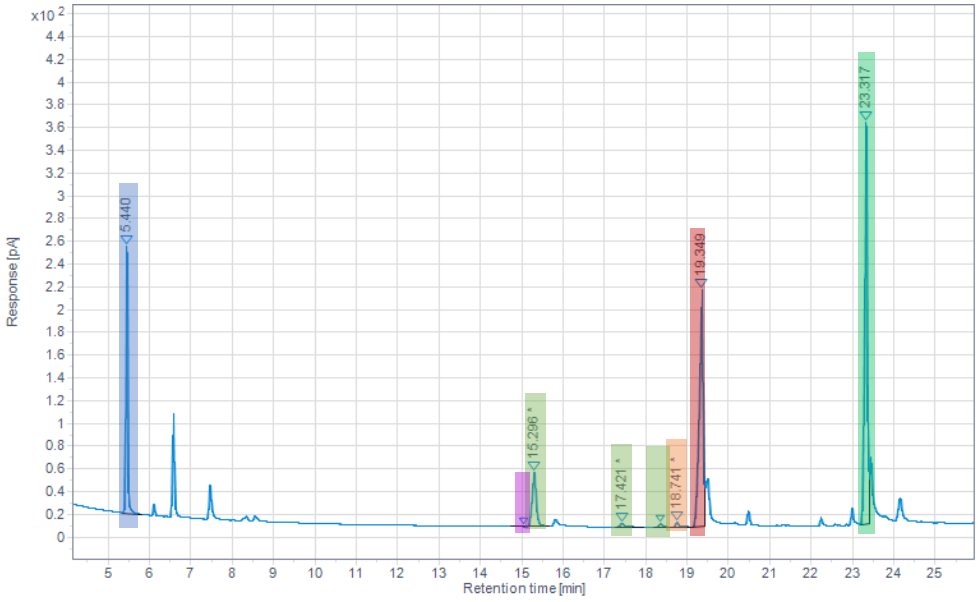

	Retention Time (min)	Surface Area	# of C	Yield (%)
Ph_3CH	5.44	602.354	19	n.a.
2.7ac	23.32	1431.650	30	30.1
2.3a	19.35	1285.246	23	35.3
2.4a	18.74	27.693	23	0.8
2.5a	15.04	2.29	23	0.1
homocoupled **2.2**	15.30, 17.42, 18.35	363.792	24	9.6

Figure 2.148. Quantitative GC-FID chromatograph of the one-pot pyrrole synthesis/arylation of **2.1a-BBN** and **2.6c** after HCl workup. *Taken from YC-2020-0023-1FID.*

One-Pot Pyrrole Synthesis/Arylation for 2.1a-BBN and Methyl *p*-Iodobenzoate

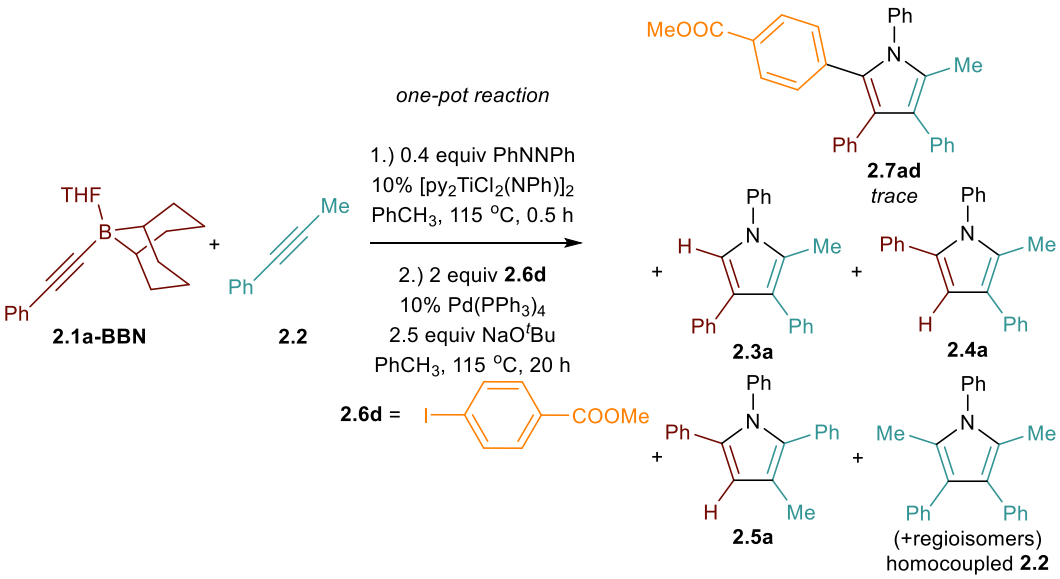

The reaction was performed following **Procedure 2.D** using **2.1a-BBN** (29.4 mg, 0.1 mmol, 1 equiv) as alkynylborane and methyl *p*-iodobenzoate (**2.6d**, 52.4 mg, 0.2 mmol, 2 equiv) as aryl iodide.

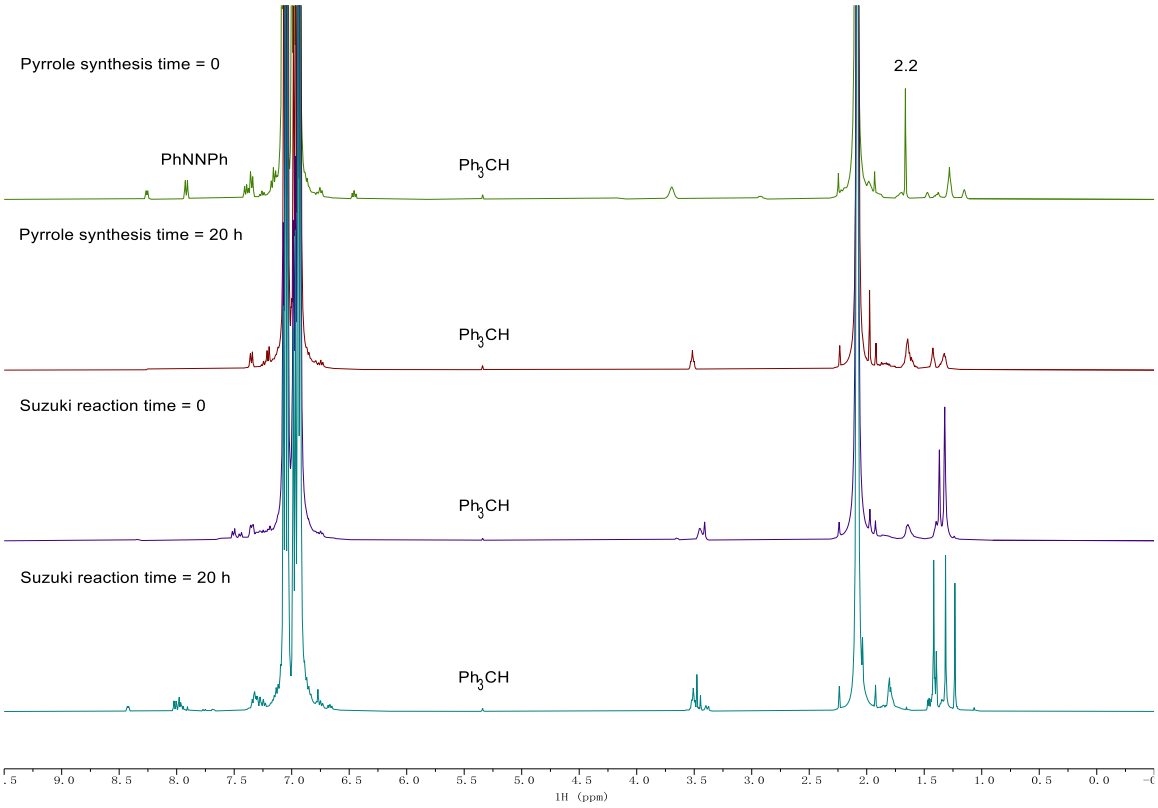

Figure 2.149. No-D ^{1}H NMR of the one-pot pyrrole synthesis/arylation of **2.1a-BBN** and **2.6d** at time = 0, time = 20 h of pyrrole synthesis, time = 0 and time = 20 h of Suzuki reaction in $PhCH_3$. *Taken from (top to bottom) (1) YC-2020-0021-NoD-Tol-0h-H; (2) YC-2020-0021-NoD-Tol-20h-H; (3) YC-2020-0021-NoD-Tol-tandem-0h-H; (4) YC-2020-0021-NoD-Tol-tandem-20h-H.*

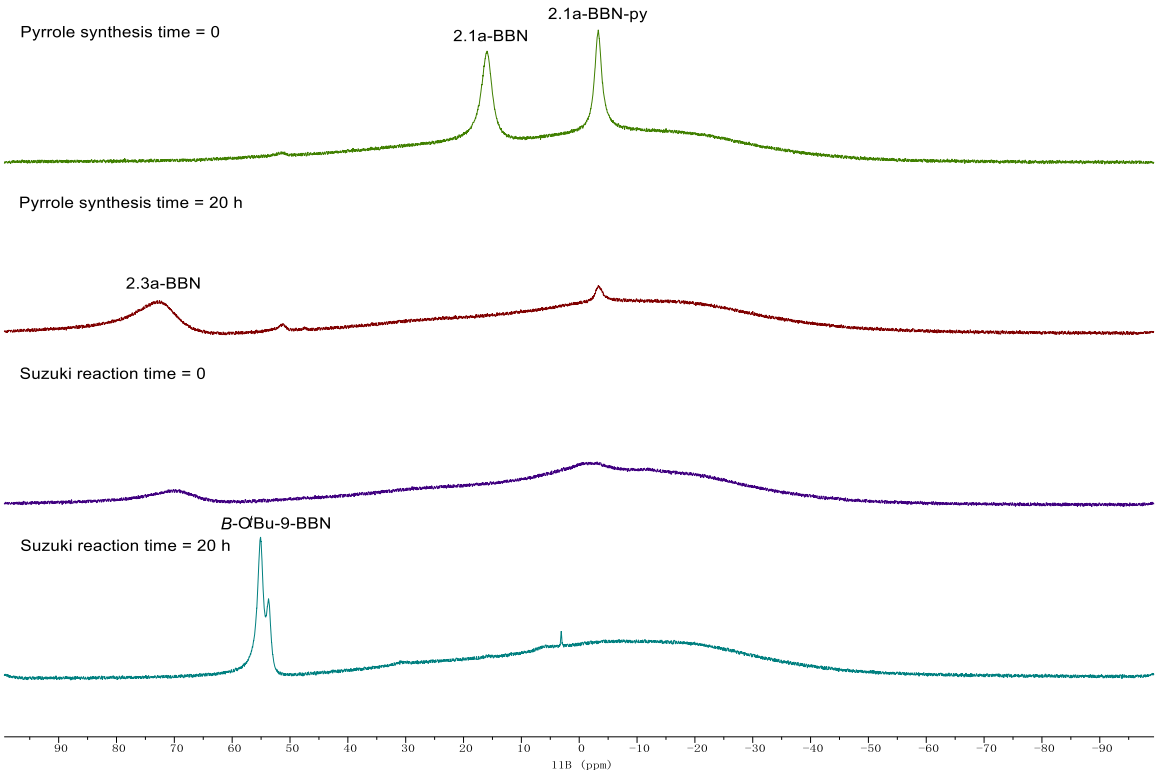

Figure 2.150. ^{11}B NMR of the one-pot pyrrole synthesis/arylation of **2.1a-BBN** and **2.6d** at time = 0, time = 20 h of pyrrole synthesis, time = 0 and time = 20 h of Suzuki reaction in $PhCH_3$. *Taken from (top to bottom) (1) YC-2020-0021-NoD-Tol-0h-B; (2) YC-2020-0021-NoD-Tol-20h-B; (3) YC-2020-0021-NoD-Tol-tandem-0h-B; (4) YC-2020-0021-NoD-Tol-tandem-20h-B.*

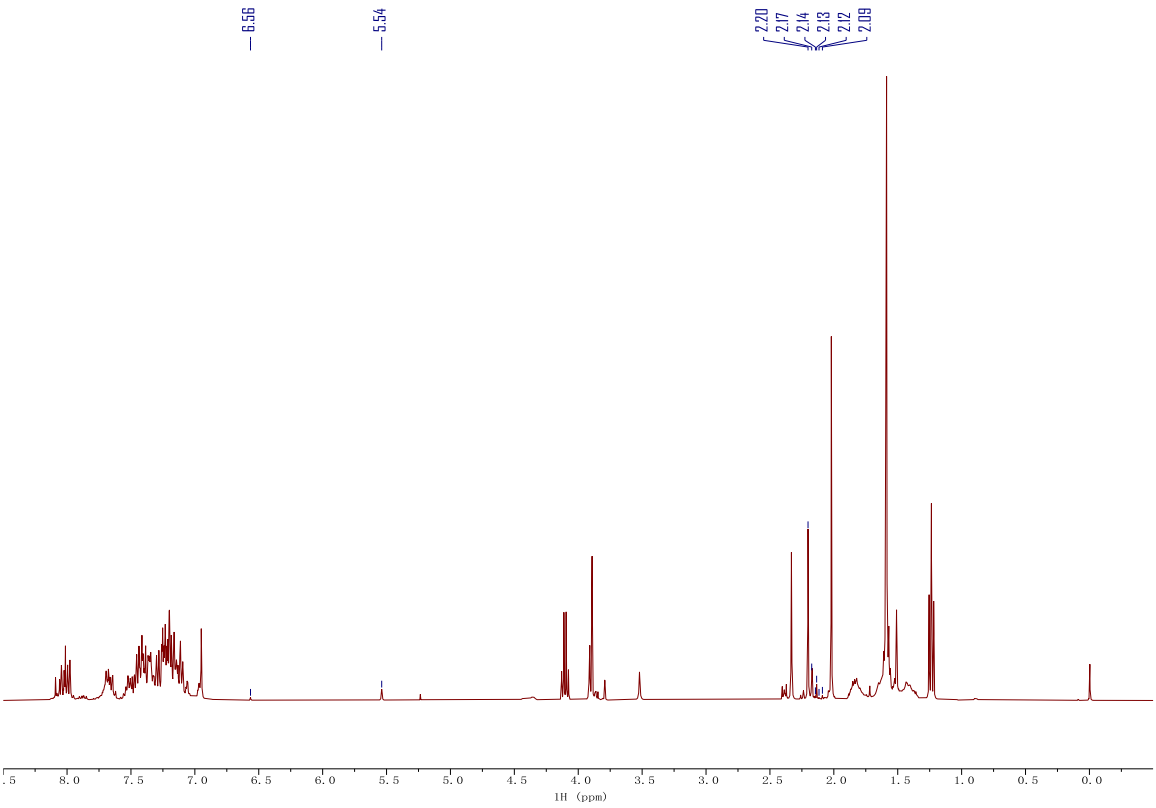

	δ (ppm)	Assignment	# of H	Peak Area	Yield (%)
Ph_3CH	5.54	Ph_3C-H	1	1904.2	n.a.
2.7ad	2.17	$Me_{pyrrolyl}$	3	1954.3	6.8
2.3a	2.20	$Me_{pyrrolyl}$	3	15225.7	53.4
2.4a	5.56	$H_{pyrrolyl}$	1	230.1	2.4
2.5a	not found	$H_{pyrrolyl}$	1	n.a.	n.d.
homocoupled **2.2**	2.14, 2.13, 2.12, 2.09	$Me_{pyrrolyl}$ (2 per molecule)	6	1414.6	2.5

Figure 2.151. ^{1}H NMR of the one-pot pyrrole synthesis/arylation of **2.1a-BBN** and **2.6d** in $CDCl_3$ after HCl workup. *Taken from YC-2020-0021-5H.*

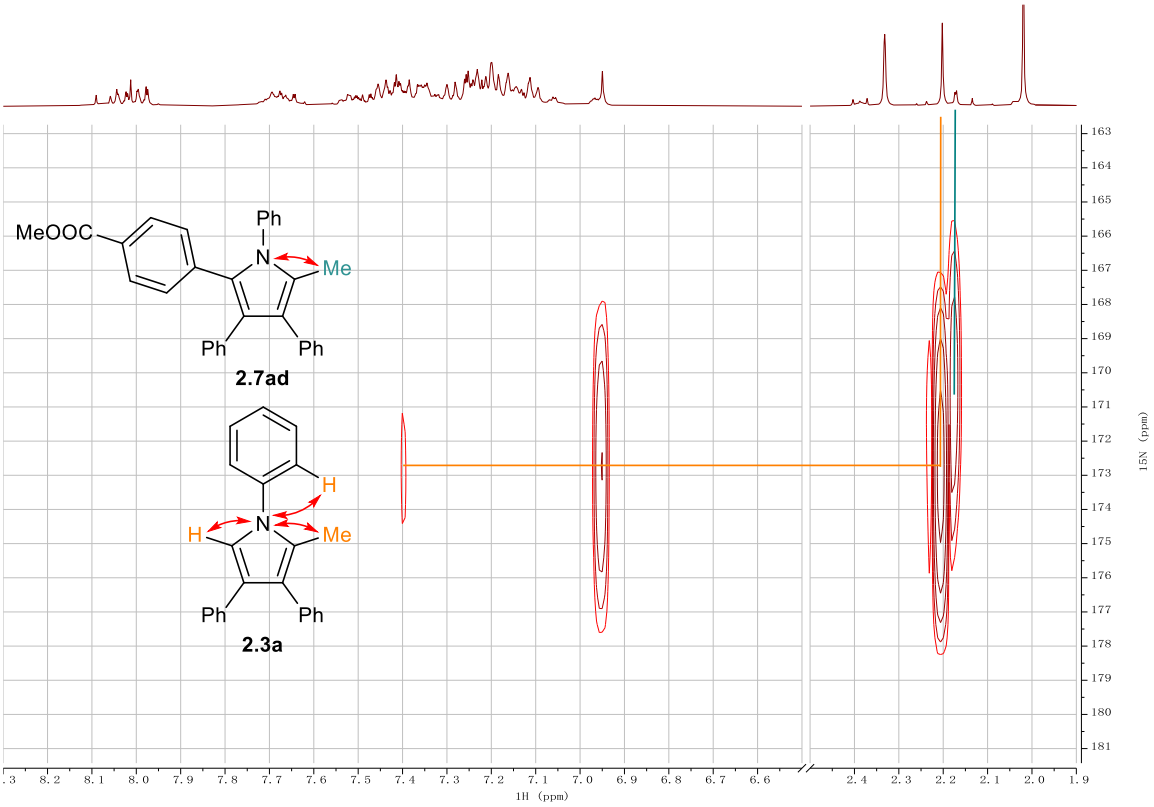

Figure 2.152. ^{1}H–^{15}N HMBC of the one-pot pyrrole synthesis/arylation of **2.1a-BBN** and **2.6d** in $CDCl_3$ after HCl workup. *Taken from YC-2020-0021-5NHMBC.*

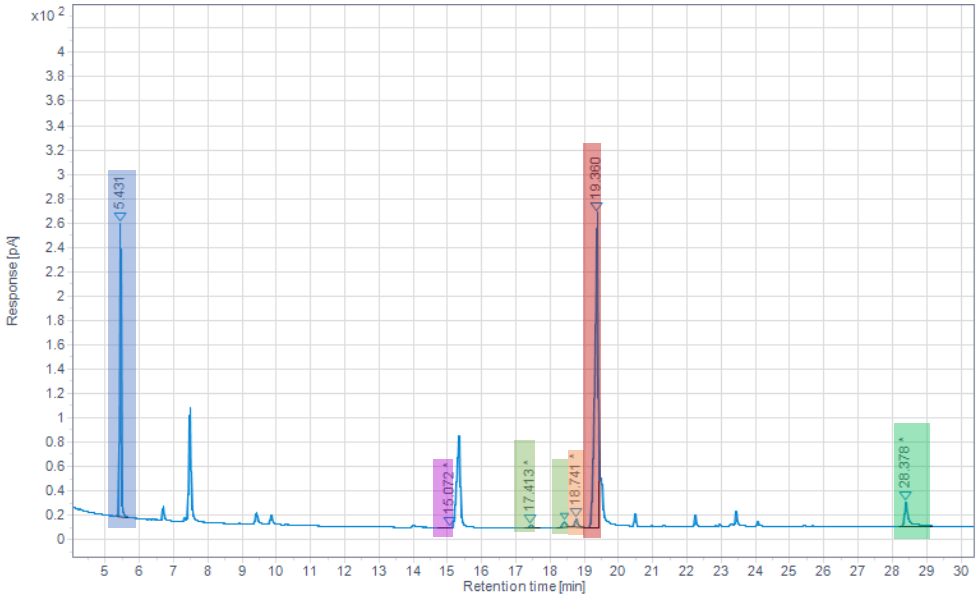

	Retention Time (min)	Surface Area	# of C	Yield (%)
Ph_3CH	5.43	596.253	19	n.a.
2.7ad	28.38	171.625	31	3.5
2.3a	19.36	1666.566	23	46.2
2.4a	18.74	42.820	23	1.2
2.5a	15.07	0.184	23	< 0.1
homocoupled **2.2**	17.41, 18.36	59.168	24	1.6

Figure 2.153. Quantitative GC-FID chromatograph of the one-pot pyrrole synthesis/arylation of **2.1a-BBN** and **2.6d** after HCl workup. *Taken from YC-2020-0021-2FID.*

One-Pot Pyrrole Synthesis/Arylation for 2.1a-BBN and *p*-Iodonitrobenzene

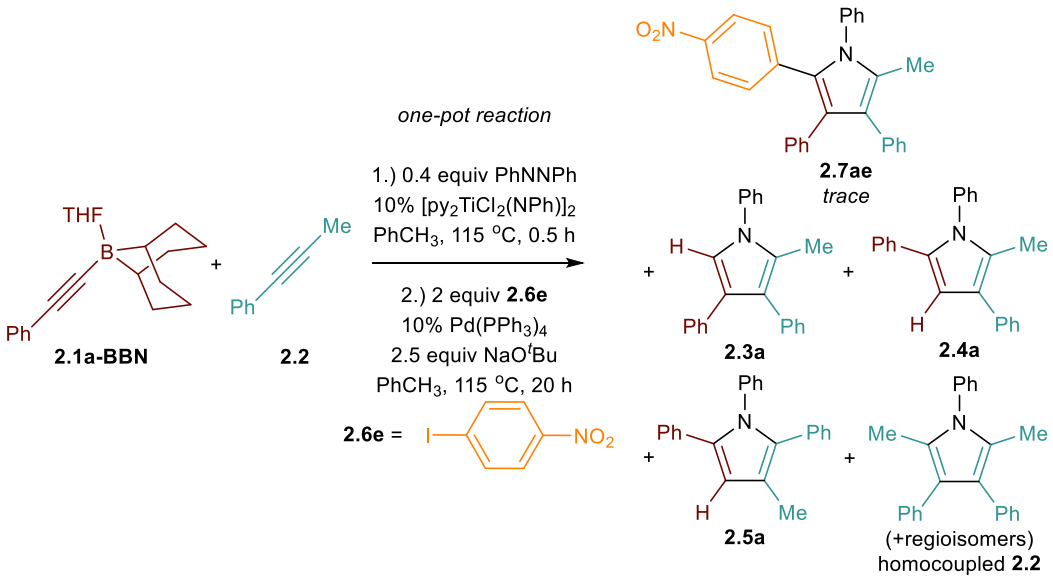

The reaction was performed following **Procedure 2.D** using **2.1a-BBN** (29.4 mg, 0.1 mmol, 1 equiv) as alkynylborane and *p*-iodonitrobenzene (**2.6e**, 49.8 mg, 0.2 mmol, 2 equiv) as aryl iodide. The extraction was performed with CH_2Cl_2/H_2O.

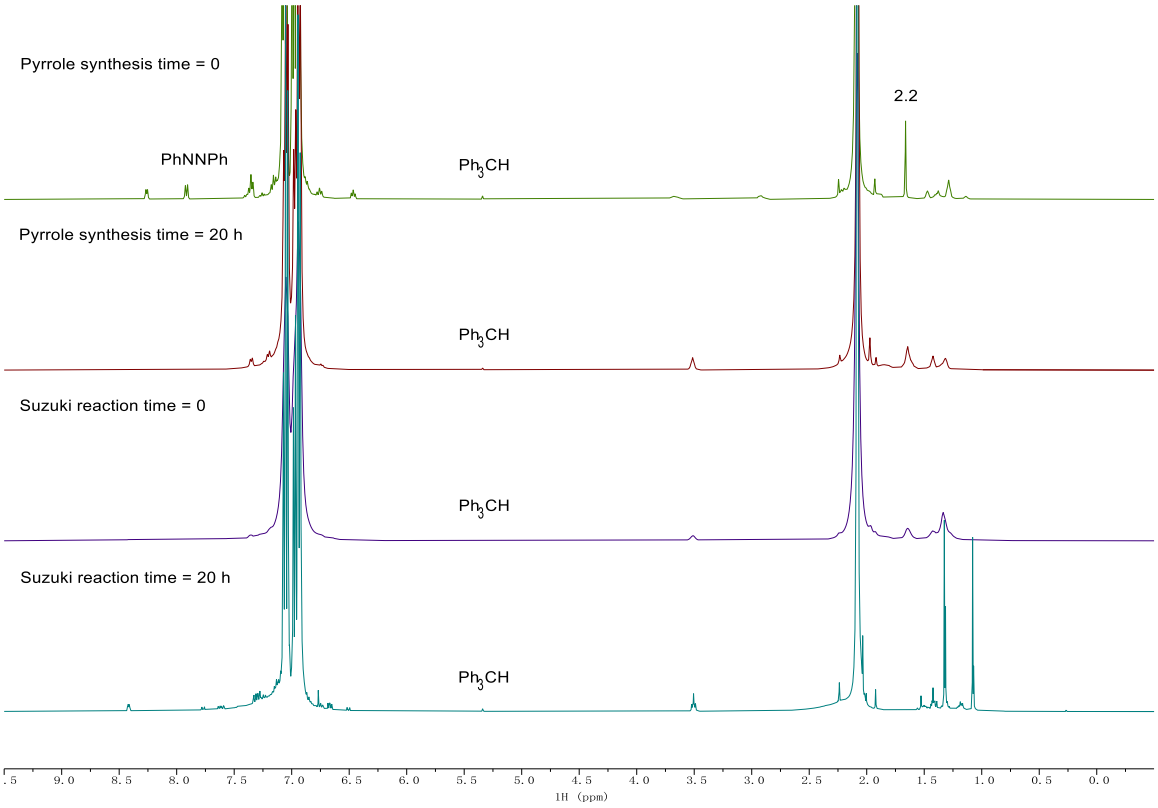

Figure 2.154. No-D ^{1}H NMR of the one-pot pyrrole synthesis/arylation of **2.1a-BBN** and **2.6e** at time = 0, time = 20 h of pyrrole synthesis, time = 0 and time = 20 h of Suzuki reaction in $PhCH_3$. *Taken from (top to bottom) (1) YC-2020-0022-NoD-Tol-0h-H; (2) YC-2020-0022-NoD-Tol-20h-H; (3) YC-2020-0022-NoD-Tol-tandem-0h-H; (4) YC-2020-0022-NoD-Tol-tandem-20h-H.*

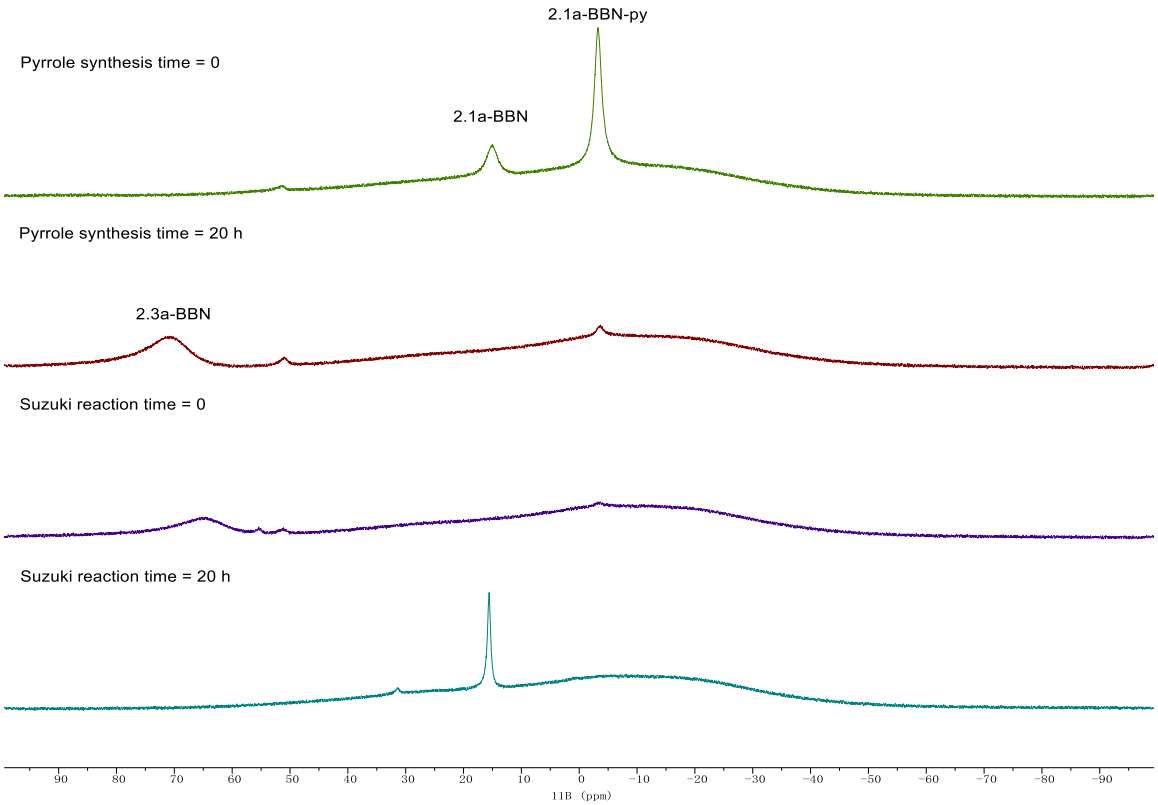

Figure 2.155. ^{11}B NMR of the one-pot pyrrole synthesis/arylation of **2.1a-BBN** and **2.6e** at time = 0, time = 20 h of pyrrole synthesis, time = 0 and time = 20 h of Suzuki reaction in $PhCH_3$. *Taken from (top to bottom) (1) YC-2020-0022-NoD-Tol-0h-B; (2) YC-2020-0022-NoD-Tol-20h-B; (3) YC-2020-0022-NoD-Tol-tandem-0h-B; (4) YC-2020-0022-NoD-Tol-tandem-20h-B.*

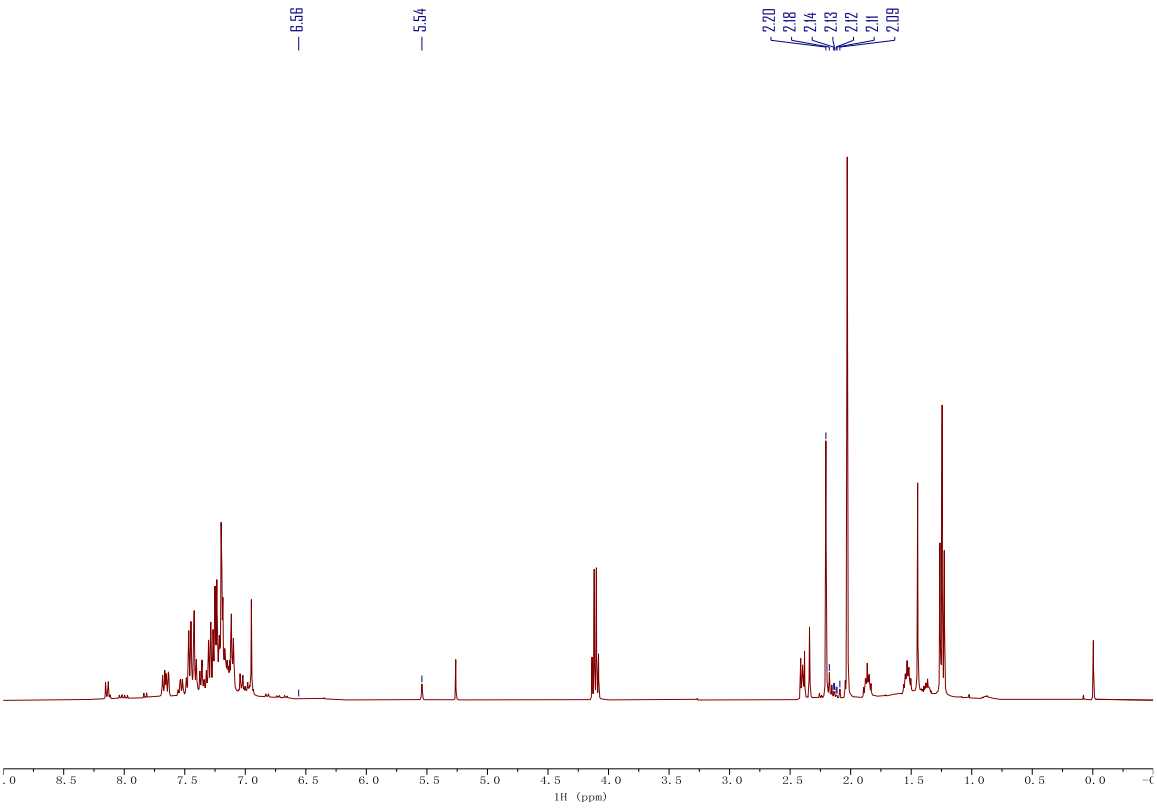

	δ (ppm)	Assignment	# of H	Peak Area	Yield (%)
Ph_3CH	5.54	Ph_3C-H	1	3084.0	n.a.
2.7ae	2.18	$Me_{pyrrolyl}$	3	2120.5	4.6
2.3a	2.20	$Me_{pyrrolyl}$	3	28226.0	61.0
2.4a	6.56	$H_{pyrrolyl}$	1	111.6	0.7
2.5a	not found	$H_{pyrrolyl}$	1	n.a.	n.d.
homocoupled **2.2**	2.14, 2.13, 2.12, 2.11, 2.09	$Me_{pyrrolyl}$ (2 per molecule)	6	2539.1	2.7

Figure 2.156. ^1H NMR of the one-pot pyrrole synthesis/arylation of **2.1a-BBN** and **2.6e** in $CDCl_3$ after HCl workup. *Taken from YC-2020-0022-5H.*

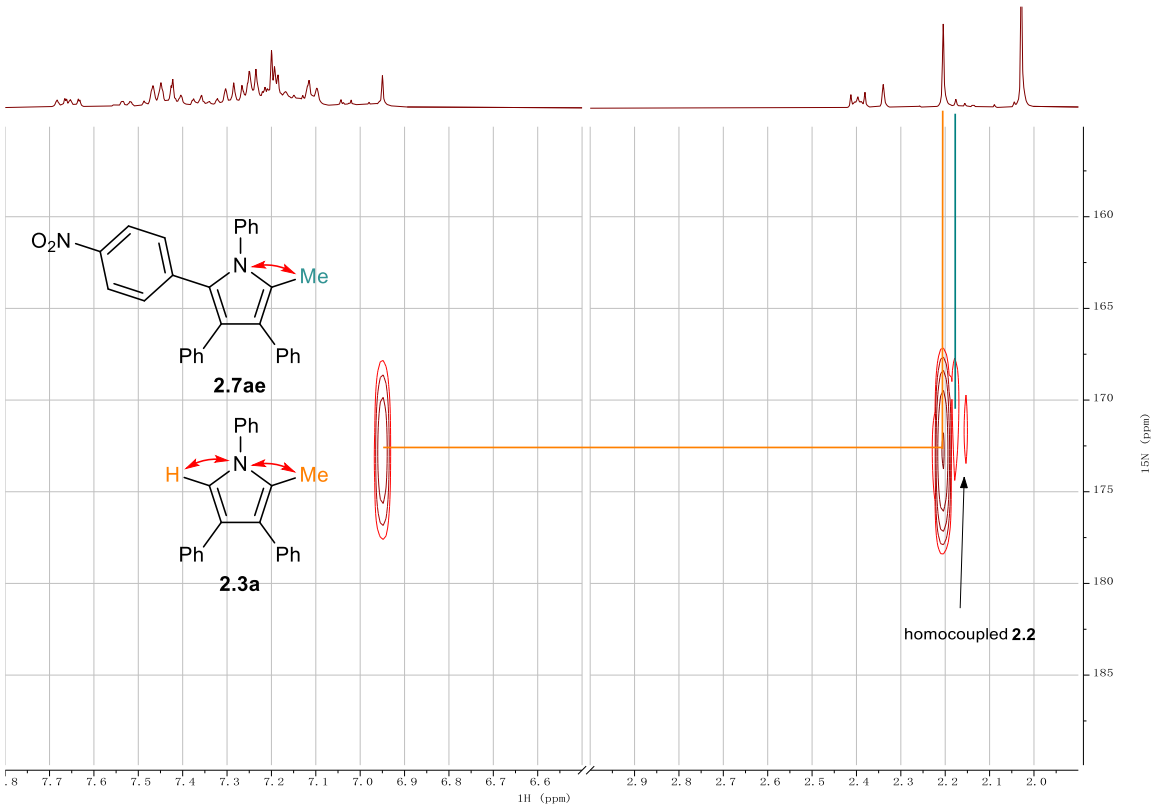

Figure 2.157. ^{1}H–^{15}N HMBC of the one-pot pyrrole synthesis/arylation of **2.1a-BBN** and **2.6e** in $CDCl_3$ after HCl workup. *Taken from YC-2020-0022-5NHMBC.*

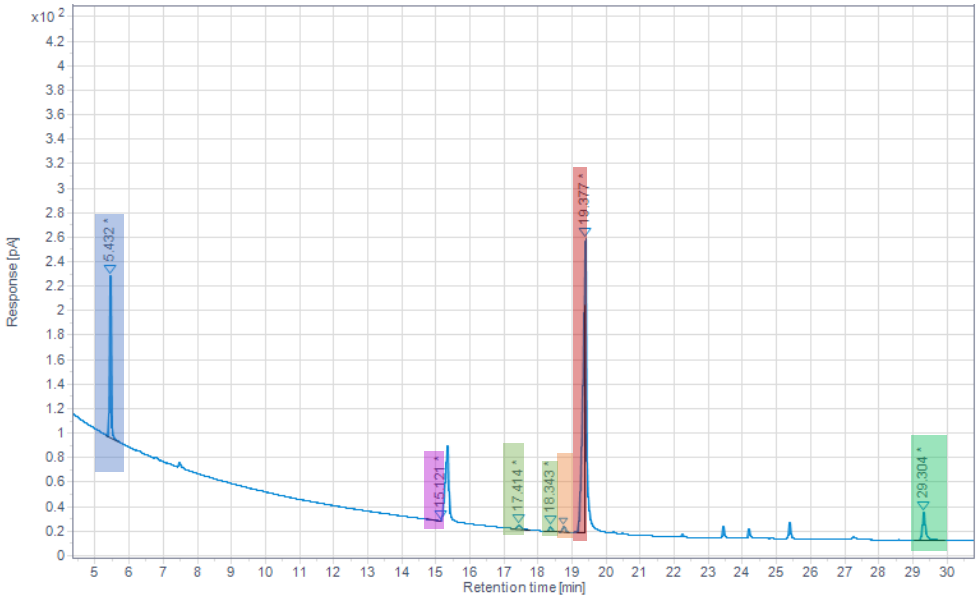

	Retention Time (min)	Surface Area	# of C	Yield (%)
Ph_3CH	5.43	336.796	19	n.a.
2.7ae	29.30	148.209	29	5.8
2.3a	19.38	1396.794	23	68.5
2.4a	18.74	27.707	23	1.4
2.5a	15.12	0.107	23	< 0.1
homocoupled **2.2**	17.41, 18.34	48.556	24	2.3

Figure 2.158. Quantitative GC-FID chromatograph of the one-pot pyrrole synthesis/arylation of **2.1a-BBN** and **2.6e** after HCl workup. *Taken from YC-2020-0022-2FID.*

2.5.10 Catalytic Pyrrole Syntheses: Hydrocarbon Alkyne Scopes (Table 2.4)

Catalytic reaction of **2.1a-BBN** with 2-butyne **(Table 2.4)**

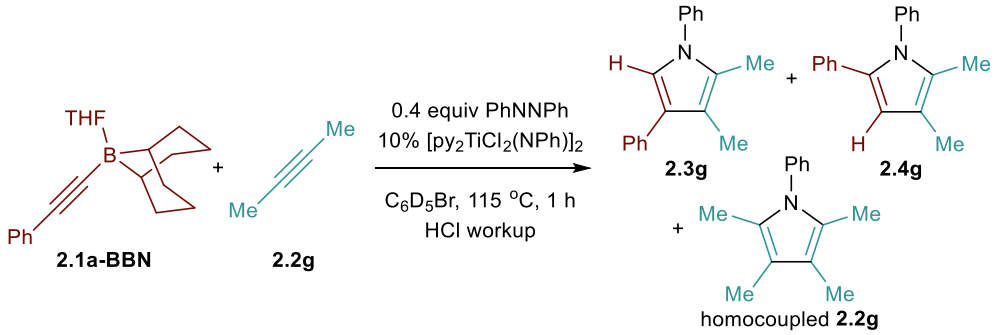

The reaction was performed following **Procedure 2.B** using **2.1a-BBN** (29.4 mg, 0.1 mmol, 1 equiv) and 2-butyne (**2.2g**, 5.4 mg, 0.1 mmol, 1 equiv) with the reaction being heated for 1 h.

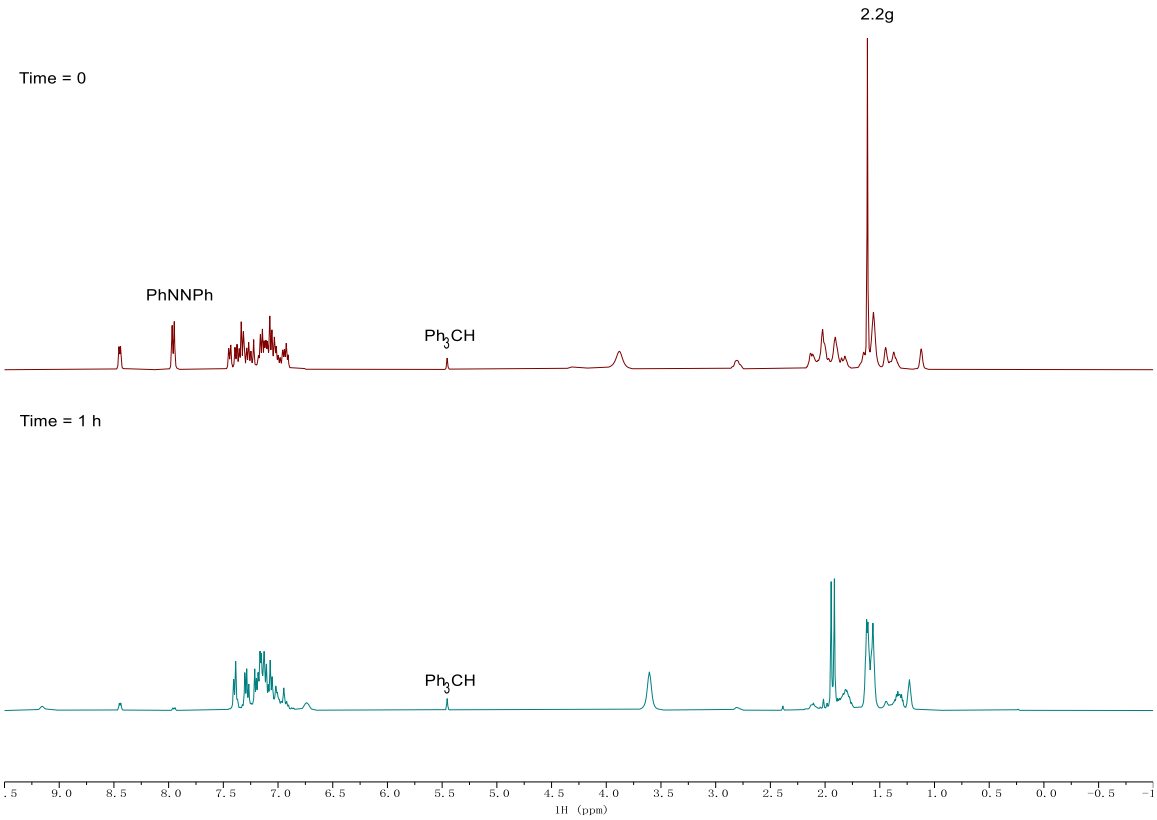

Figure 2.159. ^{1}H NMR of the reaction of **2.1a-BBN** with **2.2g** at time = 0 (top), time = 1 h (bottom) in C_6D_5Br. *Taken from (top) YC-2020-0069-0h-H and (bottom) YC-2020-0069-1h-H.*

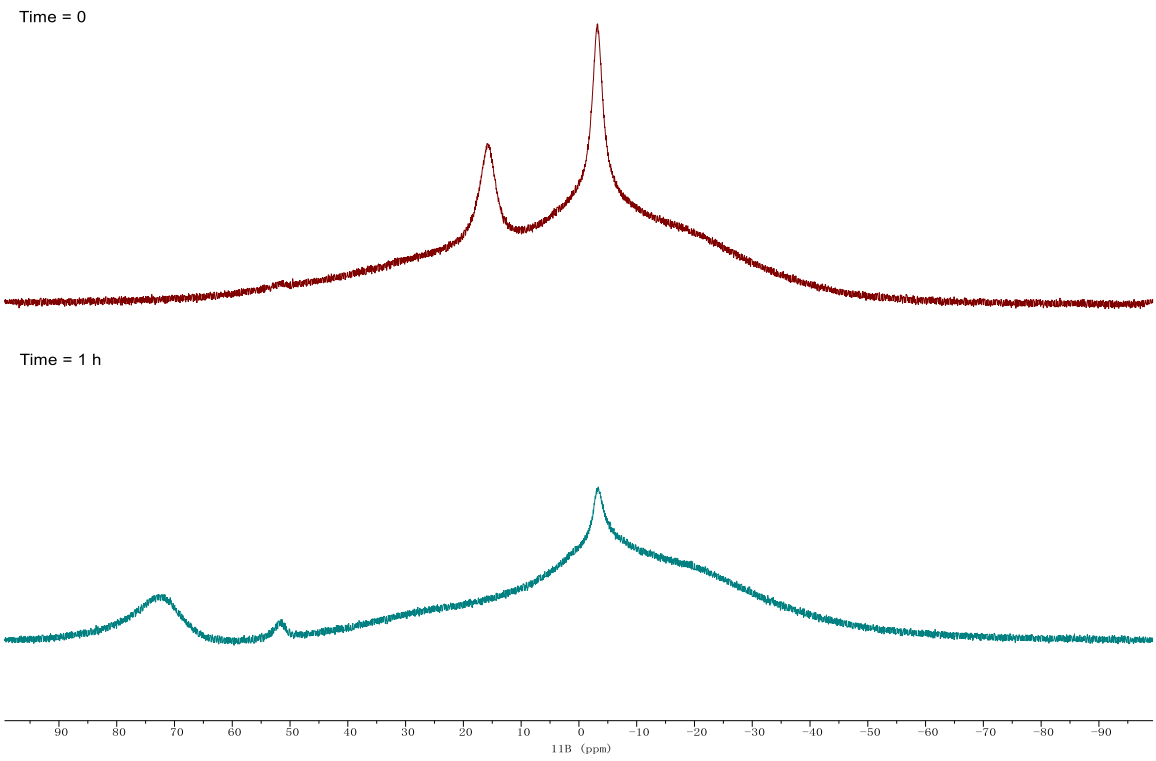

Figure 2.160. ^{11}B NMR of the reaction of **2.1a-BBN** with **2.2g** at time = 0 (top), time = 1 h (bottom) in C_6D_5Br. *Taken from (top) YC-2020-0069-0h-B and (bottom) YC-2020-0069-1h-B.*

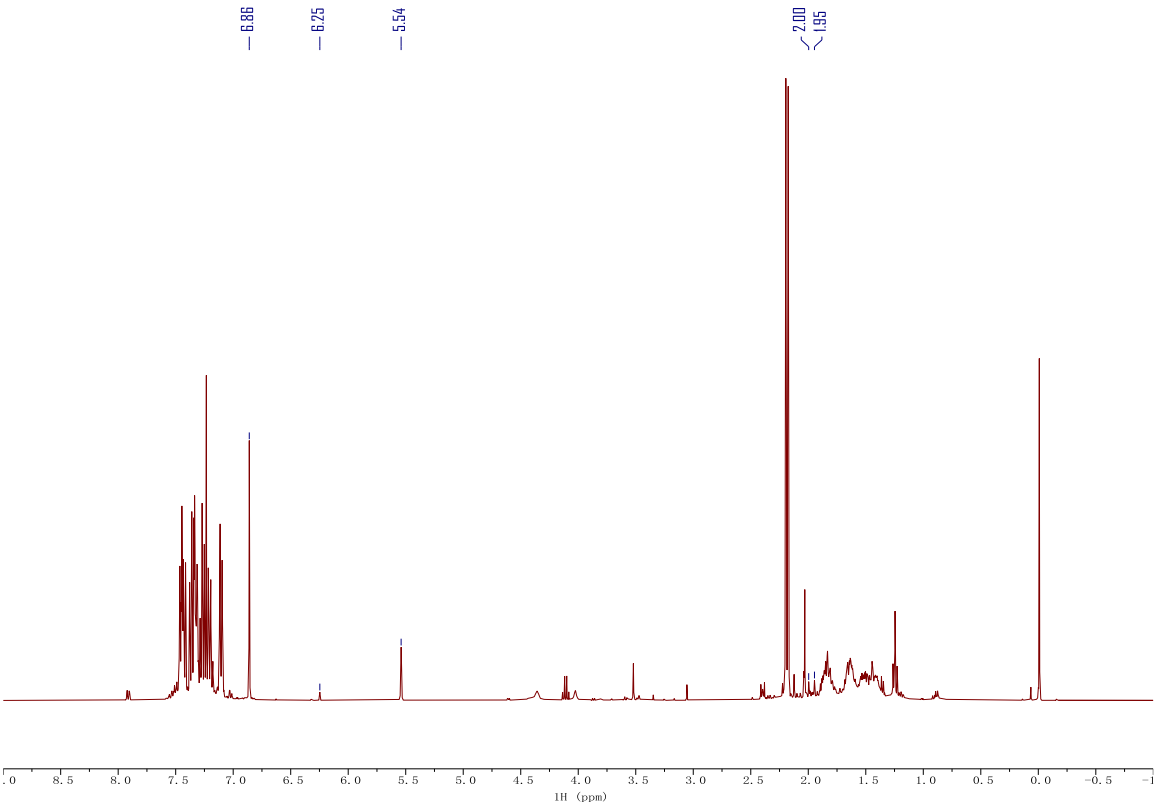

	δ (ppm)	Assignment	# of H	Peak Area	Yield (%)
Ph_3CH	5.54	Ph_3C-H	1	5760.5	n.a.
2.3g	6.86	$H_{pyrrolyl}$	1	15151.4	52.6
2.4g	6.25	$H_{pyrrolyl}$	1	597.5	2.1
homocoupled **2.2g**	2.00, 1.95	$Me_{pyrrolyl}$ (4 per molecule)	12	2685.6	0.8

Figure 2.161. ^{1}H NMR of the reaction of **2.1a-BBN** with **2.2g** in $CDCl_3$ after HCl workup. *Taken from YC-2020-0069-3H.*

Catalytic reaction of **2.1a-BBN** with 3-hexyne **(Table 2.4)**

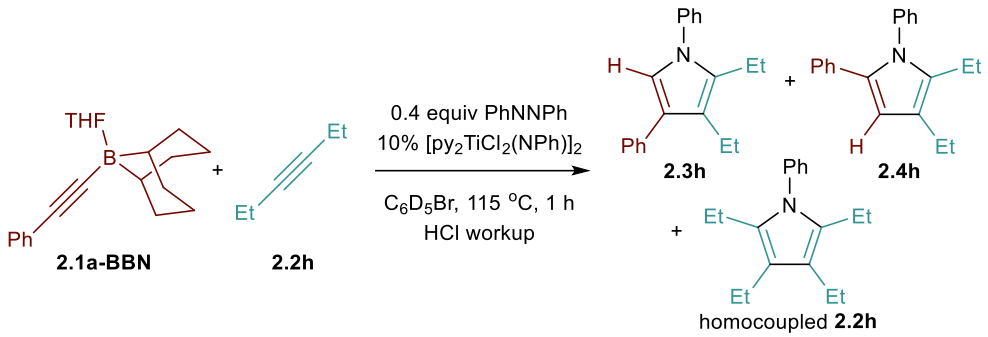

The reaction was performed following **Procedure 2.B** using **2.1a-BBN** (29.4 mg, 0.1 mmol, 1 equiv) and 3-hexyne (**2.2h**, 8.2 mg, 0.1 mmol, 1 equiv) with the reaction being heated for 1 h.

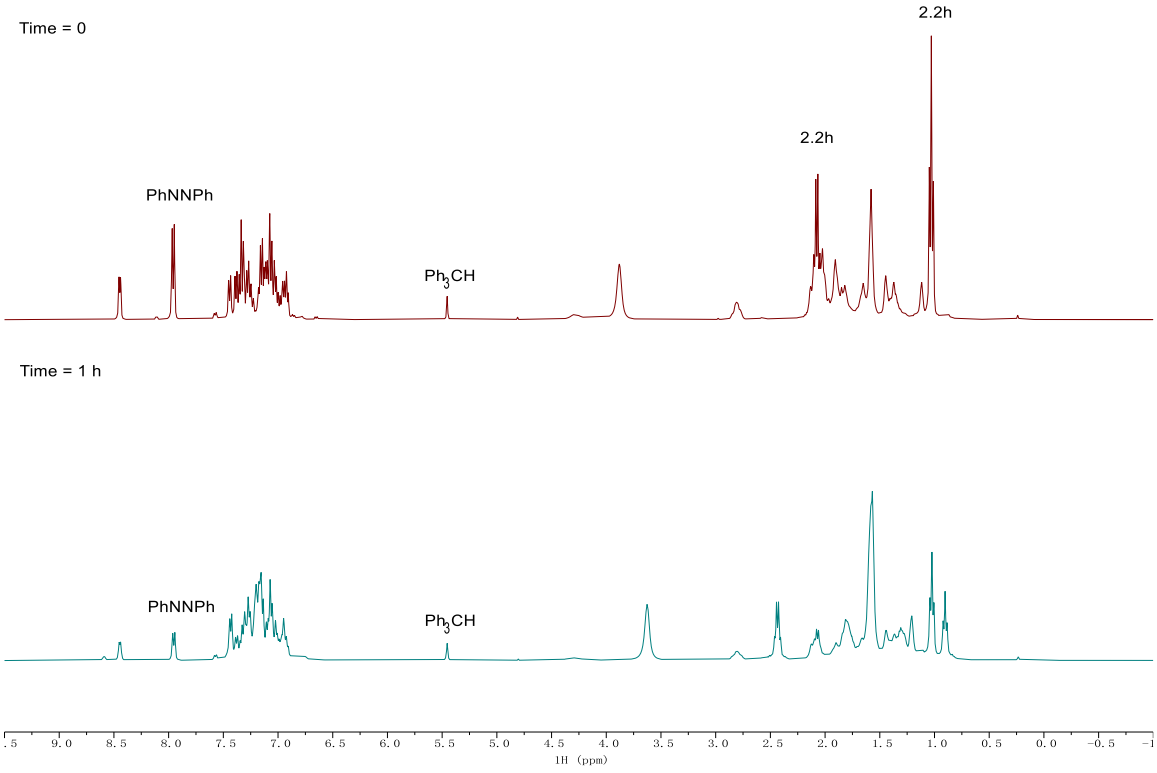

Figure 2.162. ^{1}H NMR of the reaction of **2.1a-BBN** with **2.2h** at time = 0 (top), time = 1 h (bottom) in C_6D_5Br. *Taken from (top) YC-2020-0070-0h-H and (bottom) YC-2020-0070-1h-H.*

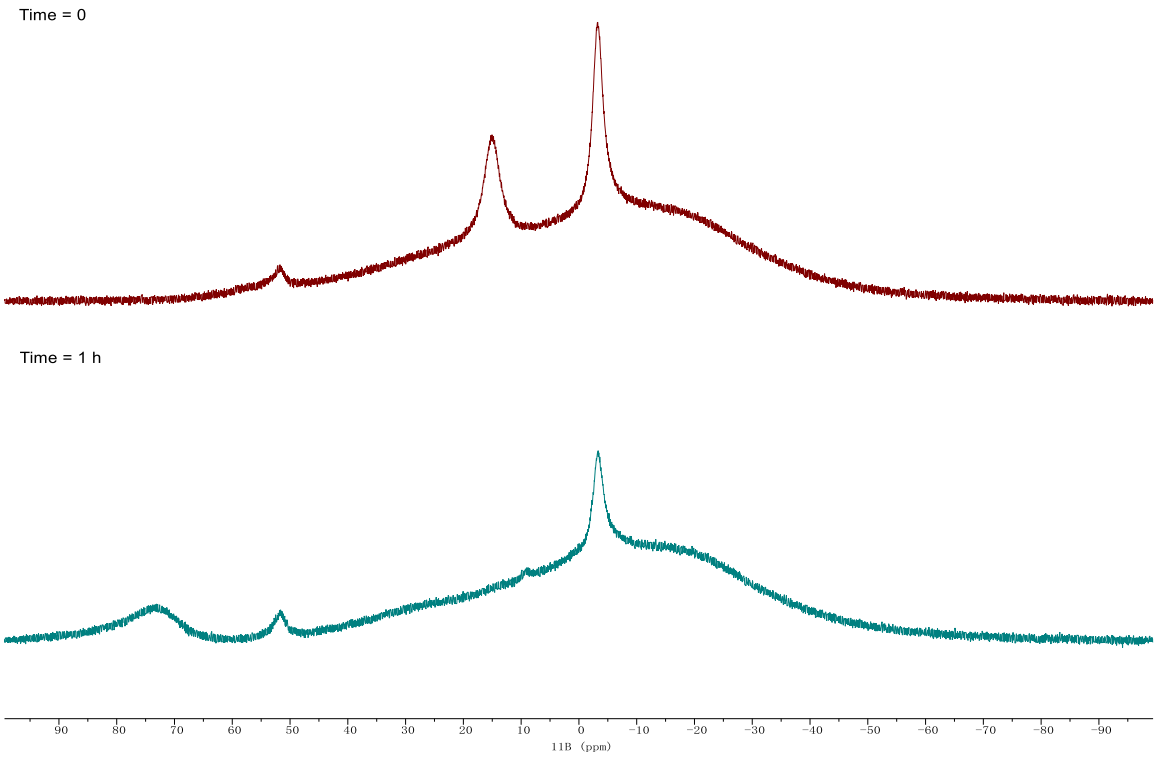

Figure 2.163. ^{11}B NMR of the reaction of **2.1a-BBN** with **2.2h** at time = 0 (top), time = 1 h (bottom) in C_6D_5Br. *Taken from (top) YC-2020-0070-0h-B and (bottom) YC-2020-0070-1h-B.*

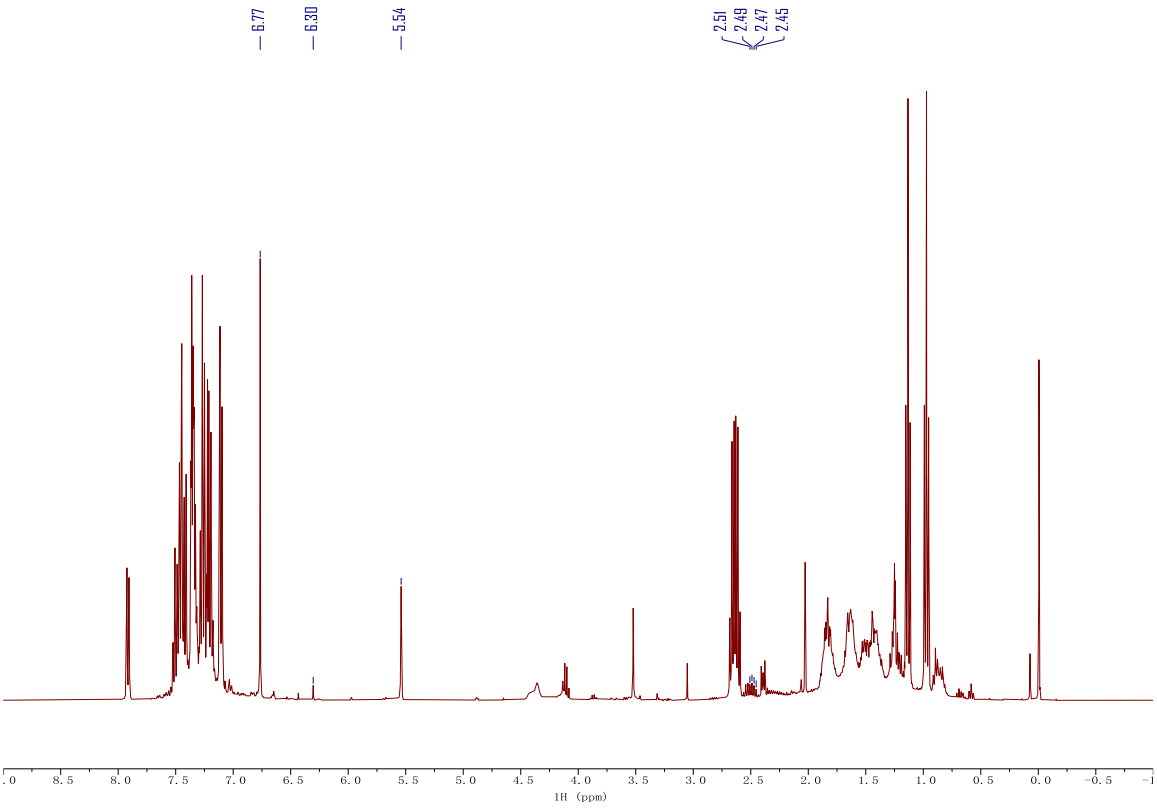

	δ (ppm)	Assignment	# of H	Peak Area	Yield (%)
Ph_3CH	5.54	Ph_3C-H	1	4143.2	n.a.
2.3h	6.77	$H_{pyrrolyl}$	1	7107.0	34.3
2.4h	6.30	$H_{pyrrolyl}$	1	348.0	1.7
homocoupled **2.2h**	2.51, 2.49, 2.47, 2.45	3,4-CH_2CH$_3$ (2 per molecule)	4	904.8	1.1

Figure 2.164. ^{1}H NMR of the reaction of **2.1a-BBN** with **2.2h** in $CDCl_3$ after HCl workup. *Taken from YC-2020-0070-3H.*

Catalytic reaction of **2.1a-BBN** with 4-octyne **(Table 2.4)**

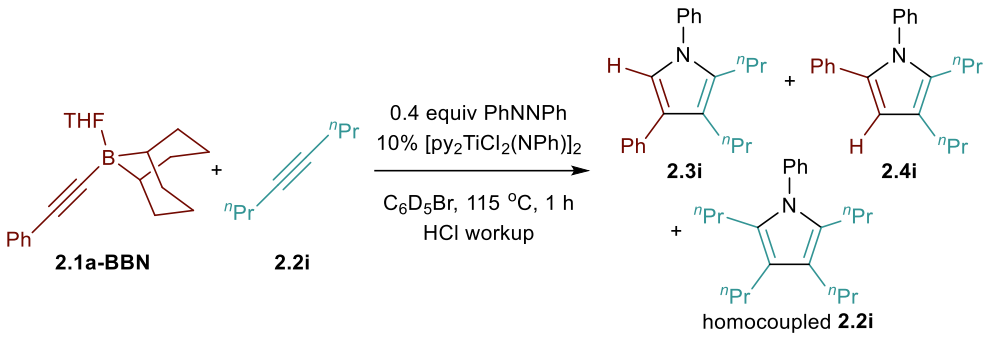

The reaction was performed following **Procedure 2.B** using **2.1a-BBN** (29.4 mg, 0.1 mmol, 1 equiv) and 4-octyne (**2.2i**, 11.0 mg, 0.1 mmol, 1 equiv) with the reaction being heated for 1 h.

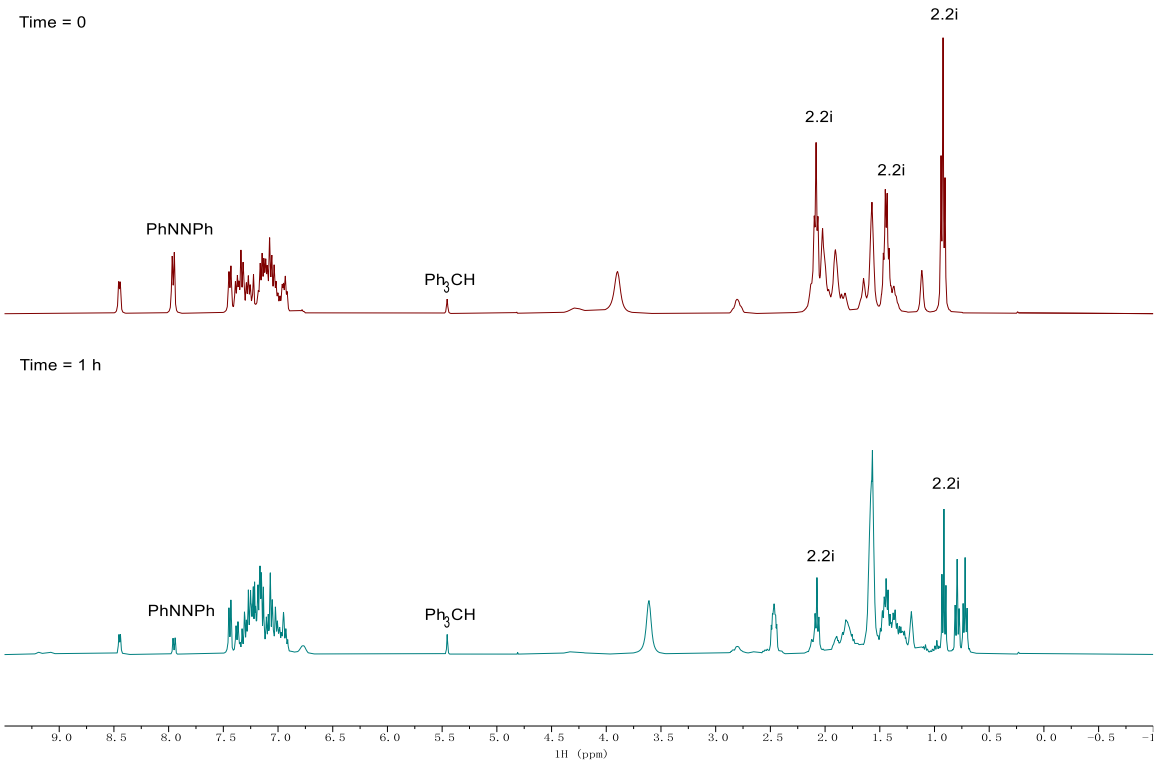

Figure 2.165. ^{1}H NMR of the reaction of **2.1a-BBN** with **2.2i** at time = 0 (top), time = 1 h (bottom) in C_6D_5Br. *Taken from (top) YC-2020-0071-0h-H and (bottom) YC-2020-0071-1h-H.*

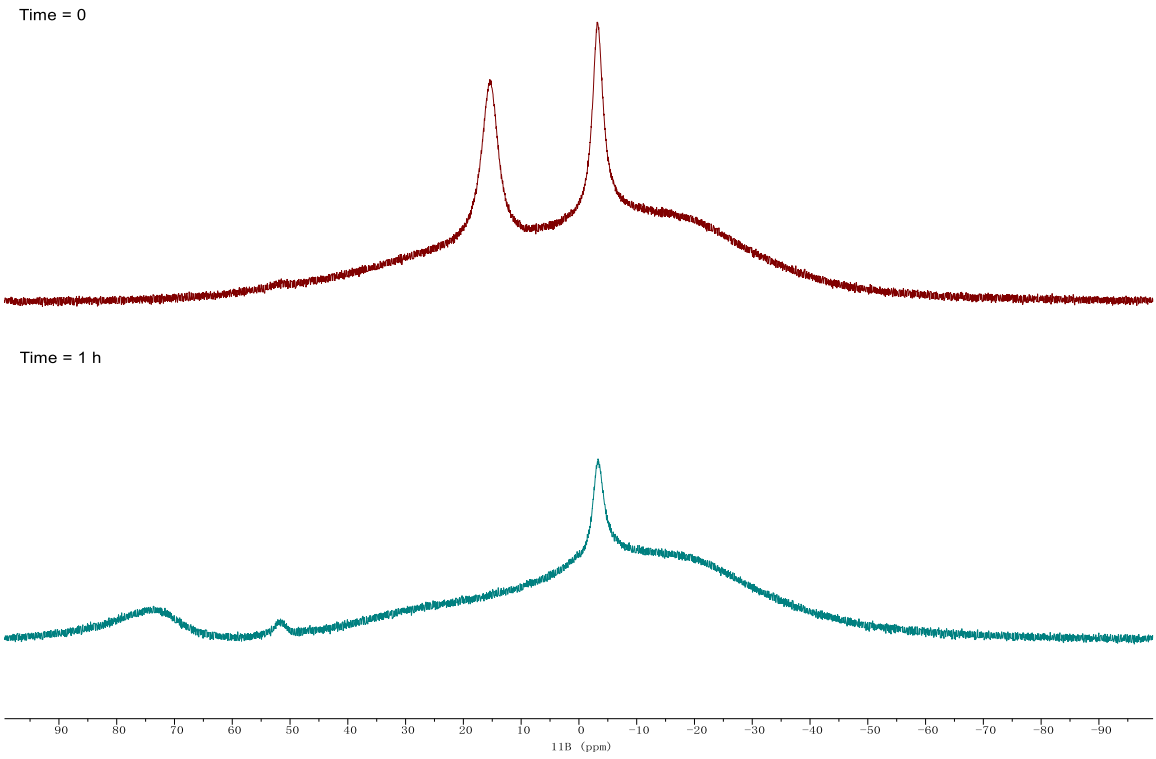

Figure 2.166. ^{11}B NMR of the reaction of **2.1a-BBN** with **2.2i** at time = 0 (top), time = 1 h (bottom) in C_6D_5Br. *Taken from (top) YC-2020-0071-0h-B and (bottom) YC-2020-0071-1h-B.*

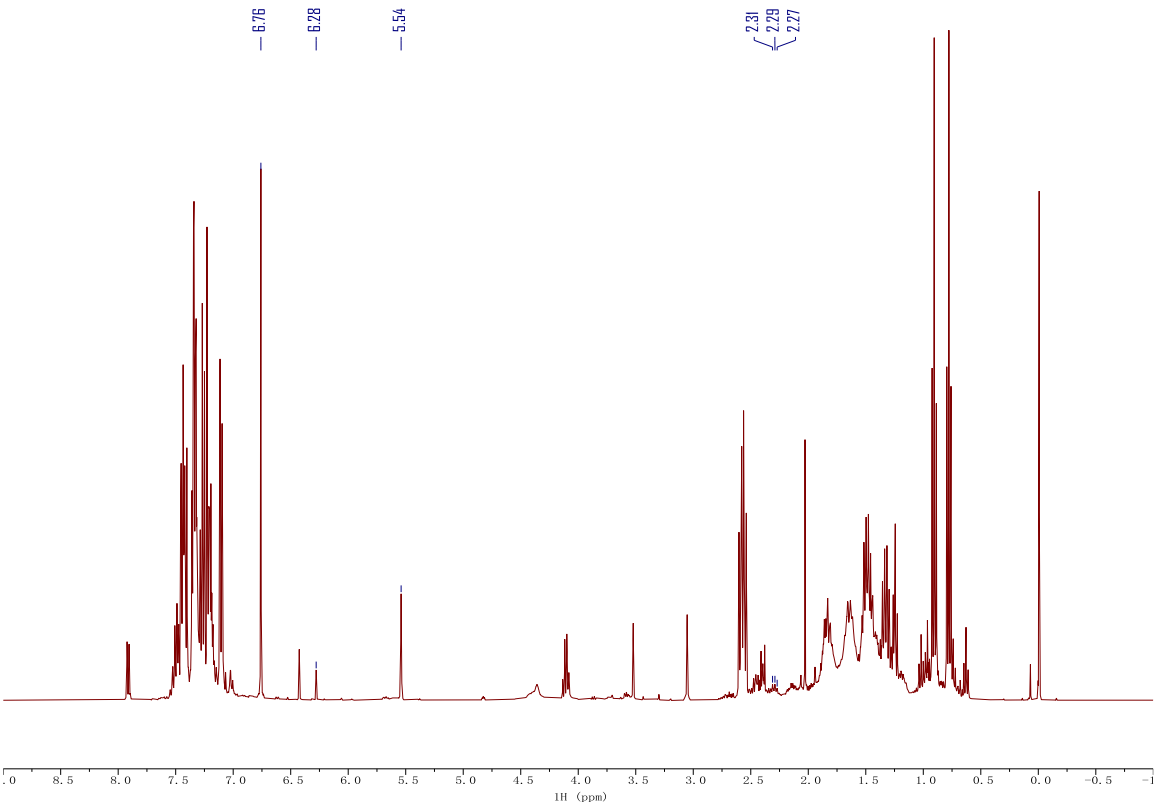

	δ (ppm)	Assignment	# of H	Peak Area	Yield (%)
Ph_3CH	5.54	Ph_3C-H	1	4788.6	n.a.
2.3i	6.76	$H_{pyrrolyl}$	1	10643.2	44.5
2.4i	6.28	$H_{pyrrolyl}$	1	808.8	3.4
homocoupled **2.2i**	2.30, 2.29, 2.27	2,5-C$H_2$$CH_3$ (2 per molecule)	4	948.7	1.0

Figure 2.167. ^{1}H NMR of the reaction of **2.1a-BBN** with **2.2i** in $CDCl_3$ after HCl workup. *Taken from YC-2020-0071-3H.*

Catalytic reaction of **2.1a-BBN** with diphenylacetylene **(Table 2.4)**

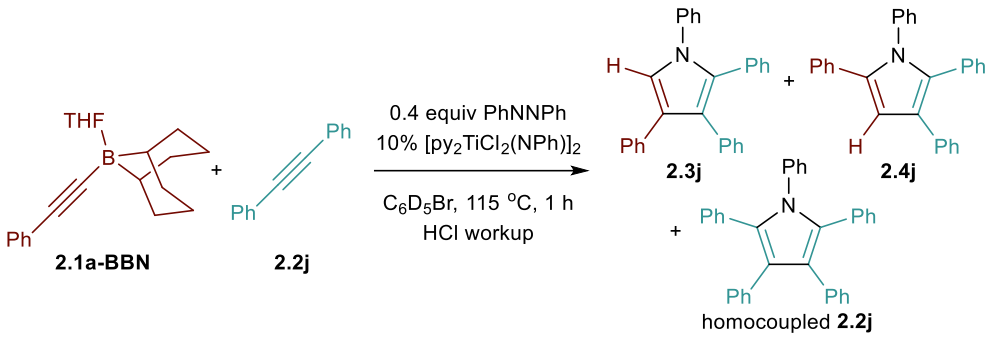

The reaction was performed following **Procedure 2.B** using **2.1a-BBN** (29.4 mg, 0.1 mmol, 1 equiv) and diphenylacetylene (**2.2j**, 17.8 mg, 0.1 mmol, 1 equiv) with the reaction being heated for 1 h. Yields were determined by GC due to peak overlapping in ^{1}H NMR spectrum after HCl workup.

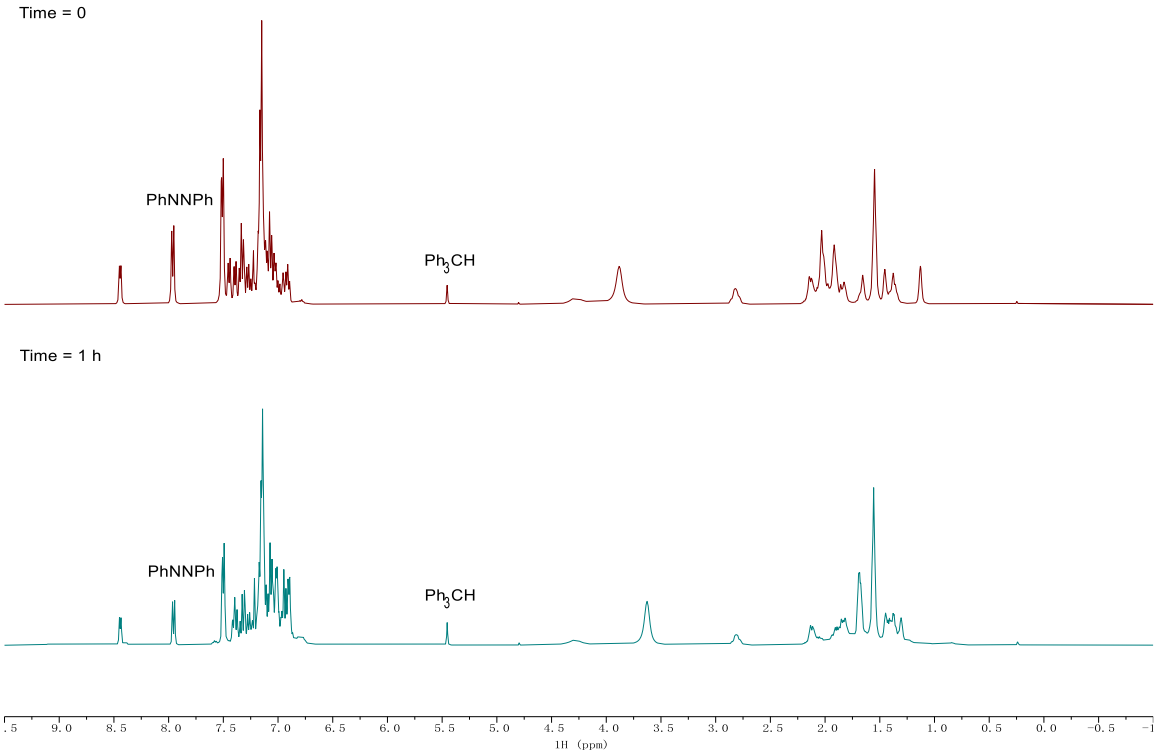

Figure 2.168. ^{1}H NMR of the reaction of **2.1a-BBN** with **2.2j** at time = 0 (top), time = 1 h (bottom) in C_6D_5Br. *Taken from (top) YC-2020-0072-0h-H and (bottom) YC-2020-0072-1h-H.*

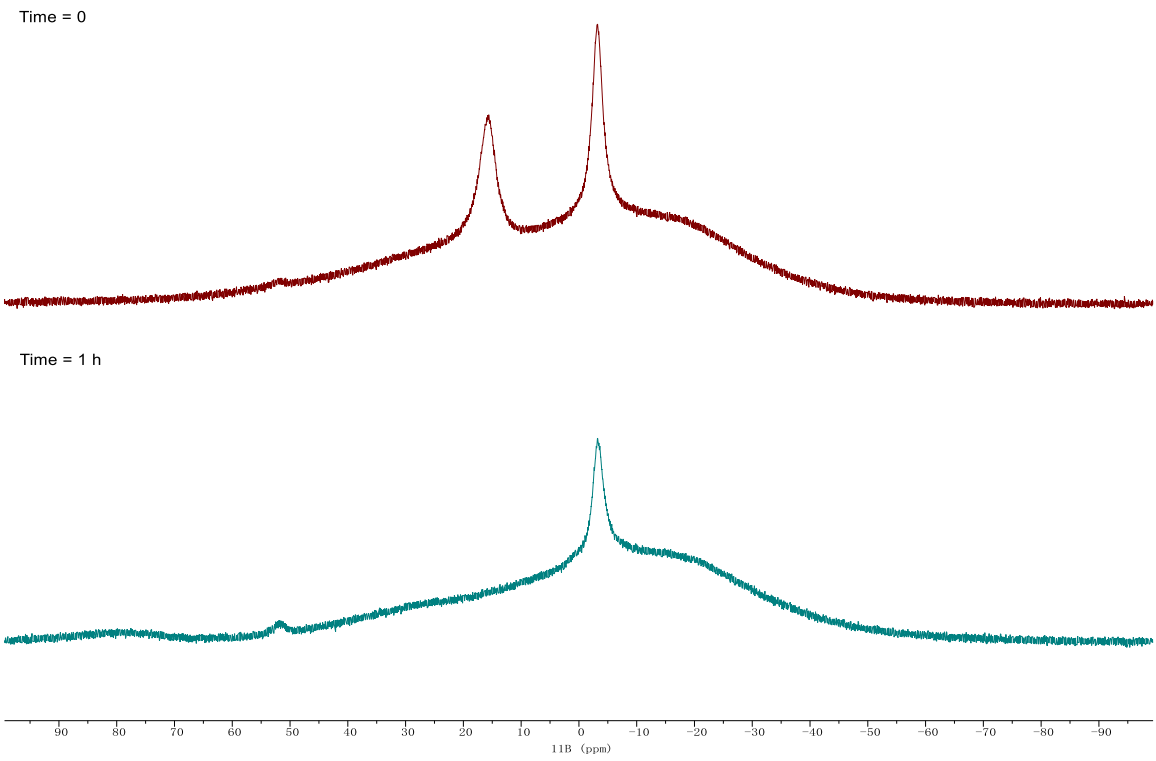

Figure 2.169. ^{11}B NMR of the reaction of **2.1a-BBN** with **2.2j** at time = 0 (top), time = 1 h (bottom) in C_6D_5Br. *Taken from (top) YC-2020-0072-0h-B and (bottom) YC-2020-0072-1h-B.*

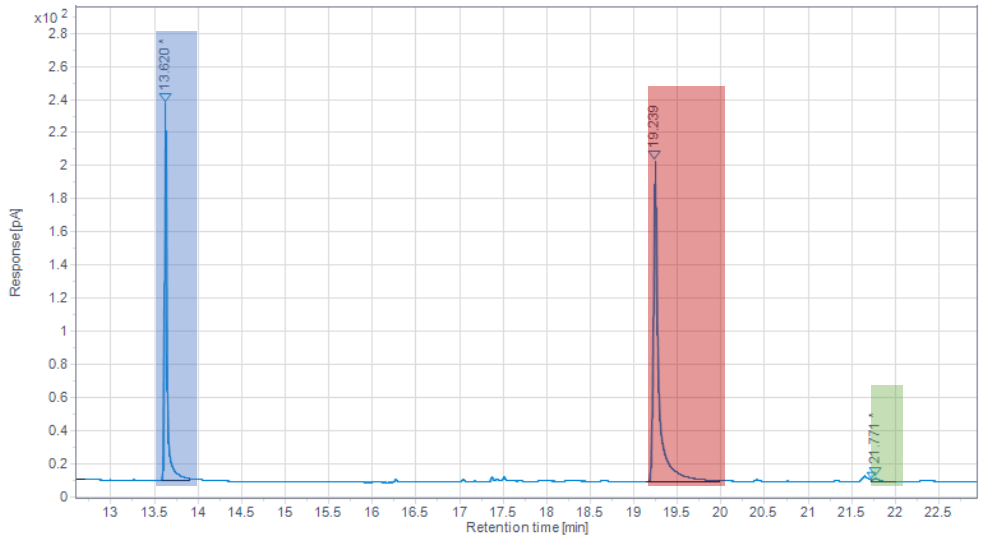

	Retention Time (min)	Surface Area	# of C	Yield (%)
Ph_3CH	13.620	434.769	19	n.a.

2.3j	19.239	791.935	28	24.7
2.4j	not found	n.a.	28	n.d.
homocoupled **2.2j**	21.771	10.684	34	0.3

Figure 2.170. Quantitative GC-FID chromatograph of the reaction of **2.1a-BBN** with **2.2j** after HCl workup. *Taken from (top) YC-2020-0072-2FID.*

Catalytic reaction of **2.1a-BBN** with 1-hexyne **(Table 2.4)**

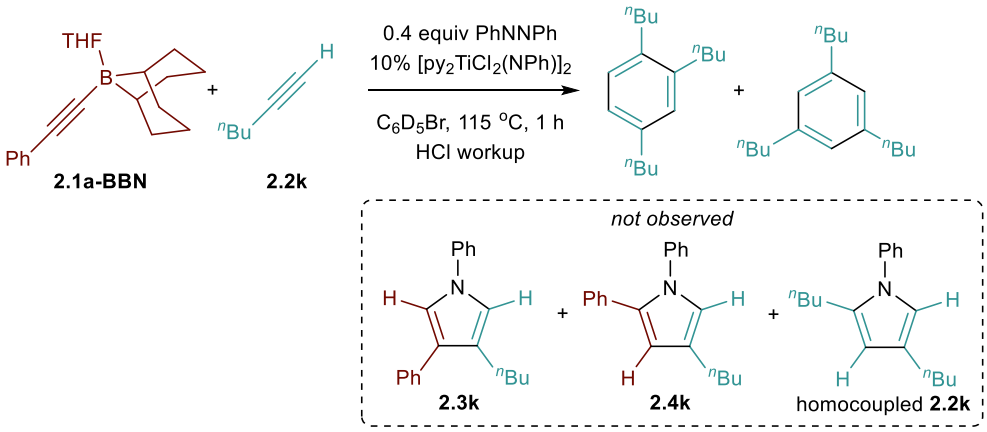

The reaction was performed following **Procedure 2.B** using **2.1a-BBN** (29.4 mg, 0.1 mmol, 1 equiv) and 1-hexyne (**2.2k**, 8.2 mg, 0.1 mmol, 1 equiv) with the reaction being heated for 1 h.

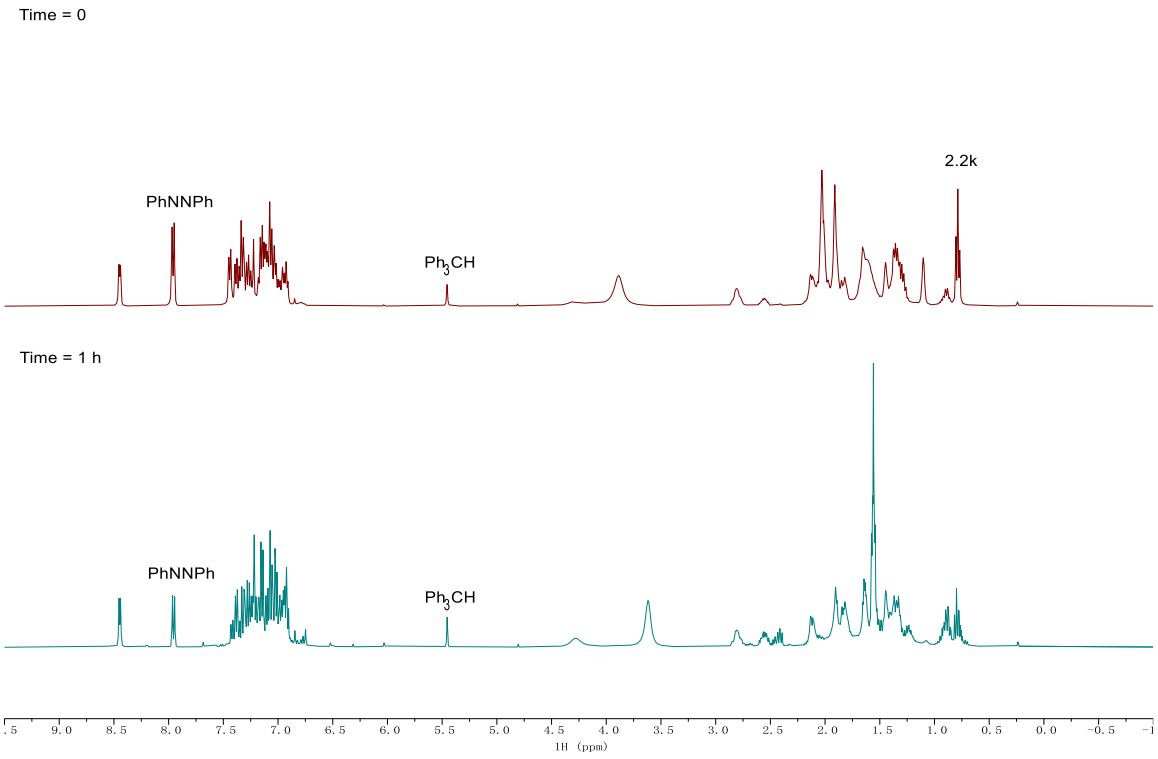

Figure 2.171. ^{1}H NMR of the reaction of **2.1a-BBN** with **2.2k** at time = 0 (top), time = 1 h (bottom) in C_6D_5Br. *Taken from (top) YC-2020-0073-0h-H and (bottom) YC-2020-0073-1h-H.*

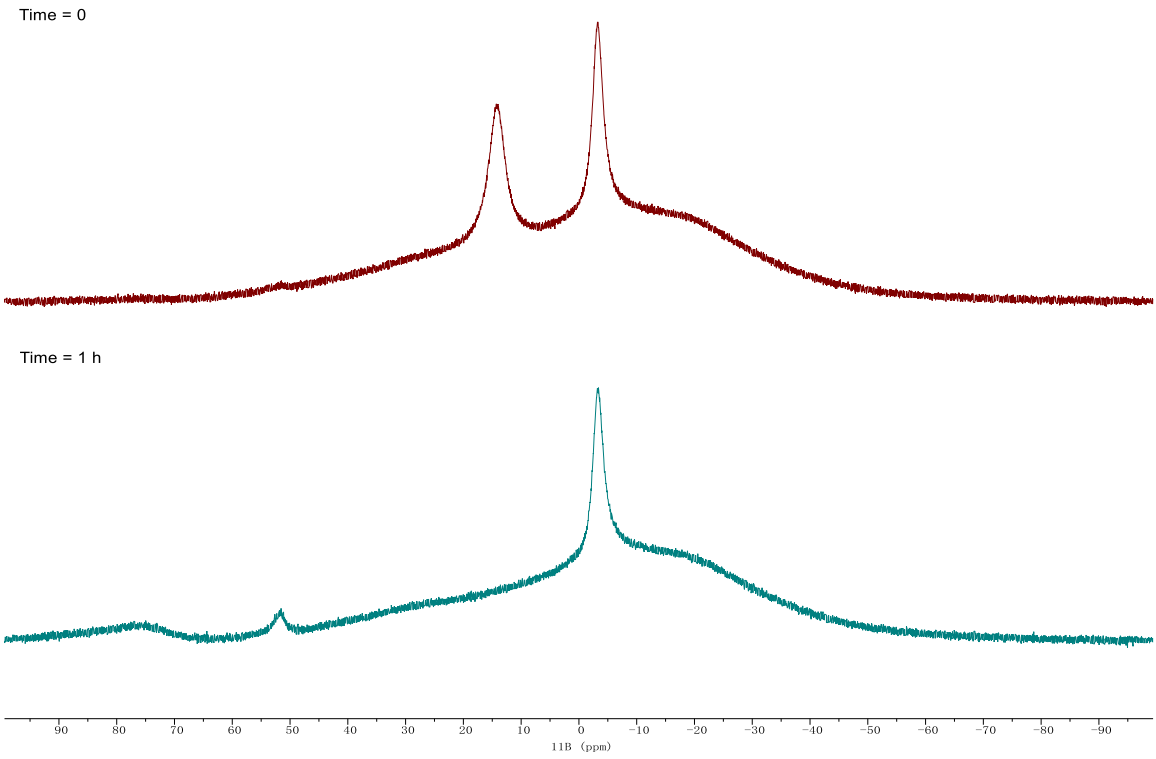

Figure 2.172. ^{11}B NMR of the reaction of **2.1a-BBN** with **2.2k** at time = 0 (top), time = 1 h (bottom) in C_6D_5Br. *Taken from (top) YC-2020-0073-0h-B and (bottom) YC-2020-0073-1h-B.*

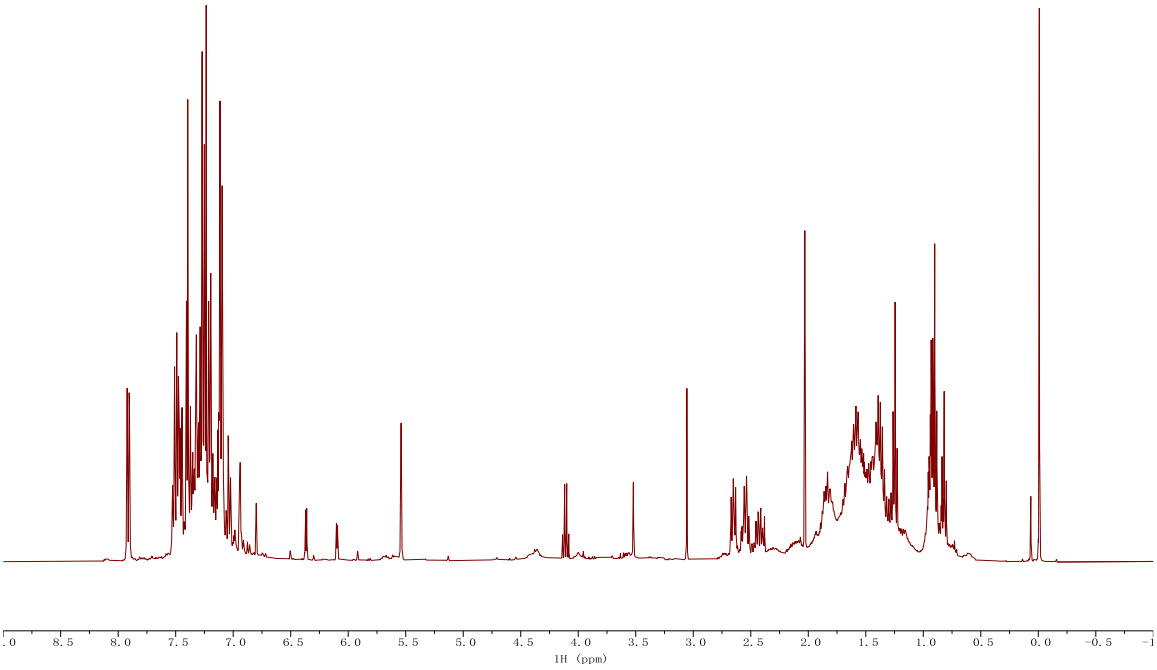

Figure 2.173. ^{1}H NMR of the reaction of **2.1a-BBN** with **2.2k** in $CDCl_3$ after HCl workup. *Taken from YC-2020-0073-3H.*

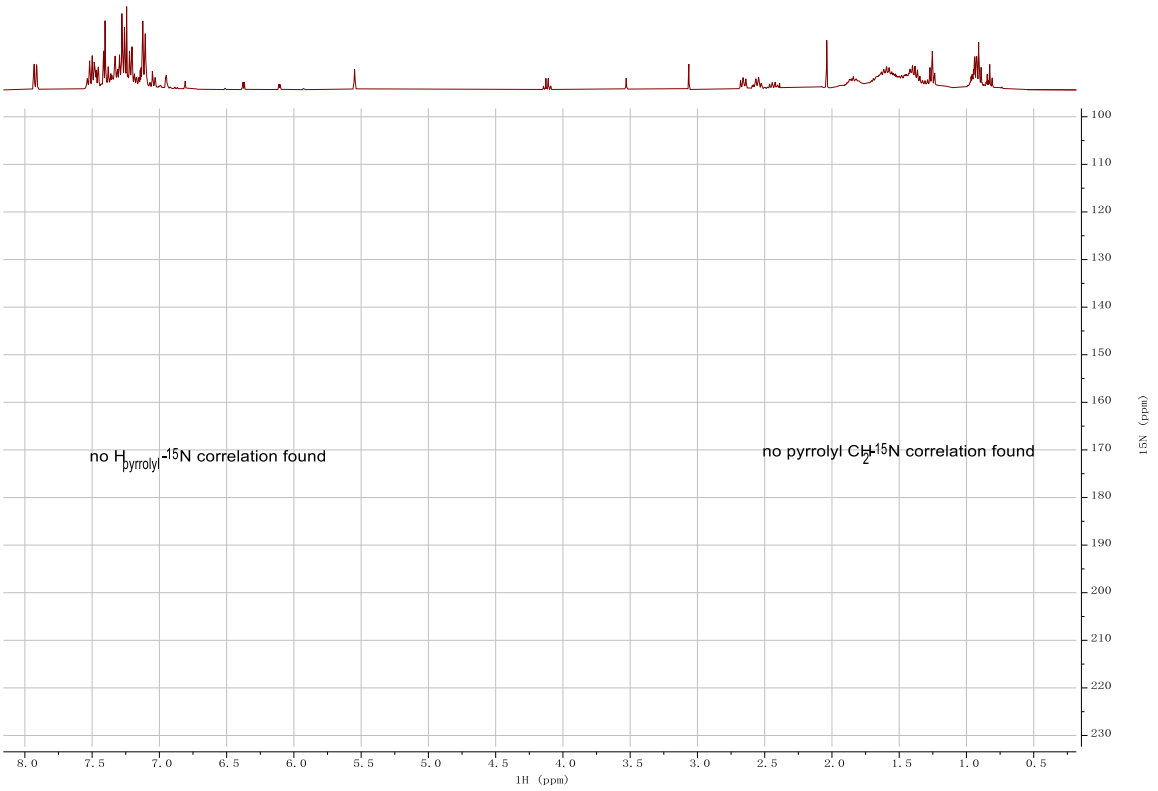

Figure 2.174. ^{1}H–^{15}N HMBC of the reaction of **2.1a-BBN** with **2.2k** in $CDCl_3$ after HCl workup. *Taken from YC-2020-0073-3NHMBC.*

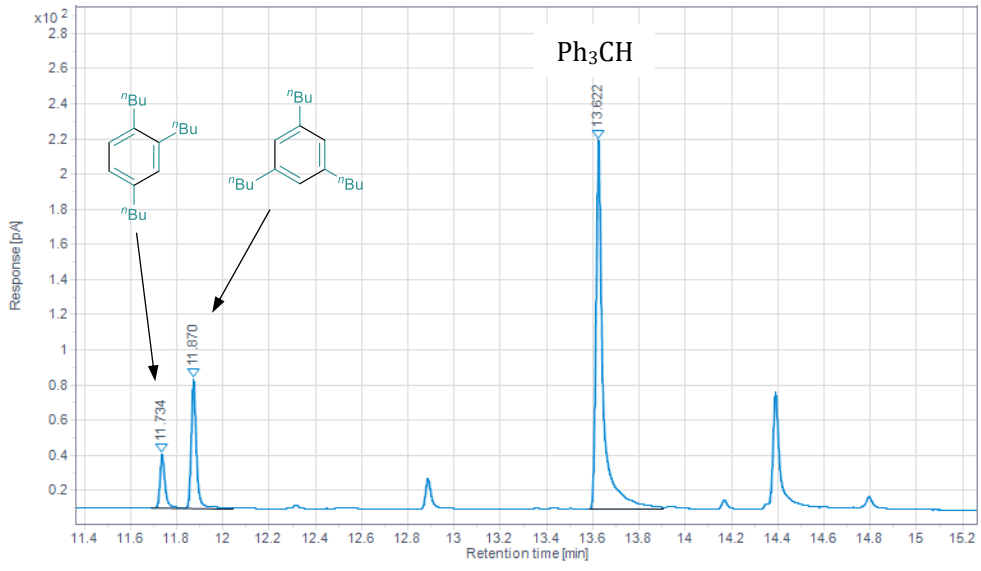

Figure 2.175. GC-FID chromatograph of the reaction of **2.1a-BBN** with **2.2k** after HCl workup. *Taken from YC-2020-0073-1FID.*

Catalytic reaction of **2.1a-SnMe$_3$** with 2-butyne **(Table 2.4)**

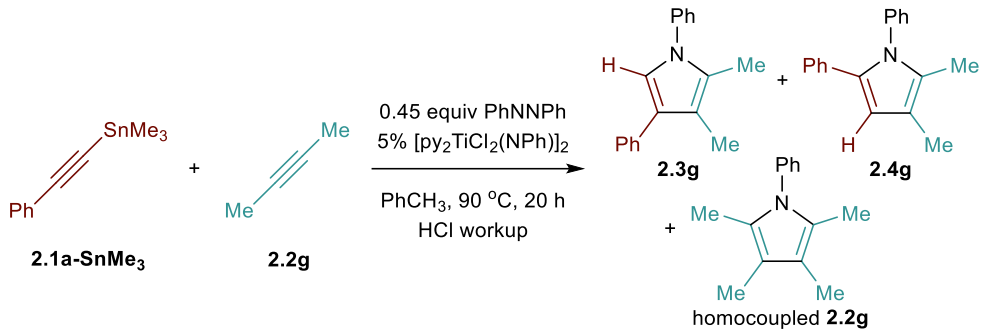

The reaction was performed following **Procedure 2.B** using **2.1a-SnMe$_3$** (26.5 mg, 0.1 mmol, 1 equiv) and 2-butyne (**2.2g**, 5.4 mg, 0.1 mmol, 1 equiv) with the reaction being heated for 20 h.

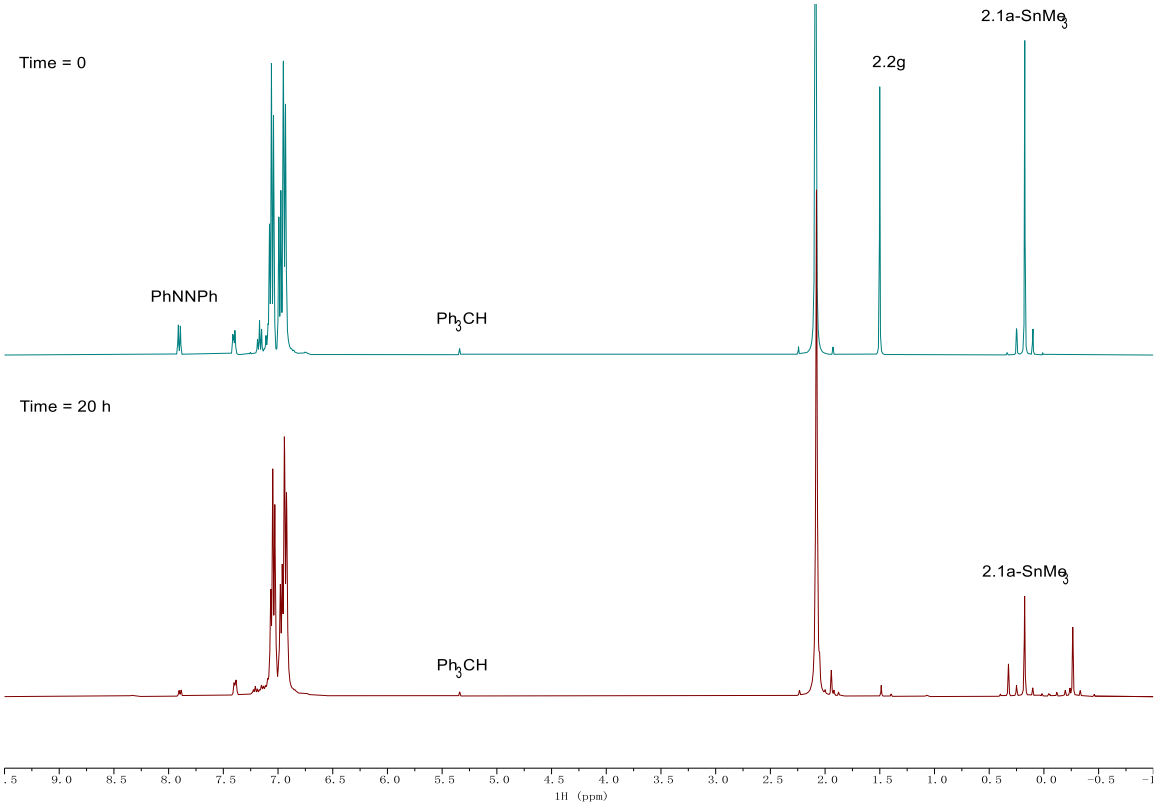

Figure 2.176. No-D ^{1}H NMR of the reaction of **2.1a-SnMe$_3$** with **2.2g** at time = 0 (top), time = 20 h (bottom) in $PhCH_3$. *Taken from (top) YC-2020-0063-2-NoD-Tol-0h-H and (bottom) YC-2020-0063-NoD-Tol-20h-H.*

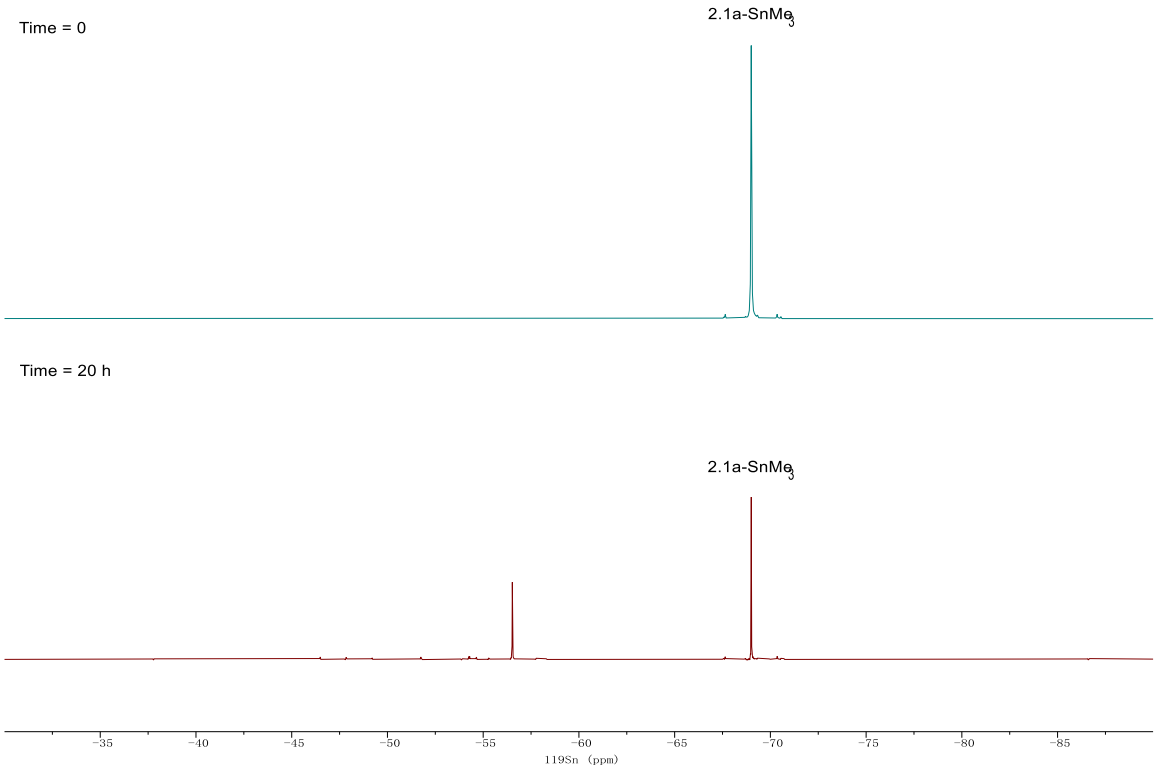

Figure 2.177. $^{119}Sn\{^{1}H\}$ NMR of the reaction of **2.1a-SnMe$_3$** with **2.2g** at time = 0 (top), time = 20 h (bottom) in $PhCH_3$. *Taken from (top) YC-2020-0063-2-NoD-Tol-0h-Sn and (bottom) YC-2020-0063-NoD-Tol-20h-Sn.*

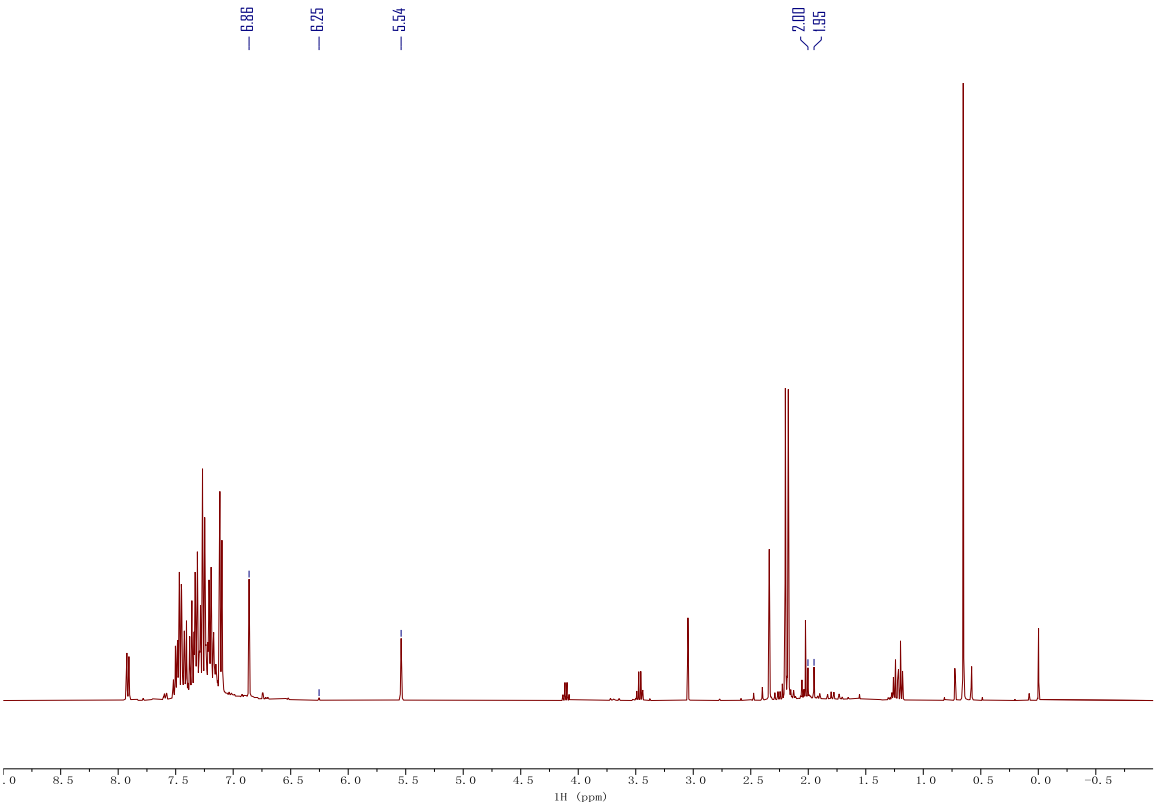

	δ (ppm)	Assignment	# of H	Peak Area	Yield (%)
Ph_3CH	5.54	Ph_3C-H	1	10245.3	n.a.
2.3g	6.86	$H_{pyrrolyl}$	1	10562.7	20.6
2.4g	6.25	$H_{pyrrolyl}$	1	401.1	0.8
homocoupled **2.2g**	2.00, 1.95	$Me_{pyrrolyl}$ (4 per molecule)	12	7329.5	1.2

Figure 2.178. ^{1}H NMR of the reaction of **2.1a-SnMe$_3$** with **2.2g** in $CDCl_3$ after HCl workup. *Taken from YC-2020-0063-3H.*

Catalytic reaction of **2.1a-SnMe$_3$** with 3-hexyne **(Table 2.4)**

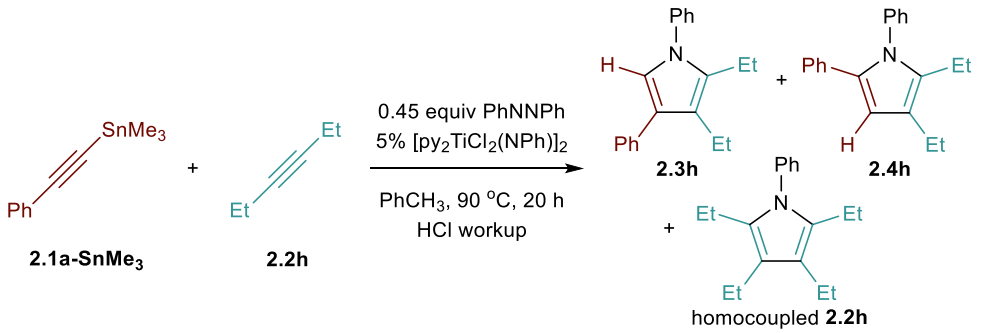

The reaction was performed following **Procedure 2.B** using **2.1a-SnMe$_3$** (26.5 mg, 0.1 mmol, 1 equiv) and 3-hexyne (**2.2h**, 8.2 mg, 0.1 mmol, 1 equiv) with the reaction being heated for 20 h.

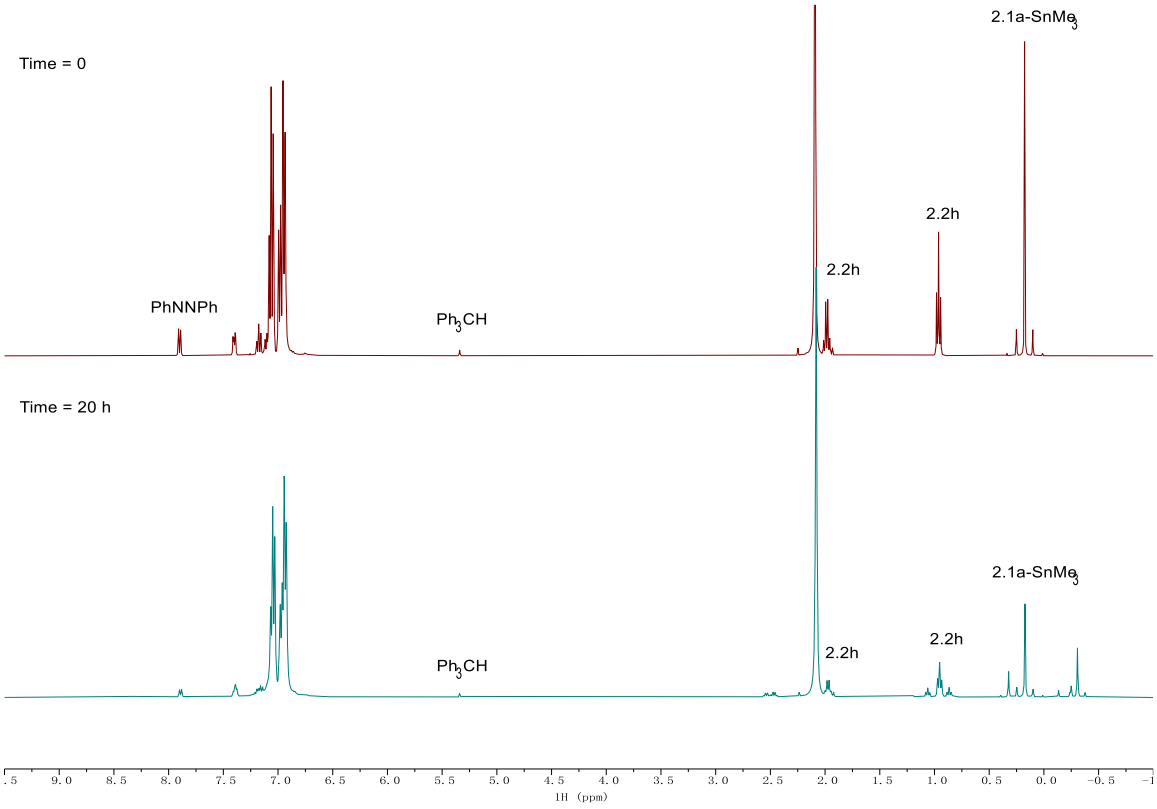

Figure 2.179. No-D ^{1}H NMR of the reaction of **2.1a-SnMe$_3$** with **2.2h** at time = 0 (top), time = 20 h (bottom) in $PhCH_3$. *Taken from (top) YC-2020-0064-2-NoD-Tol-0h-H and (bottom) YC-2020-0064-NoD-Tol-20h-H.*

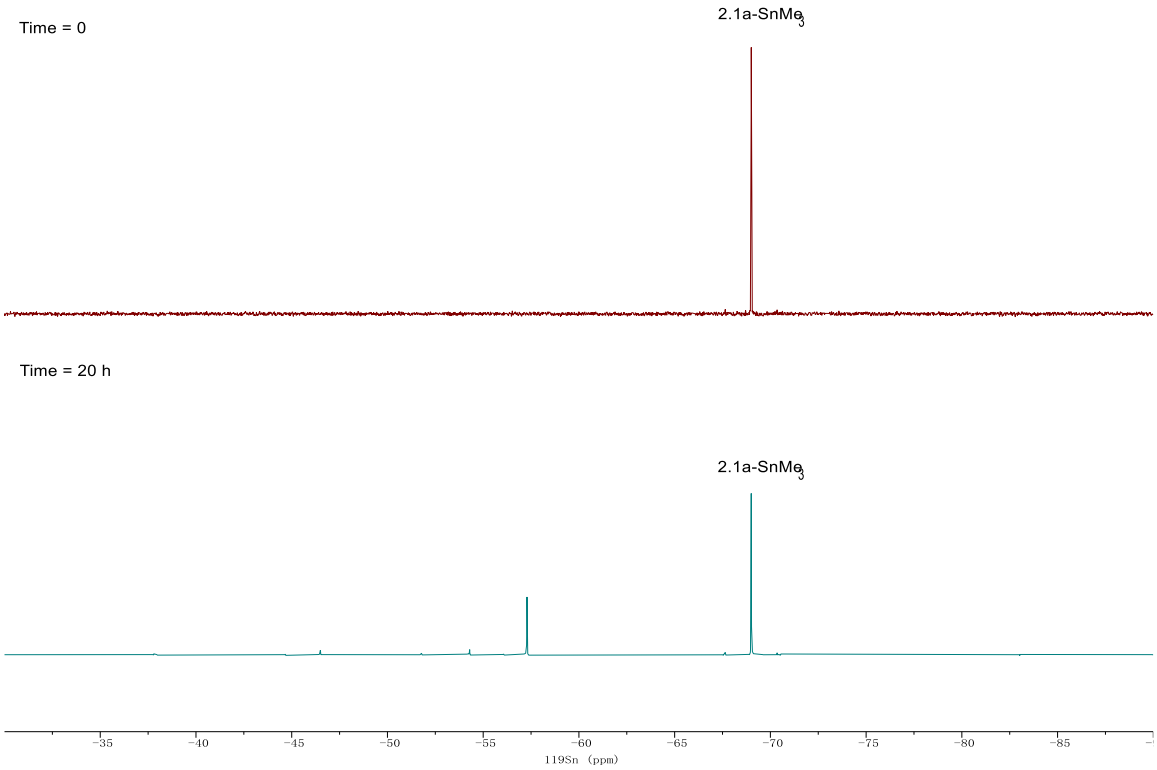

Figure 2.180. $^{119}Sn\{^{1}H\}$ NMR of the reaction of **2.1a-SnMe$_3$** with **2.2h** at time = 0 (top), time = 20 h (bottom) in $PhCH_3$. *Taken from (top) YC-2020-0064-2-NoD-Tol-0h-Sn and (bottom) YC-2020-0064-NoD-Tol-20h-Sn.*

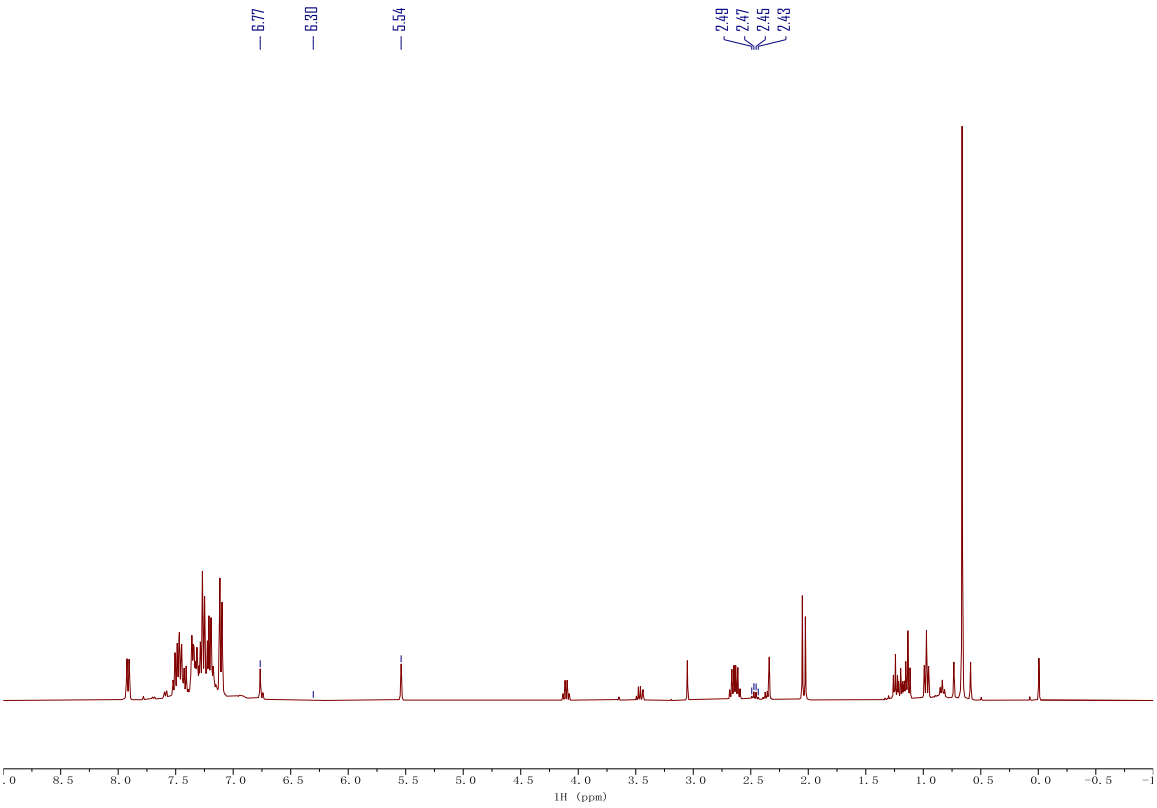

	δ (ppm)	Assignment	# of H	Peak Area	Yield (%)
Ph_3CH	5.54	Ph_3C-H	1	8048.1	n.a.
2.3h	6.77	$H_{pyrrolyl}$	1	6337.5	15.7
2.4h	6.30	$H_{pyrrolyl}$	1	240.8	0.6
homocoupled **2.2h**	2.49, 2.47, 2.45, 2.43	3,4-CH_2CH$_3$ (2 per molecule)	4	4087.2	2.5

Figure 2.181. ^{1}H NMR of the reaction of **2.1a-SnMe$_3$** with **2.2h** in $CDCl_3$ after HCl workup. *Taken from YC-2020-0064-3H.*

Catalytic reaction of **2.1a-SnMe$_3$** with 4-octyne **(Table 2.4)**

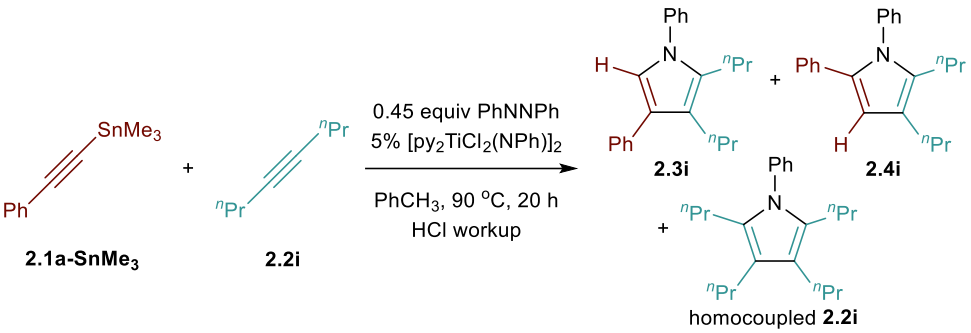

The reaction was performed following **Procedure 2.B** using **2.1a-SnMe$_3$** (26.5 mg, 0.1 mmol, 1 equiv) and 4-octyne (**2.2i**, 11.0 mg, 0.1 mmol, 1 equiv) with the reaction being heated for 20 h.

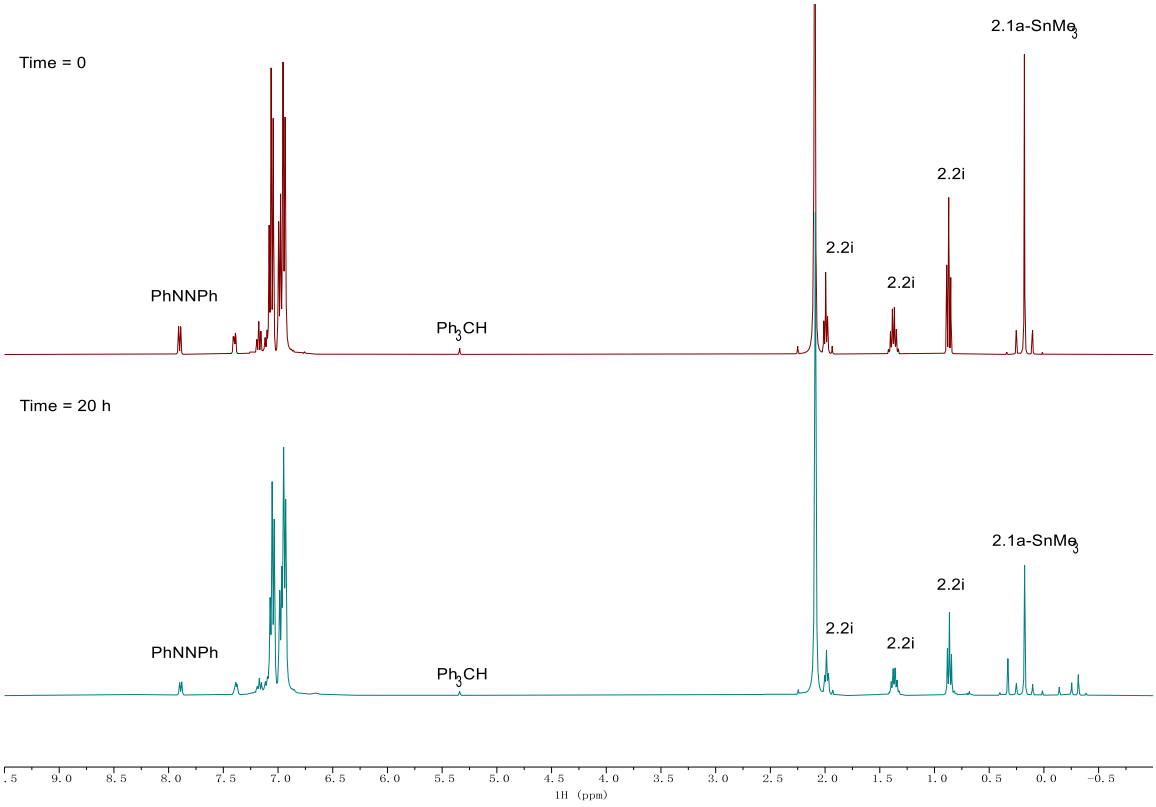

Figure 2.182. No-D ^{1}H NMR of the reaction of **2.1a-SnMe$_3$** with **2.2i** at time = 0 (top), time = 20 h (bottom) in $PhCH_3$. *Taken from (top) YC-2020-0065-2-NoD-Tol-0h-H and (bottom) YC-2020-0065-NoD-Tol-20h-H.*

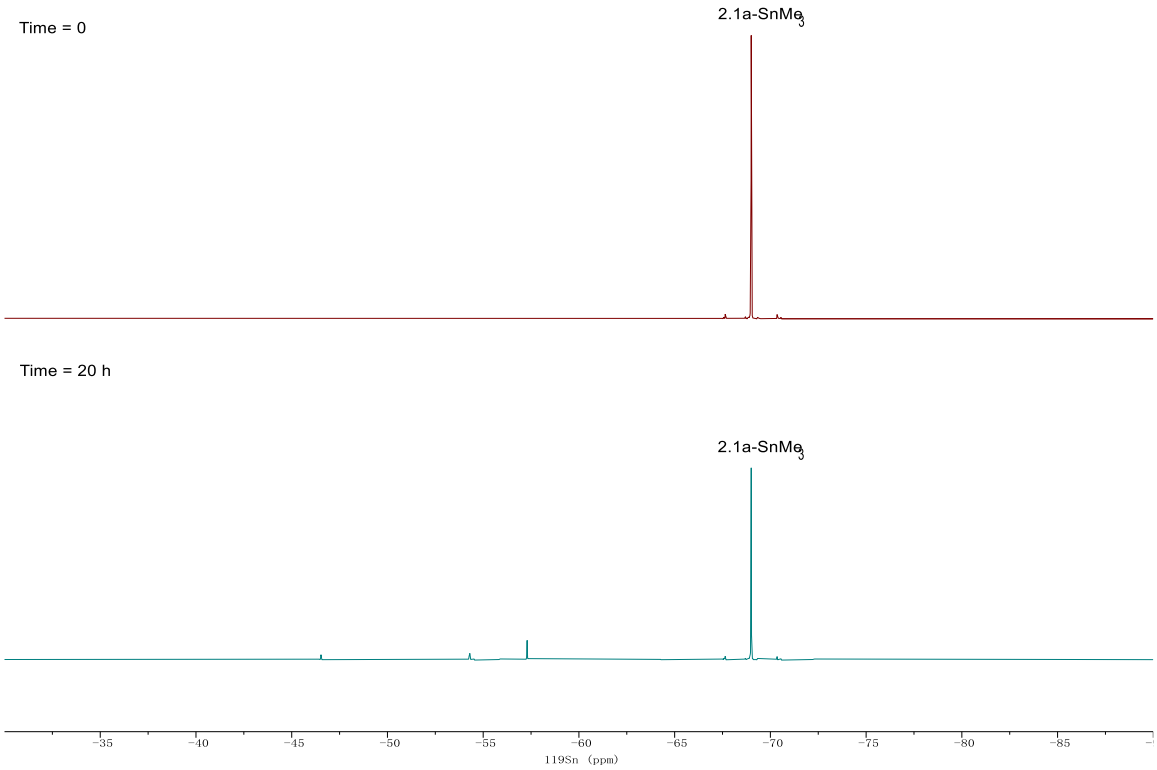

Figure 2.183. $^{119}Sn\{^{1}H\}$ NMR of the reaction of **2.1a-SnMe$_3$** with **2.2i** at time = 0 (top), time = 20 h (bottom) in $PhCH_3$. *Taken from (top) YC-2020-0065-2-NoD-Tol-0h-Sn and (bottom) YC-2020-0065-NoD-Tol-20h-Sn.*

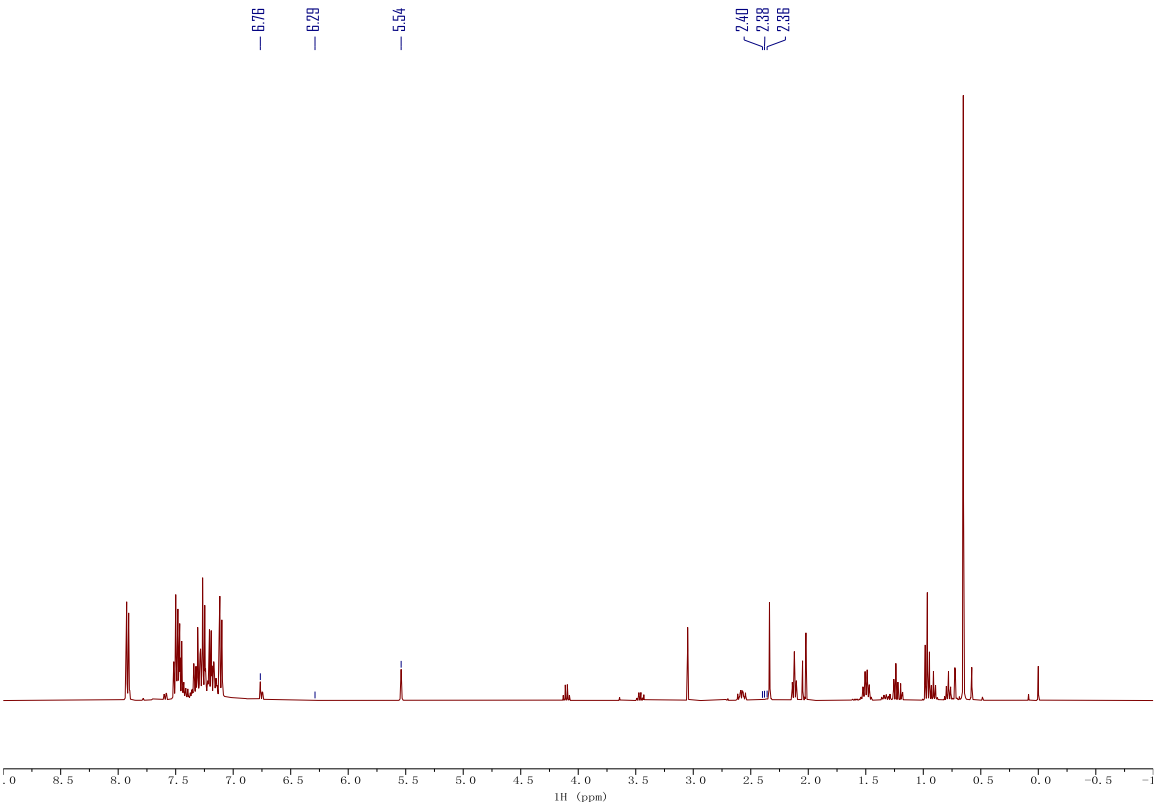

	δ (ppm)	Assignment	# of H	Peak Area	Yield (%)
Ph_3CH	5.54	Ph_3C-H	1	12272.0	n.a.
2.3i	6.76	$H_{pyrrolyl}$	1	3508.8	5.7
2.4i	6.29	$H_{pyrrolyl}$	1	81.5	0.1
homocoupled **2.2i**	2.40, 2.38, 2.36	3,4-C$H_2$$CH_3$ (2 per molecule)	4	621.2	0.3

Figure 2.184. ^{1}H NMR of the reaction of **2.1a-SnMe$_3$** with **2.2i** in $CDCl_3$ after HCl workup. *Taken from YC-2020-0065-3H.*

Catalytic reaction of **2.1a-SnMe$_3$** with diphenylacetylene **(Table 2.4)**

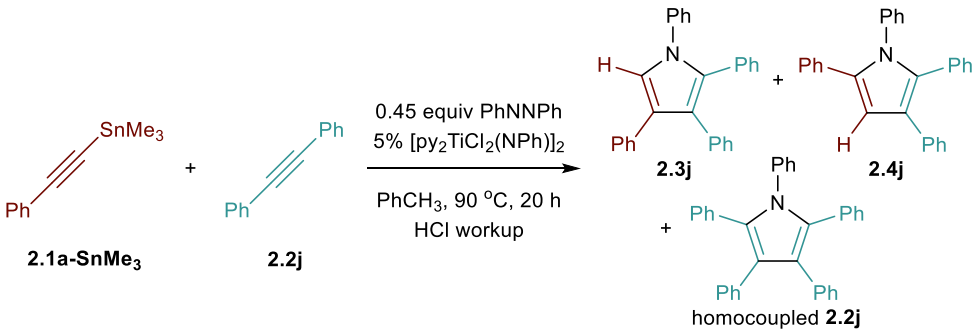

The reaction was performed following **Procedure 2.B** using **2.1a-SnMe$_3$** (26.5 mg, 0.1 mmol, 1 equiv) and diphenylacetylene (**2.2j**, 17.8 mg, 0.1 mmol, 1 equiv) with the reaction being heated for 20 h. Yields were determined by GC due to peak overlapping in ^{1}H NMR spectrum after HCl workup.

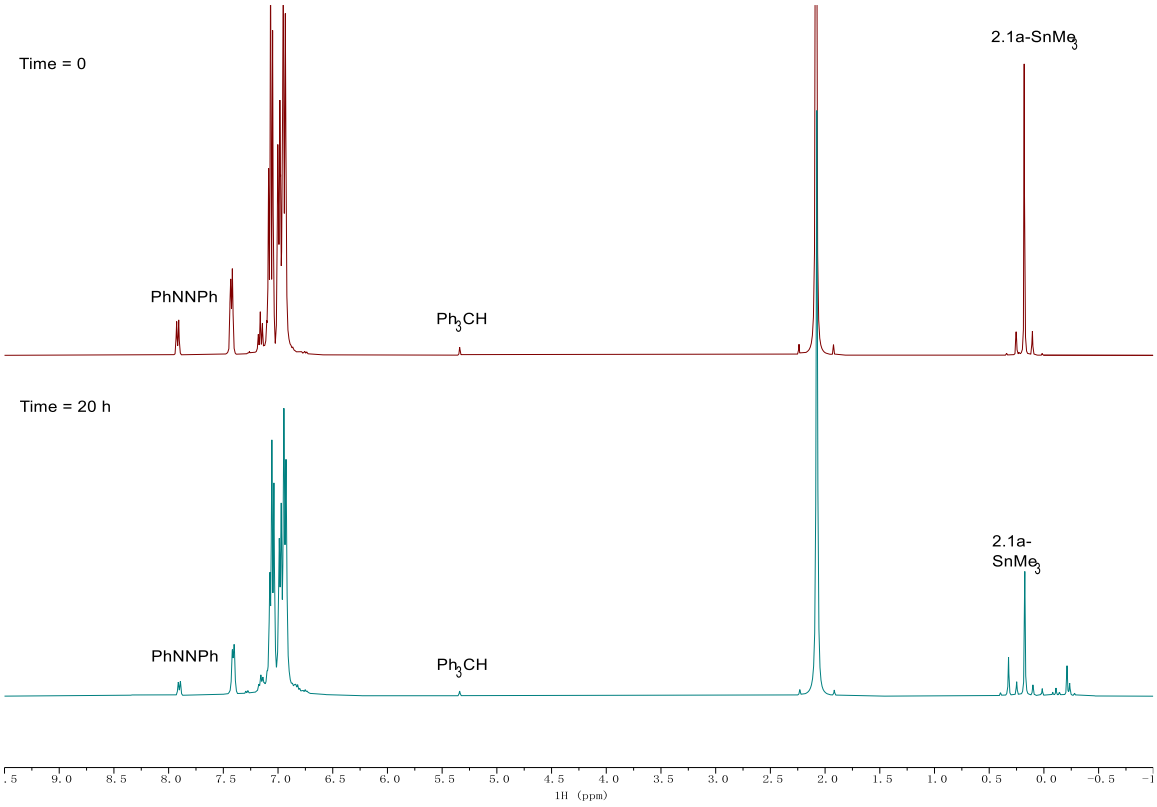

Figure 2.185. No-D ^{1}H NMR of the reaction of **2.1a-SnMe$_3$** with **2.2j** at time = 0 (top), time = 20 h (bottom) in $PhCH_3$. *Taken from (top) YC-2020-0066-2-NoD-Tol-0h-H and (bottom) YC-2020-0066-NoD-Tol-20h-H.*

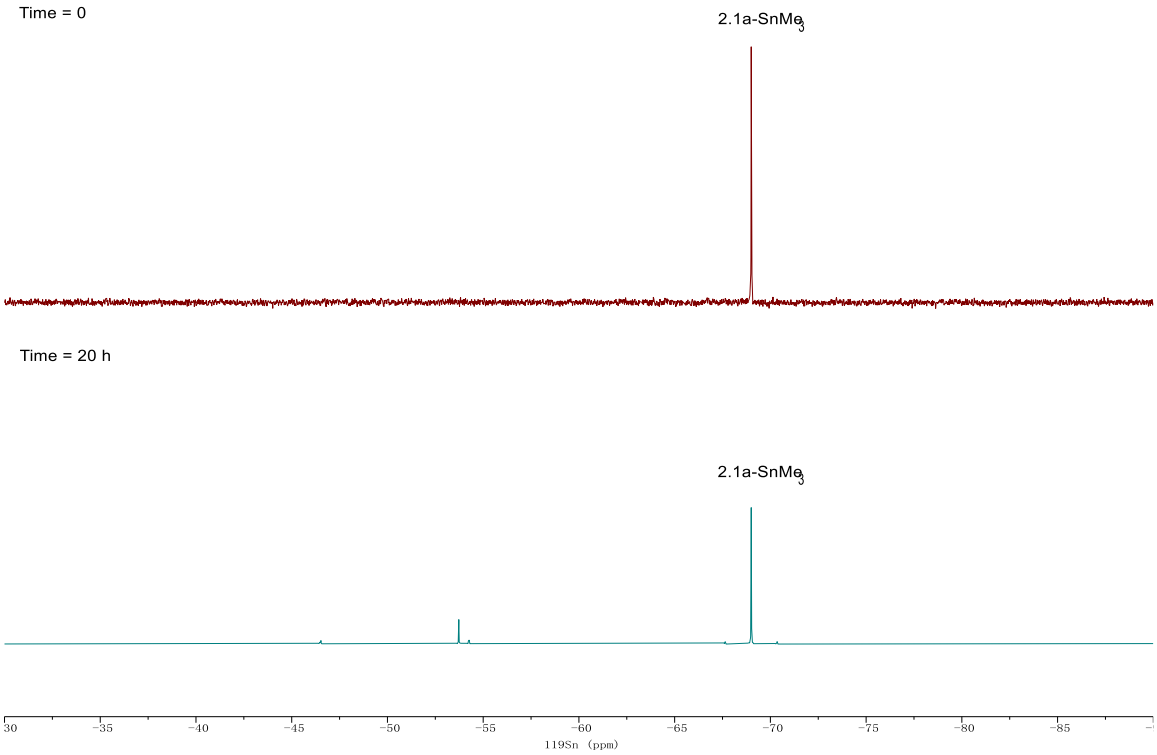

Figure 2.186. $^{119}Sn\{^{1}H\}$ NMR of the reaction of **2.1a-SnMe$_3$** with **2.2j** at time = 0 (top), time = 20 h (bottom) in $PhCH_3$. *Taken from (top) YC-2020-0066-2-NoD-Tol-0h-Sn and (bottom) YC-2020-0066-NoD-Tol-20h-Sn.*

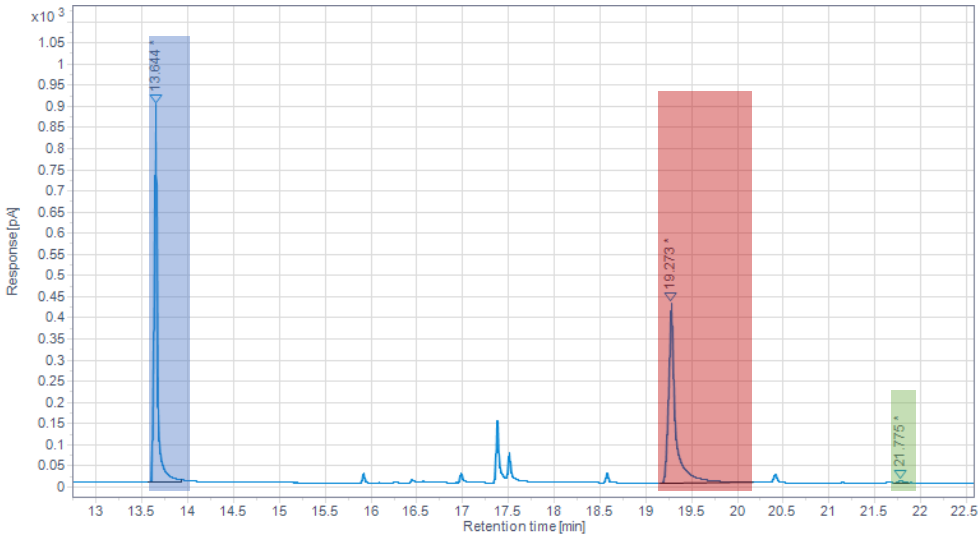

	Retention Time (min)	Surface Area	# of C	Yield (%)
Ph_3CH	13.644	2087.757	19	n.a.
2.3j	19.273	2196.968	28	14.3
2.4j	not found	n.a.	28	n.d.
homocoupled **2.2j**	21.775	25.834	34	0.1

Figure 2.187. Quantitative GC-FID chromatograph of the reaction of **2.1a-SnMe$_3$** with **2.2j** after HCl workup. *Taken from YC-2020-0066-2FID.*

Catalytic reaction of **2.1a-SnMe$_3$** with 1-hexyne **(Table 2.4)**

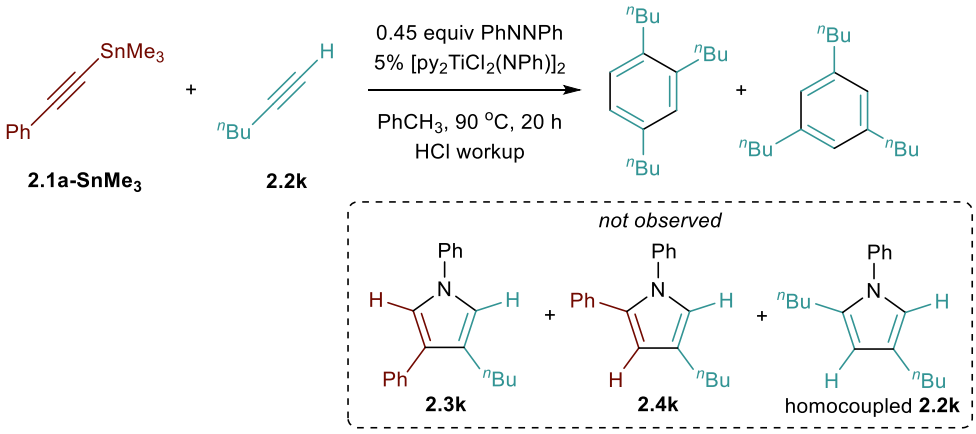

The reaction was performed following **Procedure 2.B** using **2.1a-SnMe$_3$** (26.5 mg, 0.1 mmol, 1 equiv) and 1-hexyne (**2.2k**, 8.2 mg, 0.1 mmol, 1 equiv) with the reaction being heated for 20 h.

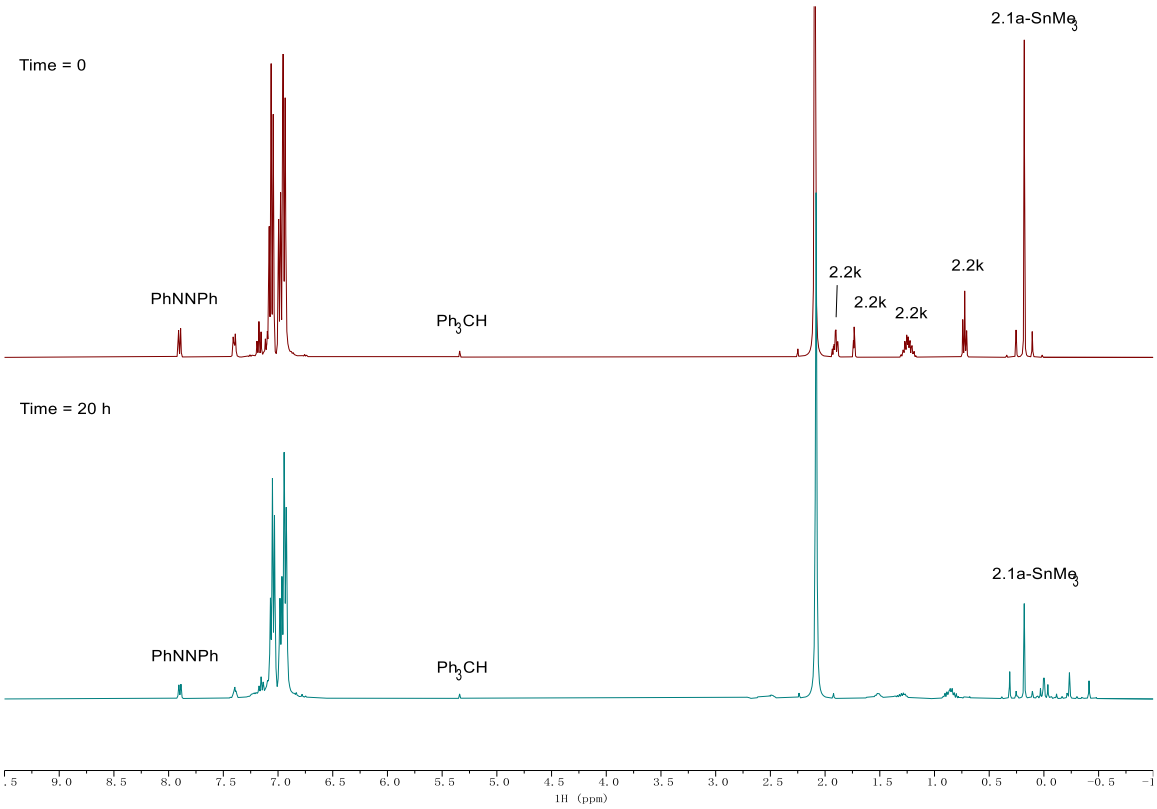

Figure 2.188. No-D ^{1}H NMR of the reaction of **2.1a-SnMe$_3$** with **2.2k** at time = 0 (top), time = 20 h (bottom) in $PhCH_3$. *Taken from (top) YC-2020-0067-2-NoD-Tol-0h-H and (bottom) YC-2020-0067-NoD-Tol-20h-H.*

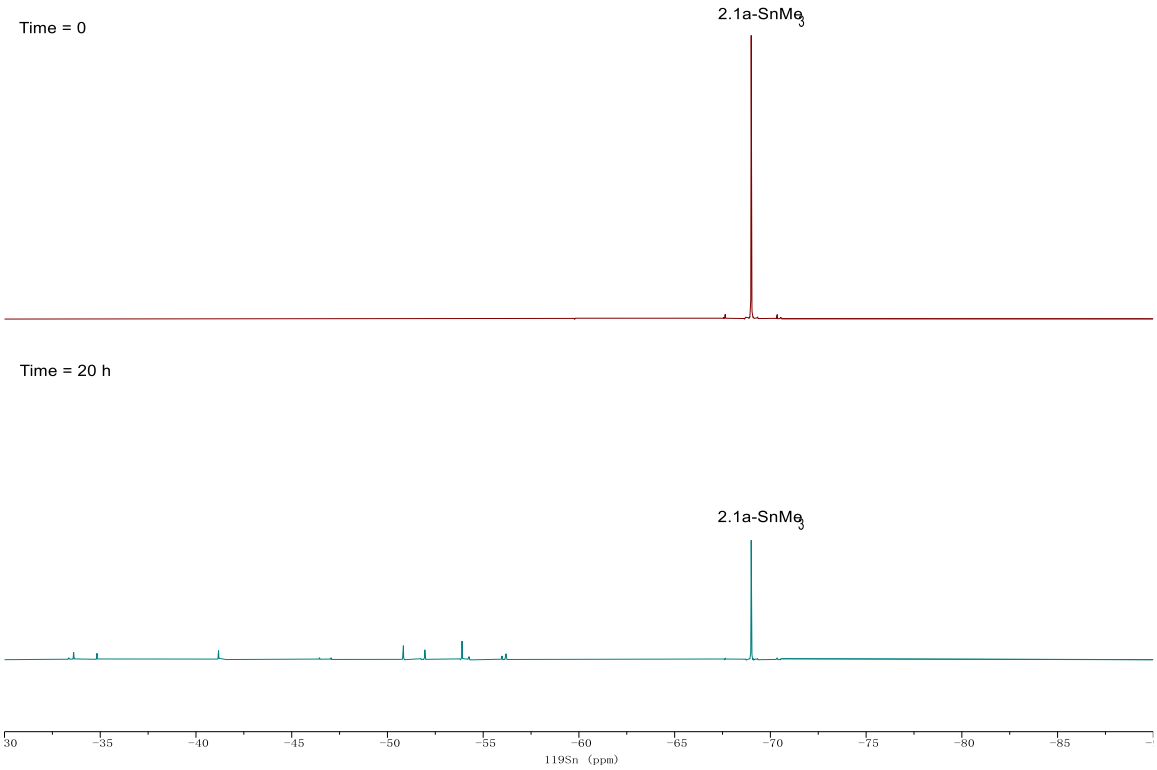

Figure 2.189. $^{119}Sn\{^{1}H\}$ NMR of the reaction of **2.1a-SnMe$_3$** with **2.2k** at time = 0 (top), time = 20 h (bottom) in $PhCH_3$. *Taken from (top) YC-2020-0067-2-NoD-Tol-0h-Sn and (bottom) YC-2020-0067-NoD-Tol-20h-Sn.*

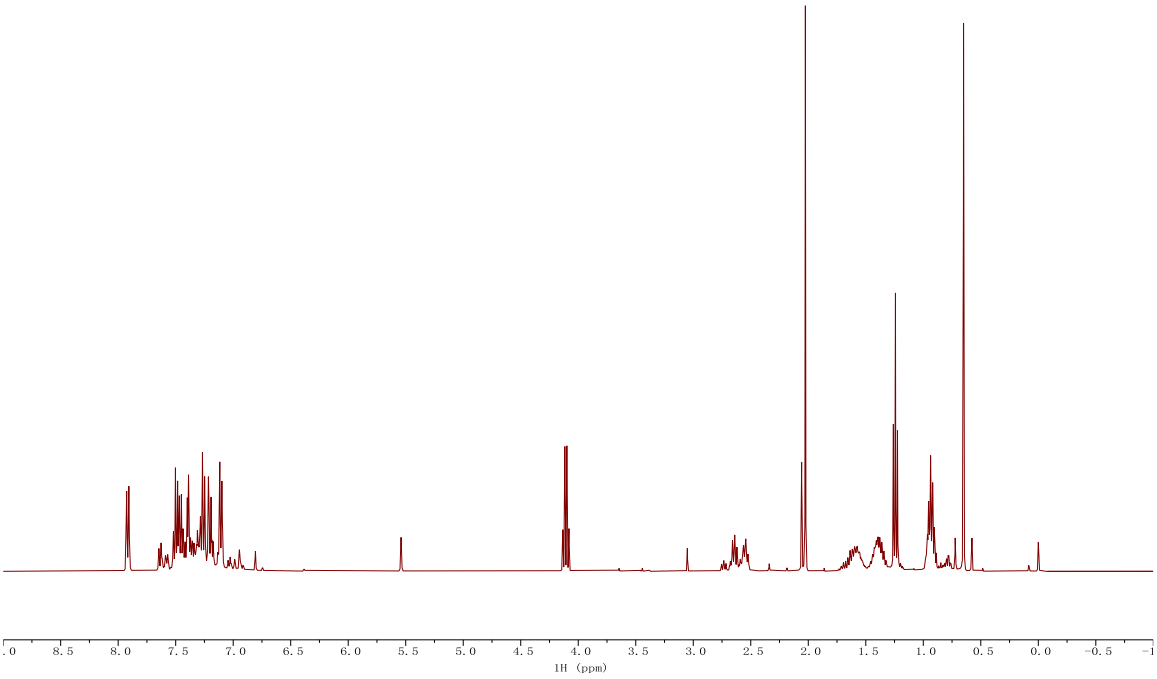

Figure 2.190. ^{1}H NMR of the reaction of **2.1a-SnMe$_3$** with **2.2k** in $CDCl_3$ after HCl workup. *Taken from YC-2020-0067-3H.*

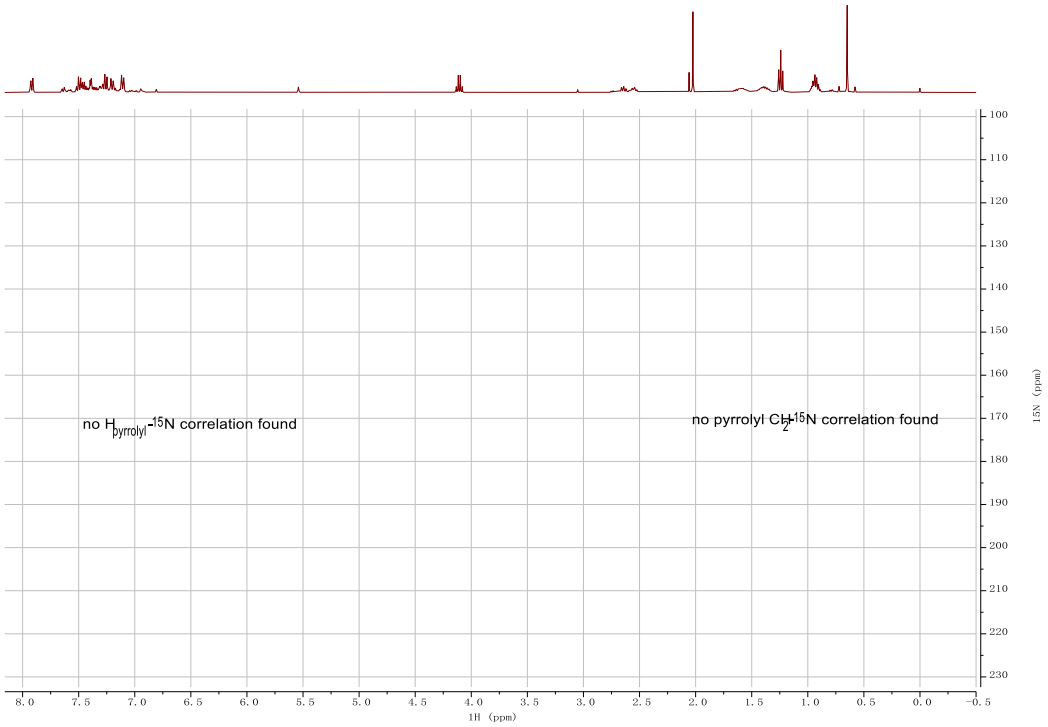

Figure 2.191. ^{1}H–^{15}N HMBC of the reaction of **2.1a-SnMe$_3$** with **2.2k** in $CDCl_3$ after HCl workup. *Taken from YC-2020-0067-4NHMBC.*

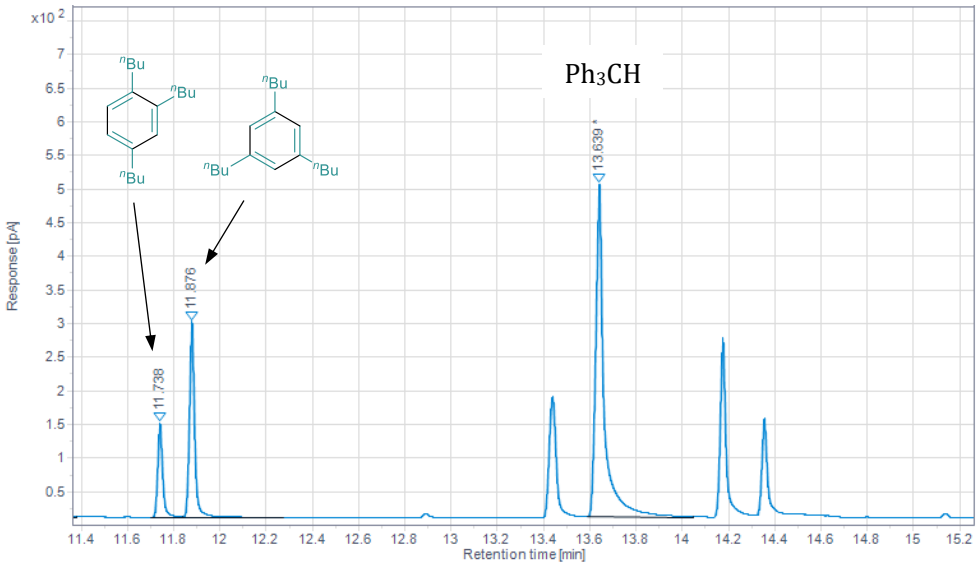

Figure 2.192. GC-FID chromatograph of the reaction of **2.1a-SnMe$_3$** with **2.2k** after HCl workup. *YC-2020-0067-2-1FID.*

Chapter 3: Generation of Masked Ti^{II} Intermediates from Ti^{IV} Amides *via* *β*-H Abstraction or Alkyne Deprotonation: An Example of Ti-Catalyzed Nitrene-Coupled Transfer Hydrogenation

Reproduced in part with permission from:

Pearce, A. J.; Cheng, Y.; Dunscomb, Rachel. J.; Tonks, I. A.

Generation of Masked Ti^{II} Intermediates from Ti^{IV} Amides *via* *β*-H Abstraction or Alkyne Deprotonation: An Example of Ti-Catalyzed Nitrene-Coupled Transfer Hydrogenation.

Organometallics **2020**, *39*, 21, 3771–3774.

3.1 Overview

Simple Ti amide complexes are shown to act as sources for masked Ti^{II} intermediates *via* several pathways, as demonstrated through the investigation of a unique Ti-catalyzed nitrene-coupled transfer hydrogenation of 3-hexyne. This reaction proceeds through reduction of azobenzene by a masked Ti^{II} catalyst, wherein both amines and 3-hexyne can serve as the hydrogen source/reductant for Ti by forming putative titanaaziridines *via* *β*-H abstraction or putative titanacyclopentynes *via* protonolysis, respectively.

3.2 Introduction

Titanium(II) complexes and intermediates play important roles in various redox reactions,[142] such as Kulinkovich cyclopropanations,[29] alkyne cyclotrimerization,[143–145] and many other annulations.[146,147] Common methods for generating low-valent metals involve reduction of metal halides or *β*-H abstraction of alkyl ligands (Figure 3.1, top).[8,148,149] In many cases, these low-valent Ti^{II} intermediates are trapped or masked via backbonding into *π*-acidic ligands. In the interest of expanding the accessibility of Ti^{II} intermediates in catalysis, we herein report the reactivity of masked Ti^{II} intermediates generated from simple Ti amides *via* *β*-H abstraction or internal alkyne deprotonation (Figure 3.1, bottom).

The η^2-titanaziridine complexes can be easily generated through *β*-H abstraction, and their insertion chemistry in the context of alkene hydroaminoalkylation catalysis is well-established.[150–152] We hypothesized that η^2-titanaaziridine complexes could alternately be considered as masked Ti^{II} species for redox transformations, in direct analogy to chemistry mediated by η^2-olefin/titanacyclopropane complexes (Figure 3.1, bottom). In fact, Rothwell demonstrated that an η^2-titanaziridine could furnish a Ti imido upon stoichiometric reaction with azobenzene.[56,153] The use of diazenes to capture these reactive species could ultimately allow for catalytic nitrene transfer reactions[32,154,155] from simple and readily available Ti amide compounds.

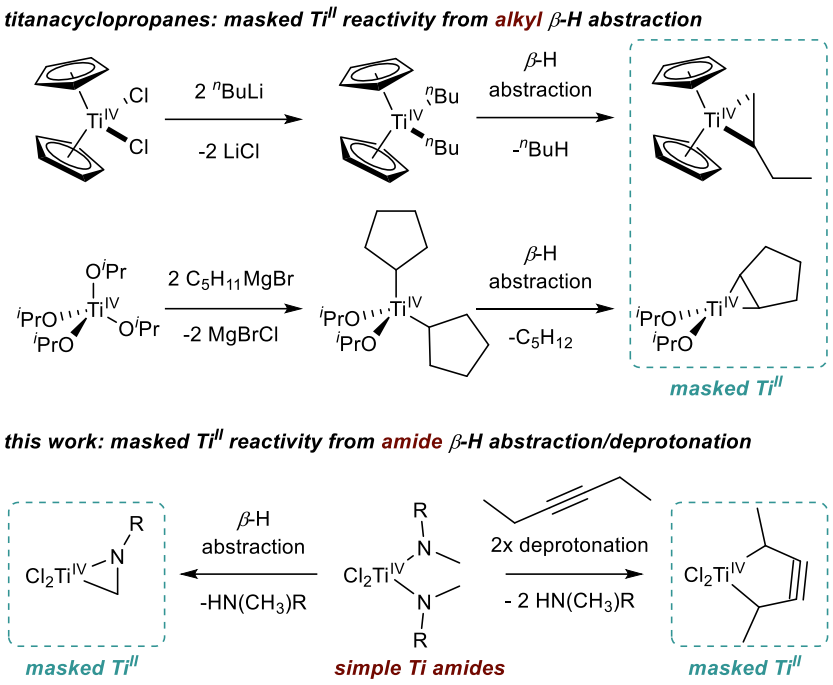

Figure 3.1. Masked Ti^{II} reagents generated *via* β-H abstraction by Ti alkyls (top) or Ti amides (bottom).

3.3 Result and Discussion

Following this hypothesis, $TiCl_2(NMe_2)_2$ was examined as a catalyst for 3-hexyne cyclotrimerization[127] as well as [2+2+1] pyrrole synthesis.[32] 3-Hexyne underwent successful cyclotrimerization with 5 mol% $TiCl_2(NMe_2)_2$ as catalyst, yielding 58% of C_6Et_6 after 22 h at 145 °C (Figure 3.2, eqn 1)—consistent with the hypothesis that Ti^{II} species could be accessed from the amide, since cyclotrimerization typically occurs through a Ti^{II}/Ti^{IV} mechanism.[156–159]

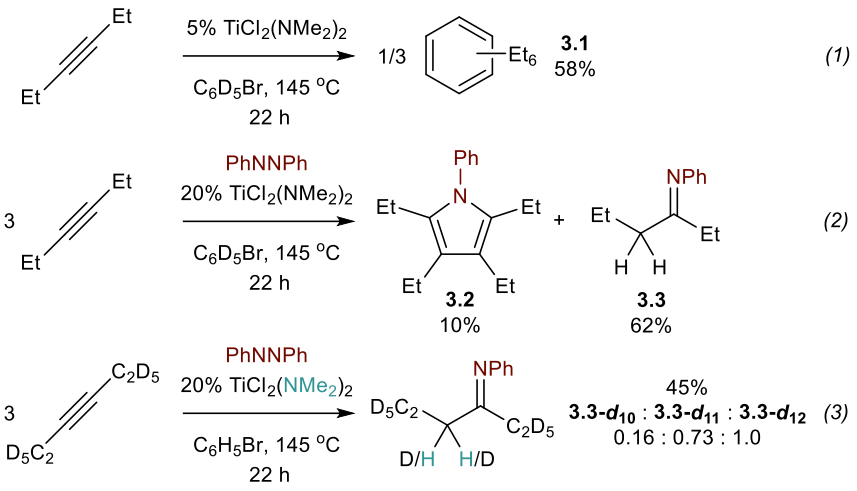

Figure 3.2. (Eqn 1) Trimerization and (eqn 2 and eqn 3) hydroamination of alkyne catalyzed by $TiCl_2(NMe_2)_2$.

Surprisingly, the attempted [2+2+1] nitrene transfer reaction (Figure 3.2, eqn 2) did not yield tetraethylpyrrole **3.2** as the major product, instead generating a mixture of (*Z*)- and (*E*)-*N*-phenylhexan-3-imine in 62% yield—the product of formal nitrene-coupled hydrogenation of the alkyne. Although metallacycle protonation by free $HNMe_2$ resulting from *β*-H abstraction could account for some imine formation, yields in excess of the catalyst loading indicates that other mechanisms and chemical species must at least partly be involved in Ti redox and hydrogen transfer.

To interrogate the source of hydrogen, reaction was carried out with perdeuterated 3-hexyne-d_{10} (Figure 3.2, eqn 3). This reaction yielded a mixture of **3.3**-d_{10}, **3.3**-d_{11} and **3.3**-d_{12} in a ratio of 0.16:0.73:1.0 (Figure 3.2, eqn 3). The predominance of **3.3**-d_{12} suggests that 3-hexyne is the major hydrogen source (*vide infra*). Meanwhile, the formation of **3.3**-d_{10} and mixed product **3.3**-d_{11} indicates that $HNMe_2$ (from *β*-H abstraction of dimethylamide ligand) also contributes a non-negligible amount of hydrogen. Notably, based on the catalyst loading, the dimethylamide ligands can account for the majority of hydrogen for **3.3**-d_{10} and **3.3**-d_{11}. However, as H/D scrambling of **3.3** with 3-hexyne can occur (see *3.5.9* for a scrambling experiment), the approximate ratio of *β*-H abstraction versus alkyne deprotonation may be underestimated. This reaction is a rare example of Ti-catalyzed transfer hydrogenation[160,161] and a unique example of nitrene-coupled transfer hydrogenation.

Based on the above, we propose the mechanism for nitrene-coupled transfer hydrogenation in Figure 3.3. Starting from $TiCl_2(NMe_2)_2$ (**3.3.A**), two pathways are possible: first, coordination of 3-hexyne to Ti and subsequent deprotonation of the propargylic C–H affords titanacyclopentyne complex **3.3.B** (pathway I). Coordination of another oxidizing *π*-acid such as azobenzene could then liberate 2,3,4-hexatriene to furnish a Ti η^2-hydrazido(2-) complex **3.3.C**. Although 2,3,4-hexatriene is not observed in reaction mixtures, metallacyclopentyne complexes of group 4 metals have been studied previously,[162–165] and this mechanism best accounts for the poor mass balance in 3-hexyne (despite 85% conversion of 3-hexyne, less than 50% 3-hexyne is converted to **3.3**), although we cannot rule out other dehydrogenation products of 3-hexyne being involved. Alternately, $TiCl_2(NMe_2)_2$ can undergo *β*-H abstraction to generate an η^2-titanaziridine **3.3.D** (pathway II), which could similarly undergo exchange with azobenzene to liberate *N*-methylformimine and generate the Ti η^2-hydrazido(2-) **3.3.C**. We have observed similar *π*-acid/azobenzene exchange with low-valent Ti halides during Ti-catalyzed isocyanide amination reactions.[166]

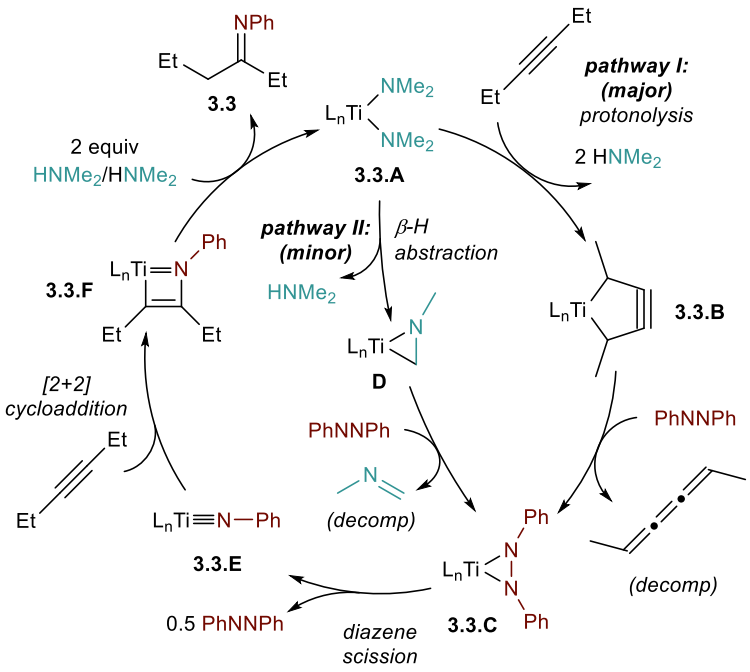

Figure 3.3. Plausible mechanism of hydroamination of 3-hexyne with azobenzene catalyzed by $TiCl_2(NMe_2)_2$. Teal and black hydrogens indicate their origin from -NMe_2 or 3-hexyne, respectively.

Ti η^2-hydrazido(2-) complexes like **3.3.C** are well-established to undergo bimetallic scission to Ti imido complexes (**3.3.E**).[32,167] From **3.3.E**, [2+2] cycloaddition of 3-hexyne yields azatitanacyclobutadiene **3.3.F**, which can undergo protonolysis by $HNMe_2$ to liberate the hydroaminated product[17,168,169] and regenerate $TiCl_2(NMe_2)_2$. $HNMe_2$ ultimately serves the role of a proton shuttle in the reaction, moving protons from either 3-hexyne or another equivalent of -NMe_2 to the imine product.

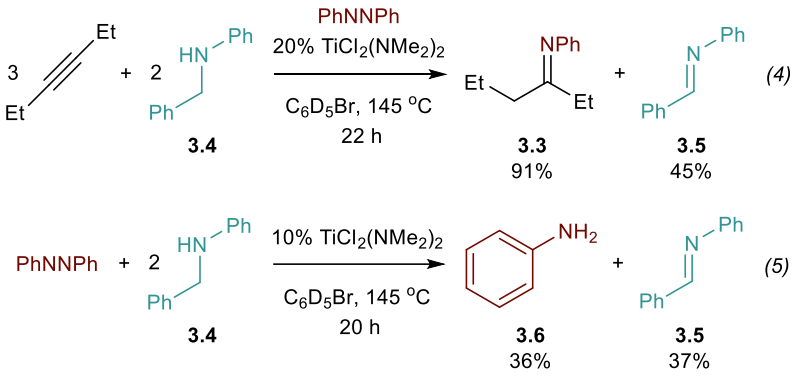

Figure 3.4. Ti-catalyzed nitrene-coupled transfer hydrogenation reactions with *N*-benzylaniline.

Prompted by these dual pathways, we hypothesized that secondary amines bearing more acidic *α*-hydrogens would be a more efficient source of hydrogen than 3-hexyne. In fact, reaction of 3-hexyne with *N*-benzylaniline (**3.4**) and azobenzene resulted in near quantitative (91% based on PhNNPh) formation of **3.3** (Figure 3.4, eqn 4), along with significant formation of *N*-phenylaldimine dehydrogenated byproduct **3.5** (45%)—indicating that *β*-H abstraction from more reactive Ti-amides can occur at rates competitive with 3-hexyne deprotonation.

Following the success of *N*-benzylaniline in the nitrene-coupled transfer hydrogenation reaction, we also investigated simple azobenzene hydrogenation[170,171] using **3.4** as a direct probe of the efficiency of transfer hydrogenation *via* solely *β*-H abstraction (Figure 3.4, eqn 5; see Figure 3.26 for full proposed mechanism). In this case, good yield (36%) of $PhNH_2$ **3.6** could be achieved upon prolonged heating, although the reaction was not as fast or efficient as those with 3-hexyne as a hydrogen source. Satisfyingly, the reactions in eqns 4 and 5 allowed observation of the dehydrogenated byproduct **3.5**: previously, *N*-methylformimine and 2,3,4-hexatriene were not detected, presumably due to their decomposition at elevated temperature.

Similar reactions catalyzed by other simple early transition metal amides, such as $Ti(NMe_2)_4$, $Zr(NMe_2)_4$, $V(NMe_2)_4$ and $Ta(NMe_2)_5$ (Table 3.1 and 3.2) were not as effective as

$TiCl_2(NMe_2)_2$, highlighting the sensitivity of this chemistry to the coordination environment and Lewis acidity of the metal.

3.4 Conclusion

In conclusion, we have discovered that Ti^{II} can be accessed from a simple Ti-diamide *via* *β*-H abstraction or alkyne deprotonation, and these elementary steps can be incorporated into a unique Ti-catalyzed nitrene-coupled transfer hydrogenation reaction. An isotope labeling study indicates that alkyne deprotonation appears more facile than *β*-H abstraction. Although these catalytic reactions are likely not of practical value, the strategy for accessing Ti^{II} synthons from low-cost and stable Ti-amide precursors will be of value to future endeavors in low-valent Ti catalysis,[8] surface organometallic chemistry of Ti,[172,173] and chemical vapor deposition of nitrogen-doped Ti thin films.[174,175]

3.5 Experimental

3.5.1 General Considerations

All air- and moisture-sensitive compounds were manipulated in a glovebox under nitrogen atmosphere. C_6H_5Br was dried over CaH_2 and distilled before passing through activated alumina and storing over activated 3 Å molecular sieves in the glovebox. C_6D_5Br was synthesized following a reported procedure[122] and passed through activated alumina before storing over activated 3 Å molecular sieves in the glovebox. $Ti(NMe_2)_4$[168,176] and $TiCl_2(NMe_2)_2$[177] were synthesized following reported procedures. 3-Hexyne, **3.4** and $TiCl_4$ were purchased from Millipore-Sigma. Azobenzene was purchased from TCI Chemicals and purified by hexane/water extraction three times. $Zr(NMe_2)_4$, $V(NMe_2)_4$, $Ta(NMe_2)_5$ were purchased from Strem Chemicals. 3-Hexyne-d_{10} was purchased from Cambridge Isotope Laboratories, Inc. ^1H, ^2H, and COSY were collected on a Bruker Avance III HD NanoBay 400 MHz spectrometer. ^1H NMR of catalytic reactions in C_6D_5Br were referenced to the proton signal of the internal standard 1,3,5-trimethoxybenzene (TMB, -OCH_3, s, 3.51 ppm). Mass spectra were collected on a Bruker BioTOF II ESI/TOF-MS spectrometer.

3.5.2 Cyclotrimerization of 3-Hexyne (Figure 3.2, eqn 1)

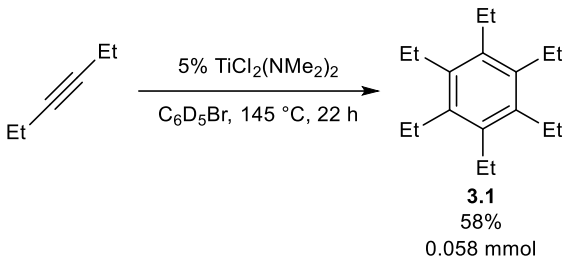

$TiCl_2(NMe_2)_2$ (3.1 mg, 0.015 mmol, 0.05 equiv), 3-hexyne (24.6 mg, 0.3 mmol, 1 equiv), 1,3,5-trimethoxybenzene (5.0 mg, 0.03 mmol, 0.1 equiv, internal standard) and 0.5 mL of C_6D_5Br were added to a J-Young NMR tube. The reaction mixture was then sealed and heated in a preheated oil bath at 145 ℃ for 22 h. ^1H NMR spectra were collected before and after heating to monitor the reaction.

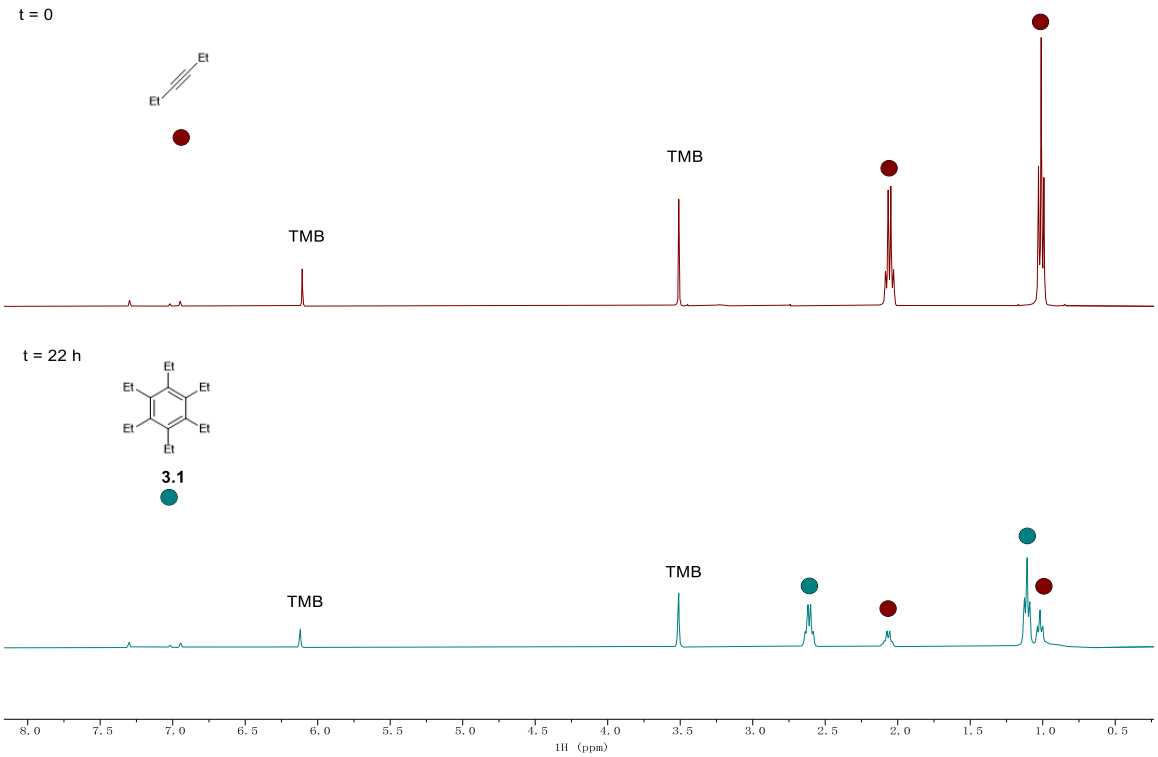

Figure 3.5. Stacked ^1H NMR spectra of $TiCl_2(NMe_2)_2$-catalyzed cyclotrimerization of 3-hexyne in C_6D_5Br. Top: t = 0. Bottom: t = 22 h. *Taken from (top) YC-2020-0055-0h-H and (bottom) YC-2020-0055-22h-H.*

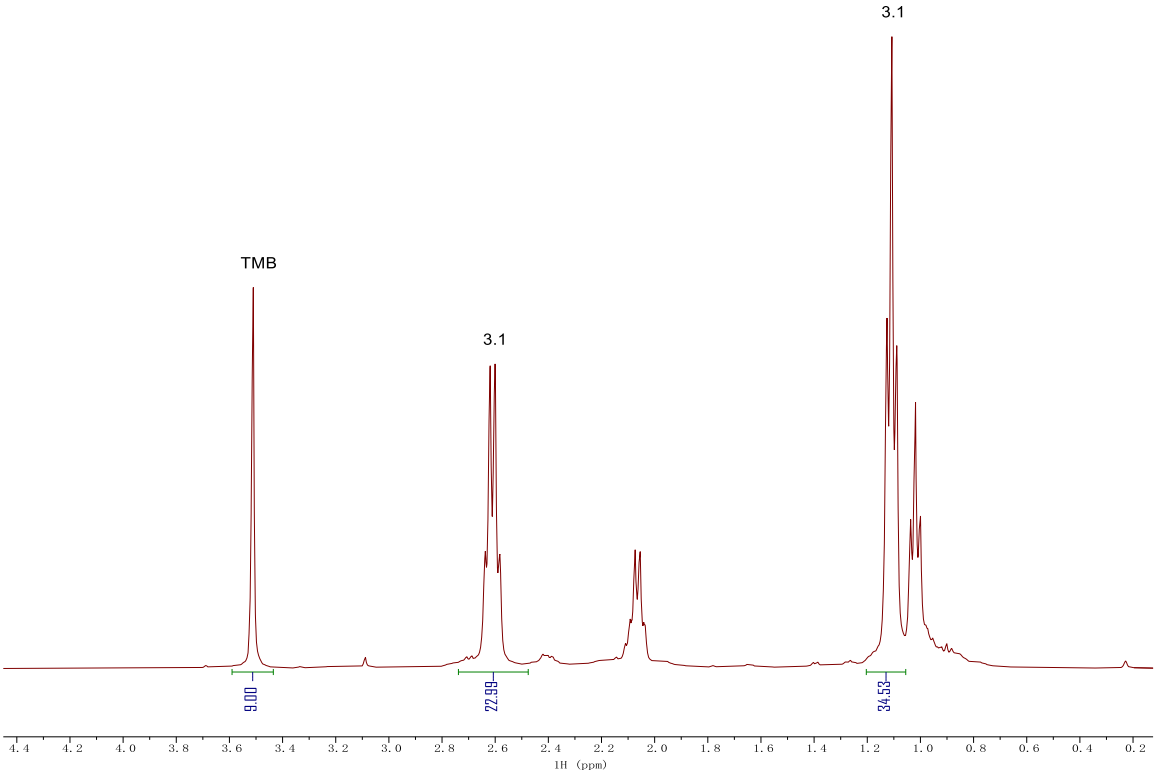

Figure 3.6. t = 22 h ^{1}H NMR spectrum of $TiCl_2(NMe_2)_2$-catalyzed cyclotrimerization of 3-hexyne in C_6D_5Br for yield calculation. *Taken from YC-2020-0055-22h-H.*

3.5.3 Hydroamination of 3-Hexyne with Azobenzene (Figure 3.2, eqn 2)

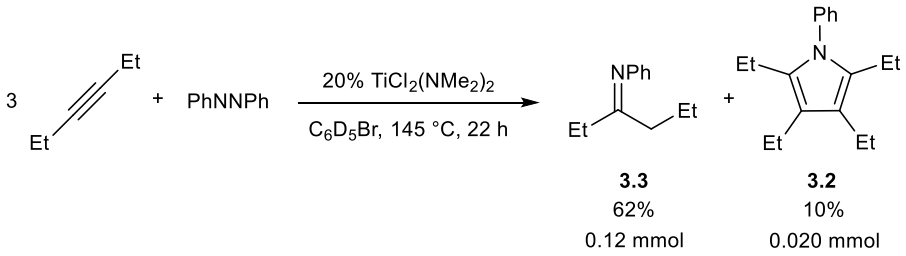

$TiCl_2(NMe_2)_2$ (4.1 mg, 0.020 mmol, 0.2 equiv), 3-hexyne (24.6 mg, 0.3 mmol, 3 equiv), azobenzene (18.2 mg, 0.1 mmol, 1 equiv), 1,3,5-trimethoxybenzene (5.0 mg, 0.03 mmol, 0.3 equiv, internal standard) and 0.5 mL of C_6D_5Br were added to a J-Young NMR tube. The reaction mixture was then sealed and heated in a preheated oil bath at 145 ℃ for 22 h. ^{1}H NMR spectra were collected before and after heating to monitor the reaction.

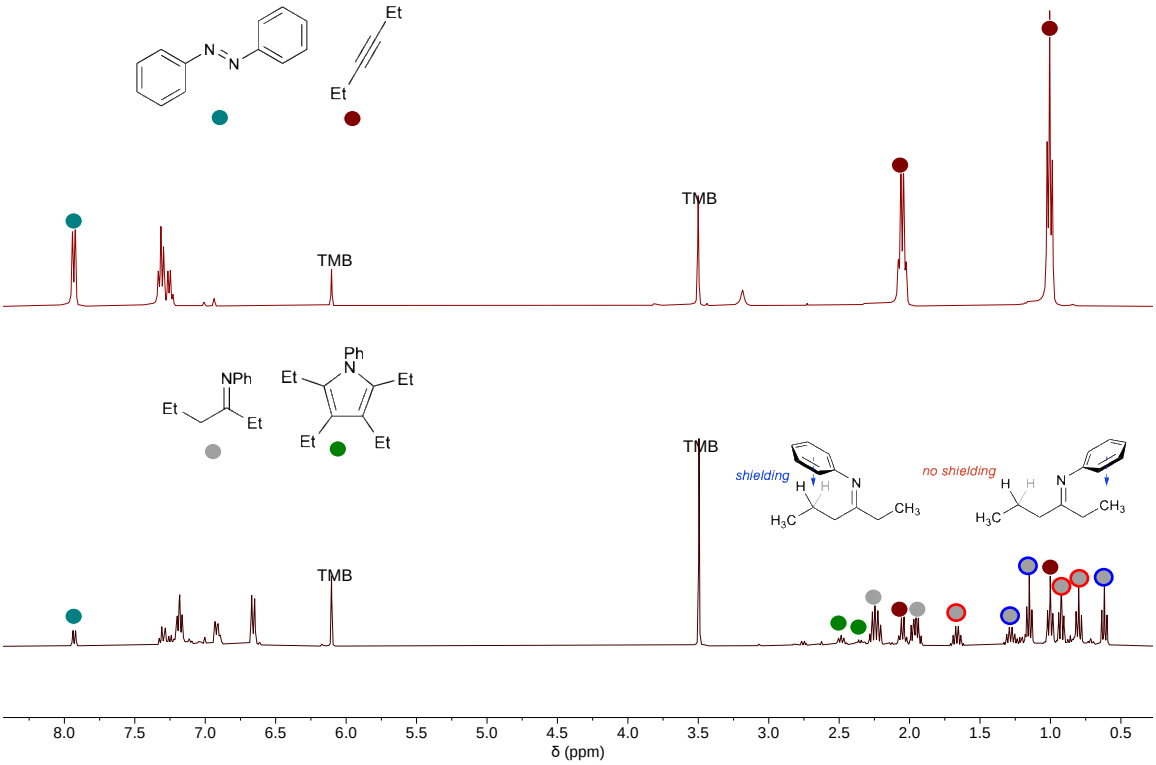

Figure 3.7. Stacked ^{1}H NMR spectra of $TiCl_2(NMe_2)_2$-catalyzed hydroamination of 3-hexyne with azobenzene in C_6D_5Br. Top: t = 0. Bottom: t = 22 h. **3.3** is a mixture of E/Z isomers (grey with blue outline = Z isomer; grey with red outline = E isomer). *Taken from (top) YC-2020-0041-0h-H and (bottom) YC-2020-0041-22h-H.*

Peak assignments can be referred to Figure 3.19 for ^{1}H-^{1}H COSY NMR of **3.3**.

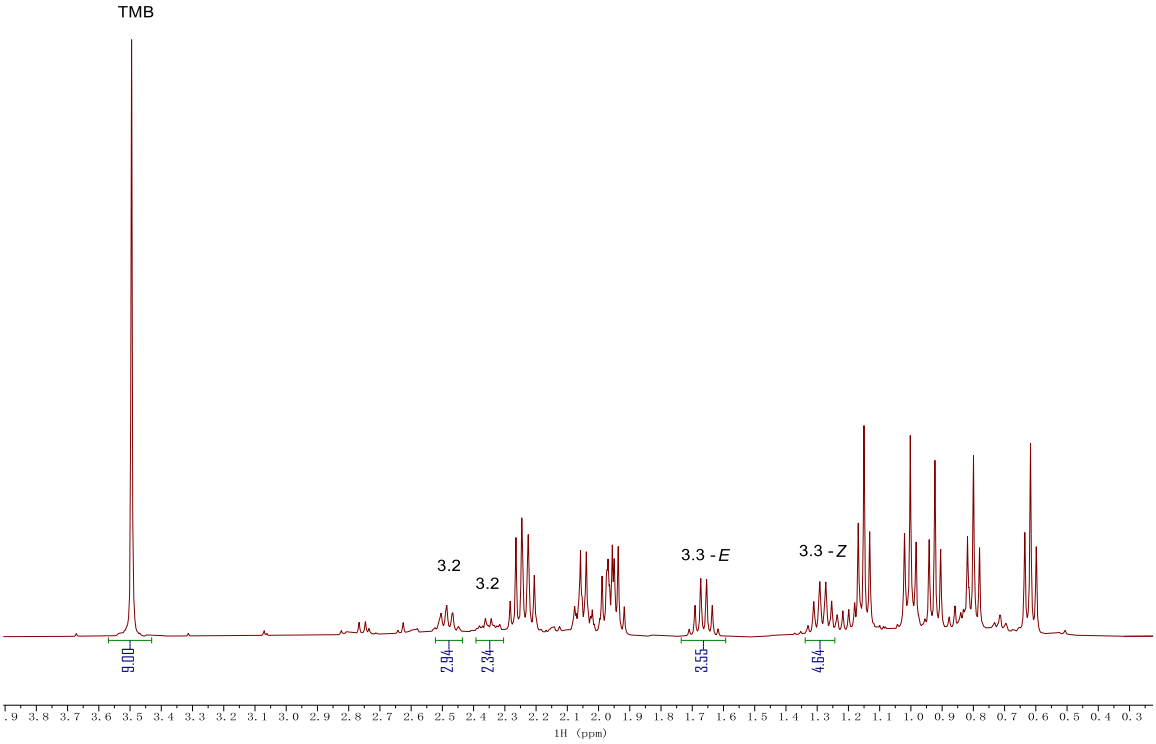

Figure 3.8. t = 22 h ^{1}H NMR spectrum of $TiCl_2(NMe_2)_2$-catalyzed hydroamination of 3-hexyne with azobenzene in C_6D_5Br for yield calculation. **3.3** is a mixture of E/Z isomers. *Taken from YC-2020-0041-22h-H.*

Example yield calculation:

TMB: $\frac{5mg}{168.19mg/mmol} = 0.0297\ mmol\ TMB \approx 0.03\ mmol\ TMB$

Imine (**3.3**):

At δ = 1.66 ppm (E isomer): $\frac{3.55\ integration}{2H} = 1.78\frac{int}{H}$

$$1.78\frac{int}{H} * 0.03\ mmol\ TMB = 0.0533\ mmol\ imine\ for\ E\ isomer$$

At δ = 1.28 ppm (Z isomer): $\frac{4.64\ integration}{2\ H} = 2.32\frac{int}{H}$

$$2.32\frac{int}{H} * 0.03\ mmol\ TMB = 0.0696\ mmol\ imine\ for\ Z\ isomer$$

$$\sum(E\ and\ Z\ isomers) = 0.1229\ mmol\ imine$$

$$\frac{0.1229\ mmol\ imine}{0.2\ mmol\ nitrene} = 62\%\ yield\ of\ the\ sum\ of\ both\ isomers$$

3.5.4 Isotope Labeling Study with 3-Hexyne-d_{10} (Figure 3.2, eqn 3)

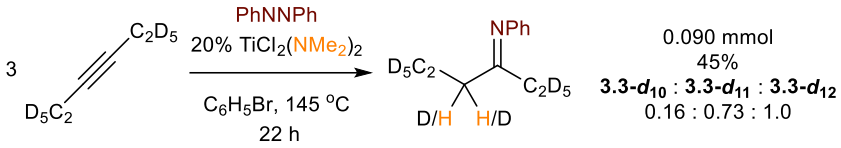

$TiCl_2(NMe_2)_2$ (4.1 mg, 0.020 mmol, 0.2 equiv), 3-hexyne-d_{10} (27.7 mg, 0.3 mmol, 3 equiv), azobenzene (18.2 mg, 0.1 mmol, 1 equiv), 1,3,5-trimethoxybenzene (5.0 mg, 0.03 mmol, 0.3 equiv, ^{1}H NMR internal standard), C_6D_6 (2.5 µL, 0.028 mmol, 0.28 equiv, ^{2}H NMR internal standard) and 0.5 mL of C_6H_5Br were added to a J-Young NMR tube. The reaction mixture was then sealed and heated in a preheated oil bath at 145 ℃ for 22 h. ^{1}H and ^{2}H NMR spectra were collected before and after heating to monitor the reaction. The reaction mixture was then poured into 5 mL of benchtop DCM, filtered. The resulting mixture containing three isotopic product isomers was characterized by ESI-MS.

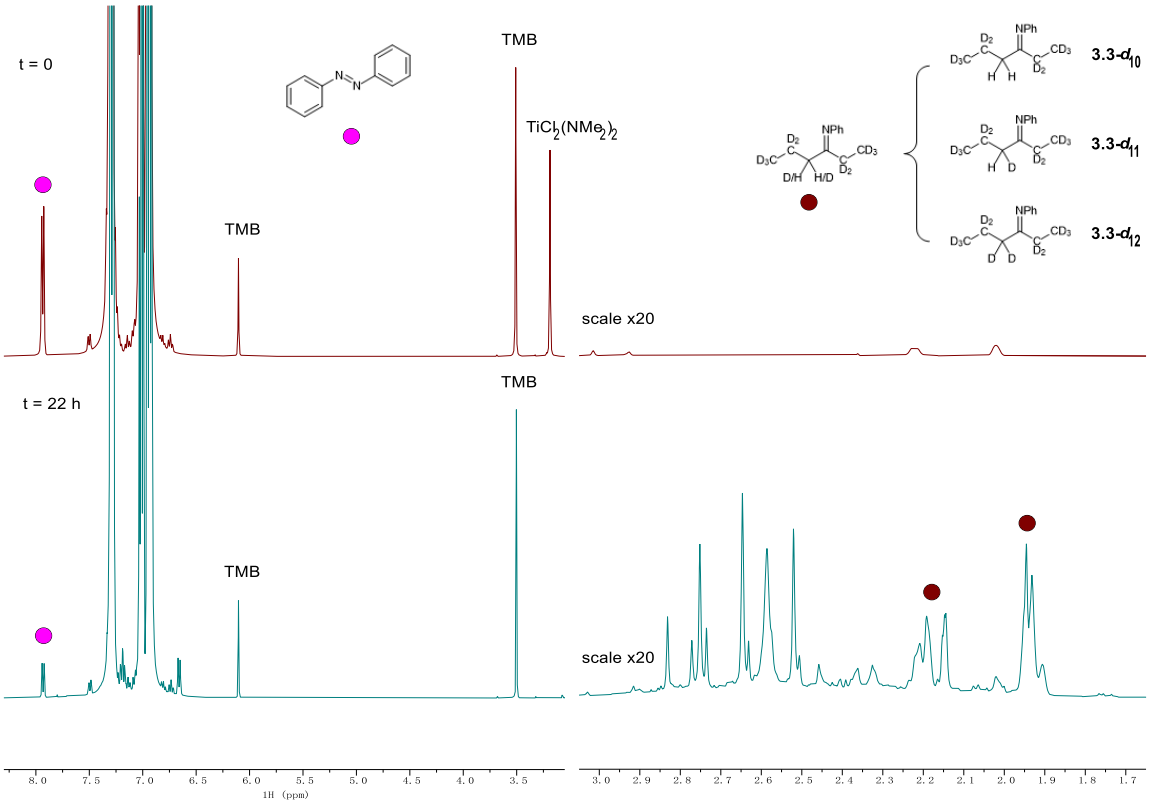

Figure 3.9. Stacked ^{1}H NMR spectra of $TiCl_2(NMe_2)_2$-catalyzed hydroamination of 3-hexyne-d_{10} with azobenzene in C_6H_5Br. Top: t = 0. Bottom: t = 22 h. **3.3-*d*$_{10}$**, **3.3-*d*$_{11}$** and **3.3-*d*$_{12}$** are mixture of E/Z isomers. *Taken from (top) YC-2020-0058-NoD-PhBr-0h-H and (bottom) YC-2020-0058-NoD-PhBr-22h-H.*

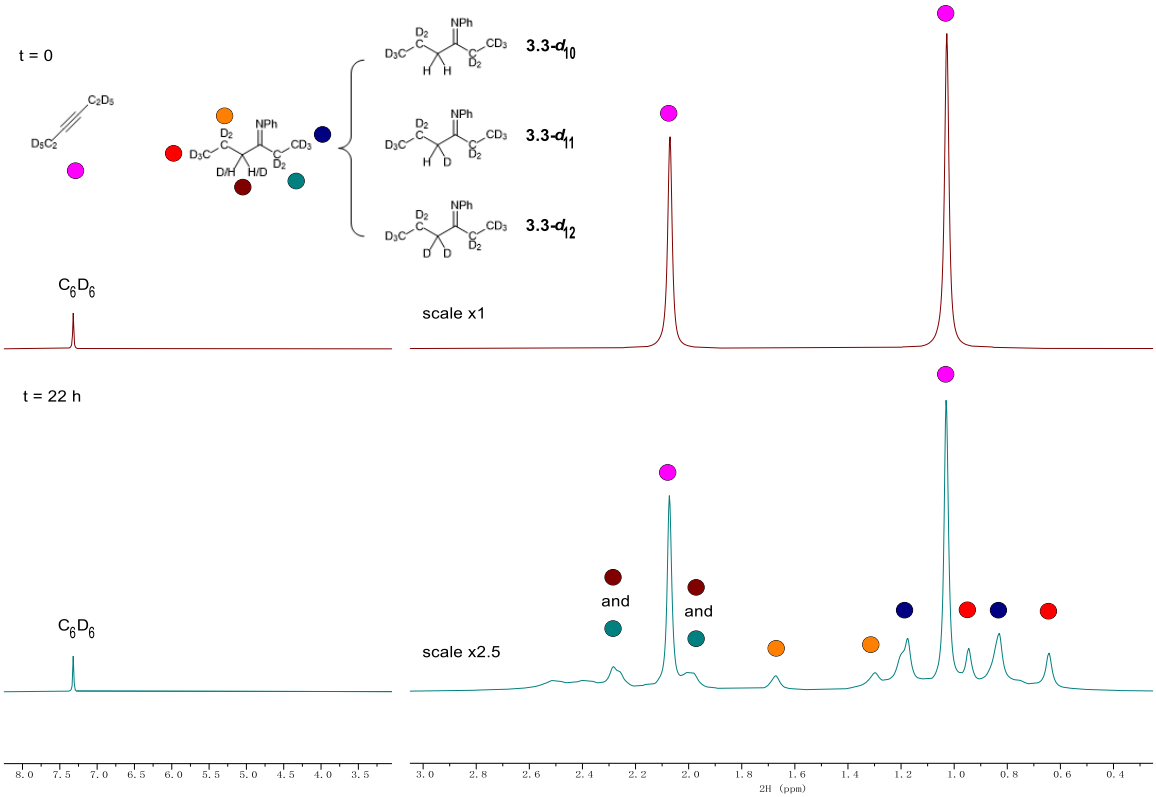

Figure 3.10. Stacked ^{2}H NMR spectra of $TiCl_2(NMe_2)_2$-catalyzed hydroamination of 3-hexyne-d_{10} with azobenzene in C_6H_5Br. Top: t = 0. Bottom: t = 22 h. **3.3-*d*$_{10}$**, **3.3-*d*$_{11}$** and **3.3-*d*$_{12}$** are mixture of E/Z isomers. *Taken from (top) YC-2020-0058-NoD-PhBr-0h-D and (bottom) YC-2020-0058-NoD-PhBr-22h-D.*

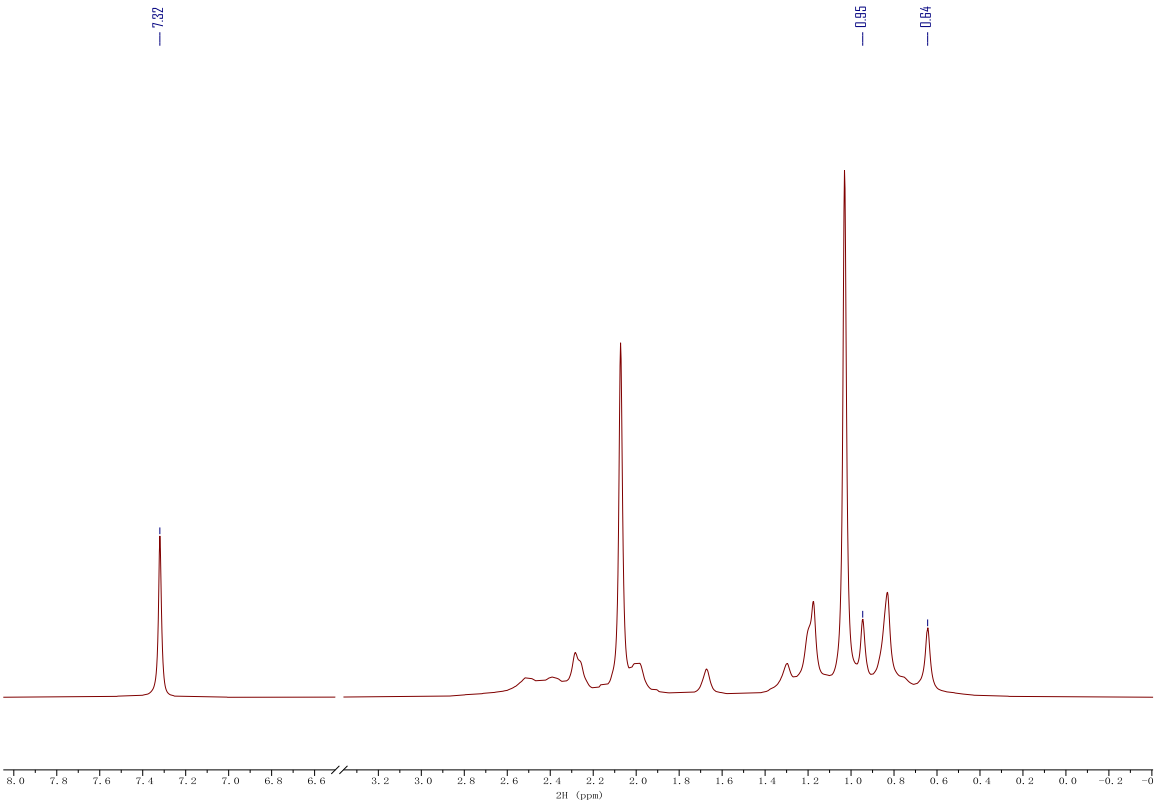

	δ (ppm)	Assignment	# of H	Peak Area	Amount (mmol)	Yield (%)
C_6D_6	7.32	Ar-D	6	5590.7	0.028	n.a.
3.3-*d*$_{10}$, 3.3-*d*$_{11}$, 3.3-*d*$_{12}$	0.95, 0.64	Imine γ-CD_3	3	8999.7	0.090	45

Figure 3.11. t = 22 h ^{2}H NMR spectrum of $TiCl_2(NMe_2)_2$-catalyzed hydroamination of 3-hexyne-*d*$_{10}$ with azobenzene in C_6H_5Br for yield calculation. The peak area of selected ^{2}H NMR peaks were calculated by Gaussian-Lorentzian fitting to omit the influence from baseline overlapping.[138] *Taken from YC-2020-0058-NoD-PhBr-22h-D.*

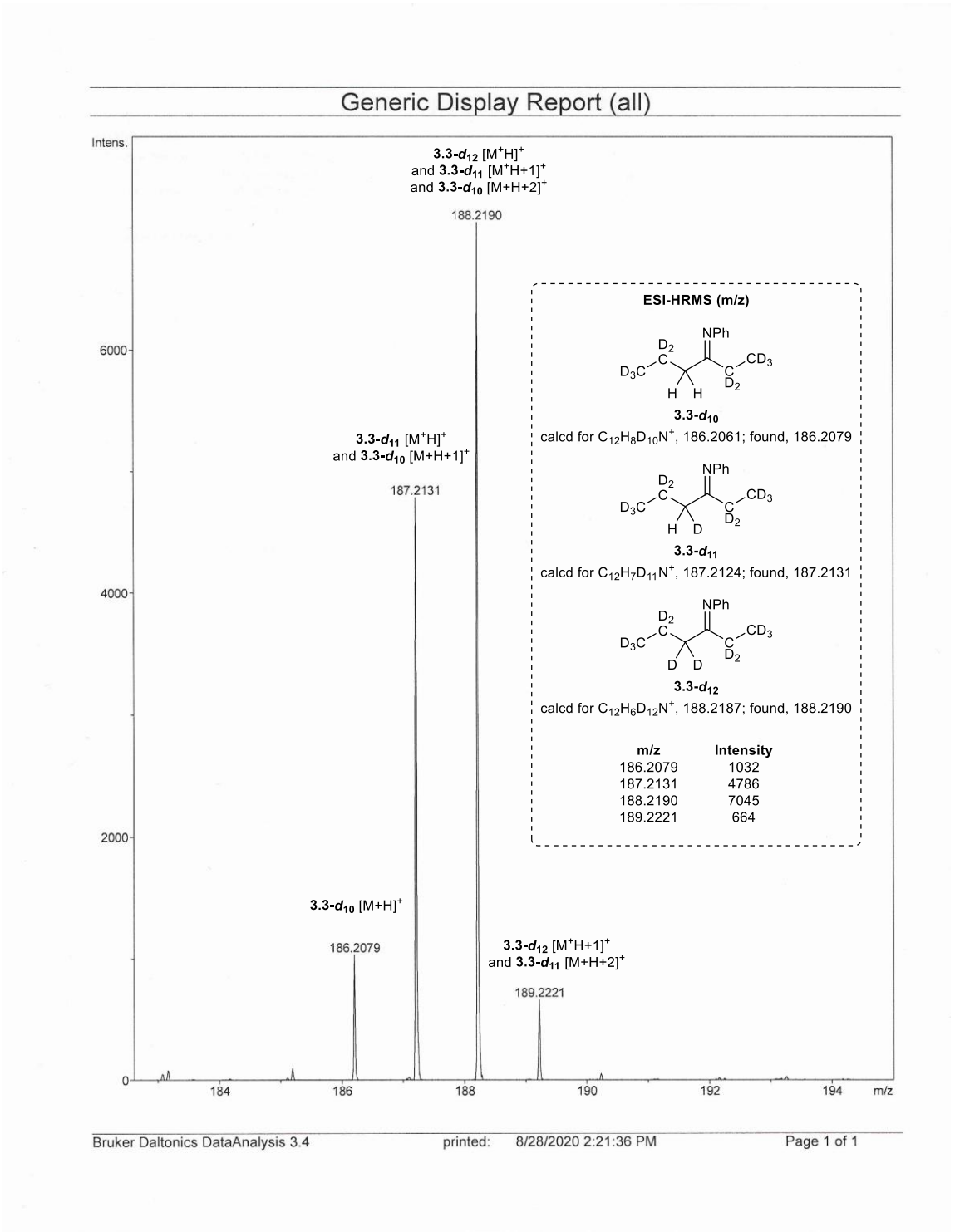

Figure 3.12. HR-ESI mass spectrum of the product mixture of $TiCl_2(NMe_2)_2$-catalyzed hydroamination of 3-hexyne-d_{10} with azobenzene. *Taken from YC0619200058highres300.*

Product ratio calculation based on ESI-MS:

Ratio of $[M+H]^+$:$[M+H+1]^+$:$[M+H+2]^+$ can be calculated based on natural element abundance.[178] $[M+H+3]^+$ was considered to be negligible in contribution.

Example: **3.3-*d*$_{10}$** ($C_{12}H_7D_{10}N$)

$[M+H]^+$ ratio = ratio of $C_{12}H_7D_{10}N$ = 1

$[M+H+1]^+$ ratio = ratio of $C_{11}{}^{13}CH_7D_{10}N$ + ratio of $C_{12}H_7D_{10}{}^{15}N$ = 0.133 + 0.004 = 0.137

$[M+H+2]^+$ ratio = ratio of $C_{10}{}^{13}C_2H_7D_{10}N$ and ratio of $C_{11}{}^{13}CH_7D_{10}{}^{15}N$ = 0.016 + 0.001 = 0.017

List of isotopic peak ratio of the compounds:

Compound	Formula	$[M+H]^+$	$[M+H+1]^+$	$[M+H+2]^+$
3.3-*d*$_{10}$	$C_{12}H_7D_{10}N$	1.00	0.137	0.017
3.3-*d*$_{11}$	$C_{12}H_6D_{11}N$	1.00	0.137	0.017
3.3-*d*$_{12}$	$C_{12}H_5D_{12}N$	1.00	0.137	0.017

Mass list

m/z	Assignment	Amount	Intensity
186.2079	**3.3-*d*$_{10}$** $[M+H]^+$	[**3.3-*d*$_{10}$**]	1032
187.2131	**3.3-*d*$_{11}$** $[M+H]^+$ and **3.3-*d*$_{10}$** $[M+H+1]^+$	[**3.3-*d*$_{11}$**] + 0.137 [**3.3-*d*$_{10}$**]	4786
188.2190	**3.3-*d*$_{12}$** $[M+H]^+$ and **3.3-*d*$_{11}$** $[M+H+1]^+$ and **3.3-*d*$_{10}$** $[M+H+2]^+$	[**3.3-*d*$_{12}$**] + 0.137 [**3.3-*d*$_{11}$**] + 0.017 [**3.3-*d*$_{10}$**]	7045

The ratio can thus be calculated as [**3.3-*d*$_{10}$**] : [**3.3-*d*$_{11}$**] : [**3.3-*d*$_{12}$**] = 0.16 : 0.73 : 1.0

3.5.5 Isotope Labeling Study with 3-Hexyne-*d*$_{10}$ and 10% Catalyst Loading

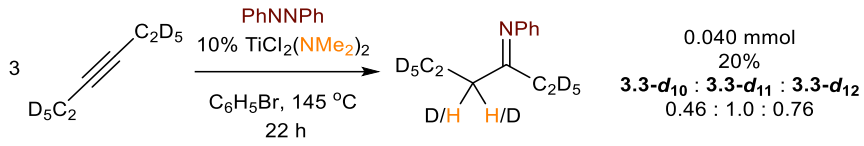

$TiCl_2(NMe_2)_2$ (2.1 mg, 0.010 mmol, 0.1 equiv), 3-hexyne-d_{10} (27.7 mg, 0.3 mmol, 3 equiv), azobenzene (18.2 mg, 0.1 mmol, 1 equiv), 1,3,5-trimethoxybenzene (5.0 mg, 0.03 mmol, 0.3 equiv, ^{1}H NMR internal standard), C_6D_6 (2.5 μL, 0.028 mmol, 0.28 equiv, ^{2}H NMR internal standard) and 0.5 mL of C_6H_5Br were added to a J-Young NMR tube. The reaction mixture was then sealed and heated in a preheated oil bath at 145 ℃ for 22 h. ^{1}H and ^{2}H NMR spectra were collected before and after heating to monitor the reaction. The reaction mixture was then poured into 5 mL of benchtop DCM, filtered. The resulting mixture containing three isotopic product isomers was characterized by ESI-MS.

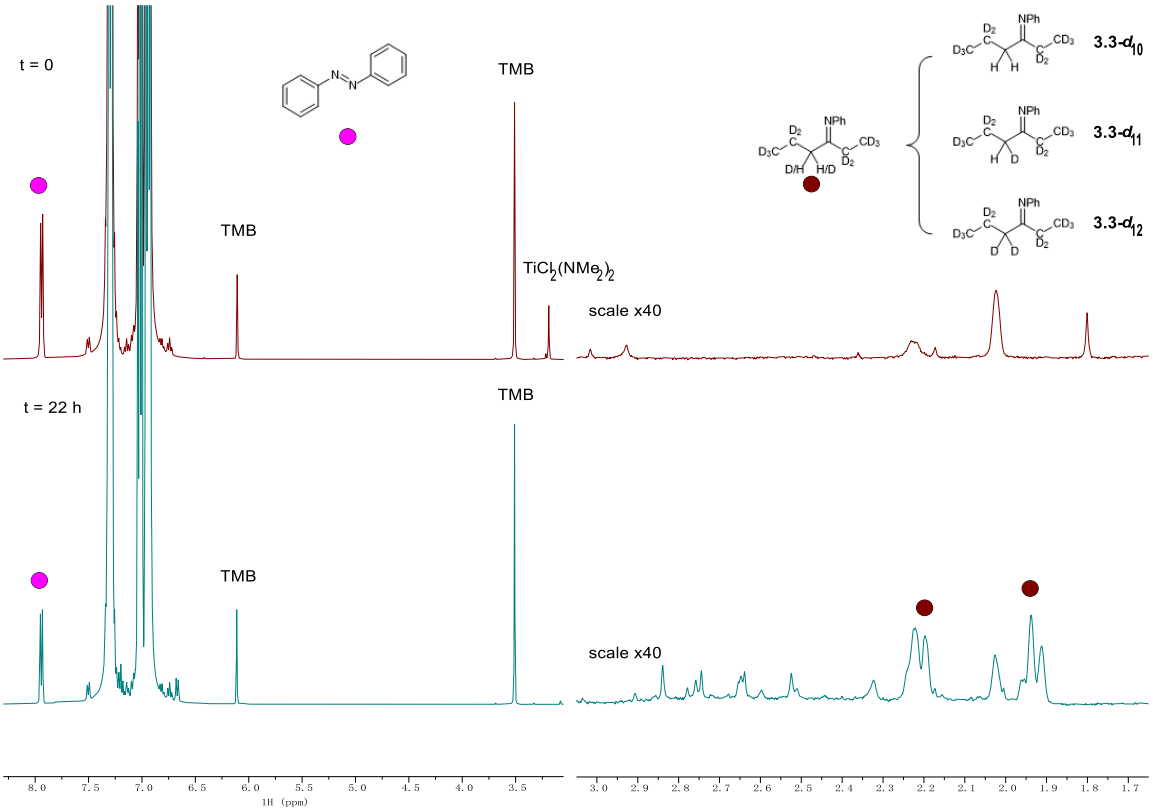

Figure 3.13. Stacked ^{1}H NMR spectra of 10% $TiCl_2(NMe_2)_2$-catalyzed hydroamination of 3-hexyne-d_{10} with azobenzene in C_6H_5Br. Top: t = 0. Bottom: t = 22 h. **3.3-*d*$_{10}$**, **3.3-*d*$_{11}$** and **3.3-*d*$_{12}$** are mixture of E/Z isomers. *Taken from (top) YC-2020-0110-NoD-PhBr-0h-H and (bottom) YC-2020-0110-NoD-PhBr-22h-H.*

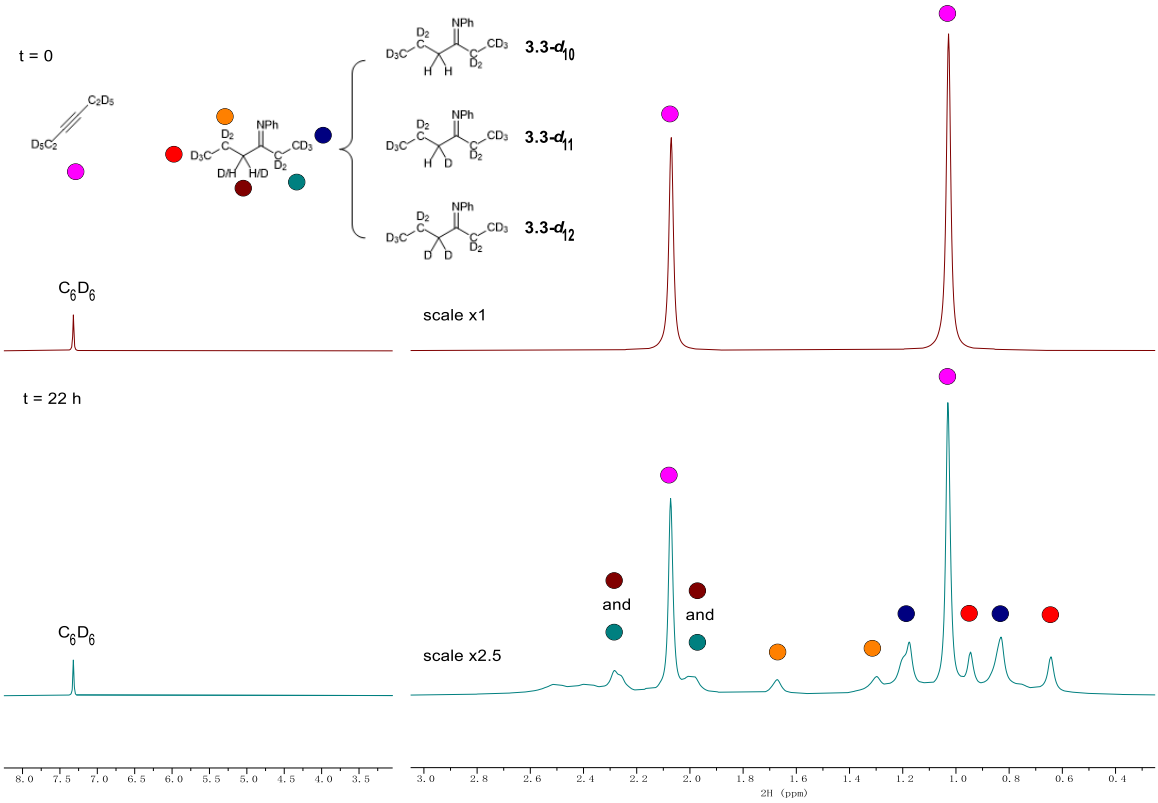

Figure 3.14. Stacked ^{2}H NMR spectra of 10% $TiCl_2(NMe_2)_2$-catalyzed hydroamination of 3-hexyne-d_{10} with azobenzene in C_6H_5Br. Top: t = 0. Bottom: t = 22 h. **3.3-d_{10}**, **3.3-d_{11}** and **3.3-d_{12}** are mixture of E/Z isomers. *Taken from (top) YC-2020-0110-NoD-PhBr-0h-D and (bottom) YC-2020-0110-NoD-PhBr-22h-D.*

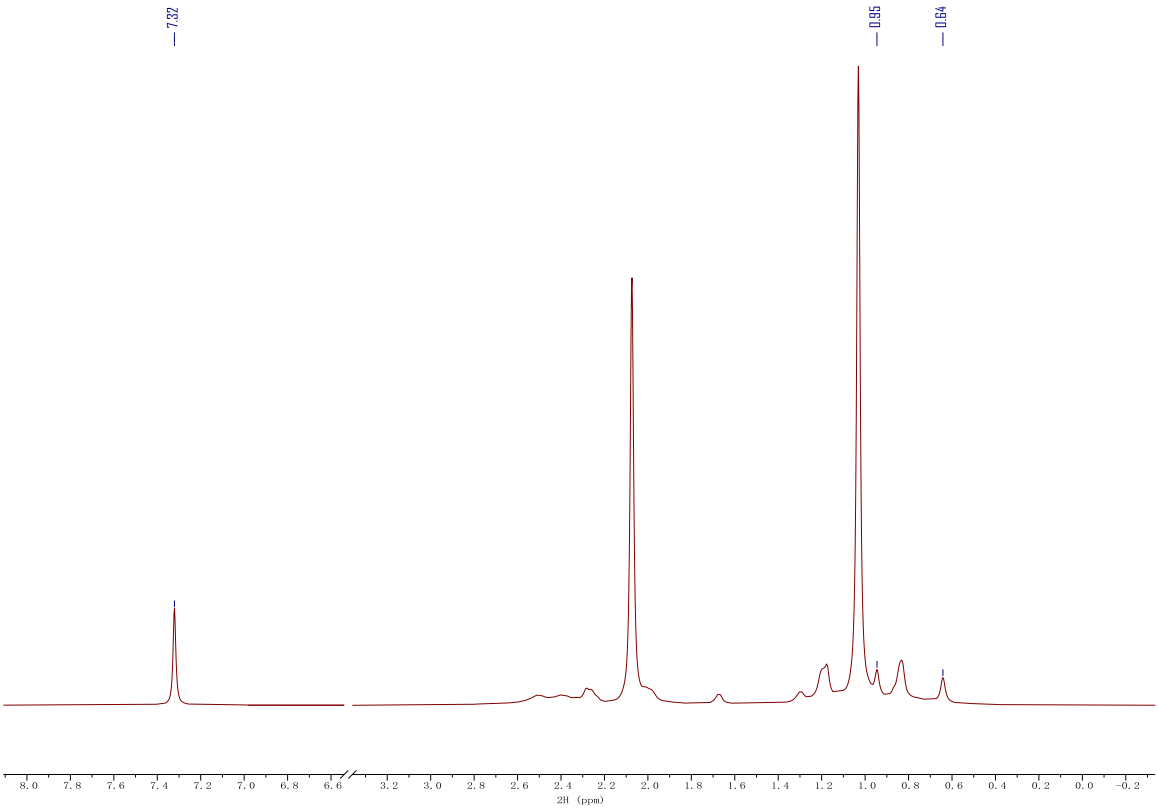

	δ (ppm)	Assignment	# of H	Peak Area	Amount (mmol)	Yield (%)
C_6D_6	7.32	Ar-D	6	4919.5	0.028	n.a.
3.3-*d*$_{10}$, 3.3-*d*$_{11}$, 3.3-*d*$_{12}$	0.95, 0.64	Imine γ-CD_3	3	3543.7	0.040	20

Figure 3.15. t = 22 h ^{2}H NMR spectrum of 10% $TiCl_2(NMe_2)_2$-catalyzed hydroamination of 3-hexyne-*d*$_{10}$ with azobenzene in C_6H_5Br for yield calculation. The peak area of selected ^{2}H NMR peaks were calculated by Gaussian-Lorentzian fitting to omit the influence from baseline overlapping.[138] *Taken from YC-2020-0110-NoD-PhBr-22h-D.*

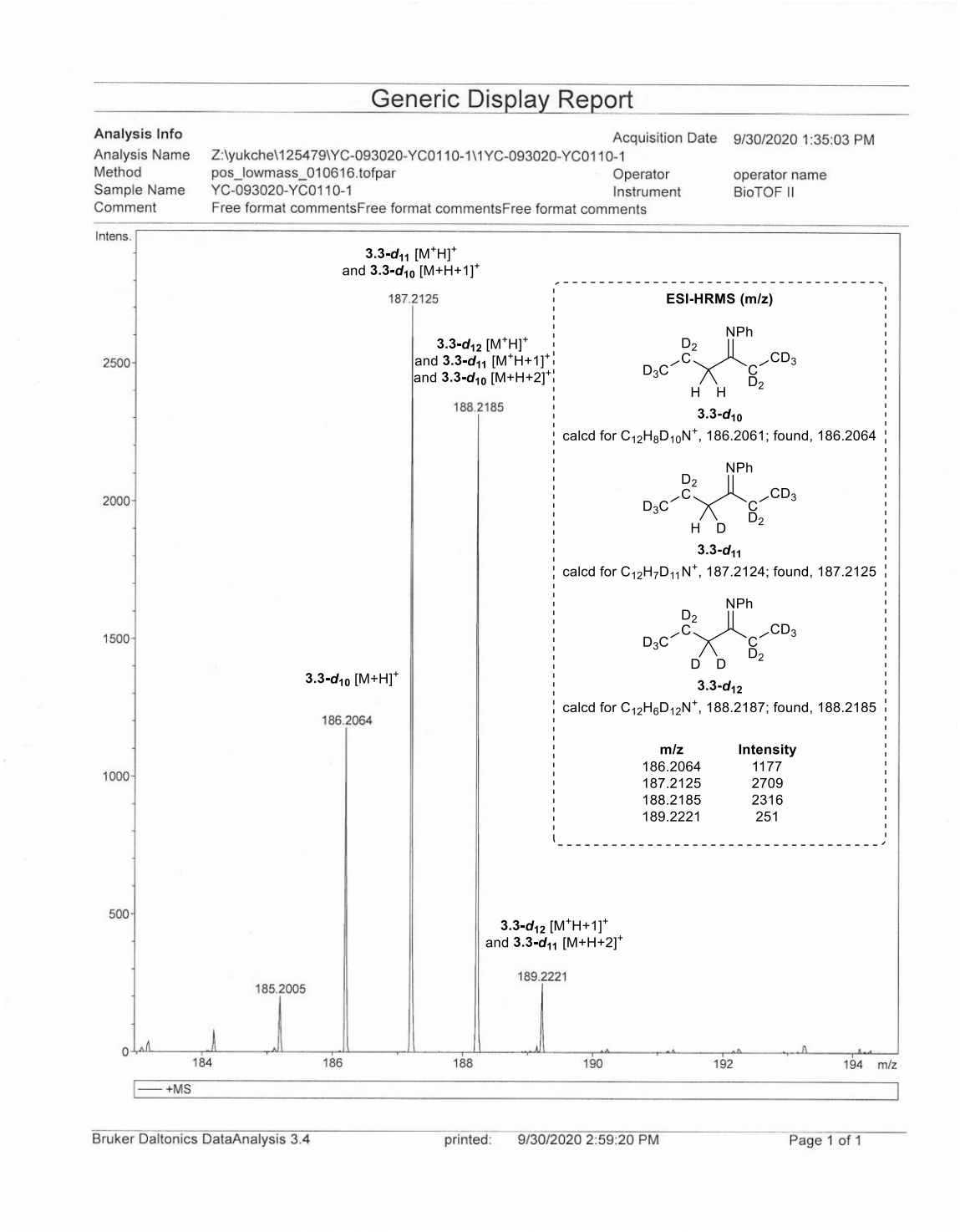

Figure 3.16. HR-ESI mass spectrum of the product mixture of 10% $TiCl_2(NMe_2)_2$-catalyzed hydroamination of 3-hexyne-d_{10} with azobenzene. *Taken from YC-093020-YC0110-1.*

Product ratio calculation based on ESI-MS:

The product ratio was determined using the same method as for eqn 3.

Mass list

m/z	Assignment	Amount	Intensity
186.2064	**3.3-*d*$_{10}$** $[M+H]^+$	[**3.3-*d*$_{10}$**]	1177
187.2125	**3.3-*d*$_{11}$** $[M+H]^+$ and **3.3-*d*$_{10}$** $[M+H+1]^+$	[**3.3-*d*$_{11}$**] + 0.137 [**3.3-*d*$_{10}$**]	2709
188.2185	**3.3-*d*$_{12}$** $[M+H]^+$ and **3.3-*d*$_{11}$** $[M+H+1]^+$ and **3.3-*d*$_{10}$** $[M+H+2]^+$	[**3.3-*d*$_{12}$**] + 0.137 [**3.3-*d*$_{11}$**] + 0.017 [**3.3-*d*$_{10}$**]	2316

The ratio can thus be calculated as [**3.3-*d*$_{10}$**] : [**3.3-*d*$_{11}$**] : [**3.3-*d*$_{12}$**] = 0.46 : 1.0 : 0.76

3.5.6 Hydroamination of 3-Hexyne with Azobenzene and 3.4 (Figure 3.4, eqn 4)

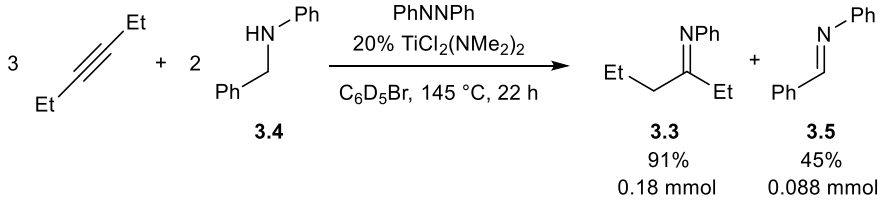

$TiCl_2(NMe_2)_2$ (4.1 mg, 0.020 mmol, 0.2 equiv), 3-hexyne (24.6 mg, 0.3 mmol, 3 equiv), azobenzene (18.2 mg, 0.1 mmol, 1 equiv), N-benzylaniline (36.7 mg, 0.2 mmol, 2 equiv), 1,3,5-trimethoxybenzene (5.0 mg, 0.03 mmol, 0.3 equiv, internal standard) and 0.5 mL of C_6D_5Br were added to a J-Young NMR tube. The reaction mixture was then sealed and heated in a preheated oil bath at 145 ℃ for 22 h. ^1H NMR spectra were collected before and after heating to monitor the reaction.

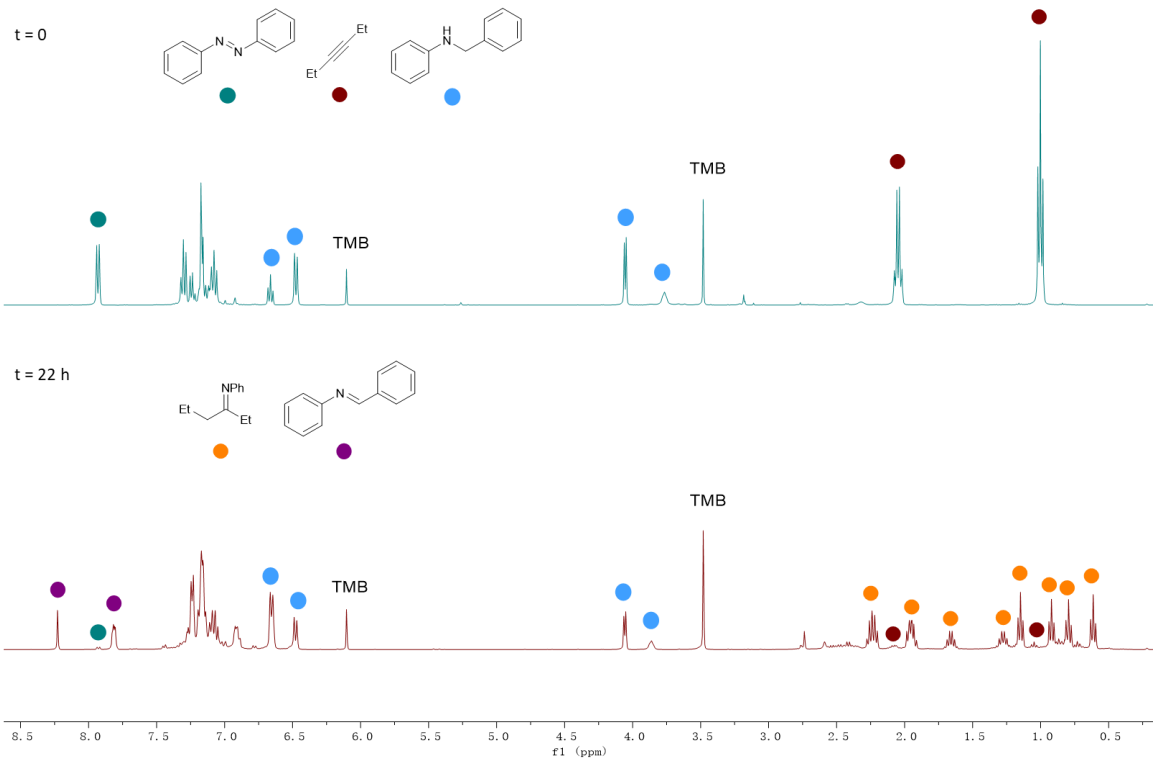

Figure 3.17. Stacked ^{1}H NMR spectra of $TiCl_2(NMe_2)_2$-catalyzed hydroamination of 3-hexyne with azobenzene and *N*-benzylaniline (**3.4**) in C_6D_5Br. Top: t = 0. Bottom: t = 1 h. **3.3** is a mixture of E/Z isomers. *Taken from (top) YC-2020-0056-0h-H and (bottom) YC-2020-0056-22h-H.*

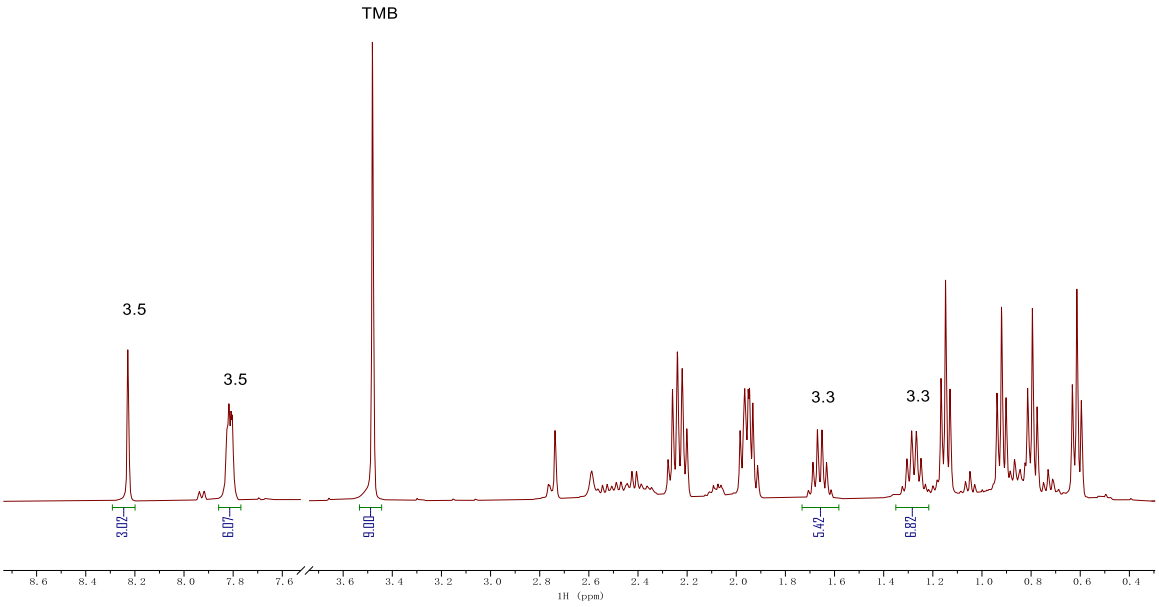

Figure 3.18. t = 22 h ^{1}H NMR spectrum of $TiCl_2(NMe_2)_2$-catalyzed hydroamination of 3-hexyne with azobenzene and *N*-benzylaniline (**3.4**) in C_6D_5Br for yield calculation. **3.3** is a mixture of E/Z isomers. *Taken from YC-2020-0056-22h-H.*

Example yield calculation:

TMB: $\frac{5mg}{168.19mg/mmol} = 0.0297\ mmol\ TMB \approx 0.03\ mmol\ TMB$

Imine (**3.3**):

At δ = 1.68 ppm (E isomer): $\frac{5.42\ integration}{2H} = 2.71\frac{int}{H}$

$$2.71\frac{int}{H} * 0.03\ mmol\ TMB = 0.0813\ mmol\ imine\ for\ E\ isomer$$

At δ = 1.28 ppm (Z isomer): $\frac{6.82\ integration}{2\ H} = 3.41\frac{int}{H}$

$$3.41\frac{int}{H} * 0.03\ mmol\ TMB = 0.1023\ mmol\ imine\ for\ Z\ isomer$$

$$\sum(E\ and\ Z\ isomers) = 0.1836\ mmol\ imine$$

$$\frac{0.1836\ mmol\ imine}{0.2\ mmol\ nitrene} = 91\%\ yield\ of\ the\ sum\ of\ both\ isomers$$

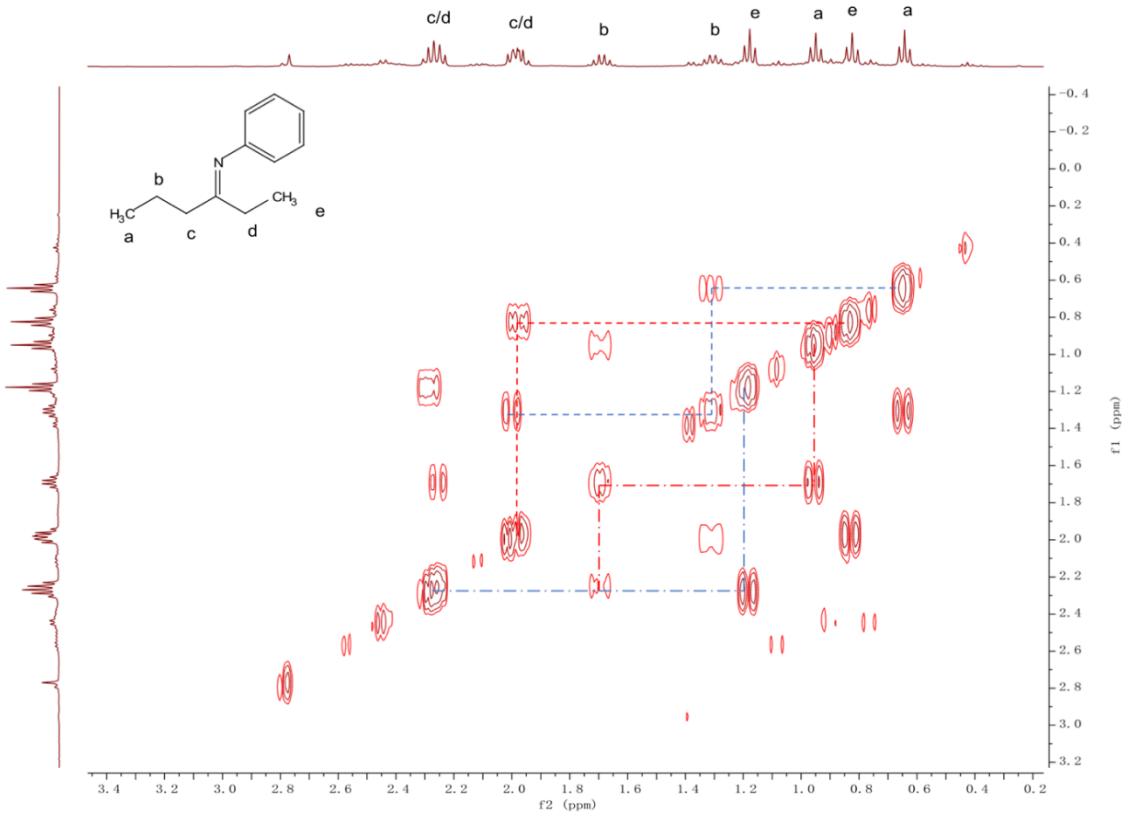

Figure 3.19. t = 22 h ^{1}H-^{1}H COSY NMR spectra of $TiCl_2(NMe_2)_2$-catalyzed hydroamination of 3-hexyne with azobenzene and N-benzylaniline (**3.4**) in C_6D_5Br for isomer proton assignments of N-phenylhexan-3-imine. *Taken from YC-2020-0056-COSY.*

3.5.7 Transfer Hydrogenation of 3.4 to Azobenzene (Figure 3.4, eqn 5)

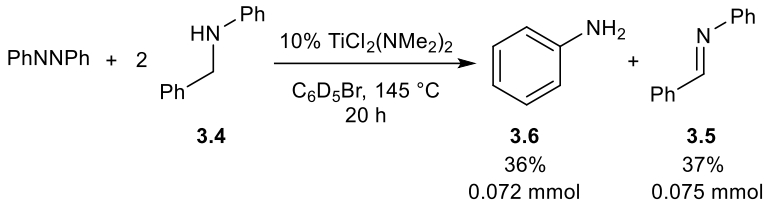

$TiCl_2(NMe_2)_2$ (2.2 mg, 0.011 mmol, 0.1 equiv), azobenzene (18.7 mg, 0.103 mmol, 1 equiv), *N*-benzylaniline (37.0 mg, 0.202 mmol, 1.96 equiv), 1,3,5-trimethoxybenzene (2.3 mg, 0.014 mmol, 0.13 equiv, internal standard) and 0.5 mL of C_6D_5Br were added to an NMR tube. The reaction mixture was then sealed and heated in a preheated oil bath at 145 °C for 20 h. ^1H NMR spectra were collected before and after heating to monitor the reaction.

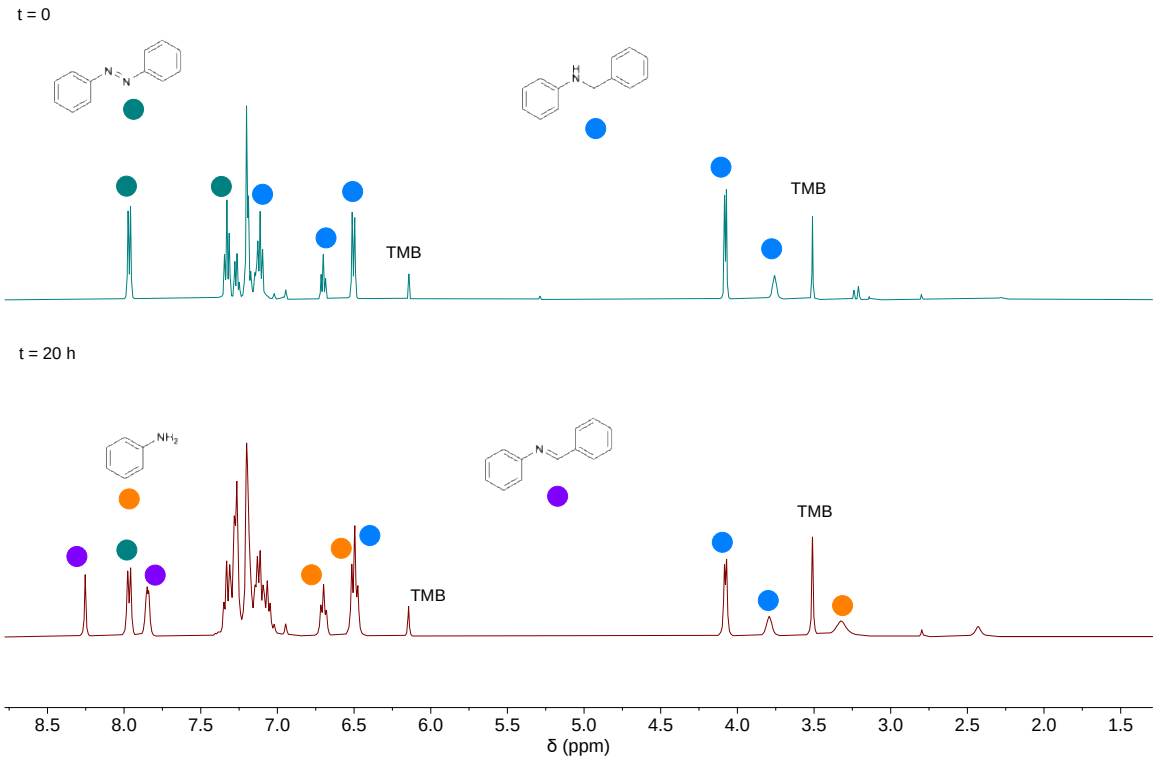

Figure 3.20. Stacked ^1H NMR spectra of $TiCl_2(NMe_2)_2$-catalyzed transfer hydrogenation of **3.4** to azobenzene in C_6D_5Br. Top: t = 0. Bottom: t = 20 h. *Taken from (top) RJD-2019-0028-1H and (bottom) RJD-2019-0028-2H.*

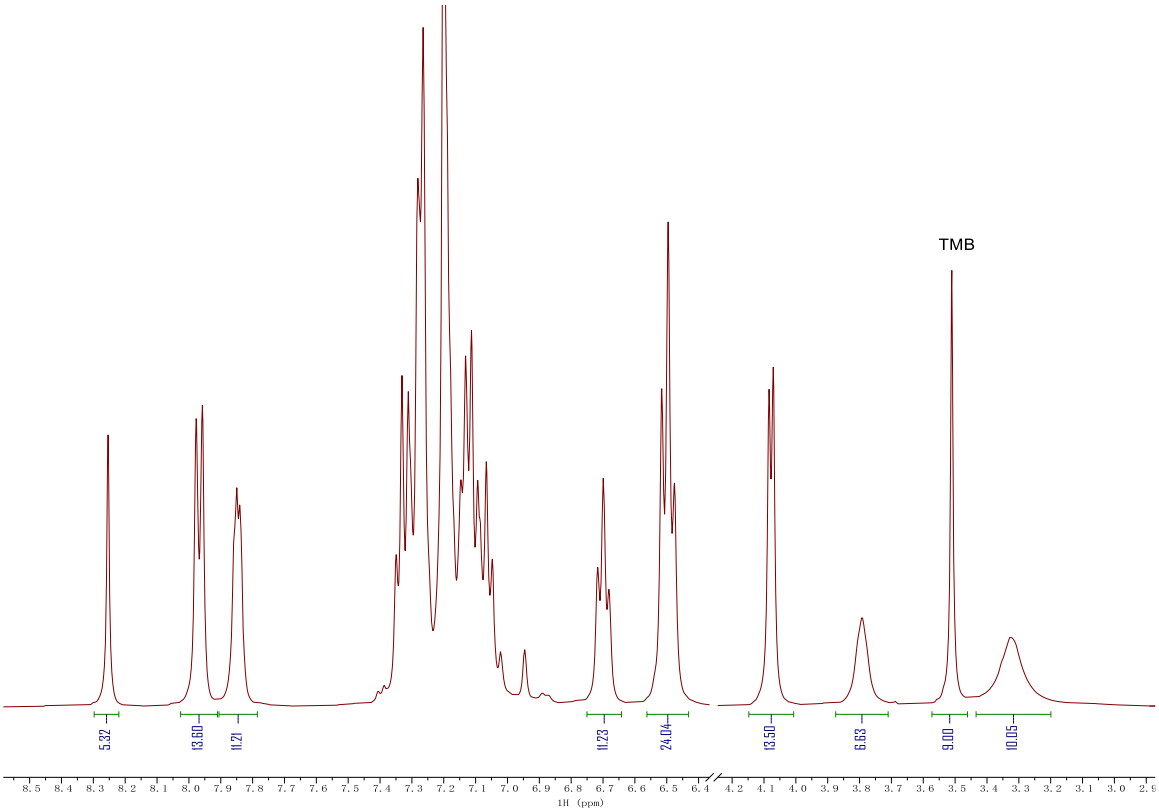

Figure 3.21. ^{1}H NMR spectrum of $TiCl_2(NMe_2)_2$-catalyzed transfer hydrogenation of **3.4** to azobenzene in C_6D_5Br for yield calculation. *Taken from RJD-2019-0028-2H.*

3.5.8 Transfer Hydrogenation of $TiCl_2(NMe_2)_2$ to Azobenzene

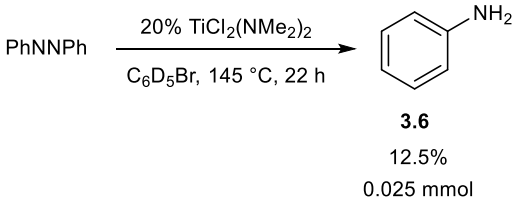

$TiCl_2(NMe_2)_2$ (4.1 mg, 0.020 mmol, 0.2 equiv), azobenzene (18.2 mg, 0.1 mmol, 1 equiv), 1,3,5-trimethoxybenzene (5.0 mg, 0.03 mmol, 0.3 equiv, internal standard) and 0.5 mL of C_6D_5Br were added to a J-Young NMR tube. The reaction mixture was then sealed and heated in a preheated oil bath at 145 ℃ for 22 h. ^{1}H NMR spectra were collected before and after heating to monitor the reaction.

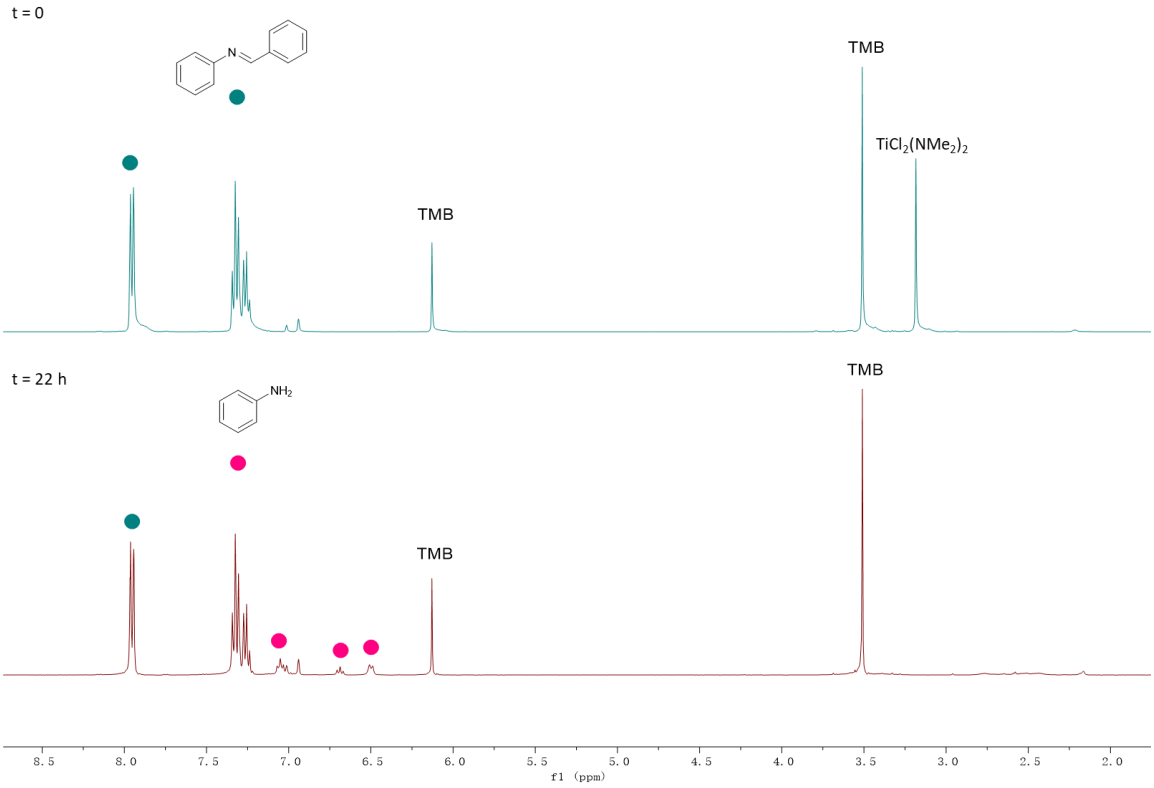

Figure 3.22. Stacked ^{1}H NMR spectra of $TiCl_2(NMe_2)_2$-catalyzed transfer hydrogenation of azobenzene in C_6D_5Br. Top: t = 0. Bottom: t = 22 h. *Taken from (top) YC-2020-0068-0h-H and (bottom) YC-2020-0068-22h-H.*

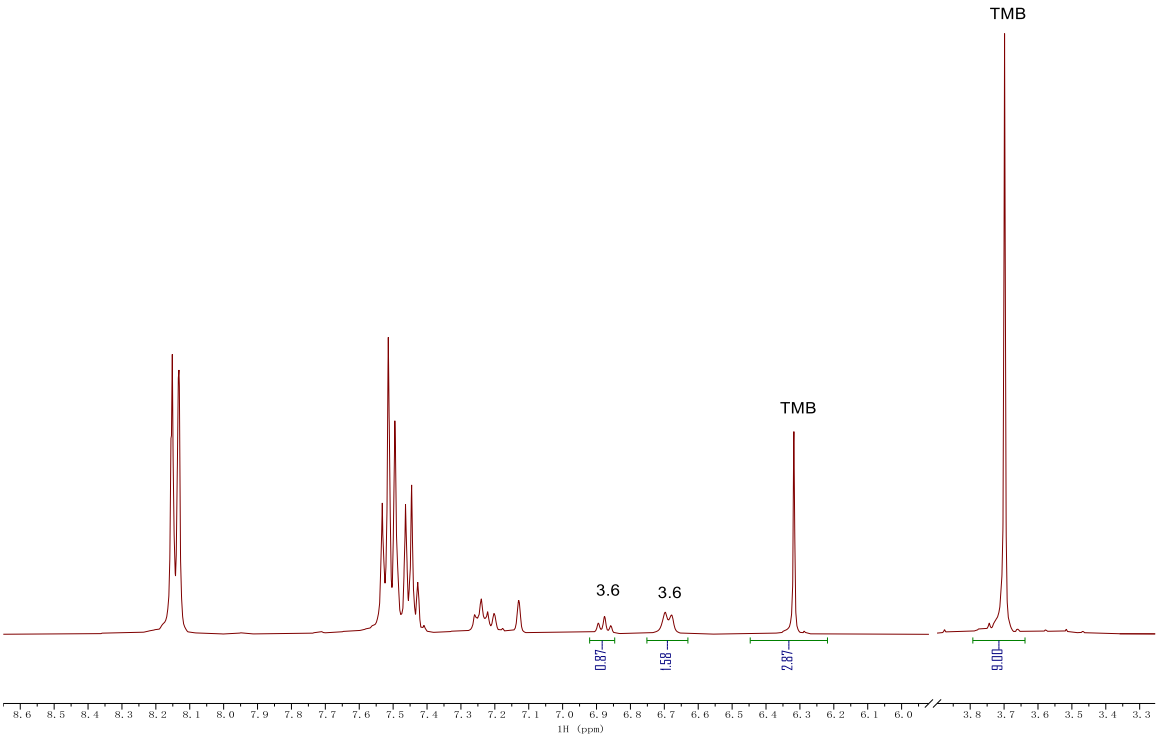

Figure 3.23. t = 22 h ^{1}H NMR spectrum of $TiCl_2(NMe_2)_2$-catalyzed transfer hydrogenation of azobenzene in C_6D_5Br for yield calculation. *Taken from YC-2020-0068-22h-H.*

The conversion of PhNNPh was 12.7%.

3.5.9 H/D Scrambling Study

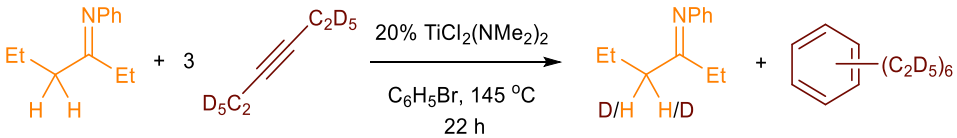

$TiCl_2(NMe_2)_2$ (4.1 mg, 0.020 mmol, 0.2 equiv), **3.3** (17.5 mg, 0.1 mmol, 1 equiv), 3-hexyne-d_{10} (27.7 mg, 0.3 mmol, 3 equiv), 1,3,5-trimethoxybenzene (5.0 mg, 0.03 mmol, 0.3 equiv, ^{1}H NMR internal standard), C_6D_6 (2.5 µL, 0.028 mmol, 0.28 equiv, ^{2}H NMR internal standard) and 0.5 mL of C_6H_5Br were added to a J-Young NMR tube. The reaction mixture was then sealed and

heated in a preheated oil bath at 145 °C for 22 h. ^{1}H and ^{2}H NMR spectra were collected before and after heating to monitor the reaction.

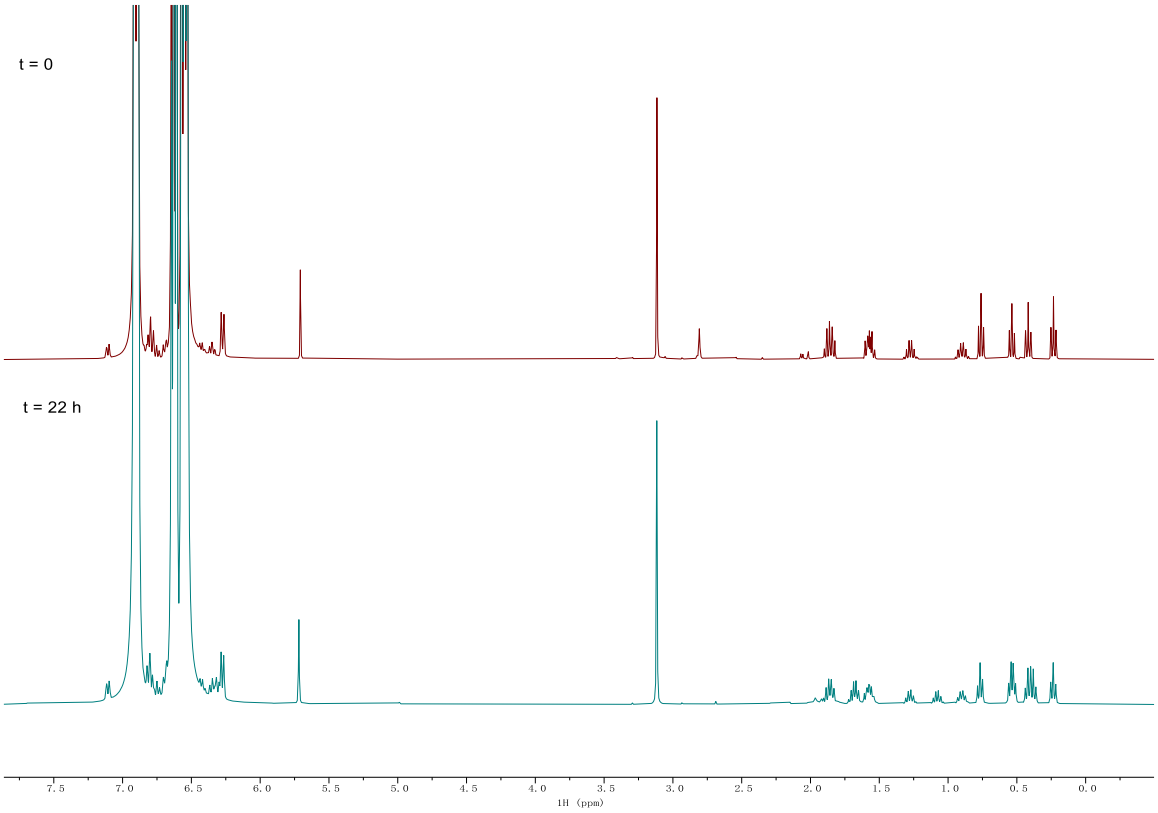

Figure 3.24. Stacked ^{1}H NMR spectra of H/D scrambling experiment of **3.3** with $TiCl_2(NMe_2)_2$ and 3-hexyne-d_{10} in C_6H_5Br. Top: t = 0. Bottom: t = 22 h. *Taken from (top) YC-2020-0088-0h-NoD-PhBr-H and (bottom) YC-2020-0088-NoD-PhBr-22h-H.*

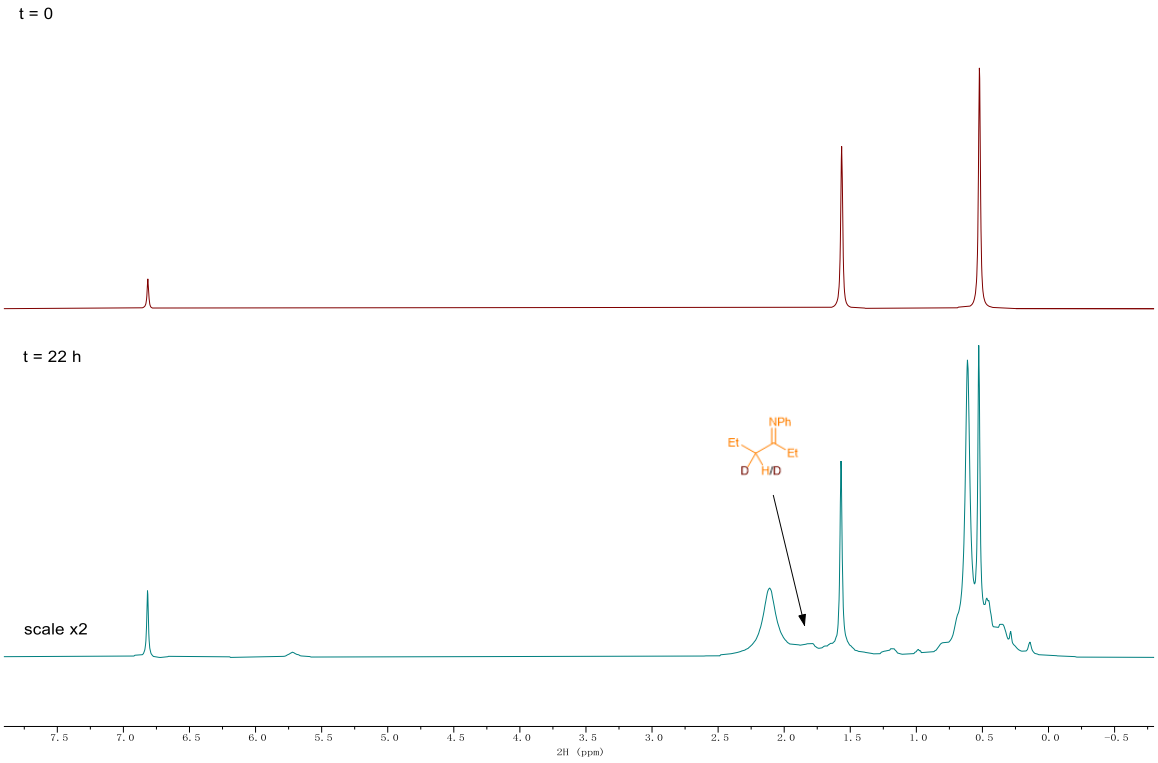

Figure 3.25. Stacked ^{2}H NMR spectra of H/D scrambling experiment of **3.3** with $TiCl_2(NMe_2)_2$ and 3-hexyne-d_{10} in C_6H_5Br. Top: t = 0. Bottom: t = 22 h. *Taken from (top) YC-2020-0088-0h-NoD-PhBr-D and (bottom) YC-2020-0088-NoD-PhBr-22h-D.*

3.5.10 Plausible Mechanism of Transfer Hydrogenation of 3.4 to Azobenzene

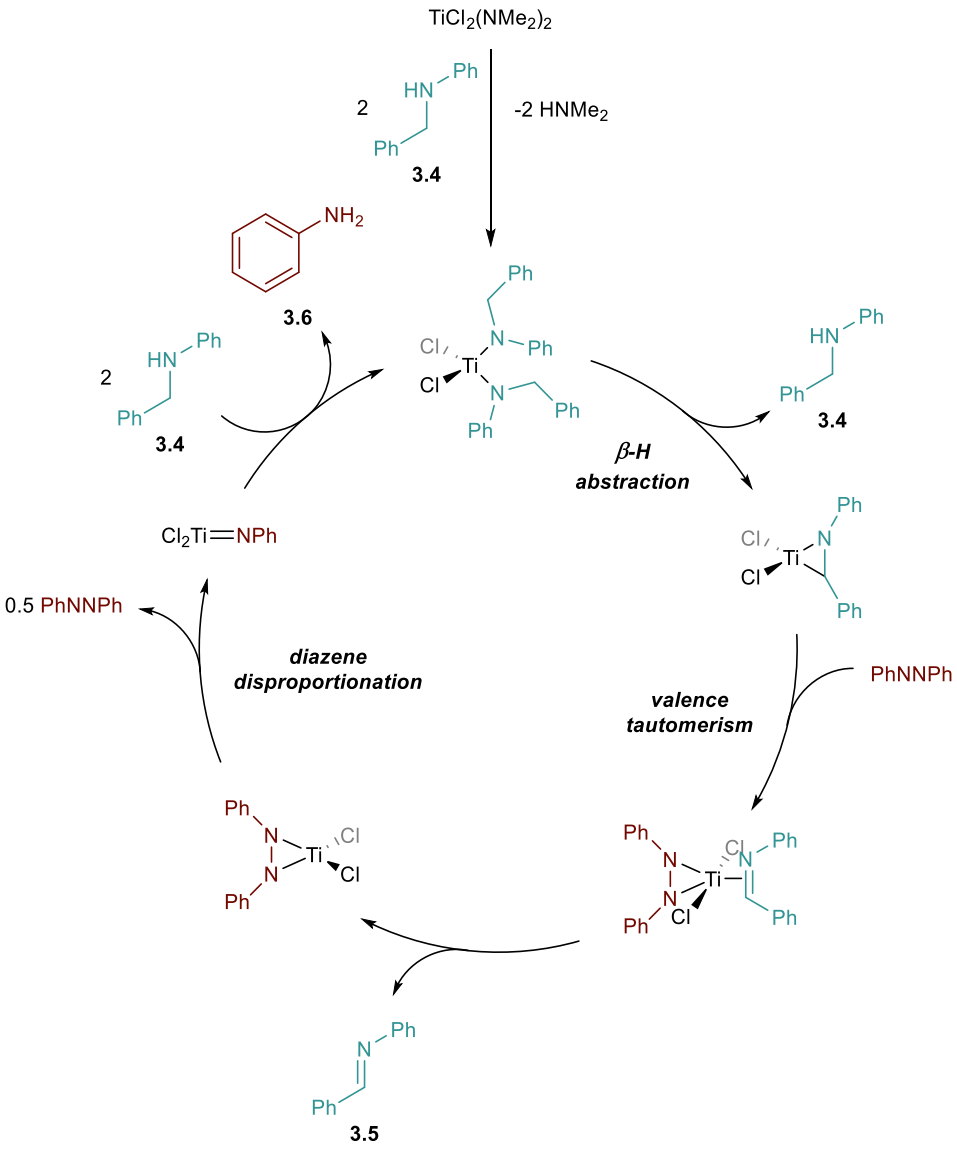

Figure 3.26. Plausible mechanism of transfer hydrogenation of **3.4** to azobenzene.

3.5.11 Metal Amide Scope for Cyclotrimerization of 3-Hexyne

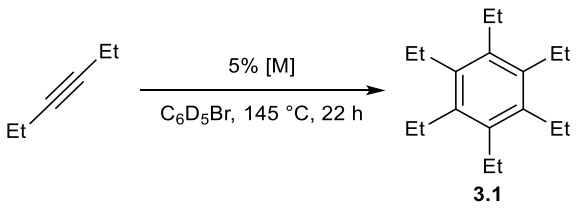

3.1

Metal amide (0.015 mmol, 0.05 equiv), 3-hexyne (24.6 mg, 0.3 mmol, 1 equiv), 1,3,5-trimethoxybenzene (5.0 mg, 0.03 mmol, 0.1 equiv, internal standard) and 0.5 mL of C_6D_5Br were added to a J-Young NMR tube. The reaction mixture was then sealed and heated in a preheated oil bath at 145 ℃ for 22 h. ^{1}H NMR spectra were collected before and after heating to monitor the reaction.

Table 3.1. Metal amide scope for cyclotrimerization of 3-hexyne.[a]

Entry	[M]	Yield
1	$TiCl_2(NMe_2)_2$	58%
2	$Ti(NMe_2)_4$	not found
3	$Zr(NMe_2)_4$	not found
4	$V(NMe_2)_4$	not found
5	$Ta(NMe_2)_5$	not found
6	$TiCl_4$	not found

[a]Yield determined by NMR.

3.5.12 Metal Amide Scope for Hydroamination of 3-Hexyne with Azobenzene and 3.4

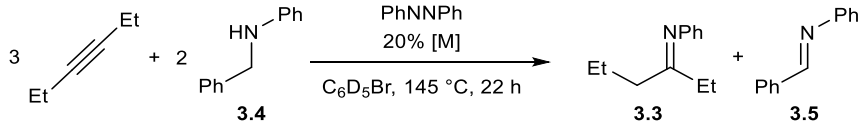

Metal amide (0.020 mmol, 0.2 equiv), 3-hexyne (24.6 mg, 0.3 mmol, 3 equiv), azobenzene (18.2 mg, 0.1 mmol, 1 equiv), *N*-benzylaniline (37.0 mg, 0.202 mmol, 2.02 equiv), 1,3,5-trimethoxybenzene (5.0 mg, 0.03 mmol, 0.3 equiv, internal standard) and 0.5 mL of C_6D_5Br were added to a J-Young NMR tube. The reaction mixture was then sealed and heated in a preheated oil bath at 145 ℃ for 22 h. ^{1}H NMR spectra were collected before and after heating to monitor the reaction.

Table 3.2. Metal amide scope for hydroamination of 3-hexyne with azobenzene and **3.4**.[a]

Entry	[M]	Amount of **3** (mmol)	Yield of **3**	Amount of **5** (mmol)	Yield of **5**
1	$TiCl_2(NMe_2)_2$	0.182	91%	0.090	45%
2	$Ti(NMe_2)_4$	0.042	21%	0.016	8%
3	$Zr(NMe_2)_4$	not found	n.a.	0.004	2%

4	$V(NMe_2)_4$	0.006	3%	0.028	14%
5	$Ta(NMe_2)_5$	0.005	3%	0.010	5%
6	$TiCl_4$	not found	n.a.	0.006	3%

[a]Yield determined by NMR.

Chapter 4: Mechanistic Study of Pyrazole Synthesis via Oxidation-Induced N-N Coupling of Diazatitanacyles

4.1 Overview

Metal-mediated inner-sphere N-N coupling is an attractive yet challenging method for N-N heterocoupling. In the past decade, oxidation-induced formal N-N reductive elimination has been achieved on various metals including Cu, Ni and Ti, while its mechanism has not been well understood. Herein, we report the kinetic and reactivity studies on Ti-mediated oxidative pyrazole synthesis from diazatitanacyclohexadiene, using inner-sphere oxidant TEMPO and outer-sphere oxidants ferrocenium (Fc^+) salts. Ti–O bond formation was found to be important in associative TEMPO oxidation as it is kinetically significant. When applying Fc^+ salts as oxidants, chloride could coordinate to Ti to allow an "inner-sphere-like" oxidation of diazatitanacycle. A unique chlorine-bridged dititanium diradical was synthesized, allowing the reactivity studies on the one-electron oxidized diazatitanacycle. A catalytic pyrazole synthesis using Cl-based photocatalyst has been attempted yet hampered by the lack of chemoselectivity on the reductive dechlorination of $TiCl_4$. This study reveals the reactivity of one-electron oxidation intermediates and Cl-based oxidants in Ti-mediated pyrazole synthesis, bringing new potential to Ti-mediated oxidative N-N coupling reactions.

4.2 Introduction

Redox non-innocent (RNI) ligands are widely presented in organometallic chemistry. Multiple roles can be fulfilled by these redox-active ligands, including serving as an electron reservoir, activating substrates, or acting as substrates toward further reactions themselves.[179] In early transition metal chemistry, RNI ligands are often crucial to unmasking low valent reactivity, where the RNI ligand can synergistically stabilize otherwise high-energy reduced states, for example through π-backbonding or ligand resonance.[8,162,180] Oxidation of a metal-RNI ligand moiety often occurs via an inner-sphere mechanism, whereby metal-oxidant bond formation occurs simultaneously with RNI ligand oxidation, such as the dihalogenative oxidation of a Zr bis(diamide) complex or the oxidation of a Ti ene-tetraamide complex by azide.[155,181–185]

Recently, our group reported an oxidation-induced N-N reductive elimination reaction (Figure 4.1, top),[61] where a diazatitanacyclohexadiene (**4.1^R**) can be oxidized by TEMPO to yield a pyrazole (**4.2^R**) through N-N coupling. In this reaction, metallacyclic ligand oxidation was critical to successful N-N coupling. Stoichiometric experiments examining the role of the system oxidation state demonstrated that a one-electron oxidized version of **4.1^R** (**4.IM1^R**)

potentially underwent disproportionation, whereby the resulting two-electron oxidized **4.IM2^{R}** underwent coupling, although we were unable to directly observe any intermediates in the reaction of simple Ti halide diazatitanacycles.

Given the rarity of N-N coupling reactions[68,186] and remaining uncertainty around the detailed mechanism of metal-mediated inner-sphere N-N coupling,[71] we sought to investigate diazatitanacycle oxidation in more depth. Herein, we report a detailed kinetic and mechanistic study of Ti-mediated oxidative pyrazole synthesis using diazatitanacyclohexadiene **4.1**, with TEMPO as a model inner-sphere oxidant and Fc^{+} salts as model outer-sphere oxidants (Figure 4.1, bottom). These studies reveal that **4.1** undergoes a rate-determining initial oxidation with TEMPO via an associative mechanism, suggesting that Ti-O bond formation has an important contribution to the reaction rate. The reactivity of a dimeric oxidized species reveals that while disproportionation may account for some pyrazole formation, a more likely pathway for N-N coupling is through a second oxidation by TEMPO. Further oxidation studies using Fc^{+} indicate that coordinating chloride counterions were required for productive reactivity. This halide effect further highlights a critical role of oxidant coordination to Ti, where the halide coordination can act as an electron transfer bridge between the oxidant and Ti.

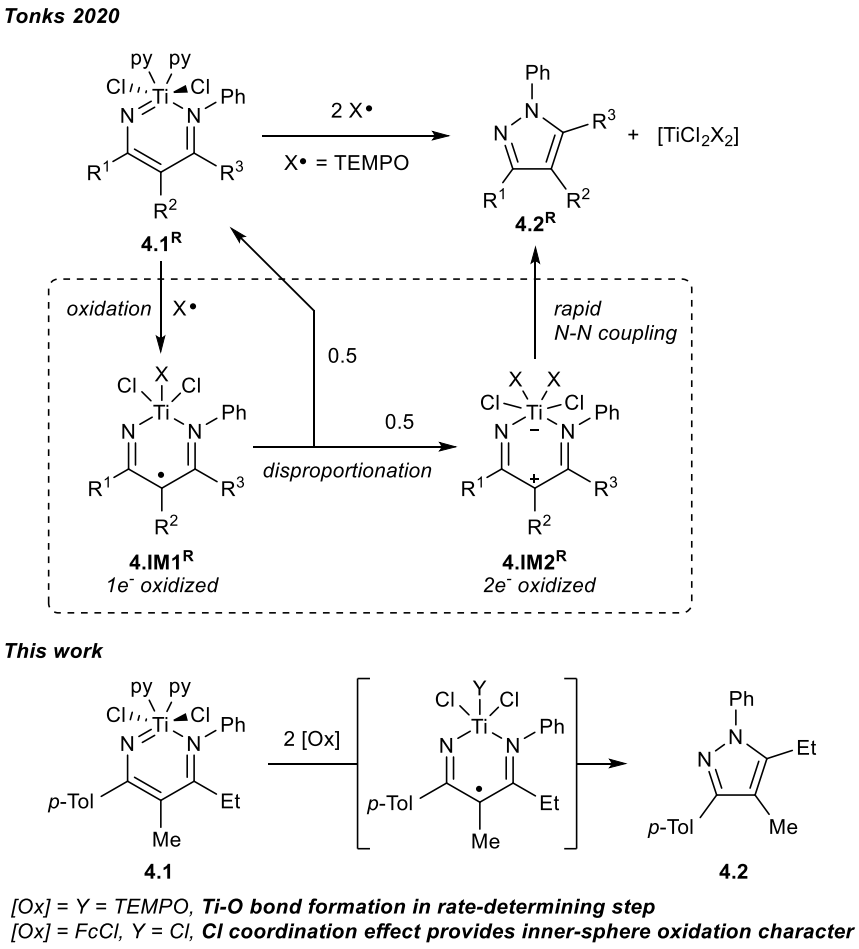

Figure 4.1. Ti-mediated pyrazole synthesis.

4.3 Result and Discussion

Our prior stoichiometric studies had implicated the intermediacy of 1- and 2-electron oxidized species in the TEMPO-induced oxidative N-N coupling of **4.1^{R}** (Figure 1, top) although we were unable to directly observe either **4.IM1^{R}** or **4.IM2^{R}**. In an effort to probe the mechanism in more detail, we first carried out kinetic studies to determine the rate law of the oxidation reaction. Under standard conditions, (Figure 4.2) TEMPO cleanly oxidizes **4.1** to form **4.2** in near-quantitative yield and time adjustment analysis (Figure 4.43) indicates a robust reaction with no product inhibition.[99,187,188]

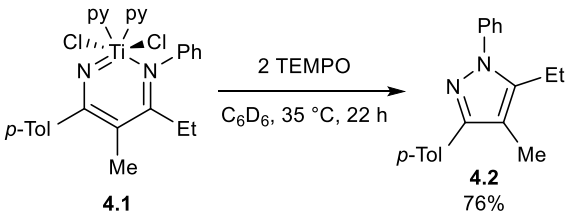

$$rate = k_{obs}\frac{[\mathbf{4.1}]^{0.7}[TEMPO]^{1}}{[pyridine]^{-2.5}}$$

Figure 4.2. Rate studies of the oxidation of **4.1** by TEMPO.

The rate profile was obtained by reaction progress monitoring through *in situ* ^{1}H NMR spectroscopy. The order of **4.1** and pyridine was obtained via variable time normalization analysis,[189] while the order of TEMPO was obtained from initial rates since the paramagnet cannot be quantitatively monitored by ^{1}H NMR spectroscopy. The reaction was found to be approximately 1st order in [TEMPO] and less than 1st order (0.7 best fit) in [**4.1**], with pyridine higher than 2nd order inhibitively (-2.5 best fit).

The 1st order dependence on [TEMPO] and the lack of observable reaction intermediates led us to hypothesize that the first oxidation of **4.1** by TEMPO was prior to the rate determining step of the reaction. However, the 0.7-order rate dependence on [**4.1**] indicates a more complex manifold for the first oxidation: this dependence could be a result of several mechanistic possibilities, including (1) a dissociation equilibrium of pyridine ligands from Ti[190] or (2) a monomer-dimer equilibrium of **4.1** (combined with pyridine loss) wherein productive reaction takes place from the monomer. In fact, dimeric diazatitanacycles lacking Lewis basic pyridine supporting ligands are synthetic intermediates *en route* to **4.1**.[61] Meanwhile, the -2.5-order dependence on pyridine suggests that the dissociation of both the two pyridines were kinetically significant, suggesting that the second pyridine dissociation was the rate determining step.

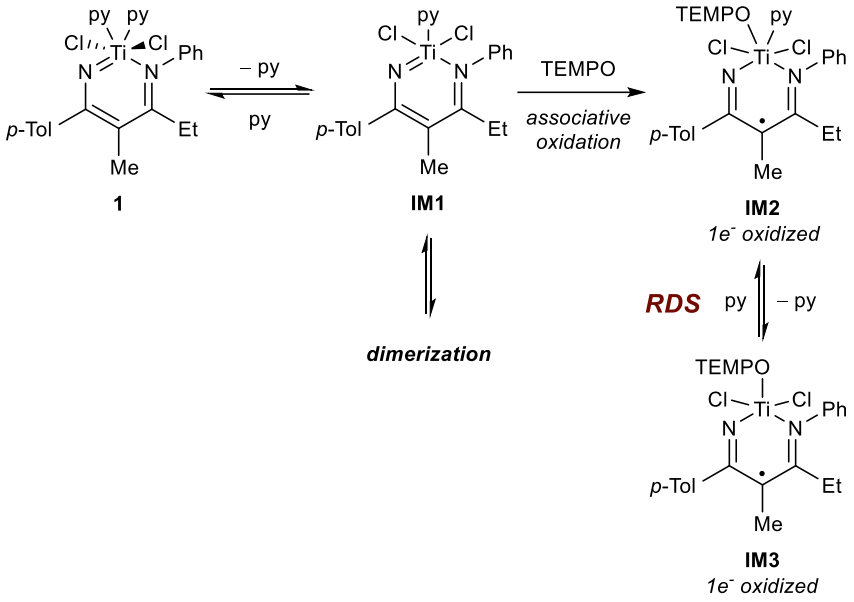

Figure 4.3. Rate determining step and hypothetical mechanistic pathways to account for the 0.7 order dependence on [**4.1**].

As a result, we turned to DOSY NMR spectroscopy to interrogate the preequilibrium structure(s) of **4.1** to address whether pyridine dissociation or **4.1** dimerization was responsible for the 0.7 order in [**4.1**] (Figure 4.3). Here, the molecular weight of solution species was determined based on the Stoke-Einstein Gierer-Wirtz Estimation (SEGWE) model.[191,192] Two concentrations (0.01 M and 0.003 M) were chosen to represent the high and low concentration conditions in the rate law study. In both concentrations, a slower diffusing signal (**4.B**) assigned to the diazatitanacyclohexadiene complex was found with estimated molecular weight (504 or 524 g/mol) close to **4.1** (553 g/mol), along with faster diffusing signal (**4.A**) with an estimated molecular weight close to free pyridine. The intensity of signal **4.A** arising from free pyridine negatively correlates with [**4.1**], indicative of a dissociation equilibrium that shifts according to [**4.1**]. In both concentration regimes the equilibrium favors the pyridine bound **4.1**, in good accordance with the saturation kinetics on [pyridine]. Importantly, the absence of any slower-diffusing signal from a higher molecular weight species indicates that a potential equilibrium between **4.1** and its dimer is likely not relevant under the reaction conditions.

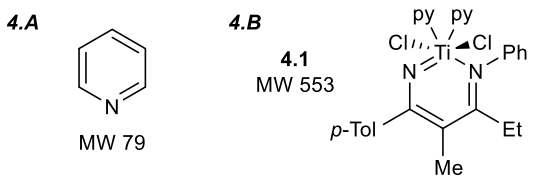

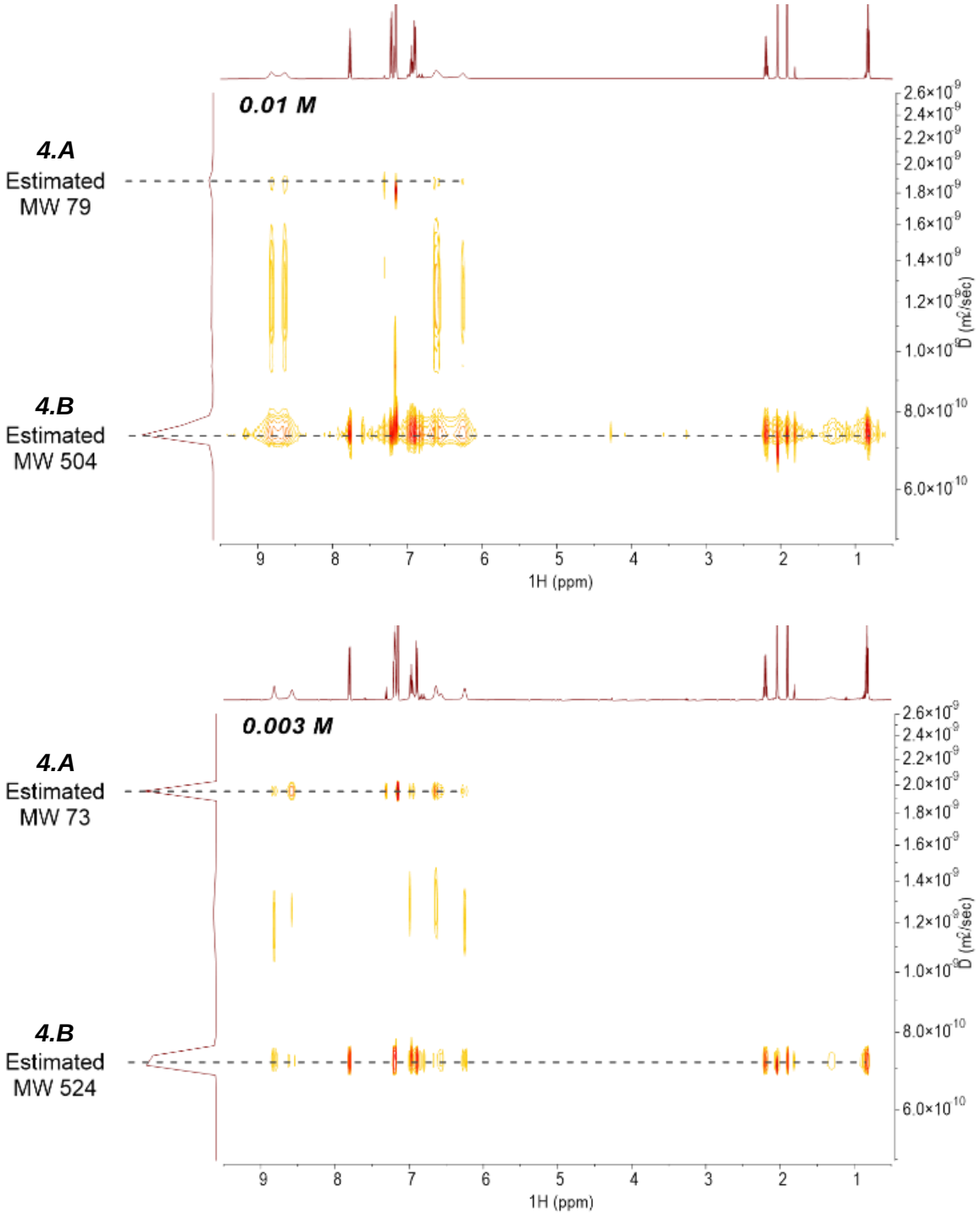

Figure 4.3. DOSY NMR spectra of 0.01 M (top) and 0.003 M (bottom) **4.1** in C_6D_6 demonstrating pyridine coordination equilibrium.

The presence of the pyridine dissociation equilibrium leads to a further question: is the vacant coordination site provided by the pyridine dissociation necessary for TEMPO oxidation? To interrogate this, TEMPO oxidation of the bipyridine (bpy) adduct **4.3** was examined, where the bidentate bpy ligand should be much harder to dissociate and thus inhibit oxidation if ligand dissociation is required (Figure 4.4). Consistent with this hypothesis, TEMPO oxidation of **4.3** led to no formation of **4.2** at 50 ℃. Self-exchange of the bpy ligand was observed in EXSY spectrum of **4.3**, prompting us investigate reaction at higher temperature where hemilability of the bpy ligand may be accessible. In fact, oxidation of **4.3** at 90 ℃ resulted in rescuing of the oxidation reactivity and a 37% yield of **4.3**. These experiments provide strong evidence that TEMPO oxidation of diazatitanacycloehexadienes requires a vacant site for Ti–O bond formation, which in this instance is provided by pyridine dissociation.

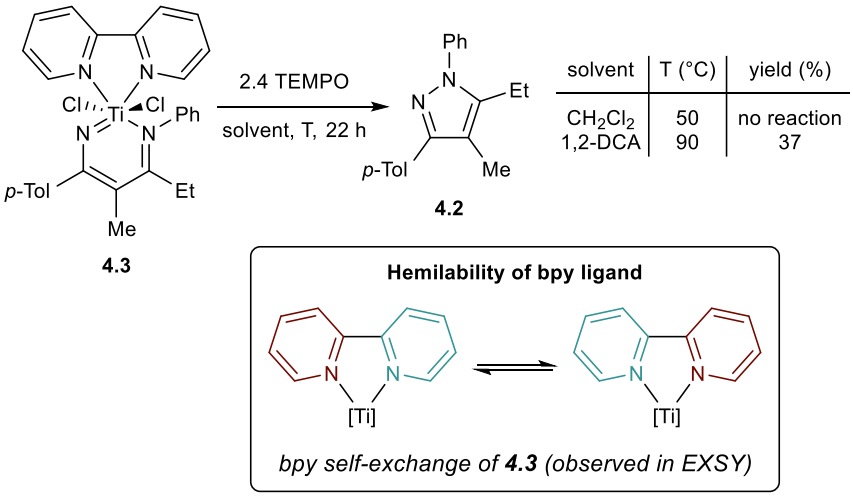

Figure 4.4. TEMPO oxidation and bpy self-exhcange of **4.3**.

After examining the rate-determining step of the mechanism through kinetic interrogation and NMR spectroscopy, we hoped to obtain further information on the post-rate determining steps by capturing the oxidized intermediates through other synthetic methods. In our previous studies, we indirectly demonstrated that one-electron oxidized species such as **4.IM1^{R}** may undergo a disproportionation mechanism *en route* to N-N coupling. However, it was unclear if this mechanism was the result of dimerization of **4.IM1^{R}** or a more complex process involving other Ti species reacting with **4.IM1^{R}**. In the oxidation reactions with TEMPO, another possibility is that the transient **4.IM1^{R}** could be captured and oxidized by TEMPO owing to the persistent radical effect.[193] Thus, we sought to synthesize a potential oxidized bimetallic analogue of **4.IM1^{R}** and examine its reactivity.

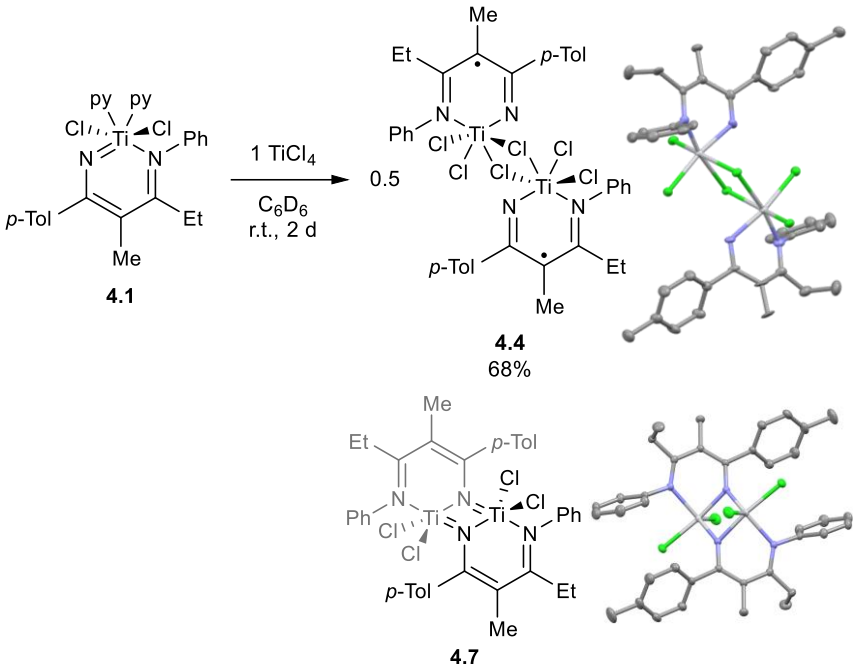

Figure 4.5. Synthesis of dititanium diradical **4.4** and an alternative possible structure **4.7**.

One-electron ligand-centered chemical oxidations of redox noninnocent d^0 metal complexes have been reported before: for example, Heyduk reported oxidation of a Zr(triamide)ClL_2 by $PhICl_2$;[37] Roberts reported oxidation of a Sc(triamide)$(THF)_3$ by Cl• from Ph_3CCl;[194] and Mashima reported oxidation of a $TaCl_3$(α-diimine) by CCl_4 or $CHCl_3$.[185] Considering that **4.1** is a relatively electron-rich Ti imido complex, we envisioned that electron-deficient $TiCl_4$ may serve as both an oxidant and pyridine abstractor when reacted with **4.1**. Reaction of **4.1** with 1 equivalent of $TiCl_4$ led to the formation of the diamagnetic bimetallic diradical **4.4** in 68% yield (Figure 4.5). **4.4** is a Ti-dimer bridged by two chloride ligands. Unfortunately, the structure is of insufficient quality for bond metric analysis, however, the connectivity of the structure displays three chloride ligands on each Ti center and the diazatitanacyclohexadiene moieties are preserved. Additionally, there is appreciable distortion of the diazatitanacyclohexadiene moiety. An alternative XRD structure was also identified from the product mixture as **4.7**, which was a pyridine-free imido-bridged titanacycle dimer. It remains unclear to us whether **4.7** is a significant component of the product mixture or a downstream decomposition product of **4.4**. However, DOSY of the product mixture showed a slow diffusing signal (897 g/mol) closer to the expected structure molecular weight of **4.4** (861 g/mol) than **4.7** (790 g/mol). The absence of faster diffusing signal indicates that **4.4** is also dimeric in solution (Figure 4.57).

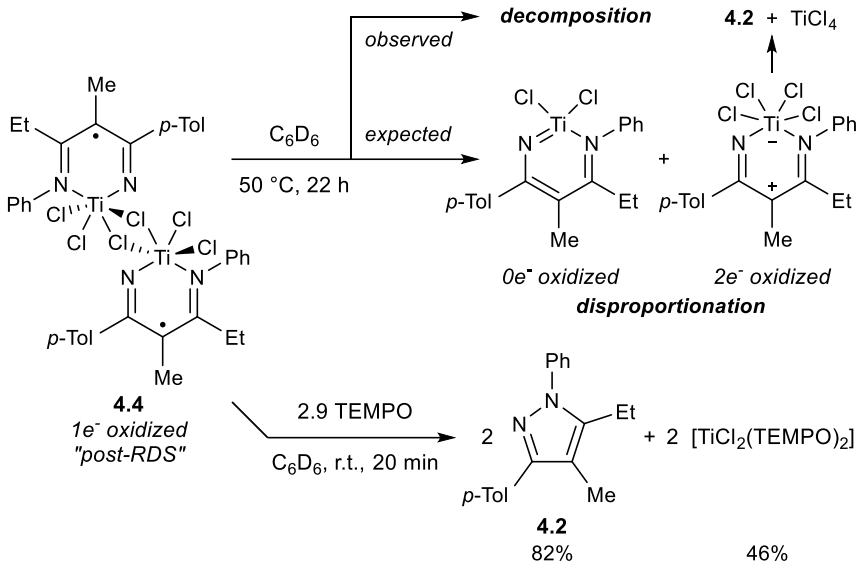

Figure 4.6. Reactivity of dititanium diradical **4.4**.

Diradical **4.4** does not undergo spontaneous thermal disproportionation to ultimately form **4.2**, but instead decomposes upon heating (Figure 4.6, top). This result in combination with the observation that ring-opening of 2-iminyl-2*H*-azirine with $TiCl_3(THF)_3$, which should form the same **4.IM1**, indicates that a dimerized **4.IM1** is likely not the predominant pathway for the formation of **4.2** and instead further oxidation of **4.IM1** by TEMPO (or another Ti species) is more likely.

Although not directly implicated as a major intermediate in oxidation of **4.1** to **4.2**, the bimetallic diradical **4.4** can nonetheless be oxidized to **4.2** by TEMPO. TEMPO oxidation of **4.4** occurs rapidly at room temperature, reaching >80% completion within 20 minutes (Figure 6, bottom). In contrast, TEMPO oxidation of **4.1** reaches only 29% yield after 2 hours (Table S1, entry 3). The rapid further oxidation of **4.4** to **4.2** is further evidence that initial oxidation of **4.1** to **4.IM1** likely occurs prior to the rate-determining step in the TEMPO oxidation of **4.1** to **4.2**.

TEMPO likely operates as an inner-sphere oxidant for these diazatitanacycles owing to the large energy difference between TEMPO and $TEMPO^{-}$.[195] In this regard, we sought to investigate whether Ti-O bond formation was critical to the oxidation process, or whether outer-sphere oxidants could also accomplish N-N bond formation. Cyclic voltammetry of **4.1** showed a semi-reversible oxidation peak ($E_{1/2}^{ox}$ = 0.22 V vs SCE, Figure 4.52b), indicating that simple Fc^{+} salts should be sufficiently oxidizing to accept an electron from **4.1**.

Attempted oxidation of **4.1** by noncoordinating Fc[B(ArF)$_4$] (ArF = 3,5-(trifluoromethyl)phenyl) resulted in no conversion to **4.2** (Table 4.1, entry 1). In contrast, oxidation of **4.1** by FcCl resulted in 50% yield of **4.2** (Table 4.1, entry 2). Oxidation of **4.3** by Fc[B(ArF)$_4$] similarly gives no conversion to **4.2** and although oxidation of **4.3** to **4.2** by FcCl proceeds, it is much lower yielding (11%) than oxidation of **4.1**. In the case of FcCl oxidations, it thus appears likely that oxidation occurs via an inner sphere-like mechanism where chloride association to form a Ti "-ate" complex precedes or is concurrent with oxidation by Fc^+. This halide-coupled oxidative electron transfer can be seen as the microscopic reverse of reductive dechlorination of M-Cl complexes with redox non-innocent ligands.[196,197] Halide coordination is supported through the addition of [^{n}Bu$_4$N]Cl to a CD_2Cl_2 solution of **4.1**, which results in a color change from deep purple to light yellow along with a clean conversion to a new species by ^{1}H NMR spectroscopy. Unfortunately, we were unable to isolate the presumed "-ate" complex for further characterization. Oxidation of diazatitanacycles by Fc[PF_6] is also possible,[61] which is consistent with an inner-sphere pathway as PF_6^- is well-known to be coordinatively noninnocent with fluorophilic and electrophilic early transition metals.[198–201]

Table 4.1. Examination of inner- vs outer-sphere oxidation with ferrocenium salts.

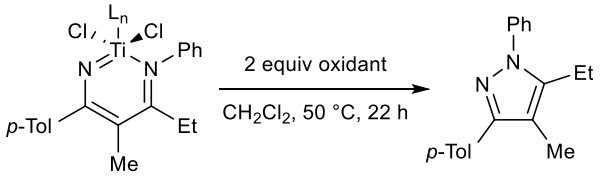

4.2

entry	[Ti]	oxidant	yield[a] (%)
1	**4.1**	FcBArF	not observed
2	**4.1**	FcCl	50
3	**4.3**	FcBArF	not observed
4	**4.3**	FcCl	11

[a]Yields were determined *via* No-D ^{1}H NMR against internal 1,3,5-$(OCH_3)_3C_6H_3$ standard.

With all of the observations above, a more detailed reaction mechanism for TEMPO oxidation of **4.1** to form **4.2** can be proposed (Figure 4.7). First, pyridine dissociation from **4.1** generates a coordinatively unsaturated diazatitanacycle **4.IM3** that undergoes inner-sphere

oxidation by TEMPO to generate a one-electron oxidized intermediate **4.IM4**. Next, the rate determining dissociation of pyridine from **4.IM4** will give **4.IM5**, which can then potentially undergo two pathways: first, **4.IM5** can be directly oxidized by another equivalent of TEMPO to form **4.2** (Path I). Alternately, **4.IM5** could undergo dimerization, generating a diradical **4.IM7** analogous to **4.4** (Path II). This diradical does not undergo disproportionation, but instead can be rapidly further oxidized by TEMPO to **4.2**. We favor the former pathway as the predominant mechanism because of the relative concentration of TEMPO radicals to **4.IM5**, which should be consumed rapidly relative to its formation since the second pyridine dissociation is rate-determining.

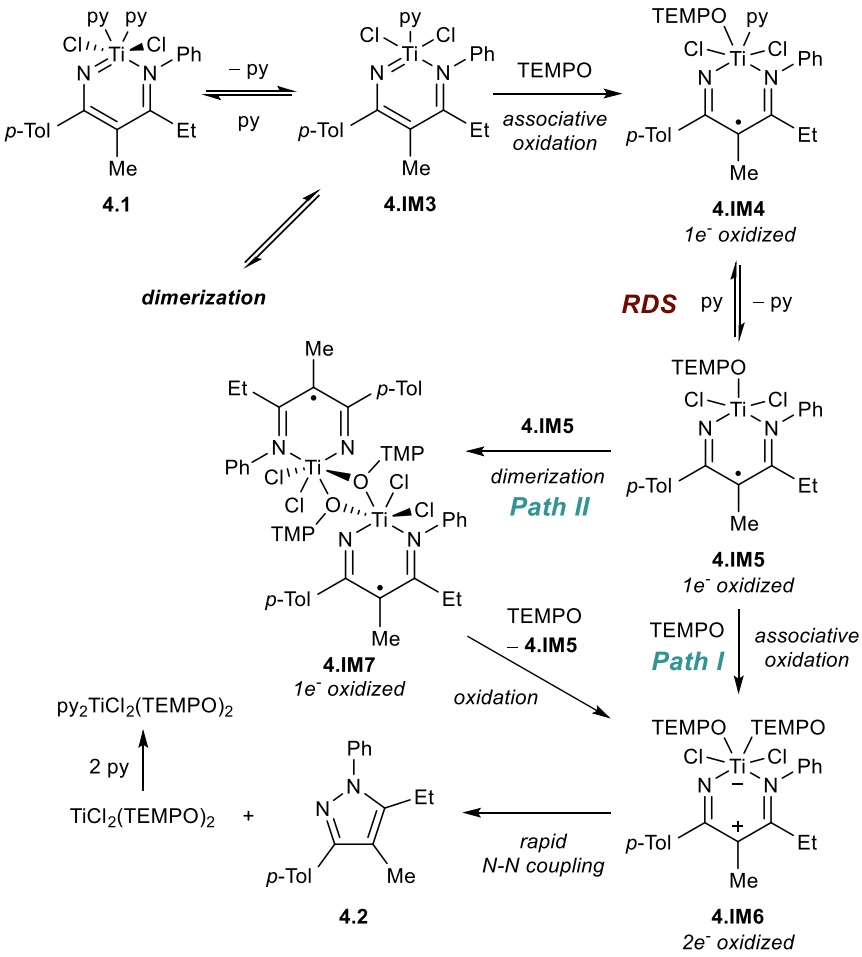

Figure 4.7. Proposed Mechanism for TEMPO oxidation of **4.1**.

Finally, building from the Fc^+ oxidation study we realized that Ti-X bond formation is necessary for oxidative N-N coupling of diazatitanacycles, and thus considered catalytic strategies that may capitalize on Ti-Cl bond formation. In our previous study, $PhICl_2$ was found

to stoichiometrically oxidize the diazatitanacycle at room temperature with good yield.[61] In the hope of searching for a catalytic Cl-based oxidant, we examined chloride-containing photooxidants. $Ce^{III/IV}$ has recently attracted wide interest as a versatile photoredox shuttle, where its photoresponsive Ce^{IV}-ligand bond can homolyze through LMCT to initiate radical catalysis.[202] In particular, $[Ce^{IV}Cl_6]^{2-}$ is attractive since it can generate Cl radical from an LMCT.[203] Oxidation of **4.1** by $(NEt_4)_2[Ce^{IV}Cl_6]$ gave the same yield under light irradiation or in the dark (Figure 4.8, top). We speculate that this oxidation occurs via chlorine atom transfer from the ground state of $[Ce^{IV}Cl_6]^{2-}$ to **4.1**, given that $[Ce^{IV}Cl_6]^{2-}$ ($E_{1/2}^{III/IV}$ = +0.41 V vs. SCE) is oxidative enough to oxidize **4.1**.[204,205] We then sought to develop a photocatalytic $Ce^{III/IV}$ oxidation of **4.1** through oxidative quenching of the highly reductive $\{[Ce^{III}Cl_6]^{3-}\}^*$ (theoretical $E_{1/2}^{*III/IV}$ = -3.07 V vs. SCE) using alkyl halides as sacrificial oxidants,[204,205] only to find the substoichiometric Ce photocatalyst failed to give turnover (Section 4.5.12). $Ru(bpy)_3Cl_2$-catalyzed photooxidation of **4.1** showed slight turnover despite the limited yield (Figure 4.8, bottom). This may originate from **4.1** acting as both the substrate and the sacrificial oxidant for the photosensitizer ($E_{1/2}(Ru^{II/I})$ = -1.33 V vs. SCE),[206,207] as **4.1** has an irreversible reduction peak offset at around -0.7 V vs. SCE (Figure 4.52c), which we tentatively assigned to the reductive dechlorination of **4.1**.

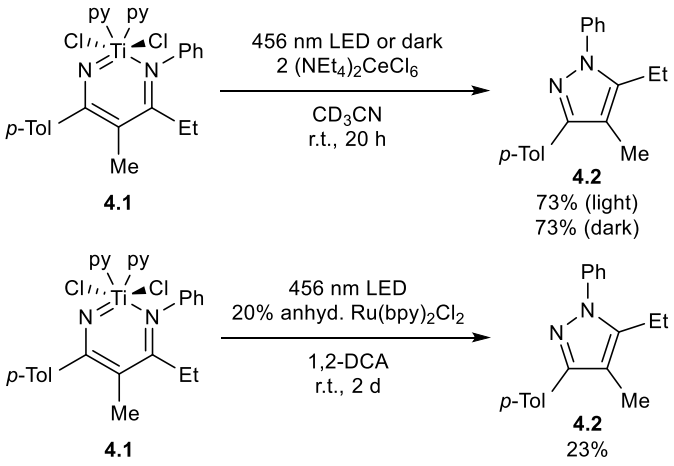

Figure 4.8. Oxidation of **4.1** by Cl-based oxidants (top) $[Ce^{IV}Cl_6]^{2-}$ and (bottom) anhyd. $Ru(bpy)_3Cl_2$.

We came to realize that the hypothetical catalytic design based on [2+2+1] multicomponent synthesis of $\mathbf{4.1^R}$ suffers from compatibility challenges among the various redox processes involved (Figure 4.9). In such a design, Ti imido **4.5** would be required for the synthesis of $\mathbf{4.1^R}$ through [2+2] cycloaddition with alkyne and the insertion of nitrile. In order to generate **4.5**,

L_2TiCl_4 needs to undergo a two-electron reduction to [Ti^{II}] followed by the diazene disproportionation with PhNNPh. A strong reductant would be required for the reduction of L_2TiCl_4 ($E_{pc}(Ti^{IV/II})$ = -1.3 V for $TiCl_4$ in DMSO).[208] However, as the most electron-deficient Ti species in the design, the other Ti intermediates, e.g. **4.1** and **4.5**, would undergo reductive dechlorination more readily than L_2TiCl_4. Thus, the hypothetical Ti catalysis can be easily poisoned by the reductant. Delicate kinetic tuning or alternative X-type ligand for the Ti catalyst will be required to overcome the compatibility challenge.

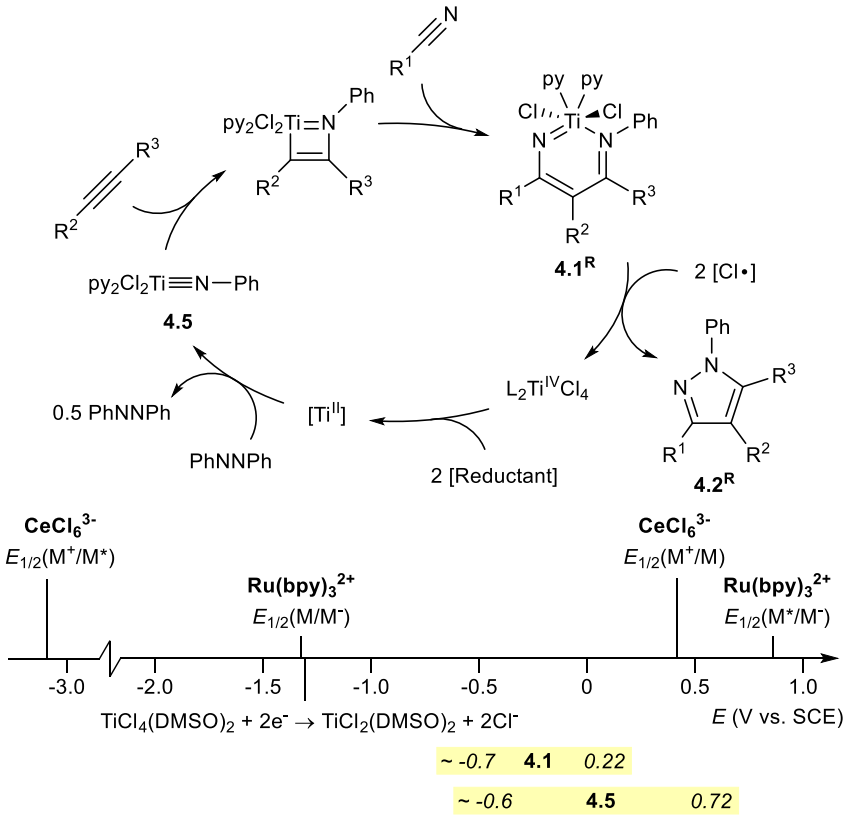

Figure 4.9. Hypothetical catalysis based on [2+2+1] synthesis of **4.1** and the reduction potentials of key species.

4.4 Conclusion

In conclusion, an investigation of the N-N coupling reactivity of diazatitanacycles engendered by different oxidants reveals an inner-sphere coordination-induced oxidation mechanism. Ti–O bond formation was found to be important in the TEMPO oxidation of **4.1** due to its involvement in the RDS. On the other hand, outer-sphere oxidant Fc^+ salts require

the presence of a coordinating anion Cl^- to provide the necessary inner-sphere oxidation character. As a comparison, FcBArF was incapable of oxidizing **4.1**. A catalytic pyrazole synthesis based on the reduction of $TiCl_4$ has been attempted as the reduction of Ti–Cl bonds is quite accessible. However, it was realized the reductive dechlorination in such a hypothetical catalysis would not be selective for $TiCl_4$ as it is the most electron-deficient Ti intermediate in the reaction. Although these transformations are currently stoichiometric, these latter reactions that result in Ti–Cl containing products may unlock future catalytic pyrazole syntheses.

4.5 Experimental

4.5.1. General Considerations

All air- and moisture-sensitive compounds were manipulated in a glovebox under nitrogen atmosphere. Alumina and molecular sieves were activated by heating at 280 ℃ under active vacuum for one week. Solvents for air- and moisture-sensitive reactions (THF, C_6H_6, CH_2Cl_2, Et_2O, *n*-pentane) were dried through activated alumina on a Pure Process Technology solvent purification system. 1,2-dichloroethane (1,2-DCA), pyridine, and CH_3CN were dried over CaH_2 and distilled before passing through activated alumina and storing over activated 3 Å molecular sieves in the glovebox. NMR solvents (CD_2Cl_2 and C_6D_6) were dried over CaH_2 or sodium metal and vacuum transferred before passing through activated alumina and storing over activated 3 Å molecular sieves in the glovebox. TEMPO was purchased from Oakwood Products, Inc. and purified by sublimation. 1,3,5-trimethoxybenzene (TMB) was purchased from Oakwood Products, Inc. and used without further purification. HMDSO was purchased from Oakwood Products, Inc. and purified by vacuum distillation. $TiCl_4$, LiHMDS, ferrocene (Fc), NEt_4Cl, PPNCl (PPN = bis(triphenylphosphine)iminium), and *n*-dodecane were purchased from Millipore-Sigma. ^{t}BuCl, ^{t}BuBr, $PhCH_2Cl$, $PhCH_2Br$ were purchased from Millipore-Sigma and purified by vacuum distillation. TBACl (TBA = tetrabutylammonium) was purchased from Tokyo Chemical Industry Co., Ltd. (TCI). NaBArF (BArF = tetrakis(3,5-bis(trifluoromethyl)phenyl)borate) was purchased from Ambeed, Inc. Anhydrous $Ru(bpy)_3Cl_2$ was prepared by treating $Ru(bpy)_3Cl_2{\cdot}6H_2O$ (purchased from Strem Chemicals, Inc.) with 3 equiv of $TiCl_4$ in CH_2Cl_2, and the precipitate was filtered and recrystallized in CH_3CN/Et_2O. $TiCl_4(THF)_2$ was prepared by dropwise addition of $TiCl_4$ into excess THF, filtration then evaporation under vacuum at room temperature for 3 days. TBABArF was prepared from cation exchange between 1 equiv NaBArF and 1 equiv TBACl in CH_2Cl_2 in a glovebox. **1**,[61]

ferrocenium chloride (FcCl),[209] FcBArF,[210] and $(NEt_4)_2CeCl_6$[211] were prepared following the reported procedures.

^1H, $^{13}C\{^1H\}$, $^{31}P\{^1H\}$, ^1H COSY, ^1H–^{13}C HSQC and HMBC, NOESY, No-D ^1H, and DOSY NMR were collected on Bruker Avance III HD NanoBay 400 MHz or Bruker Avance III HD 500 MHz spectrometers. Quantitative NMR reaction experiments were collected with the following NMR acquisition parameters: number of scan = 4, dummy scan = 0, acquisition time = 5 s, and relaxation time = 30 s (with the exception of initial rate studies due to their short time frame). Chemical shifts are reported with respect to residue protio-solvent impurity for ^1H (s, 7.16 ppm for C_6D_6; s, 5.32 ppm for CD_2Cl_2; p, 1.94 ppm for CD_3CN) and ^{13}C (t, 128.06 ppm for C_6D_6; p, 53.84 ppm for CD_2Cl_2; s, 118.26 ppm for CD_3CN). No-D ^1H NMR was referenced to the proton signal of the internal standard TMB (Ar-*H*, 3H, s, 6.08 ppm in CH_2Cl_2; s, 6.03 ppm in 1,2-DCA) or *n*-dodecane (CH_3, 6H, t, 0.85 ppm in 1,2-DCA). Baseline correction (ablative method with 5 points and 10 passes, MestReNova) were applied to NMR spectra before integrated against NMR internal standard (TMB, HMDSO or *n*-dodecane) for quantitative analysis.

456 nm and 390 nm LED light were provided by PR160L 456 nm and 390 nm LED lamps from Kessil® DiCon Fiberoptics, Inc. UVA light was provided by two black light compact fluorescent lamps (CFL) from Sleek Lighting LLC. (model 20593, 23 W). All photochemical reactions were performed at a distance of 3 cm between the reaction vessel and the light source(s). Cyclic voltammetry was collected on Pine Research Instrumentation WaveNow® Portable Potentiostat using screen-printed platinum electrodes with Ag pseudo-reference electrode (model RRPE2011PT-6).

4.5.2 Synthesis of 4.3 and Discussion on Hemilability of bpy Ligand

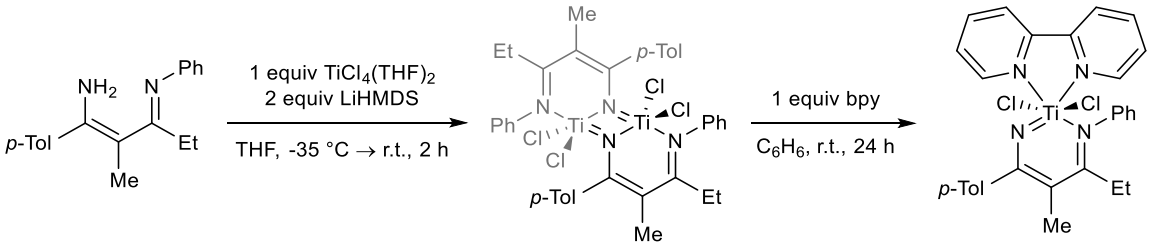

4.6 **4.7** **4.3** 28%

The procedure is adopted from a modification of the synthesis of **4.1**. **4.7** was prepared following the reported procedure.[61] In a 20 mL scintillation vial in the glovebox, a solution of

4.7 (479 mg, 1.72 mmol, 1.0 equiv) in THF (5 mL) at -30 ℃ was added dropwise to a vigorously stirring slurry of $TiCl_4(THF)_2$ (574 mg, 1.72 mmol, 1.0 equiv) in THF (5 mL) at -30 ℃ to give a deep purple solution. After 10 minutes, a -30 ℃ solution of LiHMDS (575 mg, 3.44 mmol, 2.0 equiv) in THF (3 mL) was added dropwise. The reaction was stirred at room temperature for 2 h, then the volatiles were removed by evaporation under vacuum. The residue was extracted by benzene (5 mL) and filtered through a pipet column of Celite. 2,2'-bipyridine (bpy, 269 mg, 1.72 mmol, 1.0 equiv) was added and black microcrystals formed immediately. The mixture was allowed to stand at room temperature for 1 day before being filtered and washed with 1 mL benzene three times. The resulting solid was collected as **4.3** (black microcrystals, 267 mg, 28% yield) after drying under vacuum. **4.3** is insoluble in benzene but soluble in CH_2Cl_2. 1H and 13C signal assignments were performed with the assistance of COSY, ^1H-^{13}C HSQC and HMBC spectra, where *N*-Phenyl was found to have all atoms being chemically inequivalent due to restricted rotation.

^1H NMR (400 MHz, CD_2Cl_2) δ 9.10 (dt, *J* = 5.4, 1.3 Hz, 1H, bpy Ar-*H*), 8.78 (dd, *J* = 5.2, 1.7 Hz, 1H, bpy Ar-*H*), 8.13 – 8.10 (m, 2H, bpy Ar-*H*), 7.83 (d, *J* = 7.9 Hz, 1H, bpy Ar-*H*), 7.73 – 7.63 (m, 2H, bpy Ar-*H*), 7.39 (d, *J* = 8.1 Hz, 2H, *p*-Tol Ar-*H*), 7.28 – 7.20 (m, 3H, *p*-Tol Ar-*H* and NAr-*H*), 7.08 – 7.00 (m, 2H, bpy Ar-*H* and NAr-*H*), 6.66 (tt, *J* = 7.4, 1.2 Hz, 1H, NAr-*H*), 6.47 (td, *J* = 7.6, 1.6 Hz, 1H, NAr-*H*), 5.35 (dt, *J* = 8.2, 1.5 Hz, 1H, NAr-*H*), 2.40 (s, 3H, *p*-Tol CH_3), 2.20 – 2.10 (m, 5H, CH_3 and CH_2CH$_3$), 0.82 (t, *J* = 7.5 Hz, 3H, CH$_2$CH_3) ppm.

^{13}C NMR (101 MHz, CD_2Cl_2) δ 177.48, 167.30, 152.96, 152.28, 152.02, 151.54, 150.48, 140.99, 139.17, 139.06, 134.06, 129.27, 128.88, 128.48, 127.78, 126.86, 126.49, 126.03, 125.49, 124.87, 123.11, 121.87, 121.23, 27.10, 21.48, 18.38, 12.48 ppm.

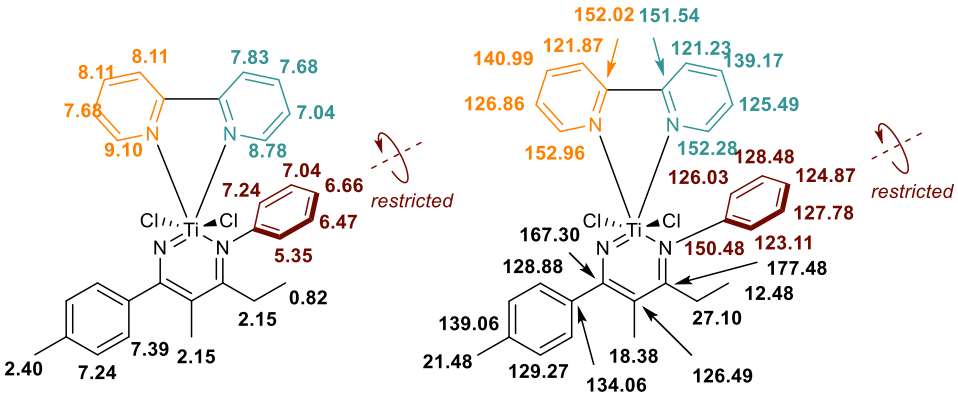

Figure 4.10. ^1H (left) and ^{13}C (right) signal assignments of **4.3**. Colors are labelled for clarity purpose to indicate the ring that the chemical shifts correspond to.

We further sought evidence of the restricted rotation of *N*-phenyl on **4.3** from NOESY NMR spectrometry. As we expected, a through-space interaction between α-H of bpy and 2-H of *N*-phenyl was observed in the NOESY spectrum of **4.3**. In addition, the EXSY signals of the *N*-phenyl on its 2-H vs. 6-H and 3-H vs. 5-H indicate that these hydrogens are in exchange of one another. Together with the distinguishable chemical shift differences of the aforementioned hydrogens, these results provide strong evidence on the restricted rotation of *N*-phenyl.

To our surprise, EXSY signals were also found between the two pyridines of the bpy ligand on the NOESY spectrum of **4.3**, indicating that the bpy can undergo self-exchange between the two pyridines. This shows that bpy is a hemilabile ligand on **4.3**. On the other hand, the differences in ^{1}H and ^{13}C chemical shifts clearly indicates that the two pyridines are chemically inequivalent due to trans effect, which requires a strong coordination to Ti. It can be deduced that the bpy ligand on **4.3** is largely intact on Ti with a weak self-exchange at room temperature, while under elevated temperature the hemilability could be enhanced and eventually lead to the dissociation of the bpy ligand.

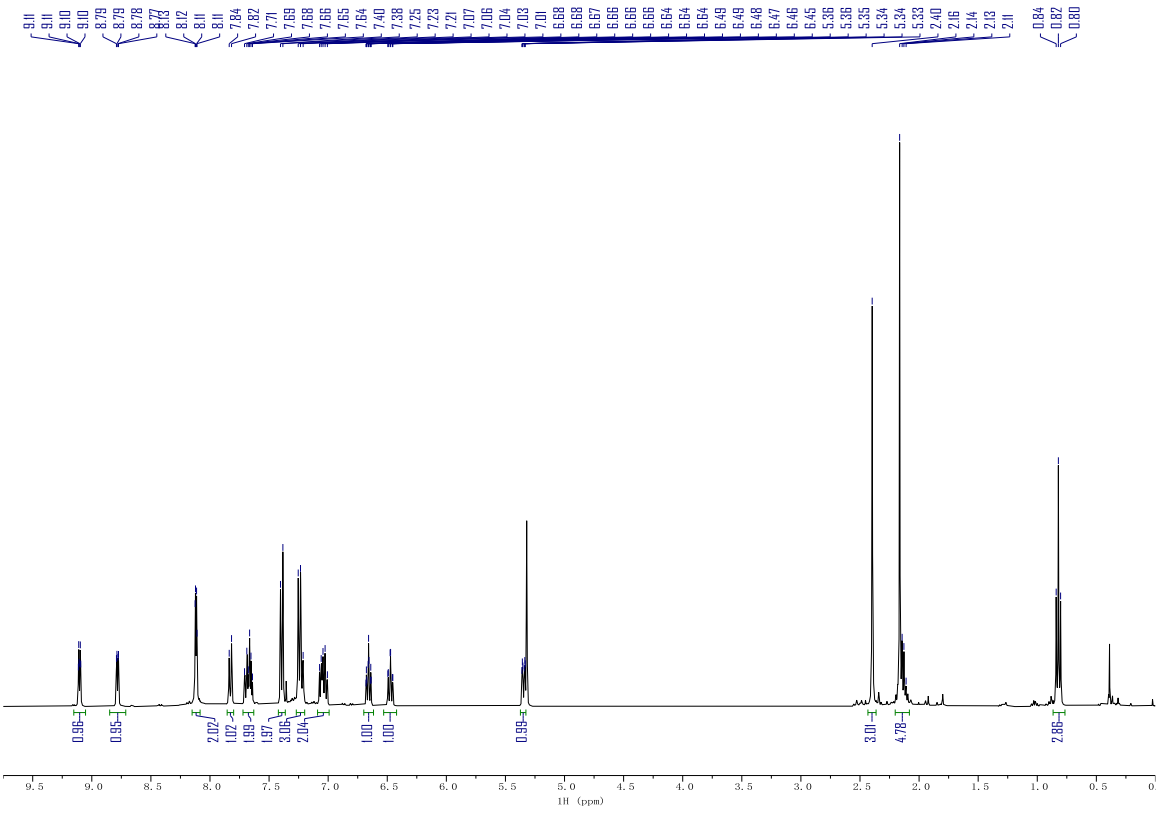

Figure 4.11. ^{1}H NMR spectrum of **4.3** in CD_2Cl_2. *Taken from YC-2021-0017-2-H.*

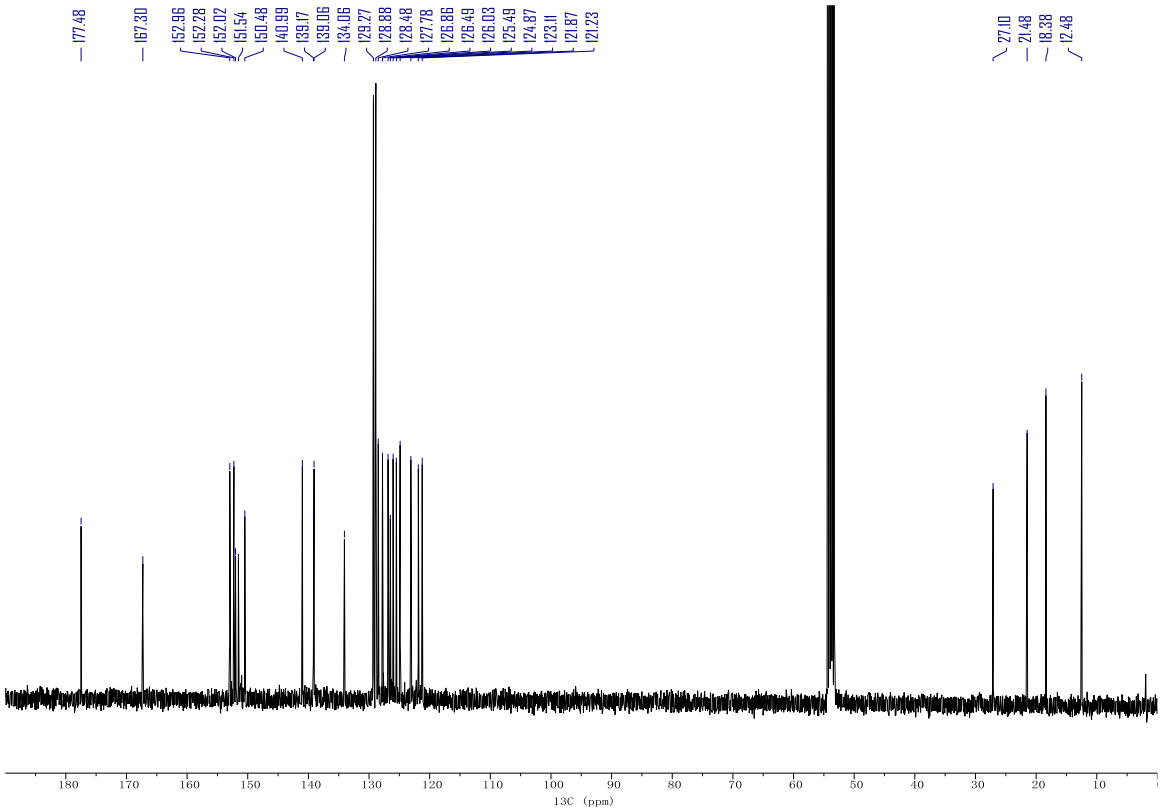

Figure 4.12. $^{13}C\{^{1}H\}$ NMR spectrum of **4.3** in CD_2Cl_2. *Taken from YC-2021-0017-2-C.*

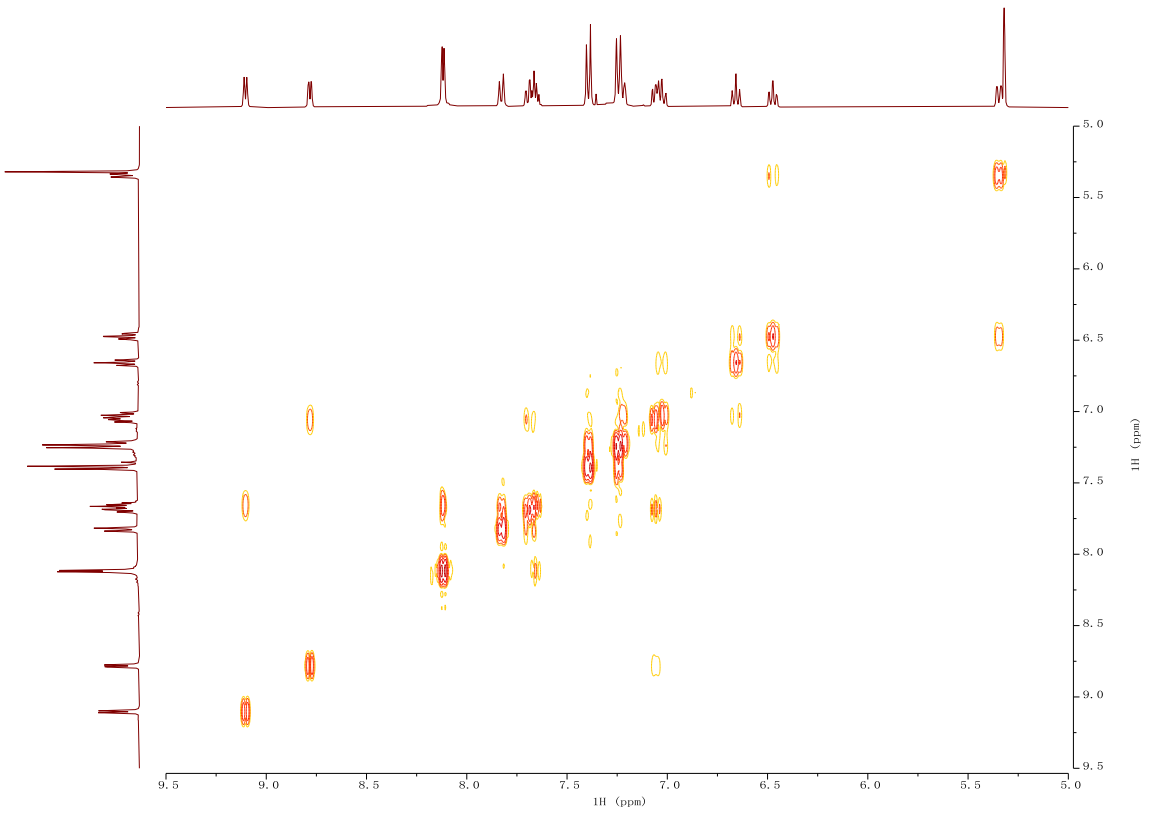

Figure 4.13. ^{1}H COSY NMR spectrum of **4.3** in CD_2Cl_2. *Taken from YC-2021-0017-2-COSY.*

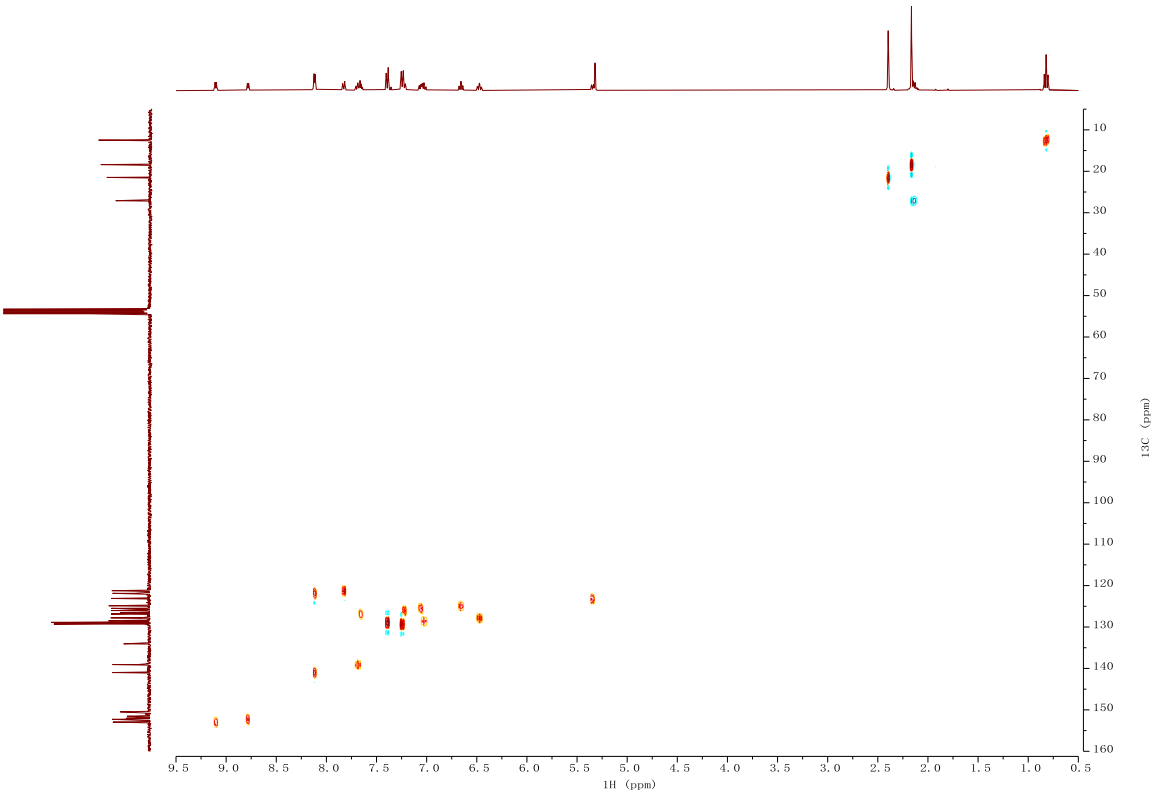

Figure 4.14. ^{1}H-^{13}C HSQC NMR spectrum of **4.3** in CD_2Cl_2. *Taken from YC-2021-0017-2-HSQC-2.*

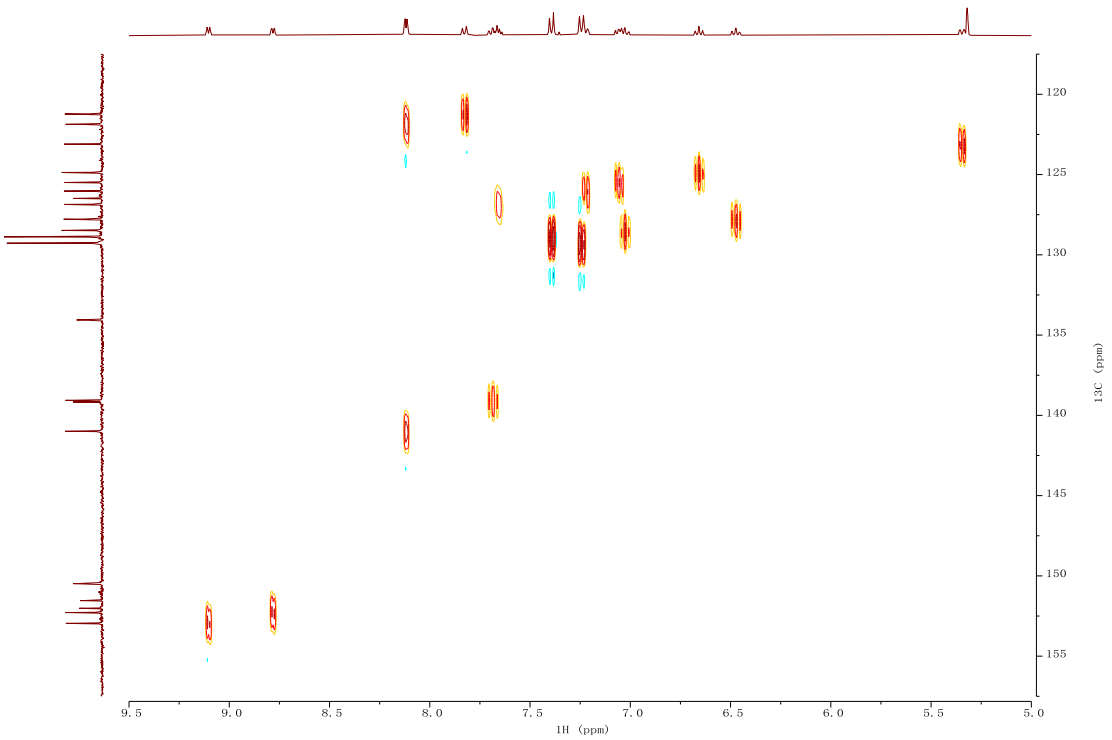

Figure 4.15. Aromatic region of ^{1}H-^{13}C HSQC NMR spectrum of **4.3** in CD_2Cl_2. *Taken from YC-2021-0017-2-HSQC-2.*

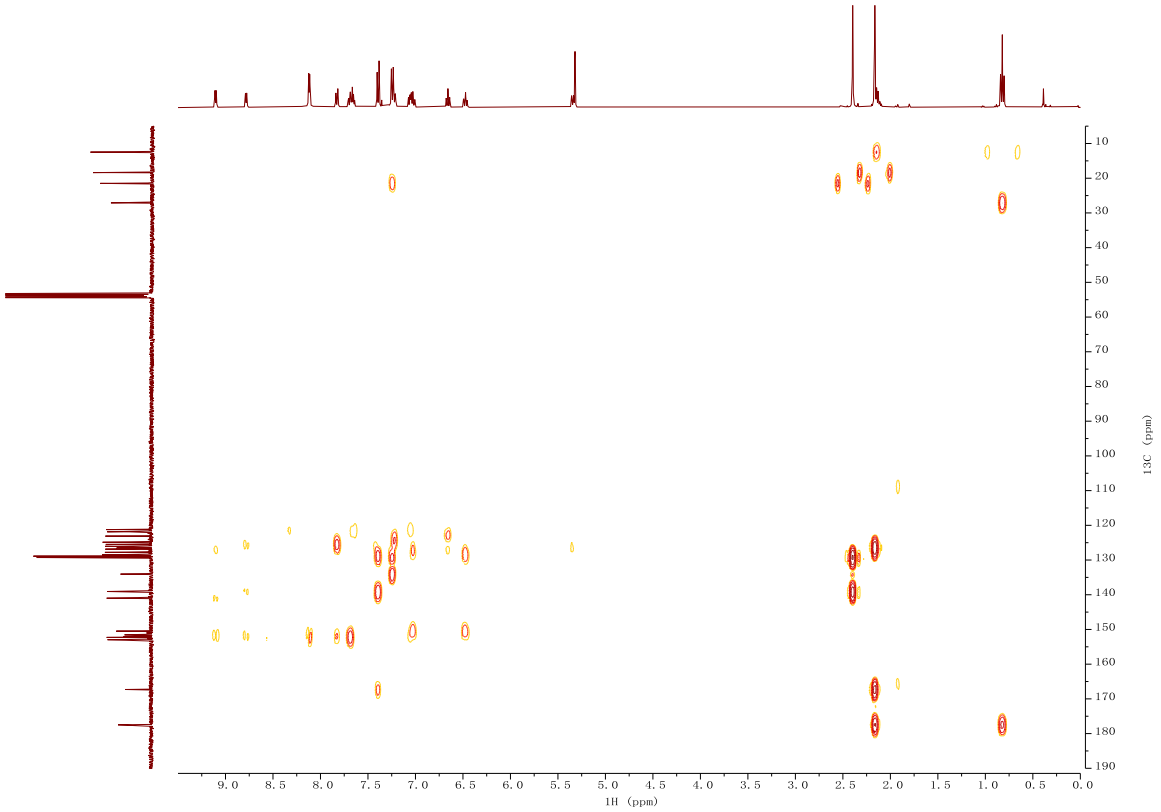

Figure 4.16. ^{1}H-^{13}C HMBC NMR spectrum of **4.3** in CD_2Cl_2. *Taken from YC-2021-0017-2-HMBC.*

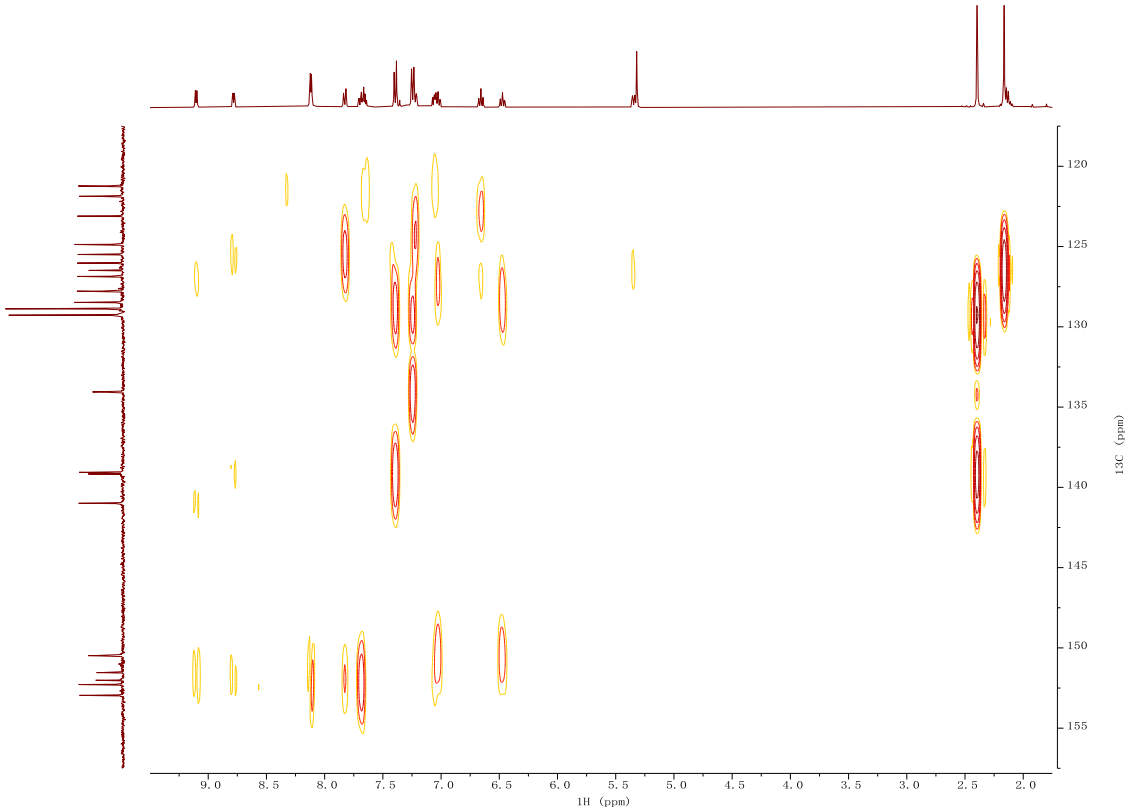

Figure 4.17. ^{13}C downfield region of ^{1}H-^{13}C HMBC NMR spectrum of **4.3** in CD_2Cl_2. *Taken from YC-2021-0017-2-HMBC.*

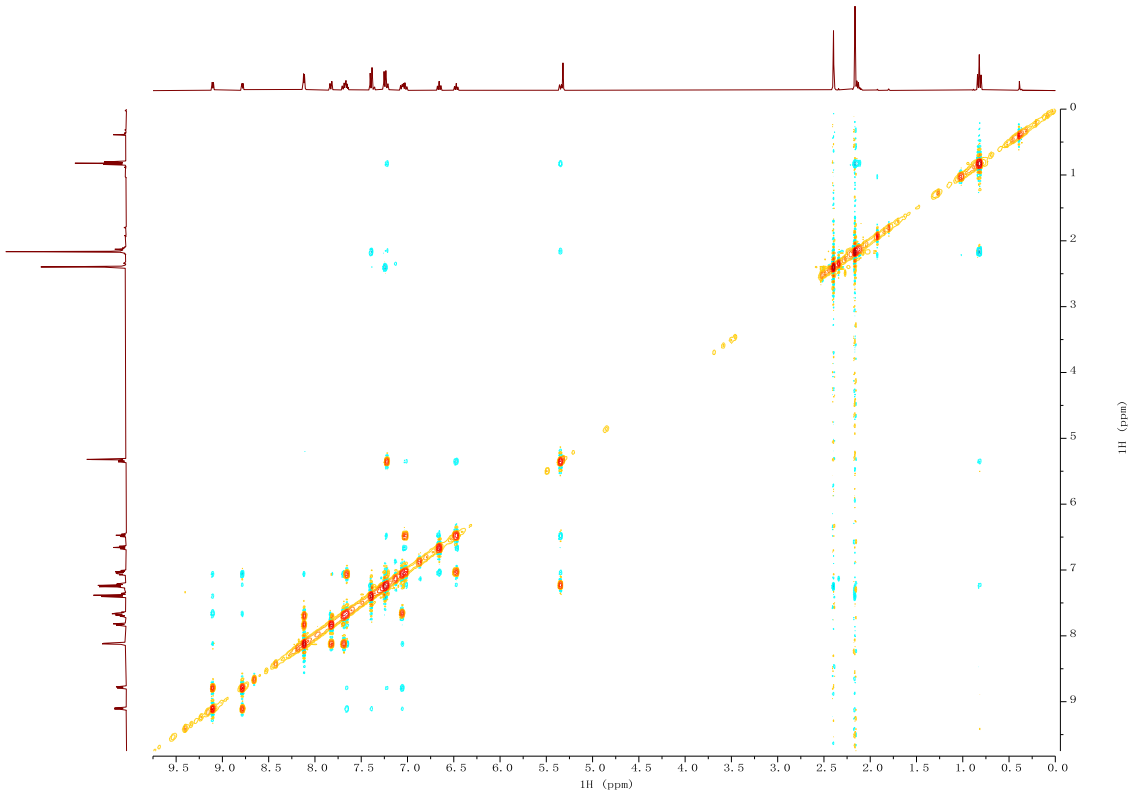

Figure 4.18. NOESY NMR spectrum of **4.3** in CD_2Cl_2 (full spectrum). *Taken from YC-2021-0017-3-NOESY.*

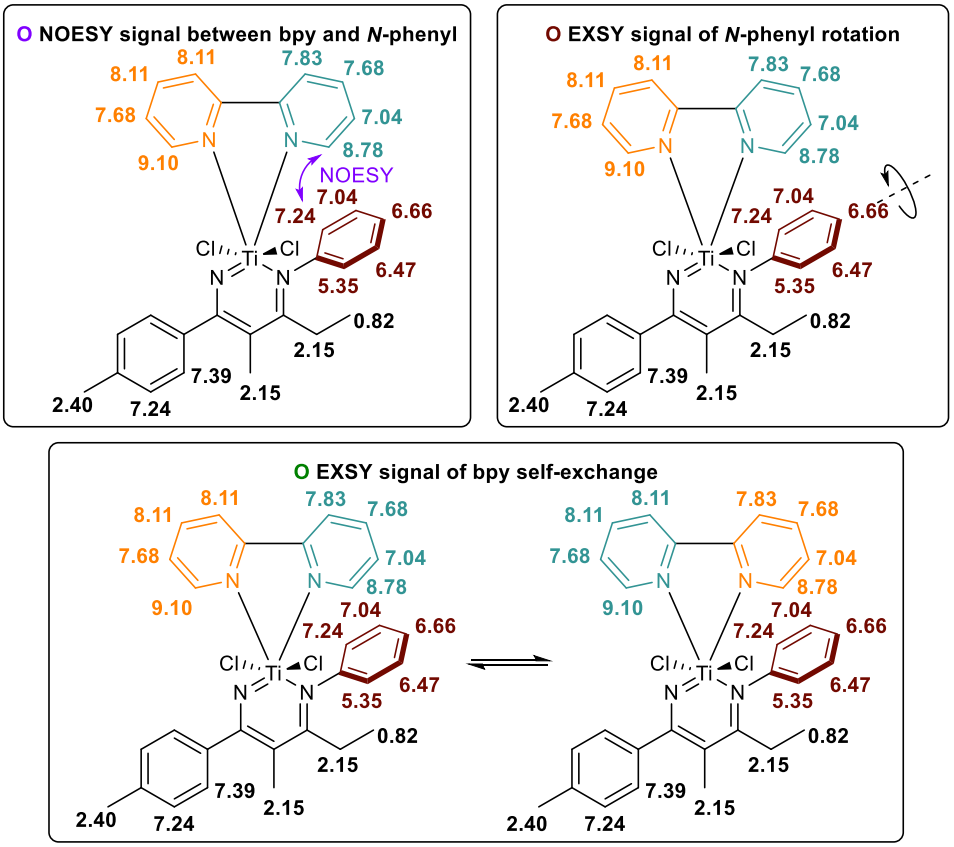
O NOESY signal between bpy and N-phenyl
8.11
8.11
7.83
7.68
7.68
7.04
9.10
8.78
NOESY
7.04
7.24
6.66
Cl
Ti
Cl
N
N
6.47
5.35
0.82
2.15
7.39
2.15
2.40
7.24
O EXSY signal of N-phenyl rotation
O EXSY signal of bpy self-exchange

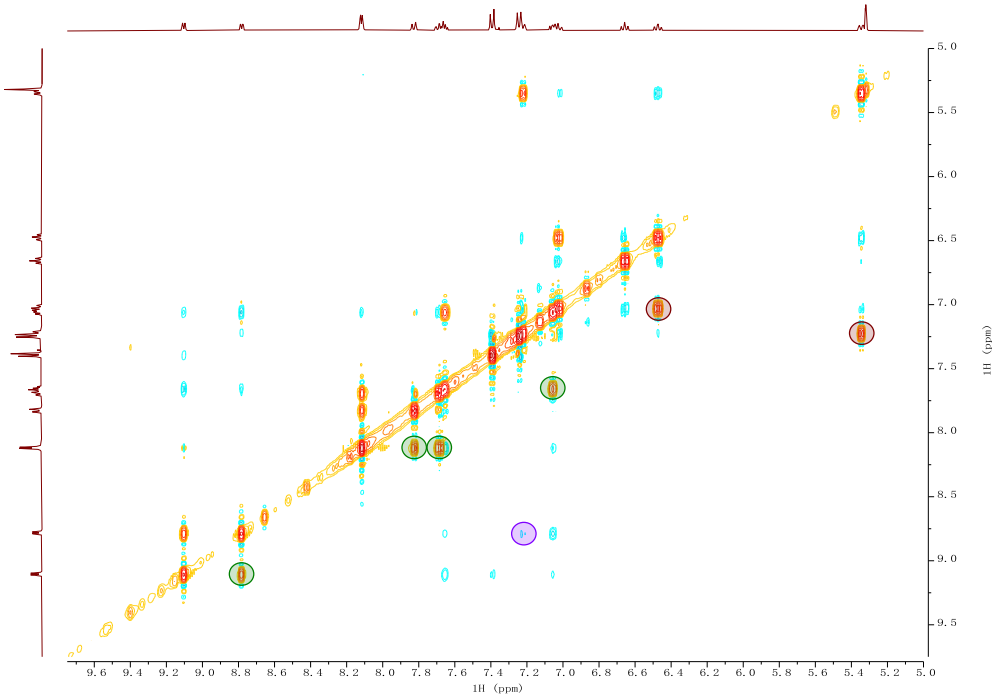
1H (ppm)
1H (ppm)

Figure 4.19. Aromatic region of NOESY NMR spectrum of **4.3** in CD_2Cl_2. Anti-phase NOESY and in-phase EXSY signal are labeled in corresponding colored circles denoting the modes of interaction. Signals on only one side of the diagonal are labeled for clarity purpose. *Taken from YC-2021-0017-3-NOESY.*

4.5.3 Synthesis of 4.4

The original design of the reaction was to use $TiCl_4$ as pyridine abstractor

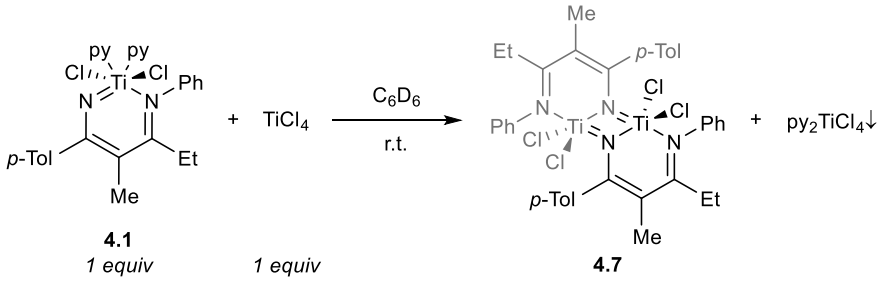

Instead, we observed the oxidation of **4.1** by $TiCl_4$

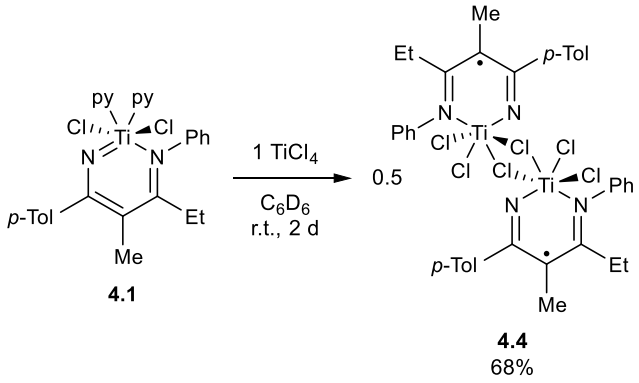

Experimental procedure is described as following. In a 4 mL scintillation vial in the glovebox, a solution of $TiCl_4$ (9.5 mg, 0.050 mmol, 1.0 equiv, measured by mass) in C_6D_6 (1 mL) was dropwise added to a stirring suspension of **4.1** (27.7 mg, 0.050 mmol, 1.0 equiv) in C_6D_6 (1 mL). The suspension immediately turned into a clear deep brown solution. The reaction was stirred at room temperature for 2 days, after which it was filtered through glass fiber filter paper, where the pale yellow precipitate was discarded. The resulting deep brown solution was the C_6D_6 solution of **4.4**.

Attempts to isolate the bulk sample of **4.4** failed as evaporation under vacuum or precipitation from excess pentane both led to decomposition to form intractable yellow mixture. However, small crystals for structure determination *via* XRD was able to be obtained by (a) slow solvent evaporation in loosely capped NMR tubes, or (b) recrystallization through vapor diffusion of pentane into the C_6D_6 solution of **4.4** (though the recrystallization needs to be stopped after a week to prevent the aforementioned precipitation from too high pentane ratio).

In the reactivity and DOSY studies, the C_6D_6 solution of **4.4** was used instead without further purification, whose concentration was determined *via* ^{1}H NMR against HMDSO internal standard (0.004 mmol, added after the filtration of reaction mixture). The reaction yield can be calculated from the concentration as 68% (0.017 mmol). Limited by the sample concentration, ^{13}C NMR signal of quaternary carbons were assigned with the assistance of ^{1}H-^{13}C HSQC and HMBC spectra.

^{1}H NMR (400 MHz, C_6D_6) δ 7.37 (d, *J* = 8.4 Hz, 4H, NAr-*H*), 7.26 (d, *J* = 7.6 Hz, 4H, Ar-*H*), 7.07 (t, *J* = 7.6 Hz, 4H, Ar-*H*), 6.95 (t, *J* = 6.9 Hz, 6H, Ar-*H*), 2.08 (s, 6H, *p*-Tol C*H*$_3$), 1.96 (q, *J* = 7.6 Hz, 4H, C*H*$_2$CH$_3$), 1.68 (s, 6H, C*H*$_3$), 0.67 (t, *J* = 7.5 Hz, 6H, CH$_2$C*H*$_3$) ppm.

^{13}C NMR (101 MHz, C_6D_6) δ 179.18, 166.08, 149.11, 139.07, 134.88, 129.64, 129.33, 128.87, 126.73, 126.27, 111.53, 27.54, 21.39, 17.06, 12.29 ppm.

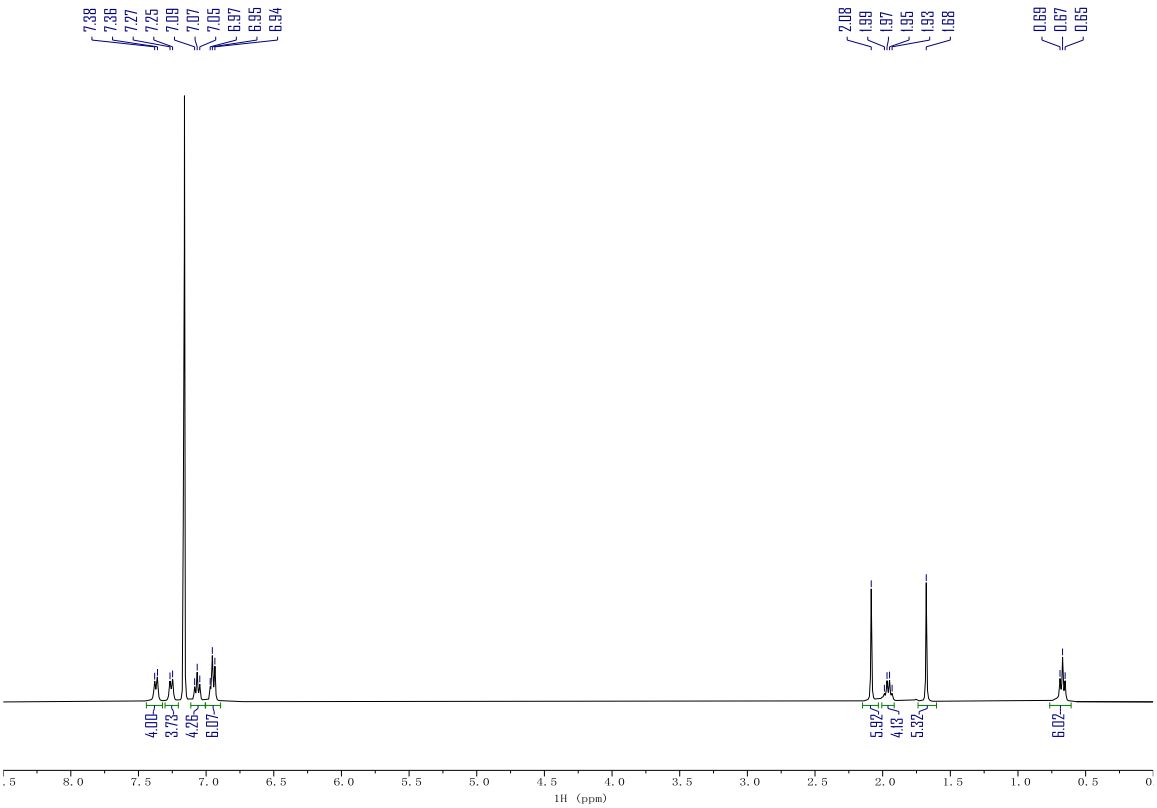

Figure 4.20. ^{1}H NMR spectrum of **4.4** in C_6D_6. *Taken from YC-2021-0224-2-H.*

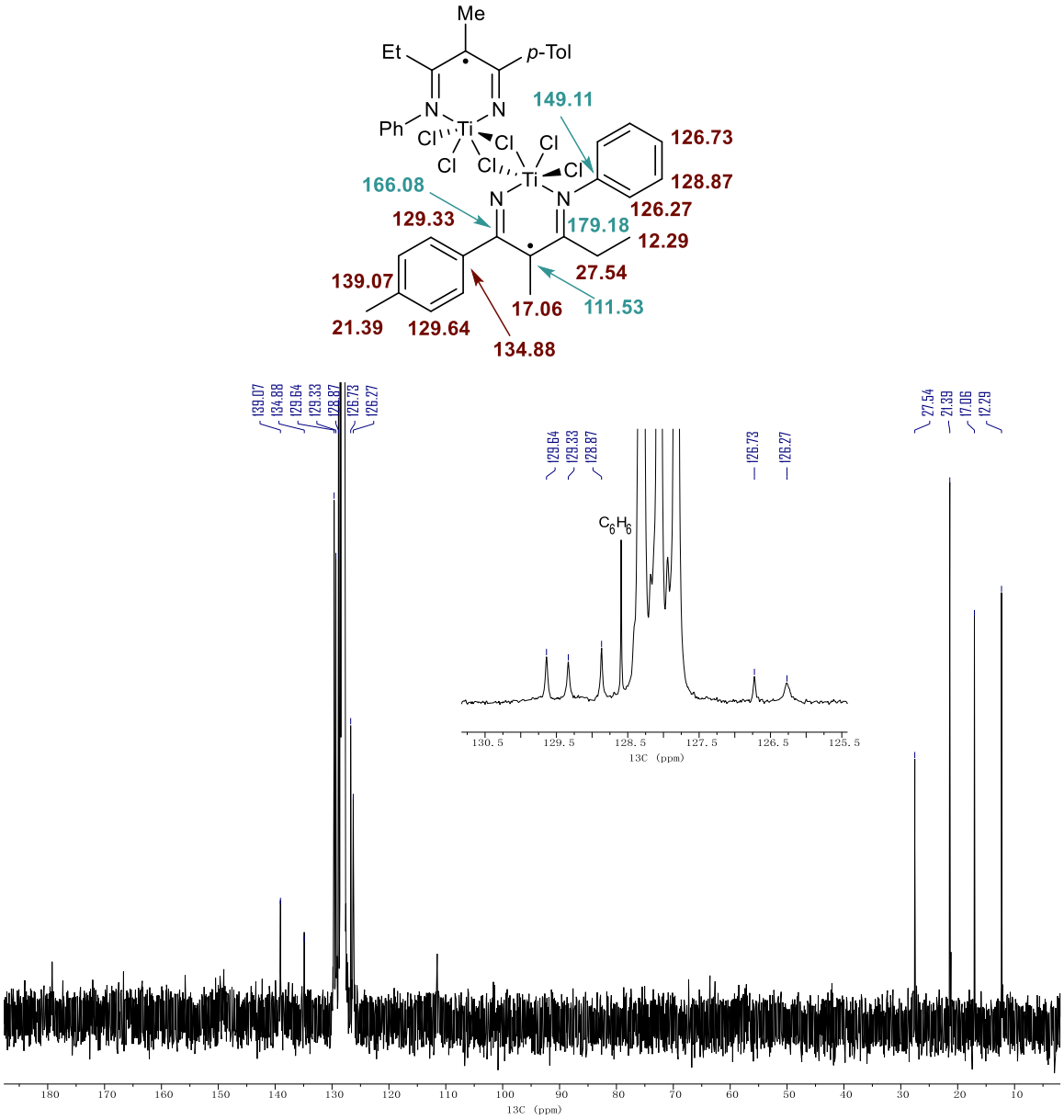

Figure 4.21. $^{13}C\{^{1}H\}$ NMR spectrum of **4.4** in C_6D_6 and signal assignments. Signals in maroon were observed in $^{13}C\{^{1}H\}$ NMR spectrum, while signals in teal were determined *via* ^{1}H-^{13}C HMBC spectrum (Figure 4.23). *Taken from YC-2021-0240-C.*

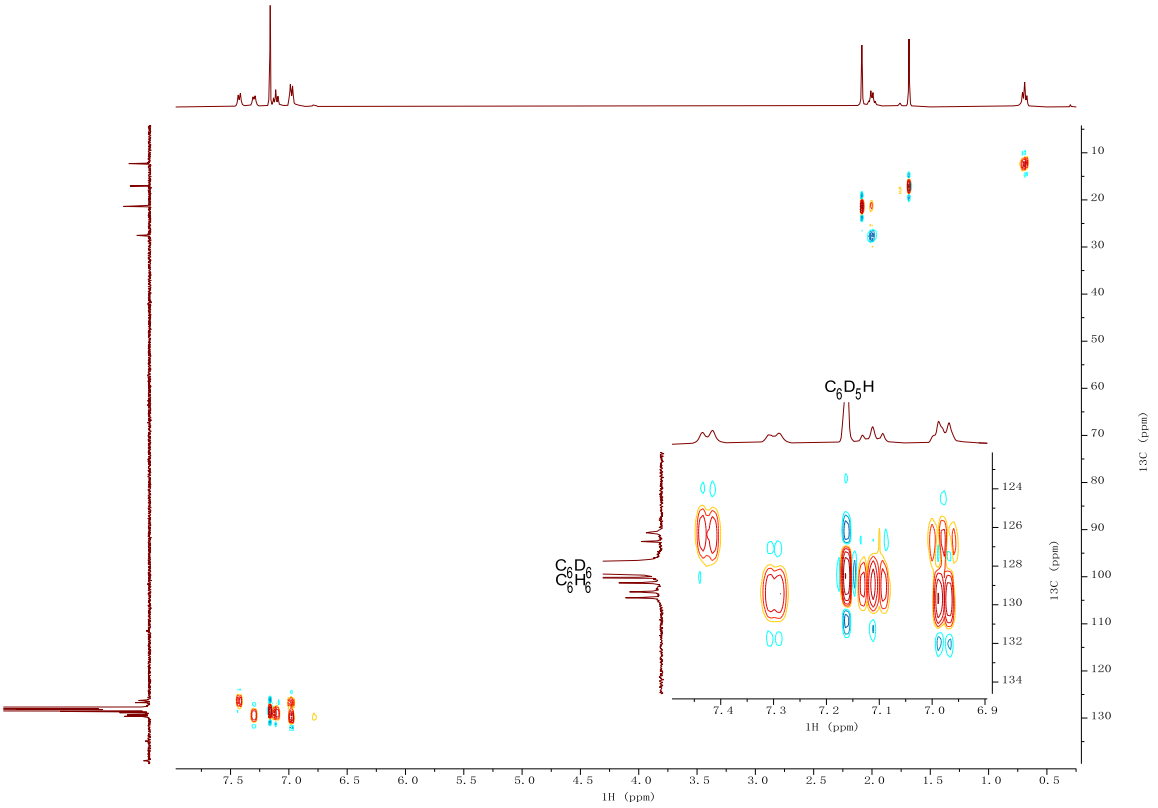

Figure 4.22. ^{1}H-^{13}C HSQC NMR spectrum of **4.4** in C_6D_6. *Taken from YC-2021-0240-HSQC.*

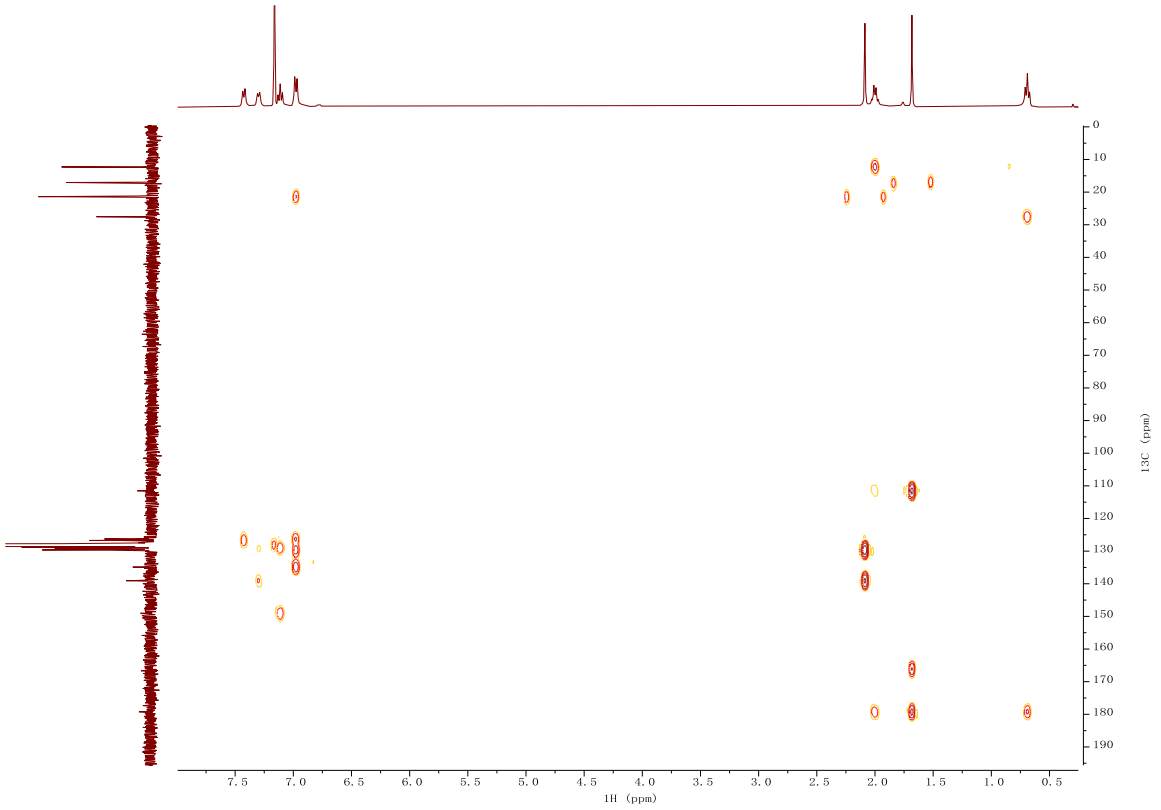

Figure 4.23. ^{1}H-^{13}C HMBC NMR spectrum of **4.4** in C_6D_6. *Taken from YC-2021-0240-HMBC.*

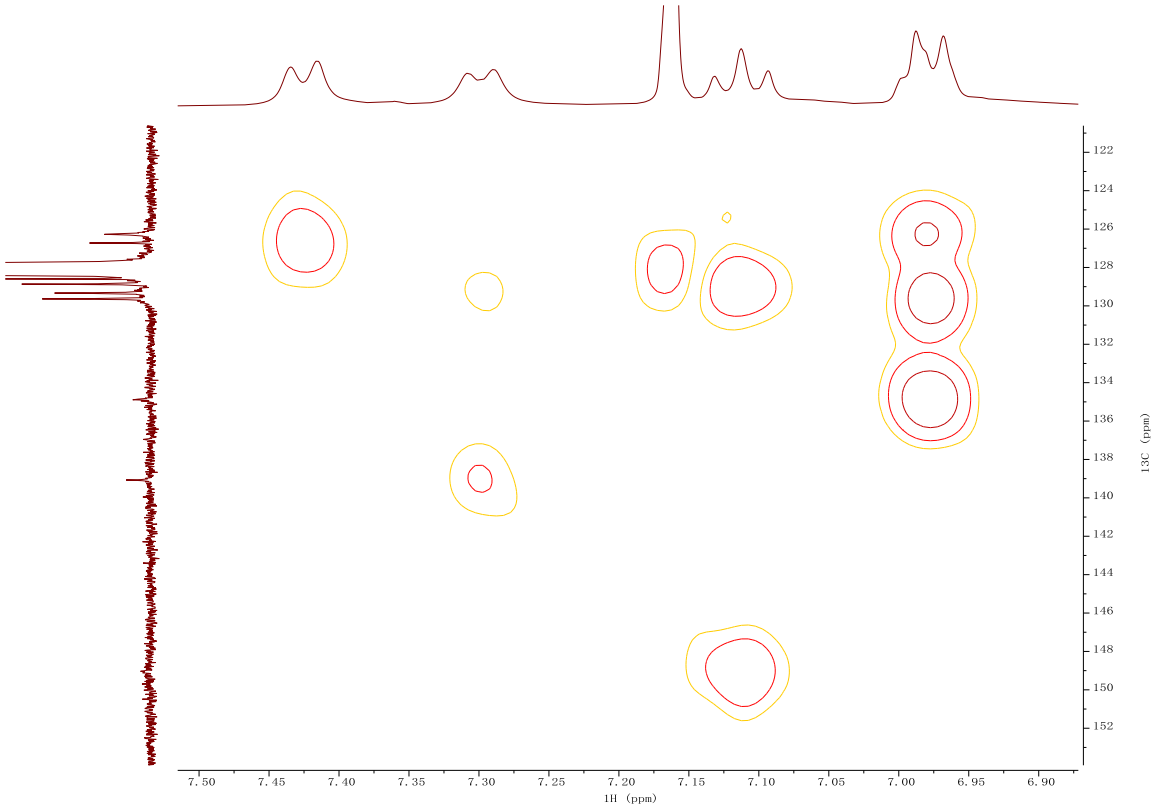

Figure 4.24. Aromatic region of ^{1}H-^{13}C HMBC NMR spectrum of **4.4** in C_6D_6. *Taken from YC-2021-0240-HMBC.*

4.5.4 Synthesis of $(PPN)_2CeCl_6$

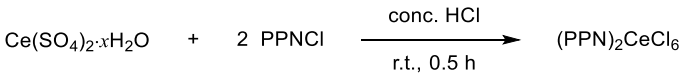

$(PPN)_2CeCl_6$ was synthesized following a modified reported procedure.[211] PPNCl (3.444 g, 6 mmol), $Ce(SO_4)_2{\cdot}xH_2O$ (1.000 g, 3 mmol), cold concentrated HCl (3 mL ,12 M) and a stir bar were added to an 25 mL Erlenmeyer flask. The reaction mixture was stirred for 5 minutes before the addition of a second aliquot of PPNCl (0.034 g, 0.06 mmol) in concentrated HCl (2 mL, 12 M). The reaction mixture was then stirred in an ice/water bath for 30 minutes. The yellowish orange precipitate was filtered, washed with acetone (3 x 3 mL), and dried under vacuum to give the crude $(PPN)_2CeCl_6$ product. Bulk $(PPN)_2CeCl_6$ (orange flake crystals, 0.400 g, 0.28 mmol, 9%) was obtained from recrystallization by re-dissolving the crude $(PPN)_2CeCl_6$ in minimum volume of hot acetonitrile and filtered. More $(PPN)_2CeCl_6$ can be

obtained from further recrystallization. Yellowish orange single crystals for XRD analysis were obtained by vapor diffusion of Et_2O into an acetonitrile solution of the crude $(PPN)_2CeCl_6$.

^{1}H NMR (400 MHz, CD_3CN) δ 7.67 (tq, J = 7.3, 1.5 Hz, 12H, Ar-H_{para}), 7.58 (ddt, J = 13.2, 6.9, 1.4 Hz, 24H, Ar-H_{ortho}), 7.52 – 7.43 (m, 24H, Ar-H_{meta}) ppm.

^{13}C{^{1}H} NMR (101 MHz, CD_3CN) δ 134.57 (t, J_{CP} = 1.5 Hz, C_{para}), 133.36 – 133.06 (m, C_{ortho}), 130.56 – 130.12 (m, C_{meta}), 128.18 (dd, J_{CP} = 107.8, 1.9 Hz, C_{ipso}) ppm.

^{31}P{^{1}H} NMR (162 MHz, CD_3CN) δ 20.78 ppm.

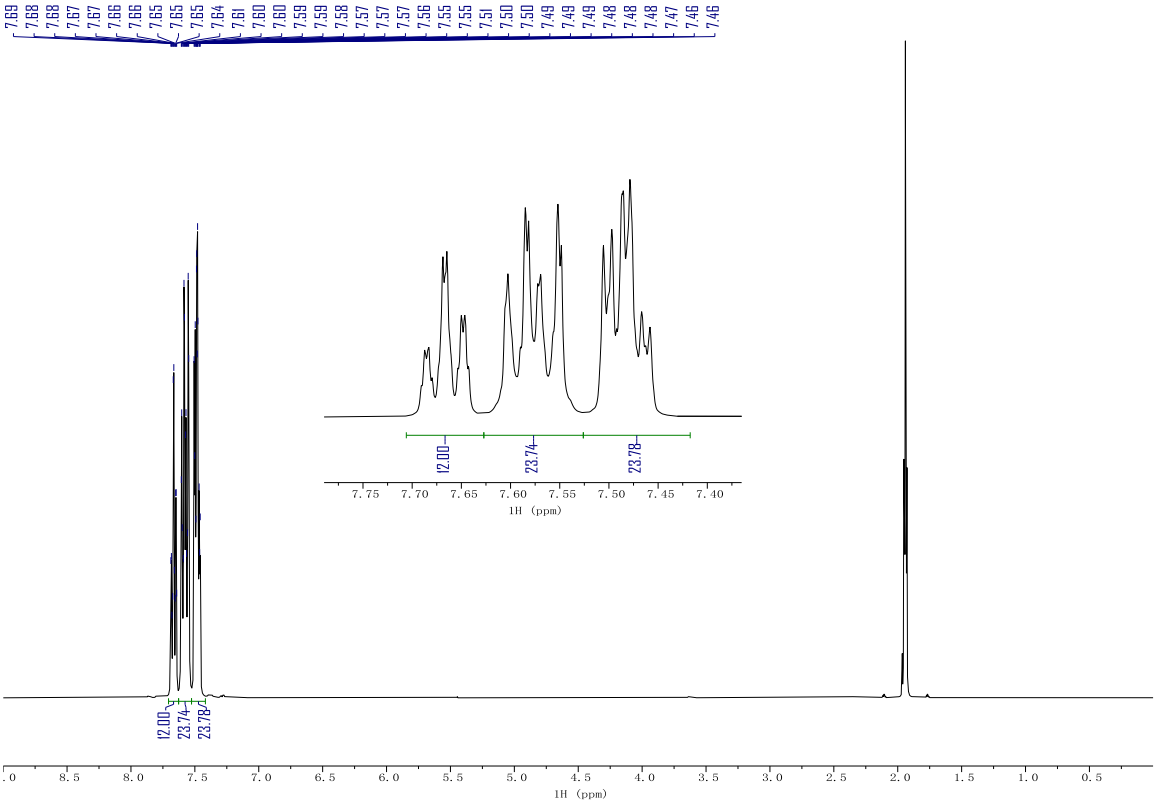

Figure 4.25. ^{1}H NMR spectrum of $(PPN)_2CeCl_6$ in CD_3CN. *Taken from YC-2022-0050-H.*

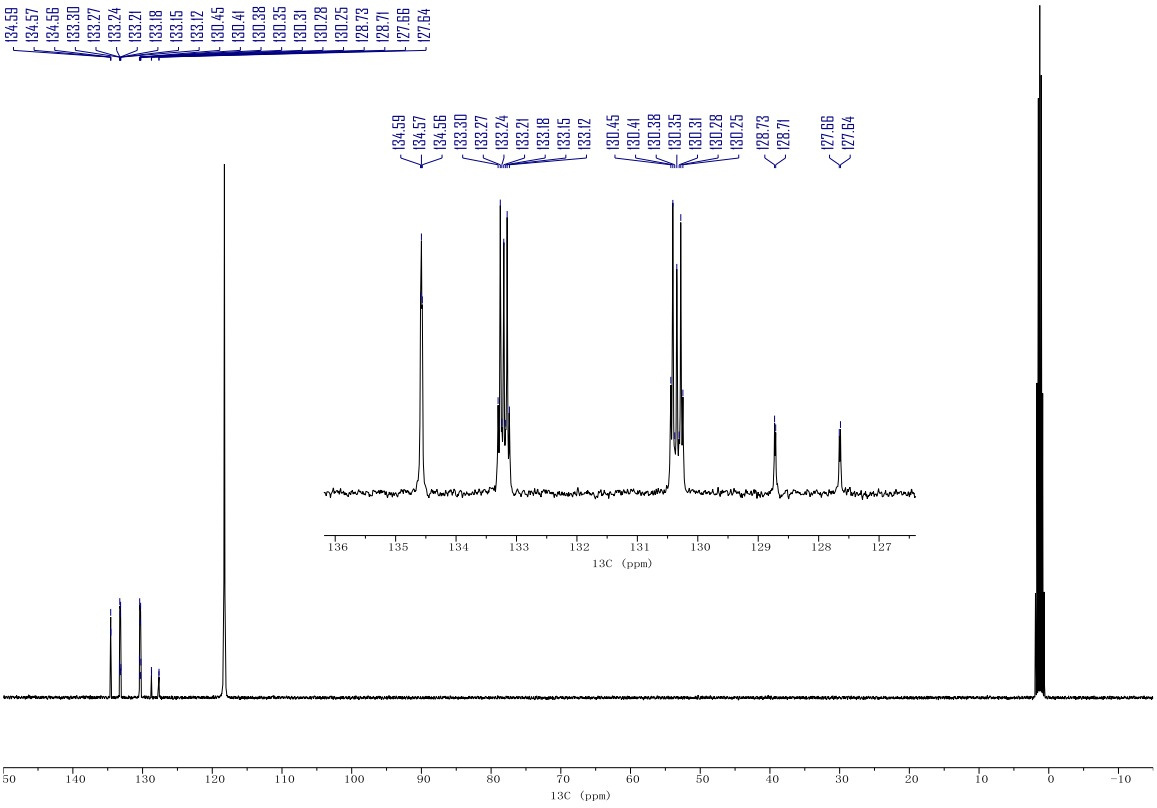

Figure 4.26. $^{13}C\{^{1}H\}$ NMR spectrum of $(PPN)_2CeCl_6$ in CD_3CN. *Taken from YC-2022-0050-C.*

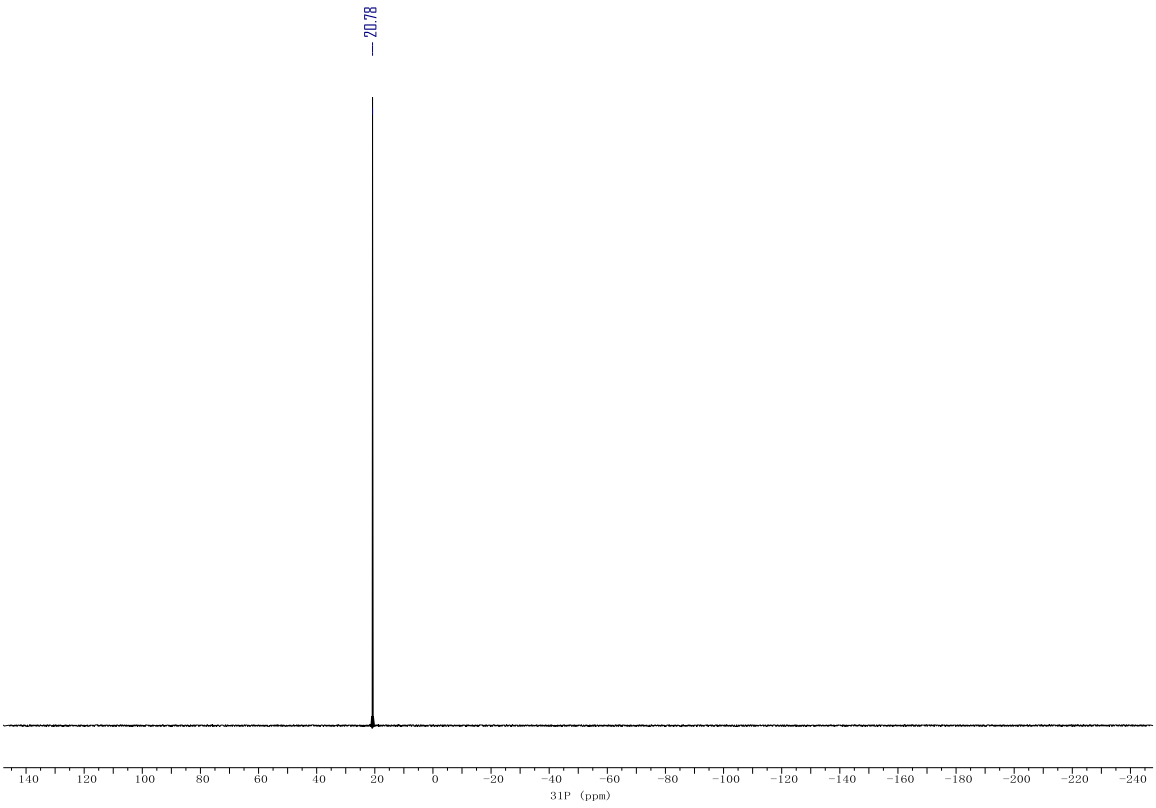

Figure 4.27. $^{31}P\{^{1}H\}$ NMR spectrum of $(PPN)_2CeCl_6$ in CD_3CN. *Taken from YC-2022-0050-P.*

4.5.5 TEMPO Oxidation of 4.1

Table 4.2. TEMPO oxidation of **4.1** under various conditions. Extended time reaction conditions and yields are noted in parentheses.

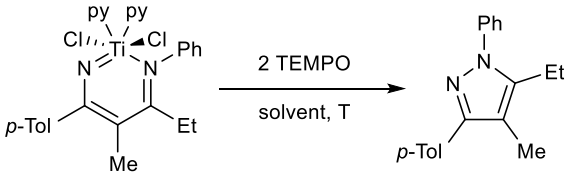

4.1 **4.2**

entry	solvent	T (℃)	time (h)	yield (%)	comments	Exp # (YC-)
1	C_6D_6	50	2	92	Control reaction of TEMPO oxidation of **4.3**	2021-0023
2	C_6D_6	35	5 (22)	61 (76)	Figure 4.2	2021-0236

3	C_6D_6	r.t.	2	29	Control reaction of TEMPO oxidation of **4.4**	2021-0023
4	CD_2Cl_2	50	5 (22)	77 (82)	Control reaction of TEMPO oxidation of **4.3**	2021-0237
5	1,2-DCA	50	2	99	Control reaction of TEMPO oxidation of **4.3**	2021-0025

4.1 (5.5 mg, 0.01 mmol, 1.0 equiv), TEMPO (3.1 mg, 0.02 mmol, 2.0 equiv), internal standard (entries 1, 3, 5: TMB, 5.0 mg, 0.03 mmol; entries 2, 4: HMDSO, 0.008 mmol, in 0.01 mL stock solution in C_6D_6), and 0.5 mL solvent were added to an NMR tube in the glovebox. The NMR tube was capped and placed in the oil bath at corresponding temperature. ^{1}H NMR spectra were collected before and after the reaction. The reaction product **4.2** matched up with the reported chemical shifts.[61] The reaction yields were determined *via* ^{1}H NMR against the internal standard.

Example NMR spectra are listed below.

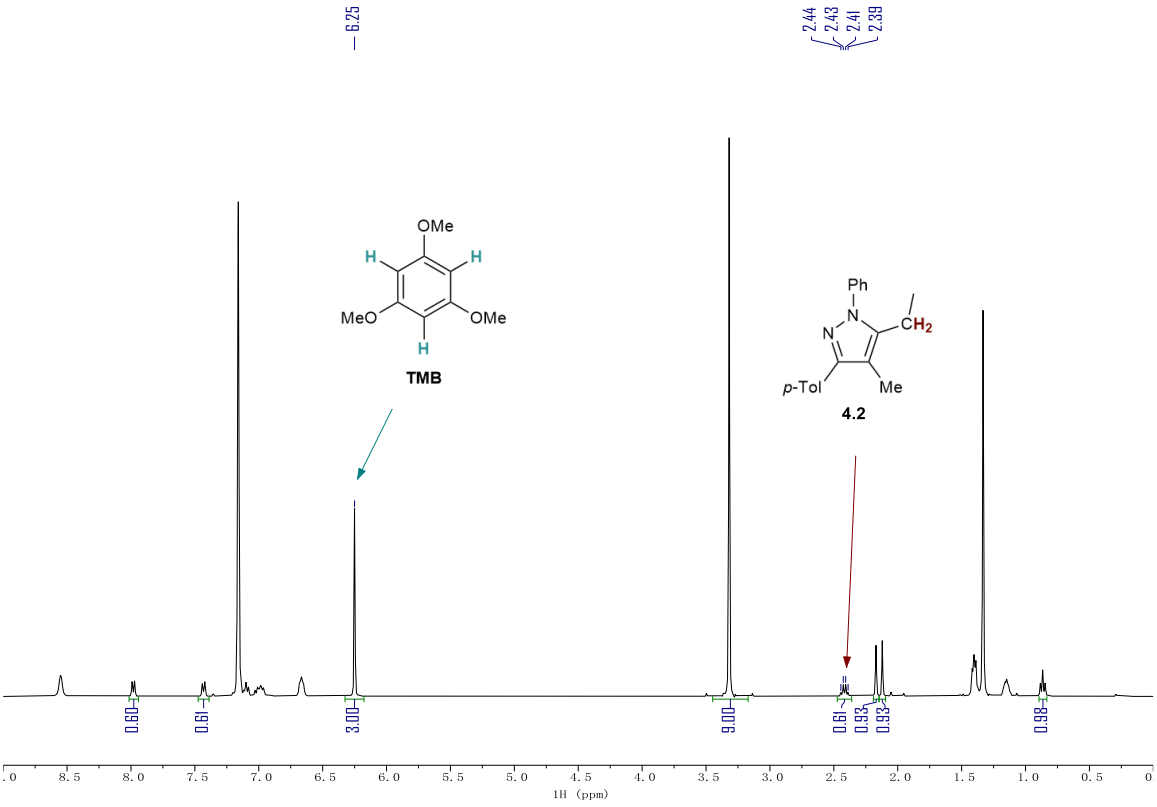

Figure 4.28. Time = 2 hours ^{1}H NMR spectrum of TEMPO oxidation of **4.1** in C_6D_6 at 50 ℃ (Table 4.2 entry 1). Peaks for yield calculation are labelled with chemical shifts and structural assignments. *Taken from YC-2021-0023.*

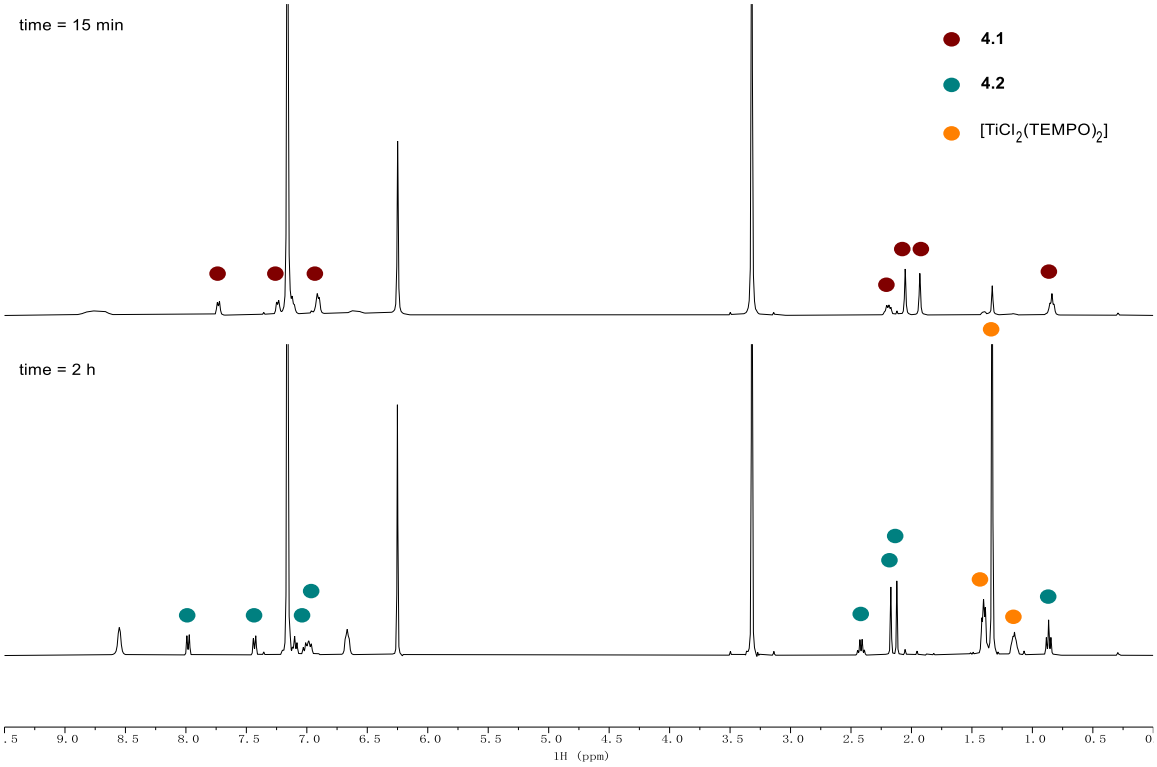

Figure 4.29. Stacked ^{1}H NMR spectra of TEMPO oxidation of **4.1** in C_6D_6 at 50 ℃ (Table 4.2 entry 1). Top: time = 15 minutes. Bottom: time = 2 hours. *Taken from YC-2021-0023.*

4.5.6 TEMPO Oxidation of 4.3

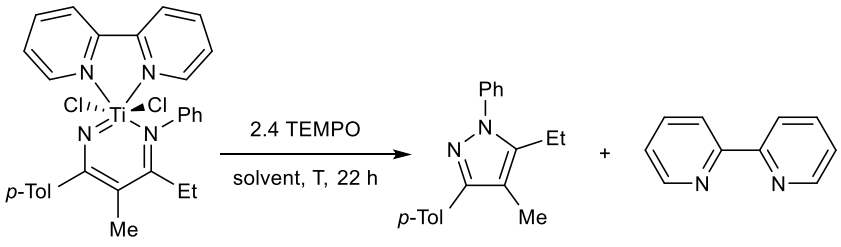

4.3 **4.2**

solvent = CH_2Cl_2, T = 50 °C — no reaction — 0%

1,2-DCA 90 °C — 37% — 54%

4.3 (5.5 mg, 0.01 mmol, 1.0 equiv), TEMPO (3.7 mg, 0.024 mmol, 2.4 equiv), TMB (5.0 mg, 0.03 mmol, internal standard), and 0.5 mL solvent (CH_2Cl_2 or 1,2-DCA) were added to an NMR tube in the glovebox. The NMR tube was capped and placed in the oil bath at corresponding temperature (50 ℃ or 90 ℃) for 22 hours. ^{1}H NMR spectra were collected before and after the reaction. The reaction yields were determined *via* No-D ^{1}H NMR against the internal standard TMB.

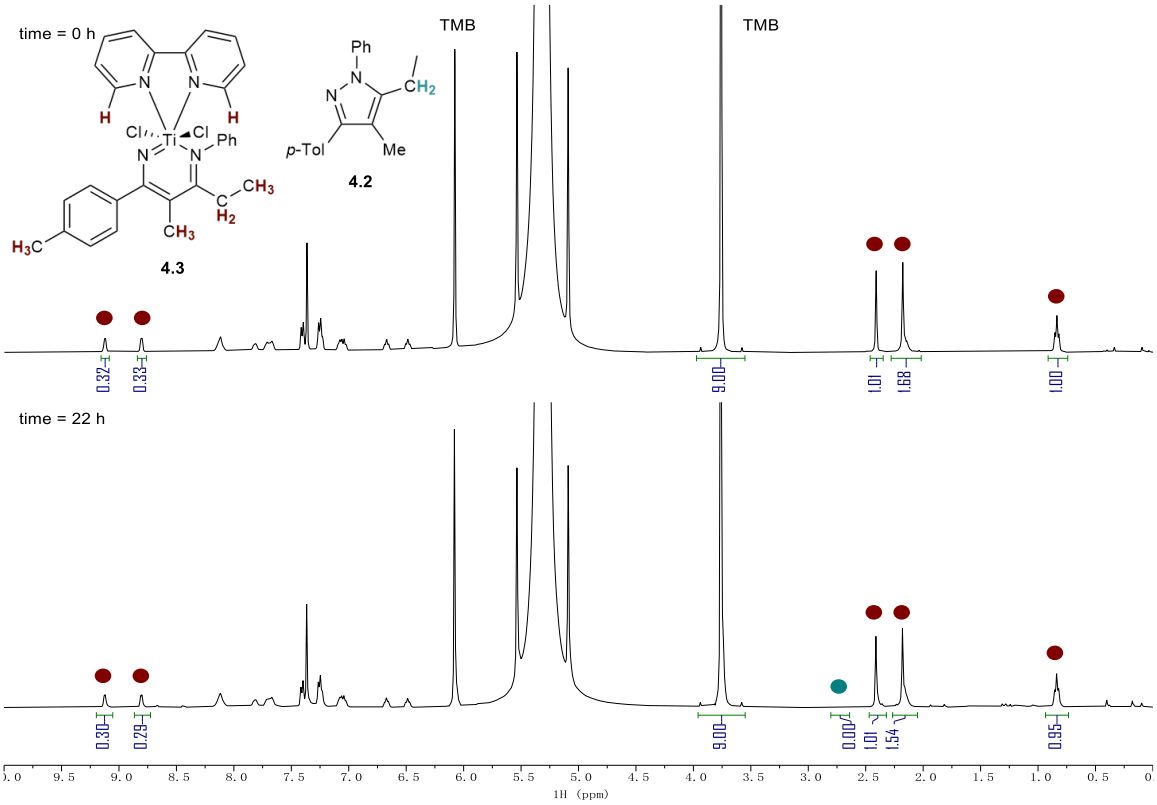

Figure 4.30. Stacked No-D ^{1}H NMR spectra of TEMPO oxidation of **4.3** in CH_2Cl_2 at 50℃. *Taken from (top) YC-2021-0019-NoD-DCM-0h-H and (bottom) YC-2021-0019-NoD-DCM-22h-H.*

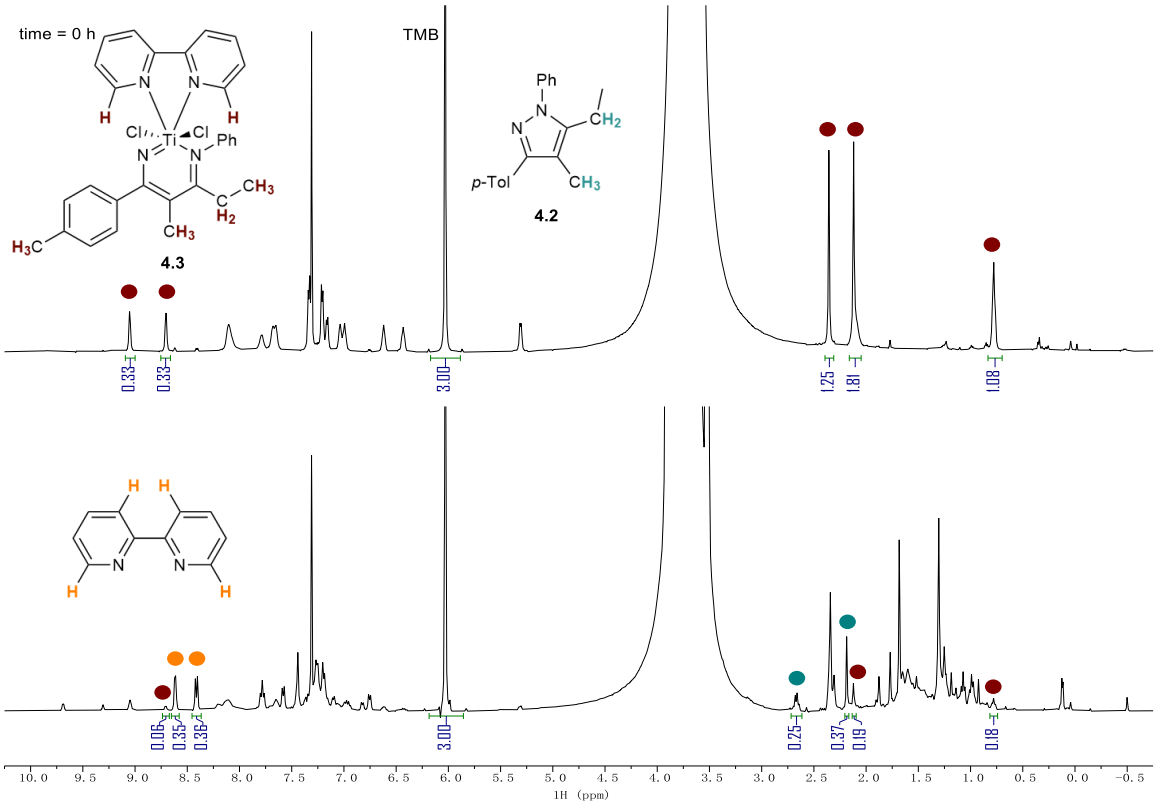

Figure 4.31. Stacked No-D ^{1}H NMR spectra of TEMPO oxidation of **4.3** in 1,2-DCA at 90℃. *Taken from (top) YC-2021-0020-NoD-DCE-0h-H and (bottom) YC-2021-0020-NoD-DCE-22h-H.*

4.5.7 Thermal Decomposition of 4.4

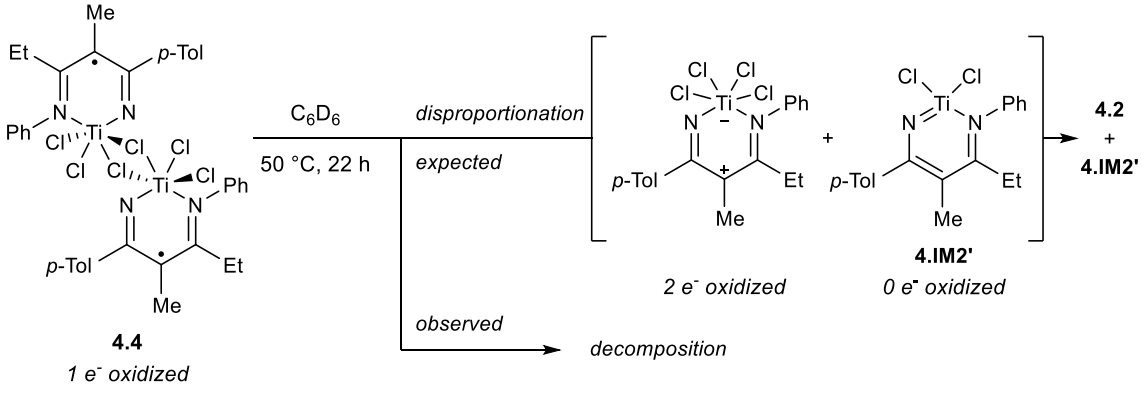

A solution of 0.5 mL C_6D_6 containing **4.4** (0.0034 mmol, determined by ^{1}H NMR against internal standard, 1.0 equiv) and HMDSO (0.008 mmol) was added to an NMR tube in the glovebox. The NMR tube was capped, taken out of the glovebox and heated at 50 ℃ for 22 hours.

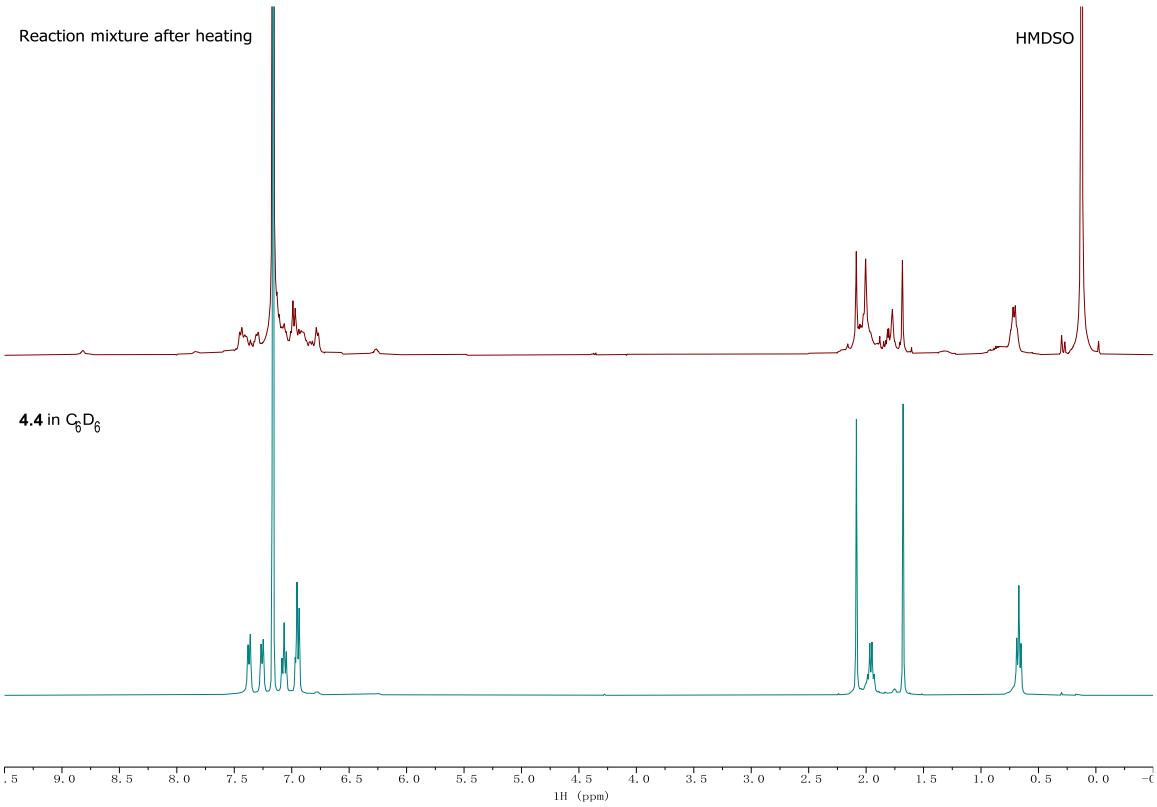

Figure 4.32. (Top) ^{1}H NMR spectrum of the reaction solution of **4.4** in C_6D_6 after heating, and (bottom) ^{1}H NMR spectrum of **4.4** in C_6D_6 as comparison. *Taken from (top) YC-2021-0246-22h and (bottom) YC-2021-0224-2-H.*

4.5.8 TEMPO Oxidation of 4.4

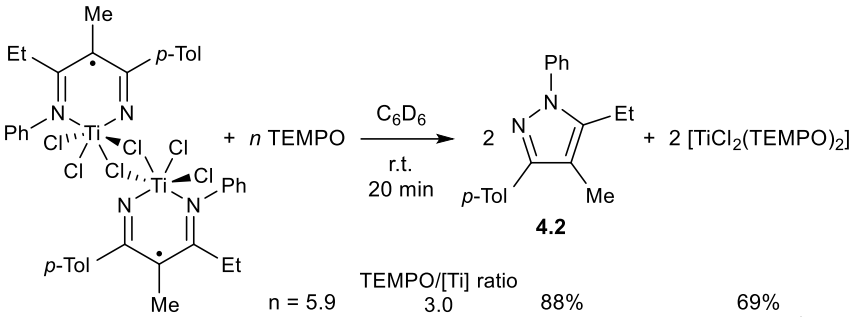

	TEMPO/[Ti] ratio		
n = 5.9	3.0	88%	69%
2.9	1.5	82% (–)	46% (↓)
1.5	0.8	25% (↓)	4% (↓)

TEMPO (0.020 mmol, 0.010 mmol, 0.0050 mmol, respectively) was added to a 0.5 mL C_6D_6 solution containing **4.4** (0.0034 mmol, determined by ^{1}H NMR against internal standard, 1.0 equiv) and HMDSO (0.008 mmol) in an NMR tube in the glovebox. The NMR tube was capped and shaken vigorously to ensure the thorough mixing. ^{1}H NMR was collected at 20 minutes. Due to the rapid reaction, time = 0 NMR was unable to be collected. Time = 30 minutes, 10 h and 20 h NMR spectra were also collected, while only minor changes have been observed. The reaction product **4.2** matched up with the reported chemical shifts.[61] The reaction yields were determined *via* ^{1}H NMR against the internal standard HMDSO.

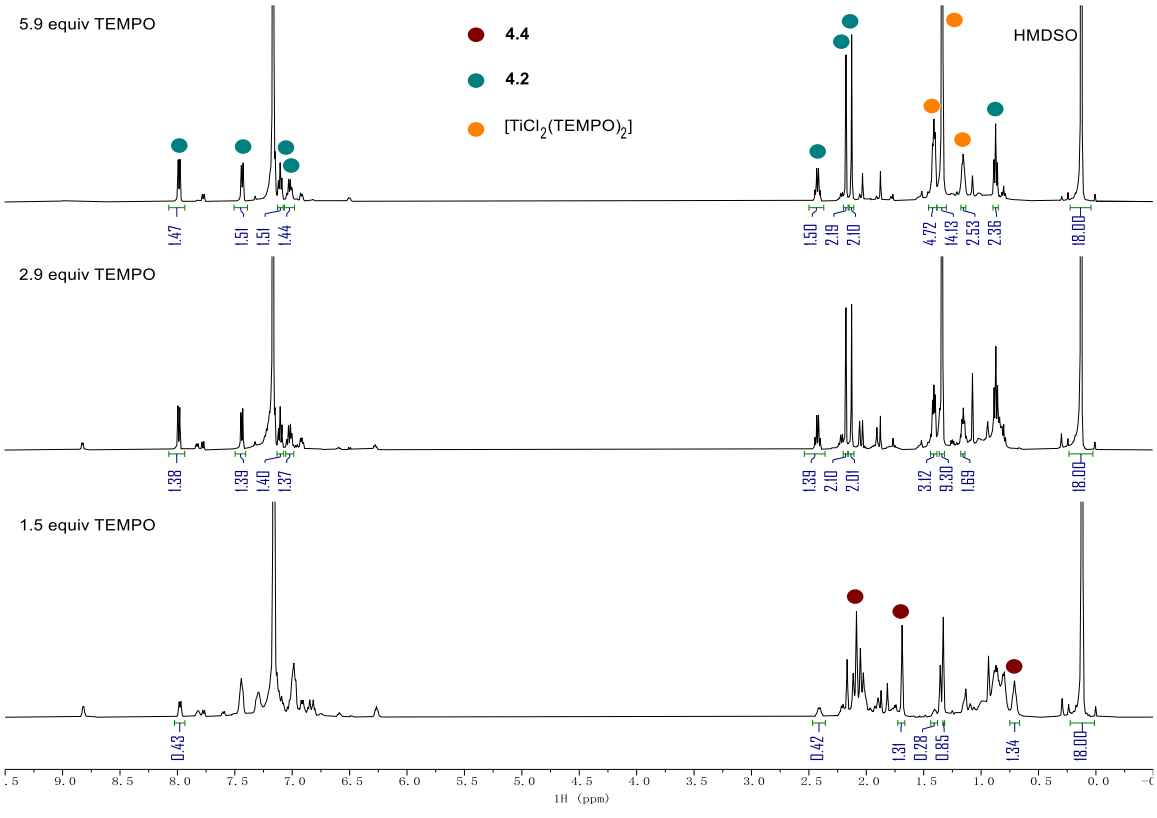

Figure 4.33. Time = 20 minutes stacked ^{1}H NMR spectra of TEMPO oxidation of **4.4** in C_6D_6 with (top) 5.9 equiv, (middle) 2.9 equiv, and (bottom) 1.5 equiv TEMPO. *Taken from (top) YC-2021-0241-2-after TEMPO-20min, (middle) YC-2021-0243-after TEMPO-20min, and (bottom) YC-2021-0244-after TEMPO-20min.*

4.5.9 FcCl Oxidation of 4.1 and 4.3

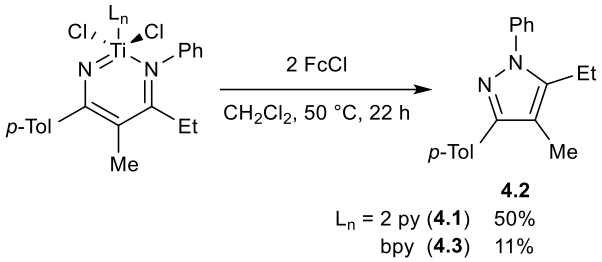

4.1 or **4.3** (0.01 mmol, 1.0 equiv), FcCl (4.4 mg, 0.02 mmol, 2 equiv), 0.5 mL CH_2Cl_2, and a stir bar were added to a 4 mL scintillation vial in the glovebox. The vial was capped and heated at 50℃ for 22 hours. TMB (1.7 mg, 0.01 mmol, internal NMR standard) was added after the reaction mixture cooled down to room temperature and taken out of the glovebox. The reaction yield was determined *via* No-D ^{1}H NMR in CH_2Cl_2 against the internal standard TMB.

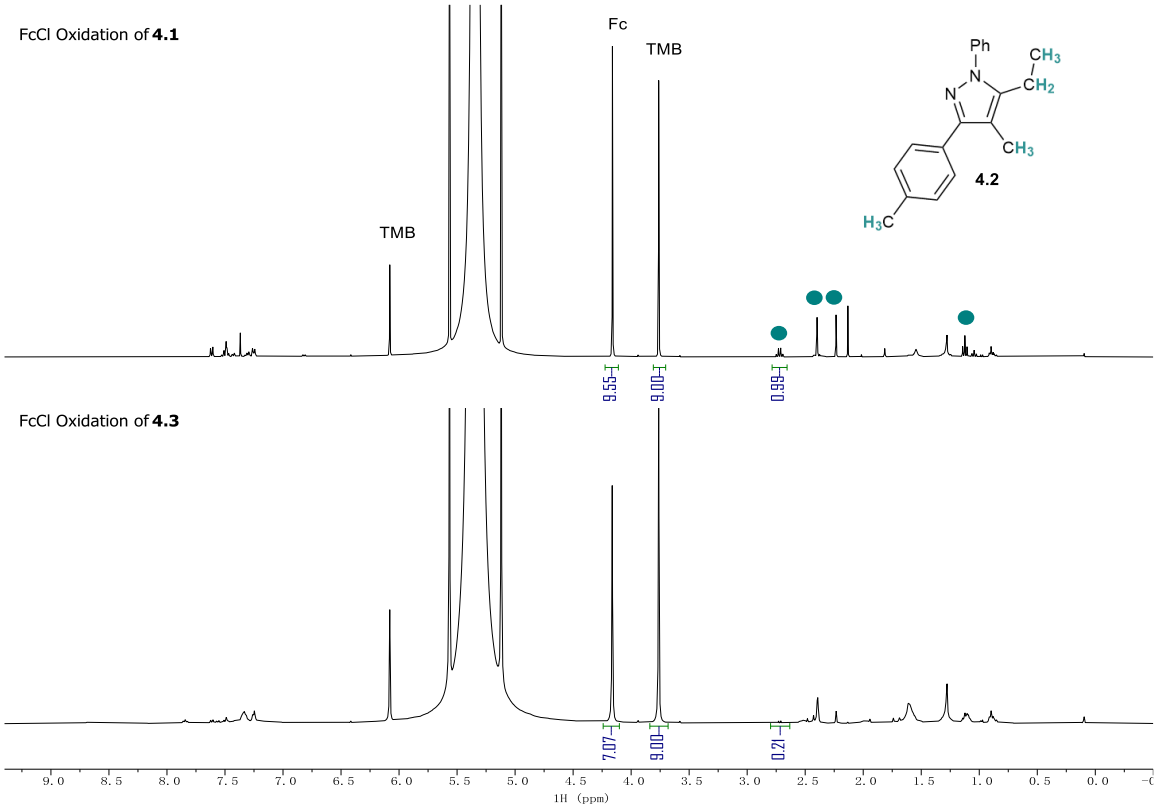

Figure 4.34. Stacked No-D ^{1}H NMR spectra of FcCl oxidation of (top) **4.1** and (bottom) **4.3** in CH_2Cl_2 after the addition of TMB. *Taken from (top) YC-2021-0155-1-NoD-DCM and (bottom) YC-2021-0156-1-NoD-DCM.*

4.5.10 FcBArF Oxidation of 4.1 and 4.3

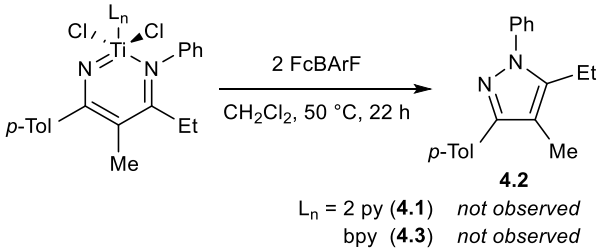

4.1 or **4.3** (0.01 mmol, 1.0 equiv), FcBArF (BArF = tetrakis(3,5-bis(trifluoromethyl)phenyl)borate, 21.0 mg, 0.02 mmol, 2 equiv), 0.5 mL CH_2Cl_2, and a stir bar were added to a 4 mL scintillation vial in the glovebox. The vial was capped and heated at 50℃ for 22 hours. TMB (1.7 mg, 0.01 mmol, internal NMR standard) was added after the

reaction mixture cooled down to room temperature and taken out of the glovebox. The reaction mixture was then extracted between CH_2Cl_2/H_2O. The organic phase was evaporated after being dried over $MgSO_4$. The reaction yield was determined *via* ^1H NMR in C_6D_6 against the internal standard TMB.

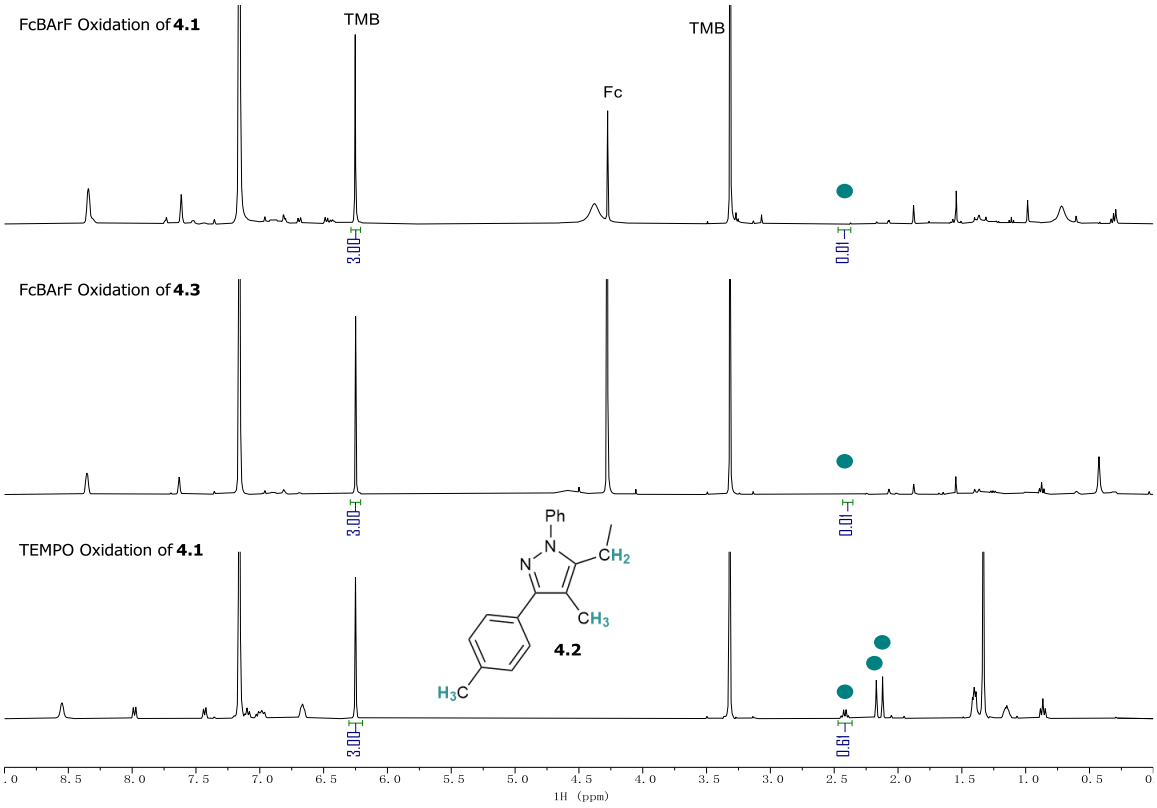

Figure 4.35. Stacked ^1H NMR spectra of FcBArF oxidation of (top) **4.1** and (middle) **4.3** in C_6D_6 after aqueous workup, and (bottom) TEMPO oxidation of **4.1** (Table 4.2 entry 1) in C_6D_6 as a comparison. *Taken form (top) YC-2021-0164-1, (middle) YC-2021-0179-1H, and (bottom) YC-2021-0023.*

4.5.11 Oxidation of 4.1 with $(NEt_4)_2CeCl_6$

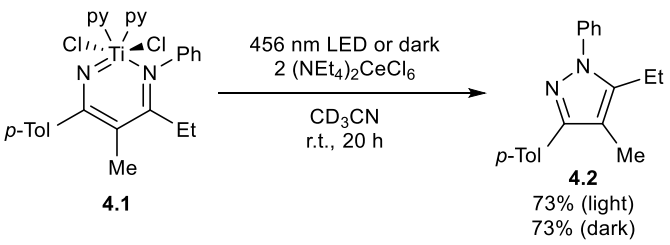

4.1 (13.8 mg, 0.025 mmol, 1.0 equiv), $(NEt_4)_2CeCl_6$ (30.7 mg, 0.05 mmol, 2.0 equiv), TMB (5.0 mg, 0.03 mmol, internal standard), 0.5 mL CD_3CN, and a stir bar were added to a 4 mL scintillation vial in the glovebox. The vial was capped, taken out of the glovebox, and stir under 456 nm LED irradiation or in the dark at room temperature for 20 hours. The reaction mixture was then transferred into an NMR tube in the glovebox, and the reaction yield was determined *via* ^{1}H NMR against the internal standard TMB.

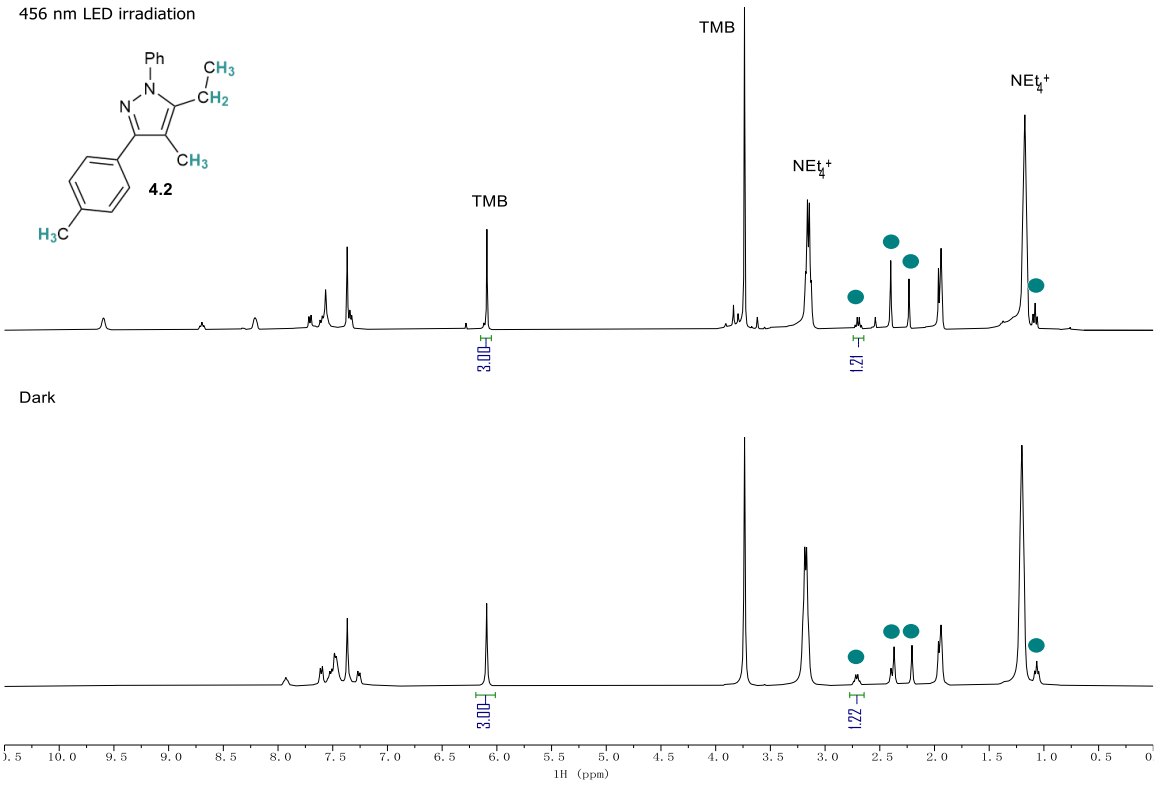

Figure 4.36. Stacked ^{1}H NMR spectra of $(NEt_4)_2CeCl_6$ oxidation of **4.1** in CD_3CN (top) under 456 nm LED irradiation and (bottom) in the dark. *Taken from (top) YC-2022-0042-20h and (bottom) YC-2022-0043-20h.*

4.5.12 Attempts on Photocatalytic Oxidation of 4.1 with $(PPN)_2CeCl_6$

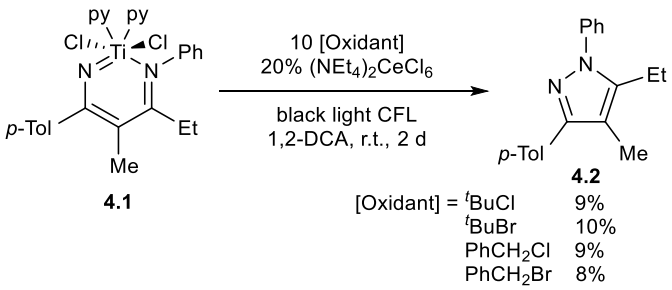

4.1 (13.8 mg, 0.025 mmol, 1.0 equiv), $(NEt_4)_2CeCl_6$ (7.1 mg, 0.005 mmol, 0.2 equiv), sacrificial oxidant (0.25 mmol, 10 equiv, ^{t}BuCl, ^{t}BuBr, $PhCH_2Cl$, or $PhCH_2Br$), a stock solution of *n*-dodecane (0.015 mmol, internal standard) in 0.5 mL 1,2-DCA, and a stir bar were added to a 4 mL scintillation vial in the glovebox. The vial was capped, taken out of the glovebox, and stir under black light CFL irradiation or in the dark at room temperature for 2 days. The reaction mixture was then transferred into an NMR tube in the glovebox, and the reaction yield was determined *via* No-D ^{1}H NMR against the internal standard *n*-dodecane. Manual baseline correction (cubic splines) was applied to improve the accuracy on yield determination due to the low reaction yield and poor NMR shimming.

The formation of one equivalent of **4.2** would consume two equivalents of $[Ce^{IV}Cl_6]^{2-}$ since $[Ce^{IV}Cl_6]^{2-}$ is a one-electron oxidant *via* chlorine atom transfer. Therefore, the low yields of **4.2** (8-10%) likely originate from the stoichiometric oxidation of **4.1** by $[Ce^{IV}Cl_6]^{2-}$, indicating the low participation of the sacrificial oxidants in the reaction.

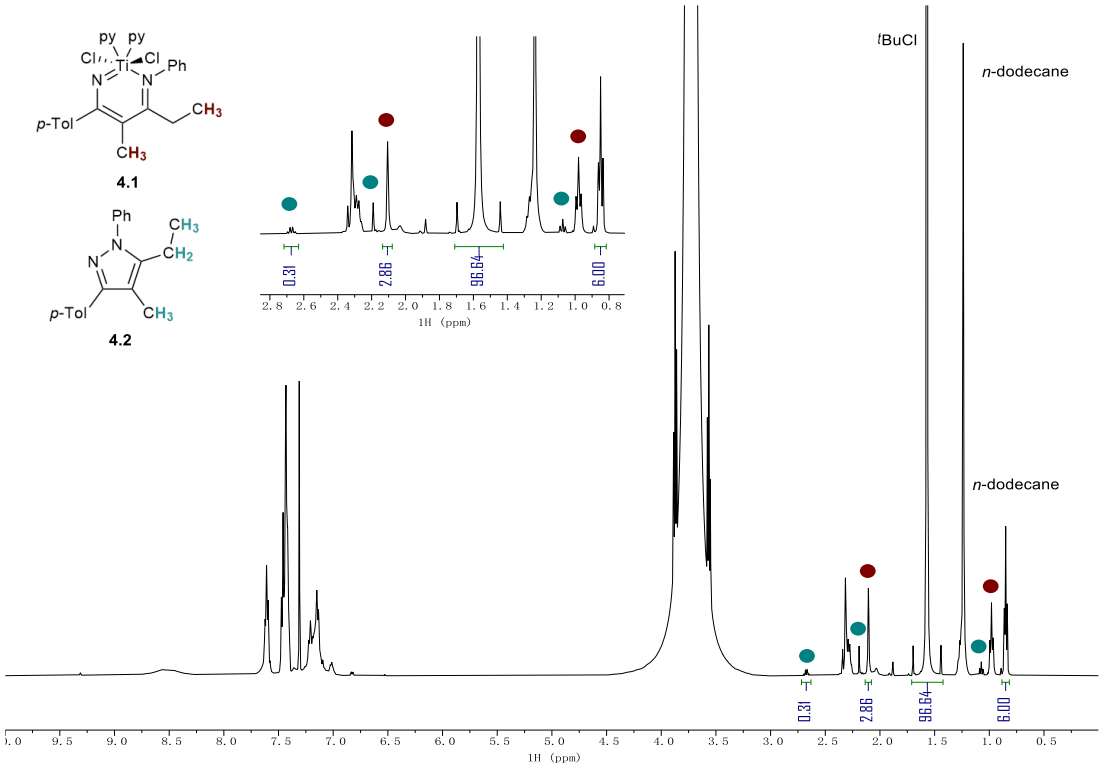

Figure 4.37. No-D ^{1}H NMR spectrum of $(PPN)_2CeCl_6$ photooxidation of **4.1** with ^{t}BuCl in 1,2-DCA. *Taken from YC-2022-NoD-DCE-0098-2d.*

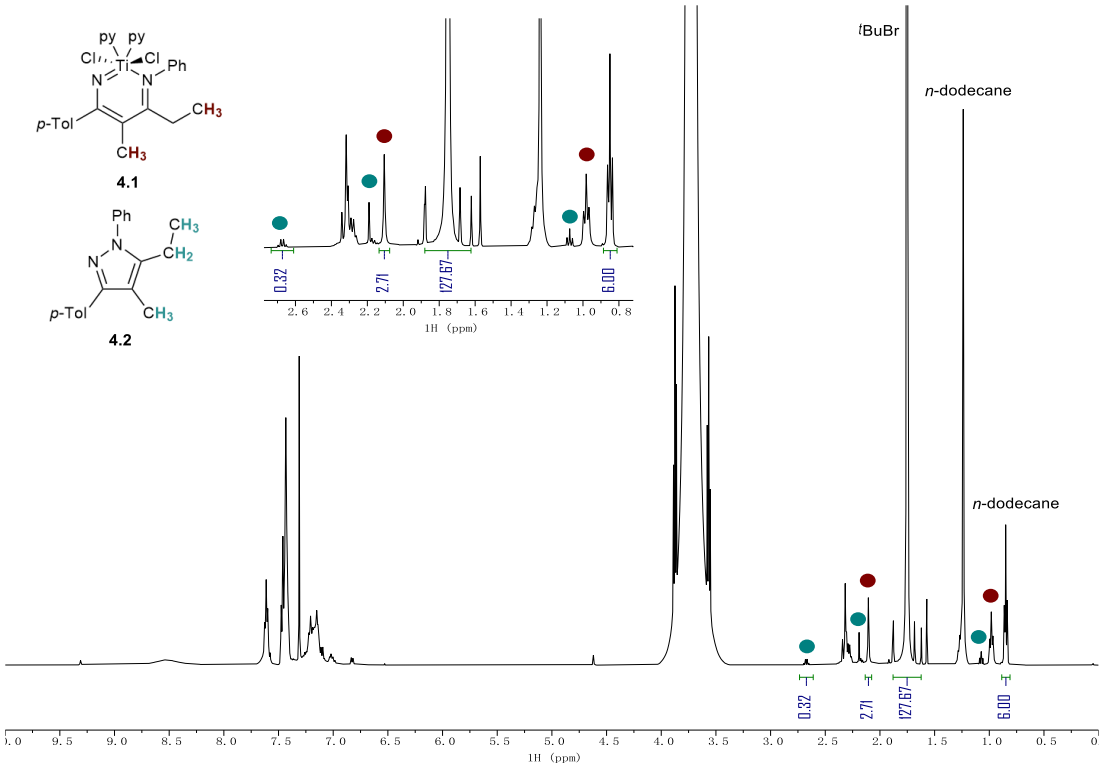

Figure 4.38. No-D ^{1}H NMR spectrum of $(PPN)_2CeCl_6$ photooxidation of **4.1** with ^{t}BuBr in 1,2-DCA. *Taken from YC-2022-NoD-DCE-0099-2d.*

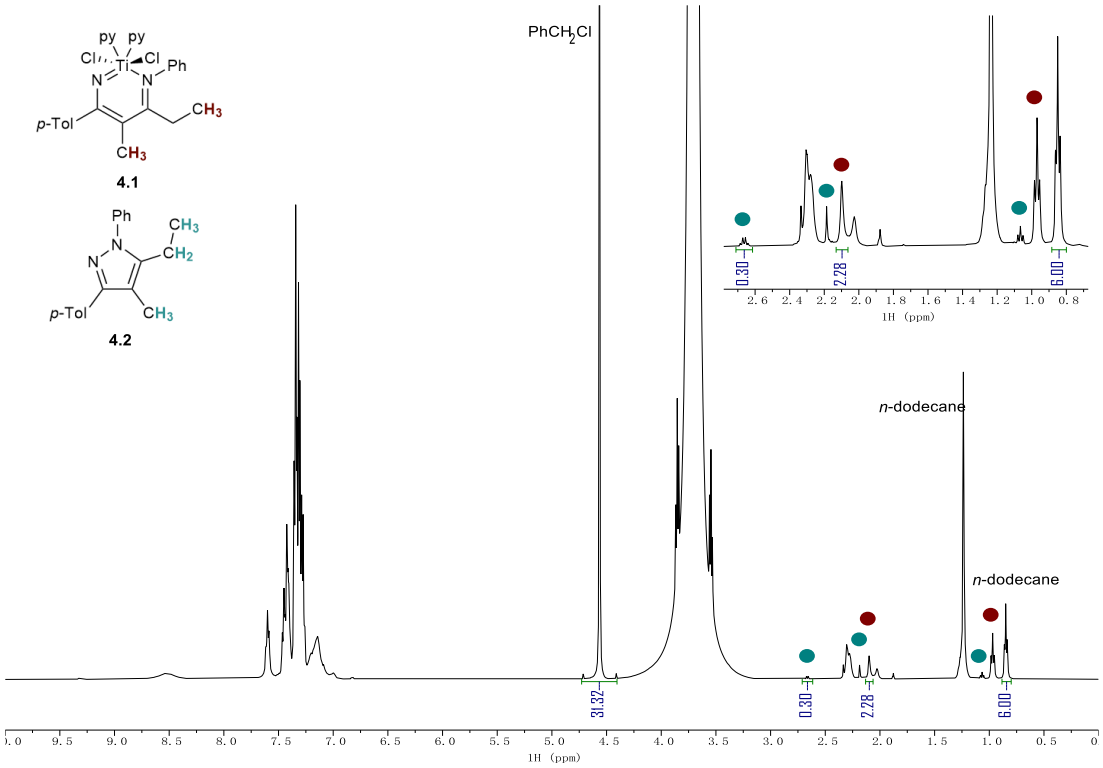

Figure 4.39. No-D ^{1}H NMR spectrum of $(PPN)_2CeCl_6$ photooxidation of **4.1** with $PhCH_2Cl$ in 1,2-DCA. *Taken from YC-2022-NoD-DCE-0100-2d.*

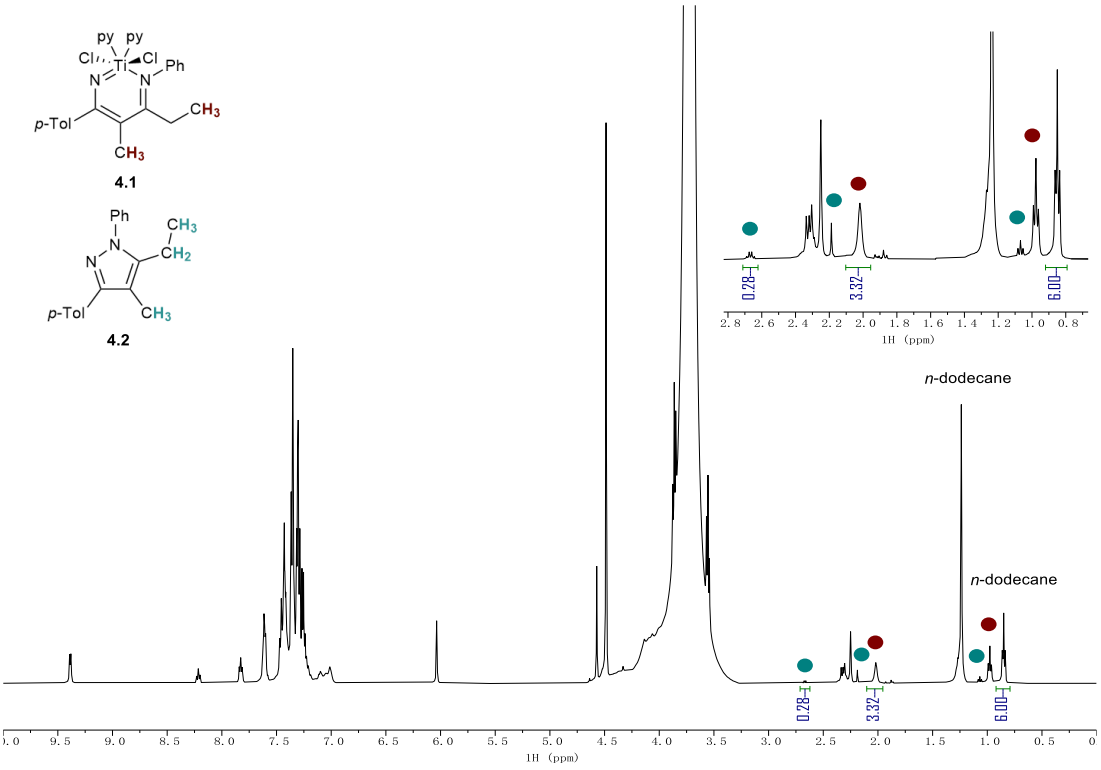

Figure 4.40. No-D ^{1}H NMR spectrum of $(PPN)_2CeCl_6$ photooxidation of **4.1** with $PhCH_2Br$ in 1,2-DCA. *Taken from YC-2022-NoD-DCE-0101-2d.*

4.5.13 Photooxidation of 4.1 with $Ru(bpy)_3Cl_2$

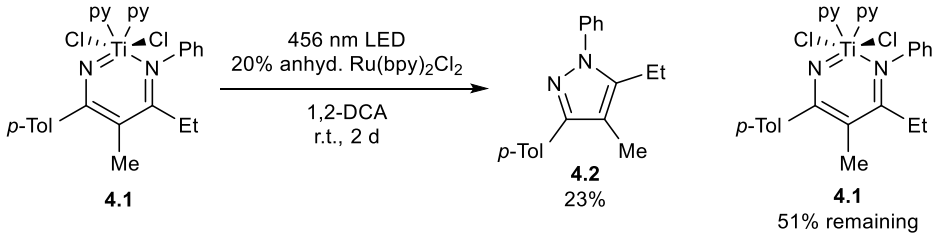

4.1 (13.8 mg, 0.025 mmol, 1.0 equiv), anhydrous $Ru(bpy)_3Cl_2$ (3.2 mg, 0.005 mmol, 0.2 equiv), a stock solution of *n*-dodecane (0.015 mmol, internal standard) in 0.5 mL 1,2-DCA, and a stir bar were added to a 4 mL scintillation vial in the glovebox. The vial was capped, taken out of the glovebox, and stir under 456 nm LED irradiation at room temperature for 2 days. The reaction mixture was then transferred into an NMR tube in the glovebox, and the reaction yield was determined *via* No-D ^{1}H NMR against the internal standard TMB. Manual baseline correction (cubic splines) was applied to improve the accuracy on yield determination due to

the low reaction yield and poor NMR shimming. Prolonged reaction time does not further increase reaction yield.

Mass balance of **4.1**:

The mass balance of **4.1** in this reaction supports that **4.1** could potentially participate in the reaction as a sacrificial oxidant besides being a substrate. The proposed catalytic cycle for this Ru photoredox turnover would be

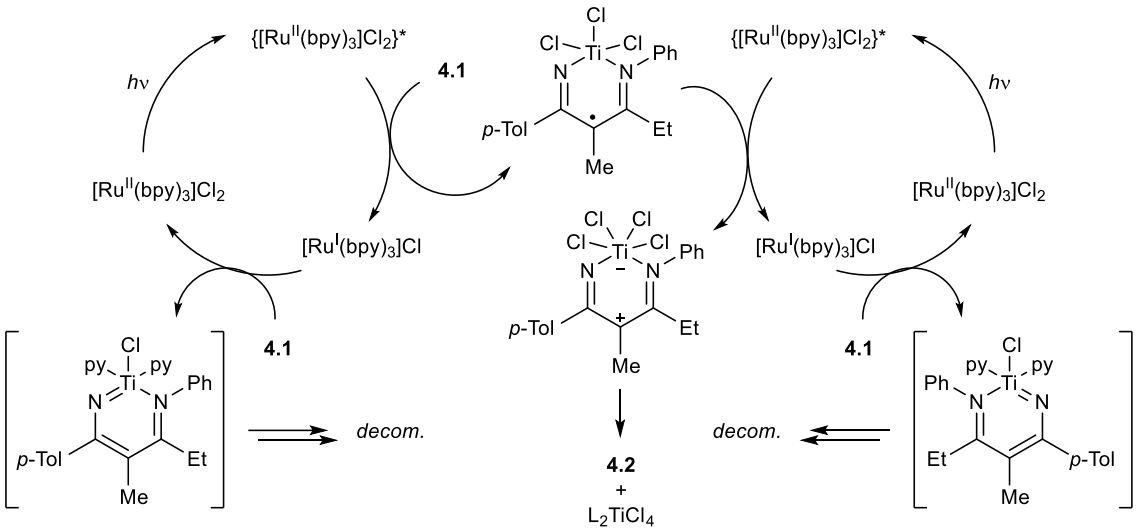

Where the formation of one equivalent of **4.2** consumes one equivalent of **4.1** as oxidation substrate and two equivalents of **4.1** as sacrificial oxidant. Considering that the last turnover of the photoredox cycle can end at $[Ru^{I}(bpy)_3]Cl$, this stoichiometric oxidation by Ru^{II} at the end-stage of the reaction can provide 10% **4.2** from 20% Ru photooxidant loading. To yield 23% **4.2**, the remaining 13% would require turnover of Ru^{I} to Ru^{II}, which would consume 26% **4.1** as sacrificial oxidant. This together with the 23% **4.1** as the oxidation substrate add up to 49%, which matches up well with the consumption of **1** in this reaction. This is supported by the reduction potential of $[Ru(bpy)_3]^{2+}$ and **4.1** (Figure 4.52c), however we were not able to observe the intermediates in the proposed mechanism.

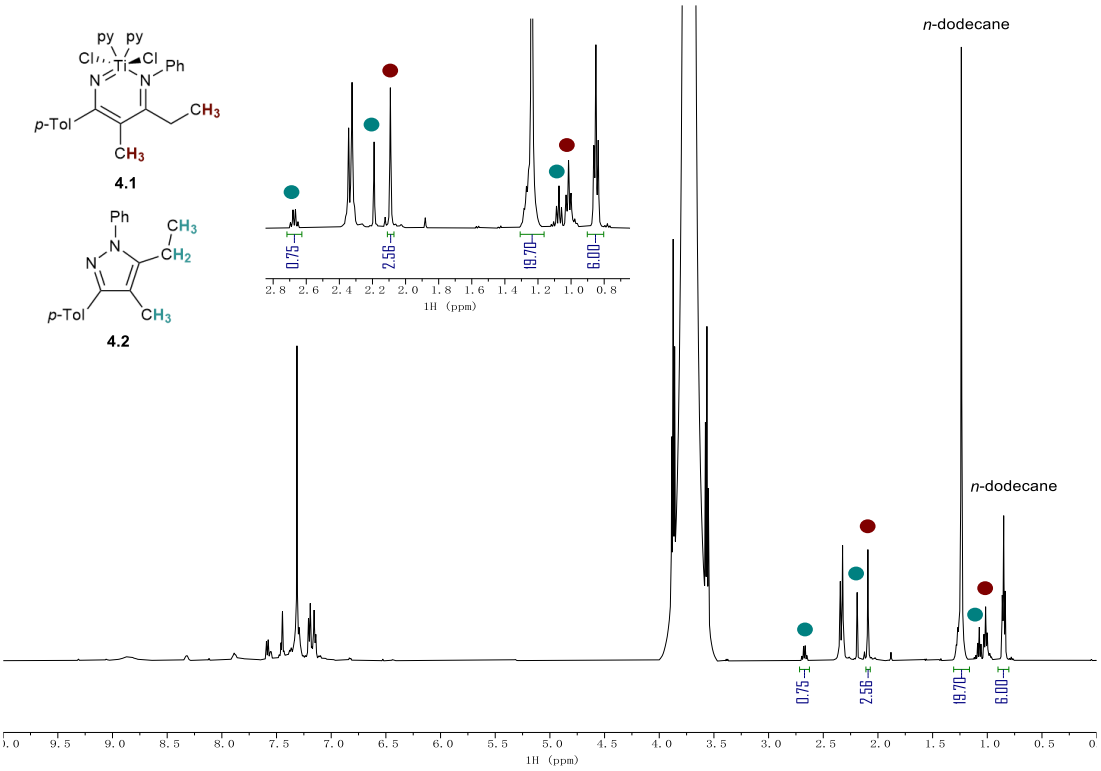

Figure 4.41. No-D ^{1}H NMR spectrum of anhydrous Ru(bpy)$_3$Cl$_2$ photooxidation of **4.1** in 1,2-DCA. *Taken from YC-2022-NoD-DCE-0102-2d.*

4.5.14 Standard Procedure for ^{1}H NMR Monitoring Kinetic Studies

TEMPO oxidation of **4.1** at room temperature (Table 4.2, entry 3) revealed that **4.1** could undergo Ti-mediated pyrazole synthesis with TEMPO slowly without heating. To obtain the optimal t = 0 data, cooling was applied to the reaction mixture to decelerate this reaction before the measurement took place.

Standard Procedure (Procedure 4):

J-Young NMR tube was cooled in a pre-cooled cold well (coolant: dry ice/acetone) in the glovebox for 30 minutes. C_6D_6 stock solution of **4.1** (0.020 mol/L), HMDSO (internal standard, 50 µL, 0.008 mol/L), and TEMPO (0.160 mol/L) were added with syringe in order. The solution was immediately frozen due to the low temperature of the pre-cooled J-Young NMR tube and high melting point of C_6D_6, preventing **4.1** from reacting with TEMPO prior to the NMR monitoring experiment. C_6D_6 was further added till the volume of the reaction solution was 400

μL. The NMR tube was capped, quickly taken out of the glovebox, and immediately cooled in an ice water bath. The reaction mixture was kept frozen during the temperature calibration of the NMR spectrometer. Shimming was performed on a C_6D_6 solution of **4.1**. When switching to samples for monitoring experiments, shimming was not performed again in order to shorten the time interval between t = 0 and the 1st acquisition. Before the measurement, the NMR tube was taken out of the ice water bath, allowed to warm up in a 35 ℃ bath for 20 seconds, shaken to mix the reactants, and injected into the NMR spectrometer. A timer was started when the NMR tube was taken out of the ice water bath to obtain a relatively accurate t = 0 time point. Multiple acquisitions were performed in automatic mode in 30 seconds interval (dummy scan = 0, number of scan = 1, acquisition time = 5 s, delay = 20 s, idle time = 5 s). The ^{1}H NMR spectra were processed using batch integration (MestReNova, integrals graph). The concentration of **4.1** and **4.2** were obtained from their peak integrals against the peak integral of HMDSO.

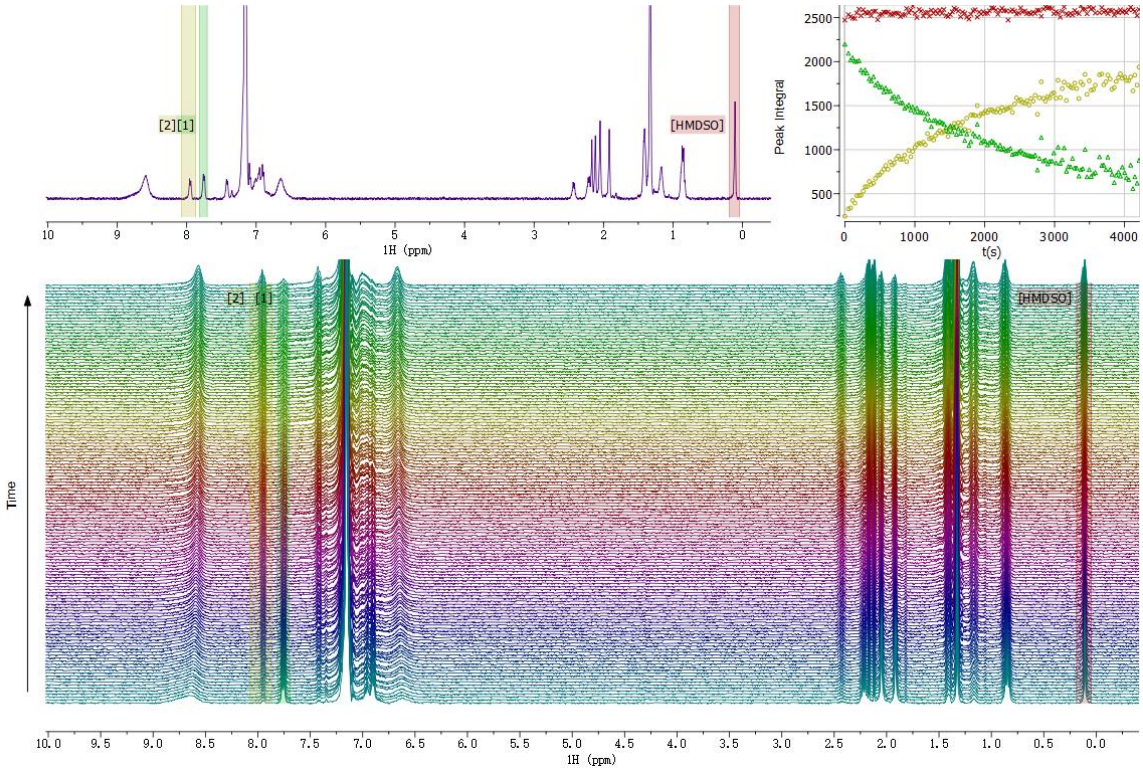

Figure 4.42. Process of example ^{1}H NMR kinetic trace from entry 1, Table 4.2. (Top left) spectrum of an example time point (the 38th time point is shown in the spectrum). (Top right) peak integral versus time plot of HMDSO (red trace), **4.1** (green trace), and **4.2** (yellow trace).

(Bottom) stacked spectra of the kinetic trace with batch integration of HMDSO, **4.1** and **4.2**. *Taken from YC-2021-0043-SameExcess.*

4.5.15 Time Adjustment Experiment and Analysis

Table 4.3. Conditions of the time adjustment experiment.

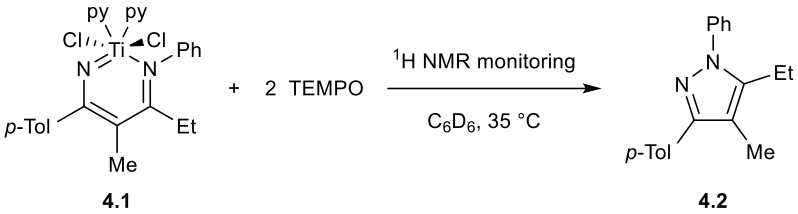

4.1 **4.2**

entry	$V_{\mathbf{4.1}}$ (µL)	[**4.1**] (mol/L)	V_{TEMPO} (µL)	[TEMPO] (mol/L)	Exp #
1	200	0.010	50	0.020	YC-2021-0043
2	120	0.006	30	0.012	YC-2021-0048

The measurements were performed following **Procedure 4** under the conditions in the table above. The consumption of **4.1** was monitored *via* ^{1}H NMR, and the concentration of **4.1** was plotted against reaction time. "Time adjusted" trace of entry 2 was obtained by plotting the consumption profile in entry 2 against an adjusted time profile (t' = t + 1600, in seconds) to allow the starting coordinate of the "time adjusted" trace locates on the trace of entry 1. The overlap of the trace of entry 1 and the "time adjusted" trace suggested that product inhibition and side reactions are kinetically insignificant in this reaction system.

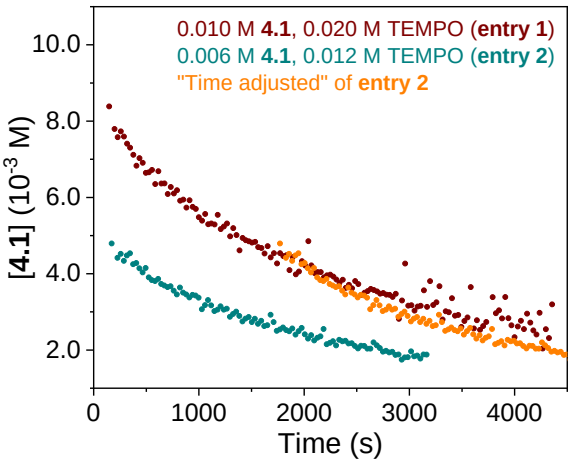

Figure 4.43. Concentration of **4.1** vs. time plots of Table 4.3 entries 1, 2, and "time adjusted".

4.5.16 Variable Time Normalization Analysis on 4.1

Variable time normalization analysis (VTNA) with varied concentration of **4.1** was performed for determination of reaction order of **4.1**:

Table 4.4. Conditions of the VTNA experiments for reaction order of **4.1**.

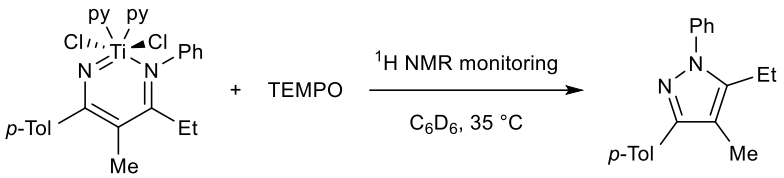

4.1 **4.2**

x mmol 0.02 mmol

entry	$V_{\mathbf{4.1}}$ (μL)	[**4.1**] (mol/L)	V_{TEMPO} (μL)	[TEMPO] (mol/L)	Exp #
1	200	0.010	50	0.020	YC-2021-0043
2	150	0.0075	50	0.020	YC-2021-0045
3	100	0.005	50	0.020	YC-2021-0046

The measurements were performed following **Procedure 4** under the conditions in the table above. The formation of **4.2** was monitored *via* ^{1}H NMR. The concentration of **4.2** (approximated via the trapezoid rule) was plotted against an adjusted time scale $\sum[\mathbf{4.1}]^{\alpha}\Delta t$ with

$$\sum[\mathbf{4.1}]^{\alpha}\Delta t = \sum_{i=1}^{n}\left(\frac{[\mathbf{4.1}]_i + [\mathbf{4.1}]_{i-1}}{2}\right)^{\alpha}(t_i - t_{i-1})$$

where α is the order of dependence on **4.1** and t is the reaction time.[34,187,188] The reaction order of **4.1** was obtained by adjusting α to allow the kinetic traces of entries 1-3 visually overlapped. α = 0.7 was found to give the best overlapped of the kinetic traces. Three characteristic VTNA plots (α = 0, 0.5, 0.7, 1) and the raw data in [**4.2**] versus time plot are shown below.

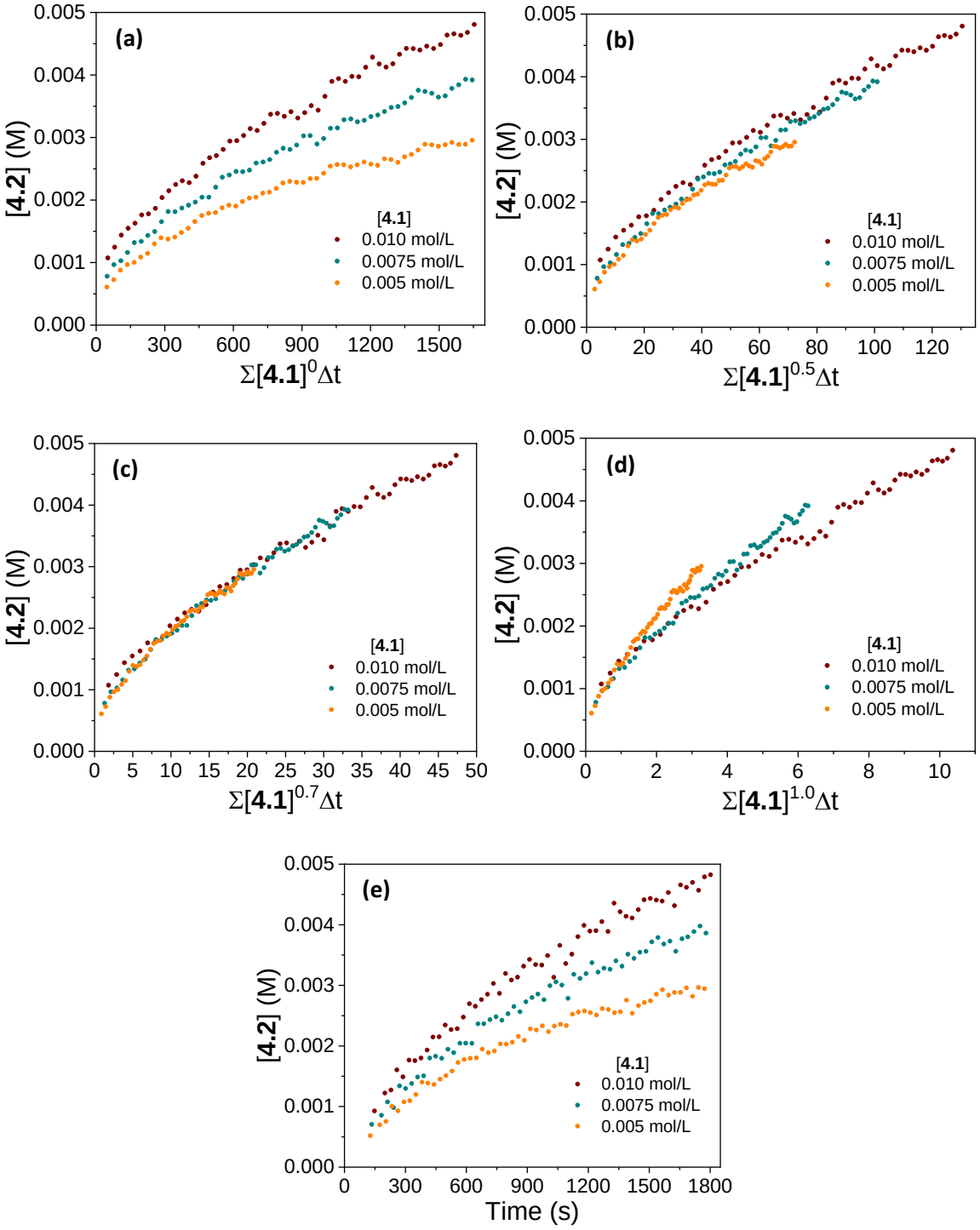

Figure 4.44. VTNA plots with α = (a) 0, (b) 0.5, (c) 0.7, (d) 1, and (e) the raw data in [**4.2**] versus time plot.

4.5.17 Variable Time Normalization Analysis on Pyridine

VTNA with varied concentration of pyridine was performed for determination of reaction order of pyridine:

Table 4.5. Conditions of the VTNA experiments for reaction order of pyridine.

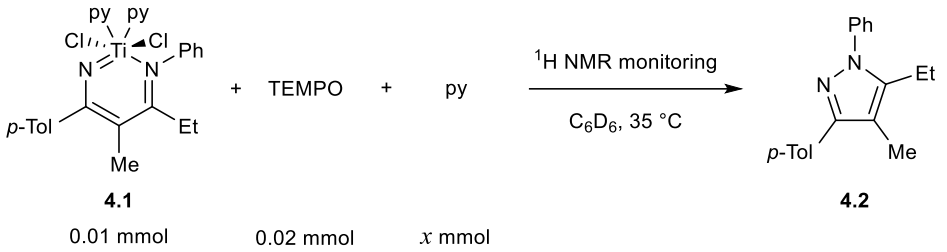

4.1 **4.2**

0.01 mmol 0.02 mmol x mmol

entry	$V_{\mathbf{4.1}}$ (μL)	[**4.1**] (mol/L)	V_{TEMPO} (μL)	[TEMPO] (mol/L)	V_{py} (μL)	$[py]_{added}$ (mol/L)	Exp #
1	200	0.010	50	0.020	0	0	YC-2021-0058
2	200	0.010	50	0.020	40	0.004	YC-2021-0218
3	200	0.010	50	0.020	100	0.010	YC-2021-0215

The measurements were performed following **Procedure 4** under the conditions in the table above. The formation of **4.2** was monitored *via* ^{1}H NMR. Due to the pyridine dissociation equilibrium, the actual concentration of pyridine is higher than $[py]_{added}$.

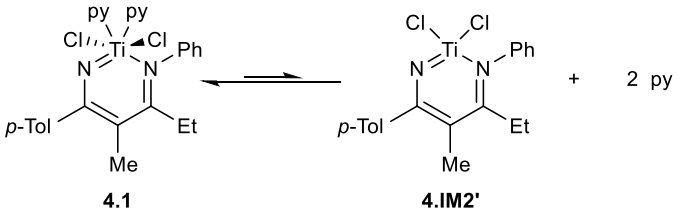

4.1 **4.IM2'**

Thus, the actual concentration of pyridine (noted as [py]) was monitored *via* ^{1}H NMR. The concentration of **4.2** (approximated via the trapezoid rule) was plotted against an adjusted time scale $\sum[py]^{\alpha}\Delta t$ with

$$\sum[py]^{\alpha}\Delta t = \sum_{i=1}^{n}\left(\frac{[py]_i + [py]_{i-1}}{2}\right)^{\alpha}(t_i - t_{i-1})$$

where α is the order of dependence on pyridine and t is the reaction time.[34,187,188] The reaction order of pyridine was obtained by adjusting α to allow the kinetic traces of entries 1-3 visually overlapped. α = -2.5 was found to give the best overlapped of the kinetic traces. Three

characteristic VTNA plots (α = 0, -1, -2, -2.5, -3) and the raw data in [**4.2**] versus time plot are shown below.

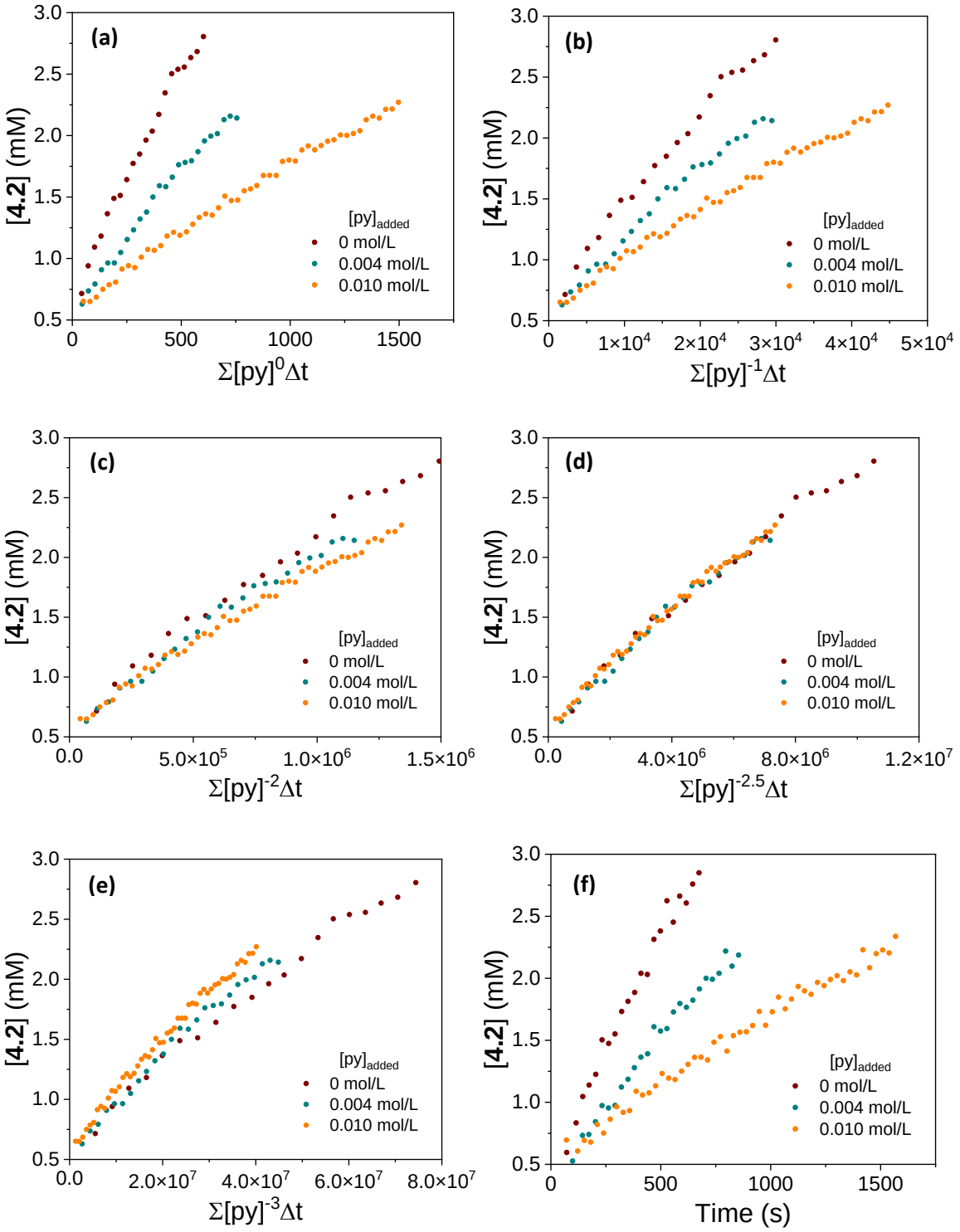

Figure 4.45. VTNA plots with α = (a) 0, (b) -1, (c) -2, (d) -2.5, (e) -3, and (f) the raw data in [**4.2**] versus time plot.

4.5.18 Initial Rate Measurements on TEMPO

Initial rate measurement with varied concentration of TEMPO for determination of reaction order of TEMPO:

Table 4.6. Conditions and results of the initial rates measurement for reaction order of TEMPO.

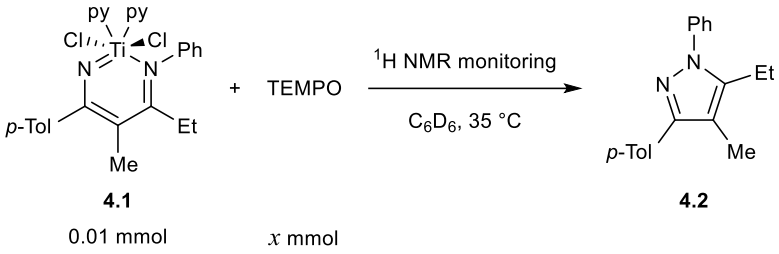

entry	$V_{\mathbf{4.1}}$ (μL)	[**4.1**] (mol/L)	V_{TEMPO} (μL)	[TEMPO] (mol/L)	$(d[\mathbf{4.2}]/dt)_{int}$ (10^{-6} mol/(L*s))	Exp #
1	200	0.010	50	0.020	4.51281	YC-2021-0043
2	200	0.010	40	0.016	4.27914	YC-2021-0047
3	200	0.010	50	0.020	4.43008	YC-2021-0058
4	200	0.010	50	0.020	4.00074	YC-2021-0081
5	200	0.010	30	0.012	3.38525	YC-2021-0084
6	200	0.010	20	0.008	2.04410	YC-2021-0085
7	200	0.010	10	0.004	1.23593	YC-2021-0086
8	200	0.010	60	0.024	5.13483	YC-2021-0087
9	200	0.010	70	0.028	5.84779	YC-2021-0088
10	200	0.010	60	0.024	4.99294	YC-2021-0089
11	200	0.010	40	0.016	3.30507	YC-2021-0090
12	200	0.010	30	0.012	2.91090	YC-2021-0091
13	200	0.010	20	0.008	2.15967	YC-2021-0092
14	200	0.010	10	0.004	1.01667	YC-2021-0093
15	200	0.010	70	0.028	5.53663	YC-2021-0095
16	200	0.010	70	0.028	6.92910	YC-2021-0096
17	200	0.010	60	0.024	5.27840	YC-2021-0097

18	200	0.010	40	0.016	3.30628	YC-2021-0098
19	200	0.010	30	0.012	2.49613	YC-2021-0099

The measurements were performed following **Procedure 4** under the conditions in the table above. The formation of **4.2** was monitored *via* ^{1}H NMR. The concentration of **4.2** was plotted against reaction time. Initial rates of the formation of **4.2**, known as d[**4.2**]/dt)$_{int}$, were obtained from the slope of the linear function fitting curve of each entry. d[**4.2**]/dt)$_{int}$ was then plotted against [TEMPO], and the experimental reaction order of TEMPO can be obtained from the power function fitting of the plot as 0.87.

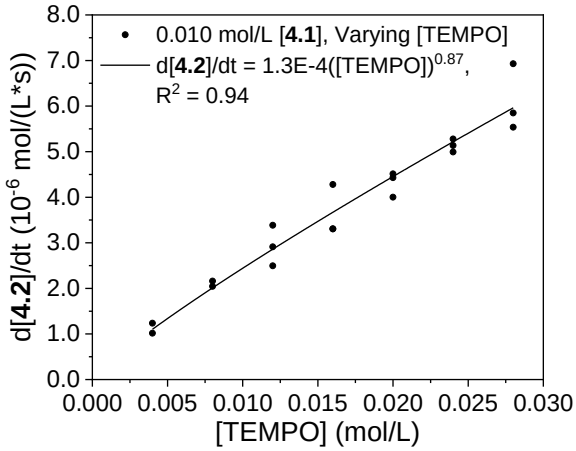

Figure 4.46. Initial rates versus concentrations of TEMPO plot and the power fitting result.

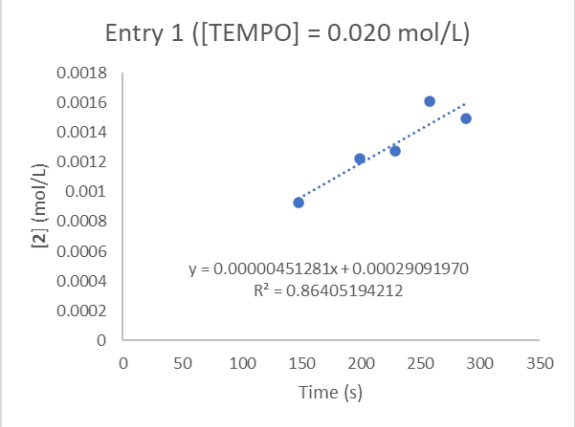
Entry 1 ([TEMPO] = 0.020 mol/L)
[2] (mol/L)
Time (s)
y = 0.00000451281x + 0.00029091970
R² = 0.86405194212

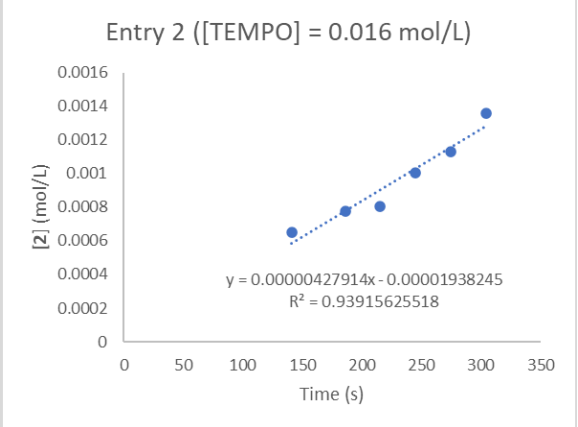
Entry 2 ([TEMPO] = 0.016 mol/L)
[2] (mol/L)
Time (s)
y = 0.00000427914x - 0.00001938245
R² = 0.93915625518

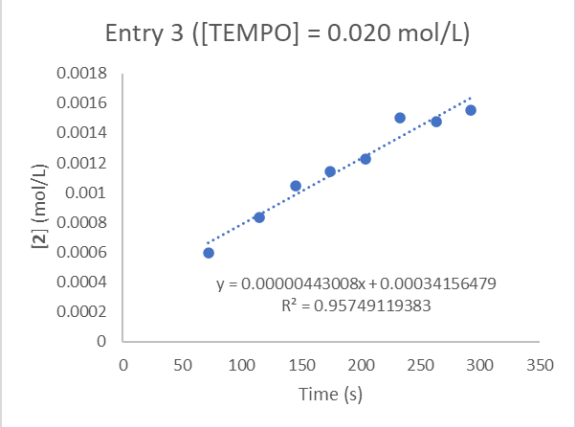
Entry 3 ([TEMPO] = 0.020 mol/L)
[2] (mol/L)
Time (s)
y = 0.00000443008x + 0.00034156479
R² = 0.95749119383

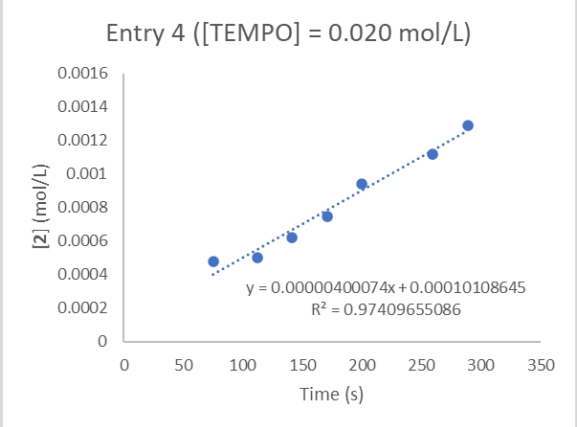
Entry 4 ([TEMPO] = 0.020 mol/L)
[2] (mol/L)
Time (s)
y = 0.00000400074x + 0.00010108645
R² = 0.97409655086

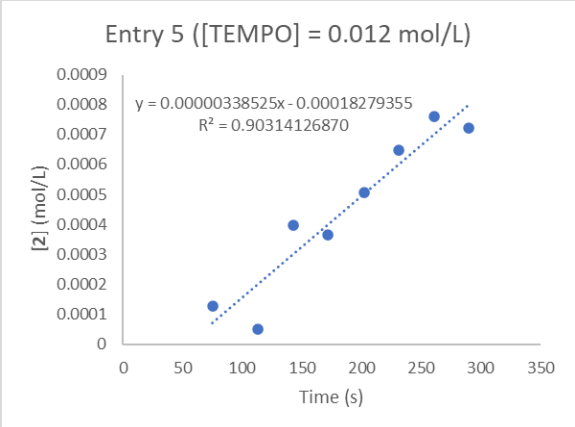
Entry 5 ([TEMPO] = 0.012 mol/L)
[2] (mol/L)
Time (s)
y = 0.00000338525x - 0.00018279355
R² = 0.90314126870

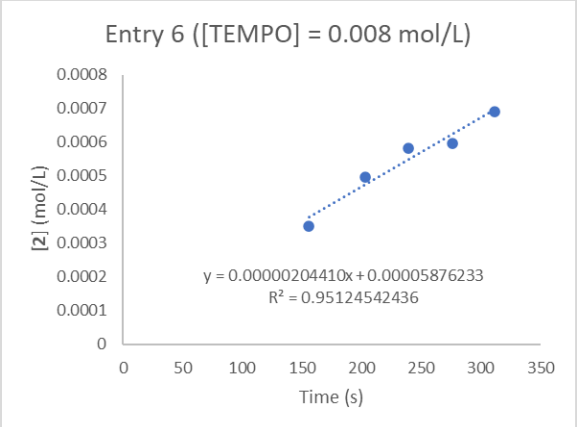
Entry 6 ([TEMPO] = 0.008 mol/L)
[2] (mol/L)
Time (s)
y = 0.00000204410x + 0.00005876233
R² = 0.95124542436

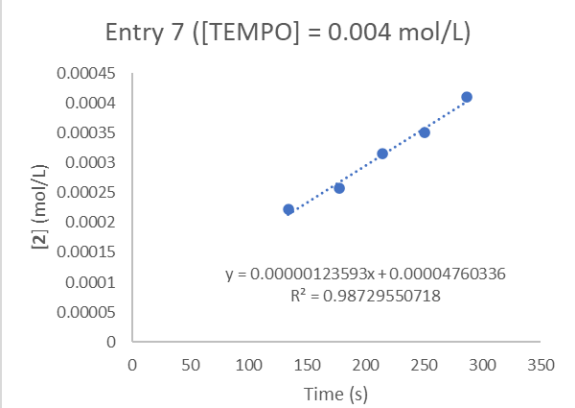
Entry 7 ([TEMPO] = 0.004 mol/L)
[2] (mol/L)
Time (s)
y = 0.00000123593x + 0.00004760336
R² = 0.98729550718

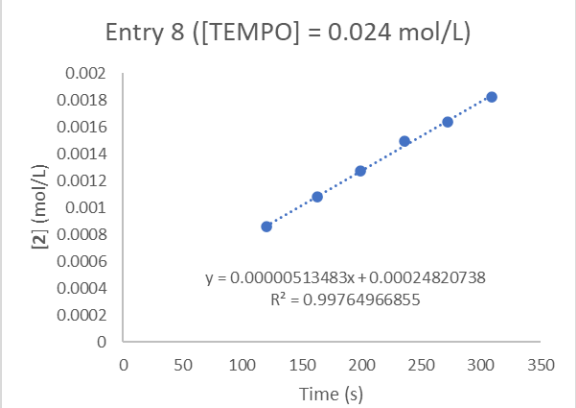
Entry 8 ([TEMPO] = 0.024 mol/L)
[2] (mol/L)
Time (s)
y = 0.00000513483x + 0.00024820738
R² = 0.99764966855

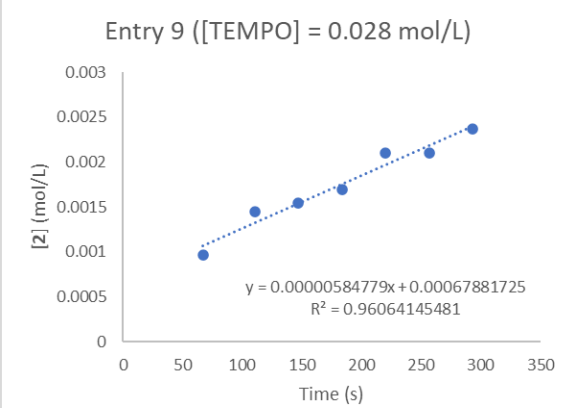
Entry 9 ([TEMPO] = 0.028 mol/L)
[2] (mol/L)
Time (s)
y = 0.00000584779x + 0.00067881725
R² = 0.96064145481

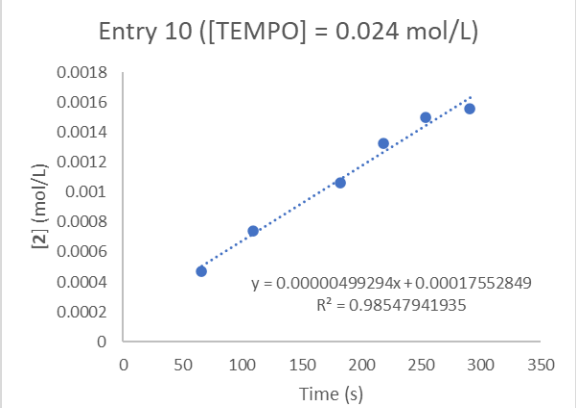
Entry 10 ([TEMPO] = 0.024 mol/L)
[2] (mol/L)
Time (s)
y = 0.00000499294x + 0.00017552849
R² = 0.98547941935

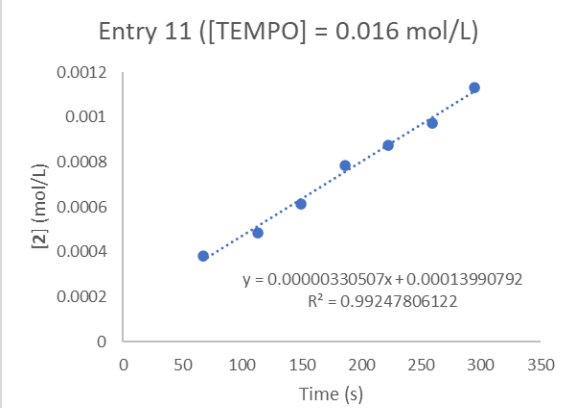
Entry 11 ([TEMPO] = 0.016 mol/L)
[2] (mol/L)
Time (s)
y = 0.00000330507x + 0.00013990792
R² = 0.99247806122

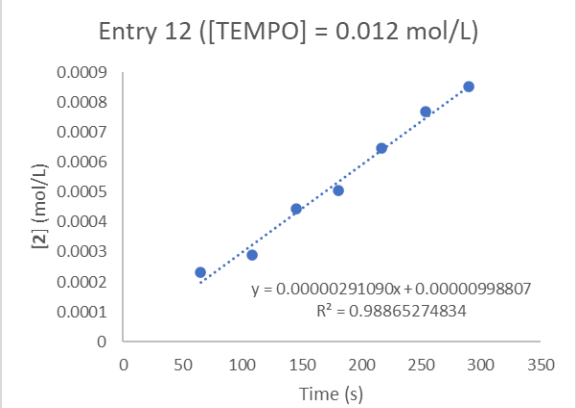
Entry 12 ([TEMPO] = 0.012 mol/L)
[2] (mol/L)
Time (s)
y = 0.00000291090x + 0.00000998807
R² = 0.98865274834

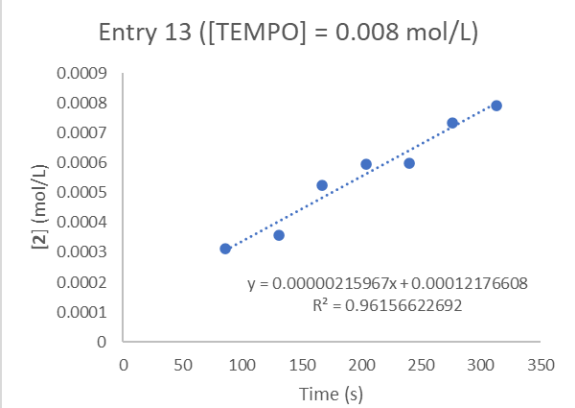
Entry 13 ([TEMPO] = 0.008 mol/L)
[2] (mol/L)
Time (s)
y = 0.00000215967x + 0.00012176608
R² = 0.96156622692

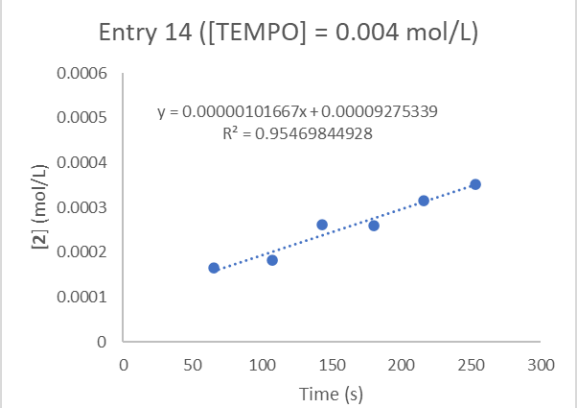
Entry 14 ([TEMPO] = 0.004 mol/L)
[2] (mol/L)
Time (s)
y = 0.00000101667x + 0.00009275339
R² = 0.95469844928

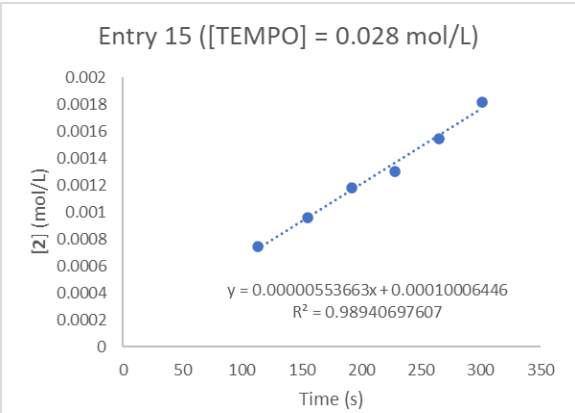
Entry 15 ([TEMPO] = 0.028 mol/L)
[2] (mol/L)
Time (s)
y = 0.00000553663x + 0.00010006446
R² = 0.98940697607

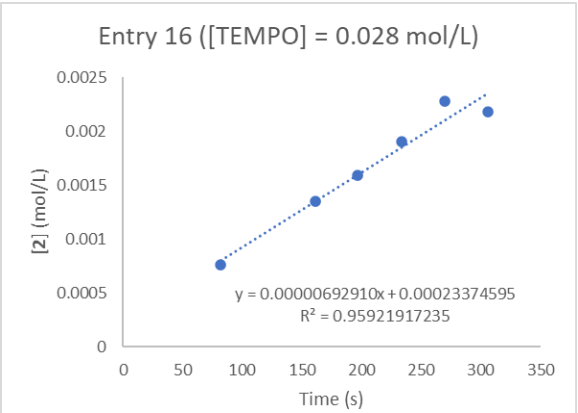
Entry 16 ([TEMPO] = 0.028 mol/L)
[2] (mol/L)
Time (s)
y = 0.00000692910x + 0.00023374595
R² = 0.95921917235

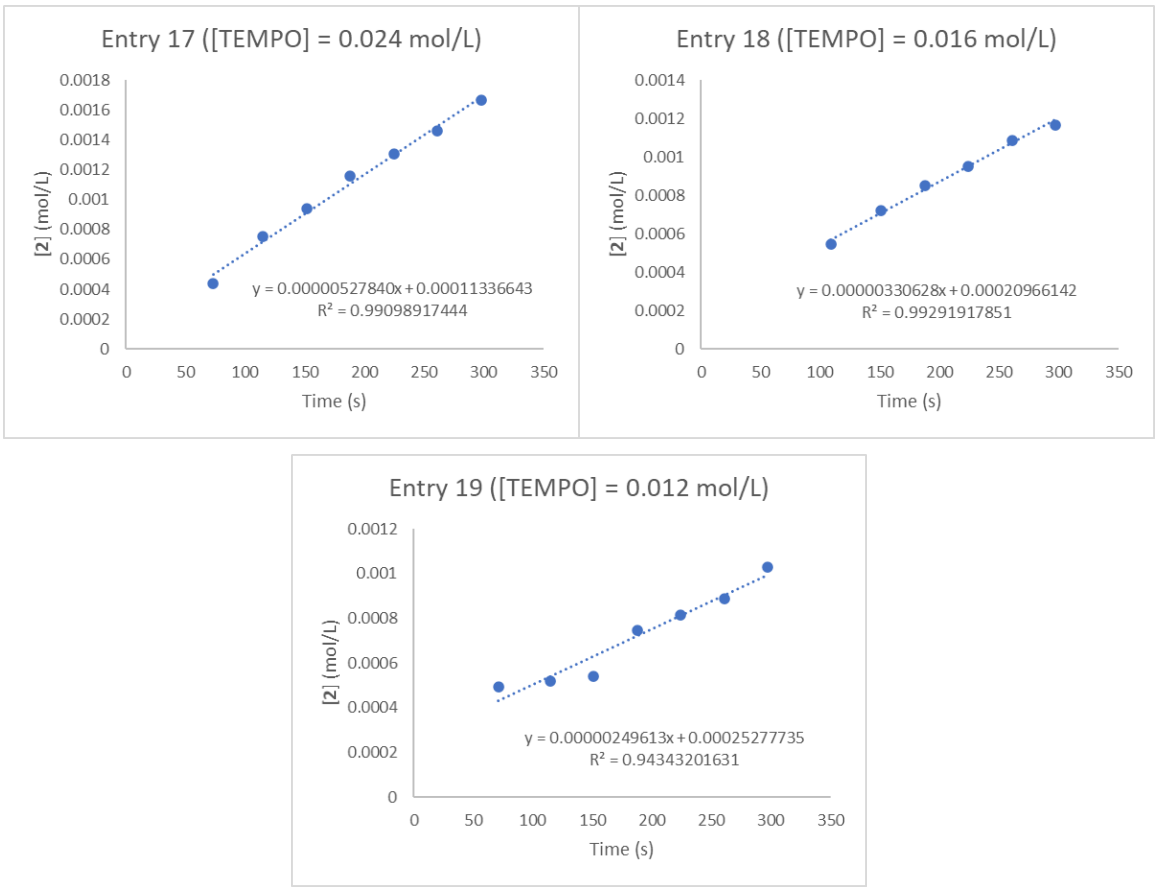

Figure 4.47. Concentrations of **4.2** versus time plots and the linear fitting results of entries 1-19 of Table 4.6.

4.5.19 Initial Rate Measurements on 4.1

Initial rate measurement with varied concentration of **4.1** provides an alternative method to VTNA for determination of reaction order of **4.1**:

Table 4.7. Conditions and results of the initial rates measurement for reaction order of **4.1**.

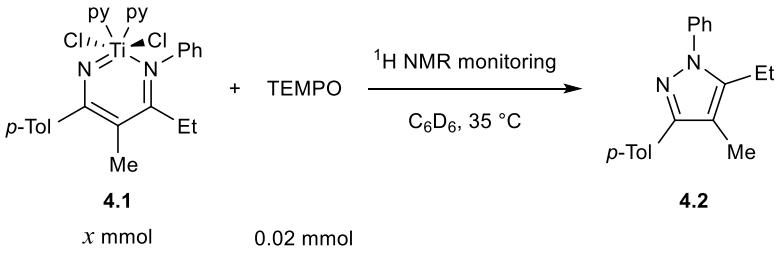

4.1 **4.2**

x mmol 0.02 mmol

entry	$V_{\mathbf{4.1}}$ (μL)	[**4.1**] (mol/L)	V_{TEMPO} (μL)	[TEMPO] (mol/L)	$(d[\mathbf{4.2}]/dt)_{int}$ (10^{-6} mol/(L*s))	Exp #
1	200	0.010	50	0.020	4.51281	YC-2021-0043
2	150	0.0075	50	0.020	3.81120	YC-2021-0045
3	100	0.005	50	0.020	3.32928	YC-2021-0046
4	120	0.006	50	0.020	3.78736	YC-2021-0049
5	80	0.004	50	0.020	1.93782	YC-2021-0050
6	160	0.008	50	0.020	4.14688	YC-2021-0052
7	180	0.009	50	0.020	4.69598	YC-2021-0053
8	40	0.002	50	0.020	1.11510	YC-2021-0055
9	160	0.008	50	0.020	4.13947	YC-2021-0056
10	180	0.009	50	0.020	4.51136	YC-2021-0057
11	200	0.010	50	0.020	4.43008	YC-2021-0058
12	140	0.007	50	0.020	3.49355	YC-2021-0060
13	120	0.006	50	0.020	4.13951	YC-2021-0061
14	100	0.005	50	0.020	2.67996	YC-2021-0062
15	80	0.004	50	0.020	2.40328	YC-2021-0063
16	180	0.009	50	0.020	3.96543	YC-2021-0064
17	40	0.002	50	0.020	1.36688	YC-2021-0067
18	60	0.003	50	0.020	1.75721	YC-2021-0068
19	60	0.003	50	0.020	2.16850	YC-2021-0069
20	60	0.003	50	0.020	2.31872	YC-2021-0071
21	40	0.002	50	0.020	1.74739	YC-2021-0072
22	20	0.001	50	0.020	0.95089	YC-2021-0074
23	20	0.001	50	0.020	1.01311	YC-2021-0077
24	80	0.004	50	0.020	2.84791	YC-2021-0078
25	100	0.005	50	0.020	3.17950	YC-2021-0079
26	120	0.006	50	0.020	3.81411	YC-2021-0080
27	200	0.010	50	0.020	4.51200	YC-2021-0081
28	20	0.001	50	0.020	1.25781	YC-2021-0082
29	140	0.007	50	0.020	4.40905	YC-2021-0083

The measurements were performed following **Procedure 4** under the conditions in the table above. The formation of **4.2** was monitored *via* ^{1}H NMR. The concentration of **4.2** was plotted against reaction time. Initial rates of the formation of **4.2**, known as $d[\mathbf{4.2}]/dt)_{int}$, were obtained

from the slope of the linear function fitting curve of each entry. d[**4.2**]/dt)$_{int}$ was then plotted against [**4.1**], and the experimental reaction order of **4.1** can be obtained from the power function fitting of the plot as 0.69, in good accordance with the reaction order of **4.1** from VTNA.

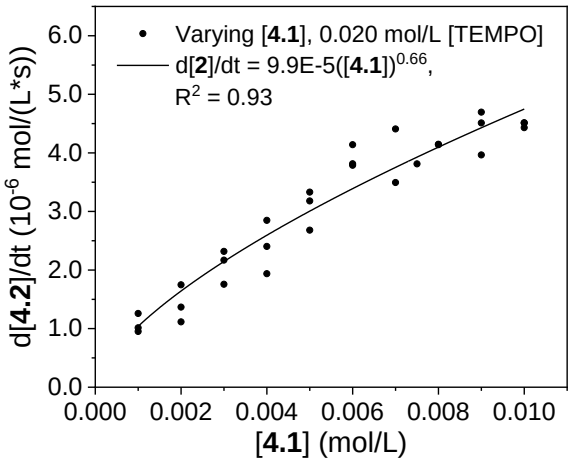

Figure 4.48. Initial rates versus concentrations of **4.1** plot and the power fitting result.

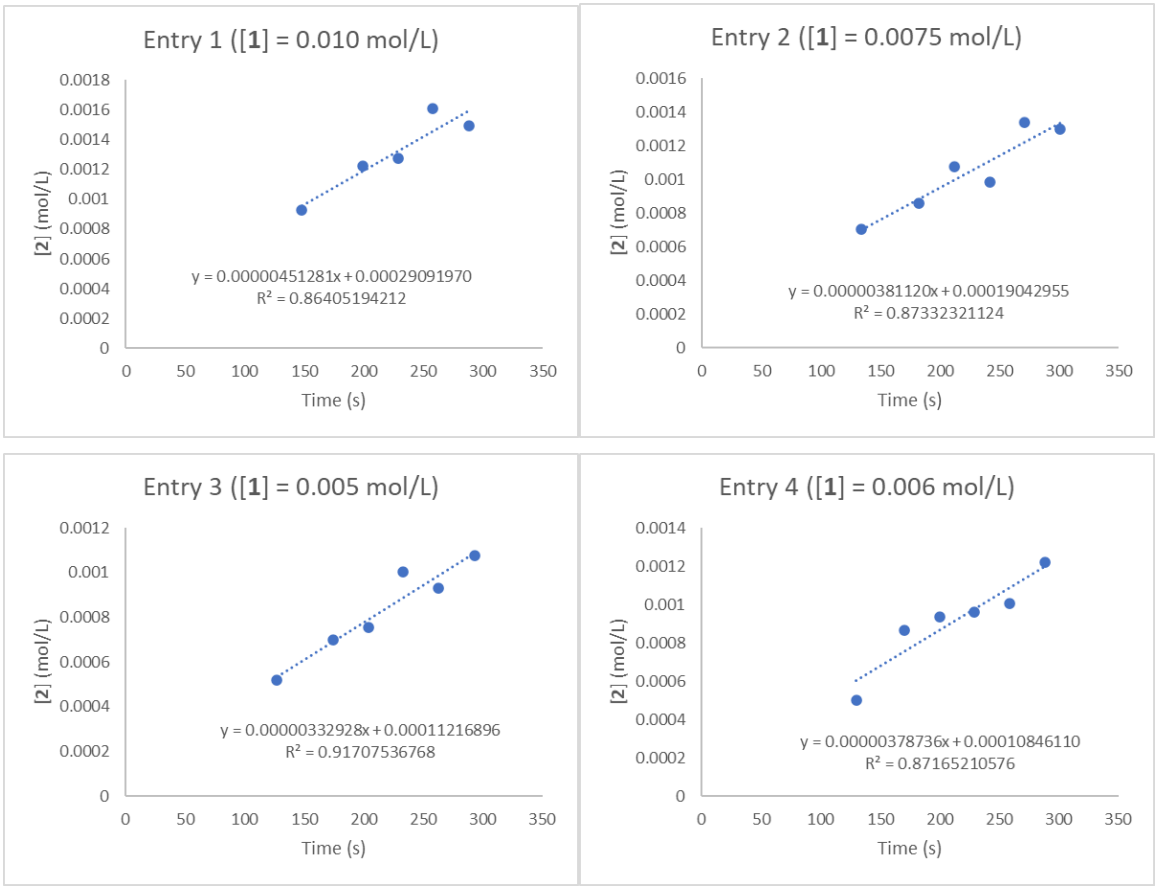

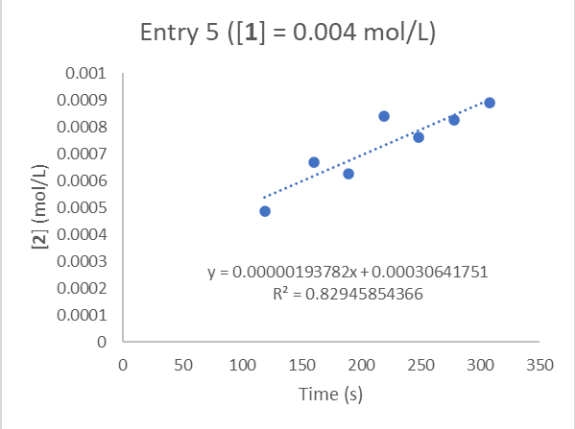
Entry 5 ([1] = 0.004 mol/L)
[2] (mol/L)
Time (s)
y = 0.00000193782x + 0.00030641751
R² = 0.82945854366

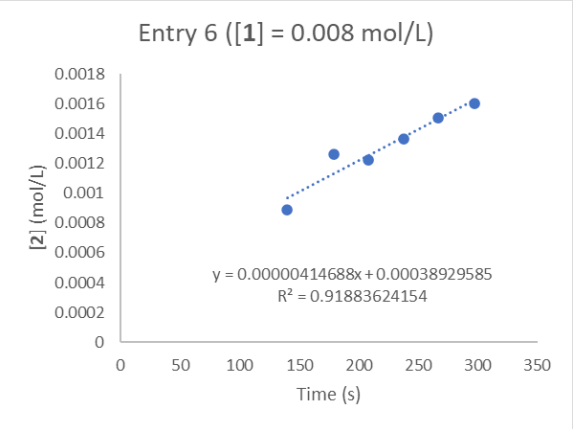
Entry 6 ([1] = 0.008 mol/L)
[2] (mol/L)
Time (s)
y = 0.00000414688x + 0.00038929585
R² = 0.91883624154

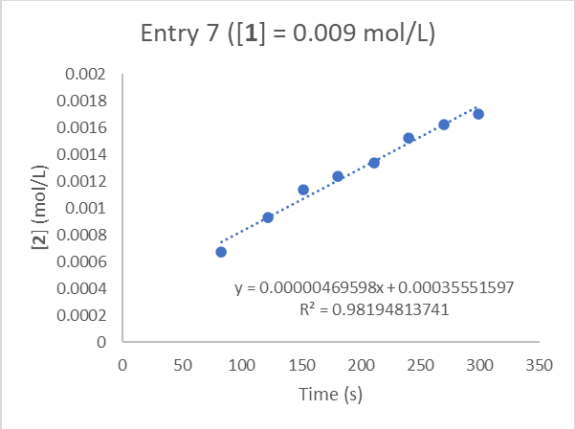
Entry 7 ([1] = 0.009 mol/L)
[2] (mol/L)
Time (s)
y = 0.00000469598x + 0.00035551597
R² = 0.98194813741

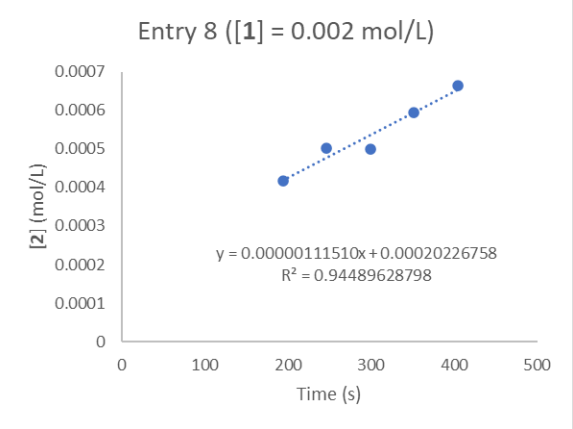
Entry 8 ([1] = 0.002 mol/L)
[2] (mol/L)
Time (s)
y = 0.00000111510x + 0.00020226758
R² = 0.94489628798

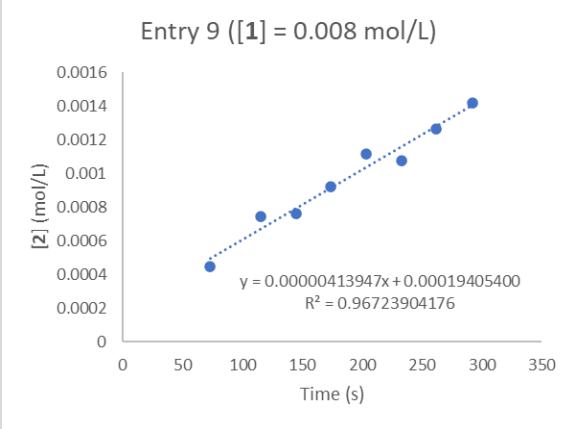
Entry 9 ([1] = 0.008 mol/L)
[2] (mol/L)
Time (s)
y = 0.00000413947x + 0.00019405400
R² = 0.96723904176

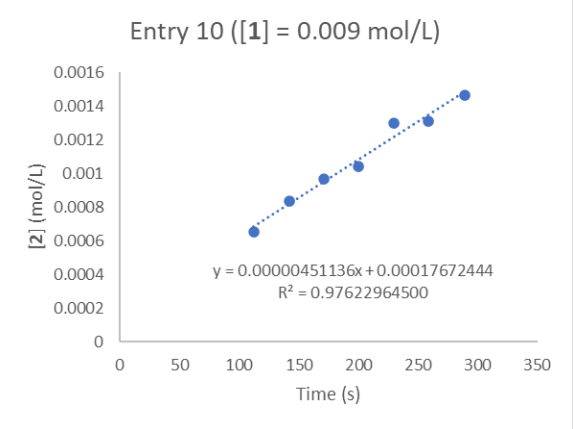
Entry 10 ([1] = 0.009 mol/L)
[2] (mol/L)
Time (s)
y = 0.00000451136x + 0.00017672444
R² = 0.97622964500

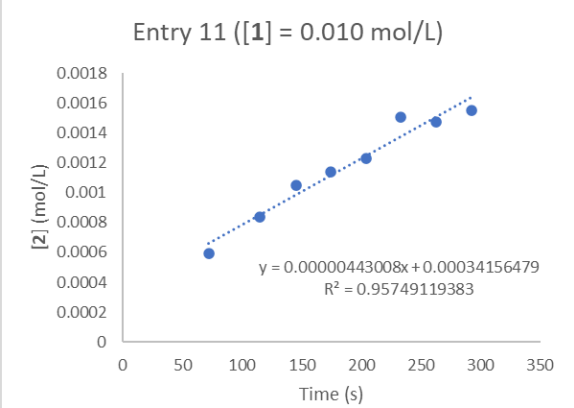
Entry 11 ([1] = 0.010 mol/L)
[2] (mol/L)
Time (s)
y = 0.00000443008x + 0.00034156479
R² = 0.95749119383

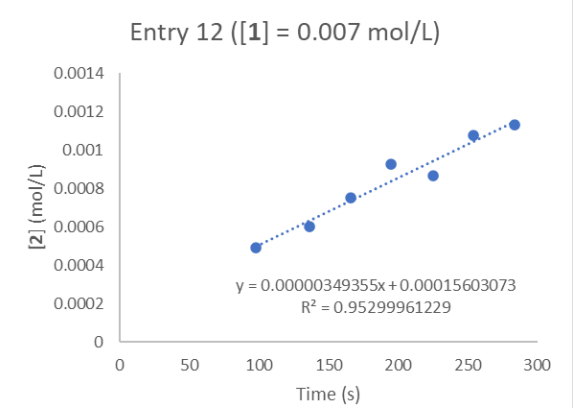
Entry 12 ([1] = 0.007 mol/L)
[2] (mol/L)
Time (s)
y = 0.00000349355x + 0.00015603073
R² = 0.95299961229

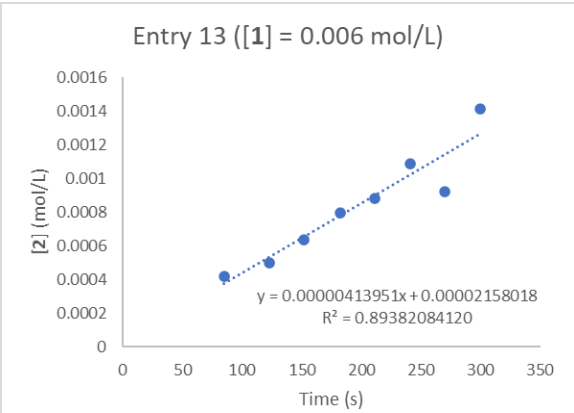
Entry 13 ([1] = 0.006 mol/L)
[2] (mol/L)
Time (s)
y = 0.00000413951x + 0.00002158018
R² = 0.89382084120

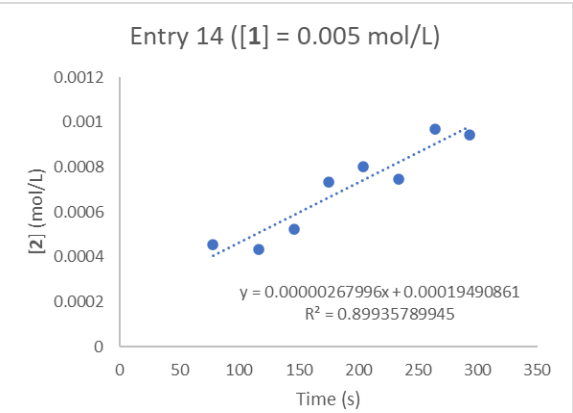
Entry 14 ([1] = 0.005 mol/L)
[2] (mol/L)
Time (s)
y = 0.00000267996x + 0.00019490861
R² = 0.89935789945

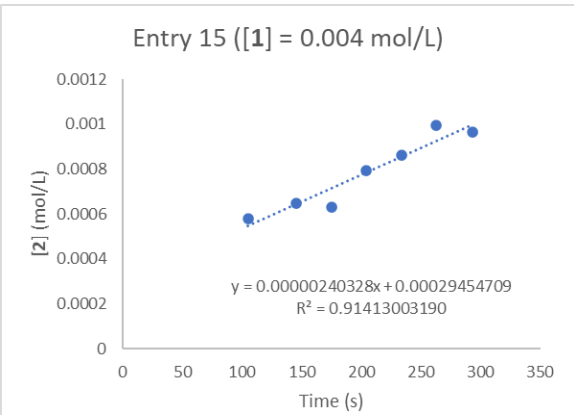
Entry 15 ([1] = 0.004 mol/L)
[2] (mol/L)
Time (s)
y = 0.00000240328x + 0.00029454709
R² = 0.91413003190

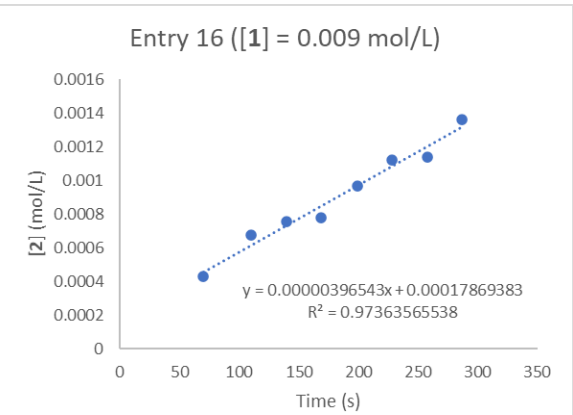
Entry 16 ([1] = 0.009 mol/L)
[2] (mol/L)
Time (s)
y = 0.00000396543x + 0.00017869383
R² = 0.97363565538

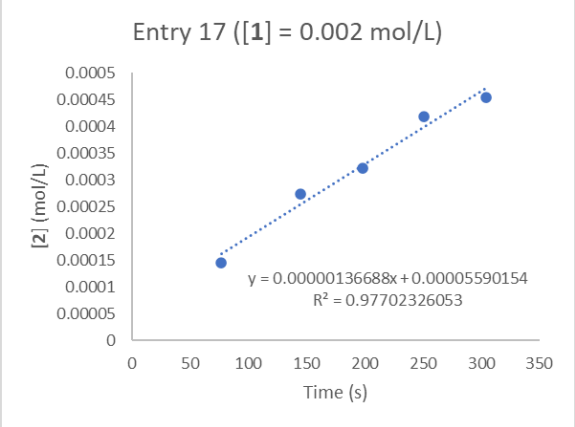
Entry 17 ([1] = 0.002 mol/L)
[2] (mol/L)
Time (s)
y = 0.00000136688x + 0.00005590154
R² = 0.97702326053

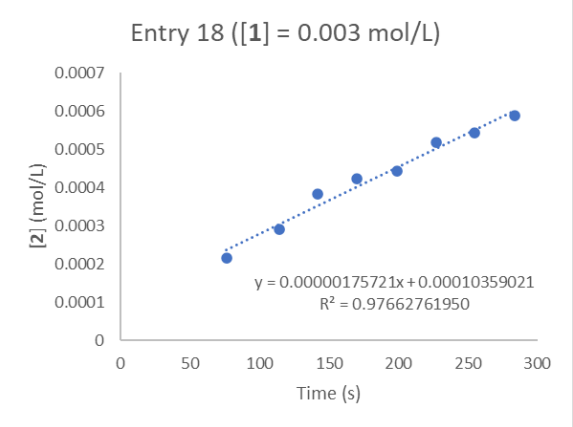
Entry 18 ([1] = 0.003 mol/L)
[2] (mol/L)
Time (s)
y = 0.00000175721x + 0.00010359021
R² = 0.97662761950

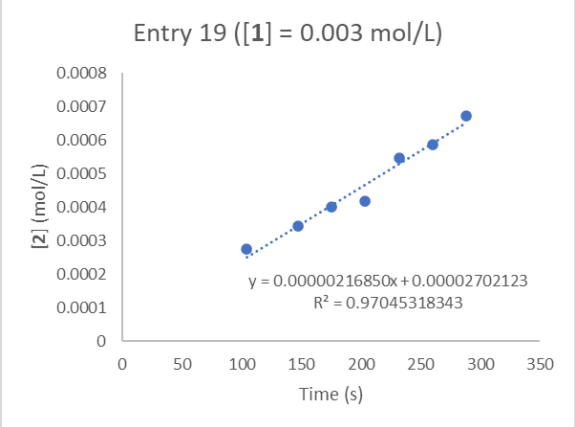
Entry 19 ([1] = 0.003 mol/L)
[2] (mol/L)
Time (s)
y = 0.00000216850x + 0.00002702123
R² = 0.97045318343

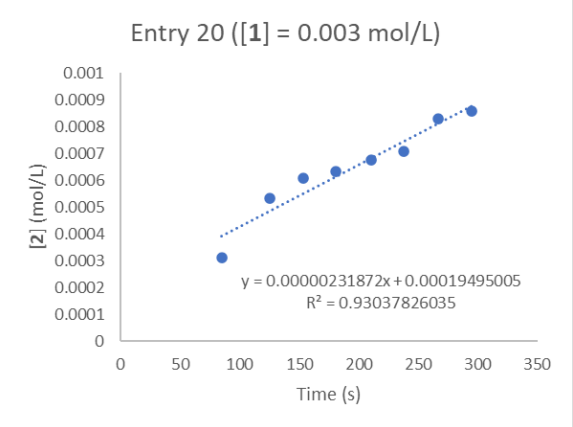
Entry 20 ([1] = 0.003 mol/L)
[2] (mol/L)
Time (s)
y = 0.00000231872x + 0.00019495005
R² = 0.93037826035

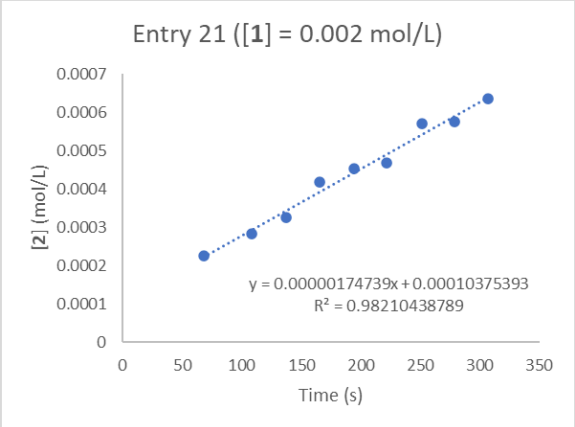
Entry 21 ([1] = 0.002 mol/L)
[2] (mol/L)
Time (s)
y = 0.00000174739x + 0.00010375393
R² = 0.98210438789

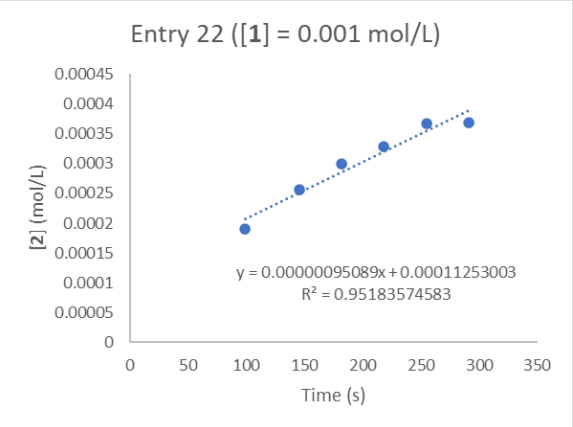
Entry 22 ([1] = 0.001 mol/L)
[2] (mol/L)
Time (s)
y = 0.00000095089x + 0.00011253003
R² = 0.95183574583

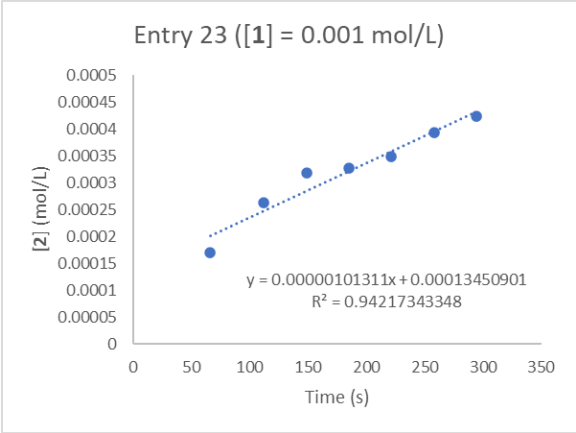
Entry 23 ([1] = 0.001 mol/L)
[2] (mol/L)
Time (s)
y = 0.00000101311x + 0.00013450901
R² = 0.94217343348

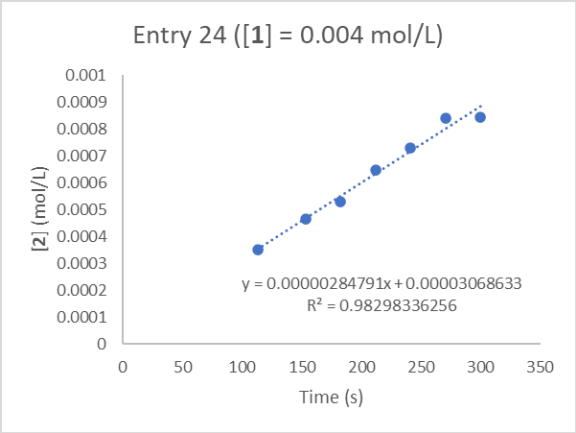
Entry 24 ([1] = 0.004 mol/L)
[2] (mol/L)
Time (s)
y = 0.00000284791x + 0.00003068633
R² = 0.98298336256

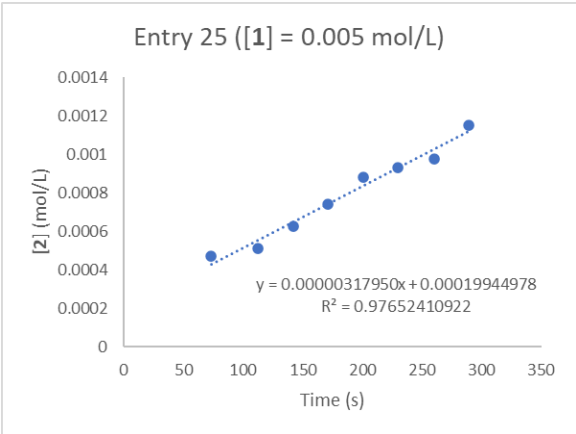
Entry 25 ([1] = 0.005 mol/L)
[2] (mol/L)
Time (s)
y = 0.00000317950x + 0.00019944978
R² = 0.97652410922

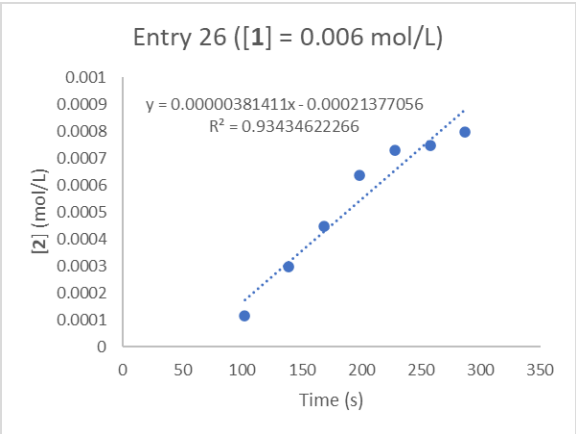
Entry 26 ([1] = 0.006 mol/L)
[2] (mol/L)
Time (s)
y = 0.00000381411x - 0.00021377056
R² = 0.93434622266

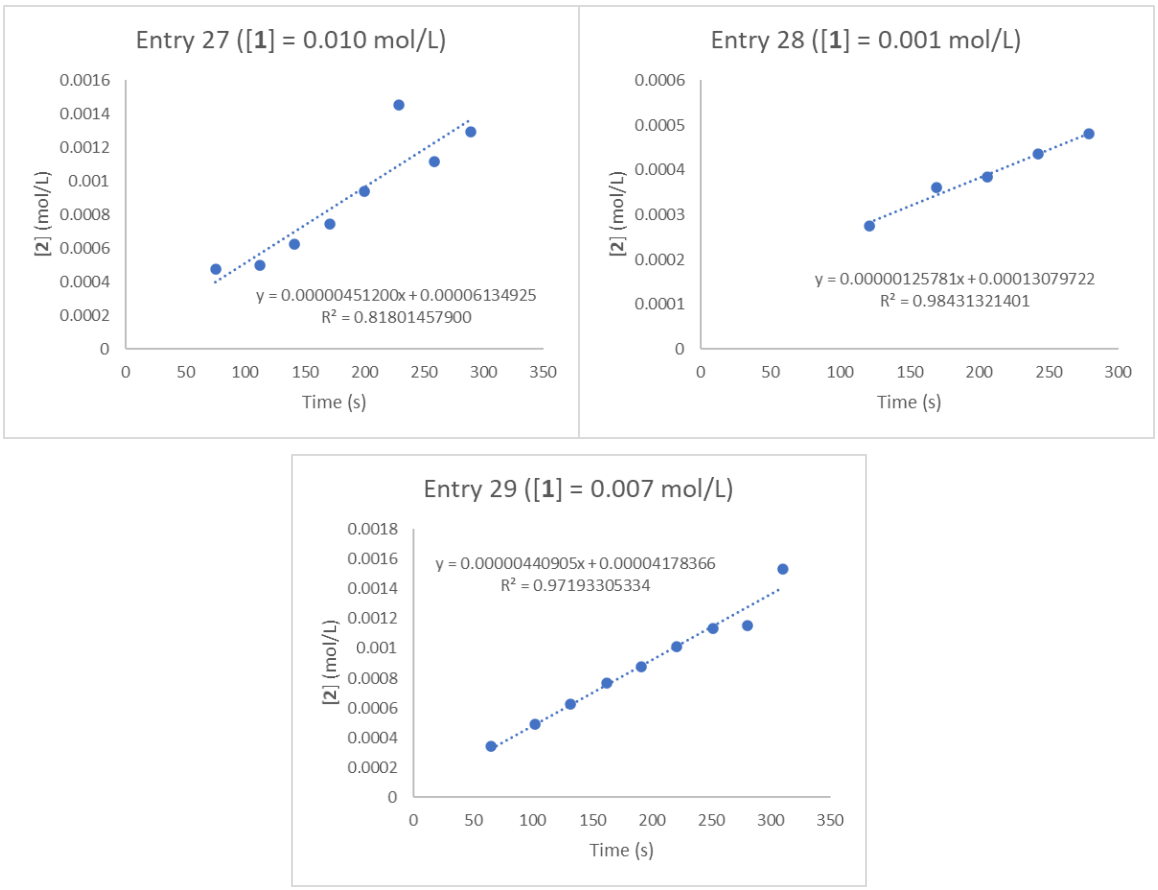

Figure 4.49. Concentrations of **4.2** versus time plots and the linear fitting results of entries 1-29 of Table 4.7. [**1**] = [**4.1**] in figure titles.

4.5.20 Initial Rate Measurements on Pyridine

Initial rate measurement with varied concentration of pyridine for determination of reaction order of pyridine:

Table 4.8. Conditions and results of the initial rates measurement for reaction order of pyridine. [**4.1**] = 0.010 mol/L, [TEMPO] = 0.020 mol/L.

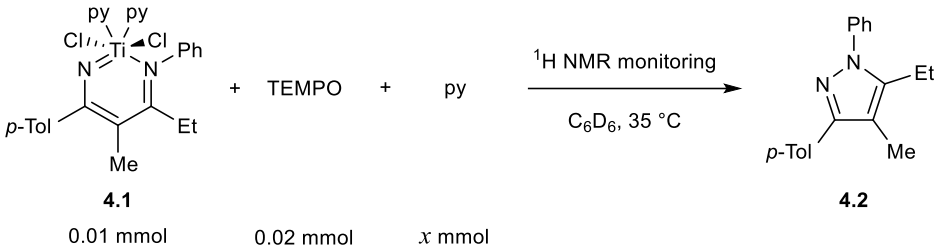

4.1 0.01 mmol | 0.02 mmol | *x* mmol | **4.2**

entry	$V_{\mathbf{4.1}}$ (μL)	V_{TEMPO} (μL)	V_{py} (μL)	$[py]_{added}$ (mol/L)	$[py]_{tot}$ (mol/L)	$(d[\mathbf{4.2}]/dt)_{int}$ (10^{-6} mol/(L*s))	Exp #
1	200	50	0	0	0.020	4.51281	YC-2021-0043
2	200	50	0	0	0.020	4.43008	YC-2021-0058
3	200	50	0	0	0.020	4.00074	YC-2021-0081
4	200	50	80	0.008	0.028	1.32008	YC-2021-0203
5	200	50	20	0.002	0.022	2.11333	YC-2021-0207
6	200	50	20	0.002	0.022	1.93393	YC-2021-0208
7	200	50	20	0.002	0.022	1.85490	YC-2021-0209
8	200	50	60	0.006	0.026	1.35995	YC-2021-0210
9	200	50	60	0.006	0.026	1.59181	YC-2021-0211
10	200	50	80	0.008	0.028	1.36139	YC-2021-0212
11	200	50	80	0.008	0.028	1.39032	YC-2021-0213
12	200	50	100	0.010	0.030	1.25980	YC-2021-0214
13	200	50	100	0.010	0.030	1.10790	YC-2021-0215
14	200	50	100	0.010	0.030	1.32768	YC-2021-0216
15	200	50	40	0.004	0.024	2.13210	YC-2021-0218
16	200	50	40	0.004	0.024	1.90133	YC-2021-0219
17	200	50	40	0.004	0.024	2.05262	YC-2021-0220
18	200	50	60	0.006	0.026	1.31148	YC-2021-0221

The measurements were performed following **Procedure 4** under the conditions in the table above, with the alternation of adding C_6D_6 stock solution of **4.1** (0.020 mol/L), HMDSO (internal standard, 50 μL, 0.008 mol/L), TEMPO (0.160 mol/L) and pyridine (0.040 mol/L) with syringe to the pre-cooled J-Young NMR tube in the glovebox before titrating to 0.4 mL by C_6D_6. The formation of **4.2** was monitored *via* ^{1}H NMR. The concentration of **4.2** was plotted against reaction time. Initial rates of the formation of **4.2**, known as $d[\mathbf{4.2}]/dt)_{int}$, were obtained from the slope of the linear function fitting curve of each entry. $d[\mathbf{4.2}]/dt)_{int}$ was then plotted against [py],

and the experimental reaction order of pyridine can be obtained from the power function fitting of the plot.

A maximum of two equivalents of pyridine can dissociate from each equivalent of **4.1** due to the pyridine dissociation equilibrium:

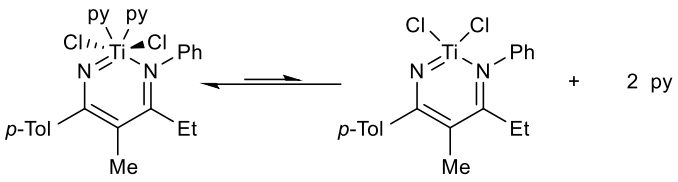

Therefore, the total concentration of pyridine in all forms ($[py]_{tot}$) at t = 0 can be obtained from:

$$[py]_{tot} = [py]_{added} + 2 \times [\mathbf{4.1}]$$

d[**4.2**]/dt)$_{int}$ was also plotted against $[py]_{tot}$, and the experimental reaction order of total equivalent of pyridine can be obtained from the power function fitting of the plot.

From both of the fittings pyridine was found to fall in the saturation region, indicating that pyridine strongly inhibits the TEMPO oxidation of **4.1**. However, the actual pyridine concentration should satisfy $[py]_{added} < [py]_{actual} < [py]_{tot}$ since pyridine is only partially bound on Ti. Thus, both the order dependence obtained using the $[py]_{added}$ and $[py]_{tot}$ have poor fitting. The order dependence on pyridine was obtained by VTNA instead.

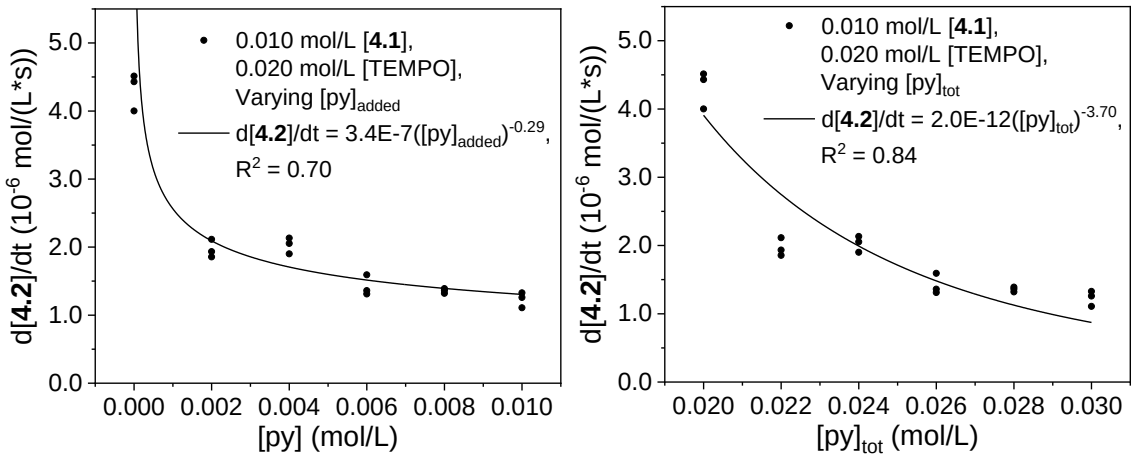

Figure 4.50. (Left) initial rates versus $[py]_{added}$ and (right) initial rates versus $[py]_{tot}$ plots and the power fitting results.

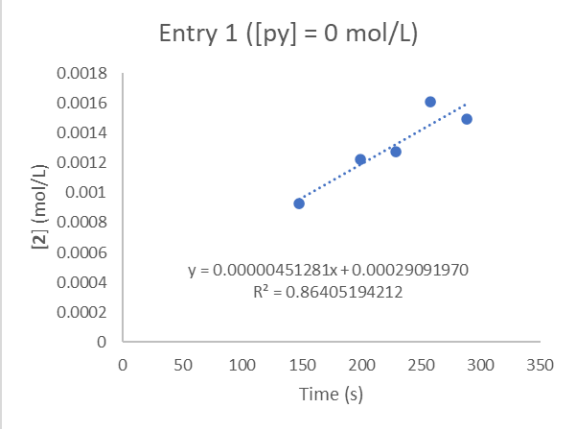
Entry 1 ([py] = 0 mol/L)
[2] (mol/L)
Time (s)
y = 0.00000451281x + 0.00029091970
R² = 0.86405194212

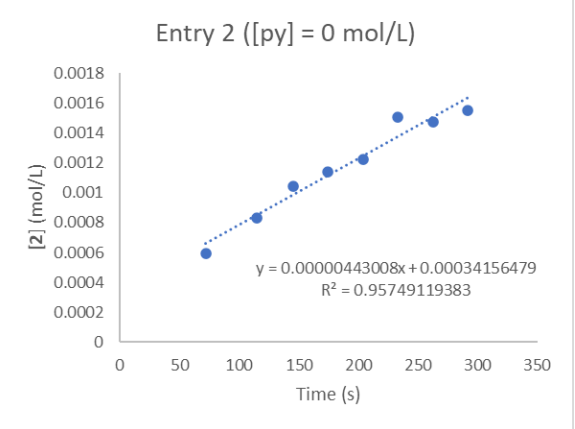
Entry 2 ([py] = 0 mol/L)
[2] (mol/L)
Time (s)
y = 0.00000443008x + 0.00034156479
R² = 0.95749119383

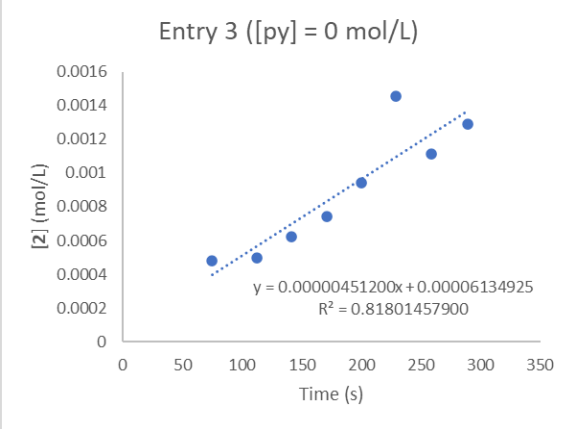
Entry 3 ([py] = 0 mol/L)
[2] (mol/L)
Time (s)
y = 0.00000451200x + 0.00006134925
R² = 0.81801457900

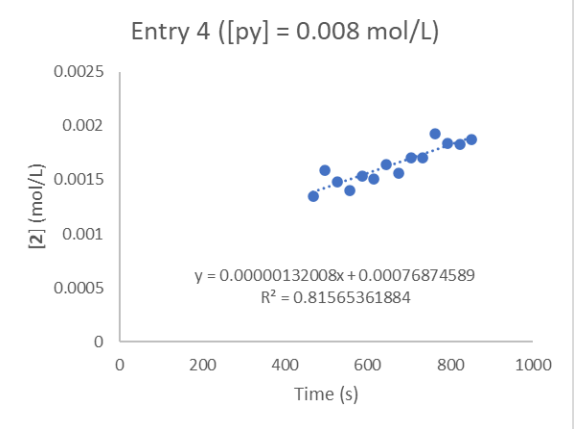
Entry 4 ([py] = 0.008 mol/L)
[2] (mol/L)
Time (s)
y = 0.00000132008x + 0.00076874589
R² = 0.81565361884

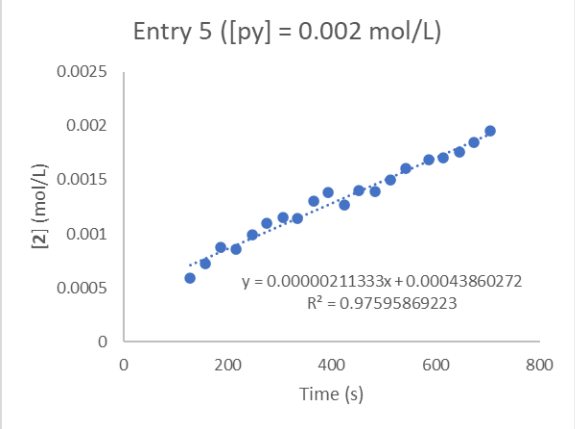
Entry 5 ([py] = 0.002 mol/L)
[2] (mol/L)
Time (s)
y = 0.00000211333x + 0.00043860272
R² = 0.97595869223

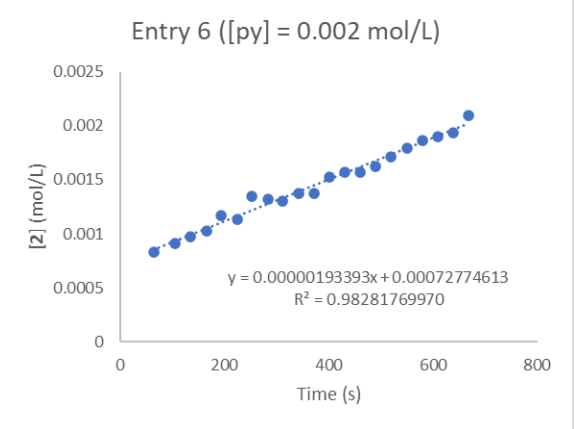
Entry 6 ([py] = 0.002 mol/L)
[2] (mol/L)
Time (s)
y = 0.00000193393x + 0.00072774613
R² = 0.98281769970

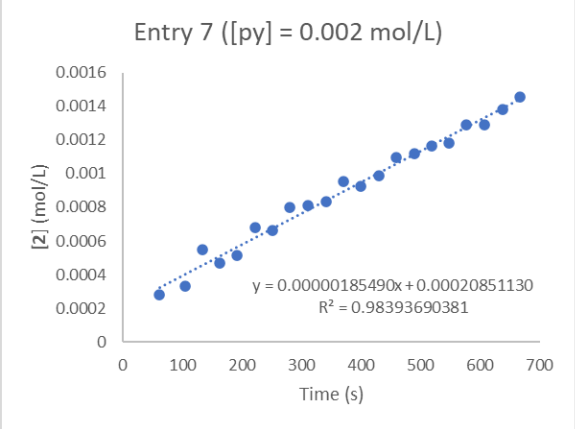
Entry 7 ([py] = 0.002 mol/L)
[2] (mol/L)
Time (s)
y = 0.00000185490x + 0.00020851130
R² = 0.98393690381

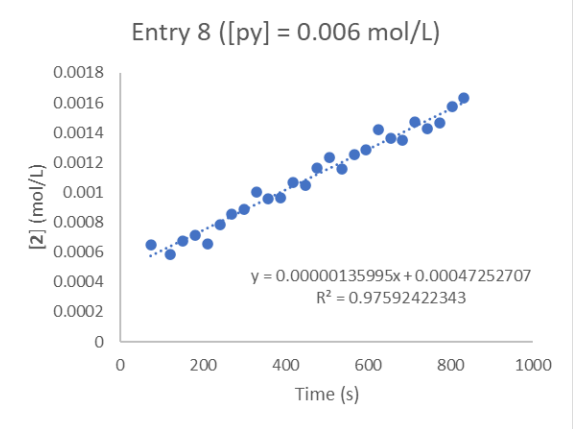
Entry 8 ([py] = 0.006 mol/L)
[2] (mol/L)
Time (s)
y = 0.00000135995x + 0.00047252707
R² = 0.97592422343

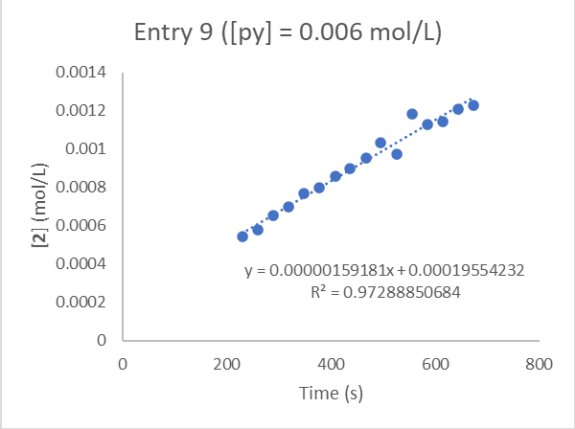
Entry 9 ([py] = 0.006 mol/L)
[2] (mol/L)
Time (s)
y = 0.00000159181x + 0.00019554232
R² = 0.97288850684

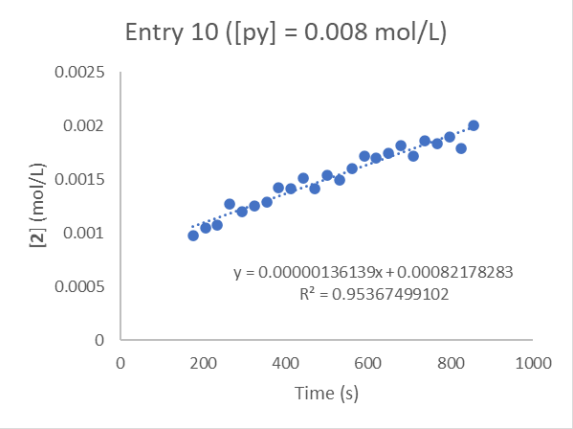
Entry 10 ([py] = 0.008 mol/L)
[2] (mol/L)
Time (s)
y = 0.00000136139x + 0.00082178283
R² = 0.95367499102

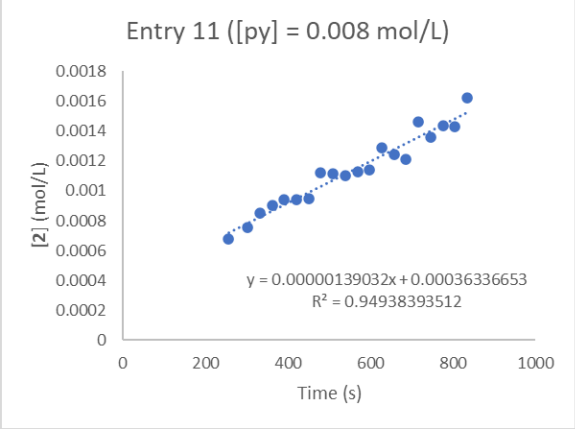
Entry 11 ([py] = 0.008 mol/L)
[2] (mol/L)
Time (s)
y = 0.00000139032x + 0.00036336653
R² = 0.94938393512

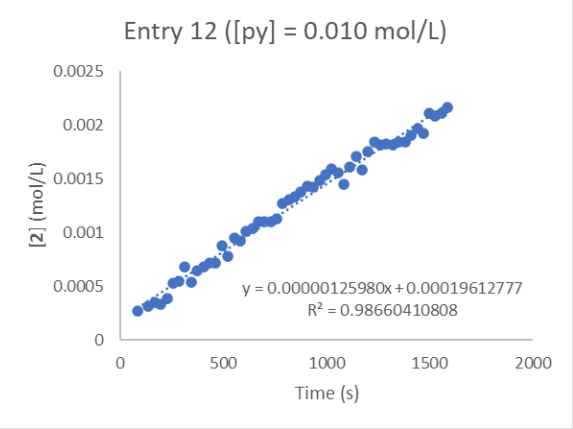
Entry 12 ([py] = 0.010 mol/L)
[2] (mol/L)
Time (s)
y = 0.00000125980x + 0.00019612777
R² = 0.98660410808

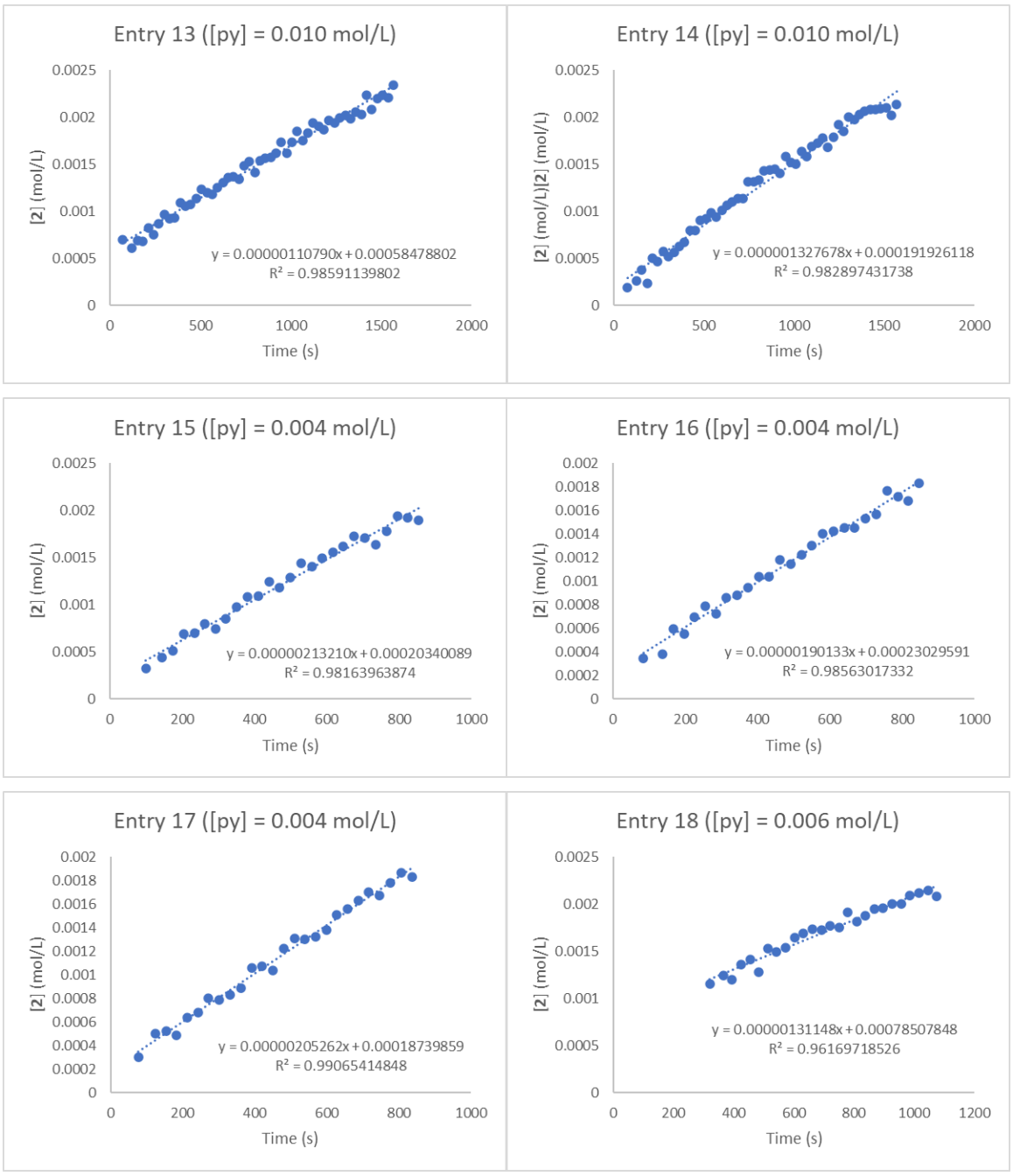

Figure 4.51. Concentrations of **4.2** versus time plots and the linear fitting results of entries 1-18 of Table 4.8. [py] refers to $[py]_{added}$ in this figure.

4.5.21 Cyclic Voltammetry of 4.1

Cyclic voltammetry of **4.1** was collected in CH_2Cl_2 with 0.1 M TBABArF as electrolyte. Fc was used as potential reference which was then converted to SCE based on reported $Fc^{0/+}$ couple vs. SCE in CH_2Cl_2.[212]

Attempts on the cyclic voltammetry measurement on **4.4** led to rapid decomposition. The color of the solution faded from deep brownish purple to light yellow upon applying both positive and negative potentials.

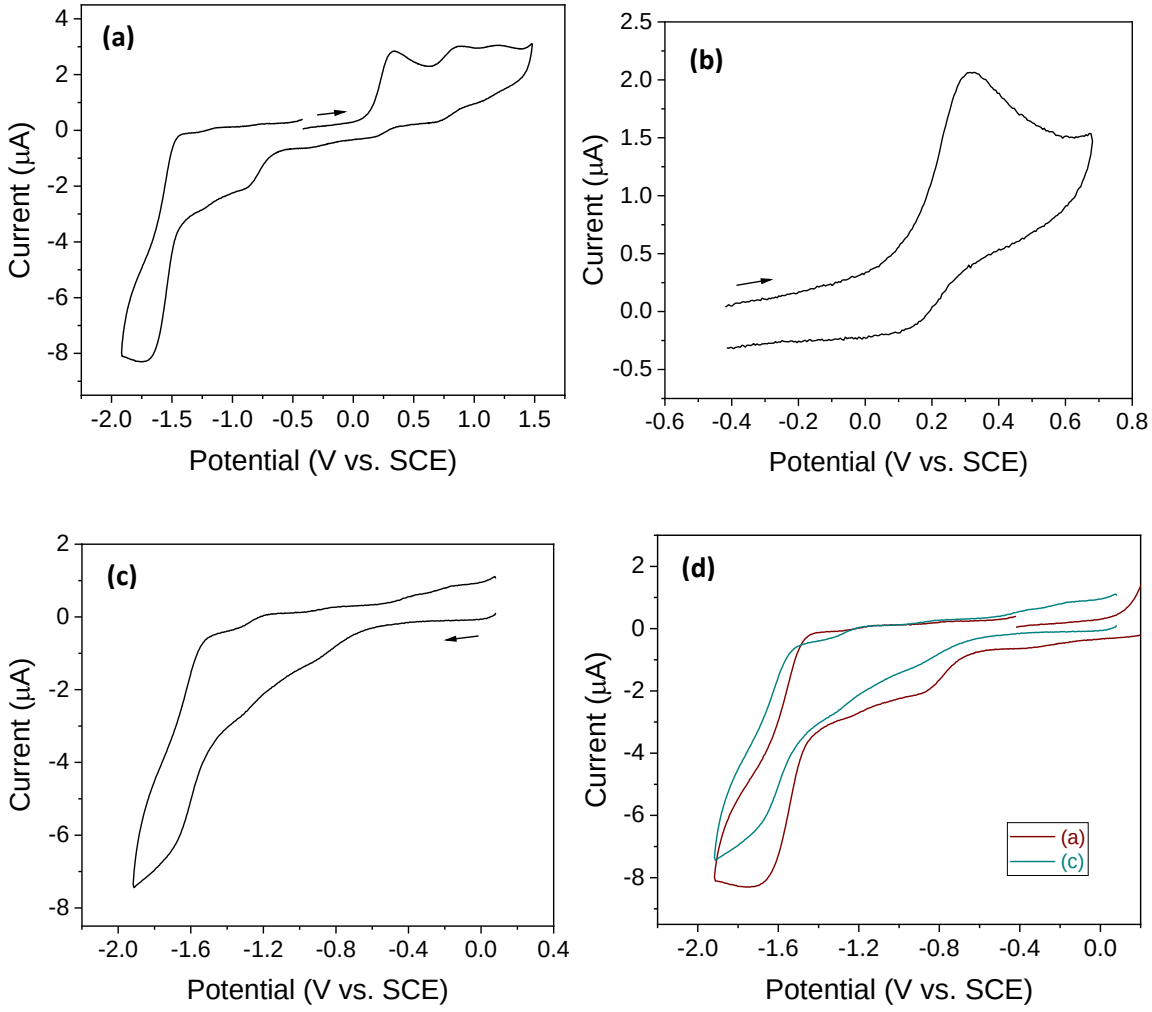

Figure 4.52. Cyclic voltammetry of **4.1** in CH_2Cl_2 with 0.1 M TBABArF, (a) full scan in positive direction; (b) oxidation scan in positive direction; (c) reduction scan in negative direction; (d) overlay of the full scan and the reduction scan. *Taken from YC EChem data: 020322 Ti metallacycle.*

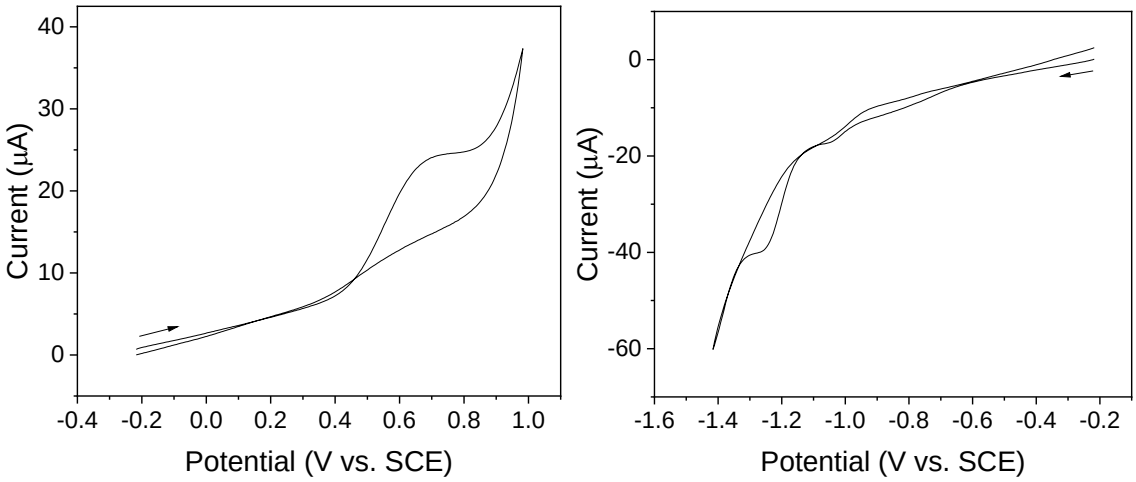

Figure 4.53. Cyclic voltammetry of **4.5** in CH_2Cl_2 with 0.1 M TBABArF, (left) oxidation scan in positive direction; (right) reduction scan in negative direction. *Taken from YC EChem data: 090522 py2Cl2TiNPh.*

4.5.22 DOSY of 4.1 and 4.4

DOSY NMR spectra were collected with first gradient amplitude = 2%, final gradient amplitude = 98%, number of points = 19 and linear ramp type. DOSY transformation was performed using Bayesian method with resolution factor = 1 and repetitions = 2. Estimated molecular weight (MW) was obtained by subjecting the diffusion coefficient (*D*) from DOSY spectra to SEGWE calculator (Manchester NMR Methodology Group, https://nmr.chemistry.manchester.ac.uk/?q=node/432).[191,192] DOSY spectra of **4.1** were collected at two concentrations: (1) 0.010 mol/L **4.1** in C_6D_6 and (2) 0.003 mol/L **4.1** in C_6D_6. DOSY spectrum of **4.4** was collected from a solution with 0.010 mol/L **4.4** in C_6D_6. DOSY of **4.3** was not collected due to the low solubility of **4.3** in C_6D_6. **4.3** is soluble CD_2Cl_2, however the estimated MW of **4.3** based on its DOSY in CD_2Cl_2 was inaccurate due to the low viscosity of CD_2Cl_2.

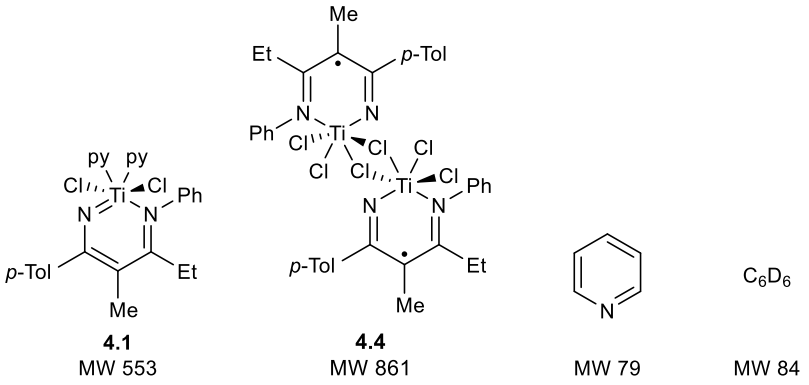

Figure 4.54. Proposed species found in DOSY studies and their MW.

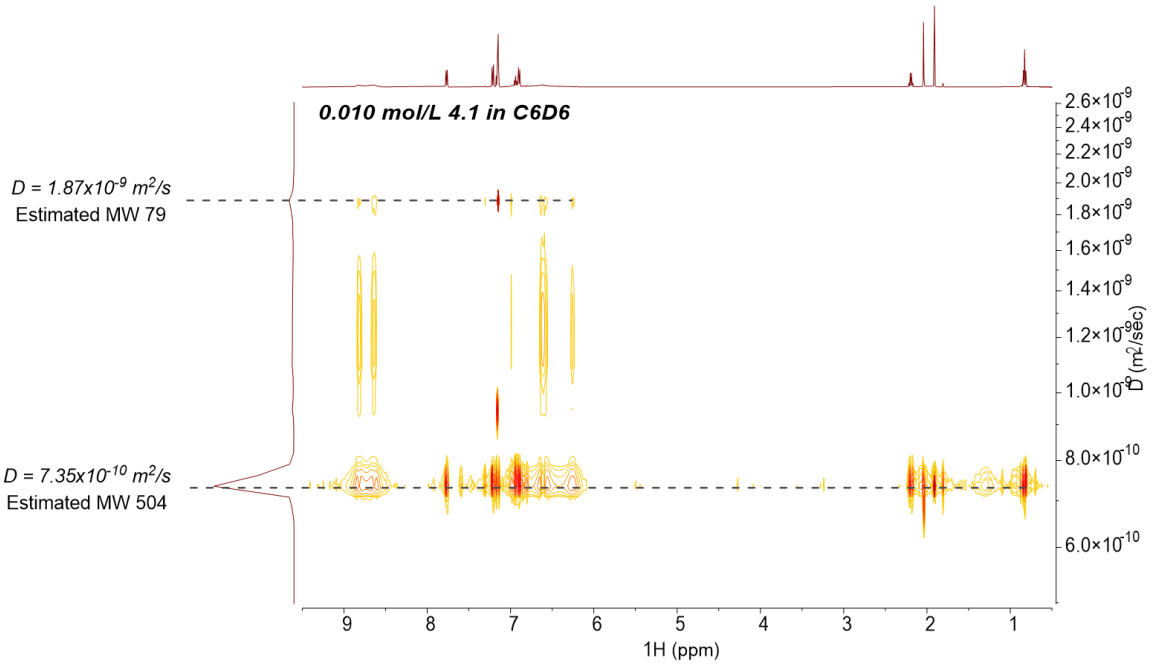

Figure 4.55. DOSY NMR spectrum of 0.010 mol/L **4.1** in C_6D_6. *Taken from YC-2021-0172-DOSY.*

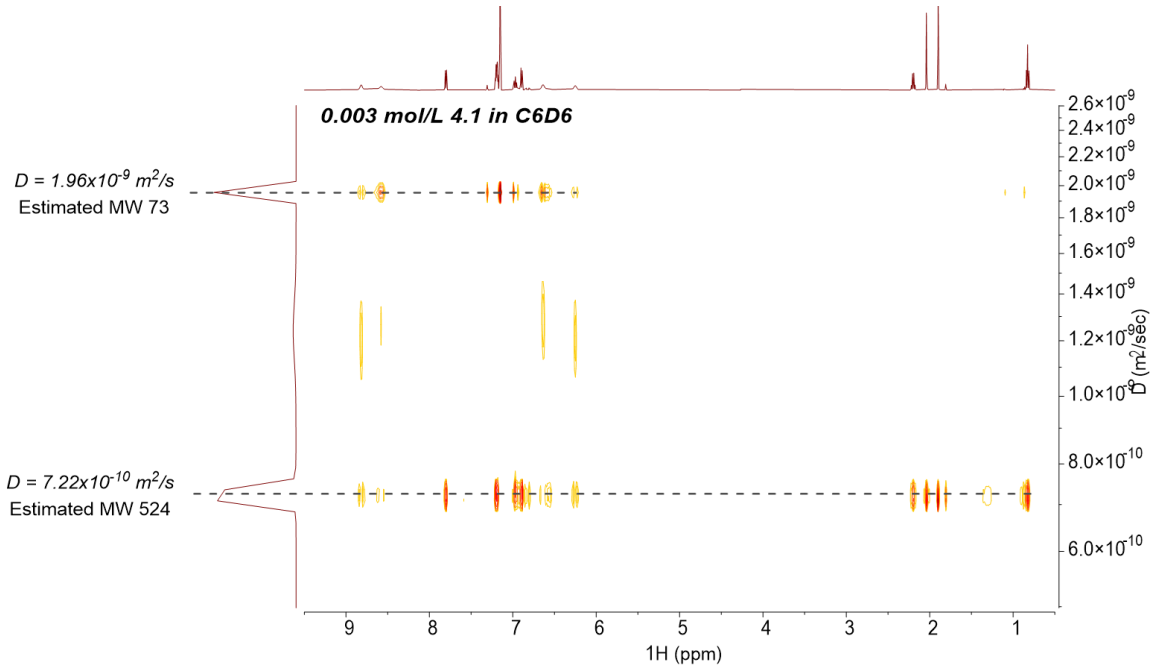

Figure 4.56. DOSY NMR spectrum of 0.003 mol/L **4.1** in C_6D_6. *Taken from YC-2021-0173-DOSY.*

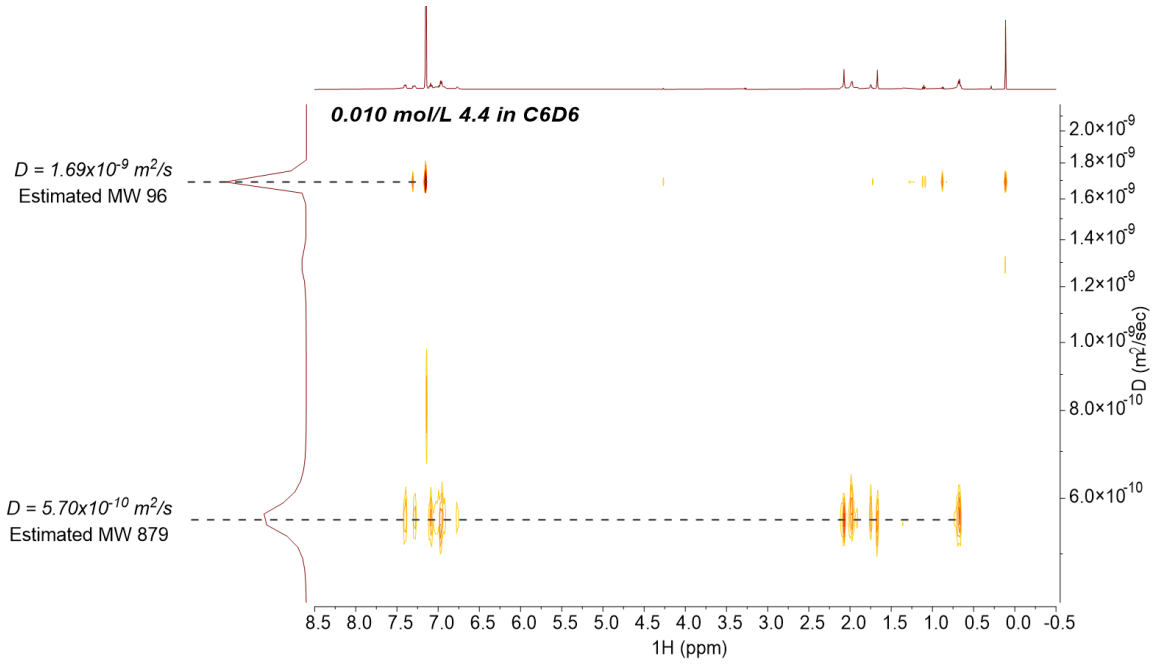

Figure 4.57. DOSY NMR spectrum of 0.010 mol/L **4.4** in C_6D_6. *Taken from YC-2021-0167-DOSY.*

4.5.23 XRD Data of 4.4 and $(PPN)_2CeCl_6$

	4.4	**4.7**	$(PPN)_2CeCl_6$
CCDC Number	?	?	?
Empirical Formula	$C_{38}H_{40}Cl_6N_4Ti_2$	$C_{38}H_{40}Cl_4N_4Ti_2$	$C_{72}H_{60}CeCl_6N_2P_4$
Formula Weight	861.24	790.34	1429.92
Temperature (K)	150(2)	150.0	150.0
a, Å	23.065(4)	9.3405(9)	10.917(3)
b, Å	11.6096(17)	9.3839(7)	12.768(4)
c, Å	15.652(2)	21.029(2)	13.254(4)
α, °	90	90	63.418(8)
β, °	109.782(6)	90.745(2)	87.010(9)
γ, °	90	90	83.337(6)
Volume, $Å^3$	3943.8(11)	1843.0(3)	1641.1(8)
Z	4	2	1
Crystal System	Monoclinic	Monoclinic	Triclinic
Space Group	$P2_1/c$	$P2_1/c$	$P\bar{1}$
d_{calc}, g/cm^3	1.451	1.424	1.447
θ Range, °	2.23 to 28.51	1.937 to 30.617	2.46 to 30.52
μ, mm^{-1}	0.845	0.757	1.079
Abs. Correction	None	Multi-scan	Multi-scan
GOF	1.099	1.130	1.047
R_1[a]	0.0832	0.0375	0.0219
wR_2[b] [I>2σ(I)]	0.2215	0.0863	0.0528

[a] $R_1 = \Sigma||F_o|-|F_c||/\Sigma|F_o|$. [b] $wR_2 = [\Sigma[w(F_o^2-F_c^2)^2]/\Sigma[w(F_o^2)^2]^{1/2}$.

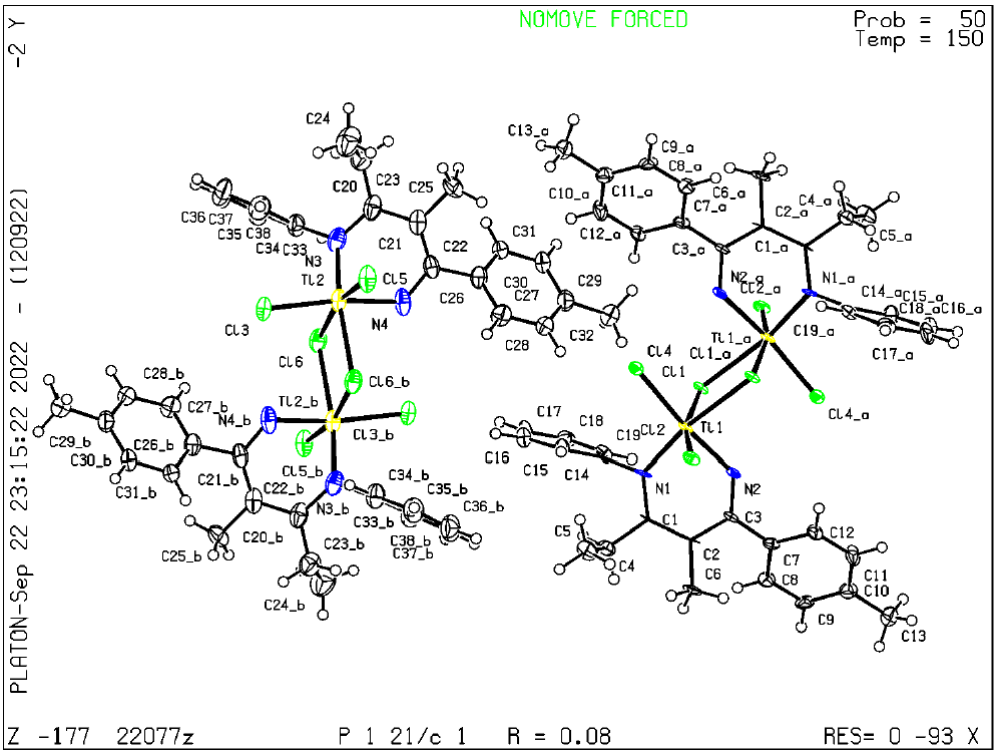

Figure 4.58. ORTEP diagram of **4.4**. Thermal ellipsoids are drawn at 50% probability.

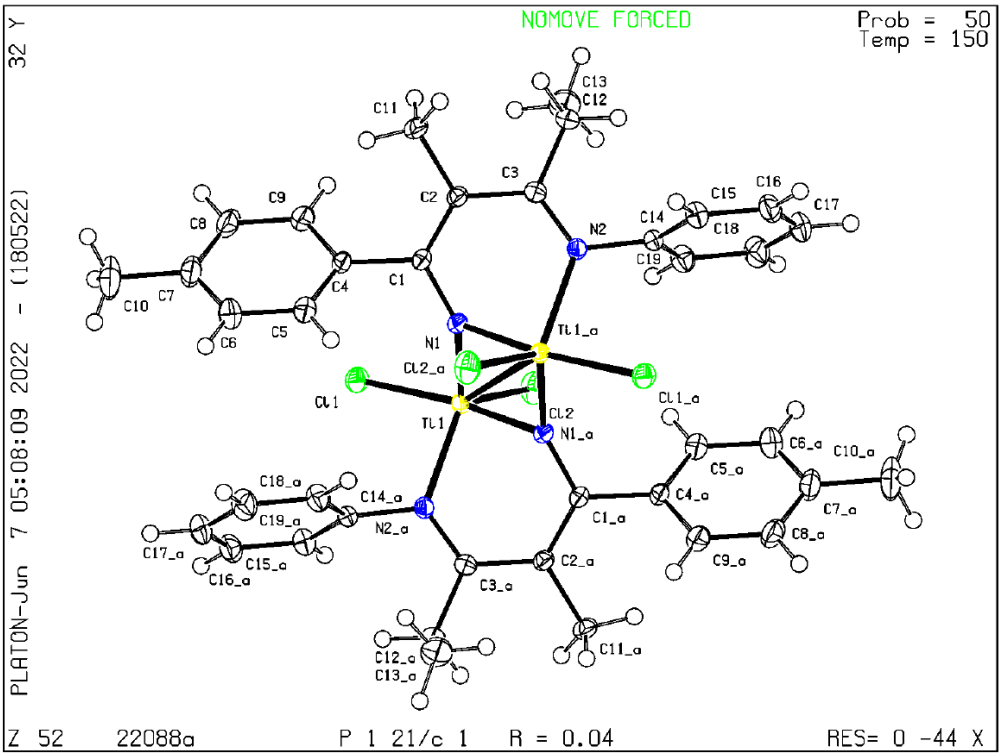

Figure 4.59. ORTEP diagram of **4.7**. Thermal ellipsoids are drawn at 50% probability.

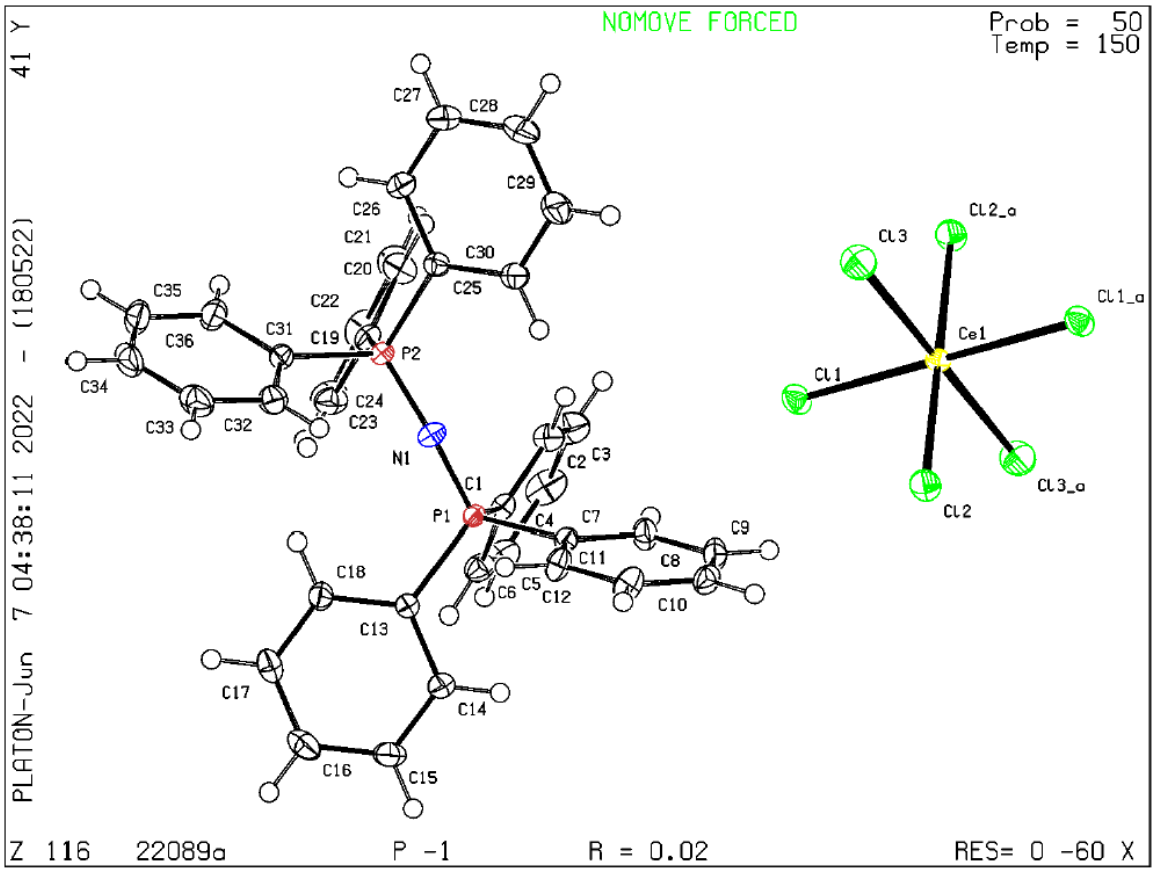

Figure 4.60. ORTEP diagram of $(PPN)_2CeCl_6$. Thermal ellipsoids are drawn at 50% probability.

Chapter 5: Synthesis of 2*H*-Indazole *via* Ti-Mediated Intramolecular N–N Coupling: Towards a General Strategy for N–N Heterocoupling

5.1 Overview

Indazoles are among the most frequently presented heteroaromatic core moieties in various pharmaceuticals. Despite being challenging, direct N–N coupling gives access to indazoles without the use of hazardous reagents with pre-formed N–N bonds such as hydrazines. Meanwhile, oxidation-induced reductive elimination of metal imido-imine or amide-amide complexes has previously been demonstrated to be a powerful method in the synthesis of 1,2-diazoles. Herein, we report the synthesis of indazole *via* Ti-mediated oxidative N-N coupling. Oxidation of 2-titanaquinazoline, *in situ* generated from deprotonation of 2-iminylaniline, generates 2*H*-indazole in good yield. The use of Cl-based one-electron oxidant ferrocenium chloride offers compatibility between the oxidation of 2-titanaquinazoline and the re-activation of oxidation product $TiCl_4$, allowing the development of a catalytic indazole synthesis. Mechanistic exploration shows that the conjugated linker has a crucial contribution to the intramolecular N-N heterocoupling by preserving the bidentate N^N ligand scaffold, while the ligand-centered oxidation of non-tethered imido-imine or amide-amide ligands results in homocoupling or scrambling due to rapid ligand dissociation. This reaction provides a method to access 2*H*-indazoles from benign reagents and new insight into the development of N–N heterocoupling reactions.

5.2 Introduction

1,2-Diazaaromatics occupy an important category as pharmaceuticals. With the addition of different targeting groups, pyrazole, indazole, and various hetero-1,2-diazoles are listed among the most frequently used aromatic cores in bioactives against various diseases.[82,213,214] Meanwhile, the synthetic methods for 1,2-diazaaromatics has traditionally relied on reactants with pre-formed N–N bond, which is crippled by their toxicity and safety concern. For example, the state-of-art syntheses of the pyrazole core in celecoxib and rimonabant utilize the Knorr condensation of hydrazines on 1,3-diketones,[82,215] and various indazole-based pharmaceuticals like pazopanib and pictilisib originates the cycloaddition of the diazo group formed *in situ*.[82,216,217] It should also be noted that 1*H*-indazoles are more prominent than 2*H*-indazoles in the drug candidate inventory, partly owing to the better synthetic accessibility of 1*H*-indazoles from cyclization of hydrazone. The recent emergence of metal-free direct N–N coupling reactions based on condensation and cycloaddition provides a new route accessing

highly functional pyrazoles and indazoles, notable ones including the Davis-Beirut reaction[218,219] and the condensation between enamide and oxime.[220–222]

Oxidative N–N coupling is another prevalent method for N–N bond formation with its use found from the industrial synthesis of hydrazine (the peroxide process)[223] to the electrosynthesis of dixiamycin B.[224] While being versatile and efficient, the majority of these methods were used to generate homocoupling product *via* the coupling of free aminyl radicals. This limits their use in the syntheses of drug candidates where high product complexity is desired. On the other hand, transition metal mediated intramolecular N–N coupling appears to be an attractive route to achieving N–N heterocoupling. However, N–N reductive elimination remains challenging, largely owing to the low N–N bond strength compared with the relatively strong metal–N bond. Regardless of the difficulties, formal N–N reductive elimination has been achieved with the assistance of oxidants and applied in the syntheses of azaaromatics with late transition metals, mainly Cu.[67,186,225,226] Notably, rich catalytic aerobic oxidation chemistry has been developed on the synthesis of pyrazole from enamine and nitrile (Figure 5.1a)[68,69] as well as 1*H*-indazole from iminylaniline (Figure 5.1b)[70] in the past decade.

Adapted from the late transition metal transformations, our group recently developed a Ti-mediated oxidative pyrazole synthesis based on the oxidation-induced reductive elimination of diazatitanacyclohexadiene **5.1** (Figure 5.1c).[61] Combining with our previous studies on the multicomponent coupling of Ti imido complexes,[9,32] tetra-substituted pyrazoles (**5.2**) can be efficiently synthesized from the one-pot sequential [2+2+1] cycloaddition-oxidation reaction from various alkynes, nitriles and Ti imido (**5.3**) through **5.1**. Alternatively, **5.1** can also be synthesized from the deprotonation of 4-azadiene-1-amine **5.3**. Designing a catalytic multicomponent pyrazole synthesis has been proved to be difficult, as it falls into a dilemma of compatibility between the oxidant for oxidation of **5.1** and the reductant for the turnover of $py_2TiCl_2X_2$ (Chapter 4). Despite being a stoichiometric reaction, Ti-mediated pyrazole synthesis has high potential in green chemistry as Ti is an earth-abundant transition metal with low toxicity.[1] We envisioned that the synthesis of **5.1** from deprotonation of **5.3** can be adapted to the synthesis of other diazatitana cycles and the subsequent oxidative N–N coupling. This offers two advantages: (1) a synthetically more accessible *β*-amino-*α*,*β*-unsaturated imine scaffold than **5.3**, and (2) potential catalytic turnover on account of the better compatibility between acid-base chemistry and oxidation.

Herein, we report the Ti-mediated synthesis of 2H-indazole (**5.6**) from 2-iminylaniline (**5.4**) through the oxidation of the *in situ* formed 2-titanaquinazoline **5.5** (Figure 5.1d). Indazole can

be synthesized using various one-electron oxidants, and a catalytic reaction has been developed using Cl-based oxidant FcCl. Further investigation on the one-electron oxidation of other Ti imido-imine and Ti bisamide complexes demonstrates the generality of Ti-mediated N–N coupling *via* ligand-centered oxidation and reveals that a conjugated linker is crucial to the intramolecular N–N heterocoupling by stabilizing the oxidized intermediates to prevent dissociation of the coupling partner before N–N bond formation.

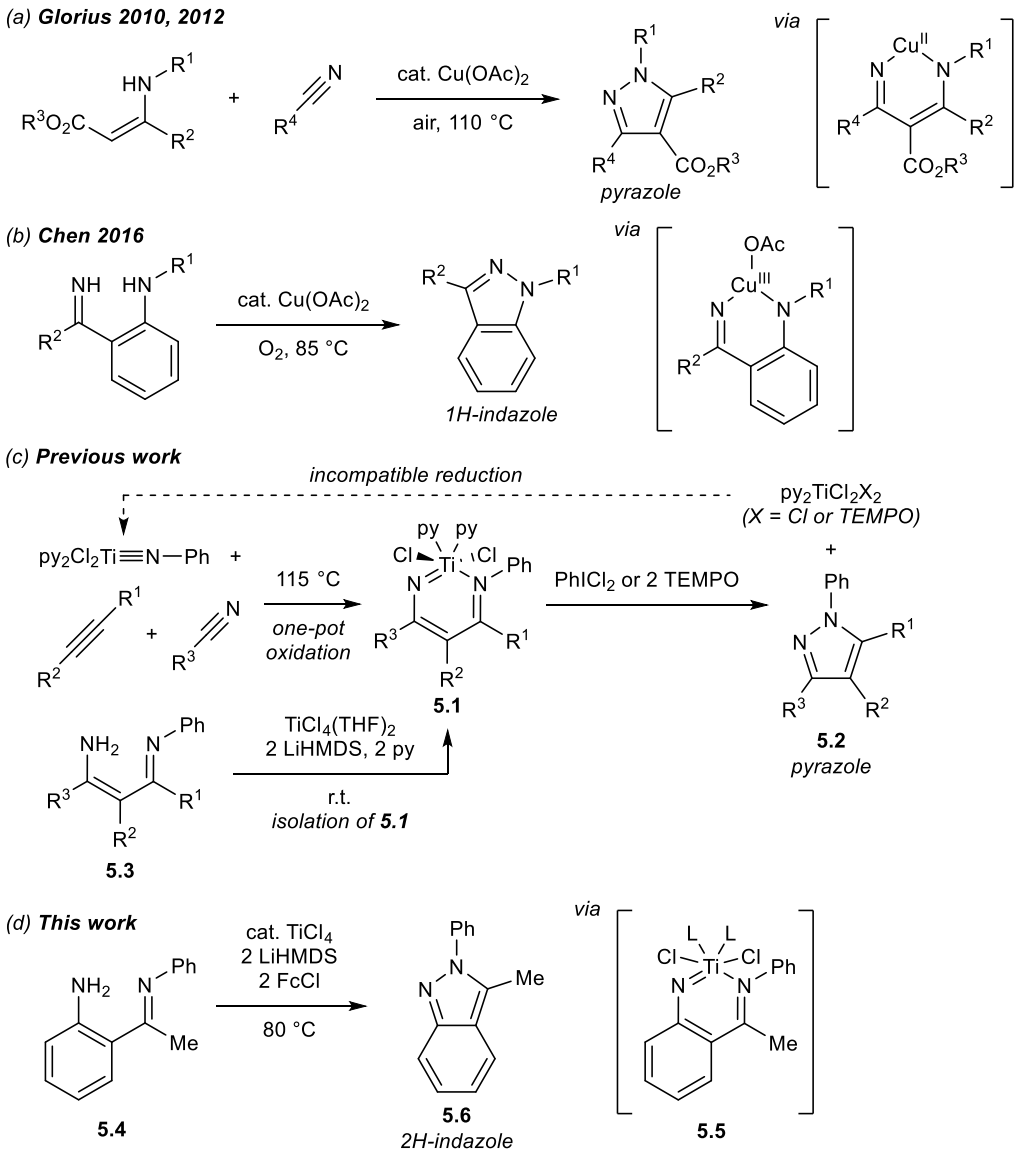

Figure 5.1. Syntheses of pyrazoles and indazoles *via* metal-mediated intramolecular N–N coupling.

5.3 Result and Discussion

The condition in our initial attempt was adapted from the synthesis of diazatitanacyclohexadiene **5.1** from **5.3**. The reaction of 2-iminylaniline **5.4** with stoichiometric $TiCl_4$ and 2 equiv LiHMDS yielded 2-titanaquinazoline **5.5** *in situ* as a bright red suspension. Two equivalents of TEMPO were added, resulting in the one-pot oxidation of **5.4** to indazole **5.6** in 9% yield (Table 5.1, entry 1). Changing the reaction solvent from THF to CH_2Cl_2 led to a dramatic increase in yield to 55-58% (Table 5.1, entry 2, 3), with the reaction product of the first step being a deep red solution instead. The solubility of **5.5** in different solvents was first suspected to be the origin of the reactivity difference. To investigate this, 2 equiv of pyridine was added as an additive after the addition of LiHMDS (Table 5.1, entry 4). The yield of indazole was lowered to 26%, despite that no precipitation was observed after the first step. It was speculated that the reactivity of **5.5** was affected by the L donor on Ti, where the presence of strong L type ligands (L = THF, pyridine) hindered the oxidation of **5.5**. In fact, pyridine was found to have an inhibitive role in the TEMPO oxidation of **5.1** that shares the similar diazatitanacyclodiene moiety (Chapter 4). Lastly, the control reactions with the absence of $TiCl_4$ (Table 5.1, entry 6) or LiHMDS (Table 5.1, entry 7) suggested that 2-titanaquinazoline **5.5** was the reaction intermediate in the Ti-mediated indazole synthesis.

Table 5.1. One-pot *in situ* Ti-mediated indazole synthesis with TEMPO and reaction condition optimization.

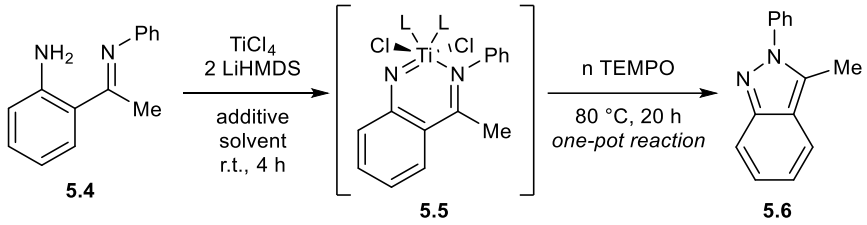

entry	solvent	additive	TEMPO equiv	yield[a] (%)
1	THF	None	2	9
2	CH_2Cl_2	None	2	55 (42)[b]
3[c]	CH_2Cl_2	None	2	58
4	CH_2Cl_2	None	4	52[d]
5	CH_2Cl_2	2 equiv pyridine	2	26

6[e]	CH_2Cl_2	None	2	not observed
7[f]	CH_2Cl_2	None	2	not observed

[a]Yields were determined *via* ^{1}H NMR against TMB internal standard unless specified. [b]Isolation yield. [c]Reaction time after the addition of TEMPO = 72 hours. [d]Yields were determined *via* GC against TMB internal standard. [e]No $TiCl_4$. [f]No LiHMDS.

Although our attempt at direct isolation of **5.5** was futile, a model compound **5.5^{bpy}** with L = 2,2'-bipyridine (bpy) can be synthesized by reacting the in situ formed **5.5** with bpy (Figure 5.2). The X-ray crystal structure of **5.5^{bpy}**, shown in Figure 5.2, shows that it has similar bond metrics to **5.1**. The Ti1–N1 distance of 2.245(3) and Ti1–N2 distance of 1.730(1) are consistent with the assignment that imido-imine has the major contribution in the imido-imine/amide-amide resonance structures of **5.1**.

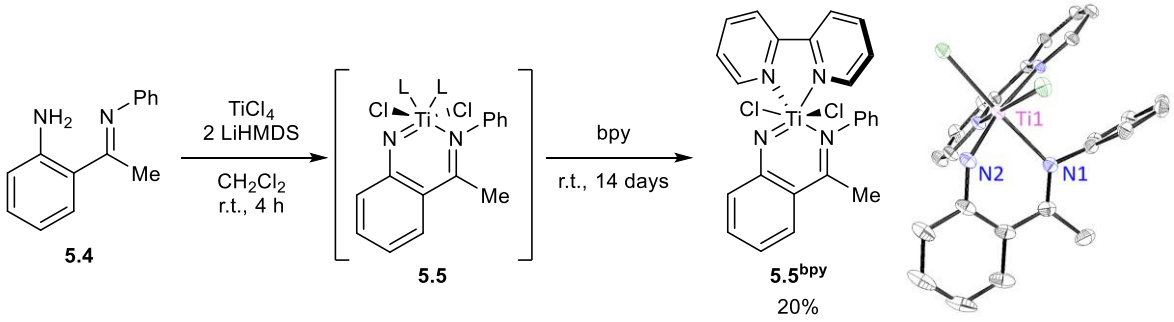

Figure 5.2. Syntheses of bpy-bound 2-titanaquinazoline **5.5^{bpy}**.

After the encouraging success in the synthesis of indazole **5.6** from 2-iminylaniline **5.4** using stoichiometric $TiCl_4$ and TEMPO, we hoped to develop a Ti-catalyzed indazole synthesis method from **5.4**. The primary obstacle in the design of a catalytic Ti redox reaction is the regeneration of the low valent Ti species due to its high reduction potential. In the hypothetical catalytic oxidation of diazatitanacyclohexadiene **5.1**, re-activation of the Ti oxidation product $TiCl_2[Ox]_2$ to Ti^{II} becomes the major challenge, where a strong reductant is required for the cleavage of the strong Ti–[Ox] bond. Our prior studies sought a solution to it by oxidizing **5.1** to $TiCl_4$ for its weak Ti-Cl bond using Cl-based oxidants (Chapter 4), yet were still unable to reduce $TiCl_4$ due to the compatibility challenges between **5.1** and the reductant (Figure 5.3 right). We envisioned that the formation of **5.5** from **5.4** *via* acid-base chemistry instead of $Ti^{II/IV}$ redox reaction can bypass the compatibility challenges between various oxidants and reductants in the design (Figure 5.3 left).

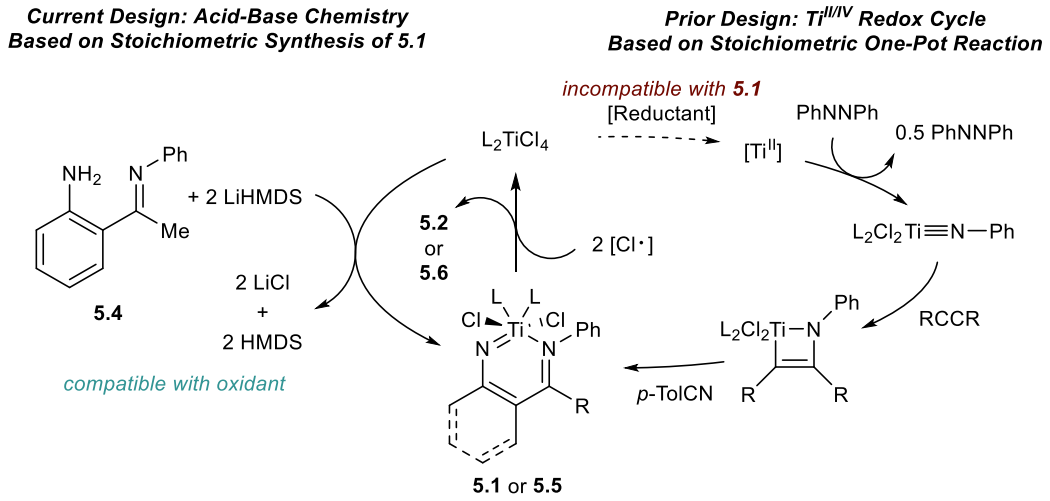

Figure 5.3. Design of a Ti-catalyzed 1,2-diazole synthesis with Cl-based oxidant.

Following the design of the Ti-catalyzed 1,2-diazole synthesis, a Cl-based oxidant compatible with the formation of **5.5** will be necessary. We first studied the oxidation of the *in situ* formed **5.5** with one-electron oxidants $(PPN)_2CeCl_6$ and FcCl (Figure 5.4, top). $[CeCl_6]^{2-}$ was previously found as a Cl radical surrogate in the oxidation **5.1**. Thus, the oxidation of **5.5** with $(PPN)_2CeCl_6$ gave a similar yield (41%) to the TEMPO oxidation of **5.5**. Our prior work revealed that outer sphere oxidant Fc^+ relied on the coordination effect of Cl^- to oxidize **5.1** in an inner sphere-like mechanism. We speculated that the successful oxidation of **5.5** by FcCl was based on the same effect, though the order of the electron transfer and the Cl^- coordination remains unclear to us. Two-electron oxidant $PhICl_2$ failed to efficiently oxidize **5.5** (Figure 5.4, bottom) due to a potential mechanism change compared to the $PhICl_2$ oxidation of **5.1**. In fact, the same yield of **5.6** can be achieved in the absence of $TiCl_4$, indicating the observation of indazole might originate from the background reaction between **5.4** and $PhICl_2$.

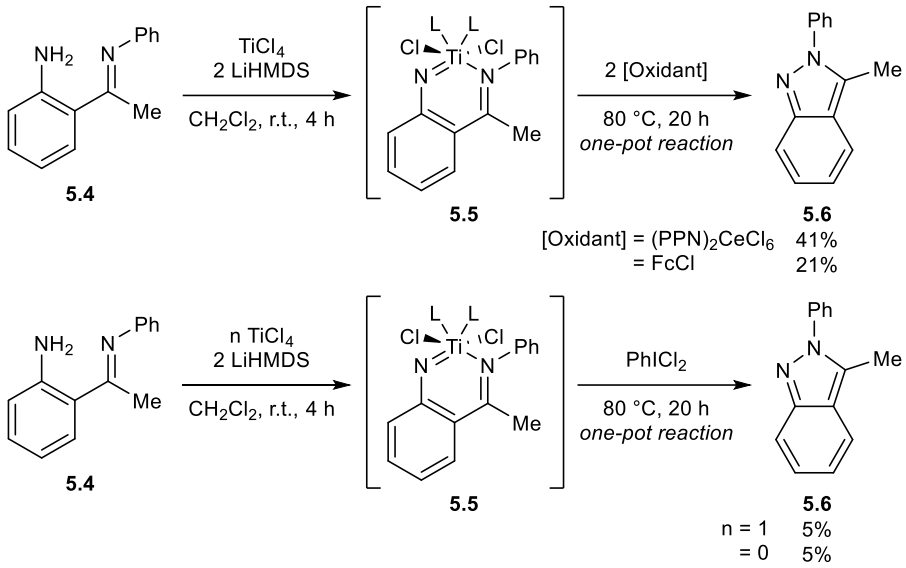

Figure 5.4. Scope of Cl-based oxidants for one-pot *in situ* Ti-mediated indazole synthesis. (Top) one-electron oxidants FcCl and $(PPN)_2CeCl_6$. (Bottom) two-electron oxidant $PhICl_2$.

The identification of Cl-based oxidants for **5.5** allowed us to design a catalytic cycle shuttling between **5.5** and $TiCl_4$. FcCl instead of $(PPN)_2CeCl_6$ was chosen as the oxidant in regard to the potential competitive formation of Ce amide complexes. 2-Iminylaniline **5.4** could be converted to indazole **5.6** in 32% yield using 10% $TiCl_4$ as the catalyst with 2 equiv LiHMDS and 2 equiv FcCl in CH_2Cl_2 (Figure 5.5). The proposed reaction mechanism starts from the coordination of **5.4** to $TiCl_4$ to form an imine-amine complex of Ti, the following deprotonation by LiHMDS generates the bidentate imido-imine Ti complex **5.5**. Oxidation of **5.5** by FcCl yields indazole **5.6** with $TiCl_4$ as the byproduct, closing the catalytic cycle. Although the yield of the pre-optimized reaction is limited, the development of a catalytic indazole synthesis demonstrates that the design combining Ti imido formation from amine and the oxidation of diazatitanacyclohexadiene is a Ti-compatible strategy for N–N cyclization of substrates bearing the *β*-amino-*α*,*β*-unsaturated imine scaffold.

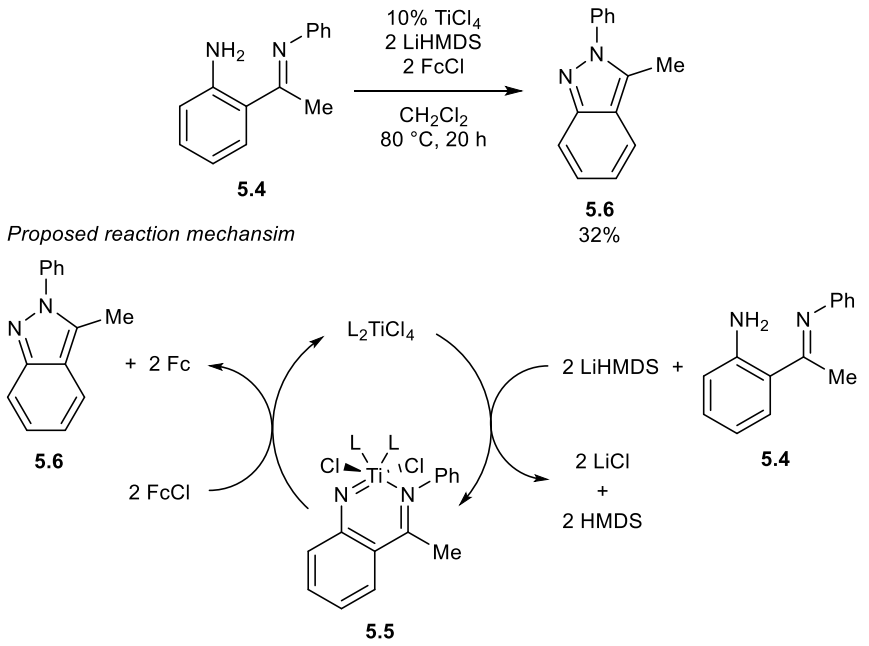

Figure 5.5. Ti-catalyzed indazole synthesis with FcCl.

The distinct difference in reactivity between $PhICl_2$ oxidation of **5.5** and **5.1** aroused our interest. We sought to gain a deeper understanding of how the extended aromatic system affects the diazatitanacyclohexadiene by examining other reaction modes **5.1** exhibited in our previous studies. The reaction between **5.1** and *C*-nitroso compounds generates α-diimines through a unique mechanism involving the sequential [4+2] cycloaddition and retro-[4+2] cycloaddition on the metallaaromatic system.[60] Surprisingly, subjecting the *in situ* formed **5.5** to nitrosobenzene (PhN=O) led to its oxidation to indazole **5.6** at 17% yield along with various diazene products (Figure 5.6). The diazenes are proposed to originate from PhN=O undergoing Mills reaction with **5.4** or nitrene heterocoupling with Ti imido on **5.5**, while no side product can be attributed to the [4+2] cycloaddition between **5.5** and nitrosobenzene. The Ti alkenylimido was proposed to serve as the diene in the [4+2] cycloaddition with PhN=O owing to the high oxophilicity of Ti, resulting in the hypothetical [4+2] adduct **5.7**. Compared to **5.1**, the dearomatization of the extended aromatic system of **5.5** renders the formation of **5.7** less favorable. The mechanism of PhN=O oxidation of **5.5** to **5.6** involving the formation of a phenylimido Ti remains unclear (see Section 5.5.8 for further discussion).

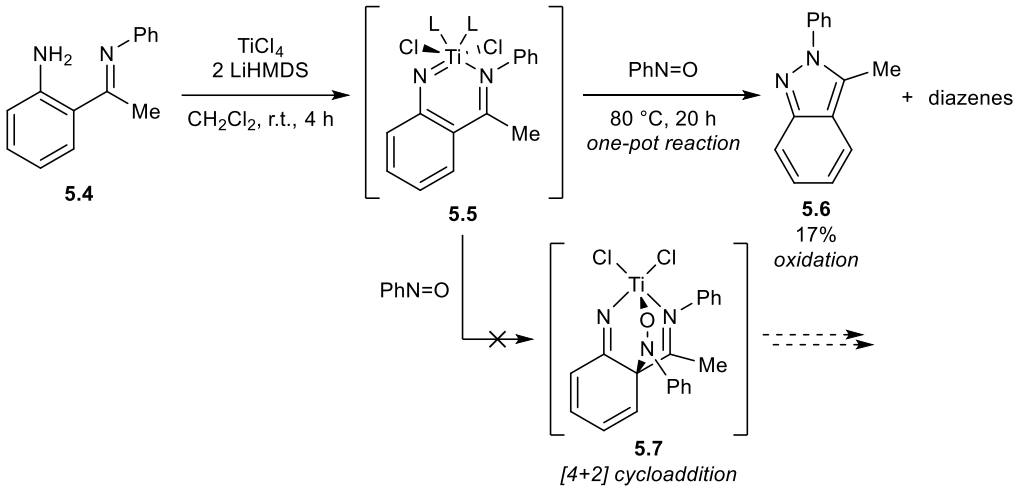

Figure 5.6. Reaction between nitrosobenzene and *in situ* formed 2-titanaquinazoline **5.5**.

During sequential one-electron oxidations, Ti complexes bearing conjugated tethered imido-imine ligands like **5.1** and **5.5** share the stabilization effect from the resonance of the conjugated system (Figure 5.7). Our previous mechanistic studies showed that in the TEMPO oxidation, the first oxidation occurred prior to the rate-determining step while the second oxidation was after, suggesting the slow intermediate was benefited from the resonance stabilization (Chapter 4). The same effect was proposed to be crucial to the oxidation of **5.5** with one-electron oxidants TEMPO, $(PPN)_2CeCl_6$, and FcCl. We were curious if a similar N–N coupling reaction can still be achieved intramolecularly on non-tethered imido-imine or amide-amide Ti complexes, using Ti as a metal template for the reactive radical intermediate.

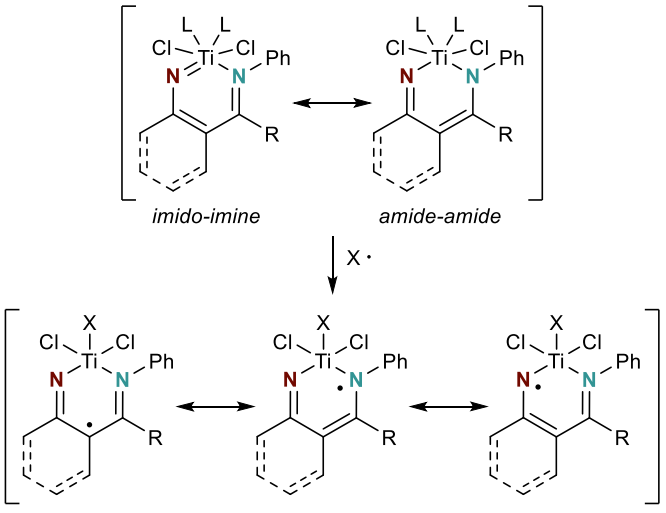

Figure 5.7. Resonance stabilization of the oxidation intermediate of Ti complex with a conjugated tethered imido-imine ligand.

The reaction of the in situ formed diimine Ti phenylimido dichloride **5.9** with TEMPO was monitored *via* quantitative ^{1}H NMR (Figure 5.8). **5.9** can be formed *in situ* through the addition of 2 equiv *N*-phenylpentan-3-imine **5.8** to the oligomeric Ti phenylimido dichloride. Immediately after the addition of TEMPO, free **5.8** was found quantitatively in the solution, indicating the full release of **5.8** from Ti (Figure 5.34). A peak assigned to Ti-bound TEMPO reached maximum yield at the 5 hours time point. On the other hand, azobenzene (PhNNPh) was formed slowly during the 24 hours at room temperature and further increase to 59% after heating, while **5.8** and [Ti–TEMPO] were unchanged during heating. It was proposed that the PhNNPh was formed *via* a dititanium bis(TEMPO) 1,2-diphenylhydrazido(2-) intermediate from the homocoupling of Ti, which was semi-stable at room temperature but underwent disproportionation readily upon heating to give PhNNPh. Although the structure of this intermediate was undefined, a similar dititanium 1,2-diphenylhydrazido(2-) complex has been reported by Floriani *et al.* in the reduction of PhNNPh by $[CpTi^{III}Cl_2]_n$,[54,55] which can be considered as the microscopic reverse process of the oxidation of Ti phenylimido to PhNNPh.

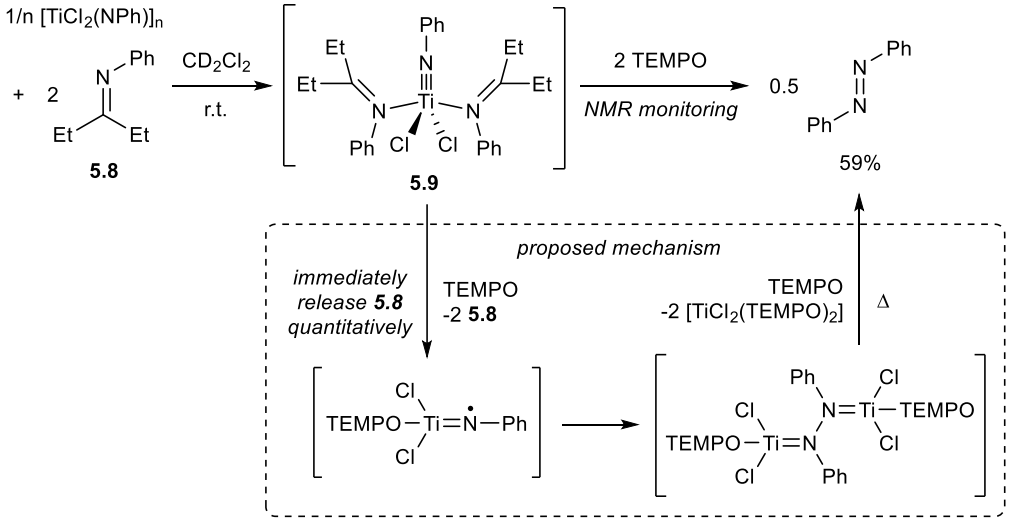

Figure 5.8. Oxidative N–N coupling of non-tethered imine-imido Ti complex.

Next, we investigated the TEMPO oxidation of Ti bisamide complexes. To our surprise, oxidation of $TiCl_2(NMe_2)_2$ with 1 and 2 equiv. TEMPO gave tetramethylhydrazine (**5.10**) in similar yields (Figure 5.9 top). The rapid TEMPO oxidation was completed in 1 hour, with prolonged reaction time giving minimum change. The side reaction of the reaction was

identified to be dichlorotitanium dimethylamide TEMPO complex **5.11** *via* the independent synthesis of **5.11** from 1:1 stoichiometric reaction of $TiCl_2(NMe_2)_2$ and TEMPO-H (Figure 5.9). These observations suggest that $TiCl_2(NMe_2)_2$ was oxidized by TEMPO rapidly to **5.11**, generating an aminyl equivalent which further underwent dimerization to yield **5.10**. We speculated that the aminyl equivalent was a free aminyl radical, as similar oxidative N–N coupling of amides to hydrazines has been observed on bismuth triamides and the triamide complexes of rare earth metals, where a free aminyl radical mechanism was supported by EPR evidence.[76,77] Meanwhile, the further oxidation of **5.11** was extremely slow but can be turned on at elevated temperature. Heating the reaction mixture at 80 ℃ led to the formation of dichlorotitanium bis(TEMPO) complex **5.12** with **5.11** being fully consumed. Although the NMR yield of **5.10** only slightly increased after heating, the actual yield of **5.10** may be much higher due to its volatility. TEMPO oxidation of $Ti(NMe_2)_4$ and $TiCl_3(NMe_2)$ were also investigated (Figure 5.9 bottom right). Despite reduced TEMPO species being formed in both reactions, $Ti(NMe_2)_4$ did not get oxidized to **5.10** at room temperature and only gave 23% yield after heating at 80 ℃ for 24 hours, while $TiCl_3(NMe_2)$ showed no productive chemistry. This indicates that the reactivity of Ti amide complexes towards TEMPO oxidation is sensitive to the coordination environment of Ti.

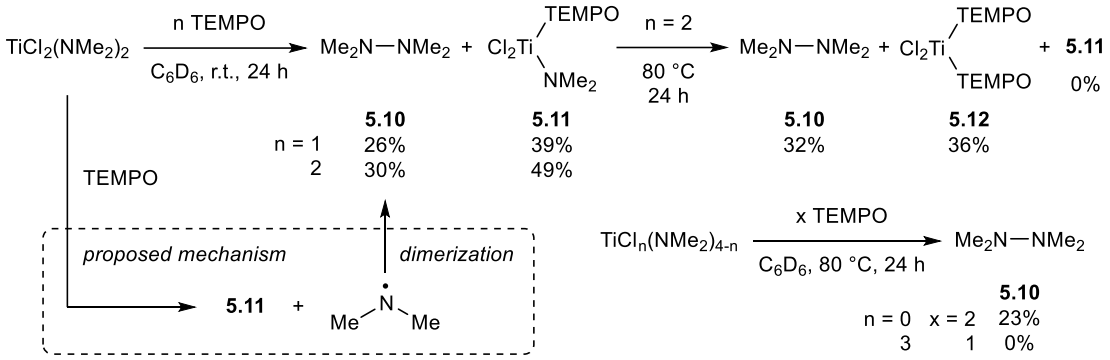

Figure 5.9. Oxidative N–N coupling of non-tethered Ti amide complexes.

Through studying the TEMPO oxidation of the aforementioned Ti imido-imine and amide-amide complexes, Ti-mediated N–N coupling through one-electron ligand-centered oxidation of Ti^{IV} complexes can be categorized into two types. When the oxidation occurs on a tethered conjugated N^N ligand, the stabilization offered by the resonance between *N*-radical and *C*-radical engenders a long-lived oxidized intermediate (Figure 5.10 left). This allows the ligand to be oxidized the second time while remaining a bidentate ligand on the Ti center, resulting in the N–N heterocoupled cyclization templated by Ti. Contrastingly, when a non-tethered

monodentate ligand is oxidized, the *N*-radical without extra stabilization leads to the disintegration of the Ti complex (Figure 5.10 right). On a non-tethered imido-imine complex, the rapid dissociation of the imine yields a Ti iminyl equivalent, eventually leading to the oxidative N–N homocoupling of the imido moiety. In the case of a non-tethered bisamide complex, the oxidation of the amide ligand releases free aminyl radical, following which a radical coupling generates hydrazine with scrambling potentially involved. The conjugation on the linker of a tethered ligand positively contributes to the selectivity in N–N heterocoupling through maintaining a bidentate scaffold, although it requires further investigation on whether this can be achieved by solely the chelate effect without the resonance stabilization.

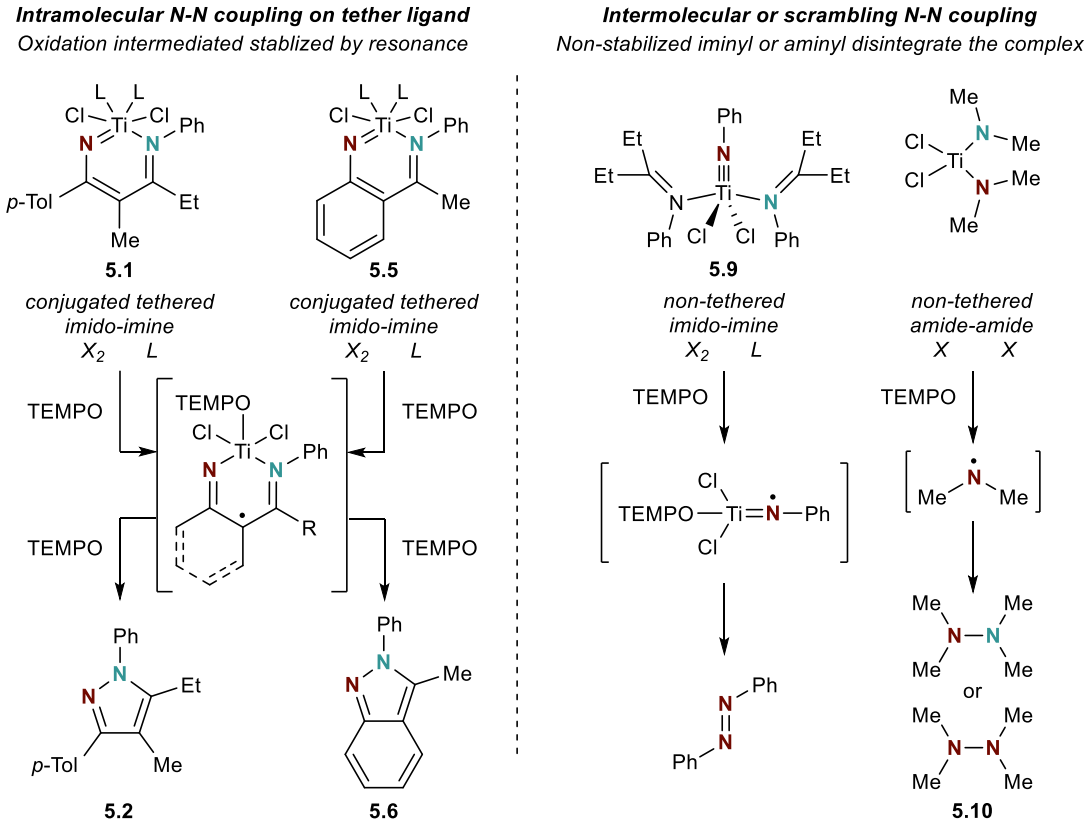

Figure 5.10. Tethered and non-tethered ligands in Ti-mediated oxidative N–N coupling with TEMPO.

5.4 Conclusions

In summary, we have demonstrated that the deprotonation 2-iminylaniline can be used as an oxidant-compatible approach to generate 2-titanaquinazoline for the stoichiometric and catalytic syntheses of 2*H*-indazole via oxidative N–N coupling. Various one-electron oxidants have been found to be efficient in the oxidation of 2-titanaquinazoline, suggesting the importance of the resonance stabilization of oxidized intermediates of diazatitanacyclohexadienes. The comparisons with non-tethered Ti imido-imine complex and bisamide complexes have shown the crucial role of the conjugated tethered linker in intramolecular N–N heterocoupling by preserving the integrity of the Ti complex. On the other hand, the oxidation of non-tethered N^N ligands will lead to the rapid dissociation of the coupling partner, leading to free *N*-radical-like reactivity where homocoupling or scrambling is dominant. The incorporation of amine deprotonation as a redox-compatible approach to access Ti imido significantly widen the potential nitrene source in Ti redox catalysis beyond the previous approaches based on the reactions of low valent Ti with diazenes or azides. While similar indazole syntheses have been established with other metals, the advance in N–N coupling methods via ligand-centered oxidation of d^0 metal complexes will promote the understanding of the reactivity and mechanistic details of the oxidation intermediates, leading to the development of new intra- and intermolecular N–N heterocoupling catalysis.

5.5 Experimental

5.5.1 General Considerations

All air- and moisture-sensitive compounds were manipulated in a glovebox under nitrogen atmosphere. Alumina and molecular sieves were activated by heating at 280 ℃ under active vacuum for one week. Solvents for air- and moisture-sensitive reactions (THF, CH_2Cl_2) were dried through activated alumina on a Pure Process Technology solvent purification system. NMR solvents (CD_2Cl_2 and C_6D_6) and pyridine were dried over CaH_2 or sodium metal and vacuum transferred before passing through activated alumina and storing over activated 3 Å molecular sieves in the glovebox. TEMPO was purchased from Oakwood Products, Inc. and purified by sublimation. 1,3,5-trimethoxybenzene (TMB) was purchased from Oakwood Products, Inc. and used without further purification. $Ti(NMe_2)_4$ and hexamethyldisiloxane (HMDSO) were purchased from Oakwood Products, Inc. and distilled under vacuum prior to use. $TiCl_4$, LiHMDS, nitrosobenzene, 2′-aminoacetophenone and ferrocene (Fc) were purchased from Millipore-Sigma. $[TiCl_2(NPh)]_n$,[227] **5.8**,[228] $TiCl_2(NMe_2)_2$,[229,230] ferrocenium

chloride (FcCl),[209] and $(PPN)_2CeCl_6$ (Chapter 4) were prepared following the reported procedures. $PhICl_2$ was prepared following the reported procedure,[231] and sequentially washed with EtOAc, Et_2O and hexanes, dried under vacuum for 3 days and stored in the freezer prior to use.

^1H, $^{13}C\{^1H\}$, ^1H–^{15}N HMBC, and No-D ^1H NMR were collected on Bruker Avance III HD NanoBay 400 MHz or Bruker Avance III HD 500 MHz spectrometers. Quantitative NMR reaction experiments were collected with the following NMR acquisition parameters: number of scan = 4, dummy scan = 0, acquisition time = 5 s, and relaxation time = 30 s. Chemical shifts are reported with respect to residue protio-solvent impurity for ^1H NMR (s, 7.26 ppm for $CDCl_3$, s, 7.16 ppm for C_6D_6; s, 5.32 ppm for CD_2Cl_2) and ^{13}C NMR (t, 77.16 ppm for $CDCl_3$), or with respect to tetramethylsilane internal chemical shift standard for ^1H NMR in $CDCl_3$ (s, 0 ppm). Baseline correction (ablative method with 5 points and 10 passes, MestReNova) were applied to NMR spectra before integrated against NMR internal standard TMB for quantitative analysis. GC-FID-MS was collected on an Agilent 8890 Custom GC Analyzer and Agilent 5977B EI MSD Bundle with an oxidation-methanation reactor (SP-1 Polyarc® System, Activated Research Company) and an FID detector for quantitative carbon detection. Automatic column chromatography was performed on a Teledyne ISCO CombiFlash® NextGen 300+ system.

5.5.2 Synthesis of 2-Iminylaniline 5.4

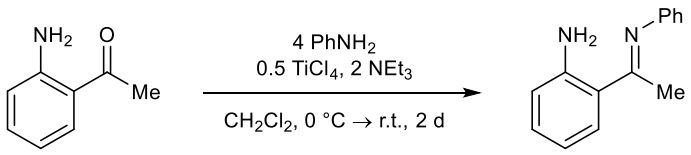

5.13 **5.4** 54%

2-(1-(phenylimino)ethyl)aniline (**5.4**) was synthesized following a modification of a reported procedure.[228] An N_2-filled 500 mL Schlenk flask equipped with a stir bar was cooled in ice/water bath. CH_2Cl_2 (150 mL), 2′-aminoacetophenone (**5.13**, 6.76 g, 50 mmol, 1 equiv), aniline (18.63 g, 200 mmol, 4 equiv), triethylamine (13.5 mL, 10.1 g, 100 mmol, 2 equiv), and $TiCl_4$ (2.73 mL, 4.74 g, 25 mmol, 0.5 equiv) were slowly added to the Schlenk flask sequentially under vigorous stirring. The ice bath was removed, and the reaction mixture was allowed to slowly warm up to room temperature and stirred for 2 days. Saturated aq. Na_2CO_3 solution was added to the

reaction mixture to quench the reaction. After stirring for another 15 minutes, the reaction mixture was extracted with CH_2Cl_2 (50 mL x 3). The organic fraction was dried with $MgSO_4$ and evaporated under vacuum. The resulting crude product contained **5.4**, $PhNH_2$ and 2′-aminoacetophenone as a mixture in roughly 1:4:0.2 ratio. $PhNH_2$ was effectively removed *via* automatic column chromatography (SiO_2, gradient CH_2Cl_2/hexanes) by identifying the UV absorption peak of PhNH2 at ~290 nm, which is absent for both **5.4** and **5.13**. Further recrystallization in hexanes yielded pure **5.4** as a yellow solid, which was dried under vacuum for 2 days prior to use. Yield: 5.76 g (54%, sum yield of 3 batches of recrystallization).

^{1}H NMR (500 MHz, $CDCl_3$) δ 7.64 (dd, *J* = 7.9, 1.6 Hz, 1H, Ar-*H*), 7.38 (dd, *J* = 8.3, 7.4 Hz, 2H, Ar-*H*), 7.22 (ddd, *J* = 8.4, 7.1, 1.5 Hz, 1H, Ar-*H*), 7.12 (tt, *J* = 7.3, 1.3 Hz, 1H, Ar-*H*), 6.84 (dd, *J* = 8.4, 1.2 Hz, 2H, Ar-*H*), 6.77 – 6.69 (m, 2H, Ar-*H*), 6.59 (s, 2H, Ar-NH_2), 2.29 (s, 3H, -CH_3) ppm.

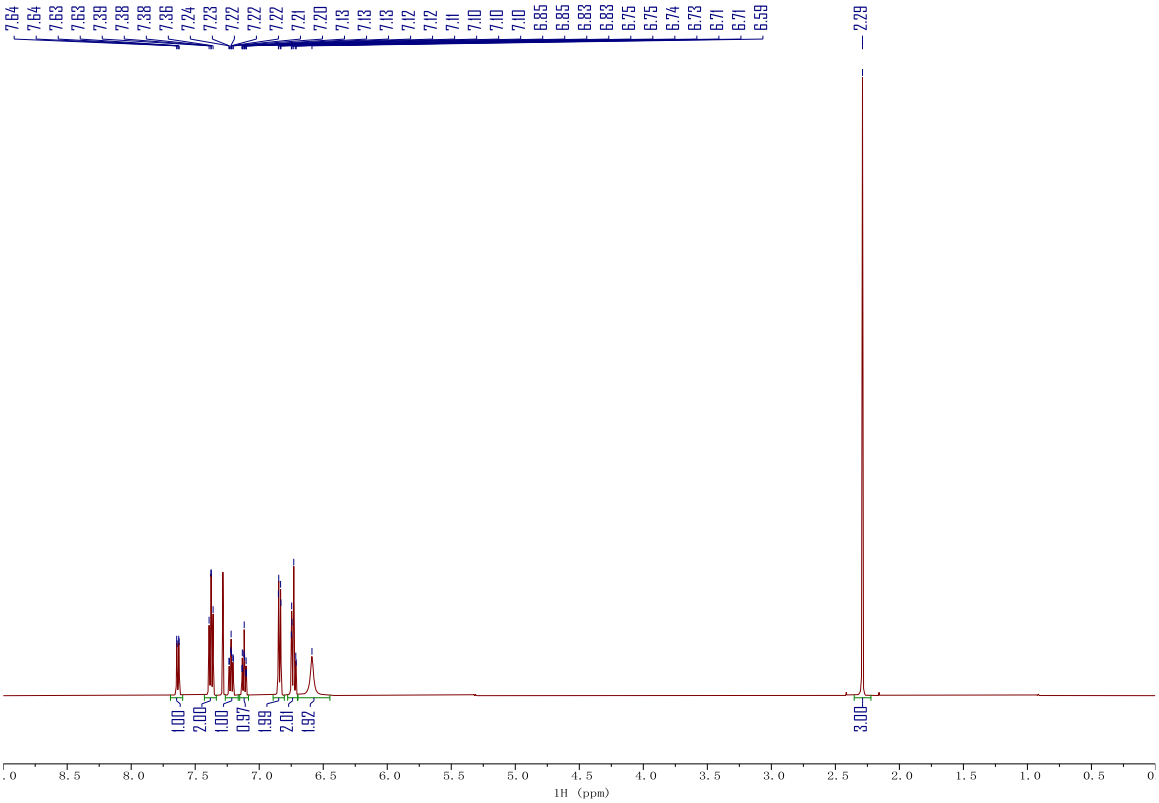

Figure 5.11. ^{1}H NMR spectrum of **5.4** in $CDCl_3$. *Taken from YC-2022-0137-recry1.*

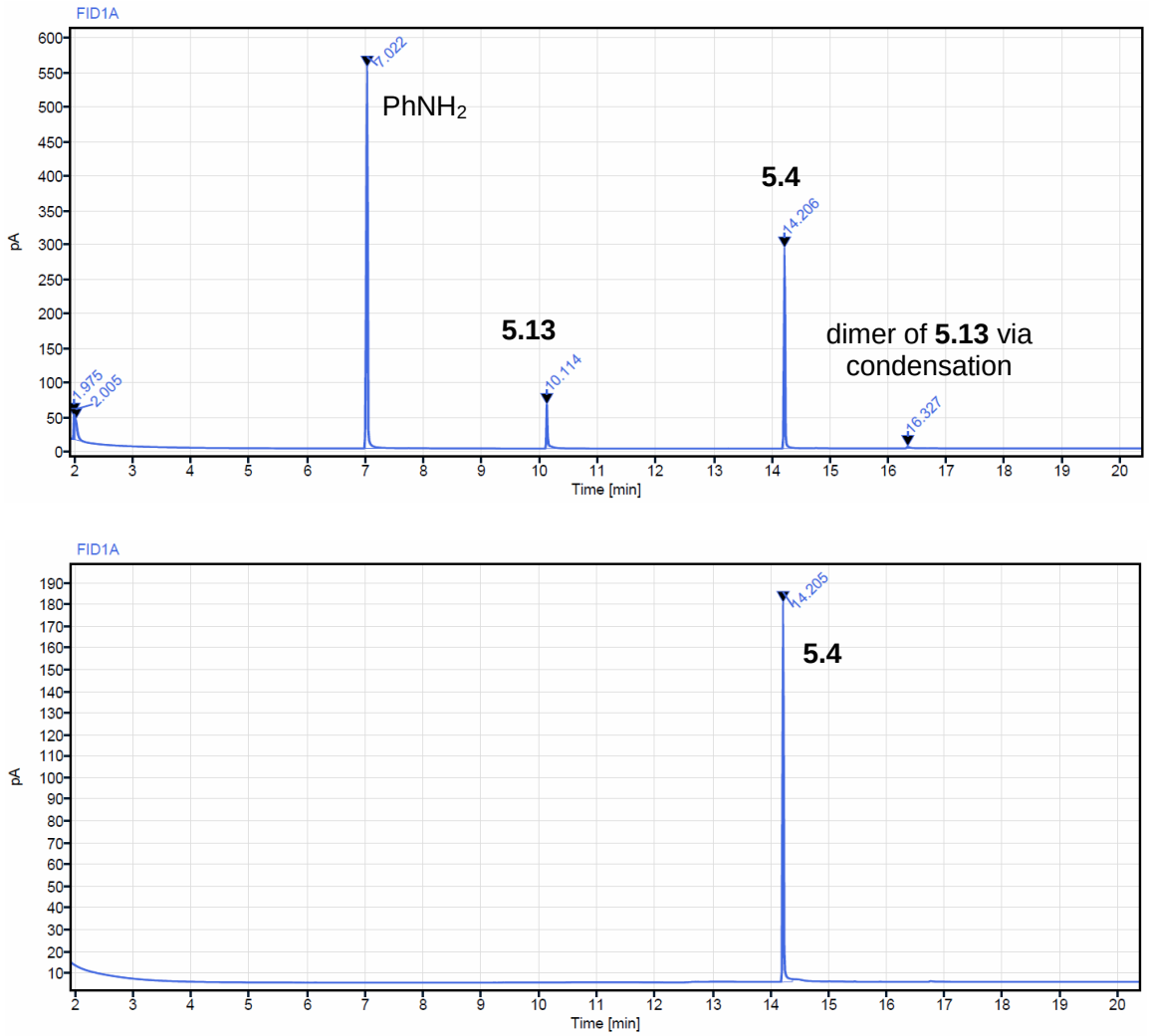

Figure 5.12. GC-FID spectra of (top) crude product and (bottom) pure **5.4**. *Taken from (top) YC-2022-0137--1 and (bottom) YC-2022-0137-recry-1.*

5.5.3 General Procedure for One-Pot Oxidation Reactions

General Procedure for One-Pot Oxidation of In Situ formed 2-Titanaquinazoline 5.5 (Procedure 5):

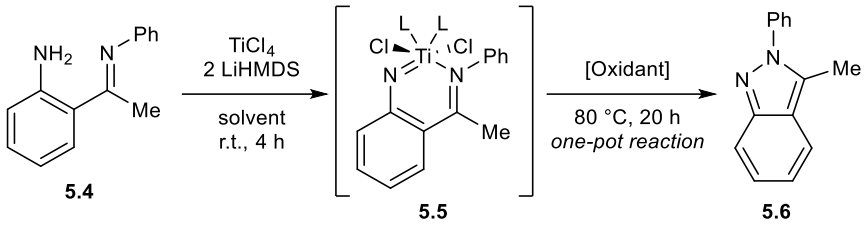

$TiCl_4$ (37.9 mg, 0.2 mmol, 1 equiv), solvent (1.5 mL), and a stir bar were added to a 4 mL scintillation vial in the glovebox. A solution of **5.4** (42.0 mg, 0.2 mmol, 1 equiv) in solvent (1 mL) was added dropwise to the reaction mixture under vigorous stirring, resulting in a bright red suspension or dark red solution depending on the solvent. A solution of LiHMDS (66.9 mg, 0.4 mmol, 2 equiv) in solvent (1.5 mL) was added dropwise to the reaction mixture under vigorous stirring. After stirring at room temperature for 4 hours, TEMPO (62.5 mg, 0.4 mmol, 2 equiv) was added to the reaction mixture, and the reaction mixture was heated at 80 ℃ for 20 hours. The vial was then taken out of the glovebox and allowed to cool down. The reaction mixture was poured into a 20 mL scintillation vial with CH_2Cl_2 (4 mL) and 5% methanolic HCl (1 mL) and extracted against 10 mL water, during which the unreacted **5.4** and **5.5** were hydrolyzed to give **5.13**. The organic fraction was dried over $MgSO_4$ and evaporated under vacuum. Quantitative characterization for yield calculation was performed with ^{1}H NMR or GC-FID-MS using TMB (50.4 mg, 0.3 mmol) as internal standard. Indazole **5.6** was identified *via* the comparison with reported ^{1}H NMR chemical shifts (^{1}H NMR)[232] or mass spectrometry (GC-FID-MS).

5.5.4 Condition Optimization of Ti-Mediated Indazole Synthesis with TEMPO (Table 5.1)

Entry 1:

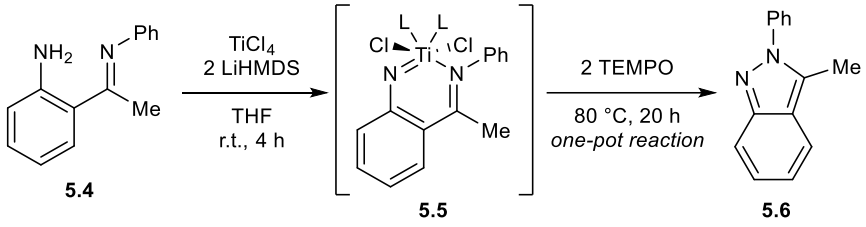

Reactions were performed following **Procedure 5** with THF as the solvent. Yield of **5.6** was determined by ^{1}H NMR as 9%.

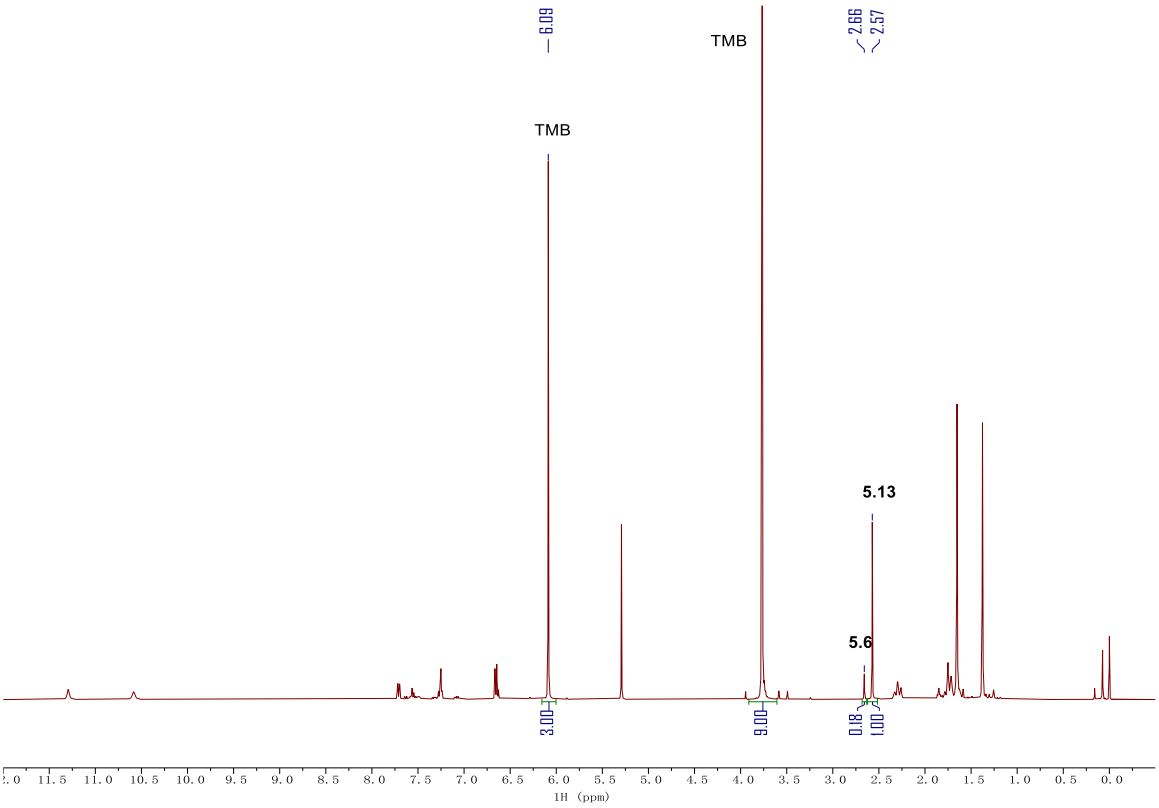

Figure 5.13. ^{1}H NMR spectrum ($CDCl_3$) of Table 5.1 entry 1 after workup. *Taken from YC-2022-0140-workup-H.*

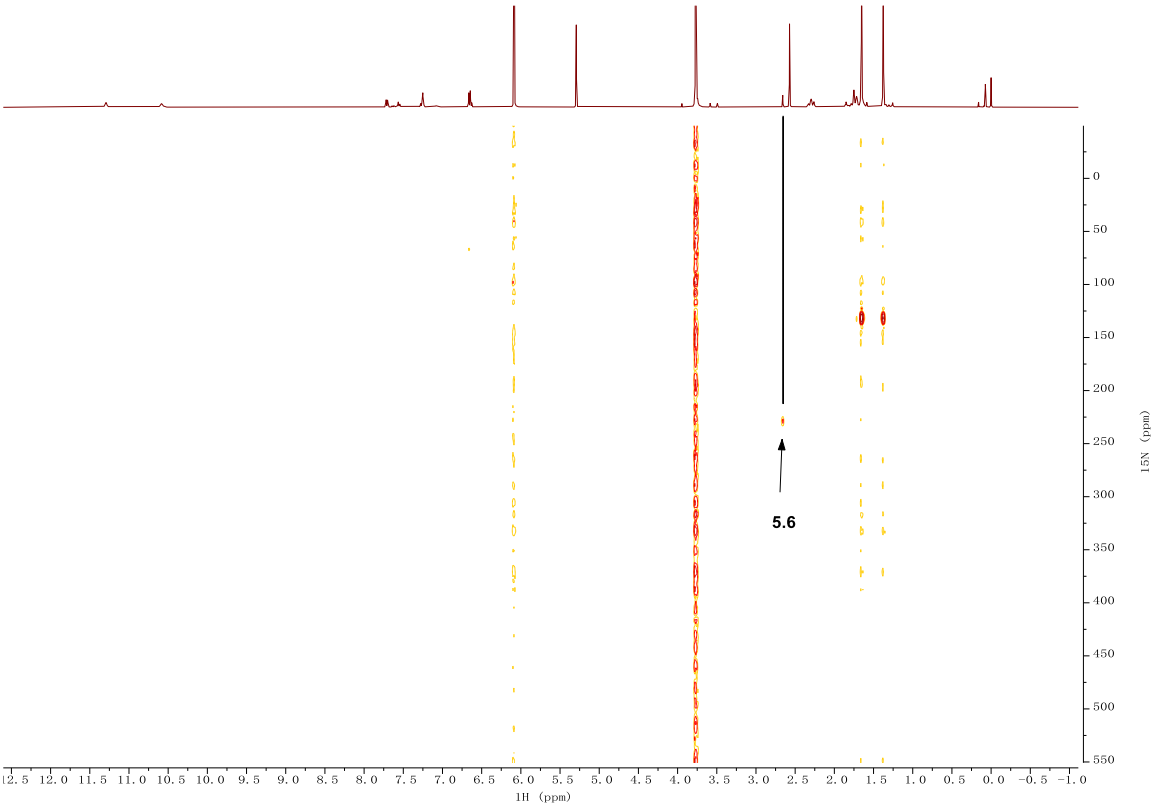

Figure 5.14. ^{1}H-^{15}N HMBC NMR spectrum ($CDCl_3$) of Table 5.1 entry 1 after workup for identification of **5.6**. *Taken from YC-2022-0140-workup-NHMBC.*

Entry 2:

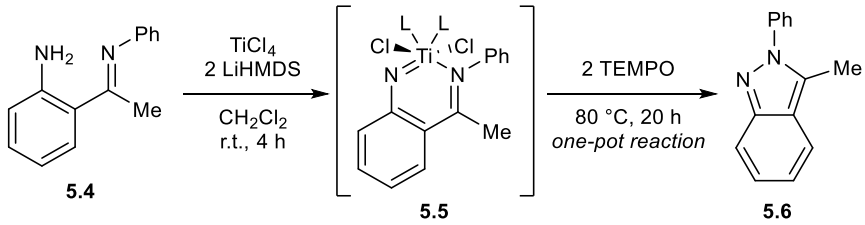

Reactions were performed following **Procedure 5** with CH_2Cl_2 as the solvent. Yield of **5.6** was determined by ^{1}H NMR as 55%.

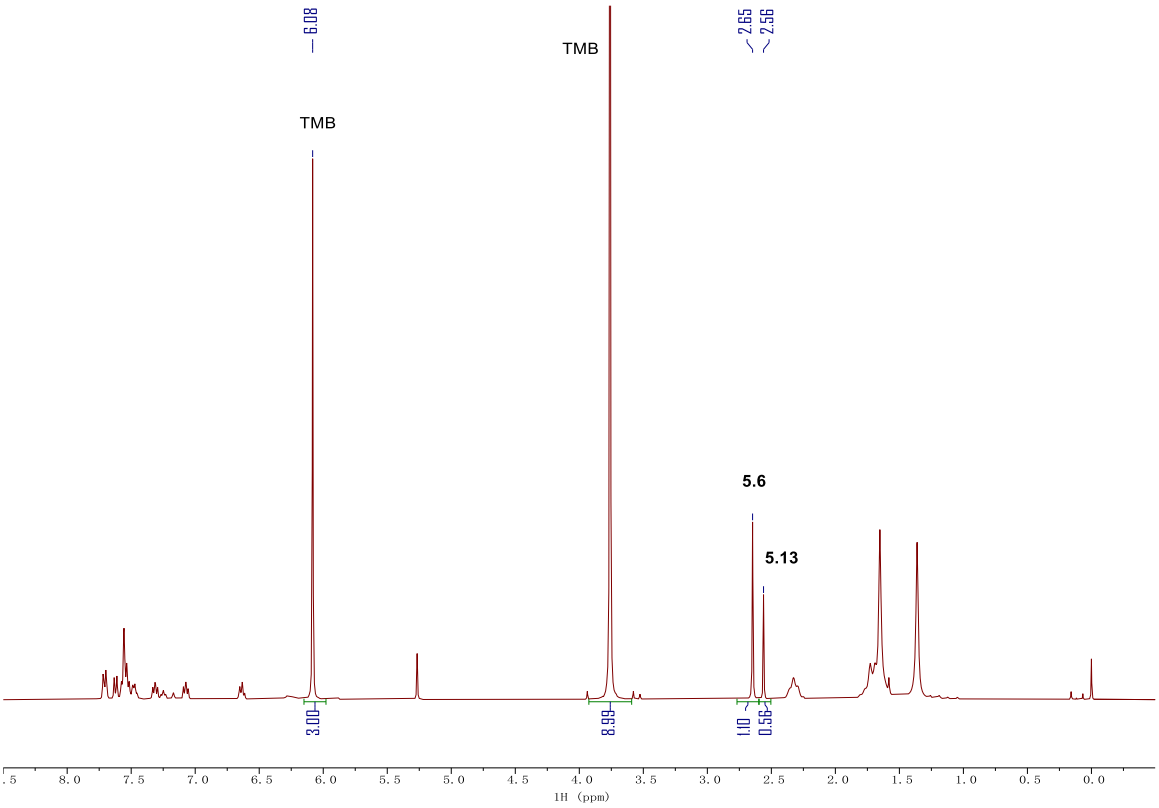

Figure 5.15. ^{1}H NMR spectrum ($CDCl_3$) of Table 5.1 entry 2 after workup. *Taken from YC-2022-0151-workup.*

Entry 3:

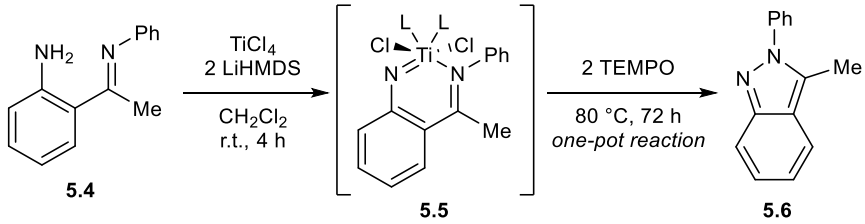

Reactions were performed following **Procedure 5** with CH_2Cl_2 as the solvent and the second step heating extended to 72 hours. Yield of **5.6** was determined by ^{1}H NMR as 58%.

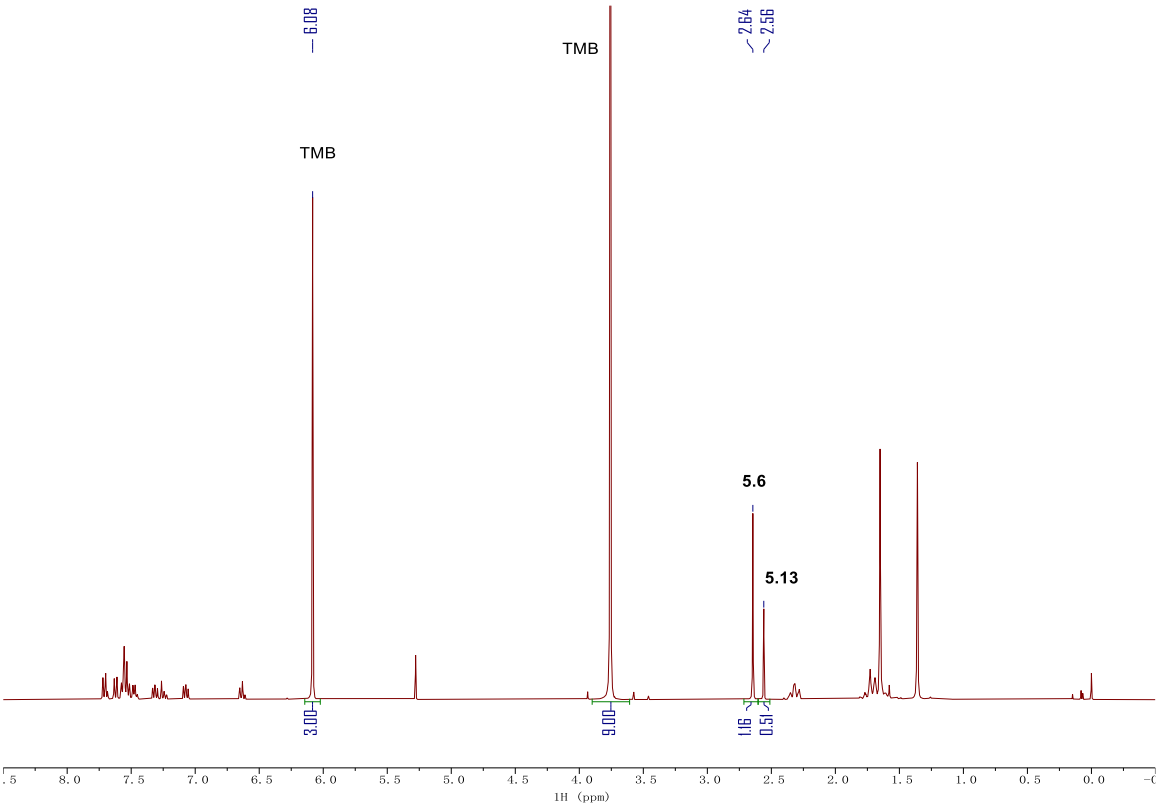

Figure 5.16. ^{1}H NMR spectrum ($CDCl_3$) of Table 5.1 entry 3 after workup. *Taken from YC-2022-0157-workup.*

Entry 4:

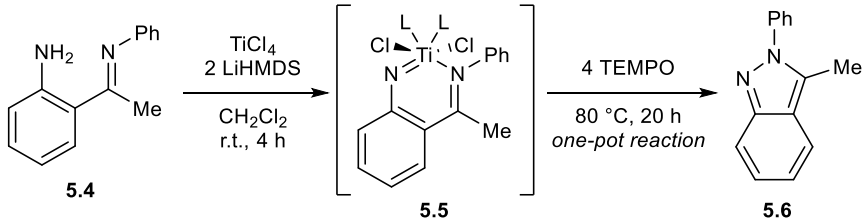

Reactions were performed following **Procedure 5** with CH_2Cl_2 as the solvent. TEMPO (125.0 mg, 0.8 mmol, 4 equiv) instead of 2 equiv was used. ^{1}H NMR was considered inaccurate for quantitative characterization due to the excessive remaining TEMPO in the product mixture. Yield of **5.6** was determined by GC-FID-MS as 52%.

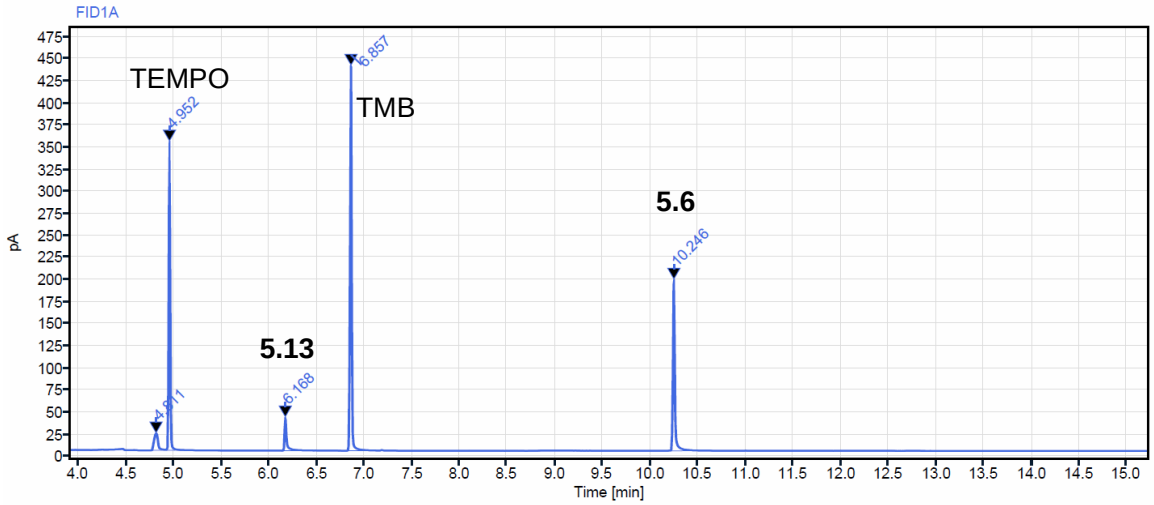

	Retention Time (min)	Peak Area	# of C	Yield (%)
TMB	6.857	510.5839	9	n.a.
5.6	10.246	273.6328	14	51.7
5.13	6.168	57.7745	8	19.1

Figure 5.17. GC-FID spectrum of Table 5.1 entry 4 after workup. *Taken from YC-2022-0159-1.*

Sample yield calculation based on quantitative carbon detection:

$$Yield\ of\ \mathbf{5.6} = \frac{Surface\ Area\ of\ \mathbf{5.6}}{\#\ of\ C\ of\ \mathbf{5.6}} \times \frac{\#\ of\ C\ of\ TMB}{Surface\ Area\ of\ TMB} \times equiv\ of\ TMB \times 100\%$$

Entry 5:

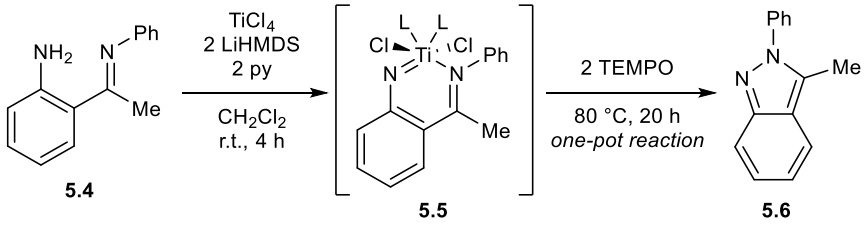

Reactions were performed following **Procedure 5** with CH_2Cl_2 as the solvent. Pyridine (31.6 mg, 0.4 mmol, 2 equiv) was added as a pre-mixed solution with the CH_2Cl_2 solution of LiHMDS. Yield of **5.6** was determined by ^1H NMR as 26%.

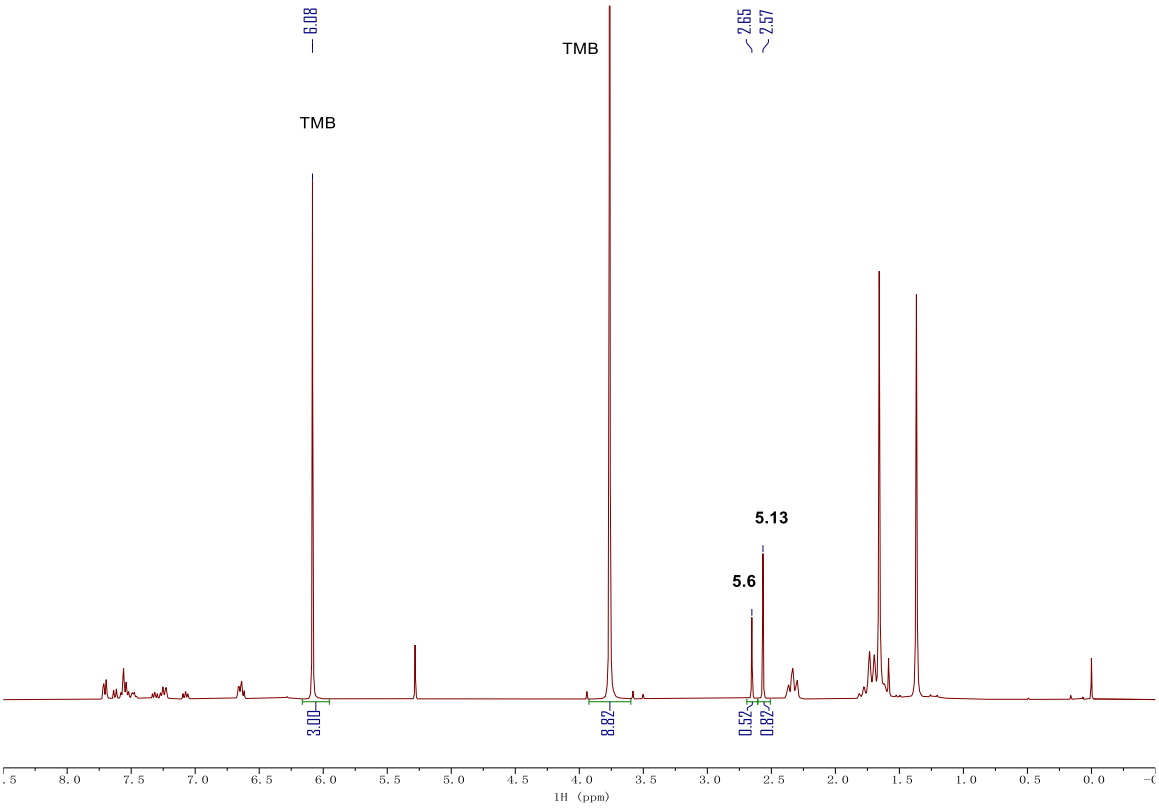

Figure 5.18. ^{1}H NMR spectrum ($CDCl_3$) of Table 5.1 entry 5 after workup. *Taken from YC-2022-0146-workup.*

Entry 6:

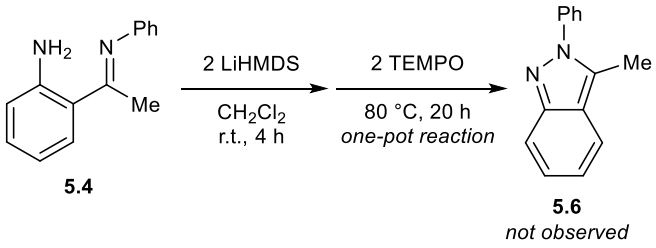

Reactions were performed following **Procedure 5** with CH_2Cl_2 as the solvent. The addition of $TiCl_4$ was skipped. **5.6** was not found in the product mixture.

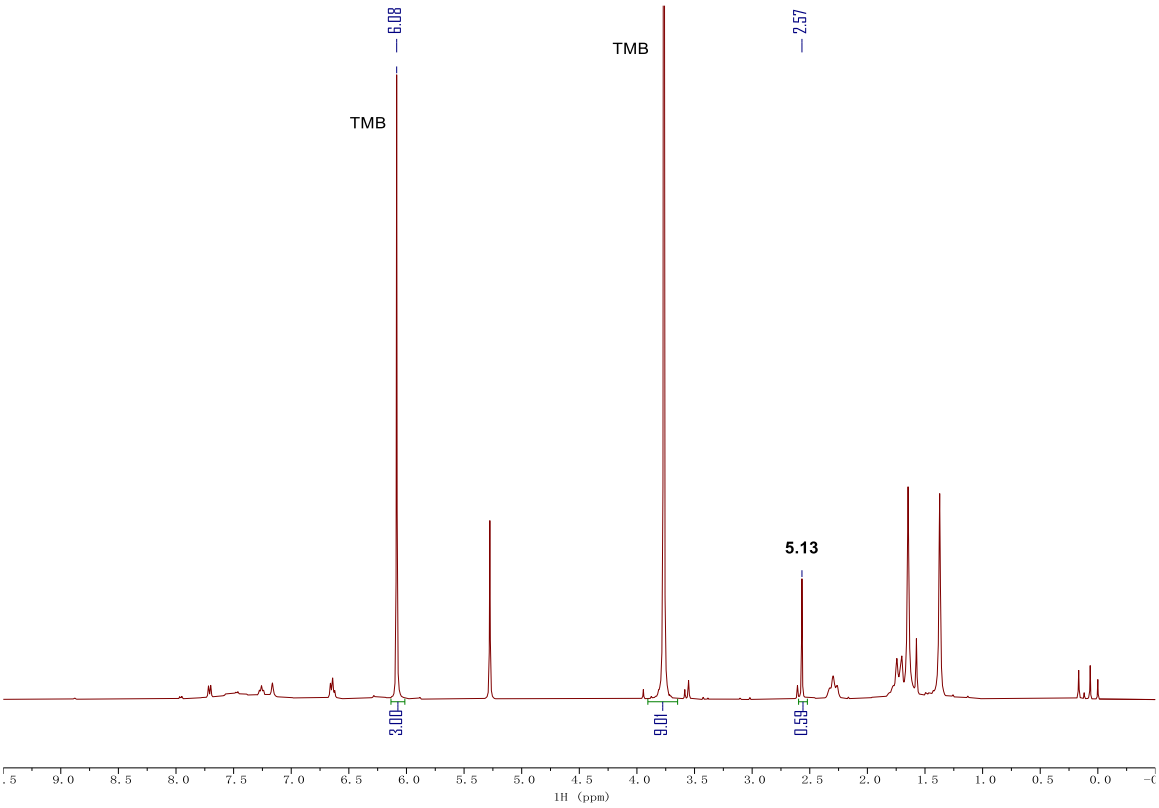

Figure 5.19. ^{1}H NMR spectrum ($CDCl_3$) of Table 5.1 entry 6 after workup. *Taken from YC-2022-0170-workup.*

Entry 7:

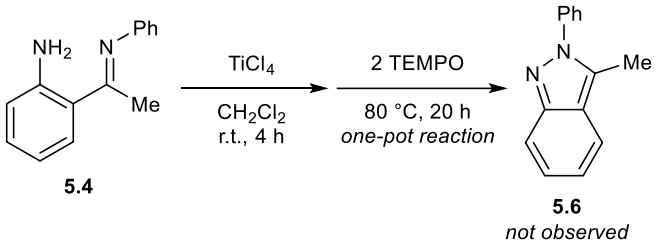

Reactions were performed following **Procedure 5** with CH_2Cl_2 as the solvent. The addition of LiHMDS was skipped. **5.6** and **5.13** were both not found in the product mixture. It was speculated that the **5.4** underwent decomposition mediated by TiCl4 as a Lewis acid, as there was no signal found in GC-FID-MS after the aqueous work (major products were aqueous soluble and lost in the extraction).

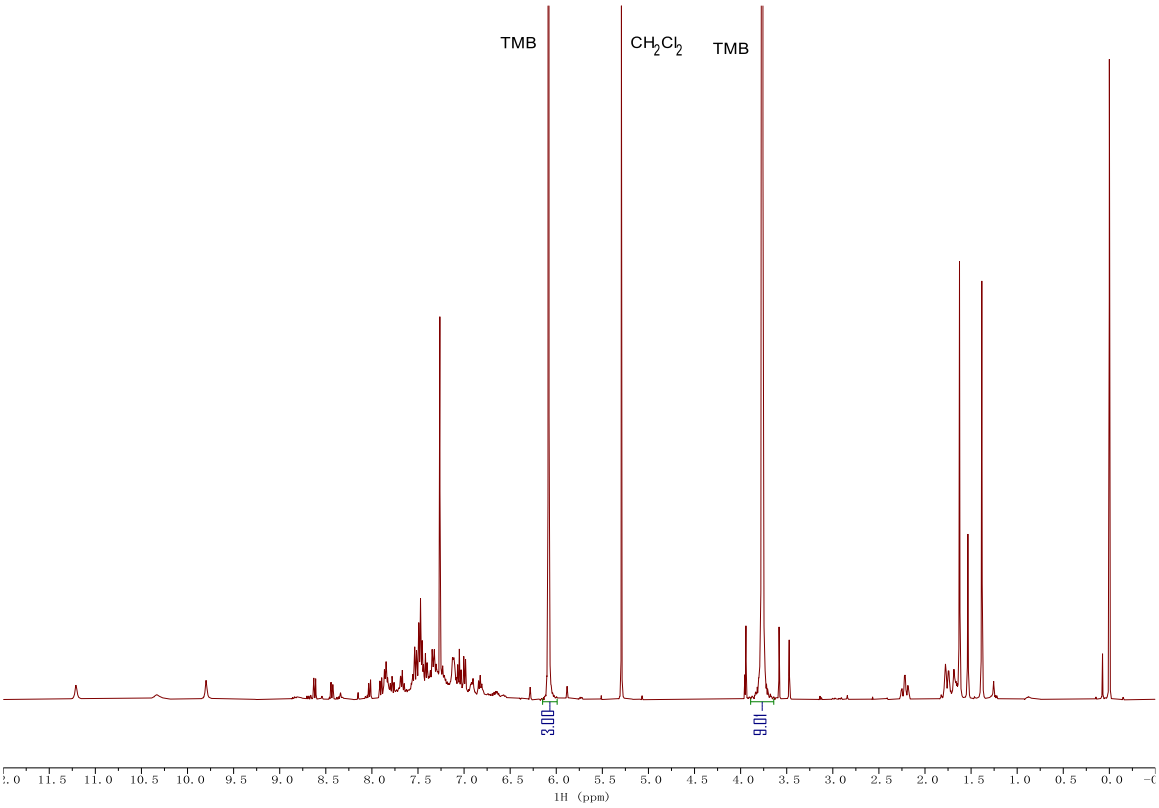

Figure 5.20. ^{1}H NMR spectrum ($CDCl_3$) of Table 5.1 entry 7 after workup. *Taken from YC-2022-0155-workup.*

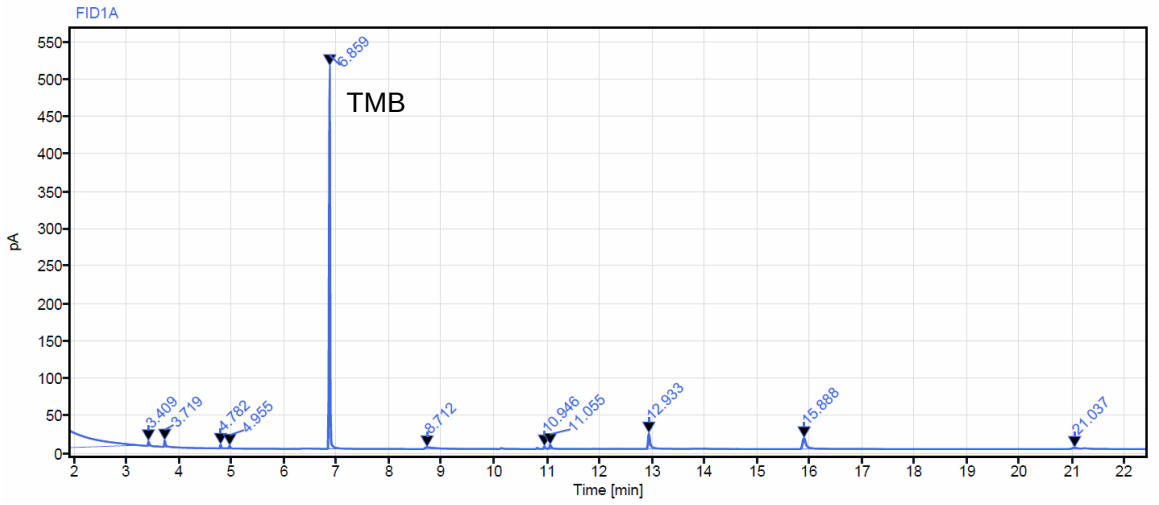

Figure 5.21. GC-FID spectrum of Table 5.1 entry 7 after workup. Expected retention time: 10.25 min (**5.6**), 6.17 min (**5.13**). *Taken from YC-2022-0155-1.*

5.5.5 Isolation Experiment of 2*H*-Indazole 5.6

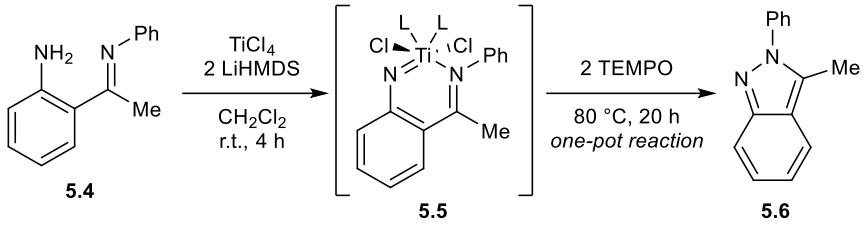

$TiCl_4$ (189.7 mg, 1.0 mmol, 1 equiv), CH_2Cl_2 (7.5 mL), and a stir bar were added to a 20 mL scintillation vial in the glovebox. A solution of **5.4** (210.0 mg, 1.0 mmol, 1 equiv) in CH_2Cl_2 (5 mL) was added dropwise to the reaction mixture under vigorous stirring, resulting in a dark red solution. A solution of LiHMDS (334.5 mg, 2.0 mmol, 2 equiv) in CH_2Cl_2 (7.5 mL) was added dropwise to the reaction mixture under vigorous stirring. After stirring at room temperature for 4 hours, TEMPO (312.5 mg, 2.0 mmol, 2 equiv) was added to the reaction mixture, and the reaction mixture was heated at 80℃ for 20 hours. The vial was then taken out of the glovebox and allowed to cool down. The reaction mixture was acidified with 5% methanolic HCl (3 mL) and extracted against 30 mL water, during which the unreacted **5.4** and **5.5** were hydrolyzed to give **5.13**. The organic fraction was dried over $MgSO_4$ and evaporated under vacuum to give the crude product. Pure **5.6** was obtained through automatic column chromatography (SiO_2, gradient CH_2Cl_2/hexanes). Yield: 87.4 mg (0.42 mmol, 42%). ^1H and ^{13}C NMR signals matched up with the reported spectra.[232]

^1H NMR (400 MHz, $CDCl_3$) δ 7.73 (dt, *J* = 8.7, 1.0 Hz, 1H, Ar-*H*), 7.63 (dt, *J* = 8.4, 1.0 Hz, 1H, Ar-*H*), 7.59 – 7.52 (m, 4H, Ar-*H*), 7.48 (ddt, *J* = 8.1, 5.6, 1.7 Hz, 1H, Ar-*H*), 7.33 (ddd, *J* = 8.8, 6.5, 1.1 Hz, 1H, Ar-*H*), 7.09 (ddd, *J* = 8.5, 6.6, 0.9 Hz, 1H, Ar-*H*), 2.65 (s, 3H, -C*H*$_3$) ppm.

^{13}C NMR (101 MHz, $CDCl_3$) δ 148.57, 139.90, 132.18, 129.30, 128.80, 127.02, 125.87, 121.73, 121.11, 120.13, 117.58, 11.25 ppm.

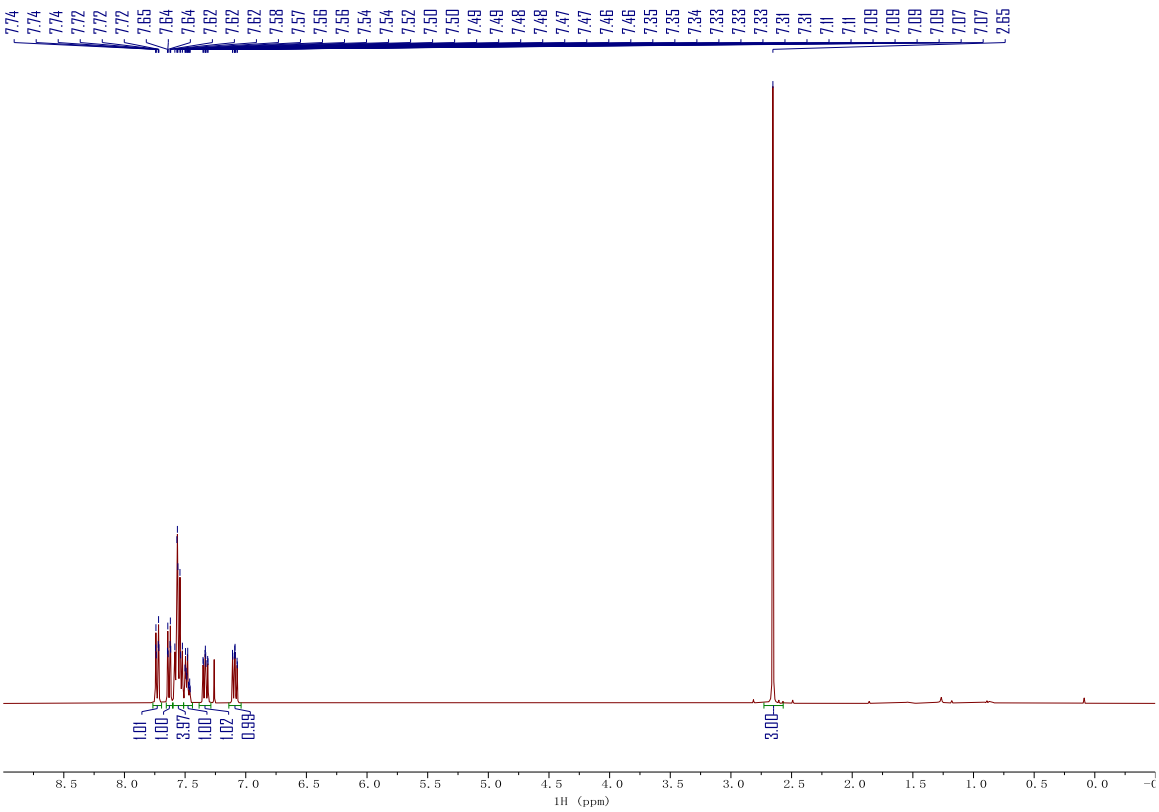

Figure 5.22. ^{1}H NMR spectrum of **5.6** in $CDCl_3$. *Taken from YC-2022-0164-isolation-H.*

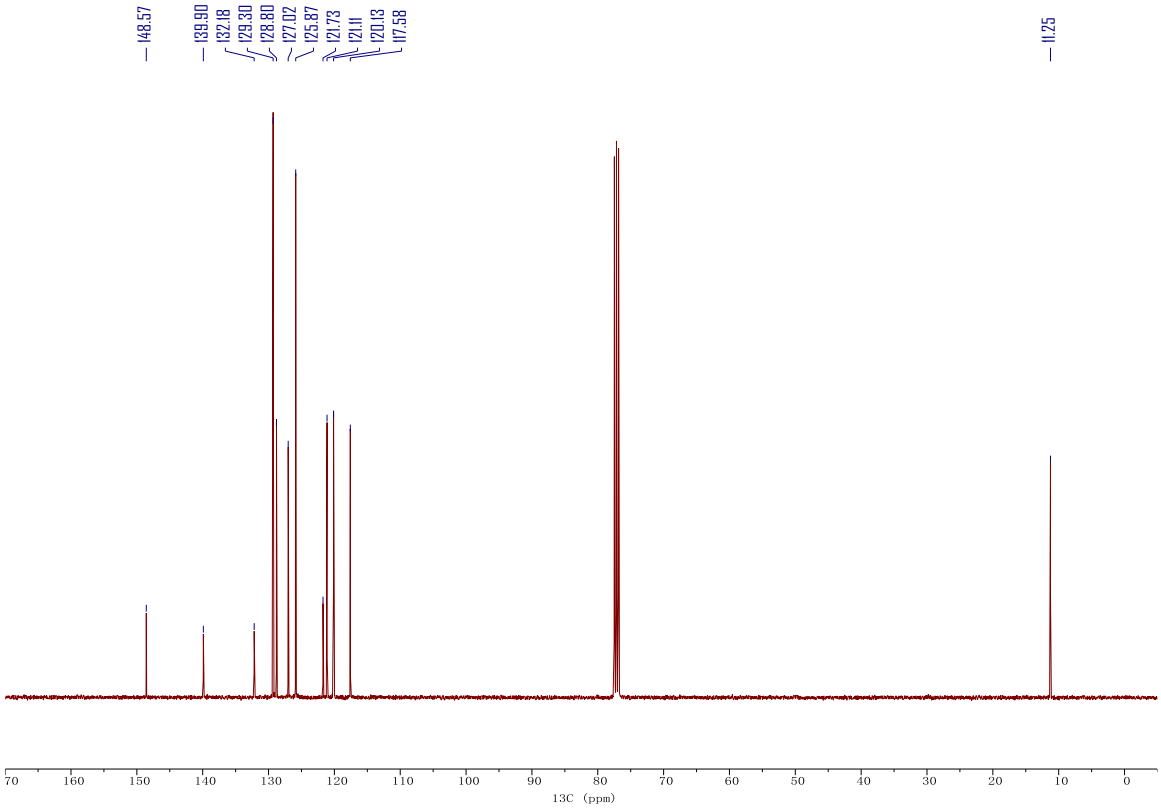

Figure 5.23. $^{13}C\{^{1}H\}$ NMR spectrum of **5.6** in $CDCl_3$. *Taken from YC-2022-0164-isolation-C.*

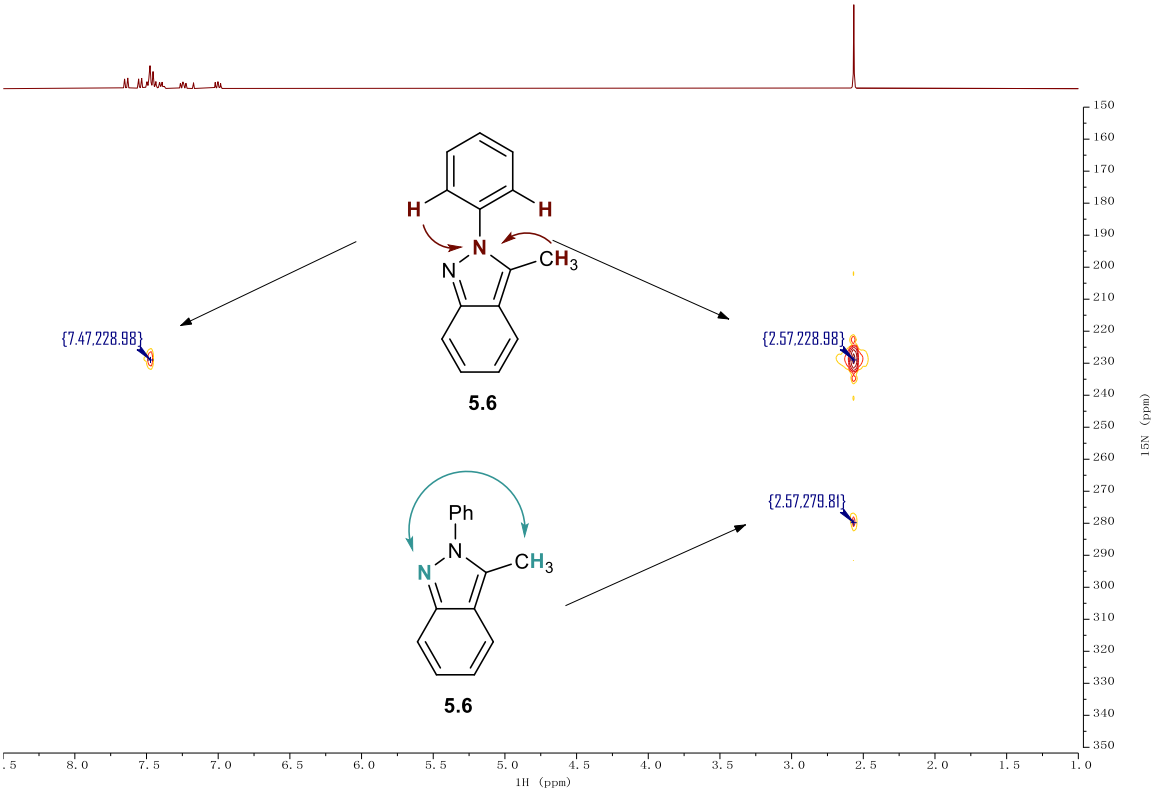

Figure 5.24. ^{1}H-^{15}N HMBC NMR spectrum of **5.6** in $CDCl_3$. *Taken from YC-2022-0164-isolation-NHMBC.*

5.5.6 Ti-Mediated Indazole Synthesis with Cl-Based Oxidants (Figure 5.4)

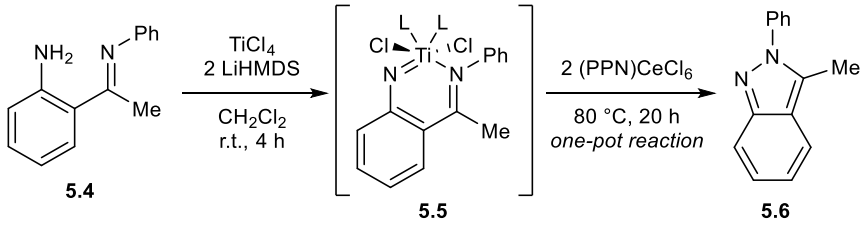

$TiCl_4$ (19.0 mg, 0.1 mmol, 1 equiv), CH_2Cl_2 (1.0 mL), and a stir bar were added to a 4 mL scintillation vial in the glovebox. A solution of **5.4** (21.0 mg, 0.1 mmol, 1 equiv) in CH_2Cl_2 (0.5 mL) was added dropwise to the reaction mixture under vigorous stirring, resulting in a dark red solution. A solution of LiHMDS (33.5 mg, 0.2 mmol, 2 equiv) in CH_2Cl_2 (0.5 mL) was added dropwise to the reaction mixture under vigorous stirring. After stirring at room temperature for 4 hours, $(PPN)_2CeCl_6$ (286.0 mg, 0.2 mmol, 2 equiv) was added to the reaction mixture, and

the reaction mixture was heated at 80 ℃ for 20 hours. The vial was then taken out of the glovebox and allowed to cool down. The reaction mixture was poured into a 20 mL scintillation vial with CH_2Cl_2 (2 mL) and 5% methanolic HCl (0.5 mL) and extracted against 5 mL water, during which the unreacted **5.4** and **5.5** were hydrolyzed to give **5.13**. The organic fraction was dried over $MgSO_4$ and evaporated under vacuum. Quantitative characterization for yield calculation was performed with ^1H NMR using TMB (50.4 mg, 0.3 mmol) as internal standard. Yield of **5.6** was determined as 41%.

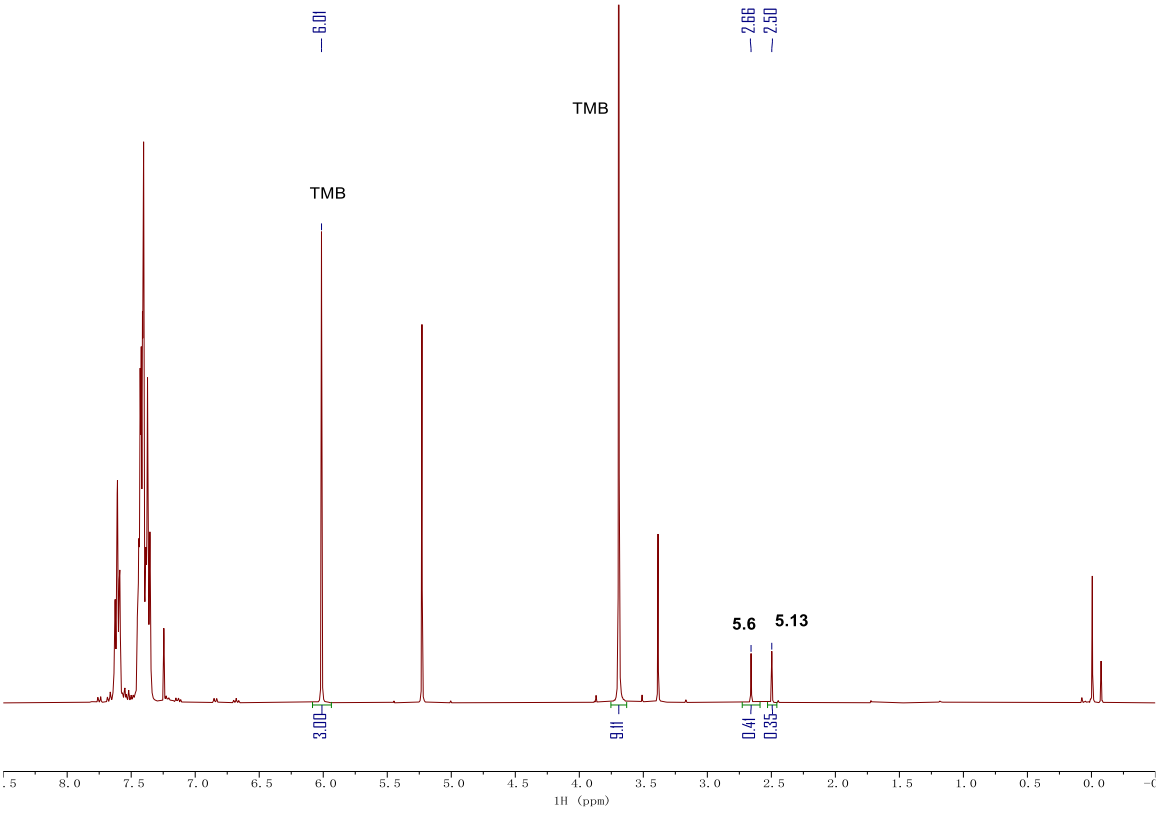

Figure 5.25. ^1H NMR spectrum ($CDCl_3$) of $(PPN)_2CeCl_6$ oxidation of **5.5** after workup. *Taken from YC-2022-0166-workup.*

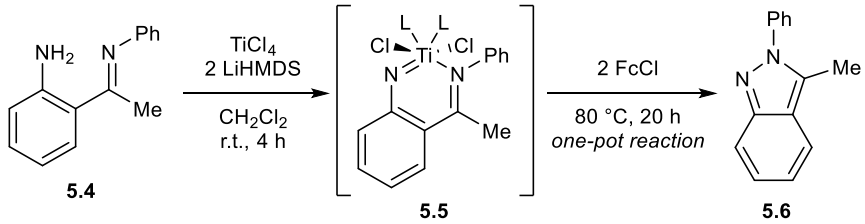

$TiCl_4$ (37.9 mg, 0.2 mmol, 1 equiv), CH_2Cl_2 (1.5 mL), and a stir bar were added to a 4 mL scintillation vial in the glovebox. A solution of **5.4** (42.0 mg, 0.2 mmol, 1 equiv) in CH_2Cl_2 (1

mL) was added dropwise to the reaction mixture under vigorous stirring, resulting in a dark red solution. A solution of LiHMDS (66.9 mg, 0.4 mmol, 2 equiv) in CH_2Cl_2 (1.5 mL) was added dropwise to the reaction mixture under vigorous stirring. After stirring at room temperature for 4 hours, FcCl (88.6 mg, 0.4 mmol, 2 equiv) was added to the reaction mixture, and the reaction mixture was heated at 80℃ for 20 hours. The vial was then taken out of the glovebox and allowed to cool down. The reaction mixture was poured into a 20 mL scintillation vial with CH_2Cl_2 (4 mL) and 5% methanolic HCl (1 mL) and extracted against 10 mL water, during which the unreacted **5.4** and **5.5** were hydrolyzed to give **5.13**. The organic fraction was dried over $MgSO_4$ and evaporated under vacuum. The solid residue was then washed by 20 mL hexanes for the removal of Fc (oxidation byproduct). Quantitative characterization for yield calculation was performed with GC-FID-MS using 1,3,5-tri-*tert*-butylbenzene ($C_6H_3{}^tBu_3$, 24.6 mg, 0.1 mmol) as internal standard. Yield of **5.6** was determined as 21%.

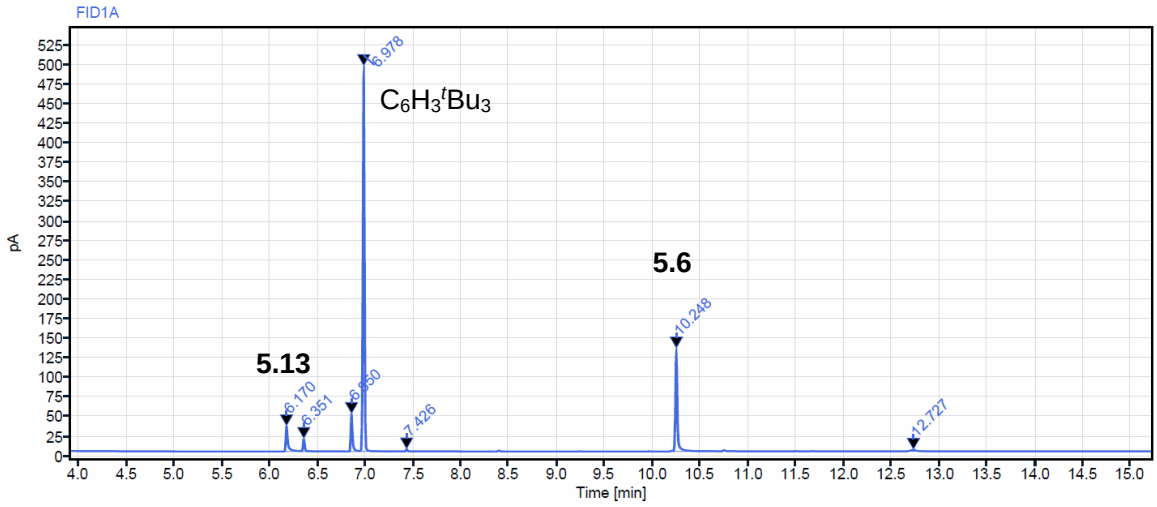

	Retention Time (min)	Peak Area	# of C	Yield (%)
$C_6H_3{}^tBu_3$	6.978	571.9360	18	n.a.
5.6	10.248	187.1971	14	21.0
5.13	6.170	51.7157	8	10.2

Figure 5.26. GC-FID spectrum of FcCl oxidation of **5.5** after workup. *Taken from YC-2022-0165-2.*

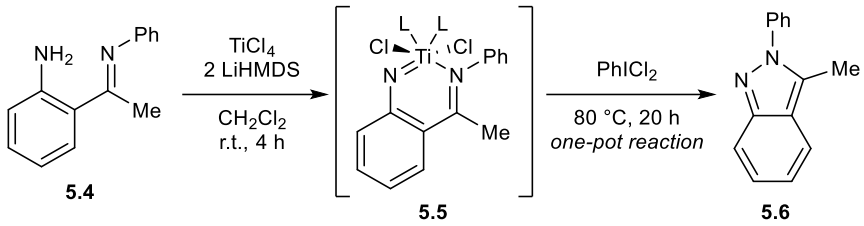

$TiCl_4$ (37.9 mg, 0.2 mmol, 1 equiv), CH_2Cl_2 (1.5 mL), and a stir bar were added to a 4 mL scintillation vial in the glovebox. A solution of **5.4** (42.0 mg, 0.2 mmol, 1 equiv) in CH_2Cl_2 (1 mL) was added dropwise to the reaction mixture under vigorous stirring, resulting in a dark red solution. A solution of LiHMDS (66.9 mg, 0.4 mmol, 2 equiv) in CH_2Cl_2 (1.5 mL) was added dropwise to the reaction mixture under vigorous stirring. After stirring at room temperature for 4 hours, $PhICl_2$ (55.0 mg, 0.2 mmol, 1 equiv) was added to the reaction mixture, and the reaction mixture was heated at 80℃ for 20 hours. The vial was then taken out of the glovebox and allowed to cool down. The reaction mixture was poured into a 20 mL scintillation vial with CH_2Cl_2 (4 mL) and 5% methanolic HCl (1 mL) and extracted against 10 mL water, during which the unreacted **5.4** and **5.5** were hydrolyzed to give **5.13**. The organic fraction was dried over $MgSO_4$ and evaporated under vacuum. Quantitative characterization for yield calculation was performed with ^1H NMR using TMB (50.4 mg, 0.3 mmol) as internal standard. Yield of **5.6** was determined as 5%.

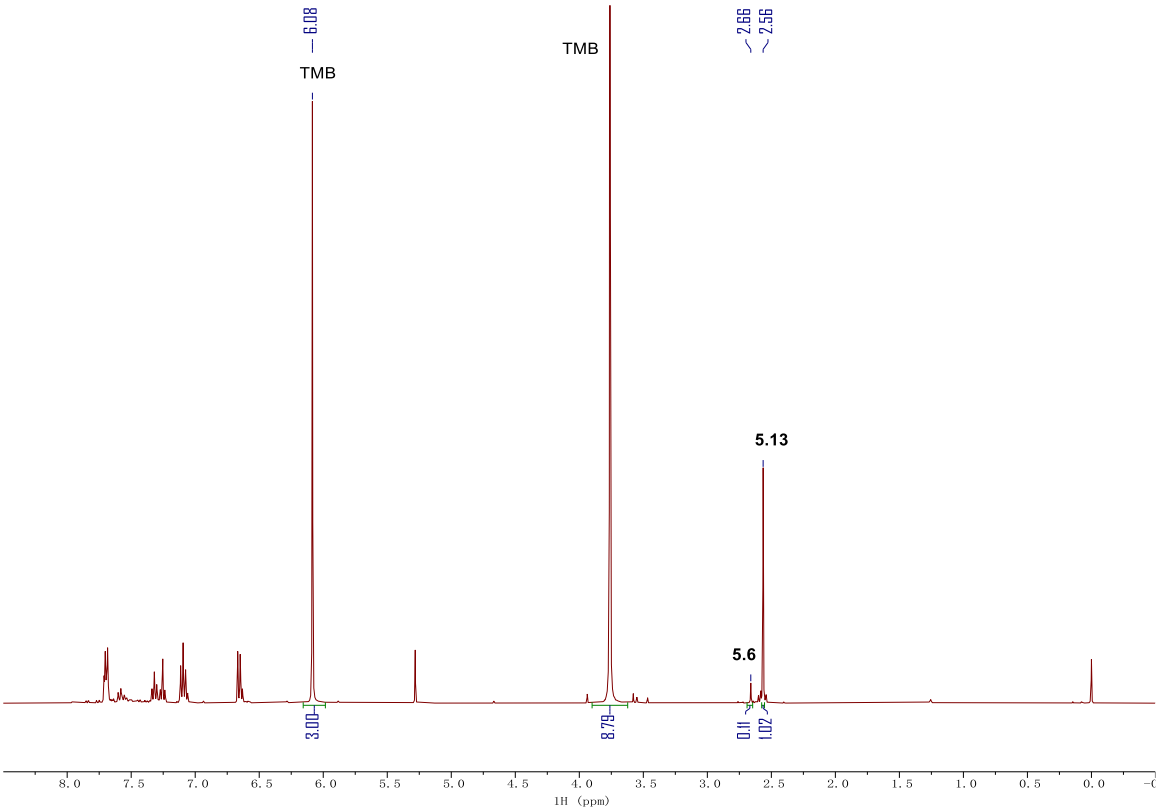

Figure 5.27. ^{1}H NMR spectrum ($CDCl_3$) of $PhICl_2$ oxidation of **5.5** after workup. *Taken from YC-2022-0150-workup.*

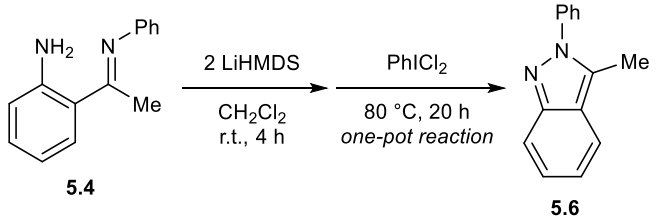

5.4 **5.6**

5.4 (42.0 mg, 0.2 mmol, 1 equiv), CH_2Cl_2 (2.5 mL) and a stir bar were added to a 4 mL scintillation vial in the glovebox. A solution of LiHMDS (66.9 mg, 0.4 mmol, 2 equiv) in CH_2Cl_2 (1.5 mL) was added dropwise to the reaction mixture under vigorous stirring. After stirring at room temperature for 4 hours, $PhICl_2$ (55.0 mg, 0.2 mmol, 1 equiv) was added to the reaction mixture, and the reaction mixture was heated at 80℃ for 20 hours. The vial was then taken out of the glovebox and allowed to cool down. The reaction mixture was poured into a 20 mL scintillation vial with CH_2Cl_2 (4 mL) and 5% methanolic HCl (1 mL) and extracted against 10 mL water, during which the unreacted **5.4** and **5.5** were hydrolyzed to give **5.13**. The organic fraction was dried over $MgSO_4$ and evaporated under vacuum. Quantitative characterization

for yield calculation was performed with ^{1}H NMR using TMB (50.4 mg, 0.3 mmol) as internal standard. Yield of **5.6** was determined as 5%.

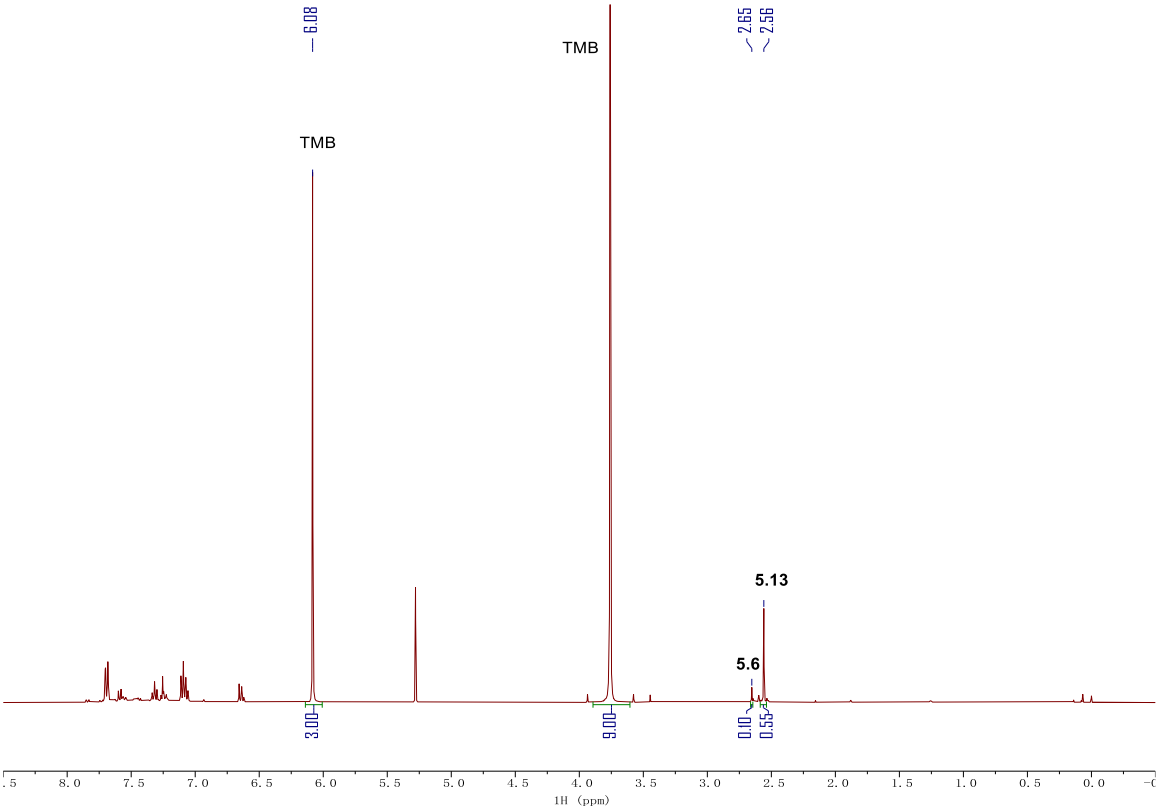

Figure 5.28. ^{1}H NMR spectrum ($CDCl_3$) of $PhICl_2$ oxidation of **5.4** without $TiCl_4$ after workup. *Taken from YC-2022-0171-workup.*

5.5.7 Ti-Catalyzed Indazole Synthesis with FcCl (Figure 5.5)

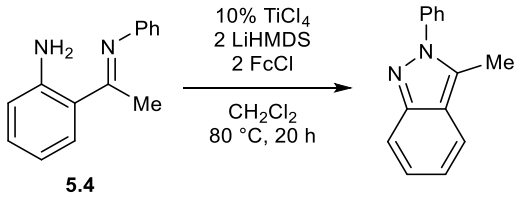

5.4 **5.6** 32%

$TiCl_4$ (7.6 mg, 0.04 mmol, 0.1 equiv), CH_2Cl_2 (3 mL), and a stir bar were added to a 20 mL scintillation vial in the glovebox. A solution of **5.4** (84.0 mg, 0.4 mmol, 1 equiv) in CH_2Cl_2 (2 mL) was added dropwise to the reaction mixture under vigorous stirring, resulting in a dark red

solution. A solution of LiHMDS (133.8 mg, 0.8 mmol, 2 equiv) in CH_2Cl_2 (3 mL) was added dropwise to the reaction mixture under vigorous stirring. FcCl (177.2 mg, 0.8 mmol, 2 equiv) was added to the reaction mixture without further wairting, and the reaction mixture was heated at 80℃ for 20 hours. The vial was then taken out of the glovebox and allowed to cool down. The reaction mixture was poured into a 20 mL scintillation vial with 5% methanolic HCl (2 mL) and extracted against 10 mL water, during which the unreacted **5.4** and **5.5** were hydrolyzed to give **5.13**. The organic fraction was dried over $MgSO_4$ and evaporated under vacuum. The solid residue was then washed by 20 mL hexanes for the removal of Fc (oxidation byproduct). Quantitative characterization for yield calculation was performed with ^{1}H NMR using TMB (50.4 mg, 0.3 mmol) as internal standard. Yield of **5.6** was determined as 32%. Further purification for pure **5.6** can be easily performed if needed as the product mixture contains only **5.6** and small amount of remaining Fc.

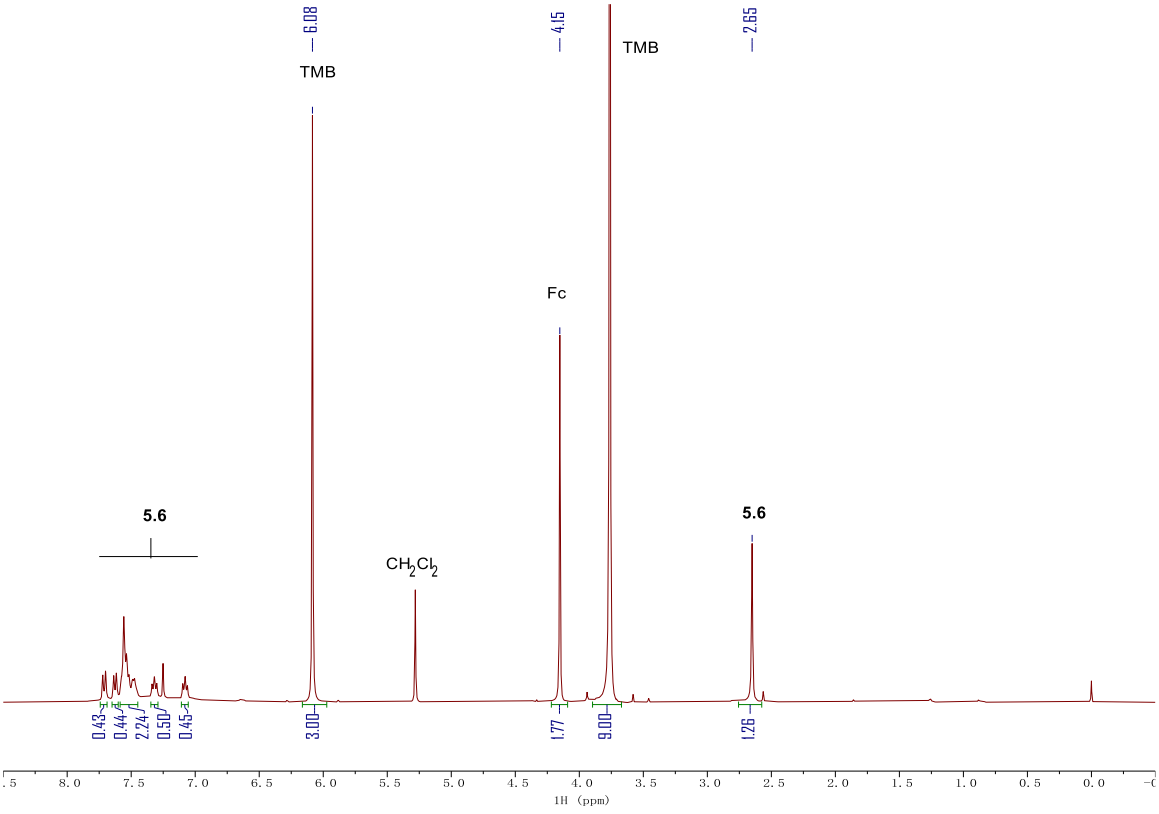

Figure 5.29. ^{1}H NMR spectrum ($CDCl_3$) of catalytic synthesis of **5.6** after workup. *Taken from YC-2022-0169-workup.*

5.5.8 Reaction Between Nitrosobenzene and *In Situ* Formed 2-Titanaquinazoline 5.5 (Figure 5.6)

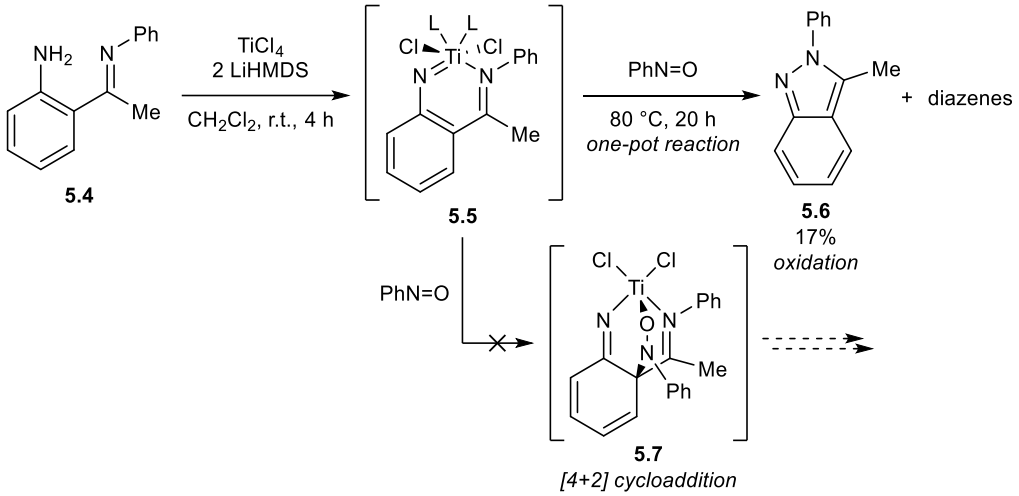

$TiCl_4$ (37.9 mg, 0.2 mmol, 1 equiv), CH_2Cl_2 (1.5 mL), and a stir bar were added to a 4 mL scintillation vial in the glovebox. A solution of **5.4** (42.0 mg, 0.2 mmol, 1 equiv) in CH_2Cl_2 (1 mL) was added dropwise to the reaction mixture under vigorous stirring, resulting in a dark red solution. A solution of LiHMDS (66.9 mg, 0.4 mmol, 2 equiv) in CH_2Cl_2 (1.5 mL) was added dropwise to the reaction mixture under vigorous stirring. After stirring at room temperature for 4 hours, nitrosobenzene (PhN=O, 21.4 mg, 0.2 mmol, 1 equiv) was added to the reaction mixture, and the reaction mixture was heated at 80℃ for 20 hours. The vial was then taken out of the glovebox and allowed to cool down. The reaction mixture was poured into a 20 mL scintillation vial with CH_2Cl_2 (4 mL) and extracted against 10 mL saturated $NaHCO_3$ aqueous solution. The organic fraction was dried over $MgSO_4$ and evaporated under vacuum. Yield of **5.6** was determined as 17% by ^{1}H NMR. Diazene **5.14** can be formed through either the condensation of nitrosobenzene on **5.4** (Mills reaction) or the nitrene heterocoupling during the imido-oxo exchange in the reaction between **5.5** and nitrosobenzene:

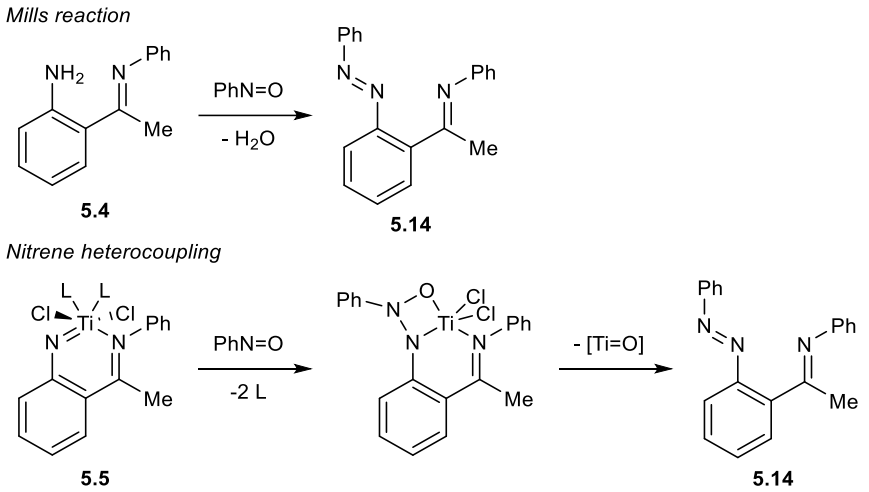

5.14 can further undergo intramolecular dehydrogenative coupling, however the structure of the product remains undefined.

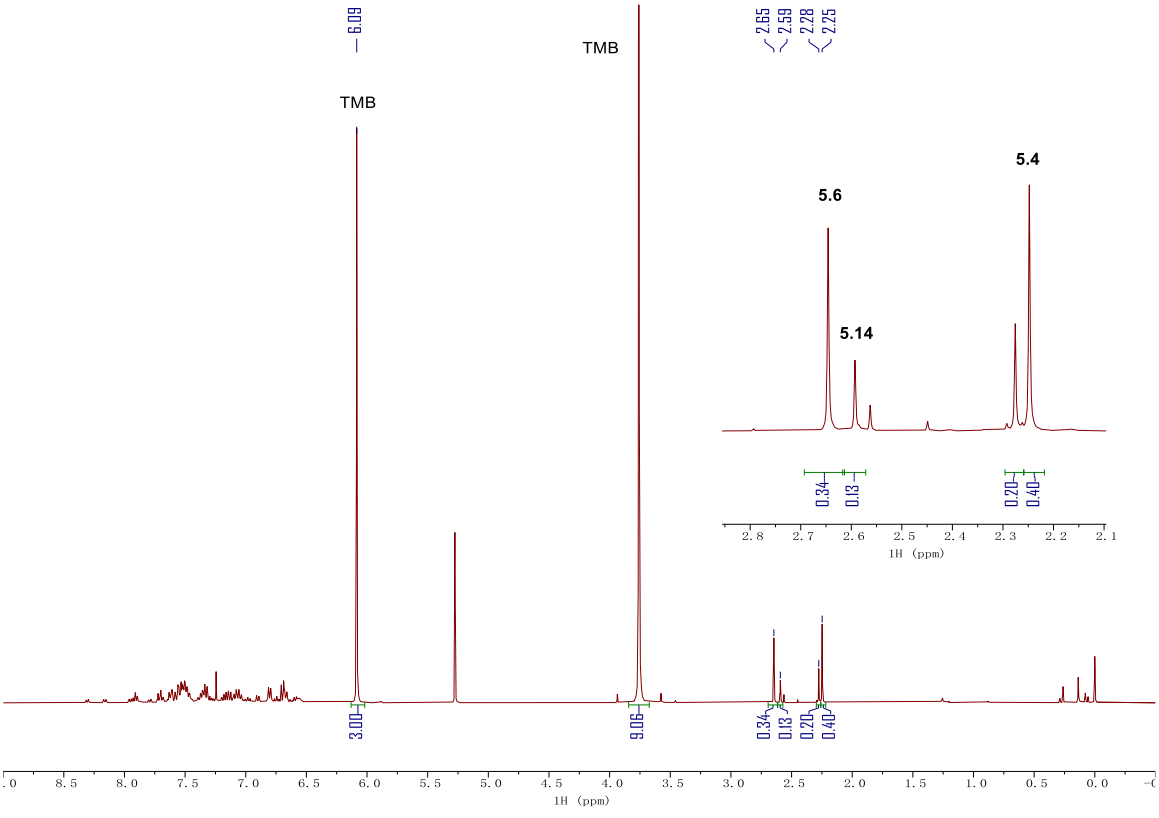

Figure 5.30. ^{1}H NMR spectrum ($CDCl_3$) of the reaction between **5.5** and nitrosobenzene after workup. *Taken from YC-2022-0167-workup.*

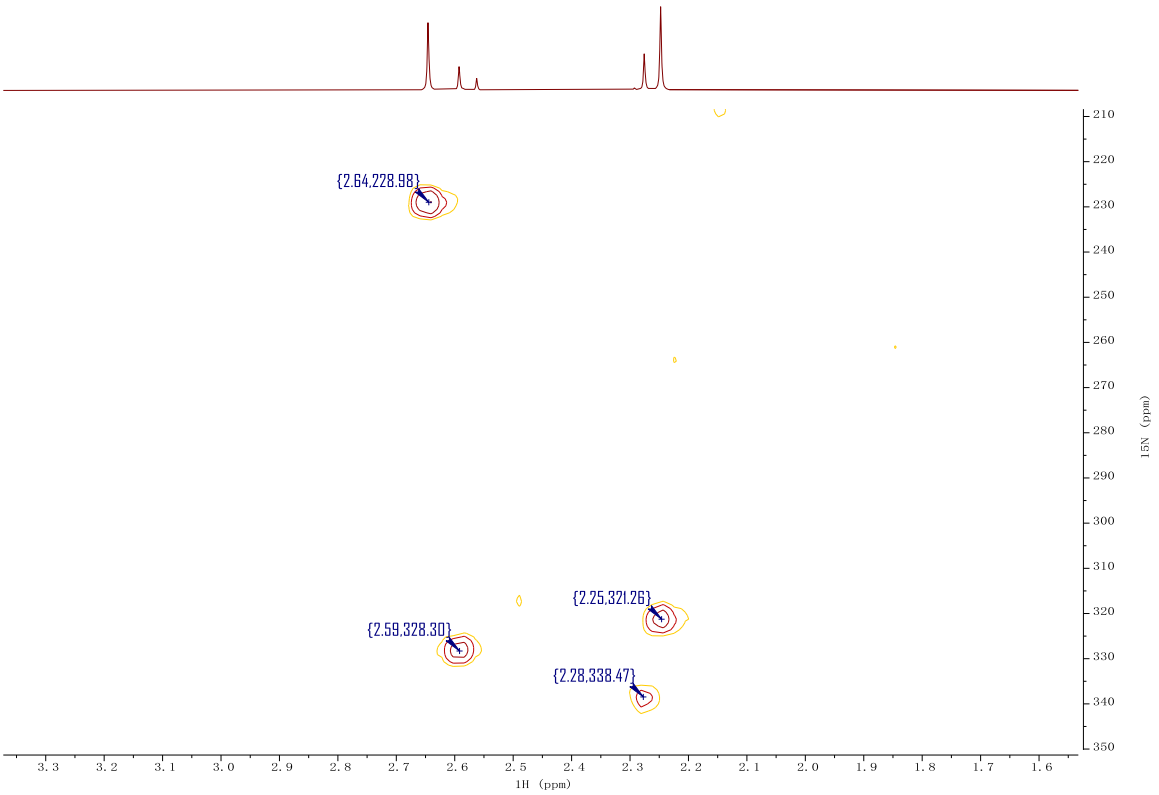

Figure 5.31. ^{1}H-^{15}N HMBC NMR spectrum ($CDCl_3$) of the reaction between **5.5** and nitrosobenzene after workup. *Taken from YC-2022-0167-workup-NHMBC.*

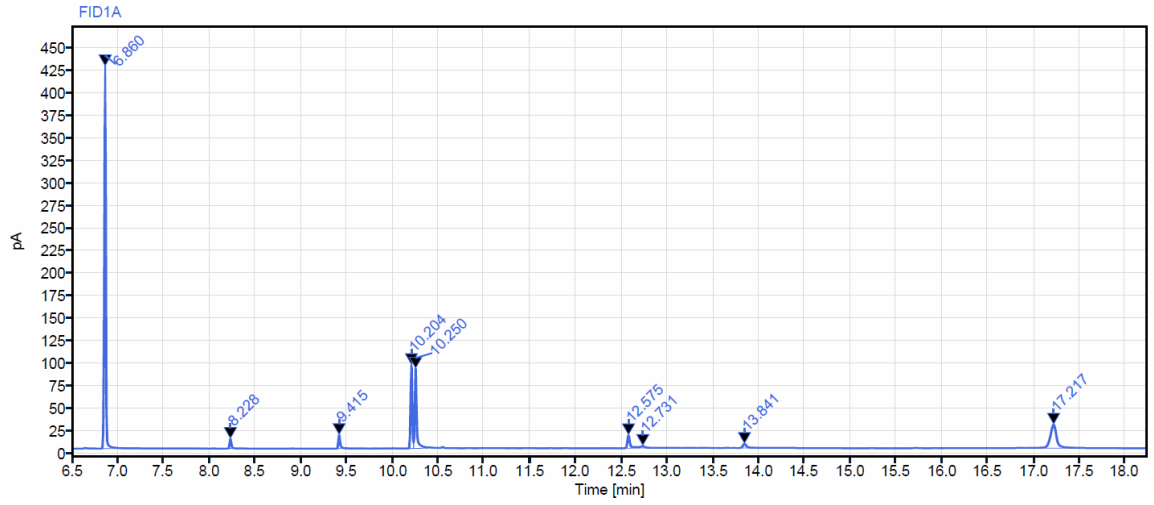

	Retention Time (min)	Peak Area	# of C	Yield (%)
TMB	6.860	476.6636	9	n.a.
5.6	10.250	112.9978	14	Overlap[a]

5.4	10.204	126.8367	14	Overlap[a]
5.14	12.575	27.6343	20	3.9
Dehydrogenative coupling of **5.14**	17.217	131.2242	20	18.6

[a]Yields of **5.6** was calculated based on NMR due to the overlapping between peaks of **5.6** and **5.4**.

Figure 5.32. GC-FID spectrum of the reaction between **5.5** and nitrosobenzene after workup. *Taken from YC-2022-0165-1.*

Peak RT: 12.561

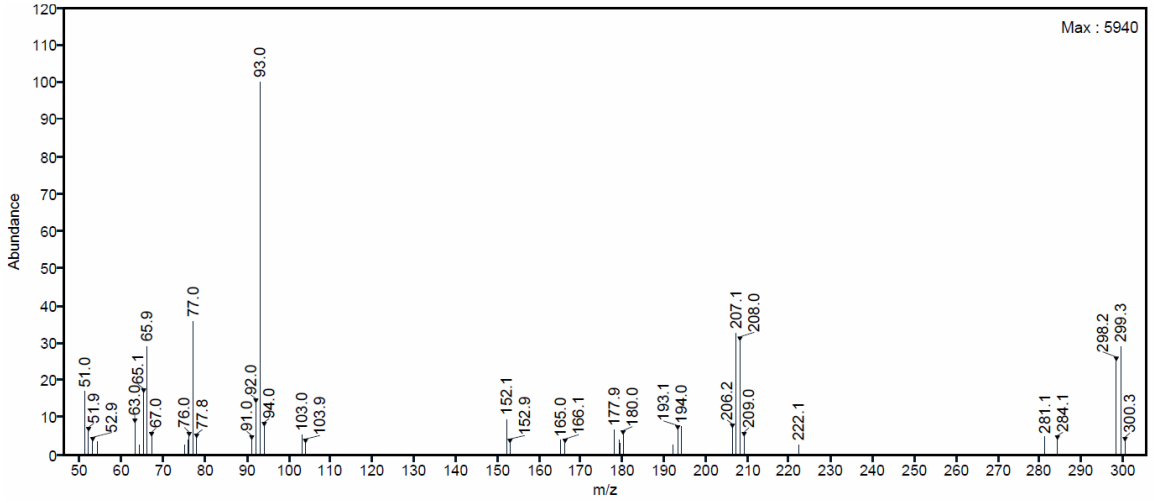

Peak RT: 17.197

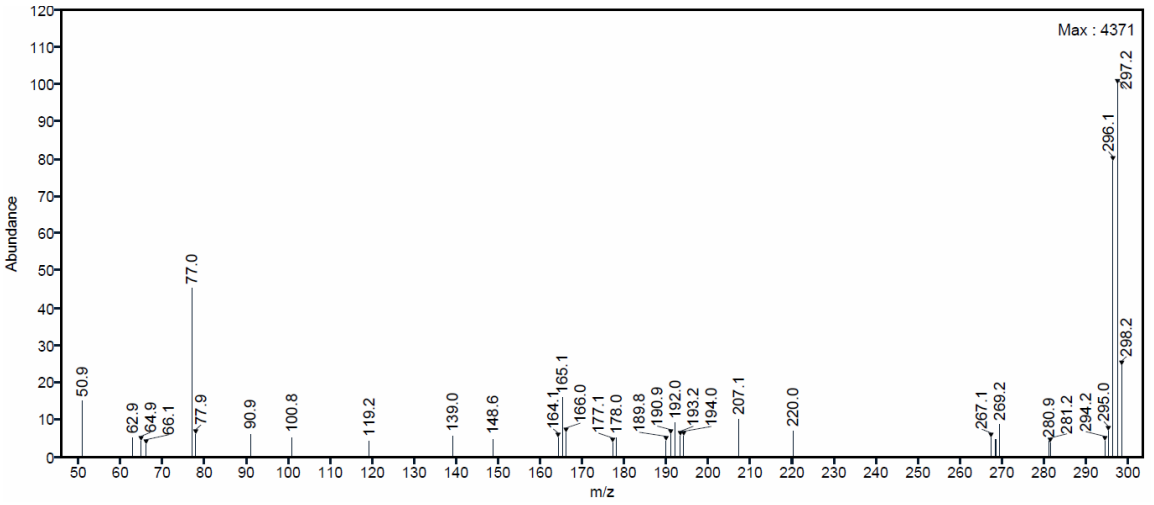

Figure 5.33. Selected GC-MS spectra of the reaction between **5.5** and nitrosobenzene after workup. (Top) retention time = 12.561 min (**5.14**); (bottom) retention time = 17.197 (dehydrogenative coupling of **5.14**). *Taken from YC-2022-0165-1.*

5.5.9 TEMPO Oxidation of Non-Tethered Ti Imido-Imine Complex (Figure 5.8)

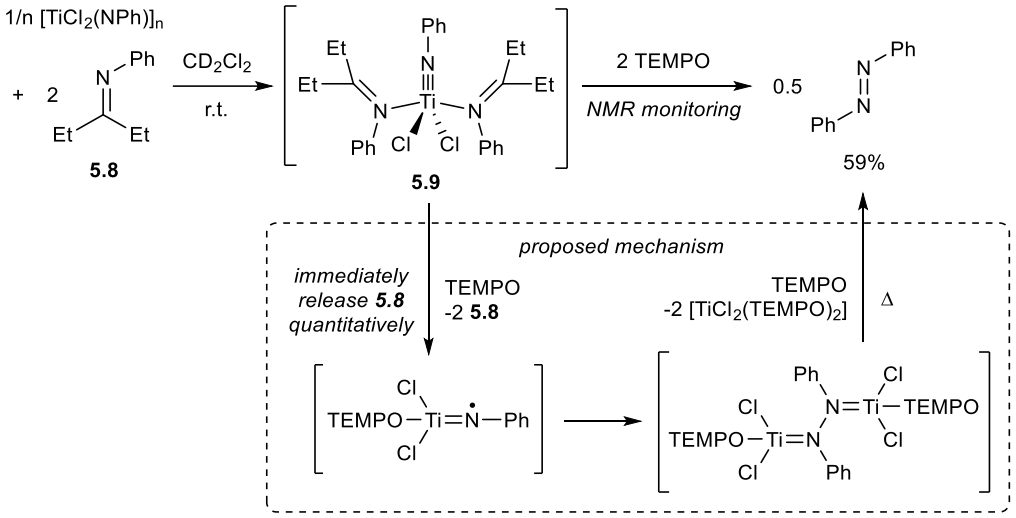

$[TiCl_2(NPh)]_n$ (10.5 mg, 0.05/n mmol, 1 equiv), *N*-phenylpentan-3-imine (**5.8**, 16.1 mg, 0.1 mmol, 2 equiv), HMDSO (16.2 mg, 0.1 mmol, 2 equiv, ^{1}H NMR internal standard), and CD_2Cl_2 (0.5 mL) were added to a J-Young NMR tube in a glovebox. The tube was capped and taken out of the glovebox. After ^{1}H NMR was taken for the reaction mixture, the NMR tube was transferred back into the glovebox. TEMPO (15.6 mg, 0.1 mmol, 2 equiv) and CD_2Cl_2 (0.1 mL) were added to the reaction mixture. The NMR tube was capped and shaken to ensure the thorough mixing of the reactants, and allowed to sit still at room temperature. ^{1}H NMR was taken at 0, 5, and 24 hours for monitoring the reaction progress. After the 24 hour time point NMR was taken, the NMR tube was put into a pre-heated 60℃ oil bath for 4 hours. ^{1}H NMR was taken after the heating. Further heating gave no change in ^{1}H NMR signals. The consumption of **5.8** after the addition of TEMPO was attributed to Ti iminyl attacking free **5.8** in the solution.

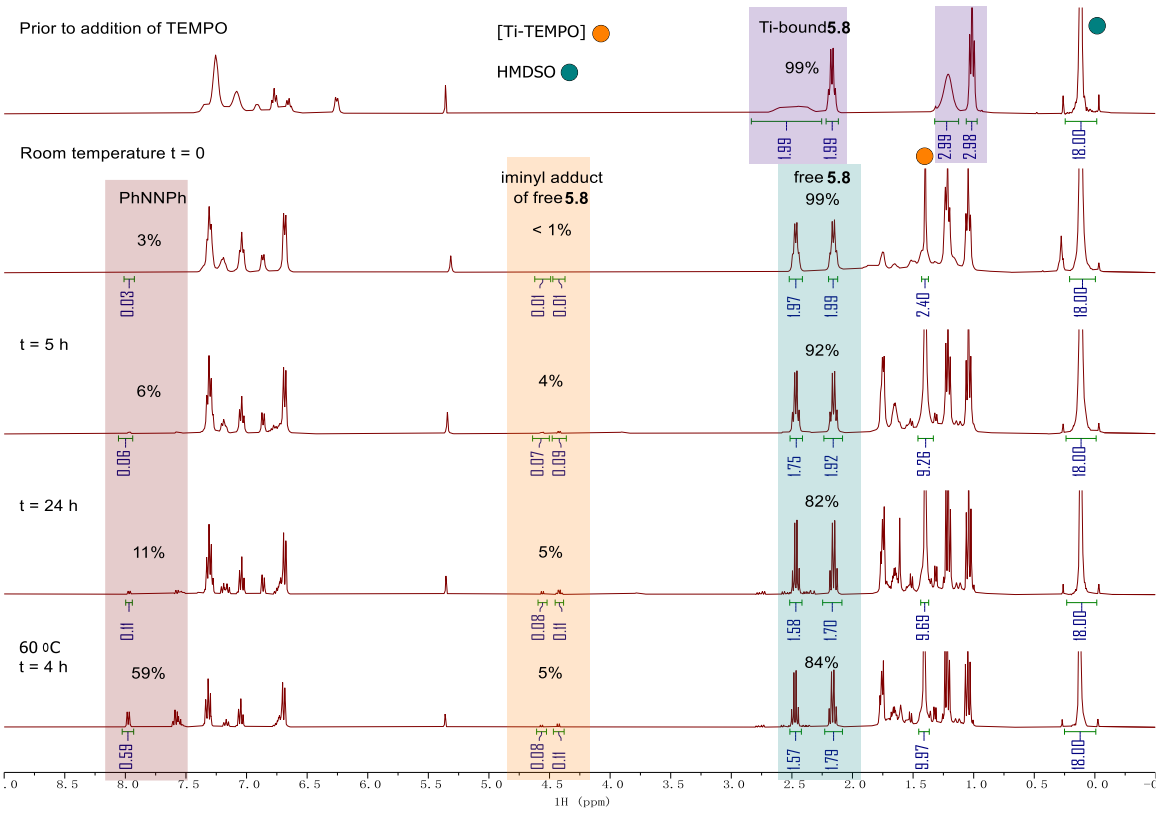

Figure 5.34. Stacked ^{1}H NMR spectra (CD_2Cl_2) of the reaction between *in situ* formed **5.9** and TEMPO. *Taken from (from top to bottom) YC-2022-0168-preTEMPO(0h), YC-2022-0168-TEMPO-0h, YC-2022-0168-TEMPO-5h, YC-2022-0168-TEMPO-24h, YC-2022-0168-TEMPO-heat-4h.*

5.5.10 Synthesis of 5.5^{bpy} (Figure 5.2)

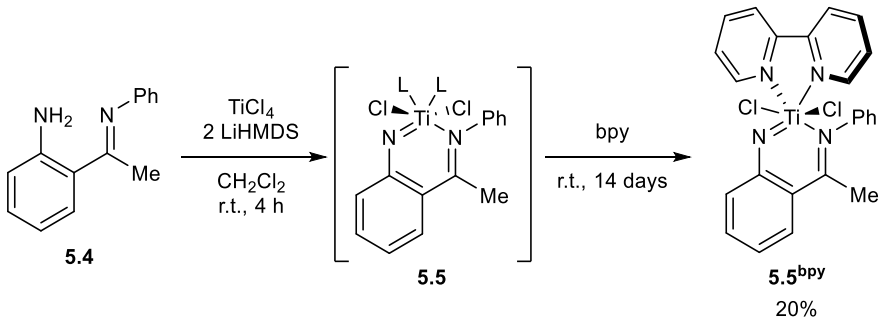

$TiCl_4$ (19.0 mg, 0.1 mmol, 1 equiv), CH_2Cl_2 (1.0 mL), and a stir bar were added to a 4 mL scintillation vial in the glovebox. A solution of **5.4** (21.0 mg, 0.1 mmol, 1 equiv) in CH_2Cl_2 (0.5

mL) was added dropwise to the reaction mixture under vigorous stirring, resulting in a dark red solution. A solution of LiHMDS (33.5 mg, 0.2 mmol, 2 equiv) in CH_2Cl_2 (0.5 mL) was added dropwise to the reaction mixture under vigorous stirring. After stirring at room temperature for 4 hours, the stir bar was removed, and 2,2'-bipyridine (bpy, 15.6 mg, 0.1 mmol, 1 equiv) was added to the reaction mixture. After shaking vigorously to allow thorough mixing, the reaction mixture was allowed to stand at room temperature for 2 weeks. Deep brown crystals were obtained by decanting the reaction solution. X-ray crystallography revealed the product structure as **5.5**^{bpy}. Yield: 9.5 mg (0.0197 mmol, 20%). NMR characterization was attempted for **5.5**^{bpy} though unsuccessful due to its low solubility.

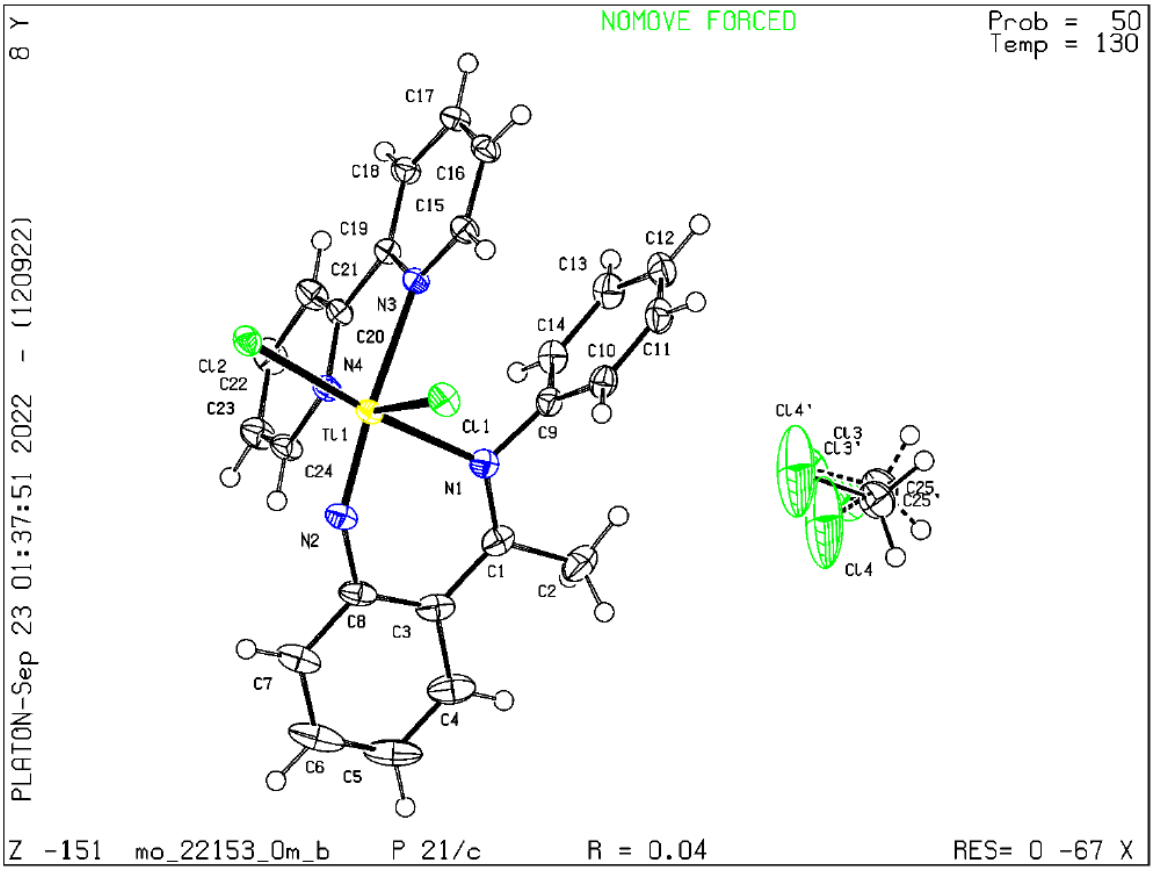

Figure 5.35. ORTEP diagram of **5.5**^{bpy}. Thermal ellipsoids are drawn at 50% probability.

	5.5^{bpy}
CCDC Number	?
Empirical Formula	$C_{24}H_{20}Cl_2N_4Ti$, CH_2Cl_2
Formula Weight	568.16

Temperature (K)	130(2)
a, Å	12.2238(8)
b, Å	8.2921(5)
c, Å	24.7315(16)
α, °	90
β, °	95.622(3)
γ, °	90
Volume, Å^3	2494.8(3)
Z	4
Crystal System	Monoclinic
Space Group	$P2_1/c$
d_{calc}, g/cm^3	1.513
θ Range, °	2.23 to 25.59
μ, mm^{-1}	0.764
Abs. Correction	Multi-scan
GOF	1.037
R_1[a]	0.0395
wR_2[b] [I>2σ(I)]	0.1048

[a] $R_1 = \Sigma||F_o|-|F_c||/\Sigma|F_o|$. [b] $wR_2 = [\Sigma[w(F_o^2-F_c^2)^2]/\Sigma[w(F_o^2)^2]^{1/2}$.

5.5.11 TEMPO Oxidation of Ti Amide Complexes (Figure 5.9)

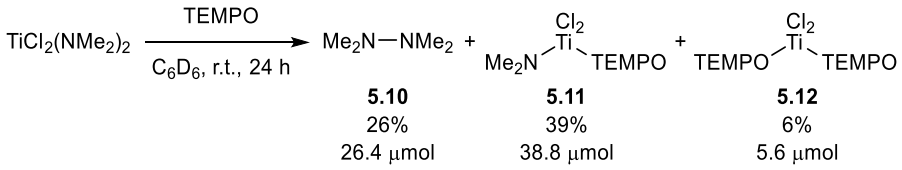

TEMPO (15.6 mg, 0.1 mmol, 1 equiv), HMDSO (16.2 mg, 0.1 mmol, 1 equiv, NMR internal standard), and C_6D_6 (2 mL) were added to an NMR tube in the glovebox. $TiCl_2(NMe_2)_2$ (20.7 mg, 0.1 mmol, 1 equiv) was added and the NMR tube was capped and sealed immediately, then shaken to allow thorough mixing. ^{1}H NMR was taken at 15 mins, 2 h, 4 h, 24 h for reaction monitoring. **5.10** was identified based on reported chemical shift. **5.11** was identified based on independent synthesis (section 5.5.12). **5.12** was identified based on ^{1}H NMR spectra of previous reported reaction in which **5.12** was the byproduct.[61]

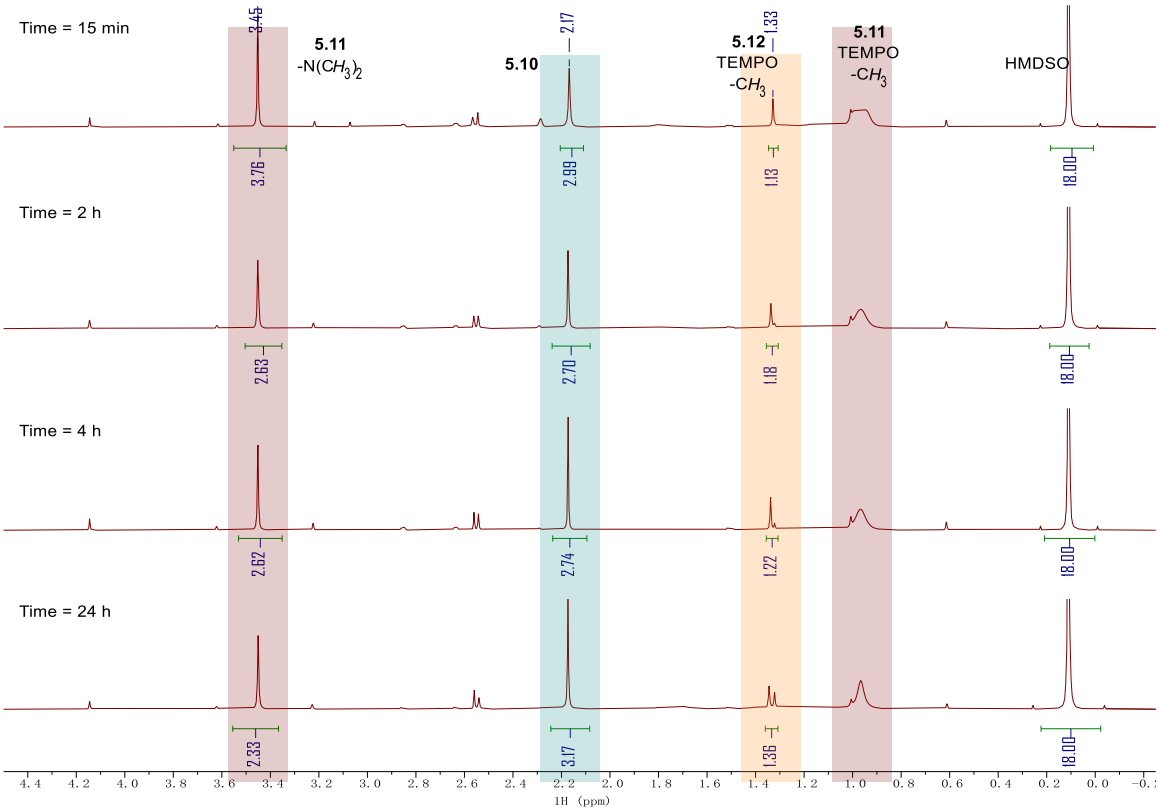

Figure 5.36. Stacked ^{1}H NMR spectra (C_6D_6) of the reaction between $TiCl_2(NMe_2)_2$ and 1 equiv TEMPO. *Taken from (from top to bottom) YC-2022-0179-0h, YC-2022-0179-2h, YC-2022-0179-4h, YC-2022-0179-24h.*

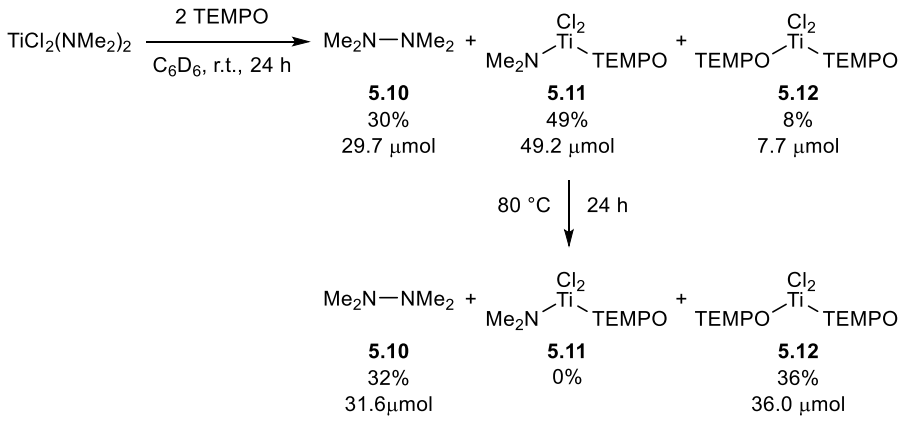

TEMPO (31.2 mg, 0.2 mmol, 2 equiv), HMDSO (8.1 mg, 0.05 mmol, 0.5 equiv, NMR internal standard), and C_6D_6 (2 mL) were added to an NMR tube in the glovebox. $TiCl_2(NMe_2)_2$ (20.7 mg, 0.1 mmol, 1 equiv) was added and the NMR tube was capped and sealed immediately, then shaken to allow thorough mixing. ^{1}H NMR was taken at 15 mins, 2 h, 4 h, 24 h for reaction

monitoring. The NMR tube was then put into a pre-heated 80 ℃ oil bath. ^{1}H NMR was taken at 1 h, 3 h, 24 h for reaction monitoring. **5.10** was identified based on reported chemical shift. **5.11** was identified based on independent synthesis (section 5.5.12). **5.12** was identified based on ^{1}H NMR spectra of previous reported reaction in which **5.12** was the byproduct.[61]

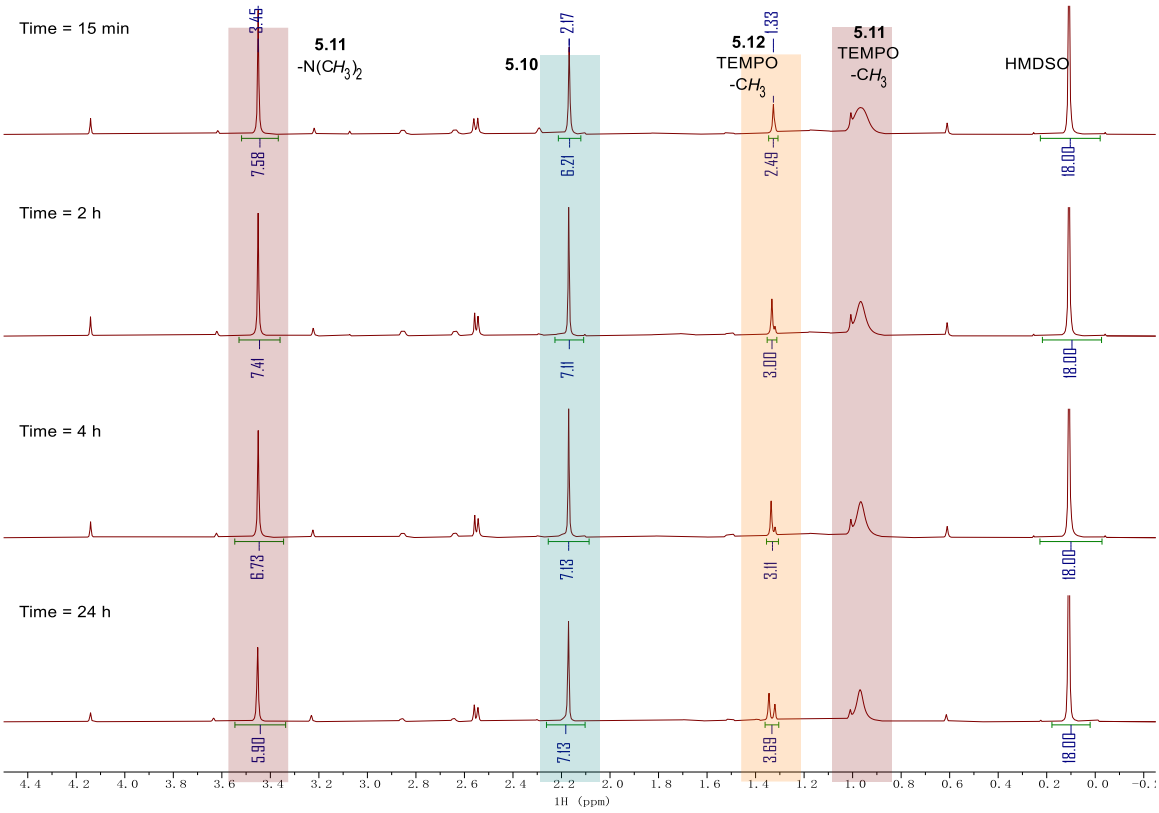

Figure 5.37. Stacked ^{1}H NMR spectra (C_6D_6) of the reaction between $TiCl_2(NMe_2)_2$ and 2 equiv TEMPO before heating. *Taken from (from top to bottom) YC-2022-0176-0h, YC-2022-0176-2h, YC-2022-0176-4h, YC-2022-0176-24h.*

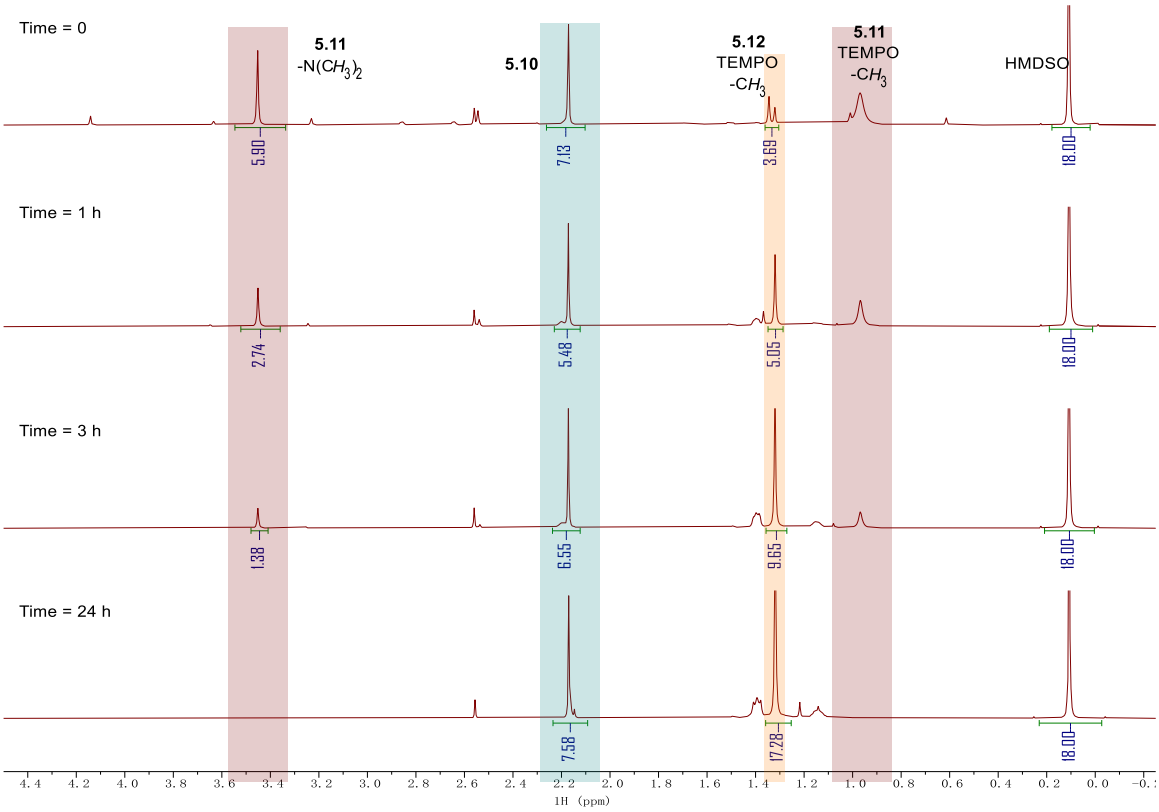

Figure 5.38. Stacked ^{1}H NMR spectra (C_6D_6) of the reaction between $TiCl_2(NMe_2)_2$ and 2 equiv TEMPO during 80℃ heating. *Taken from (from top to bottom) YC-2022-0176-24h, YC-2022-0176-80oC-1h, YC-2022-0176-80oC-3h, YC-2022-0176-80oC-24h.*

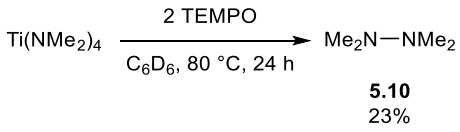

TEMPO (31.2 mg, 0.2 mmol, 2 equiv), HMDSO (8.1 mg, 0.05 mmol, 0.5 equiv, NMR internal standard), and C_6D_6 (2 mL) were added to an NMR tube in the glovebox. Ti $(NMe_2)_4$ (22.4 mg, 0.1 mmol, 1 equiv) was added and the NMR tube was capped and sealed immediately, then shaken to allow thorough mixing. ^{1}H NMR was taken at 15 mins, 2 h, 4 h, 24 h for reaction monitoring, during which no significant amount of **5.10** can be identified. The NMR tube was then put into a pre-heated 80℃ oil bath. ^{1}H NMR was taken at 1 h, 3 h, 24 h for reaction monitoring. **5.10** was identified based on reported chemical shift.

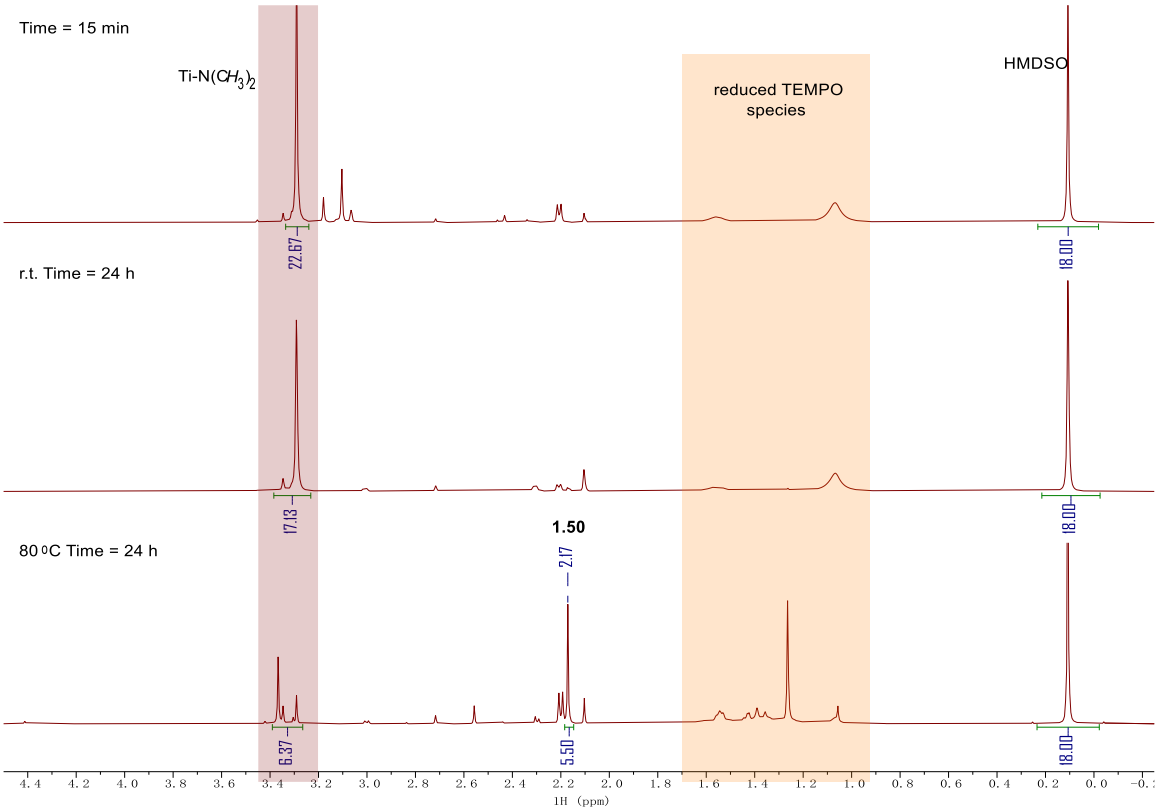

Figure 5.39. Stacked ^{1}H NMR spectra (C_6D_6) of the reaction between Ti $(NMe_2)_4$ and 2 equiv TEMPO. *Taken from (top) YC-2022-0177-0h, (middle) YC-2022-0177-24h, and (bottom) YC-2022-0177-80oC-24h.*

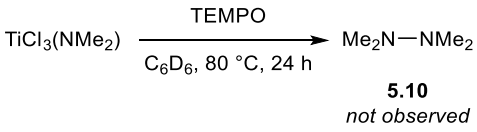

TEMPO (15.6 mg, 0.1 mmol, 1 equiv), HMDSO (16.2 mg, 0.1 mmol, 1 equiv, NMR internal standard), and C_6D_6 (2 mL) were added to an NMR tube in the glovebox. $TiCl_2(NMe_2)_2$ (20.7 mg, 0.1 mmol, 1 equiv) was added and the NMR tube was capped and sealed immediately, then shaken to allow thorough mixing. ^{1}H NMR was taken at 15 mins, 2 h for reaction monitoring. The NMR tube was then put into a pre-heated 80 ℃ oil bath for 20 h. No significant amount of **5.10** can be identified during the reaction.

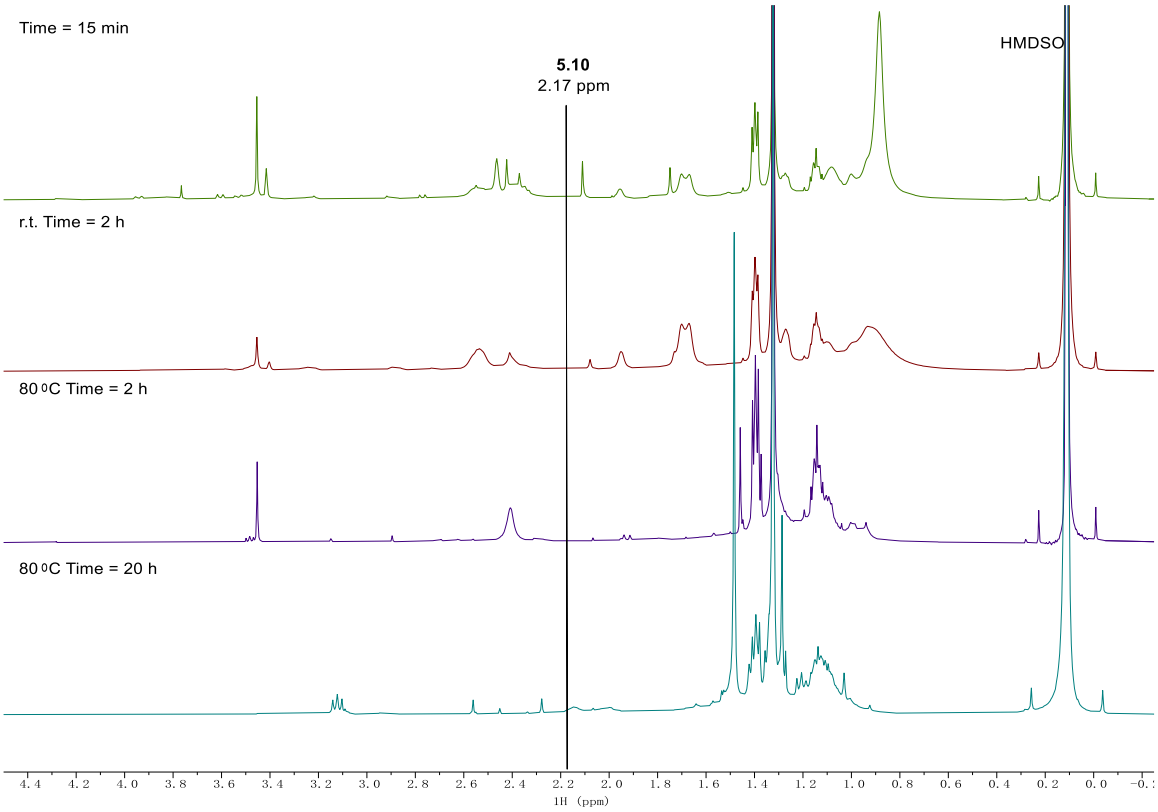

Figure 5.40. Stacked ^{1}H NMR spectra (C_6D_6) of the reaction between $TiCl_3(NMe_2)$ and 1 equiv TEMPO. *Taken from (from top to bottom) YC-2022-0180-0h, YC-2022-0180-2h, YC-2022-0180-80oC-2h, YC-2022-0180-80oC-20h.*

5.5.12 Synthesis of 5.11 from $TiCl_2(NMe_2)_2$ and TEMPO-H

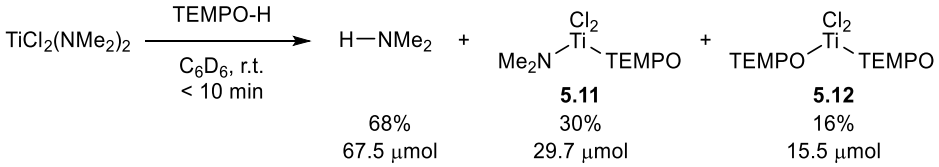

$TiCl_2(NMe_2)_2$ (20.7 mg, 0.1 mmol, 1 equiv) TEMPO-H (15.7 mg, 0.1 mmol, 1 equiv), HMDSO (16.2 mg, 0.1 mmol, 1 equiv, NMR internal standard), and C_6D_6 (0.5 mL) were added to an NMR tube in the glovebox, and the NMR tube was capped and sealed immediately, then shaken to allow thorough mixing. ^{1}H NMR was taken at 10 mins, by which time $TiCl_2(NMe_2)_2$ had been completely consumed. The reaction product was found to be a mixture of **5.11** and **5.12**. Changing the addition order to dropwise addition of TEMPO-H solution into $TiCl_2(NMe_2)_2$

solution did not lead to significant difference. ^{1}H-^{15}N HMBC showed ^{1}H-^{15}N correlation signal for the ^{1}H signal at 3.46 ppm in range with a metal-amide. The absence of ^{1}H-^{15}N HMBC signal from $HNMe_2$ can be attributed to the fast relaxation due to amine-amide exchange between $HNMe_2$ and **5.11** *via* protonolysis, shown in the NOESY NMR as the EXSY signal between 3.46 ppm and 2.24 ppm.

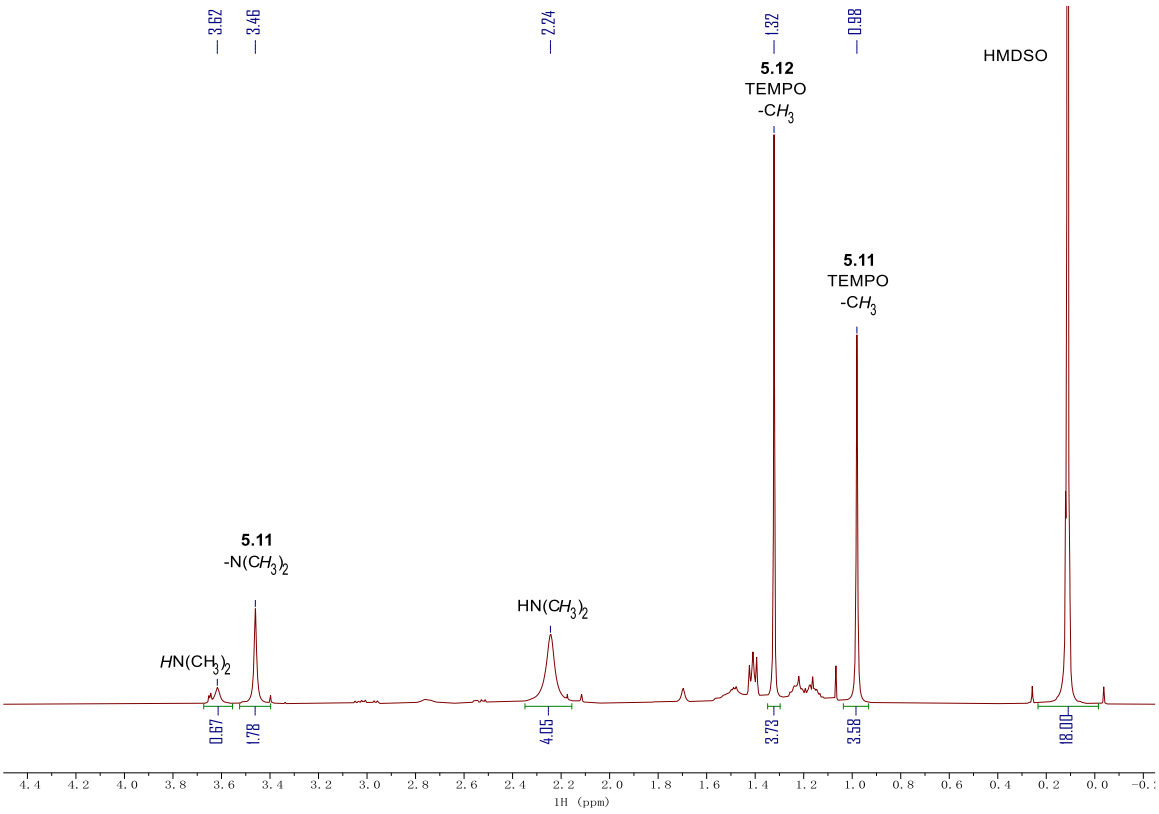

Figure 5.41. ^{1}H NMR spectrum (C_6D_6) of the reaction between $TiCl_2(NMe_2)_2$ and 1 equiv TEMPO-H. *Taken from YC-2022-0182-0h.*

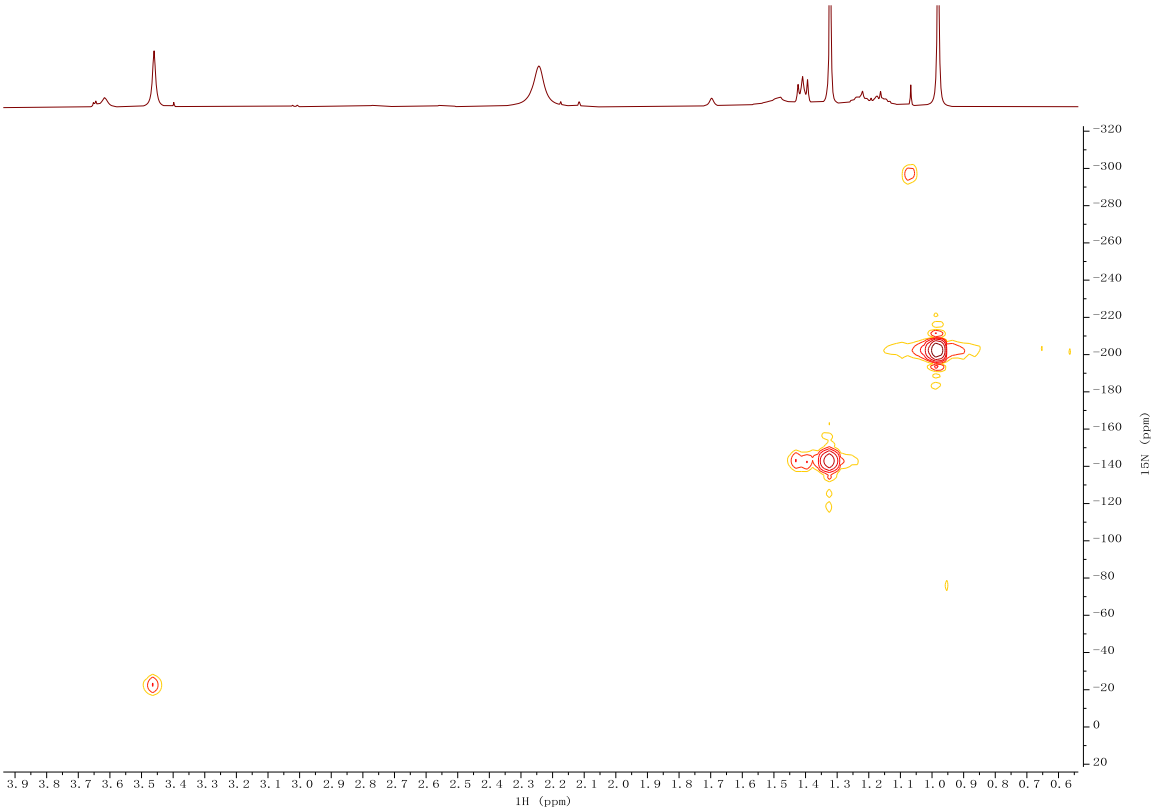

Figure 5.42. ^{1}H-^{15}N HMBC NMR spectrum (C_6D_6) of the reaction between $TiCl_2(NMe_2)_2$ and 1 equiv TEMPO-H. *Taken from YC-2022-0182-NHMBC.*

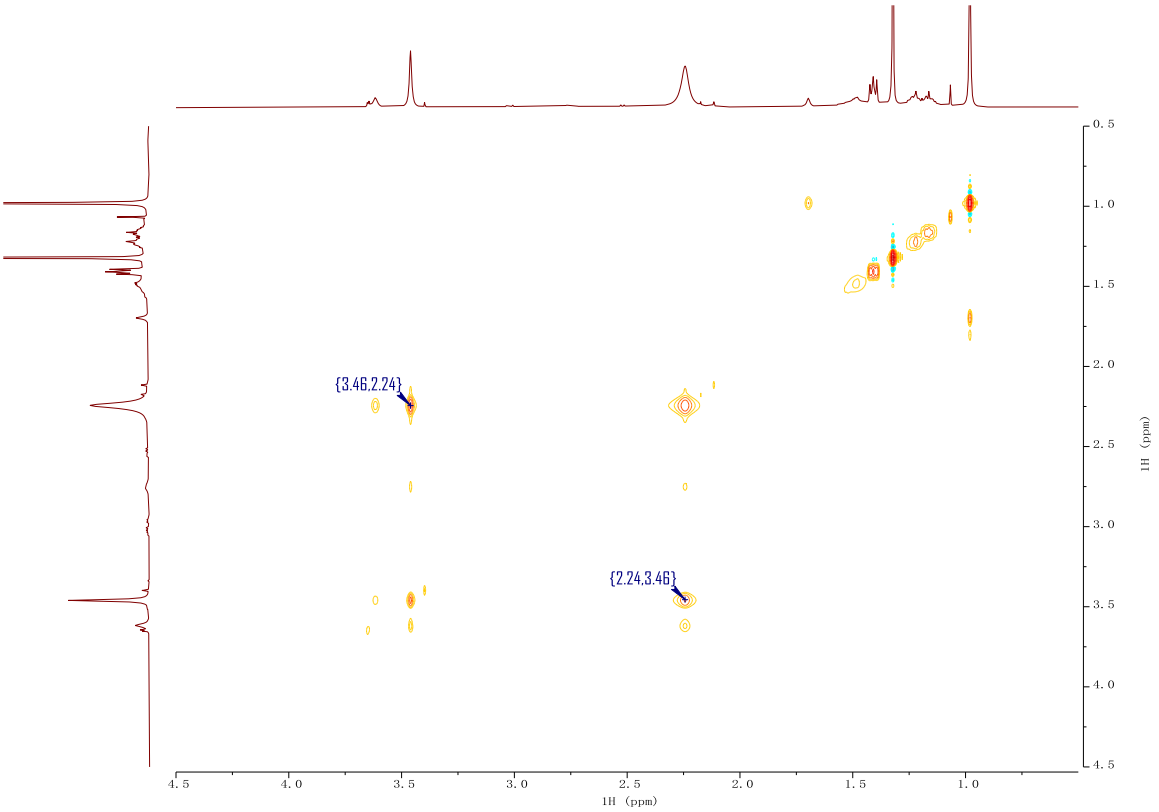

Figure 5.43. ^{1}H NOESY NMR spectrum (C_6D_6) of the reaction between $TiCl_2(NMe_2)_2$ and 1 equiv TEMPO-H. *Taken from YC-2022-0182-NOESY.*

Bibliography

(1) Odom, A. L.; McDaniel, T. J. Titanium-Catalyzed Multicomponent Couplings: Efficient One-Pot Syntheses of Nitrogen Heterocycles. *Acc. Chem. Res.* **2015**, *48* (11), 2822–2833.

(2) Sarraf, M.; Rezvani Ghomi, E.; Alipour, S.; Ramakrishna, S.; Liana Sukiman, N. A State-of-the-Art Review of the Fabrication and Characteristics of Titanium and Its Alloys for Biomedical Applications. *Bio-Design Manuf.* **2022**, *5* (2), 371–395.

(3) Hanawa, T. Biocompatibility of Titanium from the Viewpoint of Its Surface. *Sci. Technol. Adv. Mater.* **2022**, *23* (1), 457–472.

(4) Hayler, J. D.; Leahy, D. K.; Simmons, E. M. A Pharmaceutical Industry Perspective on Sustainable Metal Catalysis. *Organometallics* **2019**, *38* (1), 36–46.

(5) Mukaiyama, T.; Narasaka, K.; Banno, K. NEW ALDOL TYPE REACTION. *Chem. Lett.* **1973**, *2* (9), 1011–1014.

(6) *Handbook of Transition Metal Polymerization Catalysts*; Hoff, R., Mathers, R. T., Eds.; John Wiley & Sons, Inc.: Hoboken, NJ, USA, 2010.

(7) Parkin, G. Classification of Organotransition Metal Compounds. In *Comprehensive Organometallic Chemistry III*; Elsevier, 2007; pp 1–57.

(8) Davis-Gilbert, Z. W.; Tonks, I. A. Titanium Redox Catalysis: Insights and Applications of an Earth-Abundant Base Metal. *Dalton Trans.* **2017**, *46* (35), 11522–11528.

(9) Tonks, I. A. Ti-Catalyzed and -Mediated Oxidative Amination Reactions. *Acc. Chem. Res.* **2021**, *54* (17), 3476–3490.

(10) McGrane, P. L.; Livinghouse, T. Synthetic Applications of Group IV Metal-Imido Complex - Alkyne [2+2] Cycloadditions. A Concise Total Synthesis of (.+-.)-Monomorine. *J. Org. Chem.* **1992**, *57* (5), 1323–1324.

(11) McGrane, P. L.; Livinghouse, T. Synthetic Applications of Imidotitanium-Alkyne [2+2] Cycloadditions. A Concise, Stereocontrolled Total Synthesis of the Antifungal Agent (+)-Preussin. *J. Am. Chem. Soc.* **1993**, *115* (24), 11485–11489.

(12) Greenberg, S.; Stephan, D. W. Hydroamination as a Route to Nitrogen-Containing Oligomers. *Polym. Chem.* **2010**, *1* (8), 1332.

(13) Baranger, A. M.; Walsh, P. J.; Bergman, R. G. Variable Regiochemistry in the Stoichiometric and Catalytic Hydroamination of Alkynes by Imidozirconium Complexes Caused by an Unusual Dependence of the Rate Law on Alkyne Structure and Temperature. *J. Am. Chem. Soc.* **1993**, *115* (7), 2753–2763.

(14) Walsh, P. J.; Hollander, F. J.; Bergman, R. G. Monomeric and Dimeric Zirconocene Imido Compounds: Synthesis, Structure, and Reactivity. *Organometallics* **1993**, *12* (9), 3705–3723.

(15) Walsh, P. J.; Baranger, A. M.; Bergman, R. G. Stoichiometric and Catalytic Hydroamination of Alkynes and Allene by Zirconium Bisamides Cp2Zr(NHR)2. *J. Am. Chem. Soc.* **1992**, *114* (5), 1708–1719.

(16) Polse, J. L.; Andersen, R. A.; Bergman, R. G. Reactivity of a Terminal Ti(IV) Imido Complex toward Alkenes and Alkynes: Cycloaddition vs C−H Activation. *J. Am. Chem. Soc.* **1998**, *120* (51), 13405–13414.

(17) Müller, T. E.; Hultzsch, K. C.; Yus, M.; Foubelo, F.; Tada, M. Hydroamination: Direct Addition of Amines to Alkenes and Alkynes. *Chem. Rev.* **2008**, *108* (9), 3795–3892.

(18) Pohlki, F.; Doye, S. The Mechanism of the [Cp2TiMe2]-Catalyzed Intermolecular Hydroamination of Alkynes. *Angew. Chemie Int. Ed.* **2001**, *40* (12), 2305–2308.

(19) Straub, B. F.; Bergman, R. G. The Mechanism of Hydroamination of Allenes, Alkynes, and Alkenes Catalyzed by Cyclopentadienyltitanium-Imido Complexes: A Density Functional Study. *Angew. Chemie Int. Ed.* **2001**, *40* (24), 4632–4635.

(20) Hao, H.; Schafer, L. L. Metal–Ligand Cooperativity in Titanium-Catalyzed Anti-Markovnikov Hydroamination. *ACS Catal.* **2020**, *10* (13), 7100–7111.

(21) Johnson, J. S.; Bergman, R. G. Imidotitanium Complexes as Hydroamination Catalysts: Substantially Enhanced Reactivity from an Unexpected Cyclopentadienide/Amide Ligand Exchange. *J. Am. Chem. Soc.* **2001**, *123* (12), 2923–2924.

(22) Heutling, A.; Pohlki, F.; Bytschkov, I.; Doye, S. Hydroamination/Hydrosilylation Sequence Catalyzed by Titanium Complexes. *Angew. Chemie Int. Ed.* **2005**, *44* (19), 2951–2954.

(23) Ramanathan, B.; Keith, A. J.; Armstrong, D.; Odom, A. L. Pyrrole Syntheses Based on Titanium-Catalyzed Hydroamination of Diynes. *Org. Lett.* **2004**, *6* (17), 2957–2960.

(24) Cao, C.; Shi, Y.; Odom, A. L. A Titanium-Catalyzed Three-Component Coupling To Generate α,β-Unsaturated β-Iminoamines. *J. Am. Chem. Soc.* **2003**, *125* (10), 2880–2881.

(25) Barnea, E.; Majumder, S.; Staples, R. J.; Odom, A. L. One-Step Route to 2,3-Diaminopyrroles Using a Titanium-Catalyzed Four-Component Coupling. *Organometallics* **2009**, *28* (13), 3876–3881.

(26) Huh, D. N.; Cheng, Y.; Frye, C. W.; Egger, D. T.; Tonks, I. A. Multicomponent Syntheses of 5- and 6-Membered Aromatic Heterocycles Using Group 4–8 Transition Metal Catalysts. *Chem. Sci.* **2021**, *12* (28), 9574–9590.

(27) Gribkov, D. V.; Hultzsch, K. C. Hydroamination/Cyclization of Aminoalkenes Using Cationic Zirconocene and Titanocene Catalysts. *Angew. Chemie Int. Ed.* **2004**, *43* (41), 5542–5546.

(28) Chatt, J.; Duncanson, L. A. 586. Olefin Co-Ordination Compounds. Part III. Infra-Red Spectra and Structure: Attempted Preparation of Acetylene Complexes. *J. Chem. Soc.* **1953**, 2939.

(29) Kulinkovich, O. G.; Sviridov, S. V.; Vasilevski, D. A. Reaction of Ethylmagnesium Bromide with Esters of Carboxylic-Acid in the Presence of Tetraisopropoxytitanium. *Zh. Org. Khim.* **1989**, *25*, 2244–2245.

(30) Kulinkovich, O. G.; Kananovich, D. G. Advanced Procedure for the Preparation of Cis-1,2-Dialkylcyclopropanols - Modified Ate Complex Mechanism for Titanium-Mediated Cyclopropanation of Carboxylic Esters with Grignard Reagents. *Eur. J. Org. Chem.* **2007**, No. 13, 2121–2132.

(31) Lam, F. L.; Lee, H. W.; Wang, J.; Kwong, F. Y. Recent Advancement of Catalytic Pauson-Khand-Type Reactions. In *The Pauson-Khand Reaction*; 2012; pp 181–210.

(32) Gilbert, Z. W.; Hue, R. J.; Tonks, I. A. Catalytic Formal [2+2+1] Synthesis of Pyrroles from Alkynes and Diazenes via TiII/TiIVredox Catalysis. *Nat. Chem.* **2016**, *8* (1), 63–68.

(33) Zanda, M. SYNFORM ISSUE 2016/04. *Synfacts* **2016**, *12* (04), A48–A64.

(34) Davis-Gilbert, Z. W.; Wen, X.; Goodpaster, J. D.; Tonks, I. A. Mechanism of Ti-Catalyzed Oxidative Nitrene Transfer in [2 + 2 + 1] Pyrrole Synthesis from Alkynes and Azobenzene. *J. Am. Chem. Soc.* **2018**, *140* (23), 7267–7281.

(35) Pearce, A. J.; See, X. Y.; Tonks, I. A. Oxidative Nitrene Transfer from Azides to Alkynes via Ti(Ii)/Ti(Iv) Redox Catalysis: Formal [2+2+1] Synthesis of Pyrroles. *Chem. Commun.* **2018**, *54* (50), 6891–6894.

(36) Heins, S. P.; Wolczanski, P. T.; Cundari, T. R.; Macmillan, S. N. Redox Non-Innocence Permits Catalytic Nitrene Carbonylation by (Dadi)Ti=NAd (Ad = Adamantyl). *Chem. Sci.* **2017**, *8* (5), 3410–3418.

(37) Nguyen, A. I.; Zarkesh, R. A.; Lacy, D. C.; Thorson, M. K.; Heyduk, A. F. Catalytic Nitrene Transfer by a Zirconium(IV) Redox-Active Ligand Complex. *Chem. Sci.* **2011**, *2* (1), 166–169.

(38) Doye, S. Development of the Ti-Catalyzed Intermolecular Hydroamination of Alkynes. *Synlett* **2004**, No. 10, 1653–1672.

(39) Odom, A. L. New C–N and C–C Bond Forming Reactions Catalyzed by Titanium Complexes. *Dalton Trans.* **2005**, No. 2, 225–233.

(40) Bytschkov, I.; Doye, S. Group-IV Metal Complexes as Hydroamination Catalysts. *Eur. J. Org. Chem.* **2003**, *2003* (6), 935–946.

(41) Tillack, A.; Jiao, H.; Garcia Castro, I.; Hartung, C. G.; Beller, M. A General Study of[(H5-Cp′)2Ti(H2-Me3SiC2SiMe3)]-Catalyzed Hydroamination of Terminal Alkynes: Regioselective Formation of Markovnikov and Anti-Markovnikov Products and Mechanistic Explanation (Cp′=C5H5, C5H4Et, C5Me5). *Chem. Eur. J.* **2004**, *10* (10), 2409–2420.

(42) See, X. Y.; Wen, X.; Wheeler, T. A.; Klein, C. K.; Goodpaster, J. D.; Reiner, B. R.; Tonks, I. A. Iterative Supervised Principal Component Analysis Driven Ligand Design for Regioselective Ti-Catalyzed Pyrrole Synthesis. *ACS Catal.* **2020**, *10* (22), 13504–13517.

(43) Chiu, H. C.; Tonks, I. A. Trimethylsilyl-Protected Alkynes as Selective Cross-Coupling Partners in Titanium-Catalyzed [2+2+1] Pyrrole Synthesis. *Angew. Chemie Int. Ed.* **2018**, *57* (21), 6090–6094.

(44) Soderquist, J. A.; Colberg, J. C.; Del Valle, L. The Hydroboration of Silylacetylenes. The “Silyl-Markovnikov” Hydroboration Route to Pure (Z)-1-(2-Borylvinyl)Silanes and .Beta.-Keto Silanes. *J. Am. Chem. Soc.* **1989**, *111* (13), 4873–4878.

(45) Lefeber, C.; Ohff, A.; Tillack, A.; Baumann, W.; Kempe, R.; Burlakov, V. V.; Rosenthal, U. Darstellung Und Regioselektive Reaktionen Des Phosphinfreien Zirconocen-Alkin-Komplexes Cp2Zr(THF)(TBuC2SiMe3). *J. Organomet. Chem.* **1995**, *501* (1–2), 189–194.

(46) Stockis, A.; Hoffmann, R. Metallacyclopentanes and Bisolefin Complexes. *J. Am. Chem. Soc.* **1980**, *102* (9), 2952–2962.

(47) Seeman, J. I. Effect of Conformational Change on Reactivity in Organic Chemistry. Evaluations, Applications, and Extensions of Curtin-Hammett Winstein-Holness Kinetics. *Chem. Rev.* **1983**, *83* (2), 83–134.

(48) Chiu, H.-C.; See, X. Y.; Tonks, I. A. Dative Directing Group Effects in Ti-Catalyzed [2+2+1] Pyrrole Synthesis: Chemo- and Regioselective Alkyne Heterocoupling. *ACS Catal.* **2019**, *9* (1), 216–223.

(49) Wieland, H. Zur Kenntnis Der Tertiären Aromatischen Hydrazine Und Amine. (III). *Berichte der Dtsch. Chem. Gesellschaft* **1907**, *40* (4), 4260–4281.

(50) Wieland, H.; Lecher, H. Die Dissoziation Der Tetraarylhydrazine Und Der Diarylnitrosamine (XII). *Justus Liebig's Ann. der Chemie* **1912**, *392* (2), 156–169.

(51) Wieland, H. Zur Frage Nach Dem Intermediären Auftreten Freier Radikale Bei Chemischen Reaktionen. Der Zerfall Aromatischer Hydrazoverbindungen. *Berichte der Dtsch. Chem. Gesellschaft* **1915**, *48* (1), 1098–1112.

(52) Pugh, S. M.; Trösch, D. J. M.; Wilson, D. J.; Bashall, A.; Cloke, F. G. N.; Gade, L. H.; Hitchcock, P. B.; McPartlin, M.; Nixon, J. F.; Mountford, P. Cycloaddition Reactions of the Titanium Imide [Ti(NBut){MeC(2-C5H4N)(CH2NSiMe3)2}(Py)] with ButCP and MeCN. *Organometallics* **2000**, *19* (16), 3205–3210.

(53) Fochi, G.; Floriani, C.; Bart, J. C. J.; Giunchi, G. Azo-Complexes of Bis(Cyclopentadienyl)-Titanium and -Vanadium; Model Systems for N–N Multiple Bond Activation. *J. Chem. Soc., Dalt. Trans.* **1983**, No. 8, 1515–1521.

(54) Gambarotta, S.; Floriani, C.; Chiesi-Villa, A.; Guastini, C. Nitrogen–Nitrogen Multiple Bond Cleavage and Reduction in Diphenyldiazomethane and Azobenzene by a Titanium (III) Complex. *J. Chem. Soc., Chem. Commun.* **1982**, No. 17, 1015–1017.

(55) Gambarotta, S.; Floriani, C.; Chiesi-Villa, A.; Guastini, C. Cyclopentadienyldichlorotitanium(III): A Free-Radical-like Reagent for Reducing Azo (N:N) Multiple Bonds in Azo and Diazo Compounds. *J. Am. Chem. Soc.* **1983**, *105* (25), 7295–7301.

(56) Hill, J. E.; Profilet, R. D.; Fanwick, P. E.; Rothwell, I. P. Synthesis, Structure, and Reactivity of Aryloxo(Imido)Titanium Complexes. *Angew. Chemie Int. Ed. Engl.* **1990**, *29* (6), 664–665.

(57) Hill, J. E.; Fanwick, P. E.; Rothwell, I. P. Formation of a Terminal Aryl—Imido Compound of Titanium by Ceavage of the N=N Double Bond in Benzo[c]Cinnoline. *Inorg. Chem.* **1991**, *30* (5), 1143–1144.

(58) Heyduk, A. F.; Zarkesh, R. A.; Nguyen, A. I. Designing Catalysts for Nitrene Transfer Using Early Transition Metals and Redox-Active Ligands. *Inorg. Chem.* **2011**, *50* (20), 9849–9863.

(59) Seikel, E.; Oelkers, B.; Sundermeyer, J. Axial Functionalization of Sterically Hindered Titanium Phthalocyanines. *Inorg. Chem.* **2012**, *51* (4), 2709–2717.

(60) Frye, C. W.; Egger, D. T.; Kounalis, E.; Pearce, A. J.; Cheng, Y.; Tonks, I. A. α-Diimine Synthesis via Titanium-Mediated Multicomponent Diimination of Alkynes with C-Nitrosos. *Chem. Sci.* **2022**, *13* (5), 1469–1477.

(61) Pearce, A. J.; Harkins, R. P.; Reiner, B. R.; Wotal, A. C.; Dunscomb, R. J.; Tonks, I. A. Multicomponent Pyrazole Synthesis from Alkynes, Nitriles, and Titanium Imido Complexes via Oxidatively Induced N–N Bond Coupling. *J. Am. Chem. Soc.* **2020**, *142* (9), 4390–4399.

(62) Bour, J. R.; Camasso, N. M.; Sanford, M. S. Oxidation of Ni(II) to Ni(IV) with Aryl Electrophiles Enables Ni-Mediated Aryl–CF3 Coupling. *J. Am. Chem. Soc.* **2015**, *137* (25), 8034–8037.

(63) Kim, J.; Shin, K.; Jin, S.; Kim, D.; Chang, S. Oxidatively Induced Reductive Elimination: Exploring the Scope and Catalyst Systems with Ir, Rh, and Ru Complexes. *J. Am. Chem. Soc.* **2019**, *141* (9), 4137–4146.

(64) Lanci, M. P.; Remy, M. S.; Kaminsky, W.; Mayer, J. M.; Sanford, M. S. Oxidatively Induced Reductive Elimination from (TBu2bpy)Pd(Me)2: Palladium(IV) Intermediates in a One-Electron Oxidation Reaction. *J. Am. Chem. Soc.* **2009**, *131* (43), 15618–15620.

(65) Watson, M. B.; Rath, N. P.; Mirica, L. M. Oxidative C–C Bond Formation Reactivity of Organometallic Ni(II), Ni(III), and Ni(IV) Complexes. *J. Am. Chem. Soc.* **2017**, *139* (1), 35–38.

(66) Carsch, K. M.; DiMucci, I. M.; Iovan, D. A.; Li, A.; Zheng, S.-L.; Titus, C. J.; Lee, S. J.; Irwin, K. D.; Nordlund, D.; Lancaster, K. M.; et al. Synthesis of a Copper-Supported Triplet Nitrene Complex Pertinent to Copper-Catalyzed Amination. *Science* **2019**, *365* (6458), 1138–1143.

(67) Ueda, S.; Nagasawa, H. Facile Synthesis of 1,2,4-Triazoles via a Copper-Catalyzed Tandem Addition−Oxidative Cyclization. *J. Am. Chem. Soc.* **2009**, *131* (42), 15080–15081.

(68) Neumann, J. J.; Suri, M.; Glorius, F. Efficient Synthesis of Pyrazoles: Oxidative C–C/N–N Bond-Formation Cascade. *Angew. Chemie Int. Ed.* **2010**, *49* (42), 7790–7794.

(69) Suri, M.; Jousseaume, T.; Neumann, J. J.; Glorius, F. An Efficient Copper-Catalyzed Formation of Highly Substituted Pyrazoles Using Molecular Oxygen as the Oxidant. *Green Chem.* **2012**, *14* (8), 2193.

(70) Chen, C.; Tang, G.; He, F.; Wang, Z.; Jing, H.; Faessler, R. A Synthesis of 1H-Indazoles via a Cu(OAc)2 -Catalyzed N–N Bond Formation. *Org. Lett.* **2016**, *18* (7), 1690–1693.

(71) Ryan, M. C.; Kim, Y. J.; Gerken, J. B.; Wang, F.; Aristov, M. M.; Martinelli, J. R.; Stahl, S. S. Mechanistic Insights into Copper-Catalyzed Aerobic Oxidative Coupling of N–N Bonds. *Chem. Sci.* **2020**, *11* (4), 1170–1175.

(72) Fritsche, R. F.; Theumer, G.; Kataeva, O.; Knölker, H.-J. Iron-Catalyzed Oxidative C−C and N−N Coupling of Diarylamines and Synthesis of Spiroacridines. *Angew. Chemie Int. Ed.* **2017**, *56* (2), 549–553.

(73) Zhu, Y.; Shi, Y. Facile Cu(I)-Catalyzed Oxidative Coupling of Anilines to Azo Compounds and Hydrazines with Diaziridinone under Mild Conditions. *Org. Lett.* **2013**, *15* (8), 1942–1945.

(74) Kajimoto, T.; Takahashi, H.; Tsuji, J. CuCl-Catalyzed Oxidative Coupling Reaction of Secondary Amines with Molecular Oxygen in Pyridine. *Bull. Chem. Soc. Jpn.* **1982**, *55* (11), 3673–3674.

(75) Govindan, K.; Duraisamy, T.; Jayaram, A.; Senadi, G. C.; Lin, W.-Y. Copper-Catalyzed Oxidative Cyclization of 2-Aminobenzamide Derivatives: Efficient Syntheses of Quinazolinones and Indazolones. *Synthesis (Stuttg).* **2022**, *54* (04), 1115–1124.

(76) Zhang, L.; Xia, J.; Li, Q.; Li, X.; Wang, S. Fast Synthesis of Hydrazine and Azo Derivatives by Oxidation of Rare-Earth-Metal−Nitrogen Bonds. *Organometallics* **2011**, *30* (3), 375–378.

(77) Oberdorf, K.; Hanft, A.; Ramler, J.; Krummenacher, I.; Bickelhaupt, F. M.; Poater, J.; Lichtenberg, C. Bismuth Amides Mediate Facile and Highly Selective Pn–Pn Radical-Coupling Reactions (Pn=N, P, As). *Angew. Chemie Int. Ed.* **2021**, *60* (12), 6441–6445.

(78) Ryan, M. C.; Martinelli, J. R.; Stahl, S. S. Cu-Catalyzed Aerobic Oxidative N–N Coupling of Carbazoles and Diarylamines Including Selective Cross-Coupling. *J. Am. Chem. Soc.* **2018**, *140* (29), 9074–9077.

(79) Yin, D.; Jin, J. Transition-Metal-Free Dehydrogenative N-N Coupling of Secondary Amines with KI/KIO 4. *Eur. J. Org. Chem.* **2019**, *2019* (33), 5646–5649.

(80) Fochi, G.; Floriani, C. The Role of Titanium and Iron Complexes in the Deoxygenation of Aromatic Nitroso-Compounds. *J. Chem. Soc. Dalt. Trans.* **1984**, No. 11, 2577.

(81) Cameron, M.; Gowenlock, B. G. The Coordination Complexes of Nitrosobenzene with Tin(IV) Chloride and Titanium(IV) Chloride. *Polyhedron* **1992**, *11* (21), 2781–2782.

(82) Baumann, M.; Baxendale, I. R.; Ley, S. V.; Nikbin, N. An Overview of the Key Routes to the Best Selling 5-Membered Ring Heterocyclic Pharmaceuticals. *Beilstein J. Org. Chem.* **2011**, *7*, 442–495.

(83) Kathiravan, M. K.; Salake, A. B.; Chothe, A. S.; Dudhe, P. B.; Watode, R. P.; Mukta, M. S.; Gadhwe, S. The Biology and Chemistry of Antifungal Agents: A Review. *Bioorg. Med. Chem.* **2012**, *20* (19), 5678–5698.

(84) Walsh, C. T.; Garneau-Tsodikova, S.; Howard-Jones, A. R. Biological Formation of Pyrroles: Nature's Logic and Enzymatic Machinery. *Nat. Prod. Rep.* **2006**, *23* (4), 517.

(85) Sharma, P. S.; Pietrzyk-Le, A.; D'Souza, F.; Kutner, W. Electrochemically Synthesized Polymers in Molecular Imprinting for Chemical Sensing. *Anal. Bioanal. Chem.* **2012**, *402* (10), 3177–3204.

(86) Loudet, A.; Burgess, K. BODIPY Dyes and Their Derivatives: Syntheses and Spectroscopic Properties. *Chem. Rev.* **2007**, *107* (11), 4891–4932.

(87) Gribble, G. W. Pyrroles and Their Benzo Derivatives: Applications. In *Comprehensive Heterocyclic Chemistry II*; Elsevier, 1996; pp 207–257.

(88) Estévez, V.; Villacampa, M.; Menéndez, J. C. Recent Advances in the Synthesis of Pyrroles by Multicomponent Reactions. *Chem. Soc. Rev.* **2014**, *43* (13), 4633–4657.

(89) Gulevich, A. V.; Dudnik, A. S.; Chernyak, N.; Gevorgyan, V. Transition Metal-Mediated Synthesis of Monocyclic Aromatic Heterocycles. *Chem. Rev.* **2013**, *113* (5), 3084–3213.

(90) Pasko, C. M.; Dissanayake, A. A.; Billow, B. S.; Odom, A. L. One-Pot Synthesis of Pyrroles Using a Titanium-Catalyzed Multicomponent Coupling Procedure. *Tetrahedron* **2016**, *72* (9), 1168–1176.

(91) Miyaura, N.; Suzuki, A. Palladium-Catalyzed Cross-Coupling Reactions of Organoboron Compounds. *Chem. Rev.* **1995**, *95* (7), 2457–2483.

(92) Kotha, S.; Lahiri, K.; Kashinath, D. Recent Applications of the Suzuki–Miyaura Cross-Coupling Reaction in Organic Synthesis. *Tetrahedron* **2002**, *58* (48), 9633–9695.

(93) Liron, F.; Fosse, C.; Pernolet, A.; Roulland, E. Suzuki−Miyaura Cross-Coupling of 1,1-Dichloro-1-Alkenes with 9-Alkyl-9-BBN. *J. Org. Chem.* **2007**, *72* (6), 2220–2223.

(94) Lu, Z.; Fu, G. C. Alkyl-Alkyl Suzuki Cross-Coupling of Unactivated Secondary Alkyl Chlorides. *Angew. Chemie Int. Ed.* **2010**, *49* (37), 6676–6678.

(95) Zultanski, S. L.; Fu, G. C. Nickel-Catalyzed Carbon–Carbon Bond-Forming Reactions of Unactivated Tertiary Alkyl Halides: Suzuki Arylations. *J. Am. Chem. Soc.* **2013**, *135* (2), 624–627.

(96) Nakamura, I.; Yamamoto, Y. Transition-Metal-Catalyzed Reactions in Heterocyclic Synthesis. *Chem. Rev.* **2004**, *104* (5), 2127–2198.

(97) Farina, V.; Krishnamurthy, V.; Scott, W. J. The Stille Reaction. In *Organic Reactions*; John Wiley & Sons, Inc.: Hoboken, NJ, USA, 1997; pp 1–652.

(98) Evano, G.; Blanchard, N.; Toumi, M. Copper-Mediated Coupling Reactions and Their Applications in Natural Products and Designed Biomolecules Synthesis. *Chem. Rev.* **2008**, *108* (8), 3054–3131.

(99) Davis-Gilbert, Z. W.; Wen, X.; Goodpaster, J. D.; Tonks, I. A. Mechanism of Ti-Catalyzed Oxidative Nitrene Transfer in [2 + 2 + 1] Pyrrole Synthesis from Alkynes and Azobenzene. *J. Am. Chem. Soc.* **2018**, *140* (23), 7267–7281.

(100) Hao, H.; Thompson, K. A.; Hudson, Z. M.; Schafer, L. L. Ti-Catalyzed Hydroamination for the Synthesis of Amine- Containing p -Conjugated Materials. *Chem. Eur. J.* **2018**, *24* (21), 5562–5568.

(101) Leung, S.-W.; Singleton, D. A. Reactions of Alkynyldihaloboranes with 1,3-Dienes. 1,4-Alkynylborations and Stepwise Diels−Alder Reactions. *J. Org. Chem.* **1997**, *62* (7), 1955–1960.

(102) Yamaguchi, M.; Hirao, I. A Synthesis of Alkynyl Azacycloalkanes by the Coupling Reaction of Alkynyl Boranes and Lactams. *Tetrahedron Lett.* **1983**, *24* (16), 1719–1722.

(103) Ge, F.; Kehr, G.; Daniliuc, C. G.; Erker, G. Borole Formation by 1,1-Carboboration. *J. Am. Chem. Soc.* **2014**, *136* (1), 68–71.

(104) Kehr, G.; Erker, G. 1,1-Carboboration. *Chem. Commun.* **2012**, *48* (13), 1839–1850.

(105) Ekkert, O.; Tuschewitzki, O.; Daniliuc, C. G.; Kehr, G.; Erker, G. Reaction of Strongly Electrophilic Alkenylboranes with Phosphanylalkynes: Rare Examples of Intermolecular 1,1-Alkenylboration Reactions. *Chem. Commun.* **2013**, *49* (62), 6992.

(106) Kehr, G.; Erker, G. Advanced 1,1-Carboboration Reactions with Pentafluorophenylboranes. *Chem. Sci.* **2016**, *7* (1), 56–65.

(107) Singleton, D. A.; Leung, S. W. An Unprecedented Electronic Preference for the “Meta” Product in Diels-Alder Reactions of Ethynyldialkylboranes. [(Trimethylsilyl)Ethynyl]-9-BBN as a Reactive and Versatile Dienophile. *J. Org. Chem.* **1992**, *57* (18), 4796–4797.

(108) Silva, M. A.; Pellegrinet, S. C.; Goodman, J. M. A DFT Study on the Regioselectivity of the Reaction of Dichloropropynylborane with Isoprene. *J. Org. Chem.* **2003**, *68* (10), 4059–4066.

(109) Cauletti, C.; Furlani, C.; Granozzi, G.; Sebald, A.; Wrackmeyer, B. The .Sigma.-.Pi. Interactions in Alkynyltin(IV) Compounds Studies by UV Photoelectron Spectroscopy and Pseudopotential Ab Initio Calculations. *Organometallics* **1985**, *4* (2), 290–295.

(110) Han, H.; Schafer, L. L. Ti Catalyzed Hydroamination: A Direct Functionalization of Cu Acetylide https://doi.org/10.26434/chemrxiv.11455269.v1.

(111) Miyaura, N.; Ishiyama, T.; Sasaki, H.; Ishikawa, M.; Sato, M.; Suzuki, A. Palladium-Catalyzed Inter- and Intramolecular Cross-Coupling Reactions of B-Alkyl-9-Borabicyclo[3.3.1]Nonane Derivatives with 1-Halo-1-Alkenes or Haloarenes. Syntheses of Functionalized Alkenes, Arenes, and Cycloalkenes via a Hydroboration-Coupling Sequen. *J. Am. Chem. Soc.* **1989**, *111* (1), 314–321.

(112) Ishiyama, T.; Abe, S.; Miyaura, N.; Suzuki, A. Palladium-Catalyzed Alkyl-Alkyl Cross-Coupling Reaction of 9-Alkyl-9-BBN Derivatives with Iodoalkanes Possessing β-Hydrogens. *Chem. Lett.* **1992**, *21* (4), 691–694.

(113) Fürstner, A.; Leitner, A. General and User-Friendly Method for Suzuki Reactions with Aryl Chlorides. *Synlett* **2001**, *2001* (02), 0290–0292.

(114) Walker, S. D.; Barder, T. E.; Martinelli, J. R.; Buchwald, S. L. A Rationally Designed Universal Catalyst for Suzuki–Miyaura Coupling Processes. *Angew. Chemie Int. Ed.* **2004**, *43* (14), 1871–1876.

(115) Zultanski, S. L.; Fu, G. C. Catalytic Asymmetric γ-Alkylation of Carbonyl Compounds via Stereoconvergent Suzuki Cross-Couplings. *J. Am. Chem. Soc.* **2011**, *133* (39), 15362–15364.

(116) To the best of our knowledge, there are only three reports on sp^2-sp^2 Suzuki cross coupling of aryl-9-BBN nucleophiles: (a) Ishikura, M.; Oda, I.; Terashima, M. A Simple and Regioselective Preparation of 2- or 3-Substituted Quinoline Derivatives via Dialkylquinolylboranes. *Heterocycles* **1985**, *23*, 2375. (b) Rocca, P.; Marsais, F.; Godard A.; Queguiner, G. Connection between Metalation and Cross-Coupling Strategies. A New Convergent Route to Azacarbazoles*. Tetrahedron* **1993**, *49*, 49–64. (c) Lee, M.; Rangisetty, J. B.; Pullagurla, M. R.; Dukat, M.; Setola, V.; Roth, B. L.; Glennon, R. A. 1-(1-Naphthyl)piperazine as a Novel Template for 5-HT6 Serotonin Receptor Ligands, *Bioorg. Med. Chem. Lett.* **2005**, *15*, 1707–1711.

(117) Lennox, A. J. J.; Lloyd-Jones, G. C. Selection of Boron Reagents for Suzuki–Miyaura Coupling. *Chem. Soc. Rev.* **2014**, *43* (1), 412–443.

(118) Netherton, M. R.; Dai, C.; Neuschütz, K.; Fu, G. C. Room-Temperature Alkyl−Alkyl Suzuki Cross-Coupling of Alkyl Bromides That Possess β Hydrogens. *J. Am. Chem. Soc.* **2001**, *123* (41), 10099–10100.

(119) Dallaire, C.; Brook, M. A. The β-Effect with Vinyl Cations: Kinetic Study of the Protiodemetalation of Silyl-, Germyl-, and Stannylalkynes. *Organometallics* **1993**, *12* (6), 2332–2338.

(120) Mizoguchi, H.; Micalizio, G. C. Synthesis of Highly Functionalized Decalins via Metallacycle-Mediated Cross-Coupling. *J. Am. Chem. Soc.* **2015**, *137* (20), 6624–6628.

(121) Micalizio, G. C.; Mizoguchi, H. The Development of Alkoxide-Directed Metallacycle-Mediated Annulative Cross-Coupling Chemistry. *Isr. J. Chem.* **2017**, *57* (3–4), 228–238.

(122) Whitesides, G. M.; Ehmann, W. J. Mechanism of Formation of 1,2,3,4-Tetramethylnaphthalene from 2-Butyne and Triphenyltris(Tetrahydrofuran) Chromium(III). *J. Am. Chem. Soc.* **1970**, *92* (19), 5625–5640.

(123) Brown, H. C.; Sinclair, J. A. Organoboranes. XVIII. Reaction of Lithium Alkynes with Methyl Dialkylborinates: The Synthesis of B-1-Alkynyldialkylboranes. *J. Organomet. Chem.* **1977**, *131* (2), 163–169.

(124) Fang, G. Y.; Wallner, O. A.; Blasio, N. Di; Ginesta, X.; Harvey, J. N.; Aggarwal, V. K. Asymmetric Sulfur Ylide Reactions with Boranes: Scope and Limitations, Mechanism and Understanding. *J. Am. Chem. Soc.* **2007**, *129* (47), 14632–14639.

(125) Evans, J. C.; Goralski, C. T.; Hasha, D. L. B-[2-(Trimethylsilyl)Ethynyl]-9-Borabicyclo[3.3.1]Nonane. A New Organoboron Reagent for the Preparation of Propargylic Alcohols. *J. Org. Chem.* **1992**, *57* (10), 2941–2943.

(126) Shi, W.; Luo, Y.; Luo, X.; Chao, L.; Zhang, H.; Wang, J.; Lei, A. Investigation of an Efficient Palladium-Catalyzed C(Sp)−C(Sp) Cross-Coupling Reaction Using Phosphine−Olefin Ligand: Application and Mechanistic Aspects. *J. Am. Chem. Soc.* **2008**, *130* (44), 14713–14720.

(127) See, X. Y.; Beaumier, E. P.; Davis-Gilbert, Z. W.; Dunn, P. L.; Larsen, J. A.; Pearce, A. J.; Wheeler, T. A.; Tonks, I. A. Generation of Ti II Alkyne Trimerization Catalysts in the Absence of Strong Metal Reductants. *Organometallics* **2017**, *36* (7), 1383–1390.

(128) Beach, C. A.; Joseph, K. E.; Dauenhauer, P. J.; Spanjers, C. S.; Jones, A. J.; Mountziaris, T. J. Complete Carbon Analysis of Sulfur-Containing Mixtures Using Postcolumn Reaction and Flame Ionization Detection. *AIChE J.* **2017**, *63* (12), 5438–5444.

(129) Spanjers, C. S.; Beach, C. A.; Jones, A. J.; Dauenhauer, P. J. Increasing Flame Ionization Detector (FID) Sensitivity Using Post-Column Oxidation–Methanation. *Anal. Methods* **2017**, *9* (12), 1928–1934.

(130) Harrison, P. G.; Ulrich, S. E.; Zuckerman, J. J. Tin-119 Chemical Shifts by the Double Resonance of Organotin Compounds. *J. Am. Chem. Soc.* **1971**, *93* (21), 5398–5402.

(131) Forster, F.; Rendón López, V. M.; Oestreich, M. Catalytic Dehydrogenative Stannylation of C(Sp)–H Bonds Involving Cooperative Sn–H Bond Activation of Hydrostannanes. *J. Am. Chem. Soc.* **2018**, *140* (4), 1259–1262.

(132) Pennington, D. A.; Horton, P. N.; Hursthouse, M. B.; Bochmann, M.; Lancaster, S. J. Synthesis and Catalytic Activity of Dinuclear Imido Titanium Complexes: The Molecular Structure of [Ti(NPh)Cl(μ-Cl)(THF)2]2. *Polyhedron* **2005**, *24* (1), 151–156.

(133) Lee, C.; Zhou, J.; Ozerov, O. V. Catalytic Dehydrogenative Borylation of Terminal Alkynes by a SiNN Pincer Complex of Iridium. *J. Am. Chem. Soc.* **2013**, *135* (9), 3560–3566.

(134) Lee, C.-I.; DeMott, J. C.; Pell, C. J.; Christopher, A.; Zhou, J.; Bhuvanesh, N.; Ozerov, O. V. Ligand Survey Results in Identification of PNP Pincer Complexes of Iridium as Long-Lived and Chemoselective Catalysts for Dehydrogenative Borylation of Terminal Alkynes. *Chem. Sci.* **2015**, *6* (11), 6572–6582.

(135) Ho, H. E.; Asao, N.; Yamamoto, Y.; Jin, T. Carboxylic Acid-Catalyzed Highly Efficient and Selective Hydroboration of Alkynes with Pinacolborane. *Org. Lett.* **2014**, *16* (17), 4670–4673.

(136) Unseld, D.; Krivykh, V. V.; Heinze, K.; Wild, F.; Artus, G.; Schmalle, H.; Berke, H. Versatile Routes to Mono- and Bis(Alkynyl) Manganese(II) and Manganese(III) Complexes via Manganocenes. *Organometallics* **1999**, *18* (8), 1525–1541.

(137) Li, X.; Chen, M.; Xie, X.; Sun, N.; Li, S.; Liu, Y. Synthesis of Multiple-Substituted Pyrroles via Gold(I)-Catalyzed Hydroamination/Cyclization Cascade. *Org. Lett.* **2015**, *17* (12), 2984–2987.

(138) Petrakis, L. Spectral Line Shapes: Gaussian and Lorentzian Functions in Magnetic Resonance. *J. Chem. Educ.* **1967**, *44* (8), 432.

(139) Wang, G.-Z.; Shang, R.; Cheng, W.-M.; Fu, Y. Decarboxylative 1,4-Addition of α-Oxocarboxylic Acids with Michael Acceptors Enabled by Photoredox Catalysis. *Org. Lett.* **2015**, *17* (19), 4830–4833.

(140) Danks, T. N.; Thomas, S. E. Nucleophilic Addition to Tricarbonyliron(0) Complexes of 1-Aza-1,3-Dienes and the Production of Pyrroles. *J. Chem. Soc. Perkin Trans. 1* **1990**, No. 3, 761.

(141) Demir, A. S.; Akhmedov, I. M.; Sesenoglu, Ö. Synthesis of 1,2,3,5-Tetrasubstituted Pyrrole Derivatives from 2-(2-Bromoallyl)-1,3-Dicarbonyl Compounds. *Tetrahedron* **2002**, *58* (49), 9793–9799.

(142) Beaumier, E. P.; Pearce, A. J.; See, X. Y.; Tonks, I. A. Modern Applications of Low-Valent Early Transition Metals in Synthesis and Catalysis. *Nat. Rev. Chem.* **2019**, *3* (1), 15–34.

(143) Okamoto, S. Synthetic Reactions Using Low-Valent Titanium Reagents Derived from Ti(OR) 4 or CpTiX 3 (X = O- i -Pr or Cl) in the Presence of Me 3 SiCl and Mg. *Chem. Rec.* **2016**, *16* (2), 857–872.

(144) See, X. Y.; Beaumier, E. P.; Davis-Gilbert, Z. W.; Dunn, P. L.; Larsen, J. A.; Pearce, A. J.; Wheeler, T. A.; Tonks, I. A. Generation of Ti II Alkyne Trimerization Catalysts in the Absence of Strong Metal Reductants. *Organometallics* **2017**, *36* (7), 1383–1390.

(145) Yamamoto, K.; Nagae, H.; Tsurugi, H.; Mashima, K. Mechanistic Understanding of Alkyne Cyclotrimerization on Mononuclear and Dinuclear Scaffolds: [4 + 2] Cycloaddition of the Third Alkyne onto Metallacyclopentadienes and Dimetallacyclopentadienes. *Dalton Trans.* **2016**, *45* (43), 17072–17081.

(146) Tarselli, M. A.; Micalizio, G. C. Aliphatic Imines in Titanium-Mediated Reductive Cross-Coupling: Unique Reactivity of Ti(O- i -Pr) 4 / n -BuLi. *Org. Lett.* **2009**, *11* (20), 4596–4599.

(147) Kier, M. J.; Leon, R. M.; O'Rourke, N. F.; Rheingold, A. L.; Micalizio, G. C. Synthesis of Highly Oxygenated Carbocycles by Stereoselective Coupling of Alkynes to 1,3- and 1,4-Dicarbonyl Systems. *J. Am. Chem. Soc.* **2017**, *139* (36), 12374–12377.

(148) Roskamp, E. J.; Pedersen, S. F. The First Practical Niobium(III) Reagent in Organic Synthesis. A Convenient Route to 2-Amino Alcohols via the Coupling of Imines with Aldehydes or Ketones Promoted by NbCl3(DME). *J. Am. Chem. Soc.* **1987**, *109* (21), 6551–6553.

(149) Tsurugi, H.; Mashima, K. A New Protocol to Generate Catalytically Active Species of Group 4-6 Metals by Organosilicon-Based Salt-Free Reductants. *Chem. Eur. J.* **2019**, *25* (4), 913–919.

(150) Kubiak, R.; Prochnow, I.; Doye, S. Titanium-Catalyzed Hydroaminoalkylation of Alkenes by C–H Bond Activation at Sp 3 Centers in the α-Position to a Nitrogen Atom. *Angew. Chemie Int. Ed.* **2009**, *48* (6), 1153–1156.

(151) Eisenberger, P.; Ayinla, R. O.; Lauzon, J. M. P.; Schafer, L. L. Tantalum-Amidate Complexes for the Hydroaminoalkylation of Secondary Amines: Enhanced Substrate Scope and Enantioselective Chiral Amine Synthesis. *Angew. Chemie* **2009**, *121* (44), 8511–8515.

(152) Manßen, M.; Lauterbach, N.; Dörfler, J.; Schmidtmann, M.; Saak, W.; Doye, S.; Beckhaus, R. Efficient Access to Titanaaziridines by C□H Activation of N -Methylanilines at Ambient Temperature. *Angew. Chemie Int. Ed.* **2015**, *54* (14), 4383–4387.

(153) Durfee, L. D.; Hill, J. E.; Fanwick, P. E.; Rothwell, I. P. Formation and Characterization of H2-Imine and H2-Azobenzene Derivatives of Titanium Containing Ancillary Aryloxide Ligation. *Organometallics* **1990**, *9* (1), 75–80.

(154) Beaumier, E. P.; Ott, A. A.; Wen, X.; Davis-Gilbert, Z. W.; Wheeler, T. A.; Topczewski, J. J.; Goodpaster, J. D.; Tonks, I. A. Ti-Catalyzed Ring-Opening Oxidative Amination of Methylenecyclopropanes with Diazenes. *Chem. Sci.* **2020**, *11* (27), 7204–7209.

(155) Heins, S. P.; Wolczanski, P. T.; Cundari, T. R.; MacMillan, S. N. Redox Non-Innocence Permits Catalytic Nitrene Carbonylation by (Dadi)Ti=NAd (Ad = Adamantyl). *Chem. Sci.* **2017**, *8* (5), 3410–3418.

(156) Yamamoto, K.; Nagae, H.; Tsurugi, H.; Mashima, K. Mechanistic Understanding of Alkyne Cyclotrimerization on Mononuclear and Dinuclear Scaffolds: [4 + 2] Cycloaddition of the Third Alkyne onto Metallacyclopentadienes and Dimetallacyclopentadienes. *Dalton Trans.* **2016**, *45* (43), 17072–17081.

(157) Ozerov, O. V.; Ladipo, F. T.; Patrick, B. O. Highly Regioselective Alkyne Cyclotrimerization Catalyzed by Titanium Complexes Supported by Proximally Bridged P-Tert-Butylcalix[4]Arene Ligands. *J. Am. Chem. Soc.* **1999**, *121* (34), 7941–7942.

(158) Ladipo, F. T. SYNTHESIS AND REACTIVITY OF WELL-CHARACTERIZED LOW-VALENT TITANIUM SPECIES. *Comments Inorg. Chem.* **2006**, *27* (3–4), 73–102.

(159) Although alkyne cyclotrimerization commonly undergoes redox mechanisms, it has also been reported to occur through non-redox pathways, for example: (a) Solari, E.; Floriani, C.; Chiesi-Villa, A.; Guastini, C. Titanium Tetrachloride Binding and Making Arenes from Acetylenes: The Synthesis and X-Ray Crystal Structure of a Titanium(IV)–Hexamethylbenzene Complex. *J. Chem. Soc., Chem. Commun.* **1989**, (22), 1747–1749; (b) Musso, F.; Solari, E.; Floriani, C.; Schenk, K. Hydrocarbon Activation with Metal Halides: Zirconium Tetrachloride Catalyzing the Jacobsen Reaction Assisting the Trimerization of Alkynes *via* the Formation of η^6-Arene−Zirconium(IV) Complexes. *Organometallics* **1997**, *16* (22), 4889–4895.

(160) Hickey, A. K.; Crestani, M. G.; Fout, A. R.; Gao, X.; Chen, C.-H.; Mindiola, D. J. Dehydrogenation of Hydrocarbons with Metal-Carbon Multiple Bonds and Trapping of a Titanium(II) Intermediate. *Dalton Trans.* **2014**, *43* (26), 9834–9837.

(161) Aguilar-Calderón, J. R.; Metta-Magaña, A. J.; Noll, B.; Fortier, S. C(Sp3)−H Oxidative Addition and Transfer Hydrogenation Chemistry of a Titanium(II) Synthon: Mimicry of Late-Metal Type Reactivity. *Angew. Chemie Int. Ed.* **2016**, *55* (45), 14101–14105.

(162) Rosenthal, U.; Burlakov, V. V; Bach, M. A.; Beweries, T. Five-Membered Metallacycles of Titanium and Zirconium ? Attractive Compounds for Organometallic Chemistry and Catalysis. *Chem. Soc. Rev.* **2007**, *36* (5), 719.

(163) Suzuki, N.; Aihara, N.; Takahara, H.; Watanabe, T.; Iwasaki, M.; Saburi, M.; Hashizume, D.; Chihara, T. Synthesis and Structure of 1-Zirconacyclopent-3-Yne Complexes without Substituents Adjacent to the Triple Bond. *J. Am. Chem. Soc.* **2004**, *126* (1), 60–61.

(164) Suzuki, N.; Nishiura, M.; Wakatsuki, Y. Isolation and Structural Characterization of 1-Zirconacyclopent-3-Yne, Five-Membered Cyclic Alkynes. *Science* **2002**, *295* (5555), 660–663.

(165) Rosenthal, U.; Burlakov, V. V.; Arndt, P.; Baumann, W.; Spannenberg, A. Five-Membered Titana- and Zirconacyclocumulenes: Stable 1-Metallacyclopenta-2,3,4-Trienes †. *Organometallics* **2005**, *24* (4), 456–471.

(166) Beaumier, E. P.; McGreal, M. E.; Pancoast, A. R.; Wilson, R. H.; Moore, J. T.; Graziano, B. J.; Goodpaster, J. D.; Tonks, I. A. Carbodiimide Synthesis via Ti-Catalyzed Nitrene Transfer from Diazenes to Isocyanides. *ACS Catal.* **2019**, *9* (12), 11753–11762.

(167) Gray, S. D.; Thorman, J. L.; Adamian, V. A.; Kadish, K. M.; Woo, L. K. Synthesis, Electrochemistry, and Imido Transfer Reactions of (TTP)Ti(H2-PhN=NPh). *Inorg. Chem.* **1998**, *37* (1), 1–4.

(168) Bielefeld, J.; Doye, S. Dimethylamine as a Substrate in Hydroaminoalkylation Reactions. *Angew. Chemie Int. Ed.* **2017**, *56* (47), 15155–15158.

(169) We considered 3-hexyne as a potential protonolysis partner; however, as coordination of 3-hexyne leads to pyrrole formation, this pathway seems less likely than HNMe2 protonolysis.

(170) Zurita, D. A.; Flores-Alamo, M.; García, J. J. Catalytic Transfer Hydrogenation of Azobenzene by Low-Valent Nickel Complexes: A Route to 1,2-Disubstituted Benzimidazoles and 2,4,5-Trisubstituted Imidazolines. *Dalton Trans.* **2016**, *45* (25), 10389–10401.

(171) Brieger, G.; Nestrick, T. J. Catalytic Transfer Hydrogenation. *Chem. Rev.* **1974**, *74* (5), 567–580.

(172) Copéret, C.; Comas-Vives, A.; Conley, M. P.; Estes, D. P.; Fedorov, A.; Mougel, V.; Nagae, H.; Núnez-Zarur, F.; Zhizhko, P. A. Surface Organometallic and Coordination Chemistry toward Single-Site Heterogeneous Catalysts: Strategies, Methods, Structures, and Activities. *Chem. Rev.* **2016**, *116* (2), 323–421.

(173) Aldrich, K. E.; Odom, A. L. A Silica-Supported Titanium Catalyst for Heterogeneous Hydroamination and Multicomponent Coupling Reactions. *Dalton Trans.* **2019**, *48* (30), 11352–11360.

(174) Kim, S. J.; Xu, K.; Parala, H.; Beranek, R.; Bledowski, M.; Sliozberg, K.; Becker, H. W.; Rogalla, D.; Barreca, D.; Maccato, C.; et al. Intrinsic Nitrogen-Doped CVD-Grown TiO2 Thin Films from All-N-Coordinated Ti Precursors for Photoelectrochemical Applications. *Chem. Vap. Depos.* **2013**, *19* (1–3), 45–52.

(175) Jin, N.; Yang, Y.; Luo, X.; Xia, Z. Development of CVD Ti-Containing Films. *Prog. Mater. Sci.* **2013**, *58* (8), 1490–1533.

(176) Bradley, D. C.; Thomas, I. M. 765. Metallo-Organic Compounds Containing Metal–Nitrogen Bonds. Part I. Some Dialkylamino-Derivatives of Titanium and Zirconium. *J. Chem. Soc.* **1960**, *10* (9), 3857–3861.

(177) Benzing, E.; Kornicker, W. Dialkylamido-Titan(IV)-Chloride Und -Alkoholate. *Chem. Ber.* **1961**, *94* (8), 2263–2267.

(178) Brown, D. W.; Floyd, A. J.; Sainsbury, M. *Organic Spectroscopy*; John Wiley & Sons Inc, 1988.

(179) Lyaskovskyy, V.; de Bruin, B. Redox Non-Innocent Ligands: Versatile New Tools to Control Catalytic Reactions. *ACS Catal.* **2012**, *2* (2), 270–279.

(180) Beaumier, E. P.; Pearce, A. J.; See, X. Y.; Tonks, I. A. Modern Applications of Low-Valent Early Transition Metals in Synthesis and Catalysis. *Nat. Rev. Chem.* **2019**, *3* (1), 15–34.

(181) Ketterer, N. A.; Fan, H.; Blackmore, K. J.; Yang, X.; Ziller, J. W.; Baik, M.-H.; Heyduk, A. F. Π•−π• Bonding Interactions Generated by Halogen Oxidation of Zirconium(IV) Redox-Active Ligand Complexes. *J. Am. Chem. Soc.* **2008**, *130* (13), 4364–4374.

(182) Munhá, R. F.; Zarkesh, R. A.; Heyduk, A. F. Group Transfer Reactions of D0 Transition Metal Complexes: Redox-Active Ligands Provide a Mechanism for Expanded Reactivity. *Dalton Trans.* **2013**, *42* (11), 3751.

(183) Hananouchi, S.; Krull, B. T.; Ziller, J. W.; Furche, F.; Heyduk, A. F. Metal Effects on Ligand Non-Innocence in Group 5 Complexes of the Redox-Active [ONO] Pincer Ligand. *Dalton Trans.* **2014**, *43* (48), 17991–18000.

(184) Heins, S. P.; Zhang, B.; MacMillan, S. N.; Cundari, T. R.; Wolczanski, P. T. Oxidative Additions to Ti(IV) in [(Dadi)4–]TiIV(THF) Involve Carbon–Carbon Bond Formation and Redox-Noninnocent Behavior. *Organometallics* **2019**, *38* (7), 1502–1515.

(185) Tsurugi, H.; Saito, T.; Tanahashi, H.; Arnold, J.; Mashima, K. Carbon Radical Generation by d 0 Tantalum Complexes with α-Diimine Ligands through Ligand-Centered Redox Processes. *J. Am. Chem. Soc.* **2011**, *133* (46), 18673–18683.

(186) Diccianni, J. B.; Hu, C.; Diao, T. N−N Bond Forming Reductive Elimination via a Mixed-Valent Nickel(II)–Nickel(III) Intermediate. *Angew. Chemie Int. Ed.* **2016**, *55* (26), 7534–7538.

(187) Baxter, R. D.; Sale, D.; Engle, K. M.; Yu, J.-Q.; Blackmond, D. G. Mechanistic Rationalization of Unusual Kinetics in Pd-Catalyzed C–H Olefination. *J. Am. Chem. Soc.* **2012**, *134* (10), 4600–4606.

(188) Nielsen, C. D.-T.; Burés, J. Visual Kinetic Analysis. *Chem. Sci.* **2019**, *10* (2), 348–353.

(189) Burés, J. Variable Time Normalization Analysis: General Graphical Elucidation of Reaction Orders from Concentration Profiles. *Angew. Chemie Int. Ed.* **2016**, *55* (52), 16084–16087.

(190) Boller, T. M.; Murphy, J. M.; Hapke, M.; Ishiyama, T.; Miyaura, N.; Hartwig, J. F. Mechanism of the Mild Functionalization of Arenes by Diboron Reagents Catalyzed by Iridium Complexes. Intermediacy and Chemistry of Bipyridine-Ligated Iridium Trisboryl Complexes. *J. Am. Chem. Soc.* **2005**, *127* (41), 14263–14278.

(191) Evans, R.; Deng, Z.; Rogerson, A. K.; McLachlan, A. S.; Richards, J. J.; Nilsson, M.; Morris, G. A. Quantitative Interpretation of Diffusion-Ordered NMR Spectra: Can We Rationalize Small Molecule Diffusion Coefficients? *Angew. Chemie* **2013**, *125* (11), 3281–3284.

(192) Evans, R.; Dal Poggetto, G.; Nilsson, M.; Morris, G. A. Improving the Interpretation of Small Molecule Diffusion Coefficients. *Anal. Chem.* **2018**, *90* (6), 3987–3994.

(193) Studer, A. The Persistent Radical Effect in Organic Synthesis. *Chem. Eur. J.* **2001**, *7* (6), 1159–1164.

(194) Belli, R. G.; Tafuri, V. C.; Joannou, M. V.; Roberts, C. C. D0 Metal-Catalyzed Alkyl–Alkyl Cross-Coupling Enabled by a Redox-Active Ligand. *ACS Catal.* **2022**, *12* (5), 3094–3099.

(195) Warren, J. J.; Tronic, T. A.; Mayer, J. M. Thermochemistry of Proton-Coupled Electron Transfer Reagents and Its Implications. *Chem. Rev.* **2010**, *110* (12), 6961–7001.

(196) Bart, S. C.; Lobkovsky, E.; Chirik, P. J. Preparation and Molecular and Electronic Structures of Iron(0) Dinitrogen and Silane Complexes and Their Application to Catalytic Hydrogenation and Hydrosilation. *J. Am. Chem. Soc.* **2004**, *126* (42), 13794–13807.

(197) Bouwkamp, M. W.; Bart, S. C.; HawrelakPresent address: Department, E. J.; Trovitch, R. J.; Lobkovsky, E.; Chirik, P. J. Square Planar Bis(Imino)Pyridine Iron Halide and Alkyl Complexes. *Chem. Commun.* **2005**, No. 27, 3406.

(198) Beck, W.; Suenkel, K. Metal Complexes of Weakly Coordinating Anions. Precursors of Strong Cationic Organometallic Lewis Acids. *Chem. Rev.* **1988**, *88* (7), 1405–1421.

(199) Murphy, E. F.; Murugavel, R.; Roesky, H. W. Organometallic Fluorides: Compounds Containing Carbon−Metal−Fluorine Fragments of d-Block Metals. *Chem. Rev.* **1997**, *97* (8), 3425–3468.

(200) Honeychuck, R. V.; Hersh, W. H. Coordination of “Noncoordinating” Anions: Synthesis, Characterization, and x-Ray Crystal Structures of Fluorine-Bridged Hexafluoroantimonate(1-), Tetrafluoroborate(1-), and Hexafluorophosphate(1-) Adducts of [R3P(CO)3(NO)W]+. An Unconventional Order of An. *Inorg. Chem.* **1989**, *28* (14), 2869–2886.

(201) Alvarez, M. A.; García, G.; García, M. E.; Riera, V.; Ruiz, M. A.; Lanfranchi, M.; Tiripicchio, A. Chemistry of Highly Electrophilic Binuclear Cations. 1. Oxidation Reactions of [M2(H5-C5H5)2(CO)4(μ-Ph2PCH2PPh2)] (M = Mo, W) with [FeCp2]X (X = BF4, PF6). *Organometallics* **1999**, *18* (22), 4509–4517.

(202) Tsurugi, H.; Mashima, K. Renaissance of Homogeneous Cerium Catalysts with Unique Ce(IV/III) Couple: Redox-Mediated Organic Transformations Involving Homolysis of Ce(IV)–Ligand Covalent Bonds. *J. Am. Chem. Soc.* **2021**, *143* (21), 7879–7890.

(203) Yang, Q.; Wang, Y.-H.; Qiao, Y.; Gau, M.; Carroll, P. J.; Walsh, P. J.; Schelter, E. J. Photocatalytic C–H Activation and the Subtle Role of Chlorine Radical Complexation in Reactivity. *Science* **2021**, *372* (6544), 847–852.

(204) Yin, H.; Jin, Y.; Hertzog, J. E.; Mullane, K. C.; Carroll, P. J.; Manor, B. C.; Anna, J. M.; Schelter, E. J. The Hexachlorocerate(III) Anion: A Potent, Benchtop Stable, and Readily Available Ultraviolet A Photosensitizer for Aryl Chlorides. *J. Am. Chem. Soc.* **2016**, *138* (50), 16266–16273.

(205) Pavlishchuk, V. V; Addison, A. W. Conversion Constants for Redox Potentials Measured versus Different Reference Electrodes in Acetonitrile Solutions at 25°C. *Inorganica Chim. Acta* **2000**, *298* (1), 97–102.

(206) Prier, C. K.; Rankic, D. A.; MacMillan, D. W. C. Visible Light Photoredox Catalysis with Transition Metal Complexes: Applications in Organic Synthesis. *Chem. Rev.* **2013**, *113* (7), 5322–5363.

(207) Roth, H.; Romero, N.; Nicewicz, D. Experimental and Calculated Electrochemical Potentials of Common Organic Molecules for Applications to Single-Electron Redox Chemistry. *Synlett* **2015**, *27* (05), 714–723.

(208) Lisowska, A.; Biallozor, S. Investigations on Electroreduction of TiCl4 in Dimethylsulfoxide. *Electrochim. Acta* **1982**, *27* (1), 105–110.

(209) Adams, J. J.; Arulsamy, N.; Sullivan, B. P.; Roddick, D. M.; Neuberger, A.; Schmehl, R. H. Homoleptic Tris-Diphosphine Re(I) and Re(II) Complexes and Re(II) Photophysics and Photochemistry. *Inorg. Chem.* **2015**, *54* (23), 11136–11149.

(210) Le Bras, J.; Jiao, H.; Meyer, W. E.; Hampel, F.; Gladysz, J. . Synthesis, Crystal Structure, and Reactions of the 17-Valence-Electron Rhenium Methyl Complex [(H5-C5Me5)Re(NO)(P(4-C6H4CH3)3)(CH3)]+ B(3,5-C6H3(CF3)2)4−: Experimental and Computational Bonding Comparisons with 18-Electron Methyl and Methylidene Complexes. *J. Organomet. Chem.* **2000**, *616* (1–2), 54–66.

(211) Löble, M. W.; Keith, J. M.; Altman, A. B.; Stieber, S. C. E.; Batista, E. R.; Boland, K. S.; Conradson, S. D.; Clark, D. L.; Lezama Pacheco, J.; Kozimor, S. A.; et al. Covalency in Lanthanides. An X-Ray Absorption Spectroscopy and Density Functional Theory Study of LnCl6x – (x = 3, 2). *J. Am. Chem. Soc.* **2015**, *137* (7), 2506–2523.

(212) Connelly, N. G.; Geiger, W. E. Chemical Redox Agents for Organometallic Chemistry. *Chem. Rev.* **1996**, *96* (2), 877–910.

(213) Taylor, R. D.; MacCoss, M.; Lawson, A. D. G. Rings in Drugs. *J. Med. Chem.* **2014**, *57* (14), 5845–5859.

(214) Costa, R. F.; Turones, L. C.; Cavalcante, K. V. N.; Rosa Júnior, I. A.; Xavier, C. H.; Rosseto, L. P.; Napolitano, H. B.; Castro, P. F. da S.; Neto, M. L. F.; Galvão, G. M.; et al. Heterocyclic Compounds: Pharmacology of Pyrazole Analogs From Rational Structural Considerations. *Front. Pharmacol.* **2021**, *12*.

(215) Kotagiri, V. K.; Suthrapu, S.; Mukunda Reddy, J.; Prasad Rao, C.; Bollugoddu, V.; Bhattacharya, A.; Bandichhor, R. An Improved Synthesis of Rimonabant: Anti-Obesity Drug. *Org. Process Res. Dev.* **2007**, *11* (5), 910–912.

(216) Tian, Q.; Cheng, Z.; Yajima, H. M.; Savage, S. J.; Green, K. L.; Humphries, T.; Reynolds, M. E.; Babu, S.; Gosselin, F.; Askin, D.; et al. A Practical Synthesis of a PI3K Inhibitor under Noncryogenic Conditions via Functionalization of a Lithium Triarylmagnesiate Intermediate. *Org. Process Res. Dev.* **2013**, *17* (1), 97–107.

(217) Schmidt, A.; Beutler, A.; Snovydovych, B. Recent Advances in the Chemistry of Indazoles. *Eur. J. Org. Chem.* **2008**, *2008* (24), 4073–4095.

(218) Mills, A. D.; Nazer, M. Z.; Haddadin, M. J.; Kurth, M. J. N,N-Bond-Forming Heterocyclization: Synthesis of 3-Alkoxy-2H-Indazoles. *J. Org. Chem.* **2006**, *71* (7), 2687–2689.

(219) Zhu, J. S.; Haddadin, M. J.; Kurth, M. J. Davis–Beirut Reaction: Diverse Chemistries of Highly Reactive Nitroso Intermediates in Heterocycle Synthesis. *Acc. Chem. Res.* **2019**, *52* (8), 2256–2265.

(220) Saikia, A.; Barthakur, M. G.; Borthakur, M.; Saikia, C. J.; Bora, U.; Boruah, R. C. Conjugate Base Catalysed One-Pot Synthesis of Pyrazoles from β-Formyl Enamides. *Tetrahedron Lett.* **2006**, *47* (1), 43–46.

(221) Counceller, C. M.; Eichman, C. C.; Wray, B. C.; Stambuli, J. P. A Practical, Metal-Free Synthesis of 1H-Indazoles. *Org. Lett.* **2008**, *10* (5), 1021–1023.

(222) Wray, B. C.; Stambuli, J. P. Synthesis of N -Arylindazoles and Benzimidazoles from a Common Intermediate. *Org. Lett.* **2010**, *12* (20), 4576–4579.

(223) Schirmann, J.-P.; Bourdauducq, P. Hydrazine. In *Ullmann's Encyclopedia of Industrial Chemistry*; Wiley-VCH Verlag GmbH & Co. KGaA: Weinheim, Germany, 2001.

(224) Rosen, B. R.; Werner, E. W.; O'Brien, A. G.; Baran, P. S. Total Synthesis of Dixiamycin B by Electrochemical Oxidation. *J. Am. Chem. Soc.* **2014**, *136* (15), 5571–5574.

(225) Dai, G.; Yang, L.; Zhou, W. Copper-Catalyzed Oxidative Dehydrogenative N–N Bond Formation for the Synthesis of N,N′-Diarylindazol-3-Ones. *Org. Chem. Front.* **2017**, *4* (2), 229–231.

(226) Tang, X.; Huang, L.; Yang, J.; Xu, Y.; Wu, W.; Jiang, H. Practical Synthesis of Pyrazoles via a Copper-Catalyzed Relay Oxidation Strategy. *Chem. Commun.* **2014**, *50* (94), 14793–14796.

(227) Cheng, Y.; Klein, C. K.; Tonks, I. A. Synthesis of Pentasubstituted 2-Aryl Pyrroles from Boryl and Stannyl Alkynes via One-Pot Sequential Ti-Catalyzed [2 + 2 + 1] Pyrrole Synthesis/Cross Coupling Reactions. *Chem. Sci.* **2020**, *11* (37), 10236–10242.

(228) He, R.; Jin, X.; Chen, H.; Huang, Z.-T.; Zheng, Q.-Y.; Wang, C. Mn-Catalyzed Three-Component Reactions of Imines/Nitriles, Grignard Reagents, and Tetrahydrofuran: An Expedient Access to 1,5-Amino/Keto Alcohols. *J. Am. Chem. Soc.* **2014**, *136* (18), 6558–6561.

(229) Benzing, E.; Kornicker, W. Dialkylamido-titan(IV)-chloride Und -alkoholate. *Chem. Ber.* **1961**, *94* (8), 2263–2267.

(230) Gragert, M. M.; Tomov, A. K.; Bettonville, S.; Pannier, G.; White, A. J. P.; Britovsek, G. J. P. Biaryl Group 4 Metal Complexes as Non-Metallocene Catalysts for Polyethylene with Long Chain Branching. *Eur. J. Inorg. Chem.* **2020**, *2020* (43), 4088–4092.

(231) Zhao, X.-F.; Zhang, C. Iodobenzene Dichloride as a Stoichiometric Oxidant for the Conversion of Alcohols into Carbonyl Compounds; Two Facile Methods for Its Preparation. *Synthesis (Stuttg).* **2007**, *2007* (04), 551–557.

(232) Kondo, M.; Takizawa, S.; Jiang, Y.; Sasai, H. Room-Temperature, Metal-Free, and One-Pot Preparation of 2H-Indazoles through a Mills Reaction and Cyclization Sequence. *Chem. – A Eur. J.* **2019**, *25* (42), 9866–9869.